VOL. 458 DECEMBER 23, 1988
COMPLETE IN ONE ISSUE

12th International Symposium on Column Liquid Chromatography Washington, DC, June 19–24, 1988 Part I

JOURNAL OF

CHROMATOGRAPHY

INTERNATIONAL JOURNAL ON CHROMATOGRAPHY, ELECTROPHORESIS AND RELATED METHODS

SYMPOSIUM VOLUMES

ELSEVIER

JOURNAL OF CHROMATOGRAPHY

Scope. The *Journal of Chromatography* publishes papers on all aspects of chromatography, electrophoresis and related methods. Contributions consist mainly of research papers dealing with chromatographic theory, instrumental development and their applications. The section *Biomedical Applications*, which is under separate editorship, deals with the following aspects: developments in and applications of chromatographic and electrophoretic techniques related to clinical diagnosis or alterations during medical treatment; screening and profiling of body fluids or tissues with special reference to metabolic disorders; results from basic medical research with direct consequences in clinical practice; drug level monitoring and pharmacokinetic studies; clinical toxicology; analytical studies in occupational medicine.

Submission of Papers. Papers in English, French and German may be submitted, in three copies. Manuscripts should be submitted to: The Editor of *Journal of Chromatography*, P.O. Box 681, 1000 AR Amsterdam, The Netherlands, or to: The Editor of *Journal of Chromatography, Biomedical Applications*, P.O. Box 681, 1000 AR Amsterdam, The Netherlands. Review articles are invited or proposed by letter to the Editors. An outline of the proposed review should first be forwarded to the Editors for preliminary discussion prior to preparation. Submission of an article is understood to imply that the article is original and unpublished and is not being considered for publication elsewhere. For copyright regulations, see below.

Subscription Orders. Subscription orders should be sent to: Elsevier Science Publishers B.V., P.O. Box 211, 1000 AE Amsterdam, The Netherlands, Tel. 5803 911, Telex 18582 ESPA NL. The *Journal of Chromatography* and the *Biomedical Applications* section can be subscribed to separately.

Publication. The *Journal of Chromatography* (incl. *Biomedical Applications* and *Cumulative Author and Subject Indexes, Vols. 401–450*) has 37 volumes in 1988. The subscription prices for 1988 are:

J. Chromatogr. (incl. *Cum. Indexes, Vols. 401–450*) + *Biomed. Appl.* (Vols. 424–460):
Dfl. 6290.00 plus Dfl. 962.00 (p.p.h.) (total *ca.* US$ 3537.50)

J. Chromatogr. (incl. *Cum. Indexes, Vols. 401–450*) only (Vols. 435–460):
Dfl. 5070.00 plus Dfl. 676.00 (p.p.h.) (total *ca.* US$ 2803.00)

Biomed. Appl. only (Vols. 424–434):
Dfl. 2145.00 plus Dfl. 286.00 (p.p.h.) (total *ca.* US$ 1185.75).

Our p.p.h. (postage, package and handling) charge includes surface delivery of all issues, except to subscribers in Argentina, Australia, Brasil, Canada, China, Hong Kong, India, Israel, Malaysia, Mexico, New Zealand, Pakistan, Singapore, South Africa, South Korea, Taiwan, Thailand and the U.S.A. who receive all issues by air delivery (S.A.L. — Surface Air Lifted) at no extra cost. For Japan, air delivery requires 50% additional charge; for all other countries airmail and S.A.L. charges are available upon request. Back volumes of the *Journal of Chromatography* (Vols. 1 through 423) are available at Dfl. 230.00 (plus postage). Claims for missing issues will be honoured, free of charge, within three months after publication of the issue. Customers in the U.S.A. and Canada wishing information on this and other Elsevier journals, please contact Journal Information Center, Elsevier Science Publishing Co. Inc., 655 Avenue of the Americas, New York, NY 10010. Tel. (212) 989-5800.

Abstracts/Contents Lists published in Analytical Abstracts, ASCA, Biochemical Abstracts, Biological Abstracts, Chemical Abstracts, Chemical Titles, Chromatography Abstracts, Current Contents/Physical, Chemical & Earth Sciences, Current Contents/Life Sciences, Deep-Sea Research/Part B: Oceanographic Literature Review, Excerpta Medica, Index Medicus, Mass Spectrometry Bulletin, PASCAL-CNRS, Referativnyi Zhurnal and Science Citation Index.

See inside back cover for Publication Schedule, Information for Authors and information on Advertisements.

0021-9673/88/$03.50

Printed in The Netherlands

For contents see p. VII

3 instruments to improve your protein chromatography

1 **Pump.** A four-channel Wiz® smartpump with microprocessor calibration always gives you the flow rate you want regardless of tubing condition. Its metal construction, powered counter-rotation on the rollers, and other construction features assure years of quiet, reliable service. The three-channel Tris® pump has the same quality construction in a compact model with conventional variable speed control. Either pump can form linear gradients with only two flasks and a stirrer. For difficult separations, an optional binary/ternary programmer with memory lets you generate practically any shape gradient with minimum effort.

2 **Fraction collector.** Retriever II® is Isco's popular compact fraction collector. It holds 174 tubes but measures less than 27 x 35 cm. You can program it by time, drop, or even directly in ml if you're using a Wiz pump. It holds tubes from 10-18 mm in diameter in small, self-standing racks that allow you to handle fractions in convenient groups. Other Isco fraction collectors include the low-cost Cygnet, the big Retriever IV, and the super-smart Foxy.

3 **Detector.** Isco's UA-5® has been the performance standard for LC detectors for many years. The current model gives you a built-in 10 cm recorder, 18 wavelengths from 214 to 660 nm, removable flow cells for everything from microbore HPLC to industrial prep LC, automatic peak collection, and a fluorescence attachment. You can even use it to scan electrophoresed slab jels. If you prefer a detector with continuously variable wavelengths, choose an Isco V4 with 10,000 hour deuterium lamp life. And for economy, a Model 228 will outperform other brands and give you most of the features of a UA-5.

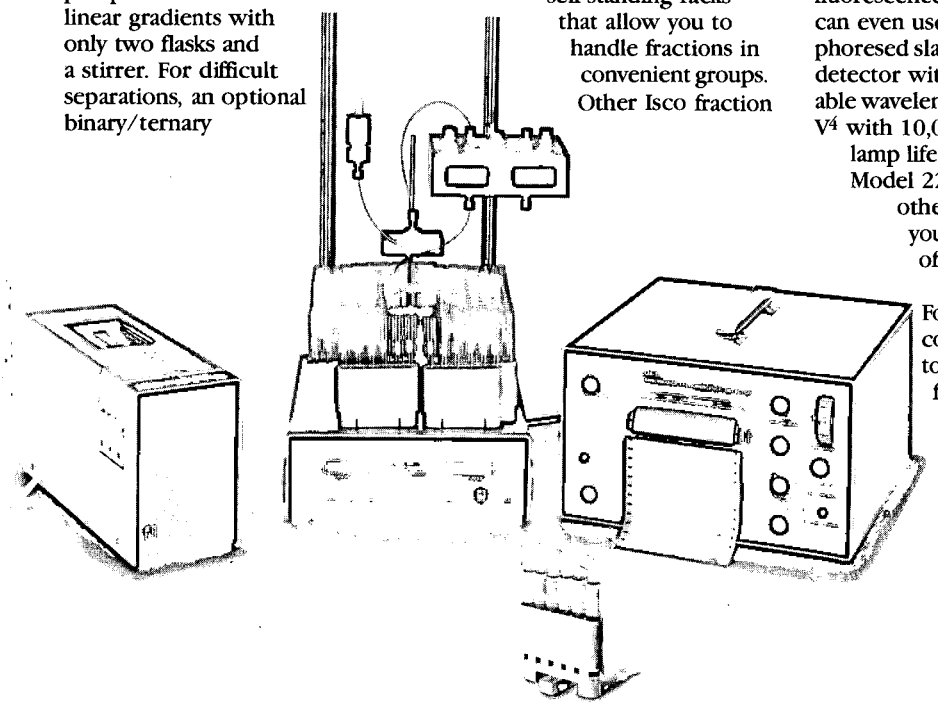

For more information, contact your distributor listed below for a free Isco catalog.

Isco, Inc.,
P.O. Box 5347,
Lincoln, NE 68505, U.S.A.

ISCO

Distributors • **The Netherlands:** Beun-de Ronde B.V. Abcoude 02946-3119 • **Hungary:** Lasis Handelsges. mbH Wien 82 01 83 • **Spain:** Iberlabo, s.a. Madrid 01 251 14 91 • **W. Germany:** Colora Messtechnik GmbH Lorch, Württ. 07172 1830 • **France:** Ets. Roucaire, S.A. Velizy (1) 39 46 96 33 • **Italy:** Gio. de Vita e C. s.r.l. Roma 4950611 • **U.K.:** Life Science Laboratories, Ltd. Luton (0582) 597676 • **Norway:** Dipl. Ing. Houm A.S. Oslo 02 15 92 50 • **Switzerland:** IG Instrumenten-Gesellschaft AG Zurich 01 4613311 • **Belgium:** SA HVL NV Bruxelles (02) 720 48 30 • **Denmark:** Mikrolab Aarhus A/S Højbjerg 06-29 61 11 • **Austria:** Neuber Gesellschaft mbH Wien 42 62 35 •

SynChropak SCD Drug Support

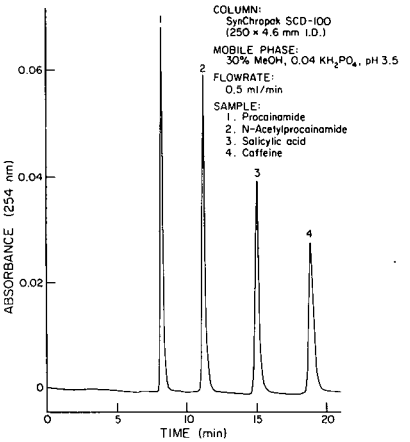

Designed to resolve small, basic molecules including therapeutic drugs by reversed phase HPLC.

- No silanol supressing additive required in the mobile phase
- Silanol deactivated
- Excellent resistance to acid hydrolysis
- Superior resolution
- Available in bulk and prepacked columns

SynChrom, Inc.
P.O. Box 310 • Lafayette, Indiana 47902-0310
(317) 423-4694
Telex: 757756

Quantitative Gas Chromatography for Laboratory Analyses and On-line Process Control

by G. GUIOCHON and C.L. GUILLEMIN

(Journal of Chromatography Library, 42)

This is a book which no chemical analyst should be without!

It explains how quantitative gas chromatography can - or should - be used for accurate and precise analysis. All the problems involved in the achievement of quantitative analysis by GC are covered, whether in the research lab, the routine analysis lab or in process control.

The discussion of the theoretical background is restricted to essentials. It is presented in a way that is simple enough to be understood by all analytical chemists, while being complete and up-to-date.

Extensive and detailed descriptions are given of the various steps involved in the derivation of precise and accurate data. This starts with the selection of the instrumentation and column, continues with the choice of optimum experimental conditions, then calibration and ends with the use of correct procedures for data acquisition and calculations.

Finally, there is almost always a way to reduce errors and an entire chapter deals with this single issue. Numerous examples are provided.

A lexicon explaining the most important chromatographic terms and a detailed index complete the book.

This is a book which should be on the library shelf of all universities, instrument companies and any laboratory and plant where gas chromatography is used.

1988 780 pages
US$ 165.75 / Dfl. 315.00
ISBN 0-444-42857-7

A brochure describing the contents of this book in detail is available on request from the publisher

Elsevier Science Publishers

P.O. Box 211, 1000 AE Amsterdam, The Netherlands
P.O. Box 1663, Grand Central Station, New York, NY 10163, USA

JOURNAL OF CHROMATOGRAPHY

VOL. 458 (1988)

JOURNAL
of
CHROMATOGRAPHY

INTERNATIONAL JOURNAL ON CHROMATOGRAPHY,
ELECTROPHORESIS AND RELATED METHODS

SYMPOSIUM VOLUMES

ELSEVIER
AMSTERDAM — OXFORD — NEW YORK — TOKYO

J. Chromatogr., Vol. 458 (1988)

The National Museum, Washington, DC, U.S.A.;
wood engraving, 1884

0021-9673/88/$03.50

Printed in The Netherlands

SYMPOSIUM VOLUME

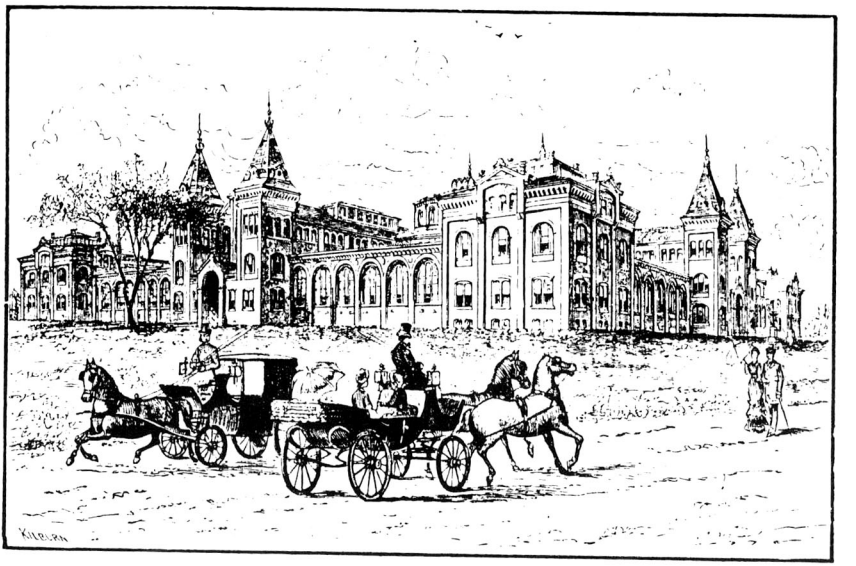

TWELFTH INTERNATIONAL SYMPOSIUM ON COLUMN LIQUID CHROMATOGRAPHY

PART I

Washington, DC (U.S.A.), June 19–24, 1988

Guest Editor

G. GUIOCHON

(Knoxville and Oak Ridge, TN)

Sponsoring Scientific Organizations

Washington Chromatography Discussion Group
Chromatography Forum of the Delaware Valley
East Tennessee Chromatography Discussion Group
San Francisco Bay Area Chromatography Colloquium
Subdivision of Chromatography and Separation Chemistry of the Division of Analytical Chemistry of the American Chemical Society
Federation of Chromatography Discussion Groups
Committee E-19 on Chromatography of the American Society for Testing and Materials
The Chromatographic Society
Arbeitskreis Chromatographie der Fachgruppe Analytischen Chemie der Gesellschaft Deutscher Chemiker
Österreichische Gesellschaft für Mikrochemie und Analytische Chemie
Koninklijke Nederlandse Chemische Vereniging
Schweizerischer Chemiker-Verband
Svenska Kemistsamfundet/Analytiska Sektionen
Societa Italiana di Biochimica Clinica
Groupement pour l'Avancement des Méthodes Spectroscopiques et Physico-Chimiques d'Analyse (G.A.M.S.)
Société Française de Chimie
The Chemical Society of Japan
The Japan Society for Analytical Chemistry
Pharmaceutical Society of Japan
The Japanese Biochemical Society
The Agricultural Chemical Society of Japan

Permanent Committee

Dr. F. Erni, Sandoz AG, Basle, Switzerland
Dr. R. W. Frei, Free University, Amsterdam, The Netherlands
Dr. G. Guiochon, University of Tennessee, Knoxville, TN, U.S.A.
Dr. Cs. Horváth, Yale University, New Haven, CT, U.S.A.
Dr. J. F. K. Huber, University of Vienna, Austria
Dr. K.-P. Hupe, Hewlett-Packard GmbH, Waldbronn, F.R.G.
Dr. B. L. Karger, Barnett Institute, Boston, MA, U.S.A.
Dr. J. J. Kirkland, E. I. du Pont de Nemours, Wilmington, DE, U.S.A.
Dr. J. H. Knox, University of Edinburgh, U.K.
Dr. H. Poppe, University of Amsterdam, The Netherlands
Dr. D. E. Westerlund, Uppsala University, Sweden

Scientific Committee

Dr. R. A. Barford, U.S. Department of Agriculture, Philadelphia, PA, U.S.A.
Dr. E. Bayer, University of Tübingen, F.R.G.
Dr. K. Benedek, Smith Kline, Philadelphia, PA, U.S.A.
Professor H. Engelhardt, University of Saarlandes, Saarbrücken, F.R.G.
Professor A. F. Fell, University of Bradford, U.K.
Dr. J. L. Glajch, E. I. du Pont de Nemours, Wilmington, D.E., U.S.A.
Professor E. Grushka, The Hebrew University, Jerusalem, Israel
Professor S. Hara, Tokyo College of Pharmacy, Japan
Professor H. Hatano, Kyoto University, Japan
Professor D. Ishii, Nagoya University, Japan
Professor J. W. Jorgenson, University of North Carolina, Chapel Hill, NC, U.S.A.
Dr. E. sz. Kováts, École Polytechnique, Lausanne, Switzerland
Professor C. Lochmüller, Duke University, Durham, NC, U.S.A.
Professor C. Lucarelli, Istituto Superiore di Sanita, Rome, Italy
Dr. R. E. Majors, EM Science, Cherry Hill, NJ, U.S.A.
Professor D. E. Martire, Georgetown University, Washington, DC, U.S.A.
Professor M. V. Novotny, Indiana University, Bloomington, IN, U.S.A.
Professor W. H. Pirkle, University of Illinois, Urbana, IL, U.S.A.
Professor F. E. Regnier, Purdue University, West Lafayette, IN, U.S.A.
Professor K. Unger, Johannes Gutenberg University, Mainz, F.R.G.
Professor M. Verzele, State University of Ghent, Belgium

Local Committee

Ms. L. A. Beaver, Food and Drug Administration, Rockville, MD, U.S.A. (Chairman)
Ms. A. Barnett, Perkin-Elmer Corporation, Rockville, MD, U.S.A.
Mr. T. Danaher, Perkin-Elmer Corporation, Rockville, MD, U.S.A.
Dr. B. Dickens, U.S. National Bureau of Standards, Gaithersburg, MD, U.S.A.
Dr. L. V. Feyns, U.S. Pharmacopeia, Rockville, MD, U.S.A.
Mr. I. Lurie, U.S. Drug Enforcement Administration, McLean, VA, U.S.A.
Dr. J. Olpin, Flow Laboratories, McLean, VA, U.S.A.
Ms. R. Parris, U.S. National Bureau of Standards, Gaithersburg, MD, U.S.A.
Dr. L. Sander, U.S. National Bureau of Standards, Gaithersburg, MD, U.S.A.
Dr. B. Shaikh, U.S. Food and Drug Administration, Beltsville, MD, U.S.A.
Dr. E. Smith, U.S. Food and Drug Administration, Rockville, MD, U.S.A.
Dr. M. P. Strickler, Waters Chromatography, Fairfax, VA, U.S.A.
Dr. P. White, U.S. Pharmacopeia, Rockville, MD, U.S.A.
Dr. S. Wise, U.S. National Bureau of Standards, Gaithersburg, MD, U.S.A.

CONTENTS

12TH INTERNATIONAL SYMPOSIUM ON COLUMN LIQUID CHROMATOGRAPHY, WASHINGTON, DC, JUNE 19–24, 1988, PART I

In articles with more than one author, the name of the author to whom correspondence should be addressed is indicated in the article heading by a 6-pointed asterisk (*)

The proceedings of the *Twelfth International Symposium on Column Liquid Chromatography, Washington, DC, June 19–24, 1988*, are published in three volumes of the *Journal of Chromatography*: Vols. 458 and 459 (1988) and 461 (1989). The Foreword to the proceedings, and information on the Sponsoring Scientific Organizations and the Scientific and Organization Committees only appear in Vol. 458. Vol. 459 is dedicated to the memory of **Dr. István Halász**, and opens with an obituary.

Journal of Chromatography, 458 (1988) XI–XII
Elsevier Science Publishers B.V., Amsterdam — Printed in The Netherlands

FOREWORD

The *Twelfth International Symposium on Column Liquid Chromatography* (HPLC'88) took place in Washington, DC, on June 19–24, 1988 at the Washington Sheraton Hotel. The vigor of research in this area of analytical chemistry and the impact of advances in chromatography on developments in many other areas of science were demonstrated by the scope of the program and the enthusiasm of the participants. The meeting was attended by over 1300 registered delegates from over 29 countries. Three parallel sessions permitted the presentation of 120 lectures and oral contributions, while another 400 posters contributions were exhibited and discussed. Discussion sessions stretched into the late evening, but were active and informative. A major exposition of instruments and products related to chromatography attracted 112 exhibitors and was attended by 500 people, in addition to the full delegates.

The success of the meeting was largely due to the high quality of its scientific program. The remarkable achievements of the chairmen of the previous symposia of this series have made the HPLC meetings the premier venue on chromatography and the meeting to attend in order to present new results and to search for new ideas. Thanks to the efforts of my predecessors and especially of Drs. Cs. Horváth and R. Majors who organized HPLC'84 and HPLC'86, the two previous symposia held in the U.S.A., it was easy to attract a large number of original contributions. The help of the members of the scientific committee in the review of the 600 abstracts submitted and in the selection of the program is gratefully acknowledged. These volumes of the *Journal of Chromatography* contain the text of many of the papers presented during the symposium and submitted by their authors for inclusion in the proceedings. They constitute the scientific core of the symposium and its legacy to the community. The permanent committee is grateful to the Scientific Editor and to the editorial staff of the *Journal of Chromatography* for their skill in producing these volumes and their efforts in doing so in such a timely fashion.

The organization of a meeting of the size of HPLC'88 is a very rewarding experience. It requires the contribution of many different people and leads to interactions which would otherwise never take place. I was fortunate to have the help and support of many colleagues, friends and associates. It is a pleasure to thank the members of my research groups at the University of Tennessee and Oak Ridge National Laboratory, and the students of Yale University who actively contributed to the smooth conduct of the meeting. Special thanks are due to Mrs. Janet Cunningham, Symposium Manager, for lending her organizational skills before and during the meeting and allowing its successful operation, and to Mr. Robert Beaudoux, the Exposition Manager, for his thoroughly professional organization of the largest exhibition ever arranged during a chromatography symposium.

Finally, it is a pleasure to acknowledge the help of Mrs. Lois Ann Beaver, who chaired the local organization committee, arranged the social functions, coordinated the work of the various parties involved, supervised the accounting and suggested successful solutions to the multitude of problems constantly raised by the organization of this important event. Her enthusiastic support was invaluable.

Shortly after HPLC'88, on August 22, 1988, Professor István Halász passed away. His personality has strongly marked the development of modern chromatogra-

phy for the last thirthy years. His influence on the scientific contributions of a few of us has been of critical importance. His lecture on "Efficiency, resolution and reproducibility in chromatography", presented at HPLC'88 on June 21, 1988, was his last scientific contribution. To his family and his friends I extend here my heartfelt sympathy. The second volume of these proceedings is dedicated to his memory.

Concord, TN (U.S.A.) GEORGES GUIOCHON

Journal of Chromatography, 458 (1988) 1–11
Elsevier Science Publishers B.V., Amsterdam — Printed in The Netherlands

CHROMSYMP. 1450

COMBINED LECTIN-AFFINITY AND METAL-INTERACTION CHROMATOGRAPHY FOR THE SEPARATION OF GLYCOPHORINS BY HIGH-PERFORMANCE LIQUID CHROMATOGRAPHY

DANILO CORRADINI*, ZIAD EL RASSI and CSABA HORVÁTH
Department of Chemical Engineering, Yale University, New Haven, CT 06520 (U.S.A.)
and
GUADALUPE GUERRA and WILLIAM HORNE
Department of Pathology, School of Medicine, Yale University New Haven, CT 06520 (U.S.A.)

SUMMARY

Human erythrocyte sialoglycoproteins, or glycophorins, were chromatographed by lectin-affinity and metal-interaction chromatography on high-performance liquid chromatographic columns. Glycophorins A, B and C were separated from other proteins and from glycophorin E by using a column containing wheat germ agglutinin, immobilized on a microparticulate silica support. The glycophorins were adsorbed on the lectin column from a mobile phase containing 0.25 *M* sodium chloride and recovered by stepwise desorption with 0.2 *M* N-acetylglucosamine solution. Glycophorins A, B and C were separated into the individual components on a silica-bound iminodiacetic acid stationary phase in the copper(II) chelate form. The separation of the glycophorins by metal-interaction chromatography was accomplished by decreasing salt gradient elution. Retention times and resolution of the individual glycophorins were sensitive to the initial sodium chloride concentration and the pH of the eluent. Addition of methanol to the eluent increased the resolution. The effects of linear, decreasing gradients of pH and methanol in 25 m*M* phosphate buffer on the resolution of glycophorins were also investigated. In both types of chromatography the mobile phases contained 0.05% (w/v) sodium dodecyl sulfate. With octylglycoside or CHAPS in the eluent glycophorins A and C could not be eluted. Sodium dodecyl sulfate polyacrylamide gel electrophoresis was used to analyze all the chromatographic results.

INTRODUCTION

High-performance liquid chromatography (HPLC) is increasingly employed in the isolation and separation of membrane proteins[1]. These high-molecular-weight

* Permanent address: Istituto di Cromatografia, C.N.R., Area della Ricerca di Roma, I-00016 Rome, Italy.

0021-9673/88/$03.50

amphiphilic molecules often contain a highly hydrophilic glycan moiety in the extracellular domain and a strongly hydrophobic amino acid sequence in their membrane-spanning domain. The peculiar molecular architecture of membrane proteins engenders particular problems in their chromatography and necessitates the use of aqueous eluents that contain surfactants to keep them in molecular dispersion and to improve their recovery[2]. Size-exclusion[2–6], ion-exchange[5,6] and hydrophobic-interaction chromatography[7,8] have traditionally been employed for the purification. In the reversed-phase chromatography[9,10] of membrane proteins hydro-organic eluents are usually much stronger, and therefore more denaturing, than those otherwise employed in the HPLC of proteins. Affinity chromatography on lectin stationary phases has also been used for the purification of membrane proteins[1,11,12]. Recently affinity chromatography and metal-interaction chromatography have been employed in the HPLC of such proteins[13–15].

In this study, glycophorins, the erythrocyte membrane sialoglycoproteins, were separated by HPLC employing the two chromatographic techniques mentioned above. These integral membrane proteins contain almost 60% (w/w) glycan, which is highly sialylated, and a hydrophobic domain of about 23 amino acids that forms the intramembraneous segment[16,17]. According to Anstee[18], human erythrocyte membranes contain at least four sialoglycoproteins, the glycophorins A, B, C and E. They have different amino acid contents and electrophoretic mobilities in sodium dodecylsulfate polyacrylamide gel electrophoresis (SDS-PAGE). In another nomenclature the letters α, δ, β and γ, are used instead of A, B, C and E, respectively[18,19].

In addition to their attraction as readily available members of an important class of membrane proteins, glycophorins are of interest because they carry a number of antigenic determinants, which are involved in blood types[18]. Further, they provide an anchoring site for the stabilizing membrane skeleton[20,21] and hence they contribute to the reversible deformability of erythrocytes. The structure of glycophorins A, B and C has been investigated and their amino acid sequences and glycosylation sites have been determined[22,23].

The interest in glycophorin structure and function prompted us to examine the possibility of a relatively rapid and straightforward HPLC procedure for the separation of the individual glycophorins. Traditional approaches by size-exclusion[24] and lectin-affinity chromatography[25] and also by preparative SDS-PAGE[19] are not only cumbersome but also rather ineffective for purifying the less abundant B, C and E forms. Recently, Blanchard *et al.*[23] have developed a method for the preparative isolation of glycophorin B and a mixture of glycophorins C and E by a combination of high-performance size-exclusion and ion-exchange chromatography with Triton X-100 in the eluent.

This paper presents the results of a study of the chromatographic conditions for the separation of glycophorins by a dual approach with high-performance metal-interaction chromatography and lectin-affinity chromatography, in which columns with microparticulate, macroporous siliceous stationary phases were used. Both techniques have already been successfully used for the HPLC of glycoproteins[26–28] and immobilized wheat germ agglutinin has been a suitable stationary phase for the isolation of glycophorins[25]. As the various glycophorins differ in their histidine contents, a Cu^{II}–iminodiacetic acid (IDA) column, which separates proteins according to their histidine content[29,30], was selected for metal-interaction chromatography.

The combination of the two HPLC techniques resulted in a relatively fast analytical and micropreparative procedure for the assay and/or purification of glycophorins.

EXPERIMENTAL

Materials

Wheat germ agglutinin (WGA), sodium chloride, *n*-octyl-β-D-glucopyranoside (octyl glucoside), N-acetyl-D-glucosamine (GlcNAc), 3-[(3-cholamidopropyl)dimethylammonio]-1-propanesulfonate] (CHAPS), 2-(N-morpholino)ethanesulfonic acid (MES), 3,5-diiodosalicylic acid (DIS) and N-2-hydroxyethylpiperazine-N′-2-ethanesulfonic acid (HEPES) were obtained from Sigma (St. Louis, MO, U.S.A.). Phosphoric acid, acetic acid, sodium and lithium hydroxide, nickel sulfate, copper(II) nitrate, the disodium salt of ethylenediaminetetraacetic acid (EDTA) and HPLC-grade methanol were purchased from Fisher (Pittsburgh, PA, U.S.A.). SDS, iron(III) chloride and IDA were obtained from Aldrich (Milwaukee, WI, U.S.A.). Two spherical silica gels having nominal particle and pore diameters of 7 μm and 300 Å, respectively, were used. They were supplied under the respective trade names of Nucleosil and Zorbax by Macherey, Nagel & Co. (Düren, F.R.G.) and DuPont (Wilmongton, DE, U.S.A.). Lithium diiodosalicylic acid (LIS) was prepared by twice recrystallizing DIS from methanol, then allowing the recrystallized DIS to react with an aqueous solution of lithium hydroxide and recrystallizing the resulting salt.

Instruments

The liquid chromatograph was assembled from a Perkin-Elmer (Norwalk, CT, U.S.A.) Series 4 solvent delivery pump, controlled by an LC terminal, Model LC-85B spectrophotometric detector, Model LCI-100 laboratory computing integrator with thermal printer and a Model 7500 laboratory computer with Chromatographics 3 software for data acquisition and reprocessing. Samples were injected by a Model 7010 sampling valve with a 100-μl sample loop from Rheodyne (Berkeley, CA, U.S.A.). A Model 110B solvent delivery pump from Beckman (San Ramon, CA, U.S.A.) was used to load the metal-interaction column with the metal of interest.

Columns

The IDA stationary phase was prepared from Nucleosil silica and the WGA was immobilized on the Zorbax silica support according to methods outlined elsewhere[26–31]. All columns were made of 100 or 60 mm × 4.6 mm I.D. No. 316 stainless-steel tubing (Handy and Harman, Morristown, PA, U.S.A.) and packed at 8000 p.s.i. Metal-interaction and lectin columns were packed from a methanol slurry and a slurry in 25 m*M* phosphate buffer (pH 6.0) containing 0.5 *M* sodium chloride and 50% (w/v) sucrose, respectively.

Protein isolation

Outdated units of erythrocytes were obtained from the blood bank of the Yale-New Haven Hospital. Erythrocytes were washed, and hemoglobin-free membranes were prepared by the method of Dodge *et al.*[32]. The LIS–phenol method[33] was employed to obtain a lyophilized extract of the glycophorins from the erythrocyte membranes.

Procedure

The IDA–silica column was washed successively with 50 ml each of water, 50 m*M* EDTA solution, methanol and water again. Thereafter, it was perfused with 100 ml of 15 m*M* copper(II) chloride solution and then washed with water to remove the unbound metal. From time to time the Cu^{II}–IDA column was regenerated by washing with 50 m*M* disodium EDTA and subsequently reloading it with the metal.

Gel electrophoresis

In each chromatographic run 10–25 fractions ranging from 0.5 to 2.2 ml were collected. They were dialyzed against water to remove excess of salt, concentrated to dryness under vacuum and subjected to discontinuous SDS-PAGE[34] with a 3.5% acrylamide stacking gel and a 10% acrylamide running gel. All reagents were of electrophoresis grade from Bio-Rad Labs. (Richmond, CA, U.S.A.). The proteins bands were rendered visible by silver staining[35].

RESULTS AND DISCUSSION

Lectin-affinity chromatography

The glycophorin extract from human red blood cells was chromatographed on the WGA column that was pre-equilibrated with 25 m*M* phosphate buffer (pH 6.0) containing 0.05% (w/v) SDS and 0.25 *M* sodium chloride. In a typical chromatographic run, 0.7 mg of glycoprotein were applied to the column, which was washed with the above buffer for 15 min in order to elute all non-glycophorins components of the sample and glycophorin E, before the tightly bound glycophorin A, B and C were eluted in a single desorption step with 0.2 *M* N-acetylglucosamine in the equilibrating buffer. The fractions taken throughout the run were analyzed by SDS-PAGE. This confirmed the composition of the peaks and showed that glycophorin E was eluted during the preceding washing step, as illustrated in Fig. 1. The results show that lectin chromatography on a WGA–silica column is an effective means of purifying the glycophorins from other proteins and of isolating pure glycophorin E.

The salt concentration in the eluent is very critical in this kind of chromatographic separation, because electrostatic interactions between the sample components and the lectin play an important role in the retention process and they are strongly affected by the salt concentrations[36]. Therefore, a certain ionic strength of the mobile phase was required in order to elute the glycophorins from the WGA column. On the other hand, when the buffer contained sodium chloride concentrations higher than 0.7 *M*, the glycophorins were very tightly bound to WGA, presumably by hydrophobic interactions, and could not be desorbed with GlcNAc. Buffers containing 0.2–0.5 *M* sodium chloride were the most appropriate in each of the pre-equilibration, washing and desorption steps.

Metal-interaction chromatography

An IDA acid column in the copper(II) chelate form was used for the separation of glycophorins A, B and C with 0.05% (w/v) of SDS in the mobile phase and a linear gradient of decreasing sodium chloride concentration. In order to find the optimal conditions, the influence of the mobile phase pH and composition, *i.e.*, concentration of methanol, nature of the surfactant and sodium chloride concentration in the starting eluent, was examined.

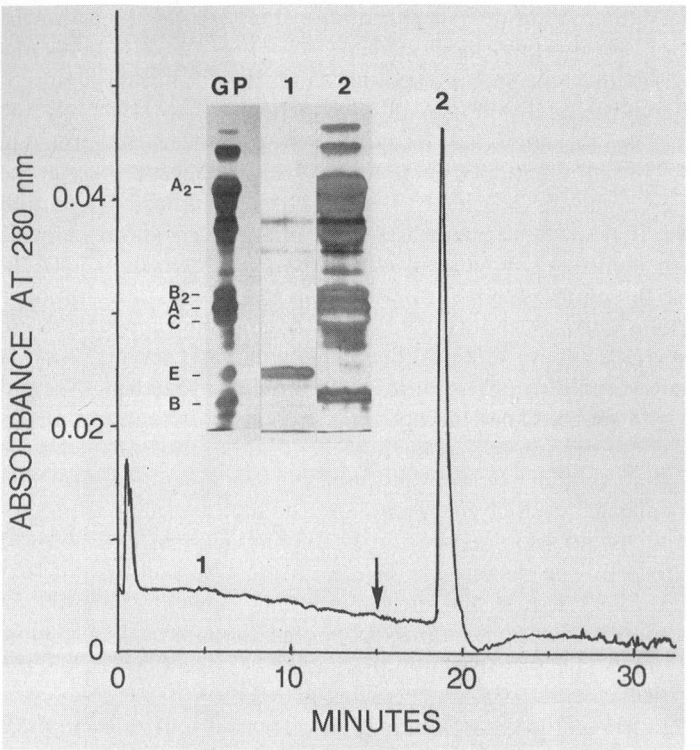

Fig. 1. Isolation of glycophorins by lectin affinity chromatography and SDS-PAGE analysis of glycophorin extract (GP) and fractions of chromatographed glycophorins. Column, 60 × 4.6 mm I.D., packed with silica-bound WGA; temperature, 25°C; flow-rate, 1 ml/min; equilibrating buffer, 25 m*M* phosphate (pH 6.0), containing 0.25 *M* sodium chloride and 0.05% (w/v) SDS. The arrow indicates the desorption step with 0.2 *M* GlcNAc in the equilibrating buffer. Sample, 0.7 mg of glycophorins in 100 μl. Inset: electropherograms of unfractionated glycophorin extract (GP), fractions containing glycophorin E (1) and the glycophorins eluted with the haptenic sugar (2). A_2, glycophorin A dimer; B_2, glycophorin B dimer; A, glycophorin A monomer; B, glycophorin B monomer; C, glycophorin C monomer; E, glycophorin E monomer.

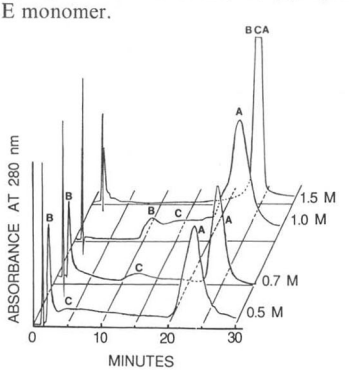

Fig. 2. Separation of glycophorins by metal-interaction chromatography with starting eluents having different sodium chloride concentrations. Column, 100 × 4.6 mm I.D., packed with Cu^{II}–IDA silica; temperature, 25°C; flow-rate, 1 ml/min; 20-min linear gradient with decreasing salt concentration from 0.5, 0.7, 1.0 or 1.5 to 0 *M* sodium chloride in 25 m*M* phosphate buffer (pH 6.0) containing 0.05% (w/v) SDS, followed by a 10-min isocratic elution with the gradient former. Sample, 0.7 mg of glycophorins in 100 μl.

The effect of the sodium chloride concentration in the starting eluent on the retention and resolution of glycophorin is evident from Figs. 2 and 3. As the chromatogram in Fig. 2 shows, the starting sodium chloride concentration significantly affects the retention and resolution of glycophorins. The effect on the chromatographic behavior of the individual glycoproteins is more clearly illustrated in Fig. 3 by plots of the adjusted retention volume *versus* the salt concentration in the starting eluent. Only glycophorin C yielded a linear plot. The adjusted retention volume of glycophorin B first slightly increases with increasing sodium chloride concentration and then increases dramatically when the latter exceeds 0.7 *M*. In contrast, the adjusted retention volume of glycophorin A shows the opposite dependence on salt concentration. Without added salt in the eluent, glycophorins were not retained on the Cu^{II}–IDA column. On the other hand, with 1.5 *M* sodium chloride in the starting eluent they were all strongly retained and were eluted together at the end of the gradient run. Fig. 3 suggests that the optimal difference in retention times is achieved when the salt concentration in the starting eluent is about 0.7 *M*. From the results, we may infer that at high salt concentrations in the eluent, electrostatic repulsion between the sialic acid-rich glycoproteins and the slightly acidic stationary phase is attenuated and, in addition to specific metal interactions, hydrophobic interactions also contribute to the retention. However, it must be pointed out that increasing salt concentrations reduce the critical micellar concentration of the surfactant and may promote association of the hydrophobic domains of the proteins. Either of these factors may affect the retention behavior of glycophorins on the Cu^{II}–IDA column.

The effect of eluent pH on the separation of glycophorins is illustrated in Figs. 4 and 5. The chromatograms in Fig. 4 show that the retention and resolution of glycophorin C is particularly pH dependent. On decreasing the pH of the eluent from 7.0 to 5.3, the retention of all glycophorins decreased, as seen in Fig. 5. At pH 5.0 or below, they all were eluted as a single peak without retention. This is in agreement with the findings[29,30] that protein retention on chelates of "soft" metals, such as copper, decreases with the pH in the range where the protonation of the amino groups in histidine residues (which are believed to be mainly responsible for retention) changes appreciably with pH. Glycophorin A was recovered in relatively pure form when the pH of the eluent ranged from 5.3 to 6.5, the best results being obtained at pH 5.3.

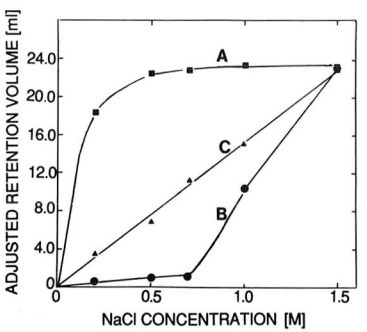

Fig. 3. Plots of adjusted retention volume of glycophorins against the concentrations of sodium chloride in the starting eluent. Conditions as in Fig. 2.

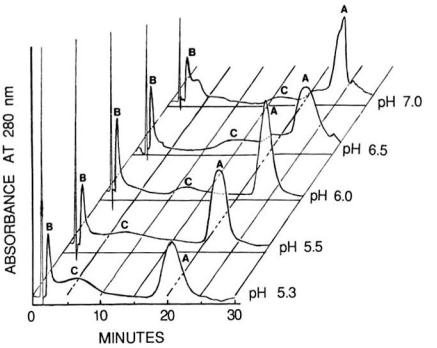

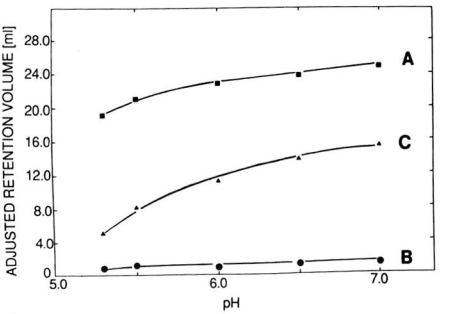

Fig. 4. Separation of glycophorins by metal-interaction chromatography with eluents of different pH. Conditions as in Fig. 2 except the starting eluent contained 0.7 *M* sodium chloride and the pH of the 25 m*M* phosphate buffer was varied.

Fig. 5. Plots of adjusted retention volume of glycophorins against the pH of the eluent. Conditions as in Fig. 4.

However, at this particular pH, glycophorins B and C were not well resolved. On the other hand, glycophorin B was obtained in pure form at pH 7.0, whereas glycophorin A and C were not well resolved. A compromise was reached by using pH 6.0, where all glycophorins were recovered in relatively pure form.

A decreasing pH gradient was also employed in some experiments. Fig. 6 illustrates the separation of glycophorins on the Cu^{II}–IDA column with a gradient of linearly decreasing pH (from 7.0 to 5.0) and salt concentration (from 0.7 to 0 *M* sodium chloride) in the eluent. According to SDS-PAGE, the first peak was pure glycophorin B and the second was relatively pure glycophorin C, whereas the third peak of glycophorin A contained traces of glycophorin C.

The effect of the addition of methanol to the eluent was examined under the conditions described above, except that the buffer was 25 m*M* phosphate, the decrease in pH was from 6.5 to 5.0 and 5 or 10% (v/v) methanol was added to the starting eluent. The results are presented in Figs. 7 and 8. With 5% (v/v) methanol in the starting eluent both the retention and resolution of glycophorins C and A increased. However, even under these conditions, no separation was obtained for glycophorins C and E. With 10% (v/v) methanol, the resolution of glycophorins A and C was poor, owing to the increased retention of glycophorin C. At the higher methanol concentration, glycophorin B present in the sample was not eluted as a sharp peak, and traces of it were found in all fractions collected throughout the chromatogram (see Fig. 8, panel 3). These results suggested the use of 5% methanol in the starting eluent. Generally, as seen in Fig. 7, the retentions of all glycophorins increase with increasing methanol concentration. This in agreement with previous observations[31] that in metal-interaction chromatography, protein retention increases with increasing organic solvent content of the mobile phase. This is probably due to weaker hydration of the metal chelate.

The ionic and non-ionic surfactants SDS, CHAPS and octylglucoside were compared for their effectiveness in the separation of glycophorins on a Cu^{II}–IDA column at concentrations of 0.05%, 0.085% and 0.87% (w/v), respectively. In these experiments, a decreasing linear salt gradient from 1.0 to 0 *M* sodium chloride in 25

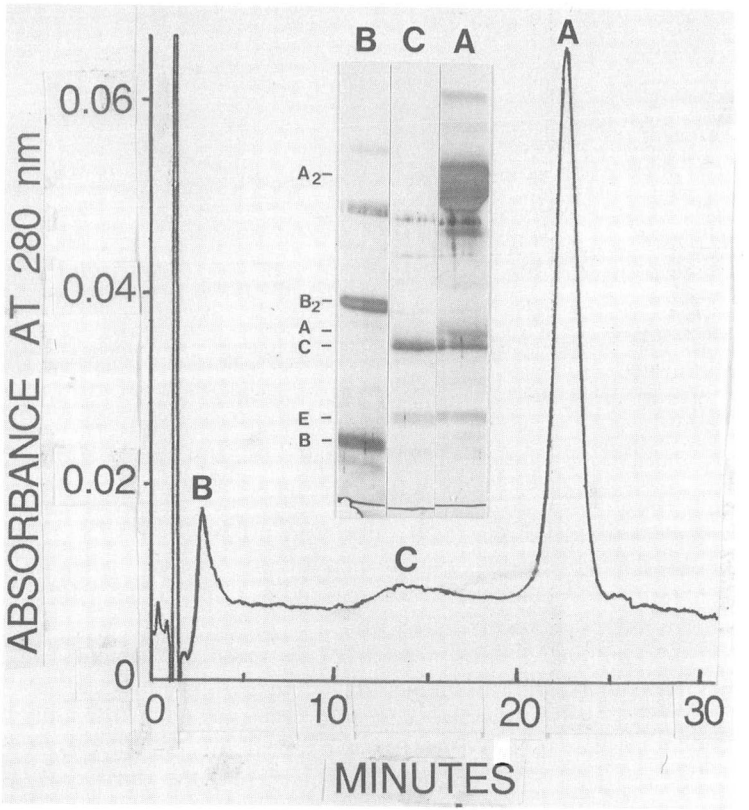

Fig. 6. Separation of glycophorins by metal-interaction chromatography. Conditions as in Fig. 2, except the starting eluent was 25 m*M* HEPES–MES–acetic acid (pH 7.0) containing 0.7 *M* sodium chloride and the gradient former was 25 m*M* HEPES–MES–acetic acid buffer (pH 5.0); both eluents contained 0.05% (w/v) SDS. Inset: electropherogram of representative fractions from peaks B, C and A. The positions of glycophorin bands are as in Fig. 1.

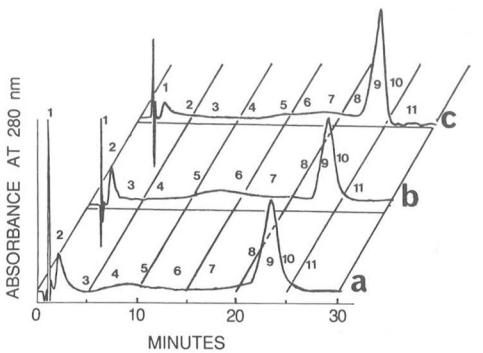

Fig. 7. Separation of glycophorins by metal-interaction chromatography with or without methanol in the starting eluent. Conditions as in Fig. 2, except starting eluent, 25 m*M* phosphate buffer (pH 6.5) containing 0.7 *M* sodium chloride, 0.05% (w/v) SDS and (a) 0%, (b) 5% and (c) 10% (v/v) methanol; gradient former, 25 m*M* phosphate buffer (pH 5.0) containing 0.05% (w/v) SDS. Numbers in the chromatogram indicate the collected fractions. Sample, 0.8 mg of glycophorins in 100 μl.

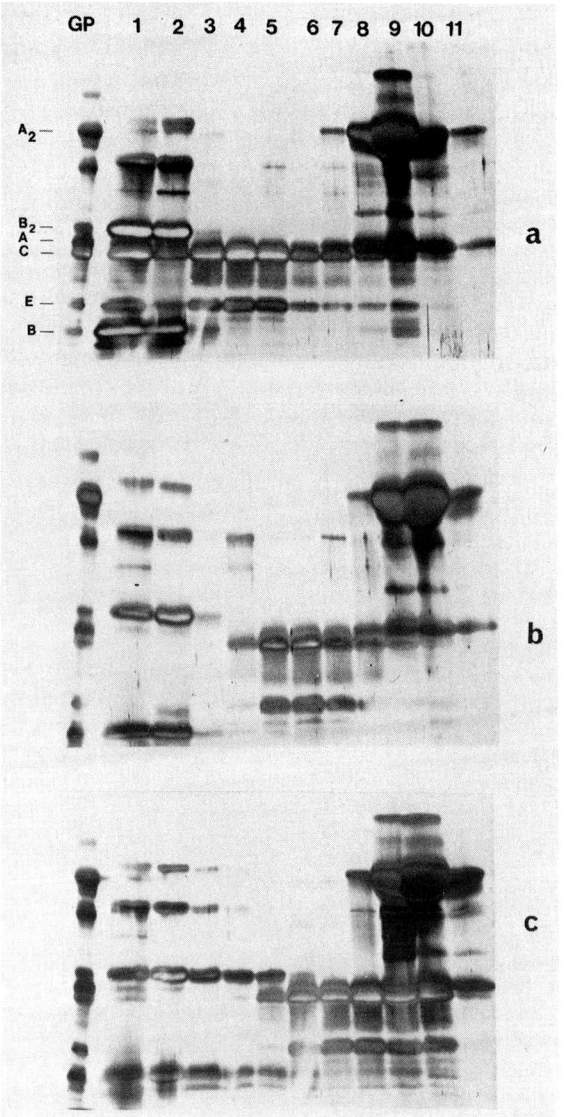

Fig. 8. SDS-PAGE analysis of fractions obtained in the metal-interaction chromatography of glycophorins under the conditions shown in Fig. 7. Panels a, b and c correspond to the chromatogram obtained with 0%, 5% and 10% (v/v) methanol, respectively, in the starting eluent. The codes for the individual glycophorins are given in Fig. 1.

m*M* phosphate (pH 6.0) was used with a 10-min isocratic elution at the end of the chromatographic run. Whereas glycophorin B was eluted close to the mobile phase hold-up time of the column with all of the surfactants tested, only eluents containing SDS were effective at desorbing glycophorins A and C from the column under our experimental conditions.

The effectiveness of different immobilized metals in separating the glycophorins was examined. Metal-interaction columns were prepared by loading the IDA–silica column with Fe^{III} and Ni^{II}. In both instances, the glycophorins were not retained at either low or high salt concentrations in the eluent in the pH range 5.0–7.0.

Our study has shown that metal-interaction chromatography is an effective method for separating integral membrane glycoproteins. The results confirmed the expectation that glycophorins A, C and B having five, three and two histidines, respectively, were retained in order of increasing number of histidine residues on the Cu^{II}–IDA column under all conditions of our experiments. The lack of separation of glycophorins C and E on the Cu^{II}–IDA column under any of the conditions tested supports previous suggestions[18] that these two glycophorins are very closely related. Depending on the desired separation, conditions can be varied to adjust the retention of glycophorin C to favor complete isolation of either glycophorin A or B or to obtain significant portions of all three glycoproteins in the pure form. When used in conjunction with the WGA column, which separates glycophorin E from the other glycophorins, the Cu^{II}–IDA column permits the rapid separation of the erythrocyte glycophorins, thus facilitating the analysis and purification of these important membrane proteins.

ACKNOWLEDGEMENTS

The authors thank George E. Palade for supporting and advancing this project and Robert Johnson for assistance with the experiments. This work was supported by Grants Nos. GM 20993, CA 21948 and GM 21714 from the National Institutes of Health, U.S. Department of Health and Human Services.

REFERENCES

1 G. W. Welling, R. Van der Zee and S. Welling-Wester, *J. Chromatogr.*, 418 (1987) 223.
2 R. S. Matson and S. C. Goheen, *J. Chromatogr.*, 359 (1986) 285.
3 E. Mascher and P. Lundahl, *J. Chromatogr.*, 397 (1987) 175.
4 G. W. Welling, K. Slopsema and S. Welling-Wester, *J. Chromatogr.*, 359 (1986) 307.
5 D. Josić, W. Hofmann, B. Wieland, R. Nuck and W. Reutter, *J. Chromatogr.*, 359 (1986) 315.
6 D. Josić, E. Mattia, G. Ashwell and J. van Renswoude, *Anal. Biochem.*, 152 (1986) 42.
7 D. Josić, W. Hofmann and W. Reutter, *J. Chromatogr.*, 371 (1986) 43.
8 J. L. Seltzer, M. L. Eschbach and A. Z. Eisen, *J. Chromatogr.*, 326 (1985) 147.
9 R. Van der Zee, S. Welling-Wester and G. W. Welling, *J. Chromatogr.*, 266 (1983) 577.
10 J. Heukeshoven and R. Dernick, *J. Chromatogr.*, 326 (1985) 91.
11 W. L. Adair and S. T. Kornfeld, *J. Biol. Chem.*, 249 (1974) 4696.
12 K. Resch, A. Loracher, B. Mahler, M. Stoeck and H. N. Rode, *Biochim. Biophys. Acta*, 511 (1978) 176.
13 D. Josić, W. Hofmann, R. Habermann, A. Becker and W. Reutter, *J. Chromatogr.*, 397 (1987) 39.
14 C. A. K. Borrebaeck, J. Soares and B. Mattiasson, *J. Chromatogr.*, 284 (1984) 187.
15 Y. Kato, T. Kitamura, K. Nakamura, A. Mitsui, Y. Yamasaki and T. Hasimoto, *J. Chromatogr.*, 391 (1987) 395.
16 R. J. Winzler, in G. A. Jamieson and T. J. Greenwalt (Editors), *Red Cell Membrane, Structure and Function*, Lippincott, Philadelphia, 1969, p. 157.
17 V. T. Marchesi, T. W. Tillack, R. L. Jackson, J. P. Segrest and R. E. Scott, *Proc. Natl. Acad. Sci. U.S.A.*, 69 (1972) 1445.
18 D. J. Anstee, *Semin. Hematol.*, 18 (1981) 13.
19 H. Furthmayr, *J. Supramol. Struct.*, 9 (1978) 79.
20 V. T. Marchesi, *Annu. Rev. Cell Biol.*, 1 (1985) 531.

21 J. A. Chassis and S. B. Shohet, *Annu. Rev. Physiol.*, 49 (1987) 237.
22 M. Tomita, H. Furthmayer and V. T. Marchesi, *Biochemistry*, 17 (1978) 4756.
23 D. Blanchard, W. Dahr, M. Hummel, F. Latron, K. Beyreuther and J.-P. Cartron, *J. Biol. Chem.*, 262 (1987) 5808.
24 H. Furthmayr, M. Tomita and V. T. Marchesi, *Biochem. Biophys. Res. Commun.*, 65 (1975) 113.
25 I. Kahane, H. Furthmayr and V. T. Marchesi, *Biochum. Biophys. Acta*, 426 (1976) 464.
26 Z. El Rassi, Y. Truei and Cs. Horváth, *Makromol. Chem., Macromol. Symp.*, 17 (1988) 305.
27 Z. El Rassi, Y. Truei, Y.-F. Maa and Cs. Horváth, *Anal. Biochem.*, 169 (1988) 172.
28 D. Josić, W. Hofmann, R. Habermann and W. Reutter, *J. Chromatogr.*, 444 (1988) 29.
29 E. Sulkowski, *Trends Biotechnol.*, 3 (1985) 1.
30 Z. El Rassi and Cs. Horváth, in K. M. Gooding and F. Regnier (Editors), *HPLC of Biological Macromolecules: Methods and Applications*, Marcel Dekker, New York, in press.
31 Z. El Rassi and Cs. Horváth, *J. Chromatogr.*, 359 (1986) 241.
32 J. T. Dodge, C. Mitchell and D. J. Hanahan, *Arch. Biochem. Biophys.*, 100 (1963) 119.
33 V. T. Marchesi and E. P. Andrews, *Science*, 174 (1971) 1247.
34 U. K. Laemmli, *Nature (London)*, 227 (1970) 680.
35 C. R. Merril, D. Goldman, S. A. Sedman and M. H. Ebert, *Science (Washington, D.C.)*, 211 (1981) 1437.
36 M. Monsigny, A.-C. Roche, C. Sene, R. Maget-Dana and F. Delmotte, *Eur. J. Biochem.*, 104 (1980) 147.

Journal of Chromatography, 458 (1988) 13–25
Elsevier Science Publishers B.V., Amsterdam — Printed in The Netherlands

CHROMSYMP. 1438

DETERMINATION OF BINDING EQUILIBRIUM CONSTANTS BY NUMERICAL SIMULATION IN ZONAL HIGH-PERFORMANCE AFFINITY CHROMATOGRAPHY

CLAIRE VIDAL-MADJAR*, ALAIN JAULMES, MICHELLE RACINE and BERNARD SÉBILLE
Laboratoire de Physico-Chimie des Biopolymères, C.N.R.S. U.M. 27, 2 rue Henry Dunant, 94 320 Thiais (France)

SUMMARY

The equation of propagation of a signal of finite concentration through an affinity column is obtained by solving the mass conservation equations of liquid chromatography. Its numerical integration allows peak simulation, curve fitting and thence the determination of the equilibrium isotherm function. This method was applied to the measurement of ligand–protein interactions in zonal elution chromatography. In the range of concentrations studied, a three-parameter isotherm equation is convenient for characterizing the binding of phenylbutazone with human serum albumin on diol-silica. The data were analyzed with two different isotherm models: the two-independent-site model with specific and non-specific interaction and the stepwise-multiple-interaction model. The effects of stationary-phase coverage and temperature were studied. From these results were determined the amount of active immobilized protein and the equilibrium constant characterizing the affinity interaction (2.6 l/μmol), which is about twice as large as the value measured in solution.

INTRODUCTION

Affinity chromatography, a powerful technique for purifying biological materials, is also an important physicochemical method for the direct evaluation of the molecular interactions between soluble and immobilized biomolecules[1]. Since its combination with high-performance liquid chromatography (HPLC), the resulting analytical method, high-performance affinity chromatography (HPAC), has gained in speed and reproducibility[2].

Two classical elution techniques are used to measure molecular interactions: the frontal and the zonal elution methods. They differ by the input injection signal. In frontal elution, the solute concentration is suddenly raised and maintained at a constant value (Dirac step function). The binding isotherm is obtained directly from the breakthrough curves when the system is at quasi-equilibrium[3]. In zonal elution, the input signal is a short rectangular pulse. This technique is generally preferred to frontal elution because of its simplicity and the small amounts of sample required. However, because of difficulties in the mathematical treatment, its exploitation was limited to the

0021-9673/88/$03.50

linear case for retention volumes extrapolated to zero sample size[1], but recently it was extended to a Langmuir-isotherm retention and an analytical expression of the elution zone was given[4,5].

In zonal elution, the retention volume and the shape of the output signal contain all the information needed to determine kinetic and equilibrium constants. It is the mass balance equations of chromatography which describe the propagation of signals through a chromatographic column[6]. They depend on the chemical equilibrium function and can be integrated by using the numerical procedures based on Godunov's method[7–9] or on Craig distribution computer modelling[10–12], without any limitations concerning the equilibrium isotherm model. These computer simulation methods were essentially developed to predict the elution behaviour under the overload conditions of preparative chromatography[13,14].

The aim of the present study is to show that the same numerical simulation approach can be used in HPAC to determine, by zonal elution, the partition isotherm characterizing the interaction of the solute and the immobilized molecule. The method is applied to a study of the interaction of a small molecule (phenylbutazone) with human serum albumin (HSA) immobilized on an HPLC support. The binding of drugs and small molecules to immobilized albumins has previously been studied by frontal elution[15,16], and bovine serum albumin (BSA) is mainly used as a chiral stationary phase in HPAC[17–22].

The characterization of the ligand interaction with the immobilized protein is useful for a better understanding of the mechanisms of separation of a small molecule on affinity columns. Moreover, the physiological importance of albumin has led to a great number of *in vitro* binding studies of drugs with albumin. It is interesting to compare the equilibrium constants, measured at the liquid–solid interface, with those of the ligand protein interacting in solutions and measured by different techniques[23], including HPLC[24], frontal analysis[24] and equilibrium/saturation methods[25,26].

THEORETICAL

The mass conservation equation of solute A during the propagation process is

$$\frac{\partial \bar{C}}{\partial t} + u \cdot \frac{\partial \bar{C}}{\partial z} - D \cdot \frac{\partial^2 \bar{C}}{\partial z^2} = -\frac{1}{V_0} \cdot \frac{\partial(\bar{Q}_A + \bar{Q}'_A}{\partial t} \tag{1}$$

where $\bar{C}$ = the total concentration of solute A in the mobile phase, z = the abscissa of the slice along the column length ($z = 0$ corresponds to the inlet, $z = L$ to the outlet of the column), t = the time elapsed from the moment of injection, u = the average velocity of the liquid phase, D = the dispersive coefficient or global diffusion parameter, V_0 = the liquid external volume, $\bar{Q}_A$ = the total amount of solute A immobilized on the solid surface by affinity, $\bar{Q}'_A$ = the total amount of solute A inside the pores, $\bar{Q}^*_A$ and $\bar{Q}'_A{}^*$ = the values of $\bar{Q}_A$ and $\bar{Q}'_A$ at equilibrium.

The kinetic effects may be written in the global expression (where α is the rate constant):

$$\frac{\partial(\bar{Q}_A + \bar{Q}'_A)}{\partial t} = \alpha\,[(\bar{Q}_A + \bar{Q}'_A) - \bar{Q}^*_A + \bar{Q}'_A{}^*)] \tag{2}$$

When equilibrium is achieved

$$\bar{Q}'^{*}_{A} = \bar{Q}'_{A} = V_i \sigma_A \bar{C} \tag{3}$$

$$\bar{Q}^{*}_{A} = \bar{Q}_{A} = f(\bar{C}) \tag{4}$$

where $f(\bar{C})$ = the equilibrium isotherm characterizing the interaction of solute A with the affinity matrix X, V_i = the liquid internal pore volume, σ_A = the permeation coefficient of solute A and $V^* = V_0 + \sigma_A V_i$.

In the absence of kinetic effects, the mass balance equation of chromatography reduces to:

$$\frac{V^*}{V_0} \cdot \frac{\partial \bar{C}}{\partial t} + u \cdot \frac{\partial \bar{C}}{\partial z} + \frac{1}{V_0} \cdot \frac{\partial \bar{Q}_A}{\partial t} = D \cdot \frac{\partial^2 \bar{C}}{\partial z^2} \tag{5}$$

The propagation of the concentration profile depends on the equilibrium between the amount of solute, $\bar{Q}_A$, and the concentration in the liquid phase (eqn. 4).

In previous papers[7,8] we have shown that it is possible to perform an approximate integration of eqn. 5 with any model of isotherm by using a numerical procedure where discrete length steps, Δz, and time steps, Δt, are used in the integration method. The dispersive effect corresponding to the second-order term is well approximated when Δz is equal to H, the height equivalent to a theoretical plate (HETP):

$$\Delta z = H = 2Dt_R/L \tag{6}$$

The chromatographic peak is then defined by the shape of the initial injection signal, the amount injected (or peak area), the global dispersive coefficient, D, and the equilibrium isotherm, $\bar{Q}_A = f(\bar{C})$; D is an apparent diffusion coefficient, accounting for the contributions to band broadening at zero concentration, including diffusion-limited kinetic effects[14].

In most cases, the ligand/albumin equilibria have been analysed according to the Scatchard model[27], assuming that the ligand is bound to classes of identical, independent binding sites. The alternative way of analysing the data is the use of a multiple-stepwise-equilibrium model[28].

In the case of the Scatchard model, the chemical equilibria may be written in the form (where the brackets [] represent concentrations, in mol/cm^3, in the liquid phase, and the braces { } surface concentrations, in mol/m^2):

$$\begin{array}{ll} A + X_1 \rightleftharpoons AX_1 & \{AX_1\} = \{X_1\}[A]\beta_1 \\ A + X_2 \rightleftharpoons AX_2 & \{AX_2\} = \{X_2\}[A]\beta_2 \\ \cdots\cdots\cdots\cdots & \cdots\cdots\cdots\cdots\cdots \\ \cdots\cdots\cdots\cdots & \cdots\cdots\cdots\cdots\cdots \\ A + X_n \rightleftharpoons AX_n & \{AX_n\} = \{X_n\}[A]\beta_n \end{array} \tag{7}$$

The corresponding isotherm is given by the equation

$$\bar{Q}_A = \sum_{i=1}^{n} \{AX_i\}S = \sum_{i=1}^{n} \bar{Q}_{X_i} \cdot \frac{[A]\beta_i}{1 + [A]\beta_i} \tag{8}$$

where β_i is the association constant between A and X_i (class i sites) $\bar{Q}_{X_i}$ is the amount in moles of class i sites, and S is the surface area of the affinity sorbent. The parameter $\bar{Q}_X$ is defined as follows:

$$\bar{Q}_X = \sum_{i=1}^{n} \bar{Q}_{X_i}$$

The second system has been used by Lagercrantz *et al.*[15,16] to analyse the binding of a small molecule to immobilized serum albumin. It involves an immobilized protein, X, carrying several sites and a low-molecular-weight ligand, A, in solution. The equilibria are as follows:

$$\begin{array}{ll} X + A \rightleftharpoons XA & \{XA\} = K_1\{X\}[A] \\ XA + A \rightleftharpoons XA_2 & \{XA_2\} = K_2\{XA\}[A] \\ & \quad = K_1K_2\{X\}[A]^2 \\ \ldots\ldots\ldots\ldots & \ldots\ldots\ldots\ldots\ldots \\ \ldots\ldots\ldots\ldots & \ldots\ldots\ldots\ldots\ldots \\ XA_{n-1} + A \rightleftharpoons XA_n & \{XA_n\} = K_1K_2 \ldots K_n\{X\}[A]^n \end{array} \tag{9}$$

where $K_1, K_2, \ldots K_n$ are the successive association constants and n the number of sites.

The expression of the equilibrium isotherm, deduced from the above equilibria, is

$$\bar{Q}_A = \bar{Q}_X[A] \cdot \frac{K_1 + 2K_1K_2[A] + \ldots + nK_1K_2 \ldots K_n[A]^{n-1}}{1 + K_1[A] + K_1K_2[A]^2 + K_1K_2 \ldots K_n[A]^n} = \bar{Q}_X y \tag{10}$$

where $\bar{Q}_A$ is the total amount of ligand bound to the matrix and y is the molar ratio between the bound ligand and the immobilized protein.

The physical meaning of both models has been discussed by Klotz and Hunston[28]. The identification of the constants of eqn. 10 with those of the Scatchard model is difficult with an analytical expression, except for K_1:

$$K_1 = \sum_{i=1}^{n} \bar{Q}_{X_i}\beta_i/\bar{Q}_X \tag{11}$$

In this work, both models will be considered as satisfactory approximations of the experimental isotherms.

EXPERIMENTAL

The reagents used were HSA (A1887, fatty-acid free) and phenylbutazone from

Sigma (St. Louis, MO, U.S.A.), diol-bonded Lichrospher Si-100 (diameter 10 μm, pore size 100 Å) from Merck (Darmstadt, F.R.G.).

The Schiff-base method was used to immobilize HSA on the diol support by the same procedure as that described previously for protein immobilization[2]. Supports of variable HSA coverage were prepared by changing the concentration of the protein solution in contact with the aldehyde support. The medium-coverage HSA sorbent was prepared from a 2-ml solution (4 mg/ml HSA) per g of diol-silica, and for the high-coverage sorbent a 10 mg/ml HSA solution was used. After protein immobilization, the excess of aldehyde groups were reduced by addition of sodium tetrahydroborate[2]. The amount of protein immobilized was determined by the Lowry method.

The HPLC system consisted of a pump (Model 2150; LKB, Bromma, Sweden), a 7125 sampling valve (Rheodyne, Berkeley, CA, U.S.A.) with a 20-μl loop and an UV detector (Model SPD 6A; Shimadzu, Kyoto,Japan), operated at 268 nm. Its response curve was linear within the whole range of solute concentrations studied.

The analogue output of the detector was connected to a digital voltmeter (Model 3497; Hewlett-Packard, Palo Alto, CA, U.S.A.), which displays the data in four digit precision. The data were stored on floppy disks. The theoretical treatments were carried out in Fortran language, using a microcomputer (Model AT2; IBM, Greenock, U.K.).

The stainless-steel column (50 mm × 4.1 mm I.D.) was vacuum-slurry-packed. It was placed in a water-bath, and its temperature was controlled within ± 0.1°C. The eluent was 0.067 M (pH 7.4) potassium phosphate buffer. The liquid volume of the column was determined from the retention time of ^2H_2O. A weak, non-specific retention was observed on the diol-silica ($k' = 0.6$), but it was larger on aldehyde-silica ($k'_0 = 2.2$ at 37°C), the activated support used for protein immobilization.

RESULTS AND DISCUSSION

Curve fitting procedure

The changes in the elution profiles obtained were studied by injecting increasing amounts of phenylbutazone into the affinity column. The partition isotherm indicates a saturation effect wich causes tailing peaks for large sample sizes (Fig. 1).

The multisite-equilibrium model. The theoretical model first assumed for the partition isotherm is that of multisite adsorption. The equation for this was introduced into the numerical integration program, and its parameters were determined from best fitting between experimental and theoretical results. For the range of concentration studied, a three-parameter isotherm is sufficient to describe the whole set of elution peaks obtained at various concentrations on the medium-coverage HSA column (Fig. 1). The isotherm equation (eqn. 8) reduces to

$$Q_A = Q_{X_1} \cdot \frac{[A]\beta_1}{1 + [A]\beta_1} + k'_2[A]V^* \tag{12}$$

where $k'_2 = Q_{X_2}\beta_2/V^*$.

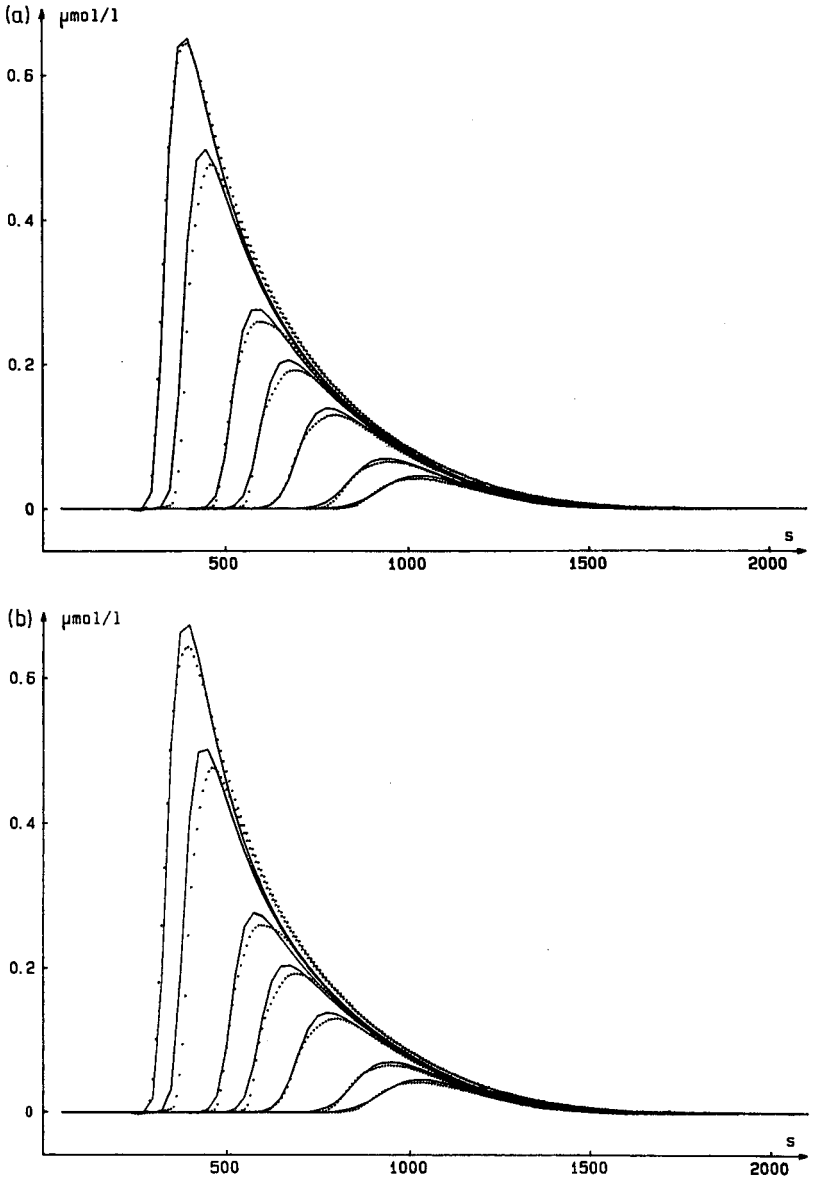

Fig. 1. Elution peak of phenylbutazone for medium-coverage immobilized HSA. Column length: 5 cm. Temperature: 37°C. Flow-rate; 1 ml/min. Eluent: 0.067 *M* phosphate buffer (pH 7.4). ....., Experimental values stored by computer data acquisition; ———, best fit of the simulated elution peak. (a) Two-independent-site isotherm model (one specific, the other non-specific); $\beta_1 = 2.6$ l/μmol; $Q_{X_1} = 6.5$ nmol; $k'_2 = 4.4$; $H = 0.55$ mm. (b) Stepwise-multiple-equilibrium-isotherm model; $K_1 = 2.7$ l/μmol; $K_2 \ldots K_5 = 0.25$ l/μmol; $Q_X = 7.5$ nmol; $H = 0.55$ mm.

The limiting capacity factor, k'_0, is then given by:

$$k'_0 = \beta_1 Q_{X_1}/V^* + k'_2 \tag{13}$$

This model describes a solute-immobilized ligand equilibrium with two groups of sites: one of high affinity and a second one of low affinity with non-specific interaction.

For the low-concentration peak a two-parameter equation fits the experimental elution peak as well as the three-parameter model, with a binding constant of $2.9 \cdot 10^{-3}$ μmol/l in the first case and $2.85 \cdot 10^{-3}$ μmol/l in the second one. The two-parameter isotherm equation is then of the Langmuir type

$$Q_A = k'_0 V^* \cdot \frac{[A]}{1 + \beta[A]} \tag{14}$$

where $\beta = \beta_1(1 - k'_2/k'_0)$. Both isotherms (eqns. 12 and 14) have equal second derivatives at the origin.

In Fig. 2, one can compare the elution peaks simulated from the Langmuir-type model (two-parameter isotherm) with those obtained from the two-site model having the same first two derivatives at the origin. The elution profiles coincide only in the low-concentration range (0–1 μmol/m^2), but marked differences between both models are observed at higher concentrations. Furthermore, the isotherm curves for both models are identical near the origin (Fig. 3). The isotherm function with two types of sites (specific and non-specific) increases linearly at high solute concentration.

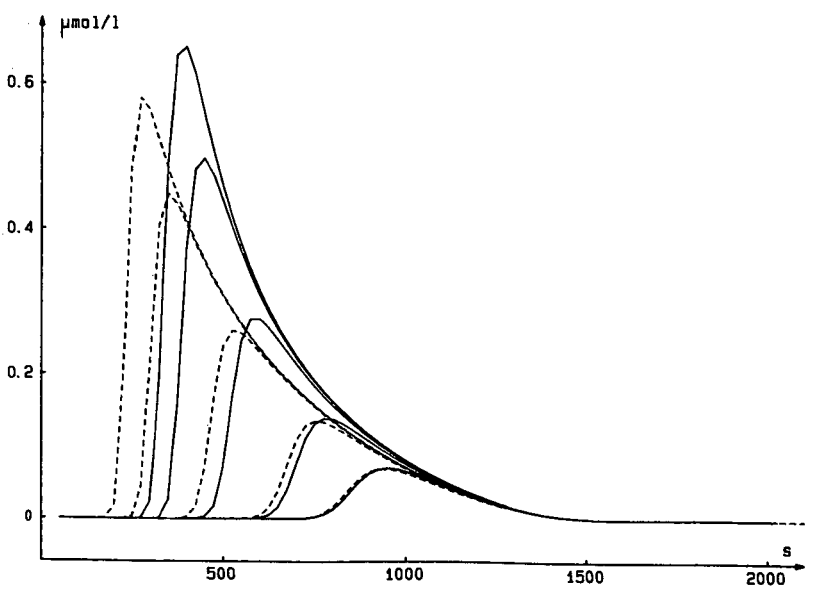

Fig. 2. Simulated elution peaks with the same first and second derivatives of the isotherm at the origin. ....., Two-parameter isotherm (eqn. 14); ———, three-parameter isotherm (eqn. 12).

Although the solute concentrations are ten times larger in the injection signal than at the column outlet, the simulation results show that the shape of the higher-concentration portion of the isotherm has only a weak influence on the low-concentration elution peaks.

The strategy of adjusting the theoretical model to the experimental one is to fit the low-concentration peak with a Langmuir isotherm. For the largest elution peaks, when important deviations between theory and experiment are observed, the three-parameter isotherm is used with the same first and second derivatives as for the Langmuir-type model.

The error of the parameters was determined according to the mathematical scheme of Phillips and Eyring[29]. The relative error at a 90% confidence level of the first derivative at zero concentration, k'_0, is 0.5%, that of the second derivative at zero concentration, k''_0, is 7% and that of k'_2 is 20%. Hence the corresponding relative errors of β_1 and Q_X are 10%.

The stepwise-multiple-equilibrium model. The data were analysed with the stepwise-multiple-equilibrium isotherm (eqn. 10). As with the previous model, good convergence of the curve fitting procedure is observed only with a three-parameter isotherm. Here, we assumed that the successive association constants, except the first one ($K_2, K_3, \ldots, K_n$) are equal. As in the previous case, the first and second derivatives at the origin must be equal to those of the Langmuir-type isotherm, determined from the low-concentration elution peaks. In this case, $Q_X K_1 = k'_0/V^*$ and $\beta = K_1 - 2K_2$. As shown in Fig. 1b, with this model, the adjustment is as good as that in Fig. 1a, where the two-independent-site model was considered.

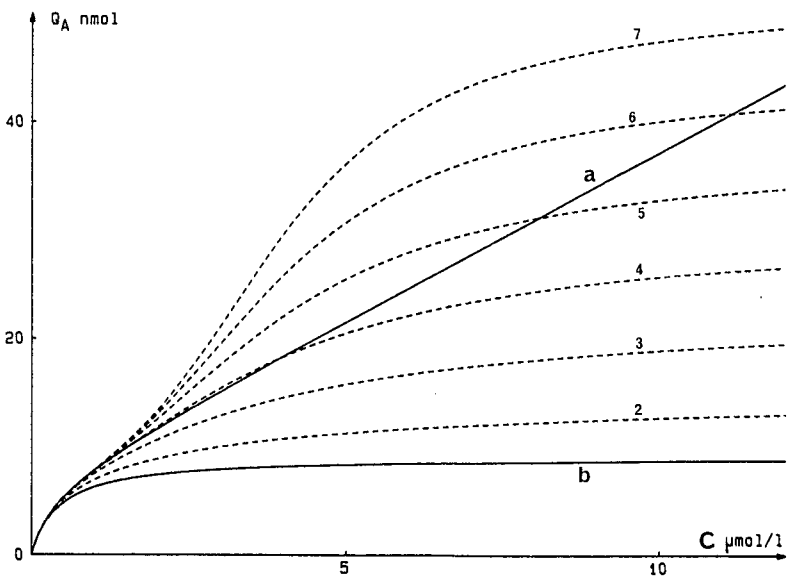

Fig. 3. Equilibrium isotherm of phenylbutazone on medium-coverage immobilized HSA. ———, (a) Independent-site-isotherm model (eqn. 12); ———, (b) Langmuir-type isotherm (eqn. 14). Same experimental conditions as in Fig. 1. ....., Stepwise multiple-equilibrium isotherm (eqn. 10). 2—7: number of steps or order of the polynomial expansion.

As in the previous case, the relative errors of K_1 and Q_X estimated at the 90% confidence level are 10%, but those of K_2 (relative error 20%) are larger.

The isotherm for this model was compared with that of the two-independent-site model used previously (Fig. 3). The best fit of the theoretical peak to the experimental one is obtained with a five-term polynomial expansion. When the order of expansion is increased, the isotherm shows two inflection points, starting with the fifth order; the presence of inflection points should generate shocks, *i.e.*, vertical parts in the calculated elution peaks, which are not observed in the experimental ones. The assumption of equal higher-order constants is unrealistic; it would be more likely for them to decrease in the order $K_2, K_3, \ldots, K_n$. However, since we could not obtain any precision in their determination, we limited the model to a three-parameter isotherm, which allows a good convergence in the determination of parameters Q_X and K_1. The value of K_2 can be taken only as a rough approximation, and only the order of magnitude is significant.

Effect of the amount of HSA immobilized

The effect of stationary-phase coverage on the binding properties of immobilized HSA was determined from the elution profiles of phenylbutazone injected at various concentrations. The equilibrium isotherm was determined on two columns with HSA immobilized in different amounts: Fig. 1a and b illustrate the peak adjustment for experiments made on the medium-coverage silica and Fig. 4 for that with high stationary-phase coverage. The results of the best fit by numerical simulation obtained with the isotherm models discussed above are summarized in Table I.

The retention volume of phenylbutazone increases in proportion to the amount of HSA immobilized within the errors of measurement of the effective amount of HSA immobilized; but the characteristics of the equilibrium isotherm are quite similar for both the medium- and high-coverage HSA–silica. The values (measured at 37°C) of the binding constant, β_1, characterizing specific interaction in the independent-site model, are equal for both HSA coverages. The capacity factor, k'_2, for non-specific interactions is roughly proportional to the amount of HSA immobilized. This shows that the non-specific sites are most probably those of the protein. Moreover, a weak retention is observed on diol-silica with a much lower capacity factor, $k'_0 = 0.6$.

The amount (in nmoles) of active protein can also be determined by this method. Its value is about half of the amount of protein effectively immobilized on the support. This is not surprising, since during the immobilization process some active groups of the protein will be bound to aldehyde-silica.

Table I also displays the constants when the experimental data are analysed with the stepwise-multiple-equilibrium model. The adjustment of the theoretical peaks obtained with this model for the high-coverage silica is almost identical to that obtained with the two-independent-site model, considered in Fig. 4 and is not given here. The binding constant, K_1, measured with the high-coverage sorbent is equal to that measured with the medium-coverage sorbent. Its value ($K_1 = 2.7$ l/μmol) is close to the binding constant ($\beta_1 = 2.6$ l/μmol) characteristic of the specific interaction between the solute and immobilized protein in the two-independent-site model (Table I).

The above results demonstrate the validity of the numerical method of determining the isotherm equilibrium from the elution peak analysis, since the equilibrium constants measured at high and medium stationary-phase coverage are in excellent agreement.

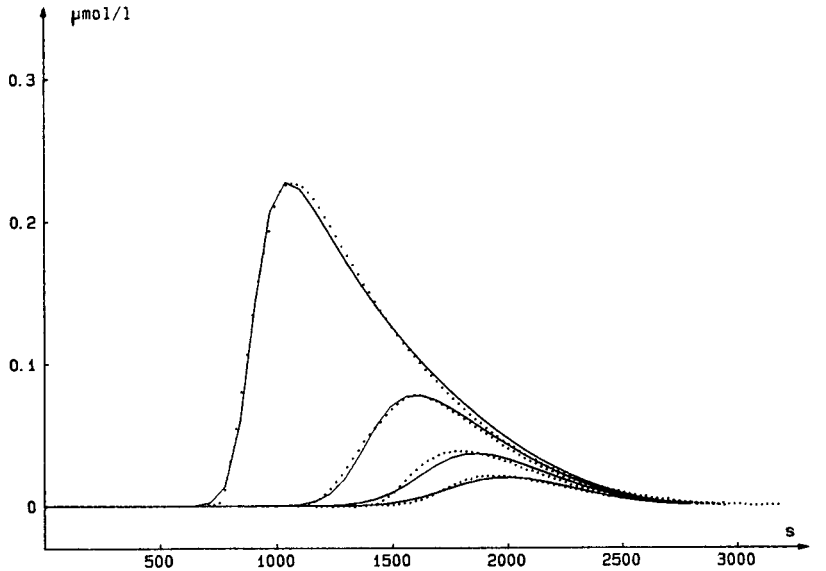

Fig. 4. Elution peak of phenylbutazone on high-coverage immobilized HSA. Column length: 5 cm. Temperature: 37°C. Flow-rate: 1.5 ml/min. Eluent: 0.067 *M* phosphate buffer (pH 7.4). ....., Experimental values stored by computer data acquisition; ———, best fit of the simulated elution peak with the two-independent-site isotherm model; $\beta_1 = 2.6$ l/µmol; $Q_{X_1} = 19$ nmol; $k'_1 = 9.1$.

Effect of temperature

The chromatographic behaviour of phenylbutazone, eluted in finite concentration in the presence of medium-coverage HSA, was studied as a function of temperature. For every temperature, the solute/immobilized HSA equilibrium isotherm was determined from the best fit of the simulated peak to the experimental one. The results are summarized in Table I. The equilibrium constants, characterizing the specific interaction of phenylbutazone with immobilized HSA, are similar for both

TABLE I

PARAMETERS OF THE EQUILIBRIUM ISOTHERM MODELS USED FOR NUMERICAL SIMULATION OF ELUTION PEAKS

Temperature and stationary phase coverage effects.

Immobilized HSA	*t (°C)*	*H (mm)*	*Two classes of independent sites*			*Stepwise multiple equilibrium*		
			Q_{X_1} *(nmol)*	β_1 *(l/µmol)*	k'_2	Q_X *(nmol)*	K_1 *(l/µmol)*	$K_2 \ldots K_5$ *(l/µmol)*
High coverage (40 nmol)	37	0.70	19.0	2.6	9.1	20.5	2.7	0.22
Medium coverage (15 nmol)	37	0.55	6.5	2.6	4.4	7.5	2.7	0.25
	30	0.64	7.9	2.9	4.4	8.8	3.0	0.25
	25	0.76	6.7	3.3	3.1	7.0	3.4	0.22
	20	1.00	5.7	4.3	5.7	6.4	4.4	0.35

isotherm models considered in this work. Their variations with temperature correspond to the Van 't Hoff plot. The molar enthalpy change, $\Delta\bar{H}$, measured from this plot, is -17 kJ/mol (standard deviation 20%).

The amount of active, immobilized protein should be independent of temperature. The calculated values are within a $\pm 20\%$ interval. This rather wide range, somewhat larger than the confidence level of 10%, is partly due to the curve fitting method, which leads to a $\approx 10\%$ error of the parameter determination. However, the main reason for this apparent discrepancy lies in the fact that the retention volumes measured on immobilized HSA are not constant and decrease perceptibly day by day. The reasons for this lack of stability are not clear. It may be due to protein degradation or to contamination by organic substances or microbial agents. The problem of the long-term stability of immobilized serum albumin is well known to column manufacturers and was carefully studied by Aubel and Rogers[22]. The advantage of the method we have developed in this work is that it allows peak shape analysis to be used to determine, at any stage, the amount of protein immobilized that is effectively reactive towards the drug.

Comparison with equilibrium measurements in solution

It is interesting to compare the association constant for phenylbutazone and HSA, measured with an immobilized protein, with the association constant measured in solution. However, prior to discussing this point, it is necessary to outline that, although the association constants of the equilibrium models are measured with the same units as those in solution, they do not refer to the same species, since some will refer to soluble HSA, others to HSA immobilized on the sorbent (eqn. 7 or 9). In affinity chromatography, we deal with heterogeneous equilibria involving surface concentrations; therefore, it is questionable to compare the data measured in affinity chromatography for solute/immobilized ligand association with those measured in the liquid phase, where one deals only with homogeneous equilibria and plain volumetric concentrations.

Moreover, the equilibrium constant, K_1, characterizing the solute/affinity sorbent interaction reflects an overall phenomenon, the interaction of the solute with the immobilized protein and with the sorbent. The contribution of the diol-silica to the total interaction is difficult to evaluate, but it seems to be small, since phenylbutazone is eluted with a weak retention and a symmetrical peak from the bare support.

The affinity constant, K_1, measured in this work (2.6 or 2.7 l/μmol, Table I), which characterizes the affinity interaction, is somewhat larger for the phenylbutazone–immobilized HSA interaction than the value measured in solution (Table II). The data in the literature were compiled from measurements made in the same solvent as in this work, and are scattered over a wide range, from 0.16 to 2.3 l/μmol. Boobis and Chignel[35] have shown that, as the concentration of albumin decreases, the binding of phenylbutazone increases. This phenomenon, which does not seem to be due to molecular aggregation at high protein concentrations, may explain the great scatter of the values for the equilibrium constants, reported in the literature, and the large value for the affinity constant characterizing the interaction of phenylbutazone with immoblized HSA.

TABLE II

COMPARISON OF ASSOCIATION CONSTANTS OF PHENYLBUTAZONE AND HSA, MEASURED BY DIFFERENT TECHNIQUES

t (°C)	$K_1 = \Sigma n_i \beta_i$ (*l*/μmol)	*HSA concentration range (%)*	*Method*
37	2.6	Immobilized	HPAC (this work)
37	0.85	0.01–0.2	Equilibrium-saturation HPLC[26]
36	2.3	Not given	Ultrafiltration[30]
37	0.16	0.2	Ultrafiltration[31]
37	0.35	0.2	Equilibrium dialysis[32]
37	0.75	0.2	Dynamic dialysis[33]
37	0.8	0.1	Fluorescence[34]
22	0.93	0.1	Ultrafiltration and equilibrium dialysis[35]
	0.20	1.0	

CONCLUSIONS

The curve fitting of the simulated theoretical profile to the experimental peak allows the determination of the equilibrium isotherm mainly for concentrations ranging from the detection threshold to the output concentration. A three-parameter-isotherm equation was found suitable to account for the peak distortions observed for phenylbutazone, when eluted from HSA, immobilized on a diol-support at a finite concentration. Two different isotherm equilibrium models were tested, but it was impossible to tell which one would fit the experimental data more closely.

The method offers a convenient way of revealing heterogeneities in affinity sites and permits the determination of the amount of immobilized protein that is active towards the solute. This parameter is an important factor for characterizing an affinity packing, especially when one considers that a decrease in the number of active protein sites occurs during the immobilization process, since some of them are bound to the support. Therefore, the amount of active protein is lower than the amount that is effectively immobilized. Moreover, the amount of active protein can readily be measured after a few solute injections, and this is useful when dealing with immobilized proteins of poor long-term stability.

Zonal elution and numerical simulation of the elution peaks also permit determination of the association constant for binding of the solute with the immobilized protein. These parameters are useful for comparing the various methods of protein immobilization and for evaluating the contributions of the support to the retention.

REFERENCES

1 G. Fassina and I. M. Chaiken, *Adv. Chromatogr. (N.Y.)*, 27 (1987) 247.
2 P. O. Larsson, M. Glad, L. Hanson, M. O. Månsson, S. Ohlson and K. Mosbach, *Adv. Chromatogr. (N.Y.)*, 21 (1983) 41.
3 L. W. Nichol, A. G. Ogston, D. J. Winzor and W. H. Sawyer, *Biochem. J.*, 143 (1974) 435.
4 F. H. Arnold and H. W. Blanch, *J. Chromatogr.*, 355 (1986) 13.
5 J. L. Wade, A. F. Bergold and P. W. Carr, *Anal. Chem.*, 59 (1987) 1286.

6 J. N. De Vault, *J. Am. Chem. Soc.*, 65 (1943) 532.
7 P. Rouchon, M. Schoenauer, P. Valentin, C. Vidal-Madjar and G. Guiochon, *J. Phys. Chem.*, 89 (1985) 2076.
8 M. J. González, A. Jaulmes, P. Valentin and C. Vidal-Madjar, *J. Chromatogr.*, 386 (1987) 333.
9 P. Rouchon, M. Schoenauer, P. Valentin and G. Guiochon, *Sep. Sci.*, 22 (1987) 1793.
10 J. E. Eble, R. L. Grob, P. E. Antle and L. R. Snyder, *J. Chromatogr.*, 384 (1987) 25.
11 J. E. Eble, R. L. Grob, P. E. Antle and L. R. Snyder, *J. Chromatogr.*, 384 (1987) 45.
12 J. E. Eble, R. L. Grob, P. E. Antle, G. B. Cox and L. R. Snyder, *J. Chromatogr.*, 405 (1987) 31.
13 L. R. Snyder, G. B. Cox and P. E. Antle, *Chromatographia*, 24 (1987) 82.
14 G. Guiochon and A. Katti, *Chromatographia*, 24 (1987) 165.
15 C. Lagercrantz, T. Larsson and H. Karlsson, *Anal. Biochem.*, 99 (1979) 352.
16 C. Lagercrantz and T. Larsson, *Biochem. J.*, 213 (1983) 387.
17 S. Allenmark, B. Bomgren and H. Borén, *J. Chromatogr.*, 264 (1983) 63.
18 S. Allenmark, B. Bomgren and H. Borén, *J. Chromatogr.*, 316 (1984) 617.
19 S. Allenmark, *J. Liq. Chromatogr.*, 9 (1986) 425.
20 B. Bomgren and S. Allenmark, *J. Liq. Chromatogr.*, 9 (1986) 667.
21 S. Allenmark, S. Andersson and J. Bojarski, *J. Chromatogr.*, 436 (1988) 479.
22 M. Aubel and L. B. Rogers, *J. Chromatogr.*, 392 (1987) 415.
23 U. Kragh-Hansen, *Pharmacol. Rev.*, 33 (1981) 17.
24 B. Sébille, N. Thuaud and J. Tillement, *J. Chromatogr.*, 167 (1978) 159.
25 B. Sébille, N. Thuaud and J. Tillement, *J. Chromatogr.*, 180 (1979) 103.
26 B. Sébille, N. Thuaud and J. Tillement, *J. Chromatogr.*, 204 (1981) 285.
27 G. Scatchard, *Ann. NY Acad. Sci.*, 51 (1949) 660.
28 I. M. Klotz and D. L. Hunston, *Arch. Biochem.*, 193 (1979) 314.
29 G. H. Philips and E. M. Eyring, *Anal. Chem.*, 60 (1988) 738.
30 K. Rehse and K. Ehlert, *Arch. Pharm. (Weinheim, Ger.)*, 318 (1985) 667.
31 J. C. McElnay and P. F. d'Arcy, *J. Pharm. Pharmacol. Suppl.*, 29 (1977) 1P.
32 J. P. Tillement, R. Zini, P. d'Athis and G. Vassent, *J. Clin. Pharmacol.*, 7 (1974) 307.
33 K. F. Brown and M. J. Crooks, *Biochem. Pharmacol.*, 25 (1976) 1175.
34 V. Maes, J. Hoebeke, A. Vercruysse and L. Kanarek, *Mol. Pharmacol.*, 16 (1979) 147.
35 S. W. Boobis and C. F. Chignell, *Biochem. Pharmacol.*, 28 (1979) 751.

Journal of Chromatography, 458 (1988) 27–44
Elsevier Science Publishers B.V., Amsterdam — Printed in The Netherlands

CHROMSYMP. 1426

HIGH-PERFORMANCE LIQUID CHROMATOGRAPHY OF AMINO ACIDS, PEPTIDES AND PROTEINS

LXXXVII*. COMPARISON OF RETENTION AND BANDWIDTH PROPERTIES OF PROTEINS ELUTED BY GRADIENT AND ISOCRATIC ANION-EXCHANGE CHROMATOGRAPHY

M. T. W. HEARN*, A. N. HODDER and M. I. AGUILAR
Department of Biochemistry, Monash University, Clayton, Victoria 3168 (Australia)

SUMMARY

The high-performance ion-exchange gradient-elution behaviour of a range of globular proteins has been investigated, using a strong anion exchanger as the stationary phase and sodium chloride as the displacer salt. Deviations were observed between the Z_c values obtained from isocratic experiments and from gradient experiments with varied gradient time and varied flow-rate. These results indicate that theoretical treatments which relate gradient and isocratic elution processes do not adequately describe the retention behaviour of protein solutes separated by ion-exchange methods. Furthermore, the experimentally observed bandwidths deviated significantly from values predicted on the basis of plate theory for low-molecular-weight molecules. The significance of these results is discussed in terms of the influence of experimental parameters on the ability of particular electrostatically interactive areas on the surface of protein solutes to control the thermodynamic and kinetic properties of these polyelectrolyte molecules during ion-exchange chromatographic processes.

INTRODUCTION

High-performance ion-exchange chromatography (HPIEC) is now a widely used and important method for the separation of peptides, proteins and polynucleotides. Despite the widespread application of the technique in the biological sciences, the mechanistic details of protein retention in the ion-exchange process have not yet been fully elucidated. This is mainly due to the complex three-dimensional structure and amphoteric nature of proteins, which leads to complex electrostatic interactions between the solute and stationary phase surface. Previous studies[1,2] on the isocratic anion-exchange elution of proteins have indicated that protein retention in HPIEC is dependent on both the number and distribution of charged sites on the protein surface.

* For Part LXXXVI see ref. 3.

0021-9673/88/$03.50

Thus, changes in mobile-phase pH and ionic strength, which will alter the surface interactive potential of the protein, can be used to manipulate the selectivity of proteins in HPIEC. The nature of the displacer ion and co-ion have also been shown to significantly influence the retention properties of proteins in HPIEC. In a previous paper[3], we reported that while the anions F^-, Cl^- and Br^- reduce protein retention as anticipated on the basis of their decreasing hydrated ionic radii and increased affinity for the stationary phase, cationic co-ions also significantly influence the retention behaviour of some proteins through preferential interactions with the solute. Furthermore, the extent of protein band-broadening under isocratic conditions depends on the choice of the anion/cation combination of the displacer salt, effects which are related to known Hofmeister effects on protein aggregation and solubility. While isocratic elution conditions offer an additional dimension for high-resolution protein purification, complex mixture are more commonly separated under gradient-elution conditions, where advantage can be taken of band-compression effects. The fundamental principles of gradient elution of low-molecular-weight solutes are now well established[4]. Mathematical expressions have been developed which relate isocratic and gradient-elution parameters under a wide range of experimental conditions and in some instances allow the accurate prediction of solute retention and bandwidth properties in ion-exchange[5,6], reversed-phase[7,8] and hydrophobic-interaction chromatography[9] of macromolecules. However, the application of models such as the linear solvent strength (LSS) approach to HPIEC of peptides and proteins has not been extensively verified, particularly with respect to the influence of solvent constituents on the ion-exchange properties of protein solutes. This paper describes the results of detailed investigations on the gradient-elution behaviour of several globular proteins in an anion-exchange chromatographic system.

EXPERIMENTAL

Apparatus

All chromatographic experiments were performed with a Pharmacia (Uppsala, Sweden) Fast Protein Liquid Chromatography (FPLC) system consisting of two P-500 syringe pumps, a V-7 injector and a 278-nm fixed-wavelength single-path UV monitor, coupled to a two-channel REC 482 pen recorder and a Perkin-Elmer (Norwalk, CT, U.S.A.) LCI-100 integrator. Isocratic and gradient elution were controlled with a Pharmacia GP-250 solvent programmer. Mono-Q prepacked strong anion-exchange columns (HR 5/5, 50 × 5 mm I.D.) were used throughout. The pH measurements were performed with an Orion Research Products (Cambridge, MA, U.S.A.) SA 520 meter, equipped with a combination glass electrode. Column effluents for gradient elapse time, t_e, measurements were collected on a Pharmacia FRAC-100 fraction collector. The conductivity of the effluent was measured with a Radiometer (Copenhagen, Denmark) Model Cdm3 conductivity meter with a Model CDC 304 glass electrode. All chromatographic separations were carried out at ambient temperatures of *ca.* 20°C.

Chemicals and reagents

Bovine erythrocyte carbonic anhydrase, sperm whale skeletal muscle myoglobin (type iii), hen egg ovalbumin (grade V) and piperazine were purchased from Sigma (St. Louis, MO, U.S.A.). Sodium chloride (AnalaR grade) was obtained from BDH (Port

Fairy, Australia). Quartz distilled water was further purified on a Milli-Q system (Millipore, Bedford, MA, U.S.A.). Buffers were adjusted to pH 9.60 with hydrochloric acid (sp. gr. 1.16, AnalaR grade), which was purchased from BDH.

Chromatographic procedures

Eluent A was a 0.02 *M* piperazine solution, adjusted to pH 9.60. Eluent B consisted of 0.02 *M* piperazine and 0.3 *M* sodium chloride at pH 9.60. Eluents A and B were filtered (0.45-μm cellulose acetate HAWP 04700, from Millipore) and degassed under vacuum. Protein solutions were prepared by dissolving purified protein in eluent A at a concentration of 5 mg/ml, unless otherwise specified. Before use, protein solutions were filtered through 0.22-μm ACRO LC13 filters (Gelman Sciences, Sydney, Australia). Protein sample sizes ranged from 5 to 1000 μg in injection volumes between 10 and 200 μl.

Protein samples were eluted isocratically, starting at 100% eluent B, and elution was repeated at decreasing concentrations of B until the elution volume was greater than 30 column volumes. Gradient elution was run from 0 to 100% eluent B under conditions of either constant flow-rate (F) and varied gradient time t_G or constant t_G and varied F. Varied-flow gradient experiments were conducted at flow-rates between 0.1 and 2.0 ml/min, while varied-gradient-time experiments were run with t_G varying between 17.1 and 171.1 min. The column dead-time, t_0, was obtained from the retention time of a salt breakthrough peak, following a 50-μl injection of 1 *M* sodium chloride in 100% eluent B (0.3 *M* sodium chloride). The gradient elapse time, t_e, required for eluent B to reach the column inlet was determined from plots of conductivity *versus* time. All data points represent the average of at least duplicate measurements.

In each type of elution experiment $\log k'$ or $\log \bar{k}$ and $\log 1/c$ or $\log 1/\bar{c}$ data were collected for each protein and subjected to an iterative regression analysis to determine the y intercept ($\log K$), slope (Z) and correlation coefficient (r^2). The various chromatographic parameters were calculated using the ChromoCalc programme series, developed in this laboratory and written in BASIC language for an IBM XT or AT computer.

RESULTS AND DISCUSSION

Retention relationships

Several studies have addressed the theoretical relationship between protein retention and mobile-phase composition in multivalent adsorption chromatography. Most work on retention optimisation and simulation has centred on reversed-phase HPLC, although more recent studies have also extended similar concepts to the hydrophobic-interaction and ion-exchange mode. For example, isocratic and gradient-elution theory, developed for simple organic acids and bases, has been adapted to evaluate the retention behaviour of polypeptides separated under regular reversed-phase conditions. It is well known that polypeptides frequently show pronounced retention dependencies on the volume fraction, φ, of the organic solvent modifier; in fact, only small changes in φ (*e.g.*, $\Delta\varphi < 0.1$) may be sufficient to encompass the solute's operational chromatographic range of $1 < k' < 100$ (refs. 10–12). This

dependency of the capacity factor, k', on the volume fraction, φ, for a polypeptide separated under regular reversed-phase isocratic conditions can be represented as

$$\log k' = \log k_0 - S\varphi \tag{1}$$

According to eqn. 1, linear dependencies of $\log k'$ on φ over relatively narrow ranges of φ, are anticipated with the intercept and slope equal to $\log k_0$ and S, respectively. However, experimental plots of $\log k'$ *versus* φ have been generally observed[10–12] to be curved rather than linear, over the operational range of mobile-phase compositions, *i.e.* over $0 < \varphi < 0.7$. This general observation is consistent with multisite binding between the protein solute and the stationary phase. The slope, S, can be used as a measure of the hydrophobic contact area established between the protein and stationary phase under specific chromatographic conditions. Evaluation of the S value, together with the $\log k_0$ value, represents critical experimental parameters in the development of structure–retention relationships and provides the basis for a quantitative approach to the optimisation of separation conditions.

Since the same reversed-phase chromatographic variables that control retention, resolution and bandwidth in isocratic elution are also relevant in gradient elution, recourse is usually to the latter elution mode, which provides a useful expedient for reducing separation times and decreasing peak volumes (σ). Several theoretical models have been developed for the prediction of the gradient-elution behaviour of small-molecular-weight solutes. For example, the retention time of a solute, t_g, of a conformationally rigid solute under linear solvent strength (LSS) gradient-elution conditions can be expressed as

$$t_g = \frac{t_0}{\beta} \log 2.3\, k_0 b + t_0 + t_e \tag{2}$$

where t_0 is the column dead-time, k_0 is the capacity factor for the peptide solute under the initial gradient conditions, t_e is the time taken for eluent B to reach the column inlet and b is the gradient steepness parameter. Evaluation of b can be easily achieved by several experiments in which different gradient times or flow-rates are used. Thus, for elution conditions with fixed column, mobile-phase composition and flow-rate the gradient steepness parameter, b, can be derived from the relationship

$$b_1 = t_0 \log \beta \Big/ \left(t_{g1} - \frac{t_{g2}}{\beta} + \frac{t_{G1} - t_{G2}}{t_{G2}} \right) \tag{3}$$

where t_{g1} and t_{g2} are the solute gradient retention times of gradient times t_{G1} and t_{G2}, respectively, and β is the ratio of the gradient times (t_{G2}/t_{G1}). However, if chromatograms are obtained at flow-rates F_1 and F_2, whilst the gradient time is maintained constant, then b values may be obtained from

$$b_1 = \log (F_2/F_1) \Big/ \left(X_1 - X_2 \cdot \frac{F_1}{F_2} \right) \tag{4}$$

where

$$X_1 = \frac{t_{g1} - t_{0,1}}{t_{0,1}} \tag{5}$$

and

$$X_2 = \frac{t_{g2} - t_{0,2}}{t_{0,2}} \tag{6}$$

By definition, LSS gradients require the value of b for all components to be constant, and this can be achieved for low-molecular-weight solutes, such as amino acids, polyaromatic hydrocarbons or drug analogues. In most gradient systems as currently used, the value of the parameter b usually varies for different polypeptides. The gradient steepness parameter, b, can also be related to the variables which quantitatively define structure–retention dependencies on LSS gradients in reversed-phase separations through the expression

$$b = \frac{SV_m \, \Delta\varphi}{Ft_G} \tag{7}$$

It is evident from eqn. 7 that changes in gradient time or flow-rate will affect the value of b and consequently alter solute selectivity (α), as reflected by changes in the S value. Conversely, both the b value and selectivity will remain constant if t_G and F are varied proportionally, provided no change in the interactive contact area of the solute occurs due to slow secondary equilibrium phenomena. Optimisation of selectivity and peak capacity can therefore be carried out through rational manipulation of these experimental variables.

In reversed-phase chromatographic systems, application of the LSS concept has proved useful for the analysis of macromolecular retention data. Similarly, extension of the LSS model to HPIEC provides a useful basis for comparing isocratic and gradient data, although the full implications of multisite interaction and orientation effects in these systems have yet to be established. For small, charged molecules, separated under isocratic ion-exchange conditions, the capacity factor, k', can be related to the concentration of the displacer salt, c, by the following empirical relationship

$$\log k' = \log K + Z \log \frac{1}{c} \tag{8}$$

where K is an ion-exchange distribution constant and Z is the tangent to the curve obtained from a plot of log k' *versus* log $1/c$. Previous studies[5] indicate that linear salt gradients may result in a non-linear dependence of k' on gradient time, a finding which is not consistent with the assumptions of LSS-type separations. Eqn. 2 can still be used in such HPIEC systems, provided the gradient is assumed to approximate the LSS condition during the time that a solute molecule migrates through a column, *i.e.* over a limited k' range, such as $1 < k' < 10$. The resultant value for t_g can then be used to

obtain a solution for b from eqns. 3 or 4. The median capacity factor, $\bar{k}$, for a particular solute, eluted under gradient conditions can then be obtained from

$$\bar{k} = 1/1.15b \tag{9}$$

where the value of $\bar{k}$ corresponds to the capacity factor for a solute band at the column midpoint. Similarly, the concentration, $\bar{c}$, of the eluting salt when the sample band has reached the column midpoint is given by

$$\bar{c} = c_0 + \left(t_g - t_0 - t_e - 0.30\frac{t_0}{b}\right)\Delta c/t_G \tag{10}$$

where $\Delta c = c_f - c_0$ and c_0 and c_f are the initial and final salt concentrations for the gradient. Values of Z and log K can then be obtained from eqn. 8 by using iterative regression analyses of plots of log $\bar{k}$ *versus* log $1/\bar{c}$.

If the physicochemical basis of isocratic and gradient elution in HPIEC is assumed to be the same, plots of log $\bar{k}$ *versus* log $1/\bar{c}$, when approximated by linear dependencies derived from the data for both isocratic and gradient experiments for a particular solute, should be superimposable. However, if the interactive properties of the protein solute are sensitive to time-dependent changes, including changes mediated by the displacer salt concentration, conformational effects, ion-binding and salt-bridging effects or other secondary equilibria, the experimental values of Z and log K, derived according to the LSS gradient model, will not coincide with the values determined isocratically. As part of further investigations on the mechanistic details of HPIEC of peptides and proteins, this paper describes the results of detailed studies on the comparative macromolecular retention behaviour in isocratic and gradient anion-exchange elution systems, using the LSS retention model summarised by eqns. 1–10 as the basis of data analysis.

The retention data for three proteins, listed in Table I, were obtained with a Mono-Q strong anion-exchange stationary phase, under gradient and isocratic elution conditions. Isocratic data were obtained at pH 9.60 with sodium chloride concentrations varying between 0 and 300 mM at a flow-rate of 1 ml/min. Gradient data were also collected at pH 9.60 with a 0 to 300 mM sodium chloride gradient. The procedure for the accumulation of gradient elution data involved either fixing the flow-rate at 1 ml/min, with t_G ranging between 17.1 and 171 min, or setting the gradient time to 17.1 min and varying the flow-rate between 0.1 and 2.0 ml/min. Fig. 1 shows retention plots of log k *versus* log $1/c$, derived from the isocratic and two sets of gradient data for the proteins listed in Table I. The slopes (Z_{comb}) of these plots and the correlation coefficient, r^2, for the combined isocratic and gradient data are also listed in Table I. Values of r^2 approaching unity, as observed for ovalbumin ($r^2 = 0.95$) in Table I, indicate that both gradient and isocratic data are highly congruent and that the LSS theory provides an accurate model of gradient elution behaviour for this protein. However, lower r^2 values for Z_{comb} were seen for carbonic anhydrase ($r^2 = 0.77$) and myoglobin ($r^2 = 0.74$). For elution systems involving monovalent displacing ions, Z is generally defined as the number of electrostatic interactions between the protein solute and the charged stationary-phase surface. Furthermore, if the desorption process were solely dependent on the concentration of displacer salt in

TABLE I

PHYSICAL PARAMETERS AND Z VALUES FOR PROTEINS USED IN THIS STUDY

Protein	*pI*	*MW*	$D_m^{\star} \cdot 10^{-10}$ (cm^2/s)	$Z_{iso}^{\star\star}$	$Z_{VF}^{\star\star\star}$	$Z_{VTG}^{\S}$	$Z_{comb}^{\S\S}$
(1) Ovalbumin (eggwhite)	4.70	43 500	4.24	7.7 (0.99)	7.4 (0.97)	9.4 (0.99)	7.3 (0.95)
(2) Carbonic anhydrase (bovine erythrocytes)	5.89	30 000	4.80	4.4 (0.99)	4.5 (0.87)	2.9 (0.98)	2.4 (0.77)
(3) Myoglobin (sperm whale muscle)	7.68 8.18	17 500	5.74	2.8 (0.98)	5.1 (0.98)	4.0 (0.94)	1.7 (0.74)

* Calculated from the Stokes-Einstein equation[29].
** Z value for isocratic data.
*** Z value for gradient varied F, constant t_G data.
§ Z value for gradient varied t_G, constant F data.
§§ Z value for combined isocratic and gradient data.

the mobile phase, it would be anticipated that similar Z values should be obtained for isocratic and gradient experiments, and that no difference should exist between gradient elution data obtained under conditions of varying gradient time and varying flow-rate. However, significant differences were observed between the three sets of data, *i.e.* Z_{iso}, Z_{VF} and Z_{VTG} for myoglobin and carbonic anhydrase.

While gradient and isocratic elution processes can be mathematically related through such theoretical treatments as the LSS model, the experimental data indicate that the two modes of elution are not directly comparable for protein solutes separated by these two HPIEC methods. The main reason for these divergencies is that different sorption/desorption dynamics will occur in each process. For example, solutes eluted isocratically are exposed throughout column migration to a constant salt concentration. In contrast, under the condition of gradient elution, as used in the current study,

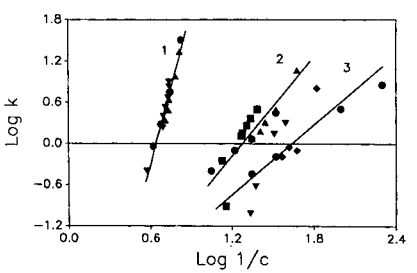

Fig. 1. Retention plots for isocratic (log k' versus log $1/c$) and gradient experiments (log $\bar{k}$ *versus* log $1/\bar{c}$) for the proteins listed in Table I. Isocratic data were derived from experiments with varied sodium chloride concentrations at pH 9.6 and a flow-rate of 1 ml/min. Gradient data were obtained with t_G varying between 17.1 and 171.1 min at a flow-rate of 1 ml/min or a constant t_G of 17.1 min and the flow-rate varying between 0.1 and 2.0 ml/min. Other chromatographic conditions are given in Experimental. See Table I for the code to protein solutes and for the derived Z_e values. For protein 1: ● = isocratic, ▲ = varying gradient time, ▼ = varying flow-rate. For protein 2: ● = isocratic, ▲ = varying gradient time, ■ = varying flow-rate. For protein 3: ● = isocratic, ◆ = varying gradient time, ▼ = varying flow-rate.

solutes are initially immobilised on the anion exchanger at low ionic strength and then subjected to either varying rates of change in the salt concentration (varied t_G and constant F) and/or varying flow-rates including a constant rate of change in the salt concentration (varied F and constant t_G). In the latter case, at very low flow-rates, the system dead-volume, t_e, becomes a major portion of the total gradient volume of the system and consequently, the gradient condition approximates a stepwise elution, *i.e.* b approaches infinity as t_G and F approach zero. Under these conditions, the sorbed solute is exposed to a smaller displacement volume, effectively at a higher rate of change of salt concentration per unit volume, rather than the more normal gradient development under elution conditions. Low flow-rates and short t_G values consequently promote increased solute presence in the mobile phase and lead to shorter elution times. Linear retention plots for log k' *versus* log $1/c$ or log $\bar{k}$ *versus* log $1/\bar{c}$ were observed for most of the varied flow-rate retention data obtained in this study. However, at very low flow-rates, such as 0.1 ml/min, data points for carbonic anhydrase and myoglobin deviate from this linear relationship, and the log k' or the log $\bar{k}$ *versus* log $1/c$ ($1/\bar{c}$) plots exhibit a curvature, particularly when $F < 0.2$ ml/min. While the effect of t_e on elution conditions may account for deviations at low k or high b values, chromatographic residence times, particularly at low b values, will also significantly influence the retention behaviour of proteins.

The influence of salts on the stability, solubility and biological activity of proteins in solution has attracted some attention[13–18]. The implications of these effects for the chromatographic behaviour of proteins in HPIEC have not yet been incorporated into a general retention model. While sodium chloride is known not to greatly influence protein structure and stability, it is clearly apparent that changes in the concentration of this salt over the ranges of gradient times adopted in this study, modify the interactive properties of different solutes, an effect which cannot be predicted on the basis of the LSS model. Furthermore, conformational changes induced by the type or concentration of the salt or pH changes in the microenvironment of the protein would be expected to give rise to changes in both Z_c and K. Where such changes are discrete rather than monotonously continuous, breaks in the log k' *versus* log $1/c$ plots will occur, leading to more than one apparent Z_c value. Such behaviour has been noted with subtilisin variants[19] as well as with several hormonal proteins[20]. The degree of solute exposure to mobile-phase constituents clearly represents a major factor contributing towards non-coincident retention behaviour for proteins eluted by gradient and isocratic HPIEC methods. The process of solute desorption is a complex interaction between the protein, the displacing salt species and the charged stationary-phase surface. If Z is also considered to be a measure of the electrostatic interaction area, A_{cont}, larger values of Z_{VTG} may be anticipated as the solute is initially sorbed in the absence of displacer salt, which should promote maximum interaction. However, this was only observed for ovalbumin and not myoglobin or carbonic anhydrase. The mechanism of protein desorption in HPIEC involves an ionic displacement hierarchy as the protein is desorbed from the charged stationary phase, in which certain charged centres on the solute surface dominate the interaction. The influence of solvent conditions on the interactive nature of these groups will thus not be solute-specific *per se*, but rather orientation- and electrostatic-contact-area-specific. As discussed elsewhere[21], these electrostatic contact areas or ionotopes define the structure–retention dependency for different proteins. It thus

follows that structurally different proteins with the same ionotopic contact area can have the same apparent retention under a particular HPIEC condition. If the protein surface structure is not influenced by the nature or the concentration of the displacer salt, similar Z values will be obtained for both isocratic and gradient experiments. However, if the interactive potential of the charged centres, which constitute the coulombic interaction area is diminished or enhanced in the presence of displacer salts, the desorption process will clearly differ between isocratic and gradient-elution conditions. This will give rise to subtle but important selectivity differences, which can be exploited in both analytical and preparative applications.

Salt-mediated changes in the surface electrostatic structure of protein solutes will also influence the kinetic properties of solute sorption and desorption, and these rate effects will be manifested as anomalous band-broadening behaviour. The LSS model was therefore further evaluated as a theoretical approach to aid in the prediction of solute bandwidth and to provide further insight into the kinetic behaviour of proteins at charged stationary phase surfaces.

Bandwidth relationships

The general plate height theory[22] provides a basis for assessing the diffusional behaviour of small molecules in chromatographic systems. Snyder and co-workers[4,5] have extended the use of retention parameters derived from their LSS model in conjunction with the plate-height theory to provide a method for predicting solute bandwidths so that overall chromatographic resolution can be evaluated and, if necessary, improved. Under chromatographic conditions of gradient elution, the resolution between two adjacent solute zones can be defined as

$$R_{s_{i/j}} = (\alpha_{i/j} - 1)\sqrt{N}\frac{k_i}{1 + k_i} \tag{11}$$

where $\alpha_{i/j}$ is the gradient separation factor (or selectivity) between two solutes, P_i and P_j, as they traverse the midpoint of the column, and N is the theoretical plate number. Furthermore, the peak capacity (PC) for a chromatographic separation of gradient time (t_G), flow-rate (F) and average resolution ($R_s = 1$), for all adjacent peaks can be expressed by

$$\mathrm{PC} = \frac{(t_G - t_0)F}{4\sigma_v} \tag{12}$$

where σ_v is the bandwidth measured in volume units (1 S.D.). When α is kept constant, maximising the peak capacity will, accordingly, optimise the resolution. The relationship between σ_v and $\bar{k}$ for linear solvent systems can be expressed as

$$\sigma_{v,\mathrm{calc}} = \frac{(0.5\bar{k} + 1)GV_m}{\sqrt{N}} \tag{13}$$

where V_m is the column void volume ($V_m = t_0F$) and G is the band-compression factor

which arises from the increase in solvent strength across the solute zone as the gradient develops along the column, given by the expression

$$G^2 = \left(1 + 2.3b + \frac{(2.3b)^2}{3}\right) \Big/ \left(1 + 2.3b\right)^2 \tag{14}$$

Under normal flow-rate conditions in gradient elution, the plate number, N, can be approximated to

$$N = \frac{D_m t_0}{C d_p^2} \tag{15}$$

where d_p is the particle diameter and D_m is the diffusion coefficient (cm^2/s) of the solute in the mobile phase, which can be expressed in terms of solute molecular weight (MW) as

$$D_m = \frac{8.34 \cdot 10^{-10} T}{\eta MW^{1/3}} \tag{16}$$

where T is the absolute temperature and η is the eluent viscosity. The Knox equation parameter, C, which accounts for resistance to mass transfer at the stationary phase surface can be estimated by

$$C = \frac{[(1 - x + \bar{k})/(1 + \bar{k})]^2}{15\rho^* a' + 15\rho^* b' \bar{k} - 19.2\rho^* x} \tag{17}$$

where x is the interstitial column fraction found[23] to be 0.62 for a Mono-Q anion-exchange column, a' is assumed to equal 1.1 and b' is the surface diffusion parameter, calculated from the relationship

$$B = a' + b'k \tag{18}$$

The Knox equation constant, B, which arises from zonal dispersion due to longitudinal diffusion, was obtained experimentally from isocratic bandwidth data at different flow-rates and substituted into eqn. 18 to obtain a value of b' equal to 0.72. The restricted diffusion parameter, ρ^*, a molecular-weight-dependent term, was calculated by using the Renkin relationship[21] so that

$$\rho^* = 1 - 2.104\rho + 2.09\rho^3 - 0.95\rho^5 \tag{19}$$

where ρ is equal to the ratio of the solute diameter to the sorbent pore diameter (d_s/d_p). The linear logarithmic relationship ($r^2 = 0.992$) found experimentally between ρ^* and solute MW for a Mono-Q column, assuming an average pore size of 800 Å and a protein molecular-weight range between 12 000 and 69 000 was

$$\log \rho^* = 0.19 - 0.06 \log MW \tag{20}$$

Although the above bandwidth relationships provide reasonable correlations with experimental data of conformationally rigid low-molecular-weight solutes, it has been found in, *e.g.* reversed-phase HPLC that the chromatographic behaviour of proteins can be much more complex than described by these equations. In the present study, these bandwidth relationships have therefore been employed to further investigate protein kinetic behaviour during high-performance anion-exchange chromatography. Application of the bandwidth eqns. 11–20, derived from the general plate-height theory, assumes that the solute migrates as a single interactive species with an invariant surface charge distribution and shape. Divergencies between experimental and theoretical bandwidths will arise when changes in surface structure occur as a result of preferential salt interactions, which may or may not lead to more specific conformational changes. If it is assumed that these secondary equilibrium processes are either very rapid or very slow compared to the solute chromatographic separation time, then the ratio between the experimentally observed bandwidth, $\sigma_{v,exp}$, and the calculated bandwidth, $\sigma_{v,calc}$, should approach unity over an optimal range of retention values, *i.e.* $1 < \bar{k} < 10$. However, there is an increasing number of examples where the average relaxation times associated with solute-dependent secondary equilibrium process, such as conformational effects, are of a magnitude comparable to the mass transfer time[25–27]. In such cases where the shape and surface characteristics of the polypeptide molecule are changing in a relatively slow, time- or condition-dependent manner, the corresponding changes in the diffusional and interactive properties of the solute will lead to differential zone migration. These increases or decreases in the kinetics of solute mass transfer properties will ultimately be revealed as experimental bandwidths that deviate significantly from values predicted by eqn. 13.

Theoretical bandwidths for the proteins listed in Table I were therefore calculated over the range of experimental conditions employed by using eqns. 13–20 and compared to the experimental peak widths as a function of the gradient steepness parameter, *b*. Fig. 2 shows plots of $\sigma_{v,exp}/\sigma_{v,calc}$ as a function of $1/b$ for experiments carried out at a constant flow-rate of 1 ml/min. In these plots, the bandwidth ratio is seen to increase with decreasing *b*. Eventually, a maximum $\sigma_{v,exp}/\sigma_{v,calc}$ value is obtained for each protein where the bandwidth ratio approaches a plateau limit and remains essentially constant with decreasing *b* values. As is evident from Fig. 2, the variation in the rate of change of displacer salt concentration, associated with differences in gradient time, dramatically affects the kinetic processes for each solute.

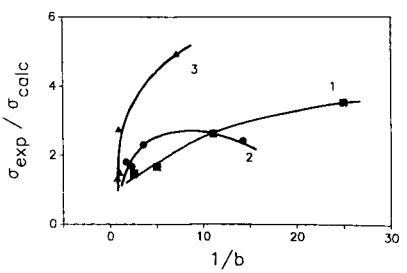

Fig. 2. Plots of $\sigma_{v,exp}/\sigma_{v,calc}$ *versus* $1/b$ for proteins listed in Table I. The dependencies shown correspond to data acquired under conditions of different gradient times at a flow-rate of 1 ml/min. $\sigma_{v,calc}$ was evaluated by using the eqn. 13. See Table I for code to protein solutes.

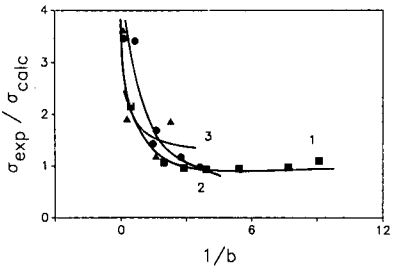

Fig. 3. Plots of $\sigma_{v,exp}/\sigma_{v,calc}$ *versus* $1/b$ for data acquired under conditions of varying flow-rates and a constant gradient time of 17.1 min. See legend to Fig. 2 for other details.

The deviation of these plots from unity indicates that the assumptions inherent in the plate-height theory do not satisfactorily accommodate these secondary equilibrium effects. Detailed explanations of the underlying reasons for solute-dependent divergencies of $\sigma_{v,exp}$ and $\sigma_{v,calc}$ for very shallow gradients, *i.e.*, small b values, have yet to be offered. However, these divergencies may arise as a consequence of solute-specific physicochemical phenomena, associated with solute solvation or changes in the approach depth of penetration of the protein at or near the Stern double layer. Values for $\sigma_{v,exp}/\sigma_{v,calc}$ in reversed-phase systems with polypeptides/proteins[7,29–31] have been reported to deviate much less from unity over similar b-value ranges. The larger $\sigma_{v,exp}/\sigma_{v,calc}$ values found for proteins eluted in ion-exchange chromatography can be related to the physiochemical nature of the kinetics of interaction between solute and sorbent surface. The solute/stationary phase electrostatic interactions in HPIEC are much stronger in terms of free energy changes than the Van der Waals interactions that dominate reversed-phase separations, *i.e.* ΔG_{iec} *versus* ΔG_{vdw} of *ca.* 20 and 4kJ/mol, respectively[32]. As a result, the differences in the affinity of the interacting groups in HPIEC will be much larger than in reversed-phase systems. This will then cause differential zonal migration of the solute band and will contribute to anomalous bandbroadening behaviour, particularly at longer column residence times.

Fig. 3 shows a plot of $\sigma_{v,exp}/\sigma_{v,calc}$ *versus* $1/b$ for the same proteins as shown in Fig. 2, where t_G was held constant at 17.1 min and the flow-rate was varied systematically between 0.1 and 2.0 ml/min. The curve shape and magnitude of the bandwidth ratios for the three non-related globular proteins were similar, and at lower

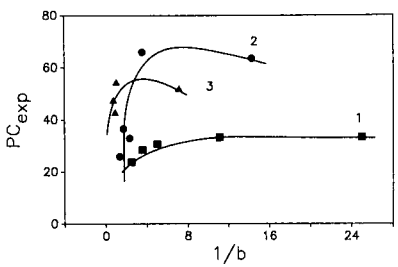

Fig. 4. Plots of peak capacity (PC) *versus* $1/b$ for data obtained under conditions of varying gradient time and a flow-rate of 1 ml/min. The PC value was determined according to eqn. 12. See legend to Figs. 1 and 2 for other details.

b-values or higher flow-rates these plots all approached unity. In general, at flow-rates of less than 0.5 ml/min, *i.e.* corresponding to large *b* values, there is a rapid increase in the bandwidth ratio. Such increases in $\sigma_{v,exp}/\sigma_{v,calc}$ have been attributed to the so-called *J*-effect[8], which is believed to be associated with rapid gradient generation, leading to stepwise elution. With decreasing flow-rate and a small t_G, the gradient elapse time, t_e, becomes a more significant proportion of the total gradient time, resulting in conditions where solute retention is governed predominately by stepwise rather than gradient elution.

This bandbroadening behaviour is also evident from analysis of the experimental peak capacity data. Fig. 4 shows plots of PC *versus* $1/b$ for the proteins listed in Table I at a constant flow-rate of 1 ml/min and varied t_G, where PC is calculated according to eqn. 12. The plots for all proteins were observed to increase to a maximum with decreasing *b*. The plots of PC *versus* $1/b$ for ovalbumin approached an apparent asymptotic limit, while the data for myoglobin and carbonic anhydrase indicated an apparent PC maximum at intermediate *b* values of 0.25–0.5, followed by decrease in PC. The relationship used to calculate $\sigma_{v,calc}$ assumes that the electrostatic surface structure of the protein solute is constant throughout its passage along the column. However, the observed differences between $\sigma_{v,exp}$ and $\sigma_{v,calc}$ (and hence the differences noted for PC_{exp}) with decreasing rates of change in sodium chloride concentration indicates that the interactive potential of the protein is, in fact, changing under the different elution conditions. This observation suggests that values calculated for various input parameters, such as D_m and the simple form of the dependency of the Knox *C* parameter on $\bar{k}$ (eqn. 17) may not adequately describe the diffusional and interactive properties of the protein solute as it passes along a charged stationary phase. Consequently, the incorporation of additional factors into bandwidth models is required to accommodate the influence of specific solute–solvent–stationary interactions and thus allow a mechanistic approach to optimisation of protein separation in HPIEC. These issues will be addressed in a subsequent manuscript.

Effect of buffer ion concentration

The magnitude of electrostatic interactions between solutes and the sorbent surface in HPIEC is clearly dependent upon several key structural and chromatographic factors. These include (i) the number and distribution of charged sites on the solute molecule that define the surface topography and contact area of the protein ionotopes that interact simultaneously with the packing, (ii) the charge density of the packing and (iii) the mobile phase composition. Of these factors, the mobile-phase composition is the easiest and most convenient to manipulate systematically. It is known that the mobile phase composition can be changed in a number of ways to influence solute retention, including variation in the type of displacer ion, ion concentration and solvent pH[1,3,33,34]. However, little has been reported on the effect of buffer ion concentration on solute retention for gradient HPIEC systems. In order to address this issue systematically, the following experimental data were obtained by simultaneously varying the concentration of piperazine in eluents A and B. Piperazine has pK_a values of 5.68 and 9.73 and at a solvent pH of 9.60 carries either a uni- or bi-valent positive charge, which may then influence chromatographic behaviour through preferential interactions with the protein solute.

Fig. 5 shows retention plots for carbonic anhydrase and ovalbumin, eluted under

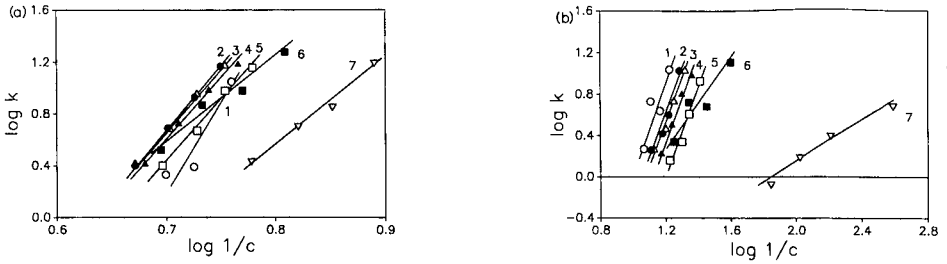

Fig. 5. Retention plots of log k *versus* log $1/c$ for (a) ovalbumin and (b) carbonic anhydrase, eluted under gradient conditions with varying piperazine buffer concentrations of 0–80 mM in eluents A and B. At each buffer concentration, retention data were obtained from four gradient times (t_G = 17.1, 34.3, 60 and 100 min) at 1 ml/min. Piperazine concentrations were as follows: (1) 0 mM, (2) 5 mM, (3) 10 mM, (4) 20 mM, (5) 30 mM, (6) 40 mM and (7) 80 mM.

gradient conditions with varying piperazine buffer concentrations. The gradient data were collected at pH 9.60, using a Mono-Q strong anion-exchange column and sodium chloride concentrations varying between 0 and 300 mM. At each buffer concentration, solute retention data were obtained for four different gradient times (t_G = 17.1, 34.3, 60 and 100 min). In Fig. 5, the high degree of parallelism between different retention plots derived for the same solute becomes immediately evident. Table II shows the Z_{obs} values obtained from each series of gradient experiments at the different buffer concentrations. The retention plots for carbonic anhydrase remain essentially parallel until a critical piperazine concentration between 30 and 40 mM is used in eluents A and B. Parallel retention plots also exist for ovalbumin between 5 and 30 mM piperazine inclusive. The existence of these parallel retention curves indicates that the interaction properties between the solute and support surface are conserved over the corresponding piperazine concentration range. Analysis of the data shown in Table II reveals that significant changes in selectivity occur for both carbonic anhydrase and ovalbumin when the piperazine concentration exceeds 40 mM or is less than 5 mM, respectively. These variations in selectivity reflect changes in both the solute surface interactive properties and the affinity of the solute for the stationary phase surface. Furthermore, the log K term in eqn. 8 is related to the equilibrium constant for the ion-exchange process, K_b, so that changes in K_b reflected in log K represent a change in both the solute affinity toward the sorbent surface and the average distance of the buffer ion from the polyelectrolyte surface. It can thus be concluded that at higher piperazine concentrations (*i.e.* 40–80 mM) the number of charged interactions between

TABLE II

PROTEIN Z_{obs} VALUES AND STATISTICAL ANALYSIS FOR VARIED PIPERAZINE CONCENTRATIONS

Protein	*Piperazine concentration (mM)*							$\bar{x} \pm 3$ *S.D.*
	0	*5*	*10*	*20*	*30*	*40*	*80*	
Carbonic anhydrase	4.0	4.4	4.1	4.1	4.2	2.0	1.0	4.2 ± 0.4
Ovalbumin	12.2	9.7	9.3	9.0	9.4	6.3	6.6	9.4 ± 0.9

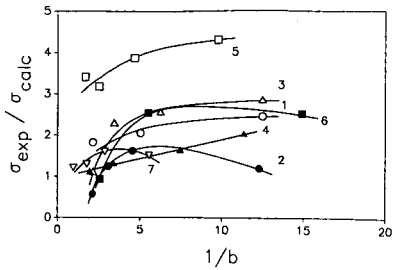

Fig. 6. Plots of $\sigma_{v,exp}/\sigma_{v,calc}$ *versus* $1/b$ for carbonic anhydrase eluted under gradient conditions and varied piperazine buffer concentrations. See legends to Figs. 2 and 5 for other details.

solute molecules and sorbent surface (Z_{obs}) is significantly reduced because of increased buffer ion competition and/or complexation of a new protein shape at the stationary phase surface. Conversely, in the case of ovalbumin at 0 m*M* piperazine, a significant increase in Z results when a decrease in the total ionic strength occurs, associated with a lack of buffer ions to complex competitively with the protein surface. Recent studies[19] on the HPIEC behaviour of subtilisin variants have documented a similar phenomena of elution-condition-dependent Z values. Further insight into the origin of this complex solute behaviour, mediated by the buffer concentration at the solute surface during gradient elution, can be obtained from bandbroadening studies. In Figs. 6 and 7 the effect of varying buffer concentration on bandwidth is shown for carbonic anhydrase and ovalbumin as plots of $\sigma_{v,exp}/\sigma_{v,calc}$ *versus* $1/b$. The curves observed are similar in shape and magnitude to those found for each protein in Fig. 2, signifying the absence of any significant new kinetic effects induced by varying the buffer concentration. Close examination of the chromatographic profiles for ovalbumin and carbonic anhydrase at different piperazine concentrations, which are shown in Fig. 8, reveals the presence of minor isoform peaks. The identity of these isoform peaks was verified by sodium dodecylsulphate polyacrylamide gel electrophoresis (SDS-PAGE) electrophoresis and isoelectrofocusing. Little change in the resolution between ovalbumin and its isoforms was observed. However, between 0 and 20 m*M* piperazine, the major peak 1 for carbonic anhydrase was well separated from those of the minor isoforms 2 and 3. However, at 30 m*M* piperazine, isoform peaks are observed to partially overlap with the major peak of carbonic anhydrase resulting in larger than predicted experimental bandwidths. As the buffer concentration is increased further the separation between carbonic anhydrase and its isoforms

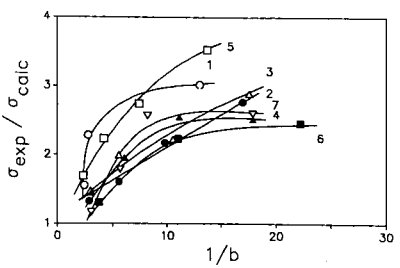

Fig. 7. Plots of $\sigma_{v,exp}/\sigma_{v,calc}$ *versus* $1/b$ for ovalbumin, eluted under gradient conditions and varied piperazine buffer concentrations. See legend to Fig. 6 for other details.

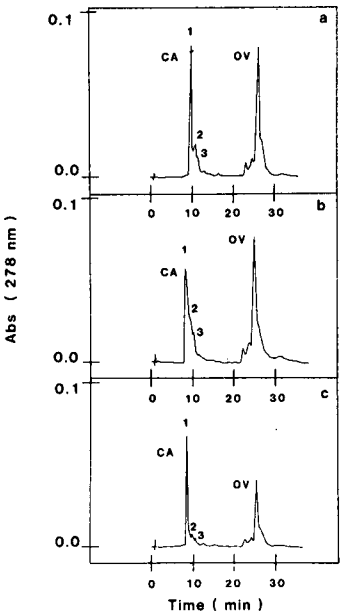

Fig. 8. Chromatograms indicating selectivity changes of carbonic anhydrase isoforms 1, 2 and 3 and of ovalbumin under gradient conditions with piperazine concentrations equal to (a) 20, (b) 30 and (c) 40 m*M*.

improves, while at 40 and 80 m*M* piperazine a decrease in the $\sigma_{v,exp}/\sigma_{v,calc}$ ratio is again observed. These trends are also evident in the peak capacity data shown in Figs. 9 and 10, where PC is plotted as a function of the inverse of the gradient steepness parameter, *b*, for carbonic anhydrase and ovalbumin, respectively.

CONCLUSION

The results of the current investigation clearly indicate that the interaction between protein solutes and the mobile-phase constituents plays a crucial role in the chromatographic behaviour of proteins in HPIEC. Furthermore, while the LSS theory

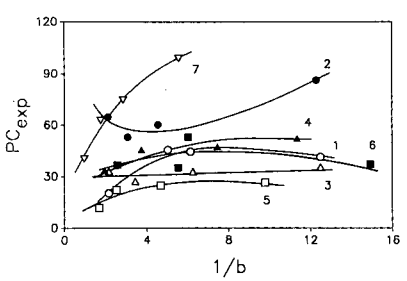

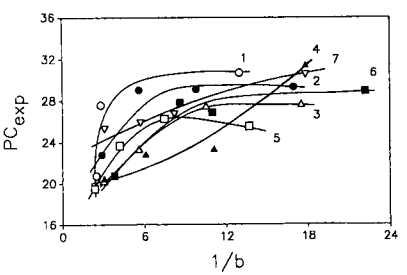

Fig. 9. Plots of peak capacity (PC) *versus* 1/*b* for carbonic anhydrase, eluted under gradient conditions and varied piperazine buffer concentrations. See legend to Figs. 4 and 5 for other details.

Fig. 10. Plots of peak capacity (PC) *versus* 1/*b* for ovalbumin eluted under gradient conditions and varied piperazine buffer concentrations. See legend to Figs. 4 and 5 for other details.

for gradient elution provides a useful basis for the analysis of the retention properties of macromolecules in HPIEC, the interactive properties of proteins are strongly influenced not only by the concentration of the displacer salt, but also by other eluent components, such as the choice and concentration of the mobile-phase buffer. The differences in the experimentally observed Z_c values in isocratic and gradient systems indicates that the orientation of the solute at the stationary phase surface can be controlled by experimental conditions. These results therefore have significant implications for the HPIEC of closely related or microheterogenous proteins. The choice of either isocratic or gradient conditions to enhance selectivity differences represents an additional parameter available for the optimisation of protein separations. It is now apparent that the concept of the coulombic interaction site or ionotype and the ability to identify their location within the surface structure of specific proteins is central to an understanding of the mechanistic basis of HPIEC of macromolecules. Studies currently in progress on the correlation of chromatographic data with the known tertiary structure of proteins, and hence, the electrostatic surface structure, will aid in the characterisation of the "molecular-docking" process between the solute and the stationary phase. The mechanistic details of this process, which is controlled by the charged groups within the ionotopic region, are required before further significant understanding of the thermodynamic and kinetic aspects of HPIEC of biological and non-biological macromolecules can be achieved. The next paper in the series will present the results of investigations into the influence of the type of displacer salt on the gradient elution of proteins in HPIEC by systematic changes in the anion or cation combination.

ACKNOWLEDGEMENTS

The support research grants to MTWH from the National Health and Medical Research Council of Australia, Australian Research Grants Committee and Monash University Special Research Fund is gratefully acknowledged. MIA is a recipient of a Monash University Postdoctoral Fellowship.

REFERENCES

1 M. T. W. Hearn, A. N. Hodder and M. I. Aguilar, *Chromatographia*, 24 (1987) 769.
2 W. Kopaciewicz, M. A. Rounds, J. Fausnaugh and F. E. Regnier, *J. Chromatogr.*, 266 (1983) 3.
3 M. T. W. Hearn, A. N. Hodder and M. I. Aguilar, *J. Chromatogr.*, 443 (1988) 97.
4 L. R. Snyder, in Cs. Horvath (Editor), *High Performance Liquid Chromatography*, Vol. 1, Academic Press, New York, 1980, p. 208.
5 R. W. Stout, S. I. Sivakoff, R. D. Ricker and L. R. Snyder, *J. Chromatogr.*, 353 (1986) 439.
6 E. S. Parente and D. B. Wetlaufer, *J. Chromatogr.*, 355 (1986) 29.
7 M. T. W. Hearn and M. I. Aguilar, *J. Chromatogr.*, 392 (1987) 33.
8 M. A. Stadalius, M. A. Quarry and L. R. Snyder, *J. Chromatogr.*, 327 (1985) 93.
9 N. T. Miller and B. L. Karger, *J. Chromatogr.*, 326 (1985) 45.
10 M. T. W. Hearn, in Cs. Horvath (Editor), *HPLC—Advances and Perspectives*, Vol. 3, Academic Press, New York, 1983, pp. 87–155.
11 M. T. W. Hearn and B. Grego, *J. Chromatogr.*, 255 (1983) 125.
12 M. T. W. Hearn and B. Grego, *J. Chromatogr.*, 266 (1983) 75.
13 F. Hofmeister, *Arch. Exp. Pathol. Pharmakol.*, 24 (1888) 247.
14 E. H. Bycher, *Chem. Weekblad*, 39 (1942) 402.
15 B. E. Conway, *Adv. Colloid Interface Sci.*, 8 (1977) 91.

16 F. A. Long and W. F. McDevit, *Chem. Rev.*, 51 (1952) 119.
17 W. A. P. Luck, in A. Pullman, V. Vasileni and L. Packer (Editors), *Water and Ions in Biological Systems*, Plenum Press, New York, 1985, p. 95.
18 P. H. von Hippel and T. Schleich, in S. N. Timasheff and G. D. Fasman (Editors), *Structure and Stability of Biological Macromolecules*, Marcel Dekker, New York, 1969, p. 417.
19 R. E. Chicz and F. E. Regnier, *J. Chromatogr.*, 443 (1988) 193.
20 M. T. W. Hearn and P. G. Stanton, in preparation.
21 M. T. W. Hearn, A. N. Hodder and M. I. Aguilar, *J. Chromatogr.*, 458 (1988) 45.
22 A. J. P. Martin and R. L. M. Synge, *Biochem. J.*, 35 (1941) 91.
23 J. K. Duncan, A. J. C. Chen and C. J. Siebert, *J. Chromatogr.*, 397 (1987) 3.
24 E. M. Renkin, *J. Gen. Physiol.*, 38 (1954) 225.
25 M. T. W. Hearn, A. N. Hodder and M.-I. Aguilar, *J. Chromatogr.*, 327 (1985) 47.
26 X. M. Lu, K. Benedek and B. L. Karger, *J. Chromatogr.*, 359 (1986) 19.
27 J. Jacobson, W. Melander, G. Vaisnys and Cs. Horváth, *J. Phys. Chem.*, 88 (1984) 456.
28 D. M. Mohilner in A. J. Bard (Editor), *Electroanalytical Chemistry*, Vol. 1, Marcel Dekker, New York, 1966, p. 241.
29 M. T. W. Hearn and M. I. Aguilar, *J. Chromatogr.*, 352 (1986) 35.
30 M. T. W. Hearn and M. I. Aguilar, *J. Chromatogr.*, 359 (1986) 31.
31 M. T. W. Hearn and M. I. Aguilar, *J. Chromatogr.*, 397 (1987) 47.
32 D. E. Metzler, *Biochemistry; The Chemical Reactions of Living Cells*, Academic Press, New York, 1977, p. 182.
33 M. A. Rounds and F. E. Regnier, *J. Chromatogr.*, 283 (1984) 37.
34 K. M. Gooding and M. N. Schmuck, *J. Chromatogr.*, 296 (1984) 321.

Journal of Chromatography, 458 (1988) 45–56
Elsevier Science Publishers B.V., Amsterdam — Printed in The Netherlands

CHROMSYMP. 1427

HIGH-PERFORMANCE LIQUID CHROMATOGRAPHY OF AMINO ACIDS, PEPTIDES AND PROTEINS

LXXXVIII*. CALCULATION OF THE AVERAGE DISTANCE BETWEEN PROTEIN SOLUTES AND THE STATIONARY PHASE DURING ISOCRATIC ANION-EXCHANGE CHROMATOGRAPHY

M. T. W. HEARN*, A. N. HODDER and M. I. AGUILAR
Department of Biochemistry, Monash University, Clayton, Victoria 3168 (Australia)

SUMMARY

This investigation deals with protein retention behaviour in high-performance anion-exchange chromatography in terms of the average distance of approach between the protein solute and the positively charged anion-exchange stationary-phase surface. The theoretical treatment is based on a modified Debye-Hückel theory for spherical impenetrable ions, where the electrostatic potential energy has been related to the chromatographic capacity factor, k'. Results are presented for three globular proteins, eluted isocratically from a Mono-Q strong anion-exchange resin with sodium choride as the displacer salt by a mobile phase with pH in the range 5.50–9.60. Analysis of experimental retention data indicates that topographically predefined, charged regions on the protein surface, called ionotopes, control the orientation and approach distance of the protein solute.

INTRODUCTION

High-performance ion-exchange chromatography (HPIEC) has emerged in recent years as an important method for the analysis and purification of peptides, proteins and polynucleotides. However, a quantitative model describing the fundamental mechanistic processes that control the ion-exchange separation of proteins on microparticulate supports coated with charged ligands is not yet available. Protein retention at ion-exchange surfaces arises from electrostatic interactions between the zwitter-ionic protein surface and the charged stationary-phase surface. Previously, a number of non-mechanistic models have been utilised to assess the retention and bandwidth behaviour of proteins derived from experimental studies with HPIEC[1–5]. These studies have typically evaluated variation in protein selectivity or band-broadening as a function of the ionic strength, mobile-phase pH or the nature of the

* For Part LXXXVII see ref. 5.

0021-9673/88/$03.50

displacer ion through changes in the electrostatic surface potential of the polyelectrolyte surface. Variation of the chromatographic experimental parameters alters the affinity of the solute for the stationary phase through changes in the overall electrostatic surface charge ratio by protonation/deprotonation or through specific electrostatic interactions of the displacer co-ions and counter-ions with surface charge groups on the protein solute or the coulombic ligand. While it is assumed that these interactions will take place at the surface of a conformationally intact protein solute, changes in the three dimensional structure of the protein, which may result from time-dependent exposure to certain chemical environments both in the mobile phase and at the stationary-phase surface during the ion-exchange process, will also clearly have significant effects on solute retention characteristics. The affinity of the solute for the stationary phase is reflected in the retention behaviour of the solute, which will thus be dependent on the relative charge distribution at the surface of both the protein and the stationary phase. Changes in these affinity dependencies will, through the contribution of mutually attractive and repulsive forces and steric bulk, influence the distance to which the protein is able to approach the stationary phase. A method has therefore been investigated for calculating the average distance of approach between a solute molecule and the ionic groups attached to the support surface during anion exchange chromatography. This procedure, which is based on a modified Debye-Hückel theory for spherical, impenetrable ions, allows the evaluation of chromatographic retention data in terms of specific geometric and thermodynamic parameters, and thus provides further mechanistic insight into the behaviour of proteins at charged surfaces in the presence of solvated ions.

EXPERIMENTAL

Apparatus

All chromatographic experiments were performed with a Pharmacia (Uppsala, Sweden) Fast Protein Liquid Chromatography (FPLC) system consisting of two P-500 syringe pumps, a V-7 injector and a 278-nm fixed-wavelength single-path UV monitor, coupled to a two channel REC 482 pen recorder and a Perkin-Elmer (Norwalk, CT, U.S.A.) LCI-100 integrator. Isocratic elution was controlled with a Pharmacia GP-250 solvent programmer. Thermostatted, prepacked Mono-Q strong anion-exchange columns (HR 5/5, 50 × 5 mm I.D.) were used throughout. The pH measurements were performed with an Orion Research Products (Cambridge, MA, U.S.A.) SA 520 meter, equipped with a combination glass electrode. All chromatographic separations were carried out at ambient temperatures of 20°C.

Chemicals and reagents

Bovine erythrocyte carbonic anhydrase, sperm whale skeletal muscle myoglobin (type iii), hen egg ovalbumin (grade v), human serum albumin, Bis-Tris, triethanolamine and piperazine were purchased from Sigma (St. Louis, MO, U.S.A.) and characterised by procedures previously established in this laboratory. Sodium chloride (AnalaR grade) was obtained from BDH (Port Fairy, Australia). Quartz-distilled water was further purified on a Milli-Q system (Millipore, Bedford, MA, U.S.A.), hydrochloric acid (sp. gr. 1.16, AnalaR grade) was purchased from BDH.

Chromatographic procedures

Eluent A was a 0.02 *M* solution of a suitable buffering ion. The buffers used were piperazine (pH 5.50 and pH 9.60), Bis-Tris (pH 6.50) and triethanolamine (pH 7.50). In all cases, eluent B was 0.02 *M* with respect to the appropriate buffer and contained 0.3 *M* sodium chloride as the displacer salt. The pH of both eluents was adjusted to the required pH by addition of hydrochloric acid. Eluents A and B were filtered (0.45-μm cellulose acetate HAWP 04700 (Millipore) and degassed under vaccum. Protein solutions were prepared by dissolving the protein in eluent A at a concentration of 5 mg/ml unless otherwise specified. Protein solutions were filtered before use through 0.22-μm ACRO LC13 filters (Gelman Sciences, Sydney, Australia). Protein sample sizes ranged from 5 to 1000 μg with injection volumes between 10 and 200 μl. At each pH, samples were eluted isocratically, starting at 100% eluent B and repeated, at decreasing concentrations of B until 5% eluent B was reached or protein elution volumes were greater than 30 column volumes.

At each mobile phase pH, log k' and log $1/c$ data were collected for each protein and subjected to an iterative regression analysis to determine the y-intercept (log K), slope (Z_c) and correlation coefficient (r^2) from the plot log k' *versus* log $1/c$. The PROTDIST program, developed in this laboratory for use on IBM XT or AT-compatible personal computers, was used for data analysis.

RESULTS AND DISCUSSION

Theoretical concepts

The mass distribution of a protein solute P with charge $\pm a$, in HPIEC under near equilibrium conditions can be described by the stoichiometric equation

$$(P^{\pm a})_m + Z_t(D^{\pm b})_s \rightleftarrows (P^{\pm a})_s + Z_t(D^{\pm b})_m \quad (1)$$

where $D^{\pm b}$ is the displacer counter-ion and the subscripts m and s represent the mobile-phase and stationary-phase component, respectively. For large polyelectrolyte molecules, such as peptides and proteins, Z_t represents the ratio of the effective surface charge to that on the counter-ion. If conditions of near-equilibrium apply for the chromatographic system, the above distribution model can be rewritten for a monovalent co-/counter-ion solvent system in terms of the dependency of the capacity factor, k', on the concentration of the displacing ion, c, such that for a generalised adsorption process

$$\log k' = \alpha + \beta[\log(1/c)] + \gamma[\log(1/c)]^2 + \delta[\log(1/c)]^3 + \ldots \quad (2)$$

In linear elution chromatography, eqn. 2 is often represented as a non-mechanistic linear expression, which describes the relationship between solute retention and the displacer ion concentration as follows

$$\log k' = \log K + Z_c \log (1/c) \quad (3)$$

where k' is the solute capacity factor, c is the concentration of the displacer ion and K is the overall distribution constant. Values of both log K and Z_c can be obtained by

evaluating the intercept and slope, respectively, of plots of log k' *versus* log $1/c$ by regression analysis. The chromatographically determined Z_c value, derived from eqn. 3, has frequently been taken to represent the number of charged interactive binding sites established between the protein solute and the stationary phase suport such that $Z_c \leq Z_t$. In anion-exchange systems, Z_c values have been found to increase with pH[3,4] and reach a maximum value at a pH which is solute-dependent. The magnitude of Z_c, the shape of the Z_c *versus* pH plots, and the relationships between Z_c and pH or ionic condition, clearly are dependent on the number of exposed charged groups and their distribution on the surface of the protein. In this context, the participation of intrinsic ion bridges between complementary charge centres within the interior or periphery of the protein or extrinsic ion bridges between solvated ions and complementary charge groups at the protein surface would be expected to have a fundamental influence on Z_c values. For example, in anion-exchange systems, operated under normal pH conditions, the non-uniform charge distribution at the surface of the protein will result in localised areas of high electrostatic potential. These regions arise as a consequence of either continuous (*i.e.* sequentially linked amino acids) or discontinuous (*i.e.* topographic through space interactions) clustering of anionic amino acids. This unique interactive patch (or patches) on the surface of the protein can thus be represented as a contour surface or ionotope. Since these regions represent the sites of highest interactive potential which orient or direct the approach of the protein to the charged surface of the stationary phase, they thus act as "docking" sites of defineable surface contact area, A_{cont}, and charge anisotropy, Z_{anis}. It is thus not surprising that many different proteins are capable of being bound to and eluted from a particular ion exchanger with the same apparent k' and even the same band dispersion. What these observations reveal is the similarity and even constancy of the shape and surface characteristics of the interactive sites of a particular set of proteins, manifested through their ionotopes, a concept which is formally analogous to the mimotope strategy recently developed for immunoaffinity chromatography[6]. The proximity and orientation with which a particular protein solute is able to approach the stationary-phase ligands will thus depend on a number of factors. These include surface charge asymmetry and the steric bulk of the protein as well as the stationary phase charge and ionic concentration gradient at the liquid–solid interface, *i.e.* the thickness of the double layer between the solid phase and the bulk solution. As chromatographic retention data is a measure of the free energy of interaction between the solute and stationary phase, the influence of experimental conditions on the approach distance and orientation of a protein solute at the charged surface can be assessed through calculation of the electrostatic potential of the protein which, in turn, allows an average approach distance to be determined. Insight into the mechanistic behaviour of proteins at an ion-exchange surface can be obtained from a number of experimental methods including (i) evaluation of the kinetics of structure–retention behaviour, (ii) analysis of isothermal behaviour and adsorption–desorption kinetics, and (iii) physicochemical treatments which provide quantitative information on protein volume or area occupancy at the surface or data on the minimum approach distance. Studies[7] on the adsortion of polyelectrolytes at charged surfaces have established that the struture of adsorbed solute layers is governed by a subtle balance between enthalpic and entropic factors. For homopolymers, such as polylysine with a repeating segmental unit, these factors include the segmental adsorption energy, the chain-con-

formation entropy, the entropy of mixing segments in a defined solvent and the interaction between segments and solvent components. Theoretical treatments have yet to be generalised to describe the behaviour at coulombic interfaces of charge asymetric, compositionally different biopolymers, which do not behave like statistical coils and which have unique tertiary or quaternary hierachial structures such as those found for globular proteins. In these more complex cases, free energy changes associated with the adsorption properties of proteins are largely determined by the extent to which their bulk conformation is retained during adsorption. If the tertiary structure is unaffected, the adsorption behaviour can be accommodated relatively simply in energetic terms and can be represented as a well-controlled interaction. For proteins which unfold upon adsorption, entropic contributions become important and sometimes dominant. Under these circumstances the orientational frequency and preference of a protein, as it approaches a coulombic surface, can be represented by a kinetically and thermodynamically favoured charge vector. This charge vector will thus correspond to the charged surface of a hypothetical ionotope of predefined interactive surface occupancy and adsorption/desorption kinetics. If it is assumed that the retention process is governed by electrostatic interactions, then Debye-Hückel theory for spherical impenetrable ions can be adapted to evaluate the behaviour of this ionised protein at an HPIEC packing surface. However, it must be recognised that, although this treatment assumes that long range Van der Waals and Lifshitz forces or hydrogen bonding effects play a minor role in the retention process, participation of these phenomena at different elution conditions will lead to second order relationships between log k' and log $1/c$ which are characteristic of changes in the surface hydrophobicity or water structure. As a consequence, non-ideality in retention behaviour analysed according to the assumptions of the Debye-Hückel theory provides insight into the influence of matrix–solute hydrophobic effects or solvation effects. These combined secondary effects can then be analysed in terms of solvophobic and/or solvation theory.

Fig. 1 shows a simplified graphic representation of the Debye-Hückel theory for spherical impenetrable ions[8], as adapted for a macro-ionic ionotope at an ion-exchange packing surface. This model assumes that the protein solute, or more accurately, the topographic region on the protein surface which interacts with the

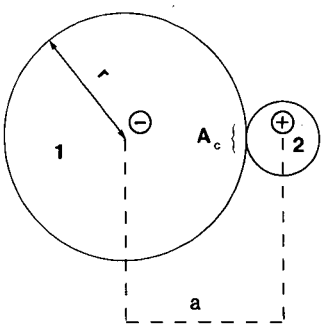

Fig. 1. Theoretical model used in the derivation of eqn. 9 to calculate the solute approach distance, a, consisting of the anionic macro-ion (1) of radius r, and the cationic stationary-phase ligand (2), which interact through the coulombic interaction area (A_c).

HPIEC ligands to create the apparent coulombic contact area, A_{cont}, of the ionotope, can be represented by a charged surface with effective radius r, and is located at the fixed centre of a co-ordinate system. Both the protein ionotope and those ions present at the solute–stationary phase interface are found in a solvent with a dielectric constant, D. The charge vector, q, associated with the ligand–solute interaction established between the stationary phase and the protein is assumed to be either evenly distributed over the macro-ionic ionotope surface or spherically symmetrical in its location. All other interacting ions found at the electrostatic binding site, which include charge support groups, buffer ions and the displacer salt, are assumed to be univalently charged and mobile relative to the central macro-ion. The probability of protein–protein interaction is assumed to be infinitesimally small. The distance, a, in Fig. 1 thus represents the average distance of closest approach between the vectorial centre of the ionotopic surface and the point charge of a univalent ligand ion at the solute–stationary phase interface.

The electrical work in placing charges on the central ion is the product of potential and charge. The work involved in adding a charge, dq, to a point with electrical potential, ψ, is

$$dW_e = \psi dq \tag{4}$$

Hence, the electrostatic free energy, W_e, can be defined in terms of a hypothetical discharge state of the protein ion such that

$$W_e = \int_0^q \psi dq \tag{5}$$

The potential at the surface where the charge is located may then be represented as

$$\psi = \left(\frac{q}{Dr}\right)\left(1 - \frac{\kappa r}{1+\kappa a}\right) \tag{6}$$

Substituting eqn. 6 into eqn. 5 and assuming that Zq is the final effective charge at the point of interest *i.e.*, the macro-ion surface

$$W_e = \int_0^{Zq} \left(\frac{q}{Dr}\right)\left(1 - \frac{\kappa r}{1+\kappa a}\right) \tag{7}$$

Integration of eqn. 7 gives

$$W_e = \left(\frac{Z^2q^2}{2Dr}\right)\left(1 - \frac{\kappa r}{1+\kappa a}\right) \tag{8}$$

By solving eqn. 8 for the a term we obtain the value for the average distance between

the protein ion and the charged ligands at the solute–stationary phase interface, *e.g.*

$$a = \left(\frac{Z^2q^2}{Z^2q^2 - 2DrW_e}\right) - \frac{1}{\kappa} \tag{9}$$

where Z is the magnitude of charge, q is the sign of the charge and r is the protein radius, which is calculated from molecular weight (MW) using the relationship

$$r = (0.39\ \mathrm{MW})^{1/3} \tag{10}$$

The quantity κ^{-1} has the dimensions of length and is referred to as the Debye length. It is an approximate measure of the thickness of the ionic atmosphere or the distance over which the electrostatic field of an ion extends with appreciable strength. The κ term can be calculated by using the following relationship

$$\kappa^2 = \left(\frac{1000\ Ne^2}{\varepsilon_0\ DkT}\right) \sum c_i Z_i \tag{11}$$

where N is Avogadro's number, e is the protonic charge, ε_0 is the permitivity in vacuum, k is the Boltzman constant and T is the temperture (K). The term $\Sigma c_i Z_i$ represents the summation of all charged species of concentration, c, and charge, Z.

If it is assumed that solute elution is carried out under conditions which maximise electrostatic interactions, then the electrostatic free energy term, ΔG_e, for ion-exchange solute retention can be considered to be equivalent to W_e. Thus, in the absence of other secondary retention phenomena the a term from eqn. 9 may be calculated by the following substitution

$$W_e = \Delta G_e = -RT \ln K_d \tag{12}$$

The equilibrium constant, K_d, for the ion-exchange process can be expanded to give

$$\Delta G_e = -RT (\ln k' - \ln \varphi) \tag{13}$$

where R is the gas constant, k' is the chromatographic capacity factor and φ is the dimensionless phase ratio, equal to the ratio of the volume of the stationary phase (V_s) to the volume of the mobile phase (V_m).

The theoretical dependence of electrostatic energy on the distance between two charged bodies is shown in Fig. 2. The right side illustrates the increasing electrostatic attractive energy of a system were two species of opposite charge are brought progressively closer together until a minimum separation distance is reached. This would be analogous to the adsorption phase of HPIEC, where the experimental conditions, such as the concentration of displacer salt and mobile phase pH, will determine the average distance between the charged protein solute and stationary-phase ligands. Conversely, the energy associated with the repulsion between two molecules of similar charge is illustrated on the left side of Fig. 2, where a decrease in the separation distance results in an increase in the repulsive energy. Solute retention in

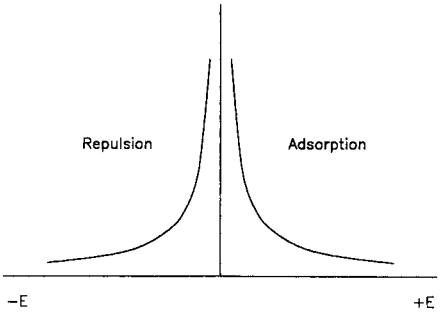

Fig. 2. Plot of the theoretical dependence of distance between two oppositely or similarly charged particles on the electrostatic energy of attraction or repulsion.

HPIEC arises from attractive electrostatic interactions, and hence the degree of repulsion depicted in Fig. 2 cannot be usually assessed from ion-exchange chromatographic data. However, these conditions will occur when proteins are chromatographed in anion-exchange systems at pH levels well below their known p*I*, *i.e.* when the surface of the protein assumes an overall positive charge, resulting in repulsion between the solute and the stationary phase. However, it is noteworthy that several examples have been reported[2,3,9] where proteins exhibit significant retention at a pH equal to or below their p*I*. The analysis of retention data in terms of the dependence of approach distance on mobile phase pH therefore provides the basis for assessing the ability of ionotopic regions at the protein surface to interact with the stationary phase, and gives greater insight into the factors that control the orientation and interaction of these topographic regions of proteins with charged surfaces in general.

Influence of pH on solute approach distance

Isocratic retention data for four globular proteins, listed in Table I, were obtained on a Mono-Q strong anion-exchange column. The proteins varied in molecular weight from 17 500 to 69 000 with p*I* values in the range 4.70–8.18. All proteins were chromatographed at a constant buffer concentration (20 m*M*) and various pH values, the sodium chloride concentration varying between 0 and 300 m*M*,

TABLE I
PHYSICAL PARAMETERS OF PROTEINS

Protein	*pI*	*MW*	*Z*			
			pH			
			5.50	*6.50*	*7.50*	*9.60*
Ovalbumin (eggwhite)	4.70	43 500	3.1	6.2	5.9	7.7
Albumin (human serum)	5.85	69 000	1.8	4.8	4.2	11.1
Carbonic anhydrase (bovine erythrocytes)	5.89	30 000	0.2	0.4	0.6	4.4
Myoglobin (sperm whale muscle)	7.68, 8.18	17 500	0.0	0.1	0.2	2.8

and at a flow-rate of 1 ml/min. Z_c values were calculated by regression analysis of plots of log k' *versus* log $1/c$ at each buffer pH. The Z_c values for each solute, which is defined as the number of charged interactions occuring between the protein solute and stationary phase, were then substituted for Zq in eqn. 9.

Figs. 3–6 show plots of the approach distance, a, as a function of the chromatographic capacity factor, k', for each protein as the mobile phase pH approaches and/or passes through their pI values. For ovalbumin and human serum albumin (Figs. 3 and 4) there is an inverse relationship between the approach distance and k'. Thus, as k' is systematically increased, a minimum a value is reached where the protein ion is thermodynamically restricted from moving any closer to the packing surface, regardless of further decreases in displacer ion concentration (*i.e.* further increases in k' values). Furthermore, the minimum a value decreases with decreasing solvent pH. This indicates that the protein ion orients itself progressively closer to the sorbent surface as the overall anionic charge on the solute surface diminishes and as the dominant interactive charge groups become more spatially isolated.

The net-charge concept has been extensively used to predict solute retention on HPIEC packings as a function of solvent pH. For an anion-exchange column, solute retention is predicted according to this concept to decrease with a decrease in solvent pH. When the solvent pH is equivalent to or below the solute pI, the solute is no longer retained on the anion-exchange column due to repulsive forces dominating the interaction between the sorbent surface and the solute molecule. However, it has been demonstrated[2,3,9] that considerable retention can occur at protein isoelectric points, a behaviour which is consistent with the intramolecular charge asymmetry on the surface accessible regions of the protein. The influence on the minimum approach distance of residual charged groups which exist at a pH close to the pI of the protein is clearly evident in Figs. 4 and 5. Human serum albumin and carbonic anhydrase have almost identical pI values of 5.85 and 5.89. On the basis of the net charge concept, similar dependencies of the a value on k' would be anticipated for these two proteins. Comparison of Figs. 4 and 5 show that human serum albumin exhibits significant retention over the entire pH range, while there is little electrostatic interaction between carbonic anhydrase and the stationary phase at pH 5.50 and 6.50. In these cases, as the solvent pH approaches and passes through the solute pI, the solute becomes

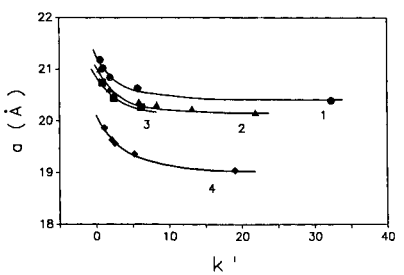

Fig. 3. Plots of approach distance, a, *versus* capacity factor, k', for ovalbumin. Data points were derived from measurements made with varying sodium chloride concentrations and solvent pH values of (1) 9.60, (2) 7.50, (3) 6.50 and (4) 5.50. See Experimental for other details.

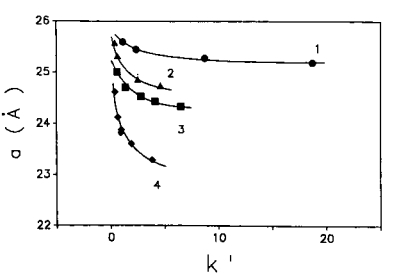

Fig. 4. Plots of a *versus* k' for human serum albumin. See legend to Fig. 3 for other details.

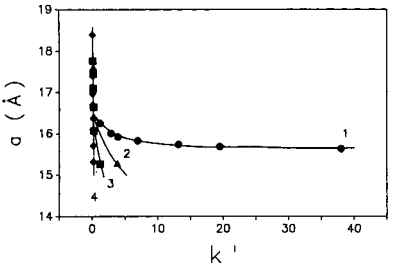

Fig. 5. Plots of *a versus k'* for carbonic anhydrase. See legend to Fig. 3 for other details.

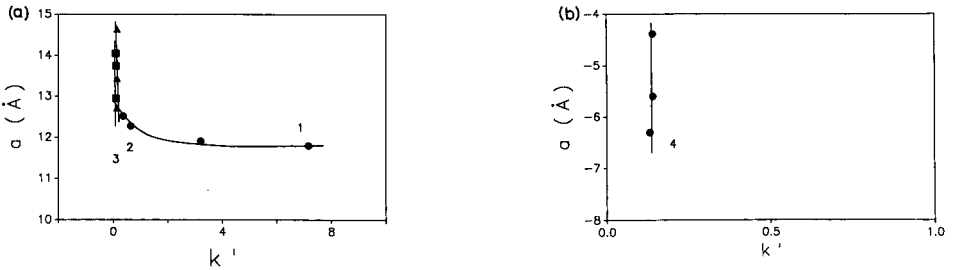

Fig. 6. (a) Plots of *a versus k'* for myoglobin with solvent pH values equal to (1) 9.60, (2) 7.50 and (3) 6.50. See legend to Fig. 3 for other details. (b) Plots of *a versus k'* for myoglobin with solvent pH equal to 5.50.

increasingly positive and this results in lower k' values for carbonic anhydrase. However, it is clearly apparent that the interactive sites or ionotopes for carbonic anhydrase and human serum albumin are significantly different, resulting in the case of human serum albumin in a closer approach to the stationary-phase ligands. Myoglobin, with a p*I* equal to 7.68, is poorly retained below pH 9.60. Indeed, as k' approaches zero, the first term in eqn. 9, which incorporates the interactive energy term, approaches a constant value. Under these conditions eqn. 9 reduces to a dependence of the *a* value on κ, and this can lead to experimental *a* values corresponding to solute repulsion from the ligand surface, as seen for myoglobin in Fig. 6b. Similar influences of pH on solute retention also have important application in the use of chromatofocusing for the separation and purification of protein samples. The choice of buffer species and pH gradient range in the optimisation of experimental conditions will significantly influence the interactive properties of protein solutes, and judicious manipulation of solvent pH would clearly enhance the separation of closely related proteins through selective changes of the surface charge.

The difference between the minima of plots for *a* versus k' for different proteins, *i.e.* the Δa *versus* k' function, provides an indication of the types of molecular changes that occur at the protein–stationary phase interface as a result of a decrease in buffer pH. In Figs. 3 and 4 the distance change between asymptotes at pH 9.60, 7.50 and 6.50 varies up to 1 Å. These differences may reflect changes in double-layer thickness, particularly since different buffer ions were used at pH 9.60, 7.50 and 6.50. Piperazine buffer was used at both pH 9.60 and 5.50 and the distances between the two curve minima for these pH values were 1.4 Å and 2.0 Å for ovalbumin and human serum albumin, respectively. Such distances are similar to those calculated for nearest-neighbour hydrogen-bonding effects for O–H distances (1.86 Å) in water[10], indicating

a difference in the thickness of the layer of solvating water molecules present at the interactive surface of either the central macro-ion or the stationary phase. Changes in the degree of protein solvation have significant implications in the conformational stability of protein solutes during HPIEC. Furthermore, substantial repulsive or hydration forces occur when solvated surfaces, such as lipid bilayers[11,13], are brought within close proximity (< 30 Å) of each other. The origin of these hydration forces has been studied[14,15] for mica surfaces, separated by distances of less than 30 Å, in a variety of electrolyte solutions. With mica, competitive adsorption between metal ions, such as Na^+ (which on adsorption strongly orients water dipoles), and H^+ ions was found to produce pH-dependent switching mechanism. The phenomenon of metal/hydrogen ion exchange at various surfaces and its correlation with short-range hydration forces has been advanced to account for thylakoid membrane stacking and unstacking in chloroplasts[16]. In ion-exchange chromatography with sodium chloride or other sodium salts as displacers a sodium/hydrogen ion switching mechanism may also be active at the solute–stationary phase interface, whereby the lowering of buffer pH from 9.60 to 5.50 causes the sorbed sodium ions at the protein surface to be replaced by hydrogen ions. This results in a decrease of the hydration forces, reflected by the observed changes in the *a* value between asymptotes at pH 9.60 and 5.50 for ovalbumin and human serum albumin in Figs. 3 and 4.

CONCLUSION

Estimation of the distance within which a protein solute can approach the charged stationary-phase surface in HPIEC provides the basis for a more detailed analysis of chromatographic retention data in electrostatic-interaction systems. The present study indicates that small changes in the charge of the interactive or ionotopic surface of the solute can strongly influence the isocratic retention behaviour of proteins through changes in the electrostatic potential. While these results would be anticipated from qualitative consideration of the amphoteric nature of protein surface structure, the current study represents a detailed quantitative approach to the analysis of these molecuar events. Identification of the ionotopic surface of proteins would clearly allow the effects of pH on the selectivity of closely eluted proteins to be more effectively exploited in ion-exchange, hydrophobic-interaction and chromatofocusing systems. The battery of experimental parameters for selectivity optimisation also includes the nature of the displacing salt and the use of gradient elution. Future papers will present the results of investigations on the influence of these parameters on the orientation of protein solutes at charged surfaces in HPIEC.

ACKNOWLEDGEMENTS

Research grants to M.T.W.H. from the National Health and Medical Research Council of Australian, Australia Research Grants Committee and Monash University Special Research Fund Committee are gratefully acknowledged. M.I.A. is a recipient of a Monash University Postdoctoral Fellowship.

REFERENCES

1 R. W. Stout, S. I. Sivakoff, R. D. Ricker and L. R. Snyder, *J. Chromatogr.*, 353 (1986) 439.
2 W. Kopaciewicz, M. A. Rounds, J. Fausnaugh and F. E. Regnier, *J. Chromatogr.*, 266 (1983) 3.
3 M. T. W. Hearn, A. N. Hodder, P. G. Stanton and M. I. Aguilar, *Chromatographia*, 24 (1987) 768.
4 M. A. Rounds and F. E. Regnier, *J. Chromatogr.*, 283 (1984) 37.
5 M. T. W. Hearn, A. N. Hodder and M. I. Aguilar, *J. Chromatogr.*, 458 (1988) 27.
6 M. Geysen, B. Shield and M. T. W. Hearn, in preparation.
7 J. Papenhuijzen, G. J. Fleer and B. H. Bijsterbosch, *J. Colloid Interface Sci.*, 104 (1985) 553.
8 C. Tanford, *Physical Chemistry of Macromolecules*, Wiley, New York, NY, 1961, p. 457.
9 M. T. W. Hearn, A. N. Hodder and M. I. Aguilar, *J. Chromatogr.*, 443 (1988) 97.
10 A. H. Narten, W. E. Thiessen and L. Blum, *Science*, 217 (1982) 1033.
11 D. M. LeNeve, R. P. Rand, V. A. Parsegian and D. Gingell, *Biophys. J.*, 18 (1977) 209.
12 A. C. Cowley, N. L. Fuller, R. P. Rand and V. A. Parsegian, *Biochemistry*, 17 (1978) 3163.
13 D. F. Evans and B. W. Ninham, *J. Phys. Chem.*, 90 (1986) 226.
14 R M. Pashley and J. N. Israelachvili, *J. Colloid Interface Sci.*, 101 (1984) 511.
15 R. M. Pashley, *J. Colloid Interface Sci.*, 83 (1981) 531.
16 J. T. Duniec, J. N. Isrealachvili, B. W. Ninham, R. M. Pashley and S. W. Thorne, *FEBS Lett.*, 129 (1981) 193.

Journal of Chromatography, 458 (1988) 57–66
Elsevier Science Publishers B.V., Amsterdam — Printed in The Netherlands

CHROMSYMP. 1527

SALT-BINDING EFFECTS IN HYDROPHOBIC-INTERACTION CHROMATOGRAPHY

R. A. BARFORD*, T. F. KUMOSINSKI, N. PARRIS and A. E. WHITE
U.S. Department of Agriculture, ARS, Eastern Regional Research Center, 600 East Mermaid Lane, Philadelphia, PA 19118 (U.S.A.)

SUMMARY

Many separations of proteins are performed on hydrophobic interaction columns. Elution is achieved with salt gradients, but anomalous elution behavior is observed often. In this investigation, we show that the binding of salt to proteins may explain these anomalies. Presumably, salt binding alters the number and distribution of protein surface groups, including charged groups. Analysis of retention data was carried out by non-linear regression until the minimum sum of squares was found between the observed capacity factor and that computed from a retention model based upon Wyman's theory of thermodynamic linkage. The relation of retention to salt concentration as described by this model is compared to surface tension models and to relative elution orders based on hydrophobicity scales.

INTRODUCTION

Previous reports from this laboratory have suggested that surface-modified siliceous packings for high-performance liquid chromatography (HPLC) represent a continuum of materials with surface tensions between about 30 mJ/m^2 and about 55 mJ/m^2 (refs. 1 and 2). Moreover, adsorption of proteins to these materials was related to the surface tensions of the packing, protein, and mobile phase. Reducing the surface tension of the mobile phase so that it is below that of the protein and higher than that of the packing promoted desorption. This is accomplished commonly in reversed-phase chromatography by the addition of organic modifiers or in hydrophobic interaction chromatography (HIC) by reducing salt concentration[3,4]. Changes in protein structure by solvent mediated denaturation altered surface tension and, therefore adsorption. However, the influence of specific salt–protein interactions was not considered. In the present investigation the binding of several milk proteins and concomitant effects on retention are evaluated using equations adapted from Wyman's theory of linked functions[5].

THEORY

Since the retentions of all proteins only varied with ammonium sulfate and not ammonium chloride, it would be prudent to adopt a mechanism involving salt binding

to a protein in order to quantitatively explain the results. Hence, following the concepts of Wyman[6–9] and Wyman and Gill[10], we have thermodynamically linked the capacity factor of a protein to the free energy of salt binding. Such methodologies involving the use of thermodynamic linkage of physical and kinetic properties of macromolecules to cosolute binding in combination with non-linear regression analysis have been used by several investigators[11–15]. With these concepts in mind, we assume a sequential binding model, *i.e.* there are essentially two classes of binding sites on proteins that are responsible for changes in retention and that all sites of one type are saturated before binding to the second type proceeds. Furthermore, we assume that equilibration among the various species is instantaneous and that the observed retention is the resultant of the individual protein species. It should be emphasized that this treatment infers nothing about binding to other site classes, but simply that it is not related to retention. Consider the following sequential equilibria:

$$P + nX \overset{K_1}{\rightleftarrows} PX_n$$

$$PX_n + mX \overset{K_2}{\rightleftarrows} PX_nX_m$$

where n and m are the number moles of ion X bound at each class of site per mole of protein, P. Then, the fraction, Q, of each species present is

$$Q(P) = \frac{[P]}{[P] + K_1[P][X]^n} \tag{1}$$

$$Q(PX_n) = \frac{K_1[P][X]^n}{[P] + K_1[P][X]^n} - \frac{K_1K_2[P][X]^n[X]^m}{K_1[P][X]^n + K_1K_2[P][X]^n[X]^m} \tag{2}$$

$$Q(PX_nX_m) = \frac{K_1K_2[P][X]^n[X]^m}{K_1[P][X]^n + K_1K_2[P][X]^n[X]^m} \tag{3}$$

Then, since

$$k'_{obs} = k'_0Q(P) + k'_1\,Q(PX_n) + k'_2\,Q(PX_nX_m) \tag{4}$$

where k'_{obs} is the observed capacity factor and k'_0, k'_1, k'_2 are the capacity factors of the respective protein salt species, as shown in Fig. 1. After substitution of eqns. 1–3 into eqn. 4, and rearrangement, the resultant expression links protein retention to salt binding:

$$k'_{obs} = \frac{k'_0}{1 + K_1[X]^n} + \frac{k'_1K_1[X]^n}{1 + K_1[X]^n} + \frac{(k'_2 - k'_1)\,K_2[X]^m}{1 + K_2[X]^m} \tag{5}$$

where [X] is the concentration of unbound salt. Here, since the protein concentration is much smaller than the salt concentration in the mobile phase, [X] is taken to be equal to the mobile phase salt concentration.

EXPERIMENTAL

Chromatography was performed at room temperature with a Model 8700XR pumping system, a Model 8750 injection system, a Model 4270 data system, all from Spectra-Physics (San Jose, CA, U.S.A.), and an Isco (Lincoln, NE, U.S.A.) UV detector set at 280 nm. The flow-rate was 1 ml/min.

Two columns were used in this study: (I) Synchropak Propyl (250 × 4.1 mm I.D.) (Synchrom, Lafayette, IN, U.S.A.) and (II) Supelco Hint LC-3 (100 × 4.6 mm I.D.) (Supelco, Bellefonte, PA, U.S.A.), both fitted with a guard column.

Buffers for chromatography were prepared with Bio-Rad (Richmond, CA, U.S.A.) grade reagents and water purified with a Continental (San Antonio, TX, U.S.A.) Modulab I system. Composition of the buffers was (A) 0.05 *M* disodium hydrogenphosphate containing 3.75 *M* urea adjusted to pH 6.0 and (B) the same buffer containing 2 *M* ammonium sulphate. These were filtered through a 0.45-μm biological filter (Alltech Assoc., Deerfield, IL, U.S.A.) before use. The amount of buffer B was varied so that the isocratic composition of the mobile phase was between 0 and 2.0 *M*.

Surface tensions were measured using the du Nouy balance technique. The instrument used was the Fisher Surface Tensiomat, Model 21 (Fisher Scientific, Pittsburgh, PA, U.S.A.). It was important to determine liquid surface tensions immediately before each run.

β-Casein, (β-CS), was isolated from milk[16] or purchased from Sigma (St. Louis, MO, U.S.A.). α-Lactalbumin, (α-LA), and β-lactoglobulin, (β-LG), were from Sigma. All proteins were greater than 90% pure as judged by sodium dodecylsulfate polyacrylamide gel electrophoresis (SDS-PAGE) based on densitometric scan at 550 nm. For HPLC, proteins were dissolved in buffer A (2 mg/ml), filtered through a 0.45-μm filter and injected (50 or 100 μl). Elution was carried out isocratically using the solvent delivery system to obtain the desired mobile phase composition.

Capacity factors (k') were calculated from the position of the peak maxima and the void volume which was taken in this study as the solvent peak.

$$k' = \frac{t_R - t_0}{t_0} = \frac{\text{mmol protein in the stationary phase}}{\text{mmol protein in the mobile phase}} \quad (6)$$

The relationships between salt concentration and k' were evaluated using a Gauss-Newton non-linear regression analysis program developed at this laboratory. Eqn. 5 was iterated to minimize the sum of square differences between measured and calculated k' values. Experimental salt values were used and n and m were the adjustable parameters[17].

RESULTS AND DISCUSSION

HPLC has been used as a tool for studying how milk proteins contribute to functional properties of foods[18,19]. In the latter study, HIC columns were used with ammonium sulfate mobile phases with an without urea as an additional mobile phase modifier. The present evaluation of salt binding effects there focused on similar systems.

Fig. 1 shows the variation of k' of β-LG with HIC column I using an ammonium

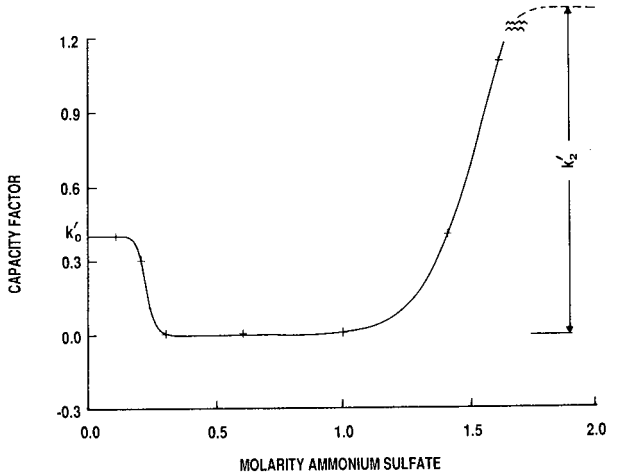

Fig. 1. Effect of ammonium sulfate concentration on retention of β-lactoglobulin. Conditions: column I; mobile phase, buffer A. (+) Data, (——) regression of eqn. 5.

sulfate–urea mobile phase (pH 6) as described in the experimental section. Data points are denoted by (+). Since, retention of proteins in HIC has been related to surface tension of the mobile phase[1,20], we determined the surface tensions of the phosphate–urea mobile phases that contained varying amounts of ammonium sulfate. Two fits of the data (+) are given in Figs. 2 and 3. The lines were obtained by the same non-linear regression analysis described in the theoretical section for analysis of the retention data. This analysis indicates that ammonium sulfate binds to urea at either one or three sites. The solution properties of urea are themselves thermodynamically complex because urea forms concentration dependent aggregates[21]. Moreover, some salts have been shown to interact with urea possibly through ion–dipole and dipole–dipole

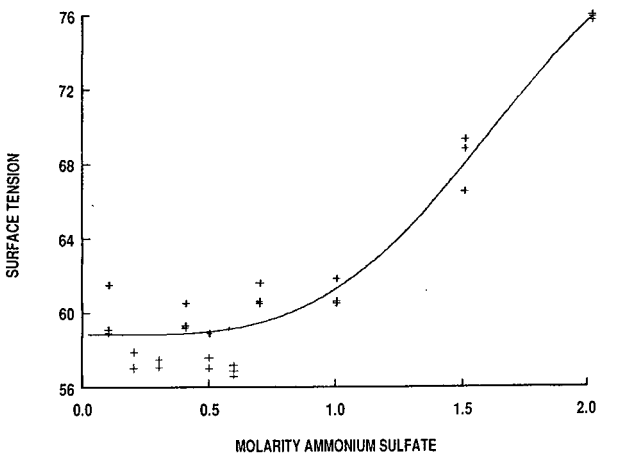

Fig. 2. Effect of ammonium sulfate concentration on surface tension of 3.75 *M* urea solutions. (+) Measured, (——) line from non-linear regression.

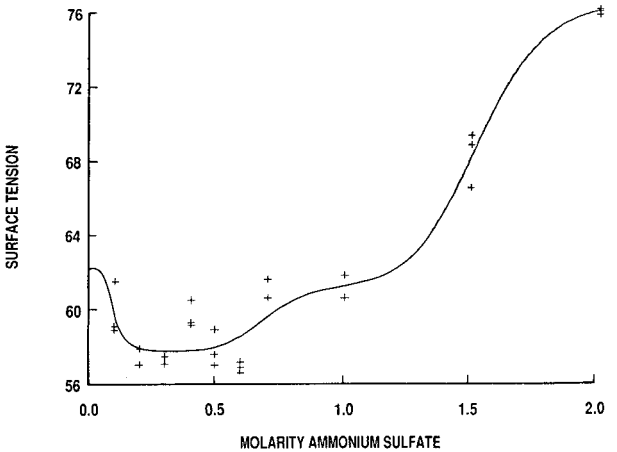

Fig. 3. Effect of ammonium sulfate concentration on surface tension of 3.75 *M* urea solution with a three binding site model.

interactions[22]. The lower root-mean-square of the three-site model (1.7 as compared to 1.1) suggests that it is more appropriate. More importantly plots of the deviation was examined for each model (not shown). The plot for the one site model was multi-phasic whereas a random deviation plot was found for the three site model. A random distribution is considered to be an appropriate criterion of goodness of fit to the data[23]. Apparently, urea species, under the conditions used in this study, are multimers with three sites that are sequentially saturated with salt. The net result is that a minimum is observed when surface tension of 3.75 *M* urea is plotted against molarity of added salt. From refs. 1–4 we see that capacity factor is related to the surface tensions of column packing (G_{sv}), protein (G_{pv}), and mobile phase (G_{mv}), by:

$$k' = C \exp\left[\frac{\sqrt{G_{pv}G_{sv}} - (\sqrt{G_{sv}} + \sqrt{G_{pv}})\sqrt{G_{mv}} + G_{mv}}{RT}\right] \tag{7}$$

Fig. 4 describes some properties of eqn. 7, assuming a G_{pv} of 70 mJ/m^2, a value that is reasonable for the whey proteins α-LA and β-LG by analogy to blood serum proteins[24]. A value of 53 mJ/m^2 was used for the packing. This is a typical value for HIC materials[1]. As mobile phase surface tension decreases, k' is predicted to decrease and reach 0 when $G_{mv} = G_{pv}$ as indicated by segment AB. Capacity factor rises again if G_{mv} continues to fall below both G_{pv} and G_{sv} (segment BC). If G_{mv} increases with further reduction in salt concentration as in Fig. 3, then k' is predicted to rise again back along segment BA. As shown clearly in Fig. 5, k' of β-LG does not respond in this manner. Mobile phase surface tension does not uniquely define a single k', so that the presence of different solute species is indicated at different salt concentrations. G_{pv} is, therefore, a variable also.

The solid line in Fig. 1 represents the excellent fit of the data by non-linear regression with eqn. 5. The root mean square was 0.01 and residual sum of squares was $6 \cdot 10^{-5}$ which demonstrates the credibility of the model for β-LG retention. Plots of protein solubility with varying pH have often been bimodal and have been explained in

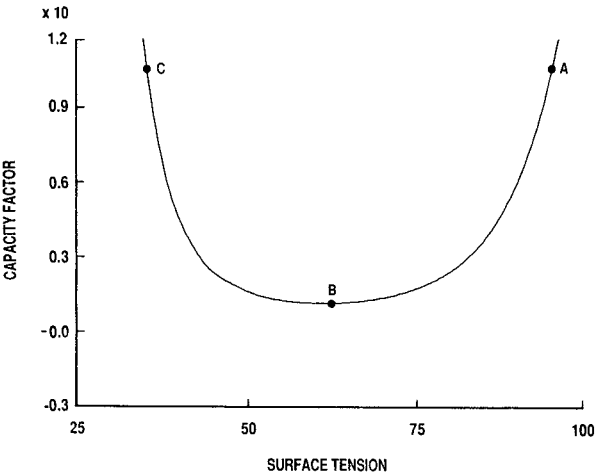

Fig. 4. Calculated curve representing effect of mobile phase surface tension on retention of protein (G_{pv} = 68 mJ/m^2); column surface tension (G_{sv} = 53 mJ/m^2).

terms of proton binding[25]. Here, binding of other ions influences retention. When ammonium chloride was substituted for ammonium sulfate, proteins were not retained at concentrations up to 4 *M*, suggesting that sulfate binding is the significant contributor to the retention profile. These data were obtained at pH above the protein's isoelectric points so that proteins had a net negative charge. This does not preclude anion binding, however, since about 80% of the positive sites[26] remain. Moreover, direct interactions between large anions and protein amide groups have been reported[16]. Cation binding may occur but it is not linked thermodynamically to retention.

The plots from regression analysis of the retention of β-CS and α-LA are given in Figs. 6A and B. As with β-LG, plots of k' do not vary exponentially with salt

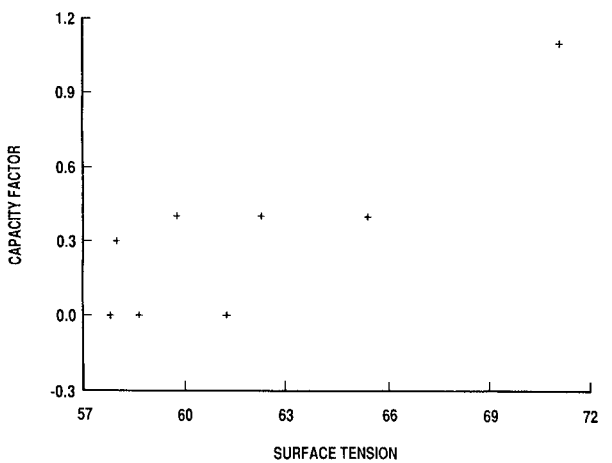

Fig. 5. Effect of surface tension on β-LG retention.

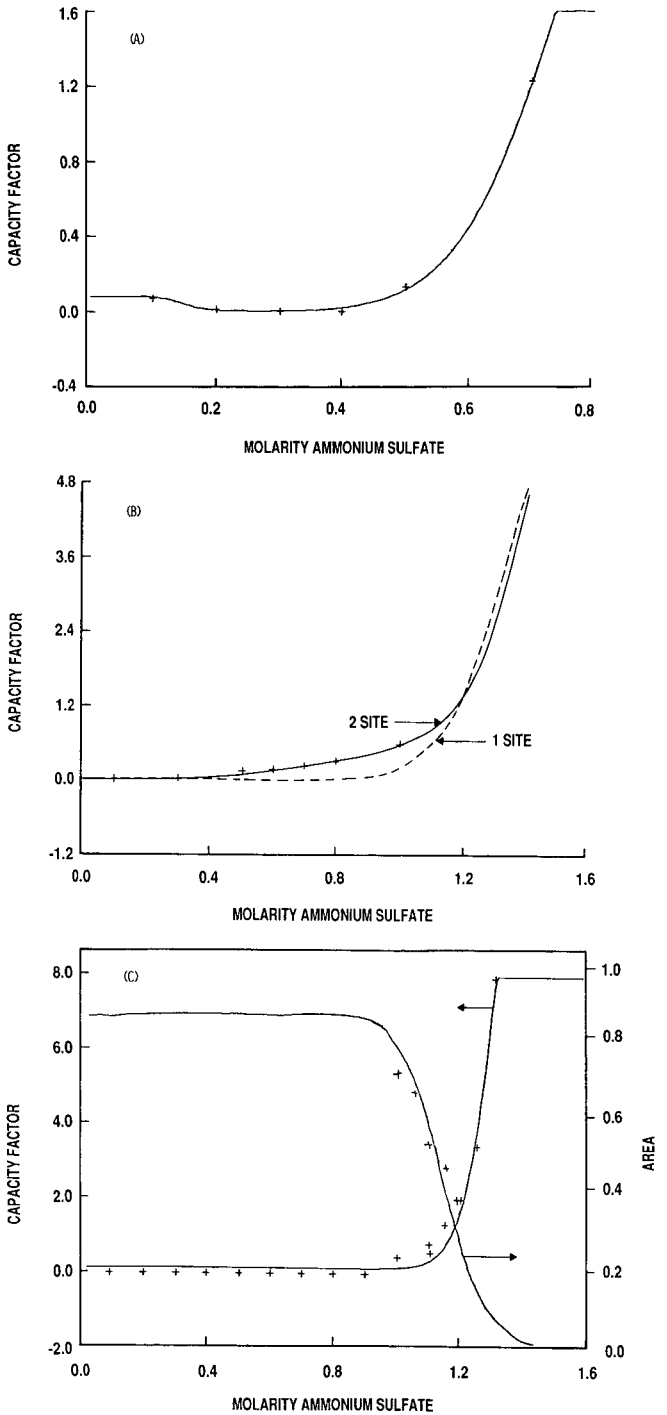

Fig. 6. Effect of ammonium sulfate concentration on retention of: (A) β-casein, (B) α-lactalbumin with (– – –) one binding site fit, and (——) two binding site fit. Conditions as in Fig. 1. (C) β-Lactoglobulin, conditions as in Fig. 1 except that no urea was used in mobile phase.

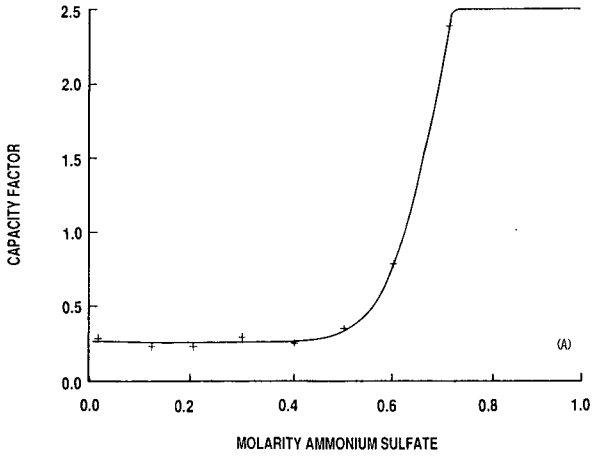

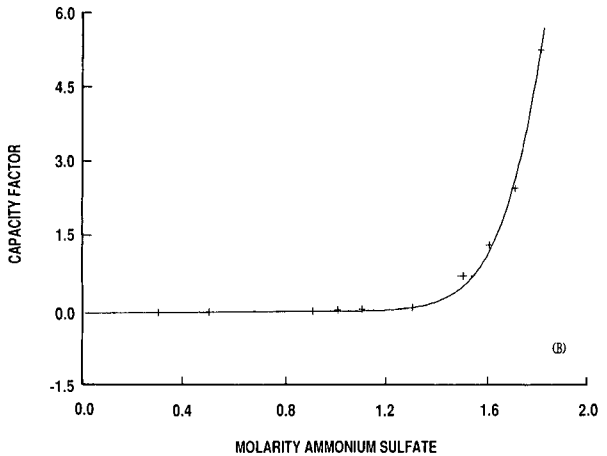

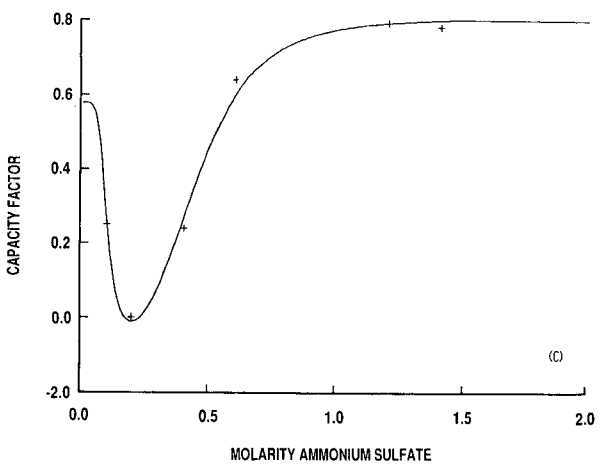

Fig. 7. Effect of ammonium sulfate concentration on retention of: (A) β-casein, (B) β-lactoglobulin, (C) α-lactalbumin. Conditions as in Fig. 1. except column I was used.

TABLE I

SALT BINDING PARAMETERS AS DETERMINED BY NON-LINEAR REGRESSION OF EQN. 5

Protein	K_1 *(l/mol)*	K_2 *(l/mol)*	n *(mol)*	m *(mol)*	k'_2	*RMS*
Column I						
β-CS	7.2 ± 1.1	1.4 ± 0.6	8	10	23 ± 6	0.2
	6.8 ± 1.6	1.2 ± 0.04	8	8	38 ± 10	0.1
β-LG	4.6 ± 0.2	0.6 ± 0.02	12	12	1.9 ± 0.3	0.01
	4.5 ± 0.1	0.7 ± 0.00	16	34	1.2 ± 0.0	0.01
α-LA	(1.1 ± 0.1)*	0.7 ± 0.02	4	12	14 ± 3.0	0.02
Column II						
β-CS	–	1.4 ± 0.0	–	12	5.3 ± 0.6	0.01
β-LG	–	0.5 ± 0.01	–	14	26 ± 7	0.1
α-LA	9.9 ± 0.8	2.2 ± 0.1	4	4	0.9 ± 0.0	0.02

* First site is different than others shown. Single site RMS = 0.2.

concentration. Elution behavior of proteins has often been treated as if there were an exponential dependence of retention on salt concentration[20,28]. The first binding site of lactalbumin occurs at higher salt concentrations than the first site for either β-LG or β-CS, and is therefore likely to be of a different type. The two site model for α-LA gave a four fold improvement in RMS analysis over the one site model.

All proteins used in this study exhibited a dramatic decrease in peak area with increased retention when they were eluted with sulfate-containing mobile phase that contained no urea. β-LG curves are given in Fig. 6C as an example.

The quantities of urea used in these experiments are insufficient to cause appreciable denaturation of β-LG or α-LA. Molarities >5 M are required to do this[29,30]. β-CS self aggregates in solution and the micelles increase in size with time. Urea promotes dissociation of these units.

Fig. 7 depicts the retention characteristics of the milk proteins on column II. Again excellent correlation of the data with the salt binding model is observed. However, the proteins exhibited different retention behavior on the two columns as can be seen by comparison of Fig. 7 with Figs. 1 and 6. Retention of proteins is lower on column II with the exception of β-LG. Table I gives values for the salt binding constants (K_1, K_2), the number of moles bound at each site class that is correlated with retention (n, m) and the estimated retention of the fully saturated salt species (k'_2). These values suggest different interaction modes on the two columns. The support matrix of column II is of the polyol type whereas column I contains amidopropyl functionality. The differences in behavior of the proteins with the two materials could result from sulfate linkages between protein and amide groups. As stated earlier direct interactions between anions and the amide dipole were reported.

Elution order is related to both column binding strength as determined by k' and by the salt binding equilibrium constant (K_1). Significant retention of these milk proteins occurs only when salt binds to the second site class. Thus in conventional HIC high salt mobile phases initially are used followed by a gradient to lower salt. For column I, β-CS has the highest K_2 and k'_2 so it is strongly retained. Salt saturated lactalbumin is more strongly adsorbed to the column than β-LG. Thus their elution order is different than is predicted from considerations of their average hydrophobicities ($H\varphi_{ave}$) as defined by Bigelow[31]. These parameters are calculated from

protein amino acid composition and are 1150 and 1230 cal/res, respectively, for α-LA and β-LG[31]. Such anomalies in elution order were observed by others[19,32] but is explained here through considerations of salt–protein interactions. β-LG has a higher k'_2 on column II but is eluted first because of its smaller salt binding equilibrium constant.

This paper demonstrates that considerations of protein, column, and mobile phase surface tensions indicate a minimum in retention *vs.* mobile phase surface tension plots when (1) the mobile phase surface tension passes below both the surface tension of the protein and of the column packing, or (2) the mobile phase surface tension passes through a minimum with composition. Moreover, salt binding modulates protein–column packing interactions so that specific salt binding effects cannot be ignored if protein retention in HIC is to be described more adequately. Furthermore the lack of correlation of retention with molecular parameters such as amino acid composition can be explained in terms of salt binding. Research is continuing to evaluate corresponding effects in reversed-phase chromatography.

REFERENCES

1 D. R. Absolom and R. A. Barford, *Anal. Chem.*, 60 (1988) 210.
2 R. A. Barford, in W. S. Hancock (Editor), *HPLC in Biotechnology*, Wiley, New York, 1988, Ch. 3.
3 R. A. Barford, B. J. Sliwinski, A. C. Breyer and H. L. Rothbart, *J. Chromatogr.*, 235 (1982) 281.
4 R. A. Barford, J. P. Cherry and R. A. Barford (Editors), *Methods for Protein Analysis*, American Oil Chemical Society, Champaign, IL, 1988, Ch. 7.
5 J. Wyman, in C. B. Anfinsen, Jr. and J. T. Edsall (Editors), *Advances in Protein Chemistry*, Academic Press, New York, 1964, p. 224.
6 J. Wyman, *Adv. Protein Chem.*, 19 (1964) 223.
7 J. Wyman, *Mol. Biol.*, 11 (1965) 631.
8 J. Wyman, *J. Am. Chem. Soc.*, 89 (1967) 2202.
9 J. Wyman, *Q. Rev. Biophys.*, 17 (1984) 453.
10 J. Wyman and S. J. Gill, *Proc. Natl. Acad. Sci. U.S.A.*, 77 (1975) 5239.
11 T. F. Kumosinski, *J. Agric. Food Chem.*, 36 (1988) 869.
12 H. M. Farrell, Jr. and T. F. Kumosinski, *J. Ind. Micro.*, 3 (1988) 61.
13 H. M. Farrell, Jr., T. F. Kumosinski, P. Pulaski and M. P. Thompson, *Arch. Biochem. Biophys.*, 265 (1988) 146.
14 S.-I. Tu, J. N. Brouillette, G. Nagahaski and T. F. Kumosinski, *Plant Physiol.*, 88 (1988) 61.
15 J. F. Rusling, C. N. Shi and T. F. Kumosinski, *Anal. Chem.*, 236 (1988) 1260.
16 J. J. Basch, F. W. Douglas, Jr., L. W. Procino, V. H. Holsinger and H. M. Farrell, Jr., *J. Dairy Sci.*, 68 (1985) 23.
17 T. F. Kumosinski, *J. Agric. Food Chem.*, (1988) in press.
18 C. V. Morr, *J. Food Sci.*, 50 (1985) 1406.
19 L. C. Chaplin, *J. Chromatogr.*, 363 (1986) 329.
20 W. R. Melander, D. Corradini and Cs. Horváth, *J. Chromatogr.*, 317 (1984) 67.
21 R. H. Stokes, *Aust. J. Chem.*, 20 (1967) 2087.
22 E. E. Schrier and R. A. Robinson, *J. Biol. Chem.*, 245 (1970) 2432.
23 L. Meites, *CRC Crit. Rev. Anal. Chem.*, 8 (1979) 1.
24 C. J. Van Oss, J. Visser, D. R. Absolom, S. N. Omenyi and A. W. Neumann, *Adv. Colloid Interf. Sci.*, 18 (1983) 133.
25 A. A. Green, *J. Biol. Chem.*, 93 (1931) 517.
26 R. K. Cannan, *Chem. Res.*, 30 (1942) 395.
27 D. R. Robinson and W. P. Jencks, *J. Am. Chem. Soc.*, 87 (1965) 2470.
28 J. L. Fausnaugh and F. E. Regnier, *J. Chromatogr.*, 359 (1986) 131.
29 T. T. Herskovitz, *J. Biol. Chem.*, 240 (1965) 628.
30 H. A. McKenzie and G. B. Ralston, *Biochemistry*, 12 (1973) 1025.
31 C. C. Bigelow, *J. Theoret. Biol.*, 16 (1967) 187.
32 A. Kato and S. Nakai, *Biochim. Biophys. Acta.*, 624 (1980) 13.

Journal of Chromatography, 458 (1988) 67–77
Elsevier Science Publishers B.V., Amsterdam — Printed in The Netherlands

CHROMSYMP. 1424

STRATEGY FOR THE IMMOBILIZATION OF MONOCLONAL ANTIBODIES ON SOLID-PHASE SUPPORTS

ROBERT S. MATSON*,* and MICHAEL C. LITTLE
Bio-Rad Laboratories, 1414 Harbour Way South, Richmond, CA 94804 (U.S.A.)

SUMMARY

Using matrices based upon Affi-Gel and Affi-Prep, we have examined conditions during the immobilization of antibodies (immunoglobulin G, IgG) that influence the performance of immunosorbents. Such conditions include: coupling pH, coupling kinetics, antibody density on the immunosorbent and the activation chemistries utilized for the immobilization process. These studies have shown that the capacity for antigen does not increase with increased antibody coupling efficiency. Presumably, increased coupling times or efficiencies lead to multi-site attachment of the antibody to the matrix, thereby causing inactivation. Immunosorbents containing low densities of IgG were found to have greater capacity for antigen on a per mole IgG basis. This suggests steric crowding of antigen at high antibody density. Finally, immunosorbents prepared through IgG carbohydrate linkages (oriented coupling) show dramatic increases in antigen capacity over those prepared by stochastic (random) coupling through IgG primary amino groups. A combination of low IgG density and oriented coupling of the IgG via the carbohydrate moiety may represent the best strategy for the preparation of immunosorbents.

INTRODUCTION

The goal in the construction of an immunoaffinity support (immunosorbent) is to immobilize the antibody to the solid-phase support without adversely affecting the antibody's function to capture antigen. Although sequestering of the antibody through the antigen binding site is not a recommended strategy most activation methods are based upon this approach, since they rely primarily on the reactivity of the immunoglobulin's free lysine residues with an activated ester or other reactive group on the support. To complicate matters further, most commercially available activated supports contain an excess of activation groups such that multi-site attachment of the antibody is assured. The results of this approach is an immunosorbent that is largely inactive, generally on the order of 1–30% of the theoretical antigen binding efficiency.

Of course, the advantage of purification by immunoaffinity chromatography

* Present address: Nuclepore Corporation, 7035 Commerce Circle, Pleasanton, CA 94566-3294, U.S.A.

0021-9673/88/$03.50

generally offsets this shortcoming. However, from an economical viewpoint, especially if one is to consider the scale-up of immunoaffinity chromatography with monoclonal antibodies, it is important to understand the immobilization process.

In these studies, we have examined both cross-linked agarose matrices such as Affi-Gel (Bio-Rad) and the polymer-based activated support, Affi-Prep (Bio-Rad) which is suitable for both analytical high-performance liquid chromatography (HPLC) and preparative chromatography. The Affi-Gel and Affi-Prep supports are N-hydroxysuccinimide (NHS)-activated matrices. The advantage of using monoclonal antibodies (MABs) rather than polyclonals is that all of the immunoglobulin G (IgG) molecules in a monoclonal population have identical primary sequence. Therefore, in altering coupling conditions one does not have to be concerned so much with the selective immobilization of different sub-populations as in the case of polyclonal antibodies. The disadvantage in using purified MAbs is that they may in fact have been isolated by affinity methods that employ harsh elution conditions, thereby reducing their native antigen, binding capacity. We will be contrasting our work on MAb immobilization with the coupling of polyclonal antibodies. They share, of course, some commonality in developing a strategy for antibody immobilization.

We have examined several factors which may influence the outcome of antibody immobilization. Principal among these is the consequence of an increased antibody ligand-matrix density. This is not a new issue since Eveleigh and Levy[1] first demonstrated that a lower density of polyclonal antibody immobilized to CNBr-Sepharose was essential in obtaining the highest antigen-binding capacity. However, this parameter has not generally been considered in the preparation of immunosorbents, especially those that are based upon other matrices using different activation chemistries. We have demonstrated the importance of ligand density; and offer methods by which the immobilization process is controlled to obtain an optimal immunosorbent. We also explored the process of oriented coupling of antibodies via hydrazide chemistry[2] to a high-performance matrix, Affi-Prep 10[3].

EXPERIMENTAL

Antibodies and antigens

Purified (98%), murine anti-tPA IgG_1 and 99+% purity tissue plasminogen activator (tPA) were experimental preparations obtained from Bio-Rad Labs. (Richmond, CA, U.S.A.). Horseradish peroxidase (HRP), type IX, was obtained from Sigma (St. Louis, MO, U.S.A.). Murine anti-HRP IgG_1 obtained from Proteins International (Rochester, MI, U.S.A.) was purified from ascites by Affi-Prep protein A affinity chromatography to near homogeneity as determined by sodium dodecyl sulphate-polyacrylamide gel electrophoretic (SDS-PAGE) analysis (data not shown). Affinity purified sheep anti-BSA IgG was obtained from Bethyl Labs. (Montgomery, TX, U.S.A.) and [methyl-^{14}C]BSA (37 μCi/mg) from Amersham (Arlington Heights, IL, U.S.A.).

Activated supports

Affi-Gel 10, Affi-Gel hydrazide (HZ), and Affi-Prep 10 were obtained from Bio-Rad Labs. Affi-Prep hydrazide was prepared from Affi-Prep 10 by quantitative displacement of NHS with hydrazine hydrate[2] by a proprietary process.

Preparation of aldo-IgG for immobilization

The oxidation of immunoglobulins was carried out as previously described[4], using sodium periodate. Essentially, IgG was dialyzed against 0.1 *M* sodium acetate, 0.15 *M* sodium chloride (pH 5.5) overnight at 25°C. To one volume of IgG dialyzate (1–10 mg/ml) was added 0.1 volume of 0.1 *M* sodium periodate, prepared in deionized water. The reactants were mixed for 1 h in the dark at 25°C. The reaction was then stopped by the addition of 20 μl of glycerol per 1.0 ml reaction mixture and the mixing was continued for an additional 30 min. The oxidized or aldo-antibody was then dialyzed against the same buffer used for coupling.

Antibodies were coupled to hydrazide supports by end-over-end mixing for 20 h at 25°C. The resulting immunosorbents were then rinsed in 0.1 *M* sodium phosphate, 0.5 *M* sodium chloride (pH 7.0) and re-equilibrated in this buffer to provide 50% (v/v) slurries. The concentration of immobilized IgG was determined indirectly from estimates of the difference in total protein input for coupling and that remaining in solution (unbound IgG) upon termination of the coupling reaction. The protein content was determined by measuring the absorbance at 280 nm.

Coupling pH studies

Anti-tPA IgG_1 (6.9 mg/ml) was prepared in the following 0.1 *M* Good's Buffers at the indicated pH: 2-(N-morpholino)ethanesulfonic acid (MES, pH 5 and 6), 3-(N-morpholino)propanesulfonic acid (MOPS, pH 6.5, 7.0, 7.5 and 8.0) and 2-(N-cyclohexylamino)ethanesulfonic acid (CHES, pH 8.5, 9.0 and 9.5). Affi-Gel 10 (1.0 ml bed volume) was prepared for coupling as previously described[3]. Equal volumes of protein solution and Affi-Gel were mixed together with constant rotation at 4°C for 12 h in polyprep columns. Each column was then washed with 8 *M* potassium thiocyanate phosphate buffered saline (KSCN-PBS), pH 7.2 and finally reequilibrated in PBS, pH 7.2 containing 0.01% Tween 20. Next, 10 ml of purified tPA (antigen) at 0.47 mg/ml PBS-Tween 20 buffer, pH 7.2 was passed over each column. Bound tPA was eluted in 3.5 *M* KSCN-PBS, pH 7.2. The results are shown in Fig. 1.

Preparative scale coupling of MAb to Affi-Gel 10

A 20.6-g amount of the anti-tPA monoclonal antibody was reacted with 3.4 l of Affi-Gel 10 at 4°C using a turbine-type propeller for efficient batch mixing. Aliquots were removed at specified times and analyzed for coupled protein. Results shown in Fig. 2 are the average of three runs.

Immobilization kinetic studies

The process of fast coupling (15 s to 10 min) of antibody to Affi-Prep 10 was carried out in the following manner. Affi-Prep 10 was rinsed in ice-cold (4°C) 10 m*M* sodium acetate, pH 4.5 and prepared as a 50% (v/v) slurry in the above buffer. Then, 400 μl of slurry was delivered into microfuge tubes to obtain 200 μl packed bed volumes upon centrifugation. The supernatant was drawn off the pelleted resin by suction and 500 μl of antibody solution (0.25–2 mg/ml) was added. Antibodies were prepared in coupling buffer, 0.1 *M* MOPS (pH 7.5) containing varying amounts of salt (0.15–3.0 *M* sodium chloride) depending upon the experiment. Rapid mixing was accomplished with the aid of a vortex mixer. For coupling times greater than 1 min

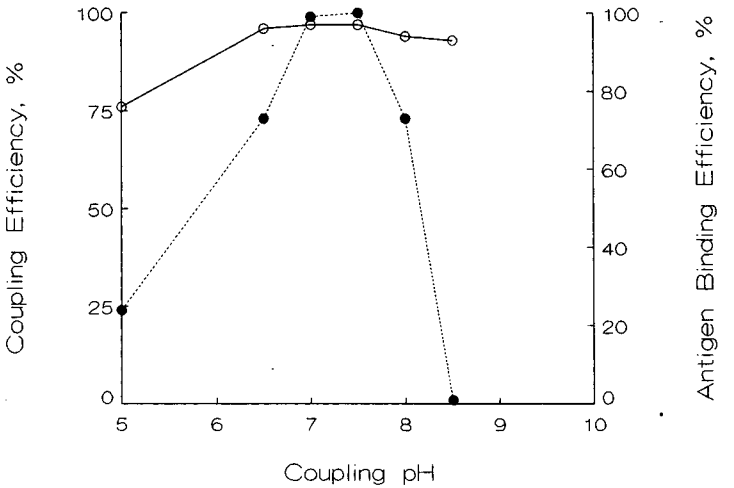

Fig. 1. The effect of coupling pH on the immobilization and activity of a monoclonal antibody. Murine anti-tPA MAb was coupled to Affi-Gel 10 under batch conditions in which the pH for coupling was varied. The tPA antigen binding efficiency for each of the immunosorbents was determined at pH 7.2. Details are provided in Experimental. ⊙ = Relative coupling efficiency (%). ● = Relative antigen binding efficiency (%).

additional mixing was accomplished by end-over-end rotation. After a specified coupling time, 100 μl of 1 *M* ethanolamine (pH 8) was added, the reaction mixture immediately mixed and the immunosorbent pelleted by centrifugation (1 min, 13 000 rpm). The supernatant was removed and placed on ice for analysis of protein content. The pelleted immunosorbent was then extensively washed, first with 0.1 *M* MOPS (pH 7.5), followed by 1 *M* sodium chloride, and finally rinsed and resuspended in antigen binding buffer as a 50% (v/v) slurry. An estimation of non-specific adsorption was

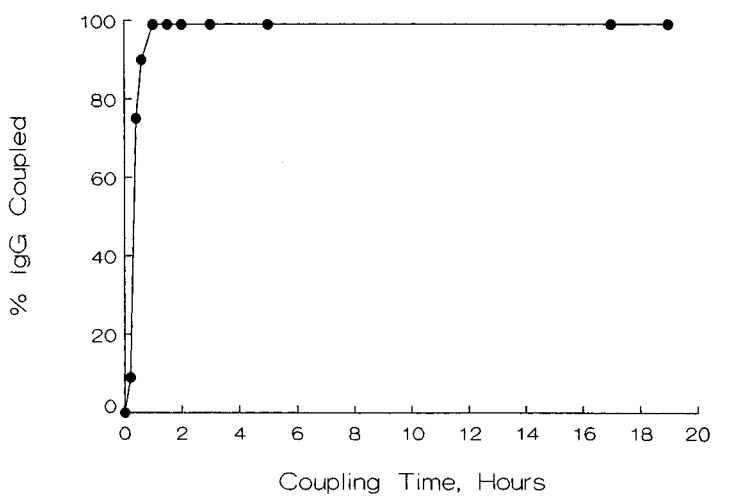

Fig. 2. Time course for preparative scale coupling of anti-tPA MAb to Affi-Gel 10.

attempted from the analysis of protein content of effluents obtained from rinsing the pelleted immunosorbent with 7M urea/1M sodium chloride. Minimal levels of protein ($\leqslant$ 1 μg/ml) were observed indicating that bound IgG was covalently coupled to the matrix.

For example, murine anti-tPA MAb (4 mg/ml) was coupled to Affi-Prep 10 in 0.1 *M* MOPS, pH 7.5 containing 0.15–3.0 *M* sodium chloride. Reactions were terminated after 10 min. Pure tPA was applied to each support and the amount bound determined by the difference between load and unbound (recovered) total protein. The results are shown in Fig. 3.

In another experiment, murine anti-HRP MAb (1 mg/ml) was coupled to Affi-Prep 10 in 0.1 *M* MOPS, pH 7.5 containing either 0.15 *M* or 2.0 *M* sodium chloride. Reactions were terminated at the specified times, beginning at 15 s. HRP was applied to each support and the extent of binding determined by the Bio-Rad ELISA peroxidase assay. The results of this study are provided in Fig. 4a and b.

RESULTS AND DISCUSSION

The effect of coupling pH

Immunoglobulins can be covalently coupled to activated, solid supports over a broad pH range without difficulty. For example, an anti-tPA IgG_1 was immobilized to Affi-Gel 10 over the pH range of 5–9.5 in an overnight (18 h) reaction at 4°C. As shown in Fig. 1, near quantitative coupling of the antibody was obtained between pH 6 and 9. However, these immunosorbents varied dramatically in their ability to effectively bind tPA antigen. Optimal antigen binding was observed only for the immunosorbents constructed from the immobilization of the MAb at coupling pH 7–7.5.

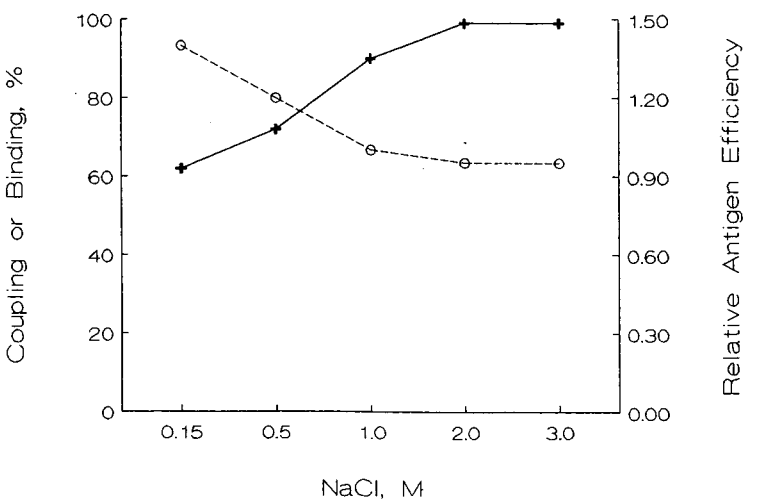

Fig. 3. Coupling efficiency *vs.* antigen binding to Affi-Prep 10. Anti-tPA MAb was coupled to Affi-Prep 10 as described in Experimental. In this case, reactions were terminated after 10 min. Pure tPA was applied to each immunosorbent and the amount bound determined by the difference between load and unbound (recovered) total protein. O = Antigen binding (%) or relative antigen binding efficiency (0.00–1.50). + = Antibody coupling efficiency (%).

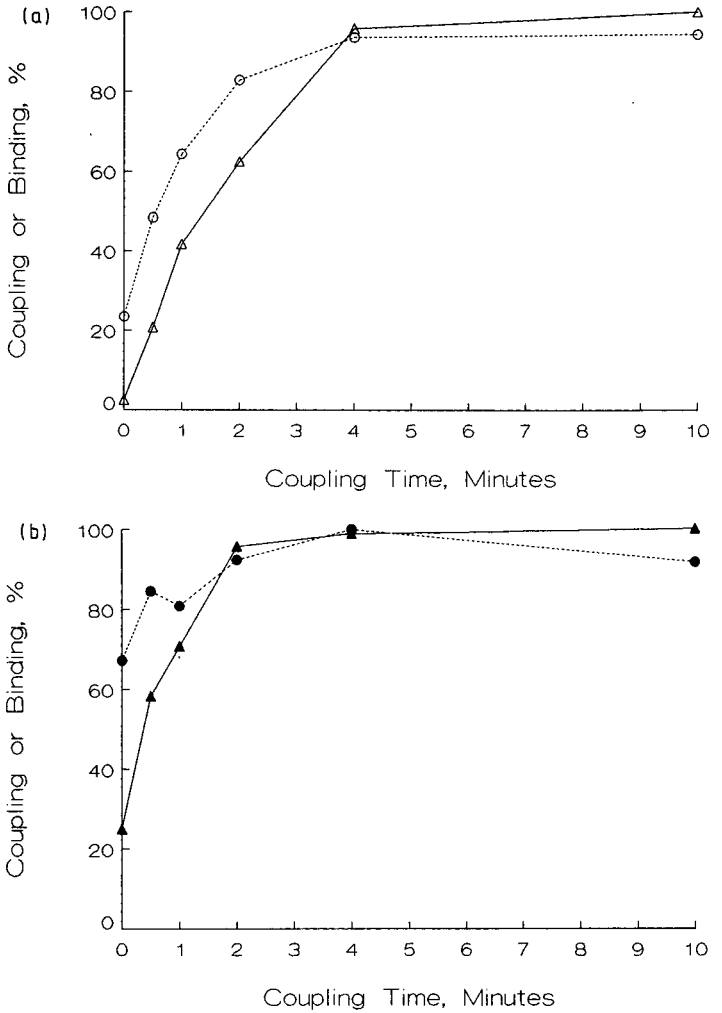

Fig. 4. The effect of coupling rate on the antigen binding capacity. (a) Anti-HRP MAb was coupled to Affi-Prep 10 in buffer containing either 0.15 *M* sodium chloride or (b) 2 *M* sodium chloride. Reactions were terminated at the specified times, beginning at 15 s. HRP was applied and the extent of binding determined by the Bio-Rad ELISA peroxidase assay. (a) △ = Antibody coupling efficiency (%); ○ = HRP binding efficiency (%). (b) ▲ = antibody coupling efficiency (%); ● = HRP binding efficiency (%).

The effect of monoclonal antibody-matrix density

Eveleigh and Levy[1] studied the effect of increased polyclonal antibody density on CNBr-Sepharose 4B and porous glass beads. They concluded from these studies that lower protein densities (*ca.* 1 mg/ml) improved the performance of the immunosorbent in terms of specific antigen binding activity (moles antigen bound/moles IgG coupled). Unfortunately, these studies cannot be regarded as definitive since the amount of CNBr was also varied over a 20-fold range in order to achieve these results. And as they report, other variables such as the activation procedure that is

operational during the immobilization process may influence the immunoreactivity of the sequestered antibody.

We have studied the antibody ligand-matrix density problem on several matrices using different activation chemistries. Three approaches have been used and will be briefly outlined here.

The first method involved using a fixed volume ratio of MAb to matrix such that the total available number of activation groups remained constant but the concentration of antibody was varied to achieve a desired ligand density. The coupling reaction was allowed to proceed to completion (Fig. 2). Any remaining reactive groups were displaced by the addition of ethanolamine. For example, the anti-tPA monoclonal antibody was immobilized onto Affi-Gel 10 (NHS) matrix at ligand densities of *ca.* 5–7 g MAb/l gel in this manner (Table I). In this particular experiment there was nearly a 2-fold increase in antigen binding efficiency when the MAb ligand–matrix density is decreased by 25%.

In the second approach, MAb was rapidly (within 10 min) coupled to the matrix, Affi-Prep 10 (NHS) by the addition of salt (Fig. 3). The result of this coupling procedure was that increased salt concentration led to an increased immobilization of MAb. At a fixed time interval such as 10 min, a series of different MAb ligand densities could be achieved by varying the input salt concentration. When the antigen binding efficiency was determined over this density range, it was found that substantially greater binding of antigen could be accomplished at the lowest MAb ligand density. This was further verified in the rapid coupling of an anti-HRP monoclonal antibody (also an IgG_1) in which enzymatic activity of the bound HRP antigen was monitored rather than mass as in the previous case. Interestingly, with the anti-HRP system little difference was found either in the amount of MAb coupled nor in the antigen binding efficiency between low salt (0.15 *M* sodium chloride) and high salt (2 *M* sodium chloride) buffers at 10 min (Fig. 4). The very early coupling times did indicate that higher salt was more effective in bringing the antibody to the solid phase for coupling. So at these earlier time points (below 2 min) the antigen capacity appeared to be better under high salt coupling conditions (Fig. 4b). The benefit gained by lower density couplings was substantially reduced with coupling time for either situation. Therefore, a similar trend in MAb ligand density *vs.* antigen binding efficiency was achieved by this approach using two different monoclonal antibodies. However, it is clear that antibodies that are even of the same isotype may interact with the matrix under different optimal coupling conditions.

TABLE I

AFFI-GEL 10 (NHS) COUPLING: EFFECT OF ANTIBODY LIGAND DENSITY ON CAPACITY FOR ANTIGEN

MAb coupled refers to the preparative scale coupling of anti-tPA MAb to Affi-Gel 10.

MAb coupled (g/l gel)	*Antigen bound/released (g/l gel)*
7.3	2.0
5.6	3.7
5.2	3.9

So in these first examples, we have attempted to optimize on the basis of coupling pH and protein-ligand density. However, as we have observed there are other factors that may influence the success of the immobilization process. In particular, one area that is not generally addressed is that of coupling kinetics. There are a number of good reasons to study kinetics in the preparation of an immunosorbent. First, longer reaction times may lead to increased inactivation of the immobilized antibody by allowing for multi-site attachments and an increased ligand density creating a steric effect that effectively reduce capacity. Furthermore, Wilchek and Miron[5] have pointed out the potential for leakage created by the immobilization of antibodies to unstable activated ester intermediates. These interactions are favorable at longer reaction times. Finally, non-specific adsorption can dramatically increase with time.

We have found that the NHS-mediated immobilization of MAbs using Affi-Gel 10 or Affi-Prep 10 is essentially complete within 1 h with proper mixing. Using more efficient methods of delivery of the antibody to the matrix, the coupling time can be reduced to approximately 10 min. For example, in earlier studies concerned with the *in situ* or on column immobilization of a rat polyclonal antibody to Affi-Prep 10 for HPLC, we could control the level of coupling by varying the flow-rate, duration and protein load. In these studies, coupling efficiency is nearly the same at 7.5 min and 85 min for similar protein loads[3].

However, the real question is what effect does this have on the antigen binding efficiency? We have examined the benefit of very rapid coupling times using high salt to enhance delivery of the immunoglobulin to the surface and found that such methods can be useful in obtaining optimal ligand densities. The action of salt upon delivery of the MAb to the matrix is presumably due to increased hydrophobic interaction of the antibody with the support. However, charge interaction phenomena with the matrix cannot be ruled out. Further studies will be necessary to delineate this effect.

Therefore it is possible to control the immobilization process to some extent from a careful study of ligand-matrix interaction. Nevertheless, the interaction remains largely a random event since the reactive lysine residues of antibodies may be distributed throughout the molecule. This approach fails particularly if these lysine residues are located in close proximity to the antigen binding site.

Oriented vs. random coupling

Recently a different strategy has been utilized. This involves sequestering of the antibody via its Fc-region. We call this oriented coupling. There are actually several ways to accomplish this event. One method involves binding the antibody to a Protein A support and then cross-linking the antibody to Protein A. For example, Philips *et al.*[6] successfully cross-linked an IgG_1 to Protein A Sepharose using dimethyl suberimidate to purify human adenosine deaminase to near homogeneity in one step.

There are some potential problems with this approach. First, not all antibodies will bind to Protein A. Second, once the antibody is bound by Protein A, the cross-linking process must be accomplished with care so as not to cause premature elution of the antibody; or inactivation by excessive cross-linking. Third, Protein A is itself expensive.

A more straightforward approach has recently been suggested by O'Shannessy and Hoffman[2], and successfully demonstrated by Little *et al.*[4]. This involves the coupling of aldo-IgG to solid-phase supports which have been activated with

a terminal hydrazide group. The aldo-IgG is generated by the sodium periodate oxidation of vicinal hydroxyl groups of the antibodies' carbohydrate moieties to aldehydes. These aldehydes are quite reactive with the matrix hydrazide. Since the reactive carbohydrates are usually located outside the antigen binding domain and no other groups within the protein will react with the matrix hydrazide, an oriented coupling is favored. The chemical bond that is formed is a hydrazone rather than a Schiff's base and does not have to be reduced for example with cyanoborohydride[7].

We have converted both Affi-Gel and Affi-Prep NHS matrices to the corresponding hydrizide (Hz) supports. Our initial studies were conducted on the cross-linked agarose matrix hydrazide; and we examined the consequences of oriented coupling for both polyclonal and monoclonal antibody-antigen pairs relative to activated supports that favor a random coupling of immunoglobulin[4]. In the case of polyclonal antibodies, dramatic increases in the antigen binding capacities were observed relative to CNBr-Sepharose. Similar results were obtained using Affi-Gel 10 (NHS). Therefore, we believe that this is a clear demonstration of the superiority afforded by the oriented coupling mechanism. In contrast, the monoclonal antibodies that we examined showed only slightly better or equivalent antigen capacity relative to those obtained on Affi-Gel 10 or CNBr-Sepharose. However, our studies have been limited to only a few examples using affinity purified species. It is possible that both the antigen binding site and the carbohydrate moiety could have been damaged during affinity purification using strongly acidic (pH 2–3) or basic (pH 9–11) conditions. Still another possibility is that excessive oxidation of the MAbs' occurred and that milder conditions for the conversion to aldo-IgG should be examined. Nevertheless, Rodwell *et al.*[8] failed to detect any significant alteration in the antigen binding affinity of periodate oxidized monoclonal antibodies.

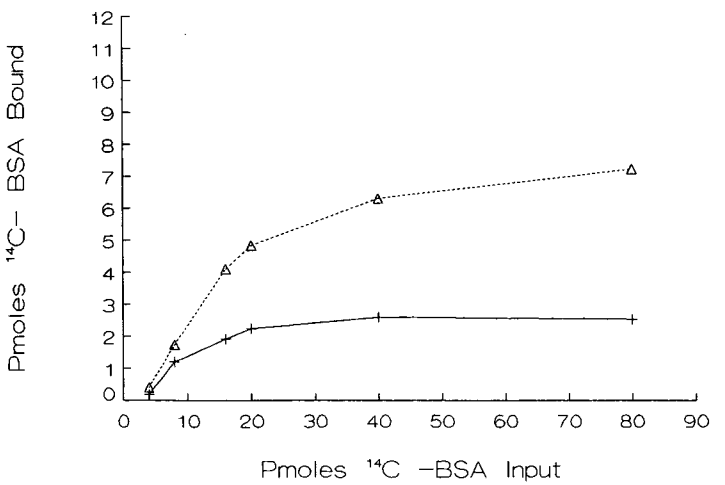

Fig. 5. Comparison of antigen binding capacities for oriented (Affi-Prep 10 HZ) *vs.* random (Affi-Prep 10) immunosorbents. Sodium periodate oxidized polyclonal anti-BSA antibody was immobilized to either Affi-Prep 10 or Affi-Prep 10 HZ and the antigen binding capacity measured using 14C-BSA. Details are described in the text. + = BSA binding to Affi-Prep 10 immunosorbent. △ = BSA binding to Affi-Prep 10 HZ immunosorbent.

There are other plausiable explanations. By definition of monoclonality, primary sequence homology is preserved. Therefore, coupling is much less random than for a polyclonal population, and large differences in antigen binding capacity from oriented *vs.* random coupling mechanisms may not be seen. On the other hand, when the immunoglobulin tends to couple through free amino residues located in close proximity to the antigen binding domain, then random coupling should lead to a substantial inactivation, while oriented coupling will allow for the successful preparation of an immunaffinity support (Fig. 5).

As previously mentioned, it is possible to convert the polymer-based Affi-Prep 10 (NHS) to the hydrazide form, Affi-Prep 10 Hz. We have found little difference in the characteristics of an immunosorbent based upon the agarose gel[4] or this polymeric Affi-Prep resin. For example, we have observed the enhanced binding capacity for immobilized polyclonal antibody that has been reported for Affi-Gel Hz (Fig. 5). In fact, this is very much the same capacity that was obtained using Affi-Gel Hz under similar antibody–ligand density and antigen load. Furthermore, the optimization

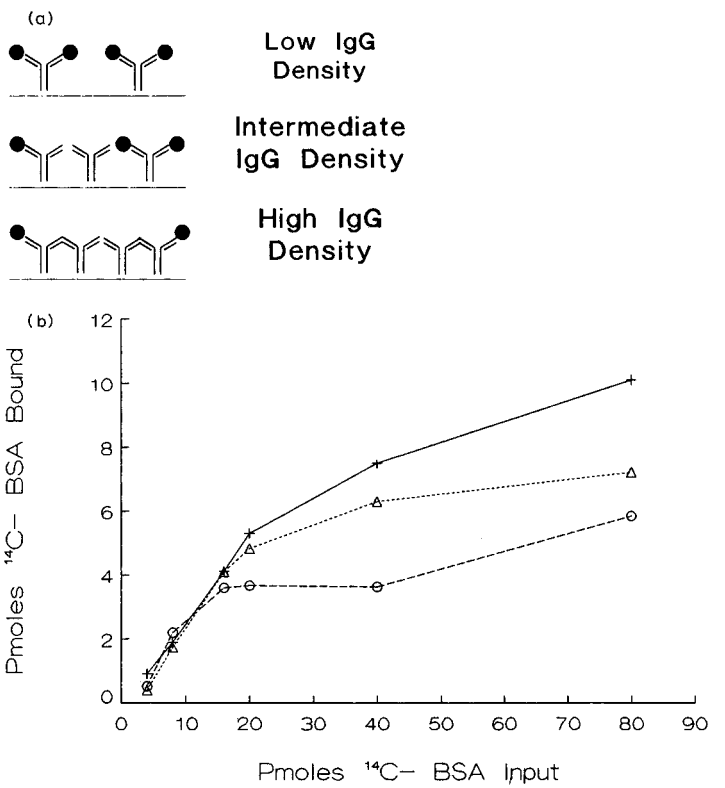

Fig. 6. (a) Artist conception of antibody ligand-matrix density relationships. Antigen molecules (closed circles) can bind freely to the antibody binding sites at low IgG density but experience steric hindrance at increased antibody density. (b) Effect of antibody ligand-matrix density on Affi-Prep 10 HZ antigen binding capacity. Anti-BSA immunosorbent was prepared at various IgG densities using Affi-Prep 10 HZ and the BSA binding capacity determined as described in the text. IgG density: ○ = 5.57 mg/ml; △ = 1.17 mg/ml; + = 0.34 mg/ml.

process should again include a regard for the antibody–ligand density because, as we have seen for CNBr or NHS-mediated coupling, lower densities lead to higher antigen capacities. In this case, antibody immobilized at 0.34 mg/ml had a 2-fold higher capacity for antigen than antibody coupled at 5 mg/ml (Fig. 6B), while the level of IgG required was reduced by 16-fold.

CONCLUSIONS

In our experiments we have attempted to focus upon those factors that are important for the preparation of an efficient immunosorbent. Presentation of the antibody to the solid-phase is critical. In particular, we have observed that monoclonal antibodies are more sensitive to coupling conditions than polyclonal antibodies. For this reason, a careful consideration of the coupling pH is especially important to obtain optimal antigen binding. Cuatrecasas and Parikh[9] in their earlier work suggested that pH control and short reaction times could be used to selectively couple one type of amino acid group over another. Indeed, this is one way in which to reduce the tendency for random coupling that results in a sterically hindered immunoligand.

An alternative to this approach is to abandon amino–ligand coupling altogether. This can be accomplished by condensation of aldehyde groups (generated by periodate oxidation of the carbohydrate moiety) with a solid-phase linked hydrazide group as suggested by O'Shannessy and Quarles[7] and subsequently demonstrated by Little *et al.*[4] for polyclonal antibodies but not for monoclonals. Nevertheless, unless there are significant differences between the kind and location of the carbohydrate moiety between monoclonal and polyclonal antibody molecules, theoretical grounds imply that this technique of oriented coupling via the Fc localized carbohydrate should work equally as well in both cases. Finally, regardless of the technique utilized for immobilization of monoclonal antibodies it is clear that the density of the antibody on the matrix is of principal importance. Steric hindrance created by crowding of adjacent antibody molecules immobilized via oriented coupling or by random coupling mechanisms leads to the same net effect, a decrease in antigen binding efficiency.

ACKNOWLEDGEMENTS

We would like to extend our appreciation to Chris Siebert and Dr. Ken Talmadge for their helpful discussions during the course of these studies.

REFERENCES

1 J. W. Eveleigh and D. E. Levy, *J. Solid-Phase Biochem.*, 2 (1977) 45.
2 D. J. O'Shannessy and W. L. Hoffman, *Biotech. Appl. Biochem.*, 9 (1987) 488.
3 R. S. Matson and C. J. Siebert, *Preparative Chromatogr.*, 1 (1988) 67.
4 M. C. Little, C. J. Siebert and R. S. Matson, *BioChromatogr.*, 3 (1988) 156.
5 M. Wilchek and T. Miron, *Biochemistry*, 26 (1987) 2155.
6 A. V. Philips, D. J. Robbins, M. S. Coleman and M. D. Barkley, *Biochemistry*, 26 (1987) 2893.
7 D. J. O'Shannessy and R. H. Quarles, *J. Immunol. Methods*, 99 (1987) 153.
8 J. D. Rodwell, V. L. Alvarez, C. Lee, A. D. Lopes, J. W. F. Goers, H. D. King, H. J. Powsner and T. J. McKearn, *Proc. Natl. Acad. Sci. U.S.A.*, 83 (1986) 2632.
9 P. Cuatrecasas and I. Parikh, *Biochemistry*, 11 (1972) 2291.

Journal of Chromatography, 458 (1988) 79–92
Elsevier Science Publishers B.V., Amsterdam — Printed in The Netherlands

CHROMSYMP. 1505

SAMPLE SIZE AND RETENTION VALUES IN HIGH-PERFORMANCE LIQUID CHROMATOGRAPHY OF BIOLOGICAL AND SYNTHETIC POLYMERS

H. ENGELHARDT*, M. CZOK, R. SCHULTZ and E. SCHWEINHEIM
Angewandte Physikalische Chemie, Universität des Saarlandes, 6600 Saarbrücken (F.R.G.)

SUMMARY

In the chromatographic separation of natural and synthetic polymers, the retention and peak broadening are strongly dependent on the sample size. Contrary to chromatography of low-molecular-weight solutes, no linear region was observed where both factors are independent of sample size. Even in gradient elution, proteins are eluted approximately 3% of the gradient time earlier when the sample size is increased by a factor of ten. With non-porous materials of small particle diameters and small surface areas, the peak broadening is markedly affected by sample size. Their advantage in efficiency compared to standard porous materials is lost at sample sizes around 100 μg. Generally, retention decreases with increasing sample size, but also the contrary has been observed. In precipitation chromatography of polystyrenes similar behaviour has been observed. Consequently, one has to be careful in qualitative identifications of polymers in mixtures of unknown concentrations and in the transfer of analytical results to preparative-scale work.

INTRODUCTION

A prerequisite for peak identification in high-performance liquid chromatography (HPLC) is the independence of retention time on the sample size. It has been shown that in LC as long as the sorption isotherm is linear, the amount adsorbed increases linearly with the amount of sample in solution. In this case the retention time and peak broadening are independent of the sample size[1]. According to Snyder[1,2], this linear range can be determined experimentally and summarized conveniently as a plot of sample retention values (capacity factor, k', or retention volume per gram stationary phase) *versus* sample size, usually on a logarithmic scale. The maximum sample size can be obtained from these semi-logarithmic plots in two ways: the maximum sample size is the one where the deviation of k' or peak width exceeds 10% of the value measured at low sample sizes (near the detection limit of the detector), or the one where the tangents to both branches of the curves cross. Consideration of preparative scale LC leads to more optimistic definitions of the maximum sample size[3], where a double logarithmic plot of plate number *versus* sample size has been proposed. The maximum sample size is designated as the one at which the slope of

0021-9673/88/$03.50

TABLE I

STATIONARY PHASES AND COLUMNS USED

Phase	*Surface area* (m^2/cm^3)	*Pore diameter* (nm)	*Column dimensions* (*mm*	*Origin*
Monospher RP-8	3	-	50 × 4	Merck, Darmstadt, F.R.G.
Monospher RP-18	3	-	50 × 4	Merck, Darmstadt, F.R.G.
LiChrospher Si 1000 RP-18	15	100	50 × 4	Merck, Darmstadt, F.R.G.
LiChrospher Si 500 RP-18	30	50	50 × 4	Merck, Darmstadt, F.R.G.
Grace 250 Acetamide	150	25	50 × 4	Silica: Grace, Worms, F.R.G. Modification[14]
Nucleosil 300 acetamide/carbamate	45	30	50 × 4	Silica: Machery-Nagel, Düren, F.R.G.
Nucleosil 300 SAX	45	30	125 × 4	Macherey-Nagel, Düren, F.R.G.
Waters Prot PAK DEAE-5PW	-	50	75 × 8	Millipore Waters, Eschborn, F.R.G.
LiChrosorb Si 100 RP-18	160	10	250 × 4.1	Merck, Darmstadt, F.R.G.

this plot is equal to -1. Up to that point, the decrease in plate number is compensated by the increase in sample size, whereas at higher sample sizes the loss in efficiency is much more rapid. Other definitions are more or less of theoretical importance, *e.g.*, the statement that "the extra peak broadening is dependent only on the total mass of solute per gram of stationary phase contained in one plate"[4].

Volume overloading may be of importance in isocratic preparative chromatography. Since proteins are usually separated with gradient elution, its influence on H and retention times can be neglected here. Sampling is done under extremely weak elution conditions and the solutes are enriched in the first zone of the stationary phase and do not migrate under these initial conditions.

The maximum sample capacity in protein analysis has not been considered so far. In some papers[5–10] one can find, in cautious wording, that in gradient elution of proteins the retention decreases slightly and continuously as the sample size is increased, but no hints of a limiting value are given. In one paper[5] independence of retention time in the range of 100 μg to 3 mg protein per gram of stationary phase was found for hydrophobic interaction chromatography, whereas a strong dependence was claimed for reversed-phase chromatography. More often the influence of the sample size on peak broadening is considered for the determination of loading capacity: here, a 75% increase in peak broadening (corresponding to a doubling of peak width) has been proposed to determine the loading capacity[11]. Semilogarithmic plots have also been used in this case.

The exact knowledge of the dependence of retention on sample size is of paramount importance for verifying chromatographic identification. The advent of nonporous materials with extremely small specific surface areas and, hence, probably reduced loading capacity, as well as the discrepancies in literature discussed above, induced us to study the sample capacity in HPLC of proteins.

EXPERIMENTAL

A Waters liquid chromatograph (gradient system 600, diode array detector 490) (Millipore, Waters Chromatographie, Eschborn, F.R.G.) with a Rheodyne 7120 sample injector (ERC, Alteglofsheim, F.R.G.) was used. For reversed-phase separations, gradients from water (containing 0.01 M trifluoroacetic acid, TFA) to acetonitrile (also with 0.1 M TFA) ranging from 20 to 75% B in 10 min were applied, and for hydrophobic interaction chromatography, gradients from 2.5 M ammonium sulphate in 0.1 M phosphate buffer pH 7 to pure phosphate buffer in 10 min. Isocratic elution was also studied (for conditions see figure legends). The flow-rate was 2 ml/min in all cases. Buffer salts and organic eluent components were obtained from various suppliers, and were at least of pro analysis quality. The columns and stationary phases are summarized in Table I together with their sources. The proteins were obtained from Sigma Chemie (Deisenhofen, F.R.G.). The solutions were prepared fresh daily and stored in ice–water.

Constant volumes (10 μl) of protein solutions of defined concentration were injected to cover the range between 1 μg and 1 mg protein per injection. To compensate for injection errors, the amounts stated have been correlated via peak areas, determined at 250 nm, to a standard solution containing 500 μg protein/10 μl. The columns were equilibrated with the corresponding protein by injection of solutions

until the peak area remained constant. The peak width at half height and retention times were determined from diode-array detector data.

RESULTS AND DISCUSSION

Dependence of peak width on sample size

For protein separations, primarily gradient elution conditions are of interest. Because H values are not defined in gradient elution, the dependence of the peak width on sample size was determined with different columns under standardized gradient conditions. Fig. 1 shows the dependence of the peak width at half height on the sample size. At low sample sizes, these values can be correlated to the particle diameters, which are 1.5 μm (Monospher), 5 μm (Acetamide) and 10 μm (Si 100, RP-18) respectively. With all columns, the peak width increased continuously with sample size, starting at very low concentrations. Over the whole concentration range, the peak width on sample size was especially pronounced with the Monospher column. This is not surprising, because with around 3 m^2 per ml of column volume this stationary phase has by far the smallest surface area. The efficiencies one may expect from these small particles (particle diameter *ca.* 1.5 μm) are soon lost with increasing sample size; at loadings above 100 μg the efficiencies of classical porous materials with particle diameters of around 5 μm are approached. The small differences in the behaviour found for the reversed-phase material (pore diameter 1000 Å) and the acetamide hydrophobic interaction material (250 Å), differing by a factor of ten in surface area, cannot easily be explained. Perhaps the kinetics of the two different sorption mechanisms plays a role in this case.

In Fig. 2 the same data are plotted on the usual semi-logarithmic scale. Here, the typical and expected curve shape was obtained. However, this plot is just a result of mathematical data transformation. Even a linear dependence of the retention or peak width on the sample size will give this typical curve when transformed to a

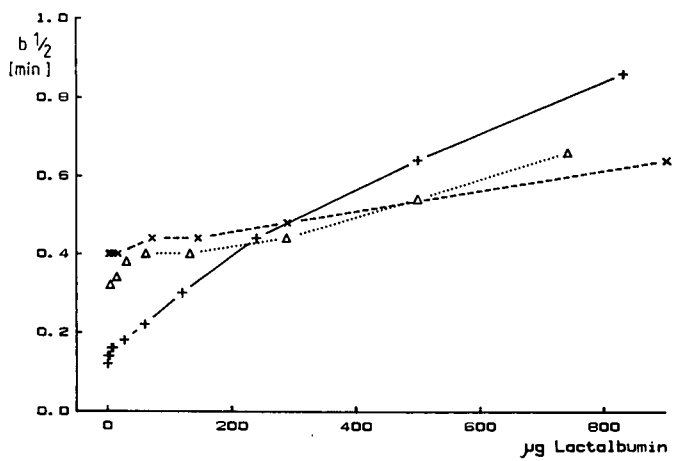

Fig. 1. Dependence of the peak width at half height on the sample size. Sample: lactalbumin. Columns: + = Monospher RP-8; △ = Grace 250 Acetamide; × = LiChrospher Si 1000 RP-18. For gradient conditions, see Experimental section.

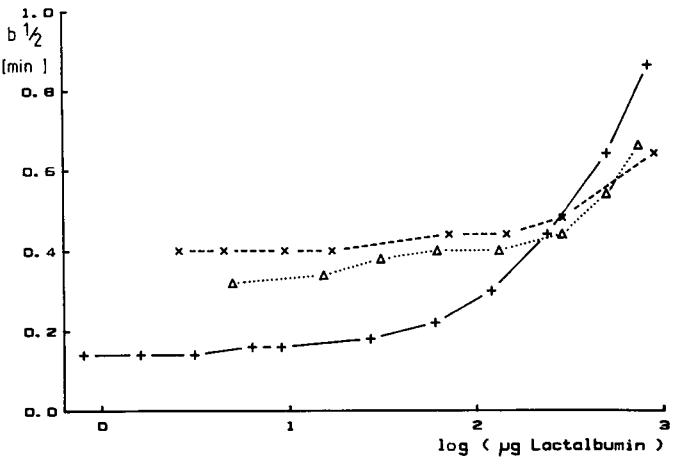

Fig. 2. Semilogarithmic plot of the dependence of peak width on sample size. Columns and conditions as in Fig. 1.

semi-logarithmic scale. The position of the bend in the curve depends only on the range of the x-axis. It is, therefore, dangerous to deduce any scientific meaning from this plot, and the place of the bend.

Dependence of retention on sample size

Under standard gradient conditions, the dependence of the elution time in the gradient on the sample size can also be used to compare stationary phases. In Fig. 3 the change in retention time with sample size is demonstrated for different stationary phases. The retention time decreases in every case with increasing sample size. Even at low sample sizes, close to the detection limit, no range of constant retention time was observed. Retention times in the standard gradient are clearly a function of the surface area per unit column volume.

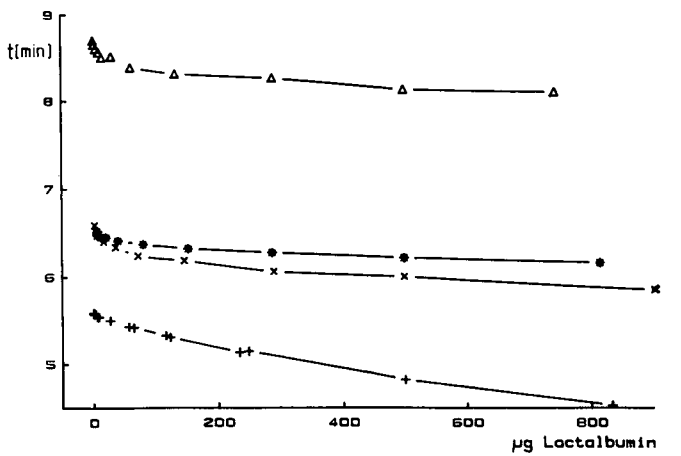

Fig. 3. Dependence of the elution time (t) in gradient elution on sample size. * = LiChrospher Si 500 RP-18; other columns and conditions as in Fig. 1.

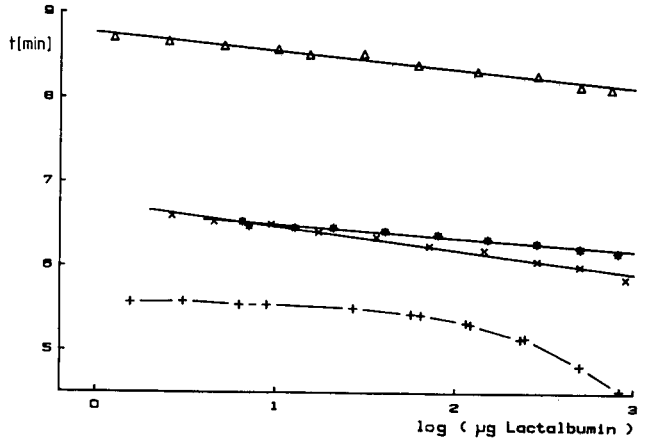

Fig. 4. Semilogarithmic plot of the dependence of elution time on sample size. Columns and conditions as in Fig. 3.

When these data are plotted in a semi-logarithmic plot, straight lines with different slopes are obtained, as shown in Fig. 4. This indicates that retention times in gradient elution always decrease by a constant value upon doubling the sample size. This means that with the exception of the Monospher column, the retention time is affected by the same factor when changing the sample size whether working in the concentration range of 1–10 µg or 0.1–1 mg. In this case, a displacement between 0.15 and 0.25 min was observed when changing the sample size by a factor of ten. Consequently, in gradient elution, variations in retention up to 3% of the gradient program time are expected. The slopes of these curves correspond to the surface area of the stationary phases and can be taken as a measure of the adsorption capacity.

Although the surface area of the Grace 250 acetamide phase is larger by a factor of 10, compared to LiChrosorb Si 1000 RP-18, the loading capacity was quite similar in both cases. This may be due to different separation mechanisms. In hydrophobic interaction chromatography (HIC), the S values (slope of log k' *vs.* eluent composition)[12,13] are lower than in reversed-phase (RP) chromatography. Consequently, the elution conditions are closer to those of isocratic chromatography, where the sample size influences retention much more strongly.

Isocratic elution

Gradient elution is the standard mode in protein chromatography. However, it is common practice, especially in HIC, to characterize the system by the slopes, S, of the plot of log k' *vs.* salt concentration in the eluent. These S values can be calculated —with some restrictions— from retention in two different gradient experiments. On the other hand, it is also possible to measure retention values isocratically. In this case, the influence of the sample size must be known. In order to evaluate this influence and to obtain some insight in the problems discussed so far, isocratic measurements were made in both HIC and RP systems. In the latter case, extreme precautions were taken to keep the eluent composition constant within a few fractions of a percent.

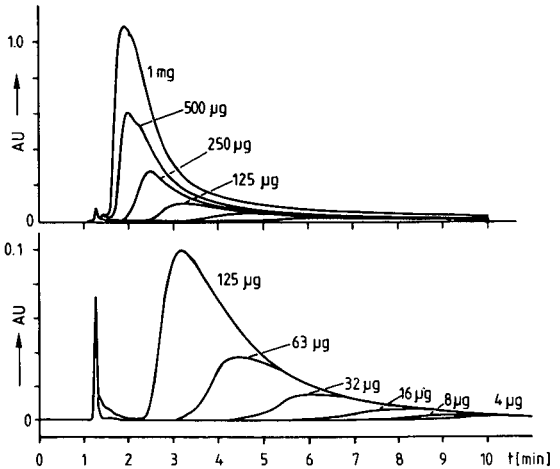

Fig. 5. Elution profiles of lactalbumin in reversed-phase chromatography. Range of sample sizes: 4 µg to 1 mg. Column: Si 500 RP-18. Eluent: 30% (v/v) acetonitrile in 0.01 *M* aqueous TFA. Lower curves, UV range 0–0.1 a.u.f.s.; upper curves, 0–1 a.u.f.s.

In Fig. 5 the change in peak shape and retention with increasing sample size is demonstrated for lactalbumin. A RP-18 column (Si 500) and 30% acetonitrile in 0.01 *M* TFA was used. If the sample sizes are increased from 4 to 125 µg, the retention times decrease from more than 10 min ($k' = 6.5$) to *ca.* 3 min ($k' = 1.5$). As expected for overloading curves, the peaks eluted for smaller sample sizes fit in the tail end of the peaks for higher sample sizes. This can be explained by a strong curvature of the adsorption isotherm, caused by inhomogeneous surface properties at different sites and with different energies of interaction. In the upper part, at lower detection sensitivity, it is quite obvious that with 1 mg sample the surface area is almost totally covered with solute and the sample breaks through ($k' = 0.5$).

Similar behaviour was observed for other stationary phases, eluent compositions and proteins. As expected, the decrease in retention time is extremely pronounced for the Monospher column. Here, the k' values decrease from *ca.* 70 for 1 µg to zero for 100 µg lactalbumin. The strongly basic lysozyme shows a behaviour similar to that of the acidic lactalbumin both in RPC and HIC. This demonstrates that this effect may not be due exclusively to overloading of residual silanol groups on the surface.

If the k' values, as determined from the peak maximum and not—as would be more correct—from the centre of mass, are plotted in the typical semi-logarithmic plot, a linear decrease of k' with sample size is observed. Fig. 6 shows the two different curves obtained for isocratic measurements with two different eluent compositions. The lower curve corresponds to measurements taken with 31% acetonitrile, the upper curve with 30% acetonitrile. The slopes are a function of the k' values. The linear sections of both curves cross at a retention value close to zero. Dividing the slopes by their corresponding ordinate intersections leads to a similar value of $-0.4\,k'$ units per decade of concentration change at normalized retention. Increasing the sample size by a factor of 10 from 1 to 10 µg gave a decrease in the k' value from 1 to 0.6 or from 10 to 6.

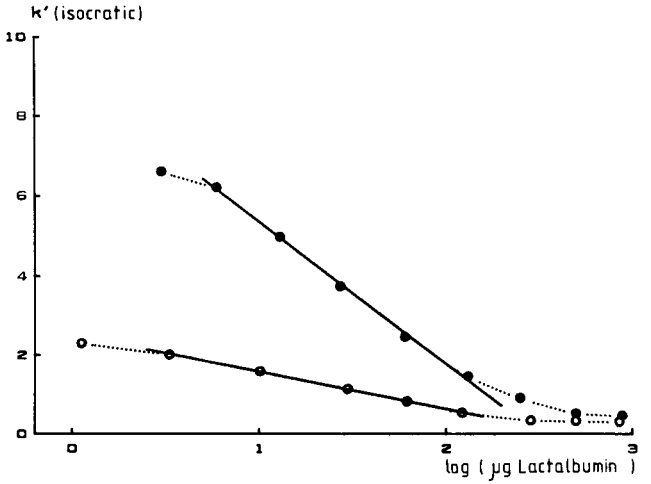

Fig. 6. Decrease in retention time for lactalbumin with sample size in reversed-phase chromatography. Isocratic elution; column and eluent as in Fig. 5. Reduced slopes: 30% acetonitrile; −0.40 (upper); 31% acetonitrile, −0.38 (lower).

Similar to Fig. 6 which shows the dependence of k' on sample size for one protein at different eluent compositions, similar reduced slopes were also obtained for different proteins on the same stationary phase. In Fig. 7 the dependence of k' on sample size is shown for three different proteins of similar molecular weight in an HIC system. The normalized slopes are very similar. The three curves do not cross close to zero but at a k' value of 1.1. If this k' value is deducted from the extrapolated one, the reduced slope is identical, −0.26, for all three proteins. This means that the slope is

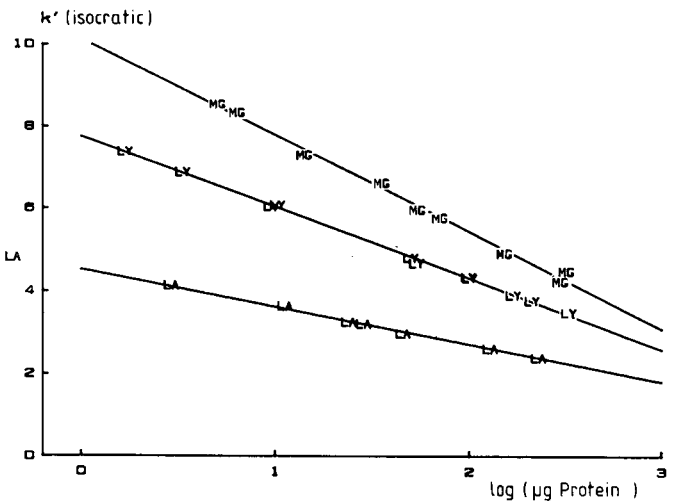

Fig. 7. Dependance of k' on sample size in HIC. Isocratic elution. Column: Nucleosil 300, 0.9 µmol/m^2 carbamate. Eluent: phosphate buffer, pH 7, with different concentrations of ammonium sulphate. Samples: MG = myoglobin, reduced slope −0.33; LY = lysozyme, reduced slope −0.22; LA = lactalbumin, reduced slope −0.20.

not only proportional to k', but increases linearily with k'. It might be possible to deduce from this slope a characteristic figure for each stationary phase.

The knowledge of this normalized dependence of k' on sample size is also important because it would be extremely difficult to compare various stationary phases under identical retention conditions. Achieving the desired k' value would require a tedious adjustment of eluent conditions. The advantage of the use of this reduced slope for stationary phase comparison is demonstrated in Fig. 8. Here, the dependence of k' on sample size is shown for four HIC columns, packed with stationary phases of different hydrophobicities. The most polar column is an acetamide column. By stepwise reaction with increasing amounts of carbamate the hydrophobicity was successively increased[14]. Stationary phase 3 was the most hydrophobic one, containing 2.2 μmol of carbamate per m^2. The relative location of the three curves in this diagram depends on the individual eluent compositions which were adjusted to get reasonable k' values.

As is seen, the normalized slope decreases with increasing hydrophobicity. This indicates that the loadability increases and that the k' values are consequently less influenced by sample size when the stationary phase hydrophobicity is increased. Increasing hydrophobicity means in this case also increasing density of carbamate groups at the surface. For proteins, this may also mean increased surface homogeneity. Surface homogeneity may be the reason why the normalized slope for the pure acetamide column—homogeneous surface coverage with a single functional group—is also relatively low (−0.17). However, this comparison should be made with some caution. The surface area of the silica support was three times as large as in the case of the mixed stationary phases. On the other hand, the column length was only one third of that for the mixed stationary phases. The surface area available for sorption in each column was, therefore, approximately the same. The slope for the acetamide phase was also only half of that for the reversed-phase systems discussed above. Consequently, the normalized slope of k' *vs.* log sample size may be a measure of the

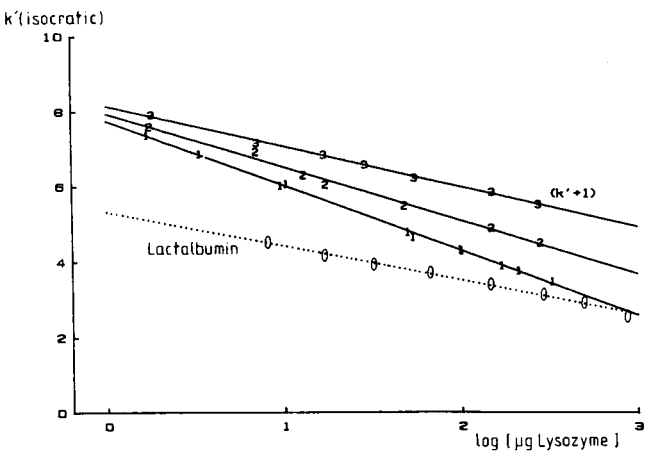

Fig. 8. Dependence of k' on sample size with different stationary phases for HIC. Curves: 1–3, lysozyme with acetamide–carbamate phases, 0.9, 1.8 and 2.2 μmol/m^2 carbamate; 0, lactalbumin with acetamide phase. Phosphate buffer, pH 7, retentions adjusted by addition of ammonium sulphate. Reduced slopes: 0 = −0.17; 1 = −0.22; 2 = −0.18; 3 = −0.17.

stationary phase hydrophobicity and homogeneity. However, further experiments are necessary to prove this.

Other separation systems

So far, only separation systems have been discussed in which hydrophobic and solvophobic interactions contribute to the retention. One of the main techniques for protein separation is ion-exchange chromotography. With the silica-based strong anion exchangers studied, the peak shapes and retention times also depend strongly on the sample size, as demonstrated in Fig. 9 for lactalbumin in the concentration range between 10 and 200 μg. The peaks are plotted in a manner similar to that used in Fig. 5, but in this case taken from gradient elution experiments[15]. Up to 50 μg lactalbumin the retention seems to be almost independent of sample size, but at higher concentrations a decrease in elution time is noticeable. The only difference between this plot and that in Fig. 5 is that here the tailing ends of the peaks do not fit in a common curve. This may indicate that retention of the protein may occur not only by electrostatic interactions. It is conceivable that, with this stationary phase, at least three different interactions may occur at different locations: the ion-exchange groups, the polar functionalities of the bonded groups and—last but not least—silanophilic interactions with residual surface silanol groups.

Proteins are always good for surprises. With polymer-based stationary phases, *e.g.*, a Waters Protein PAK DEAE-5PW column or polymer-coated phases, *e.g.*, a Baker PEI protein column the retention time of lactalbumin increases with increasing sample size, as demonstrated in Fig. 10 for the polymer-based anion exchanger. Here, the separation mechanism is also anion exchange, but no additional interaction with the matrix seems to contribute to retention. However, this does not explain why the retention increases with increasing sample size. Aggregate formation of the protein at the surface may be one explanation.

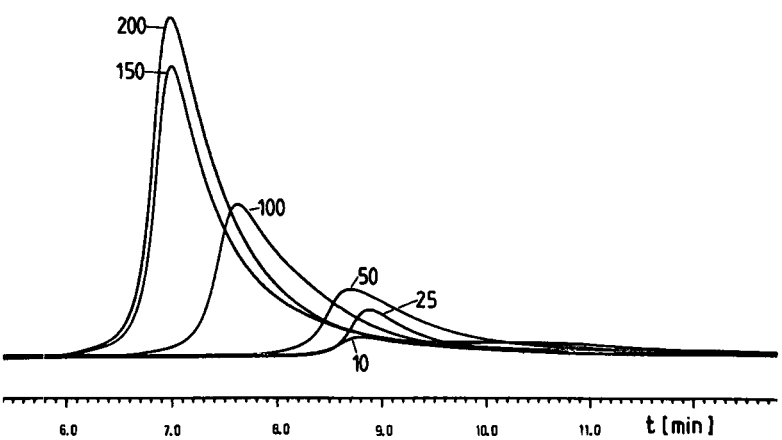

Fig. 9. Retention and sample size in ion-exchange chromatography. Stationary phase: SAX on Nucleosil 300. Eluent: 0.02 *M* phosphate buffer, pH 7; from 0 to 0.6 *M* sodium chloride in 30 min. Sample size range: 10–200 μg lactalbumin, as indicated.

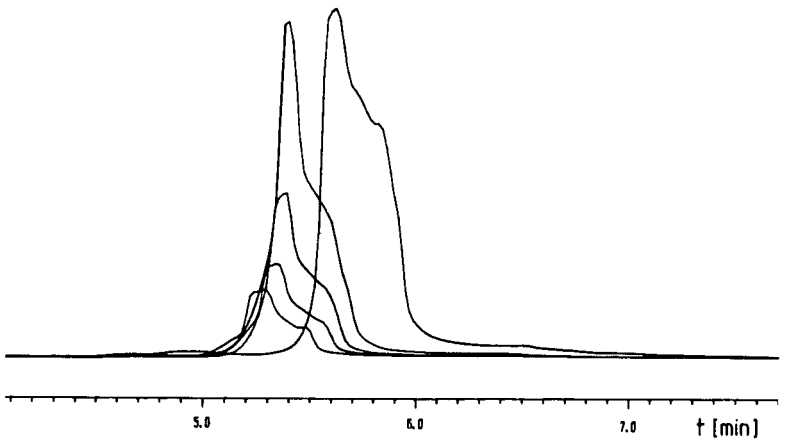

Fig. 10. Retention and sample size in ion-exchange chromatography. Stationary phase: Waters Protein PAK DEAE-5PW; eluent and samples as in Fig. 9.

Studies with polystyrenes

In the course of our studies[16] on precipitation chromatography of synthetic polymers[17] a similar influence of sample size on retention was observed for polystyrenes. Usually, in precipitation chromatography a solution of a synthetic polymer is injected into a chromatographic system with an eluent in which the polymer is insoluble. For polystyrenes, this may either be an alkane, like heptane, or an alcohol, like methanol. The polystyrene is precipitated on the stationary phase and elution is achieved in both cases by a gradient to a dissolving eluent which can be dichloromethane. In the system, where heptane is the precipitating agent and dichloromethane is the dissolving eluent, retention times decreased with increasing sample size, Fig. 11. An additional contribution of adsorption to polymer retention was observed[18]. This has been confirmed by comparing the dichloromethane concentration required for elution and the results obtained by turbidimetric titrations of the polystyrenes. In turbidimetric titrations, if polystyrenes have been precipitated by the "weaker" agent

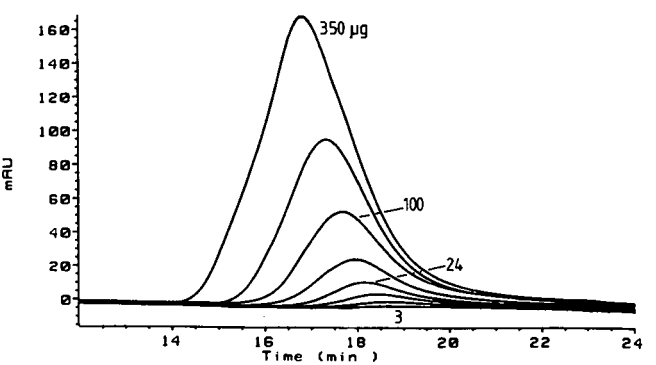

Fig. 11. Precipitation chromatography of polystyrene (mol. wt. 200 000 daltons). column: RP-18, Si 100; gradient, *n*-heptane to dichloromethane in 20 min.

heptane for redissolution of the polymer, usually lower concentrations of dichloromethane are required compared to the cases where the "harder' precipitation agent methanol has been used. In those cases, where solubility is the only mechanism and the polymers are not additionally retarded by adsorption on the stationary phase surface, the eluent composition, at which the polymer is eluted, should be identical with the solvent composition at which the polymer is precipitated in turbidimetric titrations. In Fig. 11, for elution a higher dichloromethane concentration is required than expected from turbidimetric titrations. Although a typical normal phase gradient (heptane to dichloromethane) was used, adsorption occurred even on alkyl bonded stationary phases, due to interactions with the residual silanol groups. Consequently, overloading and, hence, a decrease in retention time with increasing sample size is feasible. This corresponds to the cases in protein chromatography demonstrated in Figs. 5 and 9. The influence of sample size on retention time was much less pronounced with normal phases, *e.g.*, silica columns, due to higher loading capacities. Additionally, higher concentrations of dichloromethane were required with these columns.

Exactly the opposite influence of sample size on retention times was observed when the stronger precipitating agent methanol was used. As demonstrated in Fig. 12, the retention times increased with increasing sample size. Interaction with the surface area is not expected in this case. The eluent composition (methanol–dichloromethane) at which the polymer is eluted is, over a wide molecular weight range, identical with the solvent composition at which the polymer is precipitated in turbidimetric titrations[19]. No influence of the type of the stationary phase used was observed. As a consequence, polymer solubility must be the only separation mechanism and no additional adsorption on the stationary phase surface contributes to retention. One plausible explanation for this behaviour is that adsorption effects are diminishing at the high concentrations of the strongly eluting agent dichloromethane that are required for dissolution. The increase in retention times, and hence dichloromethane content, with sample size might be due to polymer–polymer interactions and corresponds to the results of the influence of the amount of polystyrenes in turbidimetric titrations[20]. Additionally, the polymers were eluted as colloidal suspensions[21]. This was evidenced by the fact that the peak areas were larger in this elution system than

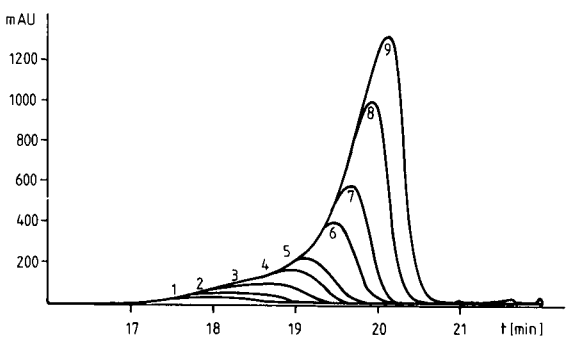

Fig. 12. Precipitation chromatography of polystyrene (MW 110 000 daltons). Influence of sample size. Column as in Fig. 11. Gradient: methanol to dichloromethane in 20 min. Sample sizes: 12.5 (1) to 400 μg (9).

when the same amount was injected in size-exclusion chromatography (SEC), where true solutions are eluted. Also the polystyrenes were detected in this case even in the visible region: the "absorption' is caused by light scattering by this colloidal solution.

CONCLUSIONS

For proteins and for synthetic polymers it was observed that the chromatographic resolution is strongly dependent on the sample size. The retention time and peak width are both affected by increasing sample size. No range was found where the retention is independent of the sample size. Even in gradient elution, variations in elution time by several percent must be dealt with. For the identification of solutes from their chromatographic retention, one must define a retention window and a corresponding concentration range in which one can work with a given system. Because of the linear dependence of retention on sample size in a semi-logarithmic plot, it is possible to calculate for each given system the change in retention time when the sample size is increased ten-fold. The change in retention is identical whether one works at low or at high concentrations.

The peak broadening and, hence, chromatographic resolution is also affected by sample size. For stationary phases with small surface areas, like the new non-porous materials with particle diameters of *ca.* 1.5 μm, the efficiencies one might expect from these materials are soon lost with increasing sample size. At a load above 100 μg the efficiencies of classical porous materials with particle diameters of *ca.* 5 μm are approached.

The dependence of retention on sample size is a function of the surface inhomogeneity. The strongest dependences on sample size are observed with reversed-phase and HIC systems. However, it is not the surface coverage that is important, but the homogeneity of the surface with which the proteins interact.

For stationary phases, where either the silica matrix has been covered or organic polymer matrices are used, surprisingly an increase in retention with sample size has been observed. Comparison of this behaviour with similar observations made in the chromatographic separation of polystyrenes leads to the assumption that proteins are also eluted as aggregates at high sample concentrations. In chromatography of proteins aggregate formation has been observed[22]. In the other cases, where multiple interaction with different active sorption sites is expected with both groups of polymers studied (synthetic and natural), the retention decreases with increasing sample size.

Further studies may lead to new types of stationary phases on which retention of polymers is, at least for a given concentration range, independent of sample size. In the meantime one must be cautious in the qualitative identification of proteins in unknown mixtures and in preparative scale work. Knowledge of the influence of sample size on retention is paramount and must be determined for each individual separation system.

ACKNOWLEDGEMENTS

We appreciate the financial support by the Deutsche Forschungsgemeinschaft, Bonn-Bad Godesberg. M. Czok is grateful for a Graduierten-Förderungsstipendium

by the government of the Saarland. We thank R. Wintringer for his help with the measurements.

REFERENCES

1 L. R. Snyder, *Anal. Chem.*, 39 (1967) 698.
2 L. R. Snyder, *Principles of Adsorption Chromatography*, Marcel Dekker, New York, 1968.
3 P. D. McDonald and B. A. Bidlingmeyer, in B. A. Bidlingmeyer (Editor), *Preparative Liquid Chromatography (Journal of Chromatography Library*, Vol. 38), Elsevier, Amsterdam, 1987, p. 27.
4 H. Poppe and J. C. Kraak, *J. Chromatogr.*, 255 (1983) 395.
5 N. T. Miller and B. L. Karger, *J. Chromatogr.*, 326 (1985) 45.
6 J. D. Pearson, N. T. Lin and F. E. Regnier, *Anal. Biochem.*, 124 (1982) 217.
7 F. L. de Vos, D. M. Robertson and M. T. W. Hearn, *J. Chromatogr.*, 392 (1987) 17.
8 Y. S. Kim, B. W. Sands and J. L. Bass, *J. Liq. Chromatogr.*, 10 (1987) 839.
9 K. K. Unger, G. Jilge, J. N. Kinkel and M. T. W. Hearn, *J. Chromatogr.*, 359 (1986) 61.
10 N. D. Danielson and J. J. Kirkland, *Anal. Chem.*, 59 (1987) 2501.
11 R. C. Williams, J. F. Vasta-Russell, J. L. Glajch and K. Golebiowsky, *J. Chromatogr.*, 371 (1986) 63.
12 L. R. Snyder, in Cs. Horvath (Editor), *High-Performance Liquid Chromatography—Advances and Perspectives*, Vol. 1, Academic Press, New York, 1980, Ch. 4.
13 J. P. Larmann, J. J. DeStefano, A. P. Goldberg, R. W. Stout, L. R. Snyder and M. A. Stadalius, *J. Chromatogr.*, 255 (1983) 163.
14 M. Czok and H. Engelhardt, *Fresenius' Z. anal. Chem.*, 327 (1987) 34.
15 E. Schweinheim, *Ph.D. Thesis*, Saarbrücken, in preparation.
16 R. Schultz, *Ph.D. Thesis*, Saarbrücken, in preparation.
17 G. Glöckner, J. H. M. van den Berg, N. L. J. Meijerink, T. G. Scholte and R. Koningsveld, *J. Chromatogr.*, 317 (1984) 615.
18 G. Glöckner, *J. Chromatogr.*, 403 (1987) 280.
19 G. Glöckner, *Chromatographia*, 25 (1988) 854.
20 G. Glöckner, *Habilitationsschrift*, TH Dresden, 1965.
21 G. Glöckner, S. Schmutzler, H. Engelhardt and R. Schultz, *Chromatographia*, 25 (1988) in press.
22 B. L. Karger, personal communication.

Journal of Chromatography, 458 (1988) 93–104
Elsevier Science Publishers B.V., Amsterdam — Printed in The Netherlands

CHROMSYMP. 1529

THERMODYNAMICS OF α-LACTALBUMIN DENATURATION IN HYDROPHOBIC-INTERACTION CHROMATOGRAPHY AND STATIONARY PHASES COMPARISON

KÁLMÁN BENEDEK*
Smith Kline and French Laboratories, King of Prussia, PA 19406 (U.S.A.)

SUMMARY

These studies present an evaluation of the role of surface hydrophobicity and temperature on the denaturation characteristics of α-lactalbumin under hydrophobic-interaction chromatography conditions, and a description of a model system to evaluate the role of chromatographic columns in the denaturation process of proteins.

The chromatographic characteristics of α-lactalbumin have been compared using commercially available poly(methyl); -(ethyl)- and -(propyl)aspartamide columns. These columns were designed for hydrophobic-interaction chromatography and represent a homologous series of stationary phases with increasing hydrophobic character. The elution profiles and retention times of α-lactalbumin have been also compared in different mobile phases and as a function of temperature. The chromatographic characteristics of the Beckman CAA-HIC column, another commercially available column for hydrophobic-interaction chromatography, have also been evaluated, permitting further insight into the effect of bonded phases on protein denaturation.

The retention time–temperature curves obtained are sigmoidal, characteristic of the classical transition curves of protein denaturation. Thermodynamic parameters of the denaturation of α-lactalbumin are calculated from the retention data and the calculated transition temperatures and free energies of denaturation are used for comparison of the different columns. The model system and the calculated thermodynamic values represent a useful method for the evaluation of such columns, and can provide an estimate of the contribution of the stationary and mobile phases to the protein denaturation process.

INTRODUCTION

Hydrophobic-interaction chromatography (HIC) is the last of the classical liquid chromatographic techniques to be converted into the high-performance

* Present address: Specialty Chemistries, Millipore Corporation, 750 Wiggins Avenue, Bedford, MA 01730, U.S.A.

0021-9673/88/$03.50

mode[1–7]. Modern HIC has been developed based on earlier work with soft organic gels[8–11], and experience with protein reversed-phase chromatography[11–16]. HIC uses descending salt gradients, most frequently ammonium sulfate, to separate the analyte from a mildly hydrophobic stationary phase. A variety of silica-based stationary phases have been developed and are used routinely for protein separations. The popularity of HIC is due to the elution conditions, which usually provide excellent mass and activity recoveries for most proteins.

It has been shown in reversed-phase chromatography that multiple peaks[16,17], peak shape distortion[18] and changes in the retention volume of a pure protein result from conformational changes[18]. It has been also shown that the magnitude of these chromatographic alterations is related to the extent of unfolding of a particular protein[18–20]. In the case of papain, two widely separated peaks have been observed. The early eluting peak was identified as the native form and the late eluting peak as the denatured form of the enzyme[17]. Since unfolding modifies structure of the protein and consequently the complementary surface, *i.e.*, the attachment points between the protein and the stationary phase, the adsorption and retention of the protein is altered. This relationship between the surface of a protein and the stationary phase defines the mechanism of separation and selectivity in all adsorption chromatographies, such as reversed-phase liquid chromatography, HIC, electrostatic interaction chromatography (EIC), metal interaction chromatography (MIC) and affinity chromatography. These techniques can sometimes detect extremely intimate modifications of the complementary surface but might be blind for major alterations of proteins if they do not affect the complementary surface[19]. A study of the role of chromatographic parameters in conformational changes can provide insight into the phenomena involved in the separation of proteins[18,20,21]. Such studies serve as a model to study the interactions between proteins and solid surfaces, an interface where it is known that protein conformational changes can occur[22].

A kinetic model for the events occurring during protein chromatography has been suggested which involves two steps[20]. The first step is the kinetically rapid initial contact of the protein with the surface, while the second step, kinetically slow, includes all further conformational events occurring until elution. It has been shown that the major cause of protein denaturation under reversed-phase chromatographic conditions is adsorption onto the stationary phase, which eventually causes denaturation[20]. When the apparent hydrophobicity of the surface is altered by the adsorption of *n*-propanol[20] or of non-ionic detergents[23] prior to separation, a greater amount of native protein is recovered. These observations led to the development of non-ionic, mild stationary phases, specifically designed for HIC[2,6,7].

In HIC the high salt content of the starting mobile phase increases the surface tension of the mobile phase, and correspondingly, the solvent–stationary phase interfacial tension. The free energy of adsorption of the protein to the stationary phase is negative. Decreasing the salt concentration thus decreases the interfacial tension and permits the elution of the protein[20].

Many experimental parameters affect the interfacial tension and can change the elution characteristics of proteins. The type and concentration of salt and the pH of the mobile phases affect retention, resolution, selectivity and peak shape. The ligand density, charge characteristics and hydrophobicity are variable parameters of the stationary phase. In low-pressure chromatography, using chemically modified soft

gels, the length of the bonded alkyl chain has a tremendous effect on the retention and selectivity of the separation[11]. Similar behavior has been observed in high-performance HIC, using stationary phases prepared by the same bonding chemistry[7]. This allows the surface hydrophobicity to be modulated by attaching *n*-alkyl homologues with different chain length[7]. The retention of proteins under identical mobile phase conditions generally increases as the hydrophobicity of the stationary phase increases. This change in the retention time varies from protein to protein and may result in significant differences in resolution and selectivity.

The temperature is a very important parameter in the modulation of column selectivity. In protein chromatography, the column temperature might affect the mass and activity recovery of proteins by altering the conformational equilibria of proteins. It has been shown that the column temperature can have a major impact on the retention behavior of certain proteins under reversed-phase[13,14,16–18] and hydrophobic-interaction chromatographic conditions[24,25]. In the HIC separation of α-lactalbumin, peak distortion and non-linear changes in retention have been observed as a function of temperature[26,27]. These anomalies have been interpreted as the result of protein denaturation. In this communication, we explore the effect of temperature on these phenomena in context with the surface hydrophobicity using four different, commercially available HIC columns. The retention time–temperature curve is sigmoidal in those cases where denaturation occurs during the chromatography. These curves are similar to the transition curves of protein denaturation studied by spectroscopic techniques, and are analyzed by the same approach.

EXPERIMENTAL

Materials

HPLC-grade water was prepared by a Milli-Q water system (Millipore). Ammonium acetate, phosphate buffered saline (120 m*M* NaCl, 2.7 m*M* KCl in 10 m*M* phosphate buffer, pH 7.4), grade III ammonium sulfate, N-2-hydroxyethylpiperazine-N′-2-ethanesulfonic acid (HEPES), and calcium-depleted α-lactalbumin were purchased from Sigma (St. Louis, MO, U.S.A.). The α-lactalbumin was prepared fresh daily as a 2 mg/l solution in water.

Equipment

A Hewlett-Packard (HP) (Palo Alto, CA, U.S.A.) Model 1090 chromatograph equipped with a diode array detector, HP 85B personal computer, DPU multi-channel integrator, HP 9121 disc drives, and an HP 7470 A graphics plotter, was used. The column temperature was controlled by immersing the column in a thermostatted water bath (Lauda RC6, Brinkmann). To improve temperature equilibration of the mobile phase, a coiled tube was inserted in the mobile phase line and immersed in the water bath.

Stationary phases

Poly(methyl)-, -(ethyl)- and -(propyl) aspartamide columns (PolyLC), were obtained from the Nest Group (Southboro, MA, U.S.A.). The Spherogel-CAA-HIC was obtained from Beckman (San Ramon, CA, U.S.A.). The aspartamide columns were 250 × 4.6 mm, while the Beckman column was 100 × 4.6 mm.

Mobile phases

Weighed amounts of the salts were dissolved in a volumetric flask, and the pH was adjusted with either glacial acetic acid or ammonium hydroxide. The premixed phosphate buffered saline (PBS) was dissolved in HPLC-grade water according to the supplier's instructions. The HPLC-grade water was degassed prior to use, and all solvents were filtered through 0.45-μm Nylon 66 filter (Rainin, MA, U.S.A.).

The following mobile phase pairs were used:

(IA) 2 *M* ammonium sulfate, 0.05 *M* ammonium acetate (pH 6)
(IB) 0.05 *M* ammonium acetate (pH 6),
(IIA) 2 *M* ammonium sulfate, 0.05 *M* HEPES (pH 7.5)
(IIB) 0.05 *M* HEPES (pH 7.5),
(IIIA) 2 *M* ammonium sulfate, PBS (pH 7.4)
(IIIB) PBS (pH 7.4)

Gradient conditions

Two different gradient systems were used for the elution of α-lactalbumin: a 25- or a 5-min linear gradient, from 0 to 100% B solvent. The flow-rate was 1 ml/min and the elution was monitored at 280 nm.

RESULTS AND DISCUSSION

The effect of temperature on the retention time of α-lactalbumin using different HIC columns

The retention times of calcium-depleted α-lactalbumin at different temperatures are shown in Fig. 1 using the poly(alkyl)aspartamide columns. Chromatography was performed at pH 6.0 using ammonium acetate in both mobile phase A and B. A 20-min descending linear gradient of ammonium sulfate was used for protein elution. A marked change in the retention time as a function of the chromatographic temperature is evident in Fig. 1 from which a number of observations can be made. First, the retention of α-lactalbumin increases with increasing stationary phase hydrophobicity. Under identical mobile phase and temperature conditions α-lactalbumin elutes first from the methyl, then the ethyl, then the propyl column. This retention behavior is expected, since elution should occur at a well defined interfacial tension, which is ultimately determined by the given protein–stationary and mobile phase combination. Because the surface tension of these stationary phases decreases with increasing hydrophobicity while the surface tension changes of the mobile phase are identical, the elution order expected to be methyl > ethyl > propyl. Second, the shapes of the retention time–temperature curves at different for each column. Under these chromatographic conditions the retention time is a linear function of the temperature on the methyl column. A slightly non-linear dependence of the retention time can be observed on the ethyl column, while a clearly sigmoid elution curve is seen on the propyl column. The latter results has previously been observed for α-lactalbumin with other HIC columns.

Effect of mobile phase conditions on the elution profile of α-lactalbumin

Retention times identical to those observed with the acetate buffer, were obtained with all columns using 50 m*M* HEPES-based mobile phases at 7.5, indicating

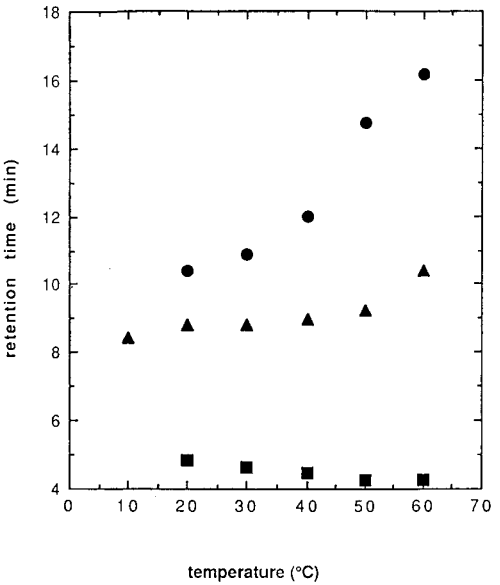

Fig. 1. Effect of surface hydrophobicity and temperature on the retention of α-lactalbumin on the poly(alkyl)aspartamide columns at pH 6.0 using the ammonium acetate-based HIC mobile phases: ■ = methyl; ▲ = ethyl; ● = propyl column. Further details on the chromatographic parameters are described in the Experimental section.

no differences between these two buffers, ionic strength and pH on the chromatograpic behavior of α-lactalbumin as a function of temperature. Next we investigated the effect of a physiological buffer system, PBS, on the chromatography of α-lactalbumin. The chromatograms of α-lactalbumin using PBS-based mobile phases at pH 7.4 are displayed in Fig. 2. At lower temperatures, α-lactalbumin elutes as a single sharp peak, which then starts to broaden as the temperature increases. At about 40°C, a new peak starts to emerge after the principal peak. At high temperatures, a single symmetrical peak, slightly broader than at low temperatures is observed. Previous studies identified the earlier eluting peak as the native conformation of α-lactalbumin, while the late eluting peak represents the denatured form[26]. The retention time shifts as a function of conformational change are in agreement with solution studies on the denaturation of α-lactalbumin. A significant increase in the Stokes radius of α-lactalbumin has been observed as denaturation progresses[28], which is accountable for increased complementary surface area, consequently longer retention time.

In Fig. 3A, the retention times of α-lactalbumin at different temperatures are displayed using a propyl column and PBS-based mobile phases. The change in the salt type and composition apparently changes the shape of the retention time–temperature curve. The curve has three characteristic segments: at low and high temperatures the retention time is a linear function of the ascending temperature and between those extremes, the retention sharply increases with increasing temperature. Similar curves were obtained using the methyl, ethyl and Beckman columns, illustrating the occurrence of a general trend.

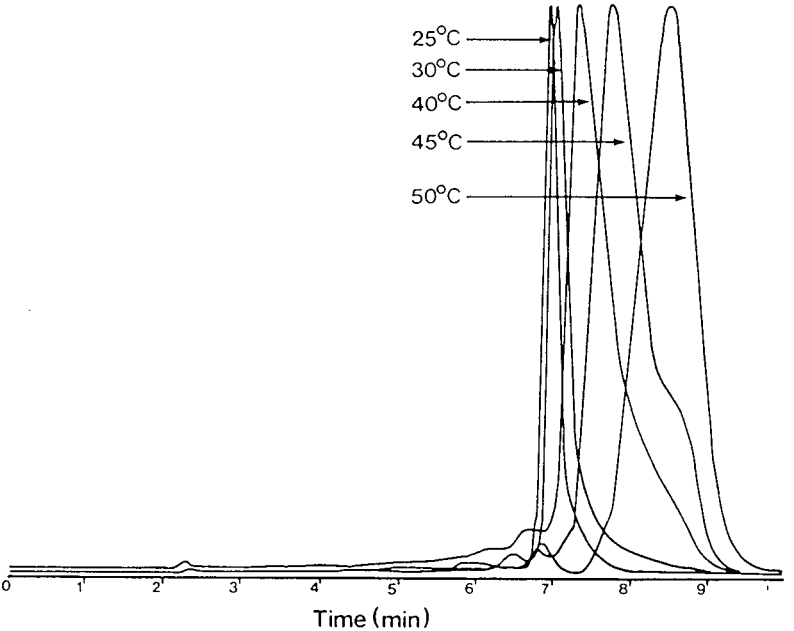

Fig. 2. Effect of temperature on the chromatograms of α-lactalbumin on the poly(propyl)aspartamide column at pH 7.4 using the PBS-based HIC mobile phases. The peak areas in the figure are not comparable because the chromatograms were normalized to better represent the characteristic change in the retention time and peak shape. Further details on the chromatographic parameters are described in the Experimental section.

These retention time–temperature curves resemble the classical thermal transition curves of α-lactalbumin denaturation obtained by spectroscopic techniques[29]. Similar transition curves have been obtained previously in reversed-phase chromatography following the temperature dependency of the peak height of ribonuclease A as a function of temperature[18]. Various parameters such as peak height, retention volume (time), peak width, peak symmetry, or the appropriate statistical moments can be used to indicate changes as a function of temperature. The appropriate parameter might differ in various applications and should be selected on the basis of its sensitivity to denaturation.

Analysis of the retention–temperature curves

Classical transition curves have been constructed for proteins in solution using spectroscopic data acquired by techniques such as UV, circular dichroism and fluorescence. The free energy of unfolding has been estimated from a two-state model, in which a native protein undergoes thermal unfolding to a denatured form.

Based on the obvious similarity between the classical transition curves and the one shown in Fig. 3A, we assumed a two-state denaturation model, and applied the classical methodology to quantitate the thermodynamic values of protein denaturation under HIC conditions.

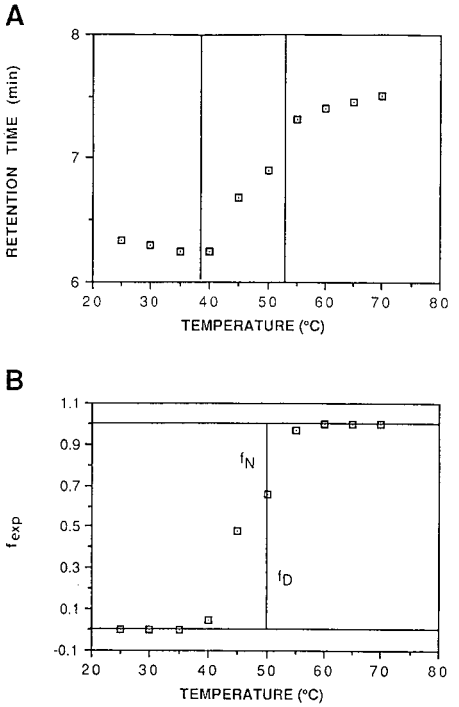

Fig. 3. (A) Effect of temperature on the retention time of α-lactalbumin on the poly(propy)aspartamide column at pH 7.4 using the PBS-based HIC mobile phases. Chromatographic conditions as in Fig. 2. (B) The transition curves of α-lactalbumin. The f_{exp} values were calculated, according the description in the text based on the data displayed in Fig. 3A.

In the present work the following simple model was used as a basis of further theoretical analysis.

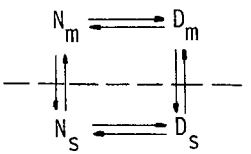

where N_m and N_s are the native forms in the mobile phase (m) and on the surface (s) respectively, and D_m and D_s are the corresponding denatured forms. The early eluting peak, at any given temperature T, corresponds to N_s and the late eluting one to D_s. We assume that the concentration ratio of the two peaks is determined by the adsorption on the stationary phase, and the conformational effects of the mobile phase can be ignored as a first approximation. Accordingly, we will concentrate on the equilibria displayed in the lower part of the model as $N_s \rightleftarrows D_s$.

In general, the fraction of the unfolded population (f_{exp}) of α-lactalbumin can be calculated from chromatographic data as follows,

$$f_{exp} = \frac{t_{exp} - t_N}{t_D - t_N} \tag{1}$$

where t_{exp} is the measured retention time and t_N and t_D are the extrapolated retention times of the native and denatured components, respectively, at temperature T if denaturation would not occur. It is known that the retention time is a linear function of the column temperature in systems where the mechanism of the retention not changing with the temperature. The extrapolated retention times have only theoretical value without any physical explanation, as in the classical denaturation studies, and they serve as numbers for further calculations.

In eqn. 1, the only experimentally determined value is t_{exp}; t_N has been calculated using linear regression. The number of data points used for the regression procedure were chosen to optimize the regression coefficient. Once the parameters (A and B) of the fitted line have been obtained from the $t_{exp} = AT + B$ equation, the t_N value can be calculated. Similarly, the t_D value can be obtained at any given temperature, using linear regression on the t_{exp} data of the high-temperature section of the transition curve.

According to the two-state model, the fractions of the native (f_N) and denatured (f_D) components can be determined as $f_N = 1 - f_{exp}$, and $f_D = f_{exp}$. The equilibrium constant of denaturation (K_d) can be expressed as

$$K_d = \frac{f_D}{f_N} = \frac{f_{exp}}{1 - f_{exp}} \tag{2}$$

In Fig. 3B the f_{exp} values calculated from the data shown in Fig. 3A have been plotted as a function of the temperature.

Effect of stationary phase hydrophobicity on the transition temperature T_{tr}

To further investigate the contribution of the stationary phase on the denaturation process, the chromatography was repeated under identical elution conditions as described in Fig. 2, using the Poly(ethyl)aspartamide, the Poly(methyl)aspartamide and the Beckman CAA-HIC columns. The retention times have been converted to f_{exp} values and the transition curves are displayed in Fig. 4. The results show that the most significant retention changes occur over a 2–4°C temperature range for the poly-(methyl) and -(ethyl) columns and these portions of the curves are parallel. The transition range for the propyl and the Beckman phase is wide, covering an approximately 20°C temperature range. This broadening can be the result one of two major causes, which were neglected above. First, it is possible that the two-state denaturation model is not quite correct, in which case conformational intermediates can exist in the transition region but the resolution of the column does not allow the separation of those species[30,31]. Secondly, it is possible that the two-state model is correct, but conformational changes in the mobile phase cannot be excluded from the model.

Based on previous results, the second explanation appears correct[26]. Wavelength ratios of the upslope side of the α-lactalbumin peak differ from those of the apex and the downslope side. The values of the upslope side are similar to the values of the native protein[26]. It was shown in previous reversed-phase liquid chromatography studies[21,32,33], that conformational refolding in the mobile phase results in a broad peak. The native form elutes in the upslope side of the peak and the denatured form in

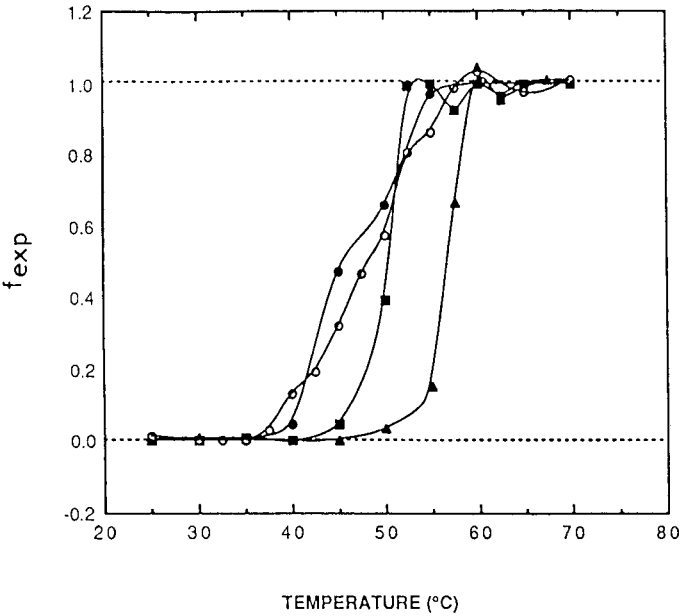

Fig. 4. Transition curves of α-lactalbumin on different HIC columns: ■ = methyl; ▲ = ethyl; ● = propyl; ○ = CAA-HIC column. Further details on the chromatographic parameters are described in the Experimental section.

the tail side of the peak. This behavior has been observed in RPLC of ribonuclease A (refs. 18 and 21) as well as in HIC of α-lactalbumin[26].

With respect to the column effects on the transition temperature of α-lactalbumin, the following observation can be made from Fig. 4. The transition temperature on the propyl column is *ca.* 46°C, on the methyl column *ca.* 50°C and on the ethyl column *ca.* 56°C. It is known that α-lactalbumin is a calcium-binding protein (binding constant K_f *ca.* 10^6–10^9)[34,35], and the removal of the Ca^{2+} ion destabilizes the structure[36]. The transition temperature decreases from about 58°C to 31°C upon removal of calcium[37]. Sodium and potassium ions also effect α-lactalbumin conformation as a function of their concentration[38]. Sodium chloride (200 m*M*) in Tris buffer at pH 8.0 has been shown to stabilize α-lactalbumin to thermal denaturation[38,39]. PBS contains 120 m*M* sodium chloride and 2.7 m*M* potassium chloride which might affect the conformation, but the ionic strength contribution of the high (2 *M*) ammonium sulfate should be dominating[40]. It is apparent that the high ammonium sulfate concentration significantly stabilizes the α-lactalbumin conformation.

The transition temperatures obtained from the different columns do not follow the order expected from surface hydrophobicity (propyl < ethyl < methyl). The negative effect of the surface hydrophobicity on the conformational stability is illustrated by the transition temperature difference obtained on the propyl and ethyl phases. The deviation, in case of the methyl column, from the order expected from homologues, might be related to differences in the coverage, the accessibility of the aspartamide groups, and/or steric hindrances.

The calculation of the free energy of denaturation (ΔG_{app})

The deduction of the f_{exp} values allows the calculation of the apparent free energy of transition, neglecting the effects of activity, by using the following equation

$$\Delta G_{app} = -RT \ln K_d = -RT \ln \frac{f_{exp}}{1 - f_{exp}} \quad (3)$$

where R and T correspond to the universal gas constant and the absolute temperature, respectively. The free energy of denaturation (ΔG_{app}) calculated from the experimental results is compared with literature data at 25°C and displayed in Table I. The higher free energy of denaturation in the presence of calcium ions clearly indicates its effect on the stabilization of α-lactalbumin. The calculated free energies of this work are in the same order of magnitude as of the cited literature data. The free energy of denaturation of α-lactalbumin for the propyl, methyl and CAA-HIC columns are similar to each other and to the values previously obtained for the calcium-depleted α-lactalbumin in solution[41]. The seemingly high ΔG_{app} value for the ethyl column suggests the most effective stabilization by the high-salt-concentration mobile phase. The values obtained are consistent with the assumption of the apoenzyme stabilization by sodium chloride and ammonium sulfate, and structural destabilization by the hydrophobic surface. These results also indicate the possibility of a mixed-mode mechanism of denaturation, involving electrostatic and hydrophobic forces. Further investigation is necessary to understand the observed anomalies which than will help to understand the phenomena involved in protein high-performance liquid chromatography.

CONCLUSIONS

The surface hydrophobicity is a crucial parameter in hydrophobic interaction chromatography of proteins. The astronomically large variety of proteins dictates the development of novel stationary phases, including ones with different hydrophobicities. The stationary phases synthesized for HIC applications are less hydrophobic than the classical reversed phases. Accordingly, one would expect less

TABLE I

FREE ENERGY OF DENATURATION OF α-LACTALBUMIN UNDER HIC CONDITIONS AT 25°C

	ΔG^* (kcal/mol)	ΔG_{app}^{**} (kcal/mol)
No Ca^{2++}	3.76	
12 m*M* Ca^{2++}	8.86	
Propyl column		5.54
Ethyl column		10.94
Methyl column		5.14
CAA-HIC column		4.28

* Conditions: pH 7.0, data from ref. 41.

** Conditions as described in the experimental section.

surface-mediated denaturation. HIC apparently represent milder chromatographic conditions for proteins than reversed-phase chromatography and biological activity is usually recovered after separation. One of the main reasons for the popularity of HIC is the erroneous belief that denaturation cannot occur in HIC. However, it must be noted that protein denaturation is a complex phenomenon depending on numerous environmental parameters such as pH, temperature, ionic strength, dipole of the solvents and the surface hydrophobicity. Certain proteins will unfold under HIC conditions if the other parameters permit.

Thermodynamic analysis of chromatographic data according to a two-state model permitted the quantitative comparison of different HIC columns. The hydrophobicity of the stationary phase affects the retention time and peak shape of proteins under hydrophobic interaction chromatographic conditions. Increasing surface hydrophobicity resulted in longer retention times applying identical mobile phases. Greater surface hydrophobicity in conjunction with high temperature favors denaturation conditions. High concentrations of ammonium sulfate, as expected, stabilize the tertiary structure of α-lactalbumin.

It has been shown that the selection of the column has a major impact on the separation, on the apparent efficiency of the column, on the denaturation and on the mass and/or activity recovery of α-lactalbumin. To understand the phenomena involved, a series of commercially available columns designed for HIC have been evaluated. Columns prepared by the same bonding chemistry and with systematically varied hydrophobicity are helpful to design and optimize separations. The thermodynamic method used for the α-lactalbumin model system may be useful for quantitative column comparison and for the evaluation of other chromatographic parameters, such as pH, column temperature and buffer type.

The primary goal of the present work was to provide a simple method to compare different columns under identical chromatographic conditions. The extension and detailed study to the quantitative characterization of surface hydrophobicity will be the subject of continuing work. Careful understanding of the role of column characteristics, such as bonding chemistry, coverage, surface area, and the weight of the stationary phase in the packed column would allow one to make quantitative evaluation of different stationary phases, and understand their roles on the retention mechanism and on the protein denaturation process.

ACKNOWLEDGEMENTS

Thanks are due to Drs. Joel K. Swadesh and Cynthia Randall for helpful suggestions and review of the manuscript.

REFERENCES

1 J. L. Fausnaugh, E. Pfannkoch, S. Gupta and F. E. Regnier, *Anal. Biochem.*, 137 (1984) 464.
2 D. L. Gooding, M. N. Schmuck and K. M. Gooding, *J. Chromatogr.*, 296 (1984) 107.
3 J.-P. Chang, Z. El Rassi and Cs. Horváth, *J. Chromatogr.*, 319 (1985) 396.
4 S. C. Goheen and S. C. Engelhorn, *J. Chromatogr.*, 317 (1984) 55.
5 Y. Kato, T. Kitamura and T. Hashimoto, *J. Chromatogr.*, 292 (1984) 418.
6 N. T. Miller, B. Feibush and B. L. Karger, *J. Chromatogr.*, 316 (1984) 519.
7 A. J. Alpert, *J. Chromatogr.*, 359 (1986) 85.

8 J. Porath, L. Sundberg, N. Fornstedt and P. Ohesson, *Nature (London)*, 245 (1973) 465.
9 B. H. J. Hofstee, *Pure Appl. Chem.*, 51 (1979) 1537.
10 S. Hjertén, *Methods Biochem. Anal.*, 27 (1981) 89.
11 S. Shaltiel, *Methods Enzymol.*, 104 (1984) 69.
12 J. D. Pearson, N. T. Lin and F. E. Regnier, *Anal. Biochem.*, 124 (1982) 217.
13 S. Y. M. Lau, A. K. Taneja and R. S. Hodges, *J. Chromatogr.*, 317 (1984) 129.
14 A. J. Sadler, R. Micanovic, G. E. Katzenstein, R. V. Lewis and C. R. Middaugh, *J. Chromatogr.*, 317 (1984) 93.
15 K. A. Cohen, K. Schellenberg, K. Benedek, B. L. Karger, B. Grego and M. T. W. Hearn, *Anal. Biochem.*, 140 (1984) 223.
16 S. A. Cohen, S. Dong, K. Benedek and B. L. Karger, in I. M. Chaiken, M. Wilchek and I. Parikh (Editors), *Affinity Chromatography and Biological Recognition*, Academic Press, New York, 1984, p. 479.
17 S. A. Cohen, K. Benedek, S. Dong, Y. Tapuhi and B. L. Karger, *Anal. Chem.*, 56 (1984) 217.
18 S. A. Cohen, K. Benedek, Y. Tapuhi, J. C. Ford and B. L. Karger, *Anal. Biochem.*, 144 (1985) 275.
19 K. Benedek, B. Hughes, M. B. Seaman and J. Swadesh, *J. Chromatogr.*, 444 (1988) 191.
20 K. Benedek, S. Dong and B. L. Karger, *J. Chromatogr.*, 317 (1984) 227.
21 X. M. Lu, K. Benedek and B. L. Karger, *J. Chromatogr.*, 359 (1986) 19.
22 J. D. Andrade (Editor), *Surface and Interfacial Aspects of Biomedical Polymers*, Vol. 2, Protein Adsorption, Plenum Press, New York, 1985.
23 K. Benedek, in preparation.
24 P. Štrop, *J. Chromatogr.*, 294 (1984) 213.
25 J. L. Fausnaugh and F. E. Regnier, *J. Chromatogr.*, 359 (1986) 131.
26 S.-L. Wu, K. Benedek and B. L. Karger, *J. Chromatogr.*, 359 (1986) 3.
27 S.-L. Wu, A. Figueroa and B. L. Karger, *J. Chromatogr.*, 371 (1986) 3.
28 Y. Hiraoka, T. Segawa, K. Kuwajima, S. Sugai and N. Murai, *Biochem. Biophys. Res. Commun.*, 95 (1980) 1098.
29 Y. Hiraoka and S. Sugai, *Int. J. Peptide Protein Res.*, 23 (1984) 535.
30 M. J. Kronman, S. K. Sinha and K. Brew, *J. Biol. Chem.*, 256 (1981) 8582.
31 M. Mitani, Y. Harushima, K. Kuwajima, M. Ikeguchi and S. Sugai, *J. Biol. Chem.*, 261 (1986) 8824.
32 A. Permyakov, L. A. Morozova and E. A. Burstein, *Biophys. Chem.*, 21 (1985) 21.
33 Y. Hiraoka and S. Sugai, *Int. J. Peptide Protein Res.*, 26 (1985) 252.
34 P. L. Privalov, *Adv. Protein Chem.*, 33 (1979) 167.
35 W. R. Melander, H. J. Lin, J. Jacobson and Cs. Horváth, *J. Phys. Chem.*, 88 (1984) 4527.
36 W. R. Melander, H. J. Lin, J. Jacobson and Cs. Horváth, *J. Phys. Chem.*, 88 (1984) 4536.
37 K. Gast, D. Zirwer, H. Welfle, V. E. Bychkova and O. B. Ptitsyn, *Int. J. Biol. Macromol.*, 8 (1986) 231.
38 W. Pfeil, V. E. Bychkova and O. B. Ptitsyn, *FEBS Lett.*, 198 (1986) 287.
39 J.-J. Schaer, M. Milos and J. A. Cox, *FEBS Lett.*, 190 (1985) 77.
40 J. CL. Van Ceunebroeck, J. Krebs, I. Hanssens and F. Van Cauwelaert, *Biochem. Biophys. Res. Commun.*, 95 (1986) 604.
41 M. Ikeguchi, K. Kuwajima, M. Mitani and S. Sugai, *Biochemistry*, 25 (1986) 6965.

Journal of Chromatography, 458 (1988) 105–116
Elsevier Publishers B.V., Amsterdam — Printed in The Netherlands

CHROMSYMP. 1439

NEW HIGH-PERFORMANCE LIQUID CHROMATOGRAPHY-BASED METHODOLOGY FOR MONITORING THE CONFORMATIONAL TRANSITIONS OF SELF-ASSOCIATING HYDROPHOBIC PEPTIDES, INCORPORATED INTO LIPOSOMES

MARÍA DEL CARMEN BAÑÓ, LORENZO BRACO* and CONCEPCIÓN ABAD*
Departament de Bioquímica i Biología Molecular, Facultades de Ciencias, Universitat de Valencia, 46100 Burjassot, Valencia (Spain)

SUMMARY

A new high-performance size-exclusion chromatographic strategy is reported for the analysis of the hydrophobic self-associating peptide gramicidin A, incorporated into artificial phospholipid vesicles (liposomes). The method is based on the direct injection of a few microlitres of the gramicidin A-containing liposome suspension into the column, which is eluted with a non-polar solvent, such as tetrahydrofuran. The type and amount of information which can be derived from this methodology have been evaluated. Using this chromatographic approach, a correlation has been unambiguously shown to exist between the organization of the peptide in the vesicles and a number of variables involved in the method of preparation of liposomes. Finally, a gramicidin A conformational transition has been monitored in the phospholipid vesicles which proved to be dependent on the class of phospholipid present in the liposome.

INTRODUCTION

In previous papers we have described the high-performance size-exclusion chromatographic (HPSEC) characterization of the dimer–monomer conformational equilibrium of the hydrophobic peptide gramicidin A (GA) in non-polar organic solvents by using an Ultrastyragel 1000-Å column, isocratically equilibrated with tetrahydrofuran (THF)[1–3]. More recently, an extension of this method has been reported which allows the analysis of the GA conformational equilibrium in more polar organic solvents, (*e.g.*, ethanol[4], and therefore the study of the interaction of this peptide with different metal cations, in particular Ca^{2+}, in terms of the dimer–monomer transition[5]. The advantages of this chromatographic methodology have been discussed previously[4].

* Present address: Department of Chemistry, Massachusetts Institute of Technology, Cambridge, MA 02139, U.S.A.

0021-9673/88/$03.50

Based on these preliminary results and taking into account the current great interest in the study of hydrophobic self-associating peptides because of their ability to form transmembrane channels in lipid bilayers[6–8], we propose in this paper a novel strategy for the HPSEC analysis of GA, incorporated into artificial phospholipid vesicles (liposomes). The method involves the direct injection of a few microlitres of the aqueous GA-containing liposome suspension into the column, equilibrated with THF, so that the vesicles are immediately disrupted, releasing the polypeptide conformational species to the eluent stream. Evidence is presented that the elution profiles obtained can provide valuable information on some features of the conformational state of GA in the liposome before injection.

On the other hand, since it has been reported that spectroscopic techniques indicate that different conformations of the peptide can exist in the phospholipid bilayers, depending on the method of liposome preparation[9–11], our attention has been primarily focused on relating the information obtained from the chromatographic analysis of the liposomes to a number of variables and experimental parameters involved in the preparation steps: the nature of the organic solvent(s), the incubation time in organic solvent, the class of phospholipid, the "age" of the liposomes, etc. Since one of the most widely used methods of incorporation of GA into the artificial vesicles is the solubilization of both lipid and peptide in an organic solvent (or solvent mixture)[12–15], a study has been first carried out in an organic solvent. The results thus obtained have later been compared with those obtained from liposomes. In addition, a slow GA conformational transition in the liposome has been directly followed as a function of the incubation time of the vesicles, which has shown to be strongly dependent on the type of phospholipid used.

Thus, the proposed HPSEC approach emerges as a rapid and accurate method which helps to provide —especially in combination with other, more conventional spectroscopic techniques— a deeper insight of the properties and organization of GA and other natural or synthetic self-associating polypeptides, incorporated into model membranes.

EXPERIMENTAL

Apparatus

The liquid chromatograph consisted of an M510 solvent-delivery system, an U6K universal injector and a 490 programmable multiwavelength detector, all from Waters Assoc. (Milford, MA, U.S.A.). The system was equipped with a 100-nm pore-size Ultrastyragel column (Ultrastyragel 1000 Å, 30 cm × 0.78 cm I.D.) from Waters. The elution profiles were recorded on a dual-channel recorder (Yokogawa Electric Works, Tokyo, Japan).

Fluorescence experiments were performed in a MPF-44B spectrofluorometer (Perkin-Elmer, Überlingen, F.R.G.) with automatic correction of excitation or emission spectra. The excitation was at 297 nm, and the emission intensity was recorded at 330 nm; the excitation and emission slits were 4 and 8 nm, respectively. The temperature was controlled within ± 0.1°C by using a Lauda Compact Thermostat MT-20 (Lauda, Königshofen, F.R.G.).

Chemicals and reagents

Gramicidin A (natural mixture) was supplied by Koch Light Labs. (Buckinghamshire, U.K.) and was used as received. Egg yolk phosphatidylcholine (PC) was from Merck (Darmstadt, F.R.G.) and purified according to the column chromatographic method of Singleton *et al.*[16]. The phospholipid gave a single spot when analysed by thin-layer chromatography. L-α-Phospatidyl-L-serine (PS) from bovine brain, tripalmitin, triolein, palmitic acid and cholesterol were obtained from Sigma (St. Louis, MO, U.S.A.) and were used without further purification. All solvents (THF, chloroform, ethanol, methanol) were of spectroscopic grade (Merck). They were passed through a 0.45-μm regenerated cellulose filter (Filtration System, Dublin, CA, U.S.A.) before use.

Procedures

All chromatographic experiments were conducted at room temperature. The column was always eluted isocratically with THF at a flow-rate of 1.0 ml/min. The injection volume was 2 μl, unless otherwise stated.

GA samples were prepared in THF, as described previously[1,2], and stirred for 1 min immediately after preparation, both in the absence and presence of lipid. Tightly stoppered 10-ml glass tubes were completely filled with the corresponding solutions to minimize hydration and stored in a dark room at 25°C until injection. GA samples, prepared in ethanol, methanol or chloroform–methanol (2:1, v/v), were stirred for 30 s, and aliquots were taken at different times and injected. Aliquots from the same samples were used when combinations of chromatographic and fluorimetric measurements were made.

Dispersions of small unilamellar vesicles (SUVs) were prepared as follows; both PC (or PS) and GA were dissolved in an organic solvent by mixing identical volumes (each 100 μl) of stock solutions. After a given time of incubation of the orgnanic GA phospholipid solution, which varied from a few seconds (referred to as zero time) to 15 h, the solvent was rapidly evaporated under a nitrogen stream and then under high vacuum overnight to remove any traces of solvents. The samples were then hydrated by the addition of 1 ml of Millipore ultrapure water, incubated for 10 min (unless otherwise stated) on ice. The sonicated material was then centrifuged for 15 min at 35 000 *g* to remove probe particles and the remaining multilamellar liposomes. The lipid/polypeptide mole ratio was 50:1. Other details of the experimental conditions used can be found in the corresponding Figure legends.

RESULTS AND DISCUSSION

Characterization of gramicidin A in organic solvents

Since the current methods of preparation of GA-containing liposomes make indiscriminate use of a relatively wide variety of organic solvents (or mixture), varying their polarity and chemical nature, we first studied the peptide conformational equilibrium as a function of incubation time in a set of solvents typically reported in the literature[9,11–15]. Fig. 1 shows as an example the elution profiles of GA samples at a concentration of 0.074 mg/ml, in THF, ethanol, chloroform–methanol (2:1, v/v) and methanol, once equilibrium had been reached.

As previously described[1–4], the peak eluted at 7.9 ml corresponds to intertwined

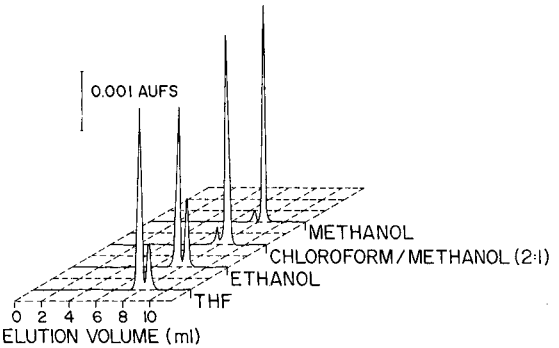

Fig. 1. Elution profiles of GA samples in different organic solvents. The samples (0.074 mg/ml) were prepared by directly dissolving the peptide in the organic solvent. After equilibrium had been reached, 2 μl were injected in all cases. Column: Ultrastyragel 1000 Å. Mobile phase; THF; flow-rate, 1.0 ml/min.

double-helical dimers, whereas that at 8.4 ml corresponds to monomers. As expected, the ratio of both conformational species dramatically varies with the solvent. In the less polar THF the predominant species at equilibrium is the dimer, whilst the monomer predominates in methanol. Fig. 2 shows the kinetic results for GA monomerization (expressed as the disappearance of double-helical dimers) in the aforementioned solvents, at 0.74 mg/ml peptide concentration. This GA concentration is the same as that used later in this work in organic solvents during the preparation of liposomes. Note that at zero time there is 100% of dimeric species because this is the conformation of the commercially available solid gramidicin sample[1]. The mass fraction of each species was directly evaluated from the heights of the peaks, as reported elsewhere[1,2]. Both elapsed time and an increase in solvent polarity result in a shift towards monomeric forms (a decrease in the mass fraction of dimers). It is clear that the time needed for equilibrium to be reached can vary from more than 20 days in THF to a few minutes in methanol. This is of particular interest, as will be later shown, since numerous methods of preparation of liposomes currently reported in the

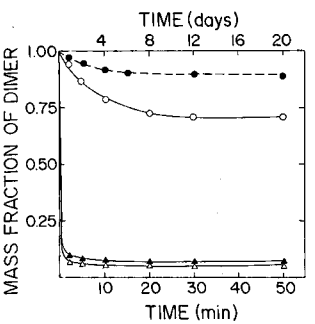

Fig. 2. Kinetic profile of the disappearance of GA double-helical dimers in THF (●), ethanol (○), chloroform–methanol (2:1, v/v) (▲) and methanol (△). The GA concentration was 0.74 mg/ml in all cases. The mass fractions of dimers, calculated from the peak heights in the chromatograms, are plotted *vs.* the time at which each aliquot was taken. The solid lines correspond to the lower axis, and the dotted line to the upper one.

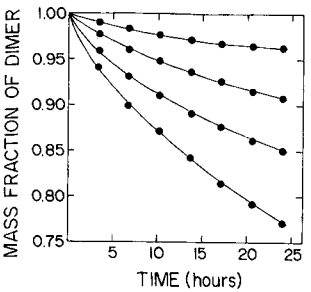

Fig. 3. PC-induced time-dependent monomerization of GA in THF. GA concentration was always 0.74 mg/ml. PC concentrations from top to bottom were: 0, 0.20, 0.33 and 0.50 mg/ml.

literature describe the incubation of the peptide in a given organic solvent during a period of time that is usually not well defined or rather arbitrarily chosen. However, even at short incubation times, the ratio of conformational species strongly depends on the solvent used (see Fig. 2). On the other hand, it was verified by means of a previously reported procedure[2] that the chromatographic results in Fig. 2 in all cases fitted a simple equilibrium model, dimer $\rightleftharpoons$ 2 monomers (results not shown).

It is well known that one of the classical methods of preparation of GA-containing liposomes consists of the simultaneous solubilization of a lipid and a peptide in an organic solvent (or mixture of solvents), followed by complete removal of the solvent and further hydration of the remaining mixed film[12–15]. Since different classes of phospholipids as well as mixtures of phospolipids with other types of lipids have been widely used for solubilization, and based on our previous observation that PC induces a time-dependent monomerization of GA in non-polar solvents[1,2], the influence of different lipid classes on the peptide conformational equilibrium in THF was next investigated. Fig. 3 shows the results obtained for the mass fraction of dimers as a function of time at 0.74 mg/ml GA for different PC concentrations. Similar to the behaviour at other GA concentrations[2], an increase in the phospholipid concentration results in a higher extent of dimer dissociation for the same incubation time. However, the equilibrium proved to be sensitive to the class of lipid used, as demonstrated by the results summarized in Table I, where a series of lipids differing in the type of polar head, chain length and degree of unsaturation are compared by means of HPSEC and fluorescence emission spectroscopy (taking advantage of the Trp residues of GA). All measurements were carried out after incubation for 10 days, the peptide concentration being as low as 0.025 mg/ml to allow reliable spectroscopic data. As deduced from the chromatographic results, the GA conformational equilibrium is drastically altered by PC towards monomeric forms, whereas it is not significantly affected by any other of the lipids assayed. This is supported by the fluorescence measurements where a clear enhancement of the peptide emission intensity (which was previously related to a strong lipid polar head–peptide interaction[2]) is again observed only for PC. Note that in the case of PS, altough the ratio of conformational species is not significantly altered, some fluorescence quenching occurs as the phospholipid concentration increases (Table I). A possible explanation for this will be given below.

However, the PS–GA system in THF proved to be particularly interesting, from the chromatographic point of view, as revealed by the elution profiles obtained. Fig.

4A depicts some actual chromatograms of PS–GA mixtures as a function of the phospholipid concentration. On the one hand the ratio of the heights of dimer and monomer peaks remains invariable (and so does the mass fraction of each species), on the other hand a peak emerging at 6.3 ml has an area which increases linearly with PS concentration, as evidenced in Fig. 4B. The expected molecular weight corresponding to a species at such an elution volume, when interpolated in the column calibration, is higher than 10^4. This suggests the presence of PS reversed micelles, presumably stabilized in THF by a strong interaction among the phospholipid polar-head dissociable groups (the PS contains an additional carboxylic group in its polar moiety relative to the PC). This assumption is supported by: (i) our own experimental chromatographic observations using other charged phospholipids (such as phosphatidic acid, results not shown), which also give in THF a peak at *ca.* 6.5 ml, and (ii) literature data indicating that natural phospholipids can exist in certain non-aqueous solvents as reversed micelles[17,18]. The PS reversed micelles seem to exclude any peptide molecule from their polar interior (since the absolute heights of the GA peaks do not change either) so that the conformational equilibrium is practically unaltered. On the other hand, these observations seem particularly exciting, because, as far as we know, this is the first time that reversed micelles of natural amphiphiles such as phospholipids are eluted from a high-performance gel permeation support, namely Ultrastyragel 1000 Å, and it undoubtedly offers new possibilities for further studies with reversed micelles of both natural and synthetic surfactants. It must be pointed out that the data in Fig. 4B do not allow a reliable determination of the critical micelle concentration (c.m.c.) for PS in THF, though the value appears to be relatively low.

Finally, the cause of the GA fluorescence quenching in the presence of PS (Table I) is not completely understood, but taking into account that there is no direct interaction between the lipid polar heads and the peptide, it seems reasonable to suggest that it may be due to a deactivation of the GA fluorophores in the excited state through direct collisions with the micelles. These differences should be taken into account in the preparation of liposomes and, in fact, they will be considered again later in this work.

Characterization of gramicidin A in liposomes

It can be concluded from the results in the previous section that the GA dimer–monomer conformational equilibrium in organic solvents is very sensitive to

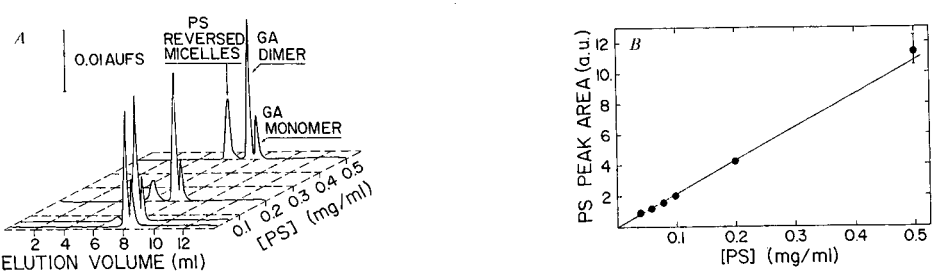

Fig. 4. (A) Elution profiles of GA in THF after 10 days of incubation, as a function of PS concentration. The GA concentration was always 0.025 mg/ml. Injection volume: 75 μl. (B) Plot of the area of the PS reverse micelles peaks (in arbitrary units) *vs.* PS concentration in THF.

a series of factors, such as the nature of the solvent (Figs. 1 and 2), peptide concentration[2], incubation time (Fig. 2), presence of lipid (Figs. 3 and 4A), lipid-to-peptide mole ratio (Fig. 3), lipid class (Table I), etc. Thus, since most of these variables have been used in a rather arbitrary way in the preparation of GA-containing liposomes reported in the literature, and they do affect the actual ratio of conformational species in organic solvents, it seems reasonable to assume that they will also influence the conformational state of the incorporated peptide. In other words, the conformation of the GA in a liposome must be somehow dependent on the "history" of how it was prepared. Altough there is some evidence of this dependence on some of the factors mentioned above[9,11], the characterization of GA incorporated in artificial phospholipid vesicles has been carried out so far only by means of spectroscopic techniques, especially circular dichroism (CD)[9,11,14,19–20]. The latter has shown that the CD spectra are not always identical but vary largely with the incorporation method and the particular experimental conditions used[9–11,14]. For example, it has recently been reported that the solvent-determined conformation of gramicidin affects some peptide properties in model membranes[11]. In this context, the HPSEC method we propose below can be considered as a new, more direct approach (valuable in itself but at the same time complementary to other spectroscopic techniques) for the monitoring of GA incorporated into liposomes, particularly its relationship with the experimental variables involved in the preparation steps. The chromatographic procedure is based on the use of the same Ultrastyragel 1000-Å column as in the previous section, equilibrated with THF. In this case, a few microlitres of an aqueous suspension of GA-containing liposomes is directly injected so that the phospholipid vesicles will be immediately disrupted on top of the column by the organic solvent, releasing both the peptide conformational species and the lipid molecules to the eluent stream. As previously reported[21], the PC molecules strongly interact with the polystyrene–divinylbenzene matrix of the support, thus being dramatically retarded during elution. However, with respect to GA, it must be pointed out that by itself this chromatographic technique does not allow a distinction between monomers and head-to-head dimers (two juxtaposed monomers)[10], since these latter species are dissociated to monomers during elution with THF[1,2]. Thus, it must be inferred that the peak referred to as monomers in the chromatograms obtained from experiments with liposomes may contain a mixture of GA molecules originally present in the liposome as both actual monomers and head-to-head dimers. Nevertheless, since the transition from double-helical dimers (peak eluted at 7.9 ml, see Fig. 1) to monomers in THF is extremely slow, as compared to the *ca.* 10 min of elution, the percentage of double-helical dimers in the chromatogram can indeed be considered as a very reliable, accurate measure of the actual percentage of these species in the original phosholipid vesicles before injection. This parameter was, in fact, used as a probe to test the influence of the experimental conditions during liposome preparation.

The first project of interest was to use the proposed strategy to find out how different organic solvents used for the simultaneous solubilization of lipid and peptide affect the organization of GA incorporated in the liposome. Fig. 5 depicts the elution profiles corresponding to the injection of 2 μl of aqueous suspension of liposomes, prepared from PC + GA in the same solvents as those used in Fig. 1. The vesicles were injected immediately after sonication and centrifugation. As is seen, two symmetrical, perfectly resolved peaks are eluted at 7.9 and 8.4 ml, their elution volumes coinciding

exactly with those of the double-helical dimer and monomer respectively, observed after injection of solutions of GA in organic solvents (see Fig. 1).

This validates the above assumption about the mechanism of disruption of the vesicles on top of the column and the elution of the GA species. Note that if the liposome had not been clearly disrupted immediately after injection, or if some interaction between GA and PC had occurred during elution, both events should have resulted in a shift of the elution volumes, a poor resolution and/or a distortion of the peaks. In addition, it was verified that essentially the same elution profiles were obtained, by direct injection of 2 μl of aqueous liposome suspension, as were obtained when liposomes were diluted 1:25 (v/v) in THF, stirred for 10 s and 50 μl of the resulting solution were immediately injected. The water in the injected sample appeared at 11.5 ml (not shown), as monitored with a refractive index detector.

Interestingly, the observed dimer/monomer ratio drastically depends on the organic solvent using during the preparation of the liposome (Fig. 5). The double-helical dimer (probe) again predominates in the liposomes prepared by simultaneous solubilization of PC and GA in the less polar solvent (THF), whereas it is clearly a minor species in those obtained from the much more polar methanol. In the vesicles prepared from ethanol the situation is intermediate, but still the dimers are predominant. Thus, there seems to exist a clear correlation between the organization of the peptide conformational species in the liposomes, as determined by HPSEC, and the original position of the GA dimer–monomer equilibrium in the organic solvent before evaporation (Fig. 1), so that the more polar the starting organic solvent(s), the lower is the proportion of double-dimeric forms in the vesicles. The fact that the mass fraction of dimers in the liposomes prepared from THF and ethanol (Fig. 5) is slightly lower than that in the corresponding original organic solvents (Fig. 1) can be explained by taking into account that during the solubilization, even if the incubation time is very short, some lipid-induced time-dependent GA monomerization may occur (see Fig 3), especially in this case, where the lipid-to-peptide mole ratio is high. This phenomenon will be considered later in more detail. However, lipid-induced monomerization does not appear to take place when methanol is present in the organic medium, probably due to the cancellation of PC–GA interactions because of the "strength" of this solvent.

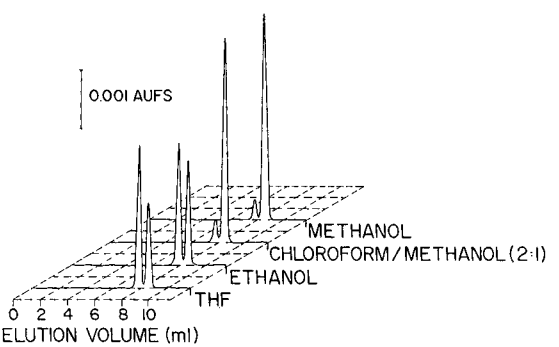

Fig. 5. Elution profiles of fresh samples of GA-containing liposomes, injected immediately after sonication and centrifugation of the vesicles. The liposomes were prepared by solubilizing the lipid and the peptide together in the organic solvent. The final GA concentration in the vesicles was 0.074 mg/ml. The injection volume was 2 μl in all cases. Column: Ultrastyragel 100 Å. Mobile phase: THF; flow-rate, 1.0 ml/min.

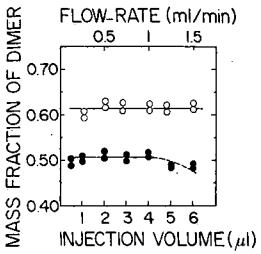

Fig. 6. Influence of the eluent flow-rate (○) and the injection volume (●) on the observed mass fraction of double-helical dimers from two different GA-containing liposome samples. GA concentration in both cases was 0.074 mg/ml.

In order to determine the interval of error due to chromatographic variables for the information obtained by means of the proposed HPSEC strategy, we determined whether changes in the flow-rate or the injection volume altered either the resolution between the dimer and monomer peaks or their ratio for a given liposome sample. Fig. 6 shows the results obtained for two liposome samples in which the dimer ratio was chosen to be different in order not to overcrowd the plot. It can be seen that neither a change in the flow-rate from 0.25 to 1.5 ml/min nor a variation in the injection volume from 0.05 to 4 μl caused any significant alteration of the value of the mass fraction of dimer within a ± 0.02 error. A very slight, artifactual decrease in the mass fraction of dimers seems to occur only for an injection volume of 5 μl or larger. It is probably due to an effect of water-induced monomerization on top of the column, since the "actual" concentration of water surrounding the GA in the injector loop is higher. In fact, we have recently shown that the addition of small proportions of water to solutions of GA in THF induces a time-dependent monomerization[3]. On the other hand, the resolution of the peaks was not affected by changes in either the flow-rate or the injection volume (not shown). In the light of these results (see Fig. 6), a flow-rate of 1.0 ml/min and an injection volume of 2 μl were selected as standard conditions for all further experimens. This allows very reliable measurements (because of the great sensitivity of the UV–VIS detector used) without damage to the column packing, as proven by the fact that the resolution after the analysis of hundreds of samples is similar to that shown in Fig. 5.

Finally, since the phospholipid and GA are usually solubilized together during the preparation of liposomes and it has been demonstrated that the peptide dimer–monomer equilibrium in organic solvent may be drastically affected by PC (see Fig. 3 and refs. 1 and 2), the influence of incubation time of the PC + GA mixture in THF on the resultant mass fraction of dimers in the vesicles was next investigated. For this purpose, aliquots were taken at different times from the lipid–peptide solution, the solvent was rapidly evaporated under a stream of nitrogen and then any traces of solvent were completely removed by rotary evaporation under vacuum overnight. The rest of the procedure followed was that described in the Experimental section. In addition, the liposomes, once prepared and sonicated, were injected immediately thereafter (which will be considered zero time for the incubation of the liposomes in water) and after 24, 48 and 72 h. Fig. 7 summarizes the chromatographic results of this experiment (solid lines), expressed in terms of the mass fraction of double-helical dimers as a function of both the incubation time in organic solvent (abcissa axis) and

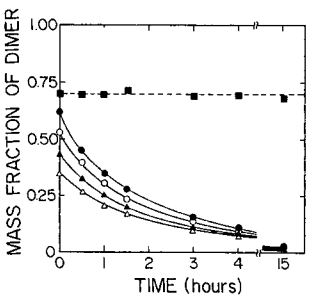

Fig. 7. Solid lines: variation of the mass fraction of double-helical dimers in GA-contaning PC liposomes as a function of both the incubation time of the lipid + peptide mixture in THF (abscissa) and the time of incubation of the vesicle suspensions, 0 (●), 24 (○), 48 (▲) and 72 h (△). The GA concentration was 0.074 mg/ml. Dotted line: mass fraction of dimers in PS liposomes as a function of the incubation time of the lipid + peptide mixture in THF. No significant change in the values was observed after incubation of the vesicles for several days.

the incubation time of the liposomes in water. The longer the incubation in THF, the lower is the rate of disappearance of double-helical dimers in the liposome. This again supports the hypothesis of a correlation between the conformational state of GA in the organic solvent before evaporation (Fig. 3) and the ratio of dimeric/monomeric species observed in the vesicles. In fact, after 15 h of incubation in THF, the remaining dimers account for less than 5% of the total GA present in the liposomes. However, a very interesting observation arises from the fact that the peptide, once the liposome is prepared, undergoes a time-dependent conformational transition, resulting in a slow, progressive decrease in the proportion of double-helical dimers (Fig. 7). This phenomenon, which we have also found to be very sensitive to incubation temperature, and its possible causes are currently under investigation, and our results will be reported elsewhere.

Based on the results in Fig. 4A and in Table I, which show that there is no interaction between PS (as opposed to PC) and GA in THF, and consequently no alteration of the dimer–monomer equilibrium due to the presence of this phospholipid in the organic solvent, it can reasonably be assumed that no variation in the mass fraction of dimers can be observed in PS liposomes, prepared by varying the incubation times of the solubilized PS + GA mixture in THF. The chromatographic results obtained with GA-containing PS vesicles are included in Fig. 7 (dotted line). In this case the liposomes were always injected immediately after sonication and centrifugation. The constant value obtained for the mass fraction of dimers as a function of the incubation time in THF corroborates the above assumption and again confirms the correlation observed in the previous experiments.

It must be pointed out that the large proportion of the mass fraction of "observed" monomers in the chromatograms may actually correspond to Urry's model of head-to-head juxtaposed dimers[22], which would emerge as monomers due to a very weak stabilization by only six hydrogen bonds, as opposed to 30 in the double-helical dimer[2,23]. Although the chromatographic strategy used cannot by itself ascertain the identity of the monomer peak in the starting liposome, we have obtained evidence supporting this assumption from the combined use of HPSEC and CD (not shown). The CD spectra of GA, incorporated into PC liposomes, clearly approach the

spectrum reported by Urry *et al.*[24] as that corresponding to the channel conformation (head-to-head dimer) both when the time of incubation in THF is increased and when the vesicles are incubated at a relatively high temperature (60°C). In both cases a simultaneous HPSEC analysis showed that the mass fraction of observed monomers approaches unity.

It should be emphasized that the results presented so far are preliminary, because they have been obtained for a particular self-associating peptide, GA, with a particular method of preparation of the liposomes. Other experimental factors involved in the preparation of the vesicles clearly remain to be analysed, such as the influence of the lipid-to-peptide mole ratio, the time of sonication of the liposomes, the incubation temperature, the presence of cations in the suspension, etc. Even more interesting is the possibility of comparing the solubilization method used with others also currently reported in the literature, such as the incorporation of GA into pre-formed vesicles, reversed-phase evaporation, etc. A great deal of additional information can be obtained by the combined use of this chromatographic method with other conventional spectroscopic techniques. For example, these approaches may help clarify the cause of the changes observed in the spectra which may be a result of conformational equilibrium when different solvents and different methods of incorporation of the peptide are used[9–11]. On the other hand, this chromatographic technique may prove to be very valuable for investigation a wide variety of other synthetic as well as natural self-associating hydrophobic peptides, incorporated in liposomes. Results of investigations of all these aspects will be the subject of future reports.

ACKNOWLEDGEMENT

This work was supported by Grant No. PB87-0996 from the Direccion General de Investigación Cientifica y Técnica (DGICYT), Spain.

REFERENCES

1 L. Braco, C. Abad, A. Campos and J. E. Figueruelo, *J. Chromatogr.*, 353 (1986) 181.
2 L. Braco, M. C. Bañó, F. Chillarón and C. Abad, *Biophys. Chem.*, 25 (1986) 297.
3 L. Braco, F. Chillarón, M. C. Bañó, M. de la Guardia and C. Abad, *Spectrochim. Acta*, Part A, 43 (1987) 1365.
4 L. Braco, M. C. Bañó, F. Chillarón and C. Abad, *J. Liq. Chromatogr.*, 10 (1987) 3463.
5 L. Braco, M. C. Bañó, A. Campos and C. Abad, *Biophys. Chem.*, 30 (1988) 93.
6 M. Colapietro, P. de Santis, A. Palleschi and R. Spagna, *Biopolymers*, 25 (1986) 2227.
7 E. W. Barret Russell, L. B. Weiss, F. I. Navetta, R. E. Koeppe II and O. S. Andersen, *Biophys. J.*, 49 (1986) 673.
8 Y. Trudelle and F. Heitz, *Int. J. Pept. Protein Res.*, 30 (1987) 163.
9 L. Masotti, A. Spisni and D. W. Urry, *Cell Biophys.*, 2 (1980) 241.
10 B A. Wallace, *Biophys. J.*, 49 (1986) 295.
11 H. Tournois, J. A. Killian, D. W. Urry, O. R. Bokking, J. de Gier and B. de Kruijff, *Biochim. Biophys. Acta*, 905 (1987) 222.
12 D. C. Lee, A. A. Durrani and D. Chapman, *Biochim. Biophys. Acta*, 769 (1984) 49.
13 J. A. Killian, A. J. Verkleij, J. Leunissen-Bijvelt and B. de Kruijff, *Biochim. Biophys. Acta*, 812 (1985) 21.
14 D. C. Shungu, J. F. Hinton, R. E. Koeppe II and F. S. Millet, *Biochemistry*, 25 (1986) 6103.
15 K. W. Short, B. A. Wallace, R. A. Myers, S. P. A. Fodor and K. Dunker, *Biochemistry*, 26 (1987) 557.
16 W. S. Singleton, M. S. Gray, M. L. Brown and J. C. White, *J. Am. Oil Chem. Soc.*, 92 (1965) 53.

17 E. A. Dennis, A. A. Ribeiro and M. F. Roberts, in K. C. Mittal (Editor), *Solution Chemistry of Surfactants*, Vol. 1, Plenum, New York, London, 1979, p. 175.
18 P. L. Luisi and B. E. Straub, *Reverse Micelles*, Plenum, New York, 1984.
19 F. Heitz, A. Heitz and Y. Trudelle, *Biophys. Chem.*, 24 (1986) 149.
20 B. A. Wallace, W. R. Veatch and E. R. Blout, *Biochemistry*, 20 (1981) 5754.
21 L. Braco, M. C. Bañó, C. Abad and A. Campos, *J. Liq. Chromatogr.*, 9 (1986) 121.
22 D. W. Urry, M. C. Goodall, J. D. Glickson and D. F. Mayers, *Proc. Natl. Acad. Sci. U.S.A.*, 68 (1971) 1907.
23 W. R. Veatch, E. T. Fossel and E. R. Blout, *Biochemistry*, 13 (1974) 5249.
24 D. W. Urry, T. L. Trapane and C. M. Venkatachalam, *J. Membrane Biol.*, 89 (1986) 107.

Journal of Chromatography, 458 (1988) 117–128
Elsevier Science Publishers B.V., Amsterdam — Printed in The Netherlands

CHROMSYMP. 1458

HIGH-PERFORMANCE LIQUID CHROMATOGRAPHIC ANALYSIS OF DNA COMPOSITION AND DNA MODIFICATION BY CHLOROACETALDEHYDE

RAM P. SINGHAL* and J. PATRICK LANDES
Department of Chemistry, Wichita State University, Wichita, KS 67208 (U.S.A.)

SUMMARY

The separation of common and modified deoxyribonucleosides derived from DNA hydrolyzates was examined under different chromatographic conditions on silica-based octadecyl (C_{18}) columns, involving hydrophobic interactions with the matrix. A novel method for the analysis of the DNA composition is described. It involves the removal of RNA contaminants and enzymatic hydrolysis of DNA, first to deoxyribonucleoside monophosphates and then dephosphorylation of the latter to deoxyribonucleosides. Hydrolysis conditions were sought to avoid deamination of dA and dC residues to dI and dU contaminants, respectively. Elution of these contaminants and the artifacts (ribonucleosides derived from RNA) is described in relation to the elution of deoxyribonucleosides. Chromatographic separation of the hydrolyzate derived from a 15-μg sample of DNA under selected separation conditions and on one high-performance liquid chromatographic column is achieved in 18 min at room temperature. Detection of modified components (and contaminants) present in minute amounts is enhanced with the use of a diode-array detector. The power of this technique lies in its ability to characterize and quantitate accurately the amount of modified species present in the DNA structure (less than 2% of all the other residues). Examples of the composition analysis of DNA derived from a prokaryote (*Escherichia coli* B) and a eukaryote (salmon sperm) are described. Details of quantitation (calibration graphs) of different nucleosides are furnished for peak-area integration by commercially available software, and spectral properties of the nucleoside in the elution buffer are described for quantitation by other means. Application of the composition analysis is shown here for probing the DNA conformation in solution by chemical means, while using chloroacetaldehyde as the modifying agent.

INTRODUCTION*

More than a decade ago, ion-exclusion and ion-exchange chromatographic methods were described for the separation of common and modified nucleosides in order to analyze the base composition of nucleic acids[1–5]. Recently, separations

* Abbreviations: dN, deoxyribonucleoside; rN, ribonucleoside; A, adenosine; C, cytidine; G, guanosine; I, inosine; T, thymidine; U, uridine; CAA, chloroacetaldehyde.

0021-9673/88/$03.50

involving hydrophobic interactions on reversed-phase chromatographic matrices have been explored in order to obtain fast and sensitive separations of the nucleosides[6–9]. The need for novel methods of DNA analysis is realized with renewed interest in the role of the modified components of DNA[10–12]. 5-Methyldeoxycytidine (m^5dC) and 6-methyldeoxyadenosine (m^6dA), the minor components of eukaryotic and prokaryotic DNAs, respectively, are present primarily in less than 2% of all the other residues[12]. In general, DNA samples are often available only in microgram amounts. Several procedures involving hydrophobic interactions have been described recently, which offer fast and sensitive methods for the separation of deoxyribonucleosides[6–9]. We recently described a microprocessor-controlled (hardware and software) high-performance liquid chromatographic (HPLC) system for data acquisition, data processing and analysis of the deoxynucleosides[13–15]. A method of DNA analysis at the sub-nanomolar level is described here. Details of the sample (DNA) purification, hydrolysis to deoxyribonucleosides, and their separation on a single reversed-phase column are reported. The study of nucleoside composition is demonstrated for probing the DNA conformation in solution by chemical means, using chloroacetaldehyde (CAA) as the modifying agent.

EXPERIMENTAL

The nucleoside separations were performed on a 250 mm × 4.6 mm I.D. column packed with 5-μm silica-based C_{18} reversed-phase chromatography material and installed with a guard column (Separation Group, Hesperia, CA, U.S.A., Model Vydac 201HS54 or Supelco, Belfonte, CA, Model Supelcosil LC-18-DB). The guard column was fitted with a 2-cm cartridge, containing 5-μm packing material. The deoxyribonucleosides and *E. coli* DNA (strain B) were purchased from Sigma (St. Louis, MO, U.S.A.). DNA from crude salmon sperm milt, obtained from Reliable Chemical (St. Louis, MO, U.S.A.) was purified in this laboratory by using Marmur's procedure[16]. The DNA sample was purified to remove RNA contaminants. The enzymes nuclease P1, pancreatic DNase I and calf intestinal alkaline phosphatase were obtained from Boehringer-Mannheim Biochemicals (Indianapolis, IN, U.S.A.) and pancreatic RNase was obtained from Worthington Biochemical (Freehold, NJ, U.S.A.).

Enzymatic digestion conditions

To remove RNA contaminants from the DNA sample, the sample was first dissolved in the buffer used for RNase digestion [50 m*M* N-tris(hydroxymethyl)-methyl-2-aminoethanesulfonic acid buffer (pH 7.7) with 0.15 *M* sodium chloride and 15 m*M* sodium citrate] and then pancreatic ribonuclease[17] (RNase) was added to the solution (0.1 enzyme unit per 1.0 A_{260} unit of DNA), followed by incubation at 45°C for 4 h. The reaction mixture was then freed from ribonucleosides by dialyzing the mixture against 20 m*M* sodium succinate buffer (pH 5.5) in microdialysis chambers (Hoefer Scientific Instruments, San Francisco, CA, U.S.A., Model EMD-101).

DNA hydrolysis was carried out with 2–4 A_{260} units (100–200 μg) of DNA in a total volume of less than 150 μl. First, the DNA was degraded to deoxyribonucleoside monophosphates by the addition of 10 μl of buffer [30 m*M* sodium acetate with 10 m*M* zinc chloride (pH 5.3)] for each A_{260} unit of DNA and an enzyme mixture

containing nuclease P_1 from *Penicillium citrinum*[18] (1 unit/μl) and pancreatic deoxyribonuclease[19] (DNase I, 0.1 unit/μl). A 1-μl volume of the enzyme mixture was added for each A_{260} unit of DNA, and the reaction mixture was incubated at 37°C for 2 h. Dephosphorylation of the deoxynucleotides was accomplished by the reaction of alkaline phosphatase. The pH of the reaction mixture was raised by the addition of 10 μl of 1 *M* sodium glycinate buffer (pH 8.0 or 8.8), then one unit of alkaline phosphatase was added for each A_{260} unit of the DNA digest, and the mixture was incubated at 37°C for 3 h.

HPLC and data processing equipment

The DNA analysis was performed with a chromatographic system consisting of (a) a manual injection valve (Rheodyne, Cotati, CA, U.S.A., Model 7125), (b) a programmable mobile phase gradient pump (Perkin-Elmer, Norfolk, CT, U.S.A., Series LC4) and (c) a diode-array effluent monitor (LKB, Bromma, Sweden, Model 2140 Rapid Spectral Detector). A minicomputer (Zenith Data Systems, St. Joseph, MI, U.S.A., Model Z-248, IBM AT-compatible) was used to operate the detection unit and also to collect and store the absorption spectrum of the effluent every 0.3 s (for example, from 220 to 300 nm) with the aid of a software program (LKB, Model Wavescan-EG).

A silica based reversed-phase C_{18} HPLC matrix of 5-μm spherical beads was used for chromatography. Separations were carried out at different temperatures and with different gradients of the mobile phase (methanol) in order to optimize the chromatographic conditions. The different elution gradient systems used for this work are described in Table I. Peak areas of the chromatogram were digitized at a wavelength of interest (*e.g.*, at 260 nm) using a commercially available software program (Nelson Analytical, Cupertino, CA, U.S.A., Model 2000, Version 3.6).

TABLE I

ELUTION GRADIENT PROGRAMS FOR THE SEPARATION OF DEOXYRIBONUCLEOSIDES

System	*Stage*	*Time (min)*	*Mode*	*Elution solvent (%)*		
				*Buffer**	*Methanol***	*THF****
A	Equil.	10	Step	100	0	0
	Start	5	Step	100	0	0
	End	15	Linear	82	18	0
B	Equil.	10	Step	95	5	0
	Start	8	Linear	78	22	0
	End	10	Linear	15	85	0
C	Equil.	10	Step	95	5	0
	Start	8	Linear	53	47	0
	End	7	Linear	15	60	25

* Buffer for system A contains 10 m*M* ammonium phosphate with 2.5% methanol (pH 5.3); buffer for system B contains 20 m*M* sodium succinate with 0.5 m*M* sodium azide (pH 5.3 or 5.5); sodium azide is routinely added to the buffer to prevent bacterial growth.

** 100% methanol.

*** 100% tetrahydrofuran.

Quantitation of each deoxyribonucleoside peak was based on the calibration graph for the reference compound which was pre-calibrated and stored in the Nelson software. From the nanomoles of the deoxyribonucleodes, the percentage nucleoside composition of DNA was derived.

Modification of DNA with chloroacetaldehyde

A DNA sample from *E. coli* (two A_{260} units) was allowed to react with 0.1 *M* chloroacetaldehyde[20] (CAA) in 0.2 *M* sodium succinate buffer (pH 5.5) at 37°C for 1 h. After the modification, the reaction mixture was extracted twice with two volumes each of diethyl ether to remove the unreacted CAA. Then the product was hydrolyzed and analyzed as described above.

RESULTS AND DISCUSSION

Effect of column temperature on the separation of deoxyribonucleosides

The results in Fig. 1 indicate that the *k'* values of the nucleosides are significantly temperature dependent from 24 to 30°C. However, no appreciable decrease in these values occurs for most species at temperatures above 30°C, that is, increasing the column temperature over 30°C does not reduce the analysis time. However, at 30°C the separation can be concluded in less time and the dG and dT pair can be more readily resolved, m^5dC —a modified component present is less than 2% of the other DNA components— is eluted close to the rG peak (deoxyinosine, dI, derived from the deamination of dA, is eluted after rG, but before dG). In analogy with the separation of nucleosides on ion-exchange and reversed-phase columns, increasing the column temperature affects the elution of purine nucleosides more than that of pyrimidine nucleosides[4,7]. As the column temperature is raised, purines exhibit less hydrophobicity; therefore, they are eluted earlier on these columns. If the objective is to measure m^5dC, separation at room temperature can yield satisfactory results. However, a chromatogram with sharper peaks results if the analysis is carried out at a temperature higher than 30°C[1,2].

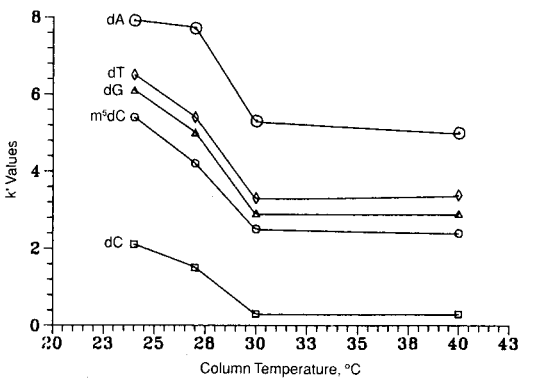

Fig. 1. Effect of temperature on the elution of deoxyribonucleosides. An authentic mixture of five nucelosides was injected into a Vydac column and elutions were carried out at different temperatures, using the same elution system (system A in Table I).

Effects of pH and mobile phase on the separation of nucleosides

Deamination of dA and dC must be avoided during DNA hydrolysis and HPLC of nucleosides. Under significantly acidic chromatographic conditions, *e.g.*, at pH 4, an acid-catalyzed deamination is observed. Similarly, under the alkaline conditions generally used for the phosphatase reaction, *e.g.*, at pH > 8, a base-catalyzed deamination of the two nucleosides occurs to a great extent. Under both conditions, deamination is further increased if the column temperature or the temperature of the phosphatase reaction is raised above 37°C (results not shown here). The separation of nucleosides (k' values) under three sets of conditions involving slightly different pH conditions (pH 5.3 *vs.* 5.5) and gradients of methanol are shown in Table II (*cf.*, Table I) for the composition of elution systems A and B). The results in columns 1 and 2 in Table II were obtained by using different methanol gradients and the same pH, whereas those in columns 2 and 3 were obtained by using the same gradient but different pH. Perhaps dC ionizes differently under two separation conditions, since dC exhibits a pK_a of 4.3. At pH 5.3, dC may exhibit some protonation, but perhaps none at pH 5.5. However, dC was eluted similarly under the three elution conditions. dA exhibits a pK_a of 3.8, far away from the two elution pH values; therefore, differences in the elution of dC and dA cannot be explained on the basis of differences in their ionizations in the elution systems used here. As noted for elution system B at pH 5.5 (Table II, column 3), ribonucleosides were eluted earlier than their deoxy derivatives. dG, a purine nucleoside, should exhibit more hydrophobicity than dT and therefore should be eluted later than the pyrimidine nucleoside. However, the results indicate that methanol abolished the hydrophobic character of dG, causing it to be eluted earlier than dT, whereas methanol failed to reduce the hydrophobic character of the other purine (dA) nucleosides to any degree.

Quantitation of chromatographic peaks

Software programs were recently described for the direct, computer-assisted acquisition and display of chromatographic data from conventional HPLC equip-

TABLE II

SEPARATION OF DEOXYNUCLEOSIDES UNDER THREE SEPARATION CONDITIONS

Nucleoside	pK_a*	k'		
		*System A*** *(pH 5.3)*	*System B*** *(pH 5.3)*	*System B**** *(pH 5.5)*
dCyd	4.3	1.7	1.6	1.7
m^5dCyd	4.4	4.6	2.8	3.0
dGuo	2.5	5.2	3.1	3.4
dThd	9.8	5.5	3.5	3.8
dAdo	3.8	7.9	4.6	4.8
Br^8Guo	–	9.6	5.2	5.4
m^6dAdo	4.2	10.2	5.7	5.9

* pK_a values are from G. W. Fasman (Editor), *Handbook of Biochemistry and Molecular Biology*, CRC Press, Boca Raton, FL, 3rd ed., 1975.

** See Table I for composition of the methanol gradient.

*** Br^8Guo, 8-bromoguanosine, used as a marker for retention time in HPLC.

ment[13–15]. Programs were written for a dual-microprocessor HPLC controller and described necessary utility routines to calibrate the instruments, and to acquire, display and store chromatographic data in real time. Here, we describe the use of commercially available software programs in order to calibrate the instrument and integrate peak areas of the chromatogram. In addition, spectral properties of the nucleosides are described here for quantitation by other means.

Relationship between the amount of nucleosides injected and the peak area originated by a software program. The standard solution of each nucleoside, prepared in the elution buffer (pH 5.5), was first assayed for its concentration by diluting a known volume of each sample, in triplicate, to a solution in which the molar absorptivity is known (*e.g.*, 0.10 *M* hydrochloric acid) and the pK_a of the nucleoside lies at least one pH unit away from the pH of the solution. Various amounts of the standard nucleoside solution were then injected and the peak areas were derived by the software and expressed in microvolts-seconds. The linear relationship between the amount of nucleoside injected and the peak area derived for each nucleoside is shown in Table III. Eqn. 1 gives the least-squares fit for the calibration graph, and eqn. 2 solves for the unknown amount of deoxynucleosides in nanomoles from the peak-area input.

Quantitation and characterization of peaks by absorption properties of the nucleosides. Spectral data and molar absorptivities (pH 5.5) at three different wavelengths for each nucleoside are listed in Table IV. This information is necessary for the characterization and quantitation of the peaks by other software programs and also manually. In the latter instance the peak area is derived[4] from the product of peak height × peak width at half maximum peak height × 1.06. Peak heights and peak widths of each nucleoside depend on several chromatographic conditions, including the flow-rate[12]. A comparison of the peak-height method with a microprocessor-contr olled, data-handling system, carried out recently, indicates a greater degree of confidence with the latter method[15]. The results of quantitation with a commercially available software program are described here (see below).

TABLE III

RELATIONSHIP BETWEEN THE AMOUNT OF NUCLEOSIDE (NANOMOLES) INJECTED AND PEAK AREA DERIVED BY SOFTWARE (NELSON ANALYTICAL, CUPERTINO, CA, U.S.A., MODEL 2000, VERSION 3.6)

Deoxyribo-nucleoside	*Eqn. 1**	*Eqn. 2**	*Correlation coefficient*
dCyd	$Y = 2.5775 \cdot 10^5 X - 2.7870 \cdot 10^5$	$X = 3.8798 \cdot 10^{-6} Y + 1.0813$	0.9996
5MedCyd	$Y = 1.7426 \cdot 10^5 X + 3.2180 \cdot 10^4$	$X = 5.7259 \cdot 10^{-6} Y - 1.842 \cdot 10^{-1}$	0.9927
dGuo	$Y = 3.5423 \cdot 10^5 X - 1.5232 \cdot 10^5$	$X = 2.8231 \cdot 10^{-6} Y + 4.3000 \cdot 10^{-1}$	0.9968
dThd	$Y = 2.8929 \cdot 10^5 X - 2.8548 \cdot 10^5$	$X = 3.4568 \cdot 10^{-6} Y + 9.8686 \cdot 10^{-1}$	0.9999
dAdo	$Y = 3.7727 \cdot 10^5 X + 5.0478 \cdot 10^5$	$X = 2.6506 \cdot 10^{-6} Y - 1.3380$	0.9999
6MedAdo	$Y = 3.8937 \cdot 10^5 X - 1.3288 \cdot 10^5$	$X = 2.5683 \cdot 10^{-6} Y + 3.4128 \cdot 10^{-1}$	0.9999

* X = nanomoles of nucleoside; Y = peak area at 260 nm.

TABLE IV

SPECTRAL PROPERTIES OF DEOXYRIBONUCLEOSIDES UNDER THE CHROMATOGRAPHY CONDITIONS

Values determined in 20 m*M* sodium succinate buffer (pH 5.5), containing 0.5 m*M* sodium azide.

Nucleoside	λ_{max} *at pH 5.5*	*Molar absorptivities at*				*pK*		
		λ_{max}	*254 nm*	*260 nm*	*280 nm*	*Basic*	*Acidic*	*dRib*
dCyd	271	9000	7030	8160	5350	4.3	none	> 13
5MedCyd	277	8500	5460	6200	7680	4.4	none	> 13
dGuo	254	13270	13270	11380	6680	2.5	9.2	12.4
dThd	267	9650	7890	9420	4630	none	9.8	> 13
dAdo	259	15000	14670	14400	1480	3.8	none	> 13
Br^8Guo*	261	15600	15040	15530	9220	–	–	–
6MedAdo	265	15400	12170	14850	7220	none	none	> 13

* Br^8Guo, 8-bromoguanosine.

Characterization of artifacts in the DNA sample

Detection of RNA contamination and deamination products of dA and dC in DNA hydrolyzates. HPLC analyses of a salmon sperm DNA hydrolyzate prior to and following RNase treatment are shown in Figs. 2 and 3. Elution systems B, also used in Table III, was used for these analyses (see Table I). Satisfactory separations of three of the four ribonucleosides (rC, rG and rA) from the deoxyribonucleosides were achieved under these chromatographic conditions. Although rU was not separated from dC, dU —a product of deamination of dC— was eluted between dC and m^5dC; it was not

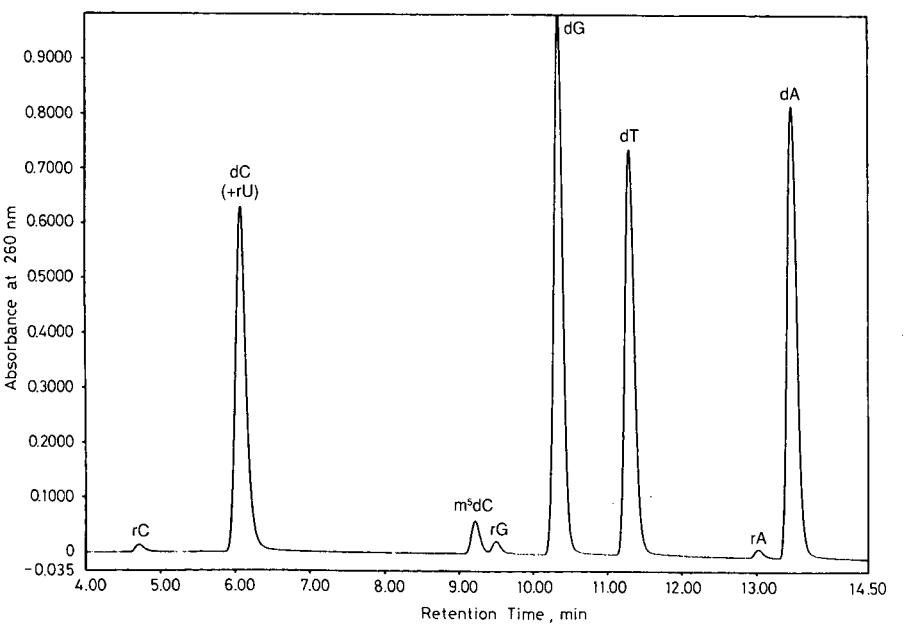

Fig. 2. Analysis of the DNA hydrolyzate, derived from salmon sperm *before* removal of the RNA contaminant. A 15-μg sample of the DNA was separated with elution system B (pH 5.5) (see Table I) at 24°C.

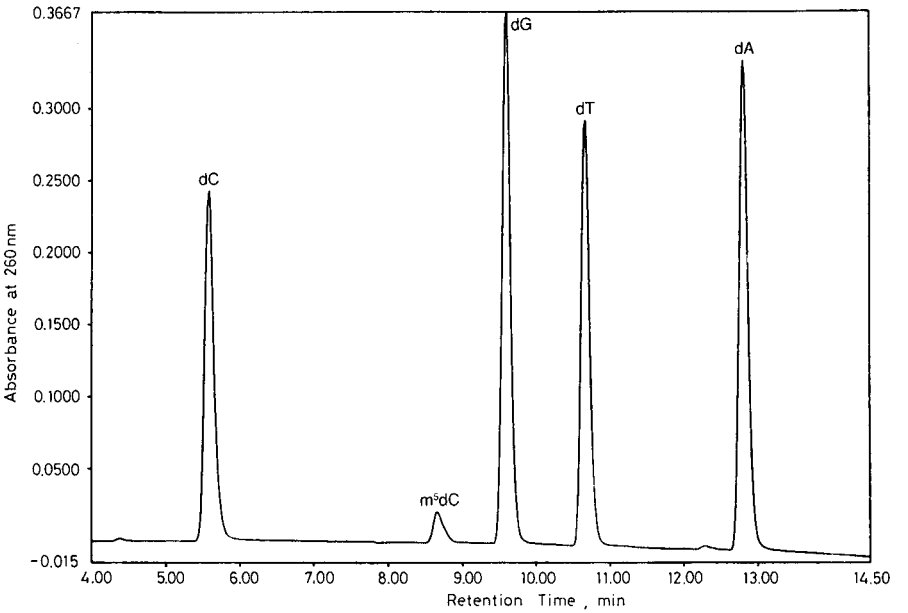

Fig. 3. Analysis of the DNA hydrolyzate, derived from salmon sperm *after* removal of the RNA contaminant by treatment with pancreatic ribonuclease, followed by dialysis. A 15-μg sample of the DNA was separated with elution system B (pH 5.5) (see Table I) at 24°C.

observed under our hydrolysis and analysis conditions. It is noted that rU and dU, which differ only by one hydroxy group, were resolved. This hydroxy group makes rU more polar and causes it to be eluted earlier than dU, but without distinction from dC, which lacks that hydroxyl function but has an additional amino group. Although rU is not separated from dC, its presence in the dC peak can be detected from the shape of the mixed peak, provided that no methanol is used in the starting eluent (results not shown). As the spectra of the two compounds differ significantly, the use of the diode-array detector aids in their identification. The DNA hydrolysis method used here showed no detectable deamination of dA resulting in dI, which was eluted between the rG and dG peaks. Deamination of dA is enhanced under any one of the following conditions: (a) presence of deaminase activity in the alkaline phosphatase, (b) phosphatase digestion carried out at pH > 8, (c) DNA concentration in amounts less than one A_{260} unit per 50 μl of the digest volume and (d) use of column temperatures above 40°C, especially with eluents of very low or very high pH, *e.g.*, in ion-exclusion chromatography[1,2]. Treatment of the DNA sample with RNase, followed by dialysis, effectively removes most RNA contaminants, as shown in Fig. 4.

Compositional analysis of DNA samples derived from two sources

The separation of the *E. coli* (strain B) DNA hydrolyzate is shown in Fig. 4. The minor component, m^6dA, was eluted after dA under our chromatographic conditions. The presence of the methyl group enhanced the hydrophobic interaction of m^6dA with the column matrix. [Although *E. coli* strain C is reported[21] to contain 1% m^5dC, no detectable amount of this residue in strain B was found in our studies.] Similarly, m^5dC

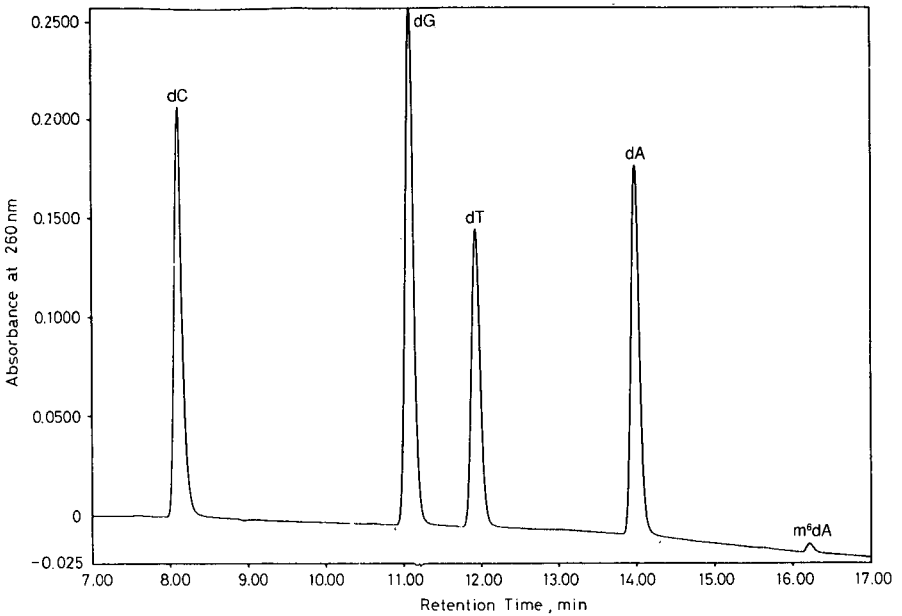

Fig. 4. Nucleoside composition analysis of a DNA sample derived from *E. coli* B. A 15-μg sample after digestion to deoxyribonucleosides was resolved with elution system C (pH 5.5) (see Table I) at 24°C.

was eluted after dC, owing to the extra methyl residue in its structure (see Fig. 3). The m^5dC peak can easily be contaminated with rG and dI contaminants, if present in appreciable amounts (see Fig. 2). Similarly, dC contents can decrease and dT contents increase at the same time by deamination of dC to dU, as dU is eluted with dT in ion-exclusion chromatography[1], although it was not observed in this study. We have recently observed, in crude DNA samples, cytosine deaminase activity responsible for the conversion of dC to dU.

Nucleoside compositions of DNA samples from two different sources, one from a prokaryote (*E. coli* B) and one from a eukaryote (salmon sperm), are shown in Table V. First, Vanyushin *et al.*[21] reported that this particular strain of *E. coli* contains 0.5

TABLE V

MOLAR NUCLEOSIDE COMPOSITION OF DNA SAMPLES

Values are derived from at least three analyses on less than one A_{260} unit (15 μg) of the DNA material.

DNA source	*Concentration (mole-%)**					
	dCyd	*m^5dCyd*	*dGuo*	*dThd*	*dAdo*	*m^6dAdo*
E. coli B	25.9 (0.4)	0.0	26.1 (0.4)	24.1 (0.1)	22.2 (0.3)	1.2 (0.3)
Salmon sperm	20.3 (0.1)	1.61 (0.03)	22.4 (0.3)	27.9 (0.2)	27.8 (0.2)	0.0

* Standard deviation in parentheses.

mole-% of m^6dA. More recently, Kuo *et al.*[6] found that this strain contains 2.5 mole-% while our results indicate that this DNA contains only 1.2 ($\pm$ 0.3) mole-% of m^6dA. Their results[6] for this DNA also differ from the data in Table V for other nucleoside contents. They report (in mole-%) dC, 26.4; m^5dC, not detected; dG, 26.7; DT, 23.4; dA, 23.6; and m^6dA, 2.5. The total content of all five nucleosides from these data equals 102.6 mole-%, whereas our values total 100%. This discrepancy can partly explain the differences between the two results. Our results differ significantly only in dA and m^6dA contents, which we find *ca.* 1.4 mole-% less for each residue than those reported by Kuo *et al*[6]. In Table V, the sum of dA and m^6dA (23.4%) narrowly fails to match the dT contents (24.1%) in *E. coli* DNA. However, considering the standard deviation associated with each residue, the difference is considered to be within the experimental error. A comparison of each residue in the Watson–Crick base pairs (*i.e.*, A = T and G = C) indicates a good correlation, well within the standard deviation.

DNA analysis of salmon milt, shown in Table V, matches very closely such analyses reported by others. For example, *Kuo et al.*[6] reported (in 100 mole-%) this DNA to contain dC, 20.4; m^5dC, 1.57; dG, 22.7; dT, 27.4; dA, 27.8; and m^6dA, not detected. In general, our results show a very good correlation with the published data for the same DNA, thus indicating the reliability of the chromatography system.

Analysis of a chloroacetaldehyde-modified DNA sample, chemical probe of the DNA structure in solution

Chloroacetaldehyde reaction with DNA. The analysis of nucleoside composition is used here to probe chemically the DNA conformation in solution, using CAA as the modifying agent. The results in Fig. 5 indicate a typical analysis of DNA, modified under the conditions described. Reaction parameters, such as CAA concentration, time, and salt concentration, were systematically studied to optimize the reaction with methylated residues in DNA (results to be reported elsewhere). The CAA reaction with *E. coli* B DNA was followed by dialysis, enzymatic hydrolysis, separation and quantitation. The extent of the etheno modification for each residue was derived from the loss in the amount of nucleoside (unreacted DNA, control experiment), while using dT as a reference residue. dT is unable to react with CAA, as it lacks an exocyclic amine function. For example, we find that in Fig. 6, the percentages of dC, dG, dA, and m^6dA residues are modified to their intermediates (e'dN) plus products (edN): 38% (dC), 6.2% (dG), 46% (dA) and 64% (m^6dA).

CAA is known to react with ribo- and deoxyribonucleosides of A and C residues. The reaction product contains an ethene bridge between the exocyclic amine nitrogen and the endocyclic nitrogen[22,23]. We have studied the reaction of CAA with methyl A, C and G derivatives. The methylated counterparts, m^6dAdo and m^5dCyd, exhibit significantly increased reactivity, owing to enhanced nucleophilicity of the exocyclic amine, as opposed to the A and C residues[24]. In normal Watson–Crick base pairing the exocyclic and endocyclic amino groups are hydrogen-bonded and therefore inaccessible. However, the regions containing methyl groups perturb the conformation of the double helix. While methylation of dA in position N-6 aborts hydrogen bonding and possibility yields a "bubble", methylation of dC at the C-5 position can induce a conformational transition from B-DNA to Z-DNA under physiological conditions[25]. The concentration of CAA determines the reactivity of C and A residues in forming an exocyclic product, and the amount of cations (Na^+ or Mg^{2+}) in the

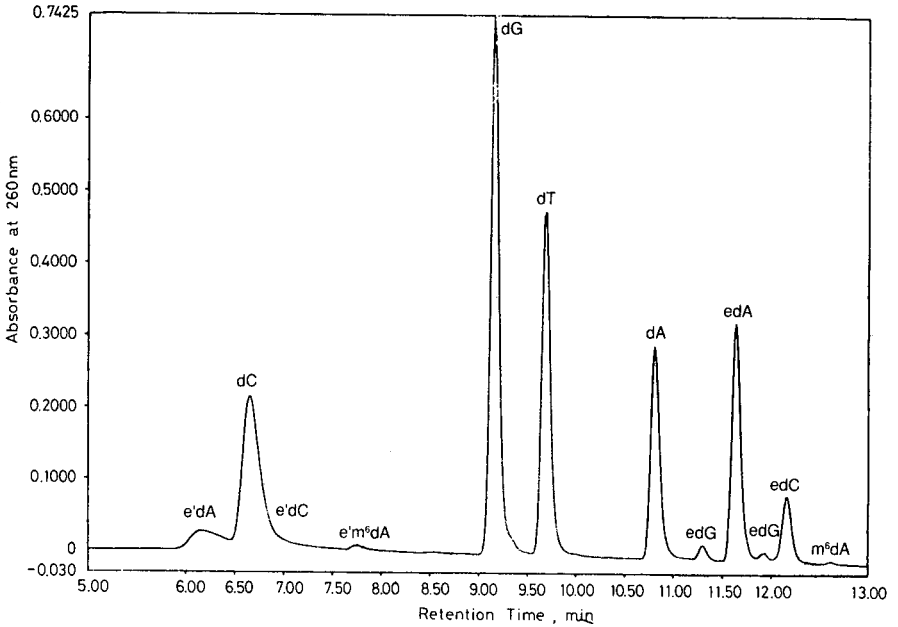

Fig. 5. Analysis of a DNA sample obtained after reaction with 0.1 *M* chloroacetaldehyde at pH 5.5 and 37°C for 1 h, followed by digestion to the nucleosides. Chromatography was carried out with elution system C (pH 5.5) (see Table I) at 24°C.

reaction mixture determines the conformation of the DNA (B-DNA *vs.* Z-DNA)[26], thus controlling the sites available for the reaction. An excessive concentration of CAA was used in the experiment described here (Fig. 6) in order to obtain a modification of the reactive residues. However, moderate reaction conditions were employed to achieve selective modification of the exposed residues in the DNA molecule.

The chromatographic system described here for the separation and analysis of DNA hydrolyzates compares favorably with the currently used methods described by others[6,9]. For example, our analyses are carried out on a single 25-cm C_{18} column as opposed to the 60-cm columns used by others. In addition, we can achieve satisfactory resolution of all five DNA components and of the artifacts at room temperature (*i.e.*, 24°C instead of 45°C) in a short analysis time (18 min instead of 40–60 min) while using only one low-ionic-strength gradient elution buffer which does not precipitate in methanol.

ACKNOWLEDGEMENT

The authors thank Mr. David Smoll for early experiments with the Vydac column. This research was supported by a grant from the National Institutes of Health (GM36099) and in part by funds from the Wesley Foundation, Wichita, Kansas (Grant T8707011).

REFERENCES

1 R. P. Singhal, *Arch. Biochem. Biophys.*, 152 (1972) 800.
2 R. P. Singhal and W. E. Cohn, *Biochemistry*, 12 (1973) 1532.
3 R. P. Singhal, *Eur. J. Biochem.*, 43 (1974) 245.
4 R. P. Singhal and W. E. Cohn, *Anal. Biochem.*, 45 (1972) 585.
5 R. P. Singhal, *Sep. Purif. Methods*, 3 (1974) 339.
6 K. C. Kuo, R. A. McCune and C. W. Gehrke, *Nucleic Acid Res.*, 8 (1980) 4763.
7 C. W. Gehrke, R. A. McCune, M. A. Gama-Sosa, M. Ehrlich and K. C. Kuo, *J. Chromatogr.*, 301 (1984) 199.
8 M. Buck, M. Connick and B. Ames, *Anal. Biochem.*, 129 (1983) 1.
9 J. S. Eadie, L. J. McBride, J. W. Efcavitch, L. B. Hoff and R. Cathcraft, *Anal. Biochem.*, 165 (1987) 442.
10 M. A. Gama-Soma, R. Y. H. Wang, K. C. Kuo, C. W. Gehrke and M. Ehrlich, *Nucleic Acids Res.*, 11 (1983) 3087.
11 A. Razin, C. Webb, M. Szyf, J. Yisraeli, A. Rosenthal, T. Naveh-Many, N. Sciaky-Gallili and H. Cedear, *Proc. Natl. Acad. Sci. U.S.A.*, 81 (1984) 2275.
12 R. P. Singhal, L. L. Mays-Hoopes and G. E. Eichhorn, *Mech. Ageing Dev.*, 41 (1987) 199.
13 R. P. Singhal and D. B. Smoll, *J. Liq. Chromatogr.*, 9 (1986) 2661.
14 D. B. Smoll and R. P. Singhal, *J. Liq. Chromatogr.*, 9 (1986) 2695.
15 R. P. Singhal and D. B. Smoll, *J. Liq. Chromatogr.*, 9 (1986) 2718.
16 J. Marmur, *J. Mol. Biol.*, 3 (1961) 208.
17 G. C. K. Roberts, E. A. Dennis, D. H. Meadows, J. S. Cohen and O. Jardetzky, *Proc. Natl. Acad. Sci. U.S.A.*, 62 (1969) 1151.
18 M. Fujimoto, K. Fujiyama, A. Kuninaka and H. Yoshino, *Agric. Biol. Chem.*, 38 (1974) 2141.
19 M. Laskowski, *Ann. N.Y. Acad. Sci.*, 81 (1959) 776.
20 W. P. McCann, L. M. Hall and W. K. Nonidez, *Anal. Chem.*, 55 (1983) 1454.
21 B. F. Vanyushin, A. N. Belozersky, N. A. Kokurina and D. X. Kodirovo, *Nature (London)*, 218 (1968) 1066.
22 J. R. Barrio, J. A. Secrist, III, and N. J. Leonard, *Biochem. Biophys. Res. Commun.*, 46 (1972) 597.
23 N. J. Leonard, *CRC Crit. Rev. Biochem.*, 15 (1984) 125.
24 R. P. Singhal, L. Brown, P. Landes and A. Maasa, unpublished results, 1988.
25 F. M. Pohland and T. M. Jovin, *J. Mol. Biol.*, 67 (1972) 375.
26 M. Behe and G. Felsenfeld, *Proc. Natl. Acad. Sci. U.S.A.*, 78 (1981) 1619.

Journal of Chromatography, 458 (1988) 129-145
Elsevier Science Publishers B.V., Amsterdam — Printed in The Netherlands

CHROMSYMP. 1415

HIGH-PERFORMANCE LIQUID CHROMATOGRAPHIC SEPARATION OF PEPTIDES ON A DIOL-GLY-PHE-PHE TRIPEPTIDE-BONDED PHASE

THOMAS C. PINKERTON* and KENNETH A. KOEPLINGER
Control Division, Building 259, Mail Stop 12, The Upjohn Company, Kalamazoo, MI 49001 (U.S.A.)

SUMMARY

The retention characteristics of some selected peptides (mol. wt. <2000 a.m.u.) have been investigated on a diol-Gly-Phe-Phe partitioning phase, bound to 5-μm porous silica. The hydrophobic, positively charged peptides can be separated with mild mobile phases, containing only acetonitrile and phosphate buffer. The peptide selectivity of the diol-Gly-Phe-Phe-bonded phase is uniquely different from that of a C_8 column. The dependence of capacity factors on mobile phase pH, ionic strength, and organic solvent concentration demonstrated that the partitioning mechanisms of the diol-Gly-Phe-Phe phase involve multifunctional reversed-phase and cation-exchange processes.

INTRODUCTION

The need for increased high-performance liquid chromatographic (HPLC) selectivity is very important in the separation and characterization of peptides. The development of small, biologically active peptide derivatives for medicinal agents and the characterization of protein fragments by tryptic mapping has created an increasing need for better resolution of complex peptide mixtures. Current HPLC technology is based principally on the one-column/one-mechanism philosophy, and in many cases, chromatographers have optimized separations to the limits of the resolving power of their columns. Currently, the strategies of using multifunctional partitioning phases and more than one column of differing selectivity are being investigated.

Peptide separations by LC have been carried out by exploiting a wide variety of separation mechanisms including size-exclusion, ion-exchange, normal-phase, and reversed-phase techniques. Reversed-phase HPLC on C_8 and C_{18} bonded phase porous silica remains the method of choice for separating peptides with molecular weights of <2000 a.m.u.[1–4]. The rapid stationary phase mass transfer of solutes on alkyl-bonded phase with small particulates (3–5 μm), and the use of aqueous organic mobile phase gradients, produce the greatest number of resolvable peaks compared to other HPLC techniques. The reversed-phase separation of peptides typically involves the use of mobile phases containing aqueous trifluoroacetic acid (TFA) in combination with acetonitrile or methanol. The TFA primarily serves to maintain a pH below

0021-9673/88/$03.50

2 in order to protonate carboxylic acid groups. In addition, TFA acts as an ion-pairing agent by association with protonated amines, thus neutralizing the molecular charge and minimizing the interaction with surface silanols. Under optimized gradient conditions, such reversed-phase separations can achieve column peak capacities (*i.e.*, the theoretical maximum number of resolvable peaks) slightly over a hundred[5]. It might appear that such a resolving power is more than adequate for separating most complex mixtures. In reality, however, the most difficult separations demand discrimination between molecules with only slight differences; and given the use of only one separation mechanism, column peak capacities in adjoining regions of a chromatogram generally go unutilized.

It is well established that reversed-phase separations exploit the solvophobic properties of solutes to generate differences in chromatographic retention. These retention characteristics are proportional to the analyte hydrophobic surface area and the mobile phase interfacial surface tension[6]. It has been demonstrated that the retention difference between small peptides on reversed-phase columns can be predicted by the linear combination of hydrophobic fragment coefficients[1,2,7]. It becomes obvious that subtle differences in amino acid sequence or peptide configuration can lead to degenerate hydrophobic surface areas, which result in overlapping chromatographic peaks. With the use of ion-pairing agents and the adjustment of pH these degeneracies can often be eliminated; however, in complicated separations, peak overlap in other regions of the chromatogram usually result. One solution to this impasse is to vary selectivity by incorporating an additional separation mechanism and/or increasing the peak capacity by adding a second dimension. This is the common strategy employed in thin-layer chromatography and two-dimensional electrophoresis, which can provide peak capacities in the thousands. For qualitative purposes, two-dimensional thin-layer techniques remain unsurpassed in resolving power; however, for accurate quantification HPLC is superior.

In an attempt to achieve greater versatility in HPLC selectivity, researchers have investigated the use of multifunctional bonded phases[8]. Multifunctional bonded phases can be classified into three categories. The first involves the delineation of physical differences, as achieved with mixed-mode size-exclusion and partitioning mechanisms. The second involves the independent partitioning of solutes with separately bonded functional groups. In this category, stationary phases bound both with ion-exchange groups and alkyl groups have been evaluated[9]. The third involves the integrated partitioning of solutes with a single bonded phase moiety which functionally invokes different partition mechanisms (*i.e.*, van der Waals dispersive forces, hydrogen bonding, ion-exchange, etc.). Most chiral bonded phases fall into the latter category, where at least three points of interaction are necessary for a bonded phase to distinguish between enantiomers. Peptide-bonded phases can also be placed in this category, because of the multifunctional nature of peptides. The well known phenomenon of peptide–peptide intermolecular interaction has prompted researchers to evaluate peptide-bonded phases as potentially valuable in multifunctional separations.

The use of tripeptide-bonded phases in HPLC was introduced by Grushka and co-workers in the late 1970s[10–12], following the lead of Corbin *et al.*[13], who earlier used a similar strategy for the gas chromatographic separation of amino acid enantiomers. Grushka and co-workers produced three tripeptide-bonded phases, Val-Ala-

Ser[10], Val-Phe-Val[11], and Val-Ala-Pro[12]. Each was bound to silica via a methylphenylethane spacer and the tripeptide was bound to the spacer by a methyl ester linkage with the carboxyl terminus, thus leaving the terminal amine free. This effectively rendered the tripeptide bonded phases weak anion-exchangers. In 1985, Howard *et al.*[14] improved the bonding synthesis of the Val-Ala-Pro phase of Grushka and evaluated the selectivity over a broad pH range in the separation of dipeptides. In that same year, Hagestam and Pinkerton[15] introduced a diol-Gly-Phe-Phe-bonded phase, where the phenylalanine moieties on the external surface of the particulate had been removed by enzyme cleavage, in order to make the packing material non-adsorptive to proteins. The packing is referred to as internal surface reversed-phase (ISRP) material and is designed for the analysis of drugs in blood plasma or serum by direct injection[16]. The ISRP columns are now commercially available from Regis, Morton Grove, IL, U.S.A.

The ISRP diol-Gly-Phe-Phe-bonded phase is distinguished by three significant differences from previous tripeptide-bonded phases. First, the carboxyl terminus is a free functional group making the packing a weak cation exchanger[17]. This is advantageous, since many blocked peptides have net positive charges, and separation reproducibility is generally enhanced when ion-pairing agents are not used. Second, the peptide is attached to an underlying diol phase. The diol phase is present in *ca.* 300 μmol/g, whereas the tripeptide is present in only 60–80 μmol/g[18]. In HPLC, the attachment of partitioning moieties to a diol phase is well established[19–21]. The advantages of using an underlying diol phase are the non-absorptivity rended to large proteins in biological samples[22] and the inactivation of residual silanols[23], which are known to produce severe tailing of amines. Third, the diol-Gly-Phe-Phe phase is bound via a carbamate linkage, which is inherently more stable[24] than the ester linkages used in previous tripeptide bonded phases[10–13].

The following study has been undertaken in order to evaluate the selectivity of the diol-Gly-Phe-Phe-bonded phase in peptide separations. Assuming one can exploit the multifunctional nature (*i.e.*, reversed-phase and cation-exchange properties) of the diol-Gly-Phe-Phe phase to improve the resolution of selected peptides, relative to conventional alkyl-bonded phases, the need to increase column peak capacity becomes important because columns with greater selective discrimination are inherently less efficient. In order to gain higher peak capacities, isolated components can be further separated off line by another type of column or different columns can coupled via switching valves for two-dimensional LC. The combined use of two-dimensional LC with columns of differing selectivity provides the greatest promise for isolating heretofore unresolved peptides, as recently demonstrated by Tanaka *et al.*[25] in a peptide separation conducted with a two-dimensional LC strategy using an alumina column and a reversed-phase column. The inclusion of multifunctional bonded phases as one dimension further enhances the flexibility and potential resolving power of such two-dimensional LC systems. It is for this reason that the multifunctional nature of the diol-Gly-Phe-Phe-bonded phase has been investigated for use in peptide separations.

EXPERIMENTAL

Chromatographic system

Chromatograph. The HPLC system consisted of a Hewlett-Packard (Palo Alto, CA, U.S.A.) 1090M liquid chromatograph with integrated ternary solvent delivery system, autosampler, column temperature controller, and photodiode-array detector. Chromatographic parameters, solvent delivery, and data acquisition were controlled by an HP9000 Model 310 computer (HPChemStation). The data was stored on either an HP 20BM hard disc or on a Bering Bernoulli 20MB removable cartridge. Retention times, peak-widths at half-height, and symmetries were determined with HPChemStation software. Additional chromatographic data including capacity factors, efficiency, selectivity, and resolution were calculated with custom macro programs, run on the HPChemStation. Hardcopy chromatograms were generated on an HP7440 plotter. Capacity factor *vs.* buffer concentration plots were created in Lotus software, run on an IBM PC.

Mobile phases. The ternary solvent system consisted of (A) deionized/photolyzed water, (B) 0.2 *M* ammonium phosphate (pH 6), and (C) acetonitrile–water (90:10). The ammonium phosphate buffer was prepared with Fisher A-685 HPLC-grade monobasic phosphate and Fisher A-686 ACS certified dibasic phosphate salts in an appropriate ratio to yield a pH of 6. The phosphate solution was filtered through a 0.2-μm Nylon filter prior to use. The water used for preparing the mobile phases was USP-grade water, which had been further purified with a MilliQ™ system (Millipore, Bedford, MA, U.S.A.). The water was then photolyzed in 2-l batches by a high-flux ultraviolet light source contained in a Barnstead (Boston, MA, U.S.A.) Organicpure™ unit. Photolysis of the water guaranteed the absence of organic impurity peaks in gradient elution with 214 nm detection. The acetonitrile used in eluent C was UV 015 grade 99.9% pure (Burdick & Jackson Labs., American Scientific Products, McGraw, IL, U.S.A.).

Columns. The diol-Gly-Phe-Phe tripeptide ISRP columns (GFF-S5-80) were purchased from Regis. The synthesis and characterization of the ISRP packing was described in detail elsewhere[18,26]. A 15 cm × 4.6 mm column (Ser. No. 22302) and a 25 cm × 4.6 mm (Ser. No. 21206) column were used throughout.

Detection. Using an HP photodiode-array detector, chromatograms were generated with optical responses at 214 nm and 254 nm. Detector settings for 214 nm included a 4-nm bandwidth and a reference wavelength region from 450 to 550 nm. Detector settings for 254 nm included a 8-nm bandwidth and a reference wavelength region from 400 to 450 nm. The photodiode-array was automatically balanced against the eluent prior to each injection to compensate for drift. The data sampling interval was typically 640 ms. When appropriate, the spectrum of each eluted component was recorded from 210 to 350 nm.

Procedures. Unless stated otherwise, general chromatographic parameters included injections of 20 μl, a flow-rate of 1.0 ml/min, and a column temperature of 40°C. For isocratic elutions, eluents A, B, and C were metered with the HP1090M solvent delivery system at constant rates.

The capacity factors of selected peptides were mapped over a range of buffer concentrations at constant pH and acetonitrile content. The peptides were chromatographed individually, in duplicate, with buffer concentrations ranging from 0.002

to 0.2 *M*. The buffer concentration was varied by metering selected percentages of eluents A and B with a constant percentage of C. When evaluating the change in capacity factor as a function of the acetonitrile concentration, eluents A and C were varied while B was held constant. In measuring the change in capacity factors as a function of pH, eluents A, B, and C were metered at constant rates, with the pH of B having been adjusted prior to the experiment with concentrated phosphoric acid.

The capacity factors (k) for each peptide were calculated in the standard fashion $k = (t_R - t_M)/t_M$, where t_R is the unadjusted retention time and t_M is the mobile phase penetration void volume. The t_M for each column was measured with a solution of sodium nitrate. The void marker was found to correspond to the first baseline perturbation observed in each chromatogram. It is presumed this perturbation was caused by conjugate salts in the peptide samples.

In order to optimize the resolution of a mixture of enzyme inhibitory peptide derivatives, a linear solvent strength gradient elution was employed with the ternary solvent system at a flow-rate of 0.7 ml/min. In all cases, an interval of at least 20 min was allowed for re-equilibration before each run. The ternary gradient program [%A–%B–%C (v/v/v) with linear elution] was as follows: start 89%–1%–10%; at 5 min, 77%–1%–22%; at 40 min, 72%–1%–27%; at 60 min, 35%–25%–40%; and at 70 min, return to initial conditions.

Peptide analytes

Fetirelin acetate (Conceral™), the proline ethylamide of luteinizing hormone releasing hormone (LHRH), was obtained from Takeda, Osaka, Japan. The remaining fetirelin derivatives were acquired from Sigma, St. Louis, MO, U.S.A.; these included LHRH (L-0507), LHRH [Gly-OH^{10}] (L-8008), LHRH des-Gly^{10} [D-Ala^6] (L-2383), LHRH des-Gly^{10} [D-Leu^6] (L-5009), LHRH des-Gly^{10} [D-Trp^6] (L-5386), and LHRH des-Gly^{10} [D-Phe^6] (L-8886). Selected amino acids, dipeptides, and tripeptides, including glycine, D-histidine, L-histidine, 1-methylhistidine, 3-methylhistidine, Gly-L-Phe, Gly-D-Phe, Gly-Gly-L-Phe, and L-Phe-Gly-Gly were obtained from Sigma. A peptide fragment mixture of dihydrofolate reductase (43–50) from *Escherichia coli*, D-Phe-Gly, D-Phe-D-Phe-Gly, D-Phe-L-Phe-Gly and derivatives of a proprietary enzyme-inhibitory peptide were obtained from The Upjohn Company. The Conceral derivatives were prepared at a concentration of 50 μg/ml in water. The enzyme-inhibitory peptide derivatives were dissolved in either absolute methanol or 50% aq. acetonitrile at concentrations ranging from 50 to 80 μg/ml.

RESULTS AND DISCUSSION

General selectivity of the diol-Gly-Phe-Phe ISRP columns

The retention characteristics for a wide variety of low-molecular-weight drugs have been determined on the ISRP columns[15–17]. The diol-Gly-Phe-Phe-bonded phase favors the retention of aromatic compounds[16] and separates species primarily by a reversed-phase mechanism. The reversed-phase properties have been established from linear plots of log k *vs.* fraction of organic solvent in the eluent[17]. The hydrophobic partitioning on an ODS column is not a good predictor of retention on the tripeptide-bonded phase, as shown by Sams and Evec[27] with the separation of 21 drugs. However, the diol-Gly-Phe-Phe-bonded phase exhibits a broader range of

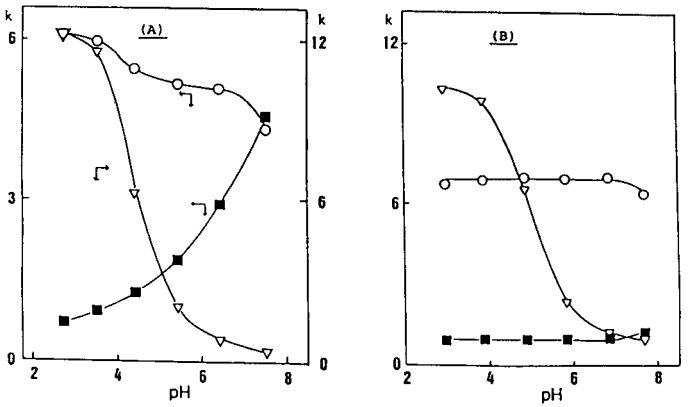

Fig. 1. Dependence of capacity factors of methylparaben (○), *p*-toluic acid (▽), and phenethylamine (■) on the pH of the mobile phase, observed with (A) diol-Gly-Phe-Phe column and (B) phenylsilica column; and mobile phases of (A) 0.1 *M* potassium phosphate buffer (ionic strength 0.2), (B) 0.1 *M* potassium phosphate buffer (ionic strength 0.20) – acetonitrile (80:20). Flow-rate, 1.0 ml/min; column size, 15 cm x 4.6 mm; detection, 220 nm. From ref. 17.

retentions than an alkyl-bonded phase and greater selectivity for some compounds. The carboxylic acid terminal of the diol-Gly-Phe-Phe acts as a weak cation exchanger and provides strong selective control for aromatic amines. Nakagawa *et al.*[17] demonstrated the secondary ion-exchange properties of the diol-Gly-Phe-Phe-bonded phase by contrasting it with a phenyl-bonded phase silica. Using *p*-toluic acid and phenylethylamine, Nakagawa *et al.*[17] plotted the change in capacity factors as a function of mobile phase pH on the two columns. As can be seen in Fig. 1, the capacity factor of *p*-toluic acid on both columns increases in a sigmoidal fashion as the pH is lowered. This is consistent with analyte protonation and reversed-phase partitioning of the neutral molecule. Phenethylamine, on the other hand, is positively charged in the pH range studied and is not well retained on the phenyl column over this range (Fig. 1). On the diol-Gly-Phe-Phe-bonded phase the capacity factor of the phenethylamine is seen to increase as the pH is raised. This implies that the carboxylic acid groups on the bonded phase become a weak cation exchanger as the groups are deprotonated. The retention of methylparaben, a neutral molecule, does not change appreciably with pH (Fig. 1). The ion-exchange properties of the diol-Gly-Phe-Phe-bonded phase are further exemplified by the change in capacity factors as a function of ionic strength, shown in Fig. 2. As the ionic strength increases, the capacity factors of the *p*-toluic acid on both columns increases slightly, as expected for reversed-phase partitioning. For the phenethylamine, as the ionic strength is decreased the capacity factor on the diol-Gly-Phe-Phe-bonded phase increases almost fifteen times over that of the phenyl column, indicating the distinct secondary cation-exchange properties of the peptide bonded phase. The retention of neutral compounds (methylparaben and phenol) remain constant with change in eluent ionic strength.

First peptide separations on ISRP columns

The separation of small biologically active peptides on diol-Gly-Phe-Phe ISRP columns was first demonstrated by Nakamura[28]. Using a 5 cm × 4.6 mm ISRP

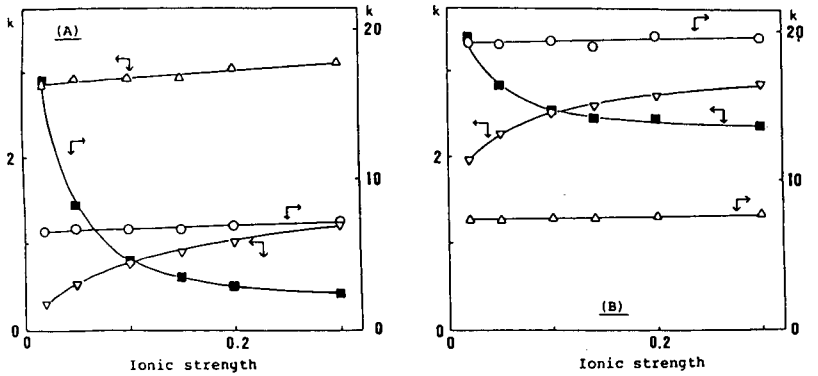

Fig. 2. Dependence of capacity factors on the ionic strength of the mobile phase at a constant pH of 6.7 with (A) diol-Gly-Phe-Phe column and (B) phenylsilica column; and mobile phases of (A) potassium phosphate buffer, (B) potassium phosphate buffer–acetonitrile (90:10). Symbol △ is for phenol. (For other information see Fig. 1.)

column, he measured the retention characteristics of a variety of proteins and peptides under both isocratic and gradient conditions (Table I). Small peptides exhibited retention, while the proteins with molecular weights > 14 000 a.m.u., were excluded and not adsorbed to the packing. Fig. 3 illustrates the resolution of four peptides by gradient elution. The amino acid sequences of peptides separated by Nakamura, and of fetirelin and DHFR investigated in this study, are shown on p. 136.

TABLE I

RETENTION CHARACTERISTICS OF SELECTED PROTEINS AND PEPTIDES ON A 5-cm DIOL-GLY-PHE-PHE COLUMN

Proteins and peptides separated by Nakamura[28] on a 5 cm x 4.6 mm ISRP column at a flow-rate of 1 ml/min with (A) an isocratic mobile phase of 0.1 *M* phosphate buffer (pH 6.7)–acetonitrile (80:20) and (B) a linear gradient of eluent A to B in 20 min, where A is 0.1 *M* phosphate buffer (pH 6.7) and B is 0.1 *M* phosphate buffer (pH 6.7)–acetonitrile (80:20). From ref. 28.

	mol. wt.	t_R *(min)*	
		A	*B*
Lysozyme	14 000	0.3	0.4
Bovine serum albumin	68 000	0.4	0.4
Catalase	240 000	0.4	0.4
Thyroglobulin	670 000	0.5	0.5
β-Lactoglobulin	18 400	0.6	0.5
Oxytocin	1007	1.1	3.2
Met-Enkephalin	574	1.3	1.5
Angiotensin II	1046	1.7	2.8
Neurotensin	1673	1.9	7.6
Angiotensin I	1297	2.0	11.2
Bradykinin	1060	5.3	14.6
Met-Lys-Bradykinin	1320	16.8	32.8

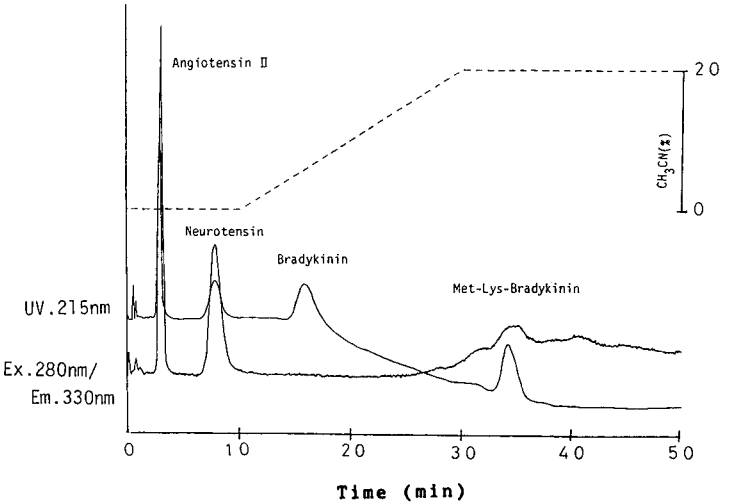

Fig. 3. Separation of biologically active peptides on a 5-cm diol-Gly-Phe-Phe column with linear gradient elution from eluent A to B, where A is 0.1 *M* phosphate buffer (pH 6.7) and B is 0.1 *M* phosphate buffer (pH 6.7)–acetonitrile (80:20). Flow-rate, 1 ml/min. (From ref. 28).

Angiotensin I
Asp-Arg-Val-Tyr-Ile-His-Pro-Phe-His-Leu
Angiotensin II
Asp-Arg-Val-Try-Ile-His-Pro-Phe
Bradykinin
Arg-Pro-Pro-Gly-Phe-Ser-Pro-Phe-Arg
Oxytocin

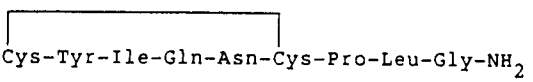

Neurotensin
Glu-Leu-Tyr-Glu-Asn-Lys-Pro-Arg-Arg-Pro-Tyr-Ile-Leu
Methionine enkephalin
Tyr-Gly-Gly-Phe-Met
Fetirelin
pGlu-His-Trp-Ser-Tyr-Gly-Leu-Arg-Pro-$NHCH_2CH_3$
Dihydrofolate reductase fragment (43–50)
Gly-Arg-His-Thr-Trp-Glu-Ser-Ile

All of these peptides have one or more of the aromatic amino acids (Phe, Tyr, or Trp), and some have one or more of the basic amino acids (Lys, Arg, or His).

Capacity factor mapping of fetirelin

Fetirelin is the proline ethylamide derivative of LHRH having a molecular weight of 1167 a.m.u. The peptide has nine amino acids, a pyroglutamyl group at the N terminus, and an ethylamide group blocking the carboxyl end. The hydrophobic

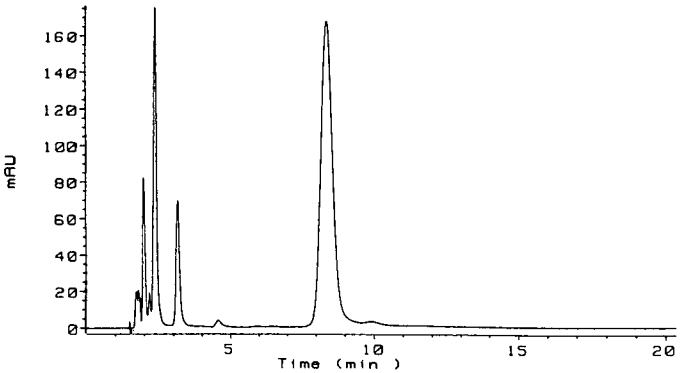

Fig. 4. Separation of fetirelin and degradation products on a 15-cm diol-Gly-Phe-Phe column with an isocratic mobile phase of 0.16 *M* ammonium phosphate (pH 6.1)–acetonitrile (82:18). Flow-rate, 1.0 ml/min; temperature 40°C; detection, 214 nm.

character of the peptide is primarily due to the Trp and Tyr, and its positive charge to His and Arg. The elution of fetirelin from a 15 cm x 4.6 mm diol-Gly-Phe-Phe column with a mobile phase of 0.16 *M* ammonium phosphate (pH 6.1)–acetonitrile (82:18) is shown in Fig. 4. Degradation products in the fetirelin sample are seen to be well separated.

By chromatographing derivatives of fetirelin one gains insights into its retention behavior relative to specific amino acid substitution. Modification of the sixth position with amino acids of increasing hydrophobicity, Ala < Leu < Phe < Trp, produces a proportional increase in the retention of the derivative on the diol-Gly-Phe-Phe-bonded phase. As shown in Table II, the increase in capacity factors parallel an increase in contribution to the log of the octanol–water partition coefficient (P)[2], and in the amino acid lipophilicity coefficient f, developed by Rekker[7]. Plots of f *vs.* log k or log P *vs.* log k for Leu, Phe, and Trp show linear relationships with correlation coeffficients of 0.95 and 0.99, respectively. This indicates that the diol-Gly-Phe-Phe reversed-phase partitioning responds systematically to a recognizable change in the molecular hydrophobic surface area. The capacity factors of fetirelin derivatives

TABLE II

RETENTION CHARACTERISTICS OF FETIRELIN DERIVATIVES

P is the amino acid octanol–water partition coefficient[2]. f is the lipophilicity side chain contribution according to Rekker[7]. k is the capacity factor of each fetirelin derivative determined on a 15-cm diol-Gly-Phe-Phe ISRP column under isocratic conditions by constant metering of the eluents A, B and C at 50%, 30% and 20%, respectively.

Amino acid substitution in sixth position	*log P*	*f*	*k*
D-Alanine	−2.94	0.53	6.56
D-Leucine	−1.71	1.99	7.21
D-Phenylalanine	−1.43	2.24	12.58
D-Tryptophan	−1.04	2.31	22.45

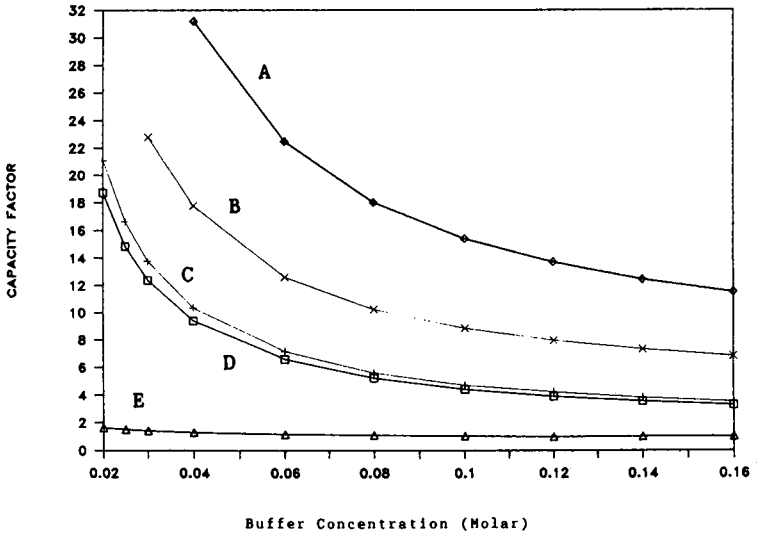

Fig. 5. Change in capacity factors of fetirelin derivatives as a function of mobile phase ionic strength at constant pH on a 15-cm diol-Gly-Phe-Phe column in isocratic elution with 0.16 *M* ammonium phosphate (pH 6.1)–acetonitrile (82:18). Other conditions same as in Fig. 4. (A) [D-Trp][6], (B) [D-Phe][6], (C) Conceral, (D) [D-Ala][6], and (E) [Gly-OH][10].

with Gly or Ala in the same position did not fall on this line, indicating these groups are too small to produce a significant change in hydrophobic surface area.

The effect of charge on the retention of the fetirelin derivatives is illustrated by the change in capacity factors as a function of mobile phase buffer concentration at constant pH (6.1) and acetonitrile concentration (Fig. 5). As expected, the capacity factors of the positively charged peptides increase with decreasing ionic strength in accordance with a cation-exchange partitioning mechanism. A decrease in pH produces a proportional increase in capacity factor of each peptide as a result of an increase in positive charge, brought on by further protonation. When the ethylamide group on the end is replaced by glycine with a free carboxylic acid terminal group [Gly-OH[10]], the molecular charge is neutralized, and the capacity factor does not increase with decreasing ionic strength (Fig 5).

Dihydrofolate reductase fragments

Another instance of the diol-Gly-Phe-Phe-bonded phase selectivity is illustrated with the separation of an *E. coli* dihydrofolate reductase (DHFR) fragment (43–50) and its N-formylated Trp derivative. Trp confers hydrophobic character on the fragment, while a positive charge is provided by Arg and His. The positive charge is offset by the negative charge produced by Glu and the C-terminal Ile. The separation, monitored with a photodiode-array detector, shows that the DHFR fragment is eluted at 8.2 min and the N-formylated Trp derivative is eluted at 9.6 min (Fig. 6). The N-formylated Trp derivative was clearly identified by its characteristic absorbances at 243 nm and 297 nm[29]. The peak at 2.9 min is an unidentified diastereomer of the DHFR fragment. This separation illustrates the selectivity difference produced on the

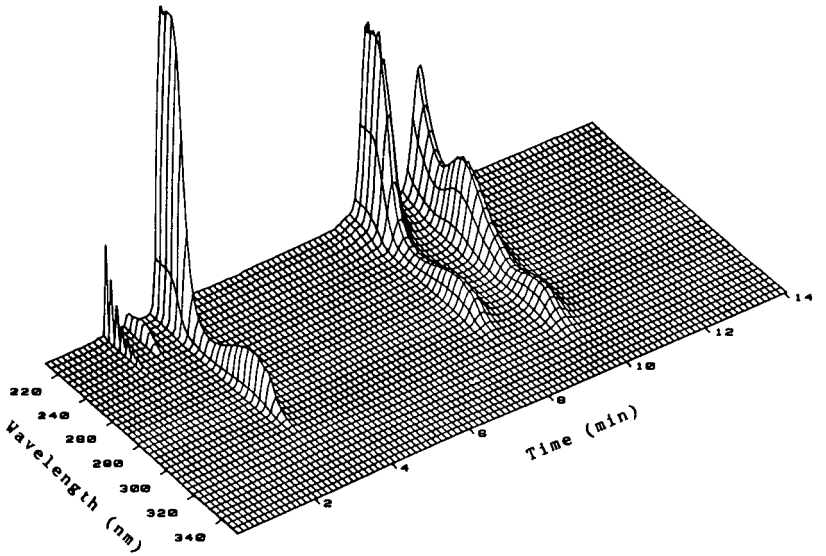

Fig. 6. Separation of DHFR (43–50) and the N-formyl-Trp derivative on a 15-cm diol-Gly-Phe-Phe column with an isocratic mobile phase of 95.5% 0.02 *M* ammonium phosphate buffer (pH 6.1)–acetonitrile (95.5:4.5). Flow-rate, 1.0 ml/min; temperature, 40°C; photodiode-array detection.

diol-Gly-Phe-Phe-bonded phase by a slight structural variation in a hydrophobic amino acid. By contrast, the components were difficult to resolve on an alkyl-bonded phase with conventional methods.

Enzyme-inhibitory peptide derivatives

Further selective discrimination can be illustrated with the separation of a synthetic mixture of peptide analogues and fragments, associated with a proprietary enzyme-inhibitory peptide. The peptide components range in molecular weight from about 450 to 940 a.m.u., and are protected on one end by a *tert.*-butyloxycarbonyl group and on the other end by methylpyridine. Hydrophobic interaction is provided by a phenylalanine residue, and positive charge by a histidine group. Fig. 7 shows a conventional isocratic separation of the mixture on a 25 cm x 4.6 mm Spherisorb C_8 column with a mobile phase of acetonitrile aqueous solution, 0.05 *M* in TFA and 0.04 *M* in triethylamine (40:60). Fig. 8 shows a ternary gradient separation of the same mixture on a 15 cm x 4.6 cm diol-Gly-Phe-Phe-bonded phase with an ammonium phosphate buffer (pH 6.1) and aq. acetonitrile. The gradient program maintains a constant buffer concentration of 0.002 *M* for the first 40 min of the chromatogram which is overlapped by a linear gradient elution with aq. acetonitrile. The program ends with a steep gradient increase in ionic strength, necessary to elute the last components. The details of the gradient program are given in the experimental section.

The numbering of the components is indicated by the elution order of the alkyl-bonded phase separation, thus illustrating discrimination by differences in the hydrophobic surface area of the analytes. The elution order on the diol-Gly-Phe-Phe phase is significantly different from that on C_8. The separation on the peptide-bonded phase is brought about by the multifunctional mechanisms of reversed-phase and

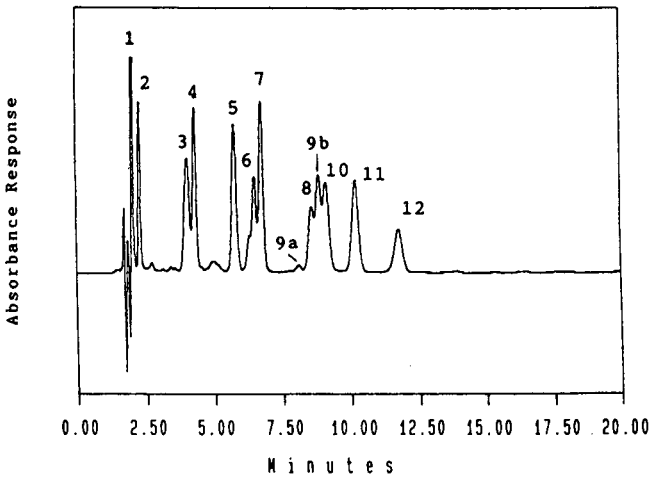

Fig. 7. Separation of an enzyme-inhibitory peptide mixture on a 25-cm Spherisorb C_8 column with an isocratic mobile phase of acetonitrile–aq. solution of 0.05 *M* in TFA and 0.04 *M* in triethylamine (40:60). Flow-rate, 1.5 ml/min; detection, at 254 nm.

cation-exchange chromatography. Components 1 and 2 are eluted early from the C_8 column and last from the diol-Gly-Phe-Phe column. These two components are unique in that the N-terminus is deblocked, thus providing an additional positive charge for the cation-exchange interaction on the diol-Gly-Phe-Phe phase. Component 13 is not eluted from the C_8. Components 8, 9a, 9b and 10 are eluted from the C_8 column in the same region, while the diol-Gly-Phe-Phe-bonded phase separation of these components differ greatly in their retention times, and the elution order is reversed. Components 9a and 9b are diastereomers, differing only in the configuration of the phenylalanine group; whereas 8 and 10 are isomers differing only in the position of a methyl group on the histidine residue (Fig. 9).

It may be postulated that the methyl group on the 3-methylhistidyl derivative (component 10) contributes more to the hydrophobic surface area of the molecule

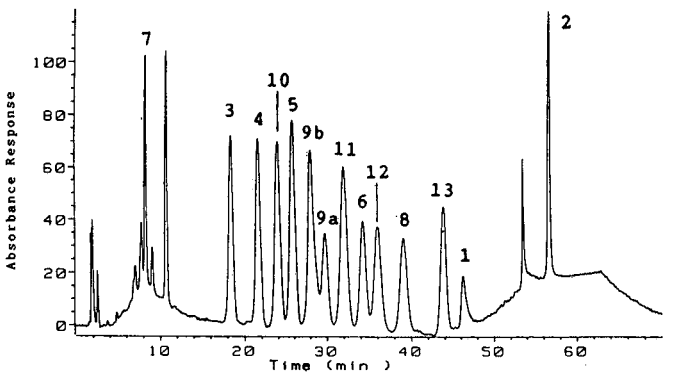

Fig. 8. Separation of the same peptide mixture as in Fig. 7 on a 15-cm diol-Gly-Phe-Phe column by gradient elution (see text for details). Components numbered according to elution order in Fig. 7.

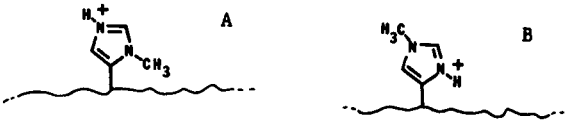

Fig. 9. Partial structures of (A) 1-methylhistidyl peptide derivative (component 8); (B) 3-methylhistidyl peptide derivative (component 10).

than does the 1-methylhistidyl derivative (component 8), where one might envision the methyl group being more imbedded in the molecule. This is consistent with the results of the C_8 separation, where one would expect the more hydrophobic molecule to have a greater retention. Conversely, on the diol-Gly-Phe-Phe-bonded phase the 1-methylhistidyl derivative (component 8) is much more strongly retained than the 3-methylhistidyl (component 10) derivative. This implies that the cation-exchange mechanism plays a critical role and that the more exposed the charged group is or the greater the differences in pK_a values, the greater is the partitioning interaction. This hypothesis is further supported by the change in capacity factors as a function of pH of the mobile phase, shown in Fig. 10. As the pH decreases from 7 to 5, the capacity factors increase as the methylhistidyl groups become more protonated. Below pH 5 the capacity factors drop off as the carboxylic acid terminal of the diol-Gly-Phe-Phe-bonded phase is protonated, thus eliminating its cation-exchange capacity. Also, the greater cation-exchange interaction of the 1-methylhistidyl derivative (component 8) is indicated by a greater increase in capacity factor compared to the 3-methylhistidyl derivative (component 10) with decreasing ionic strength of the mobile phase (Fig. 11). The degree of reversed-phase interaction is exhibited by the increase in capacity factors of the two components as a function of the acetonitrile content of the mobile

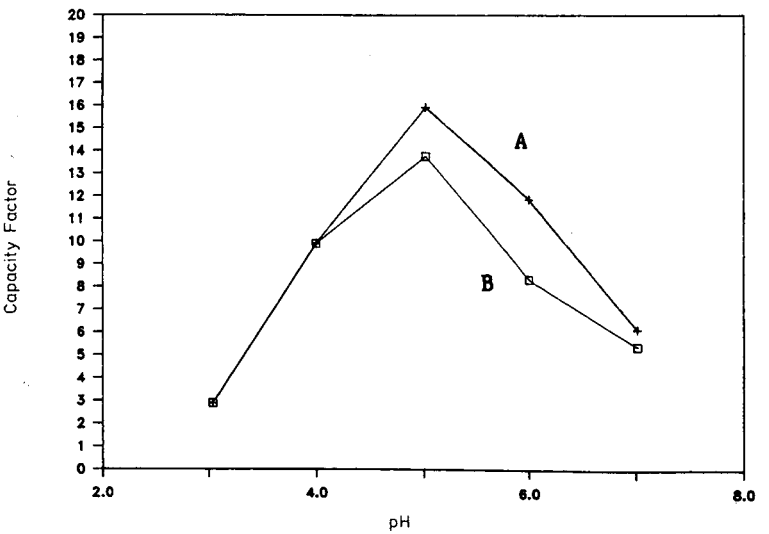

Fig. 10. Change in capacity factors of (A) 1-methylhistidyl and (B) 3-methylhistidyl derivatives as a function of pH with a 0.05 *M* ammonium phosphate–acetonitrile (82:18) isocratic mobile phase on a 25-cm diol-Gly-Phe-Phe column. Flow-rate 1.0 ml/min; temperature, 40°C.

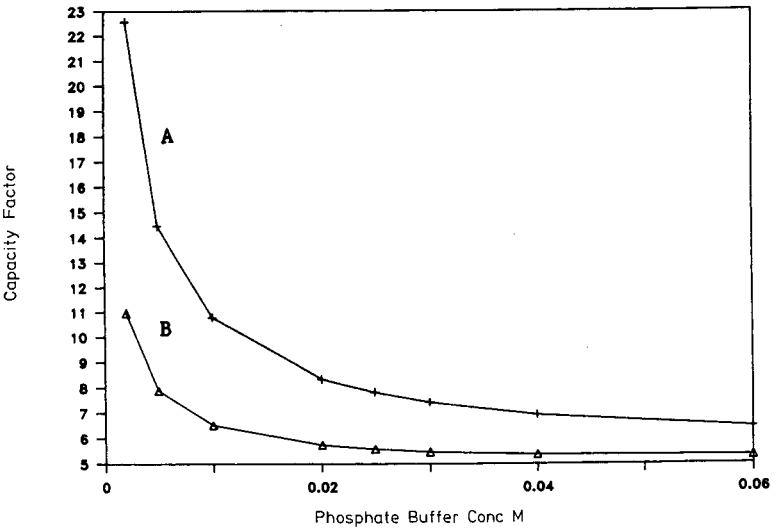

Fig. 11. Change in capacity factors of (A) 1-methylhistidyl and (B) 3-methylhistidyl derivatives as a function of mobile phase ammonium phosphate concentration at a constant pH of 6 and acetonitrile concentration of 18% with isocratic elution from a 15-cm diol-Gly-Phe-Phe column. Flow-rates 1.0 ml/min; temperature, 40°C.

phase (Fig. 12). Plots of log k *vs.* percent acetonitrile for the two components are linear and parallel with correlation coefficients of 0.99 and with indentical slopes of -0.05.

Amino acids, dipeptides, and tripeptides

Table III shows retention data for the elution of selected amino acids, dipeptides, and tripeptides for a 25 cm x 4.6 mm diol-Gly-Phe-Phe-bonded phase column under weak mobile phase conditions. As one can see, the amino acids glycine and phenylalanine and the dipeptides are not well retained. Although a retention time difference can be observed between 1-methylhistidine and 3-methylhistidine, they would not be resolved from one another. The glycylphenylalanine enantiomers are not distinguished from each other, but are slightly more retained than the D-phenylalanylglycine isomer; however, neither would be separable from one another. In like manner, the isomeric pair glycylglycyl-L-phenylalanine and L-phenylalanylglycylglycine exhibits a slight difference in retention, yet not enough to achieve resolution. On the other hand, the D-phenylalanyl-L-phenylalanylglycine and D-phenylalanyl-D-phenylalanylglycine diastereomers would be baseline resolved. This indicates that free amino acids, dipeptides, and some tripeptides could likely be resolved from larger peptides. However, minor modification in these small peptides will not enable separation of these isomers, except in the case of tripeptide diastereomers with sufficient hydrophobicity.

Column performance

Although the diol-Gly-Phe-Phe packings can provide unique selectivity for the separation of various peptides, the columns are inherently less efficient than alkyl-

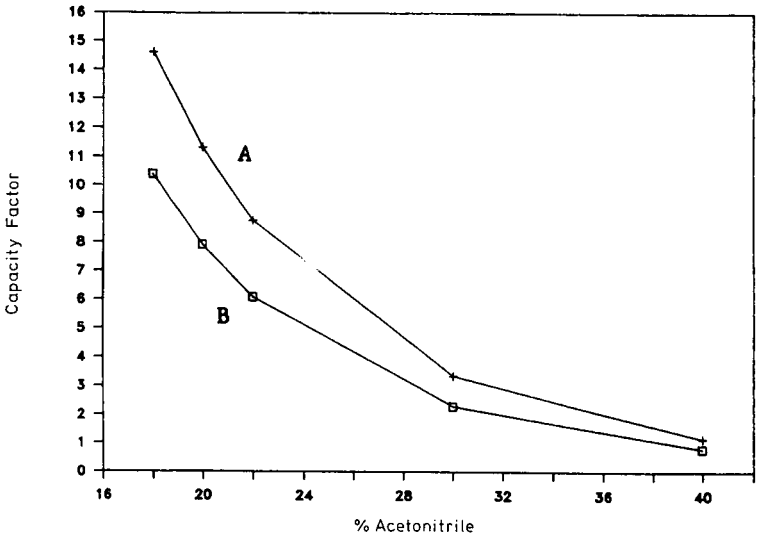

Fig. 12. Change in capacity factors of (A) 1-methylhistidyl and (B) 3-methylhistidyl derivatives as a function of mobile phase acetonitrile concentration combined with an aqueous 0.04 *M* ammonium phosphate buffer (pH 6) with isocratic elution from a 25-cm diol-Gly-Phe-Phe column.

TABLE III

SEPARATION OF SELECTED AMINO ACIDS, DIPEPTIDES, AND TRIPEPTIDES ON A DIOL-GLY-PHE-PHE-BONDED PHASE COLUMN

The separations were performed on a 25 cm x 4.6 mm diol-Gly-Phe-Phe ISRP column under isocratic conditions by constant metering of solvents A, B and C at 94%, 1% and 5%, respectively.

	t_R (min)	k
Amino acids		
L-Glycine	2.73	0.44
L-Phenylalanine	3.24	0.71
L-Histidine	11.59	5.10
3-Methylhistidine	13.34	6.03
1-Methylhistidine	13.88	6.31
Dipeptides		
D-Phe-Gly	3.05	0.61
Gly-L-Phe	3.20	0.68
Gly-D-Phe	3.20	0.68
Tripeptides		
Gly-Gly-L-Phe	2.94	0.55
L-Phe-Gly-Gly	3.10	0.67
D-Phe-L-Phe-Gly	5.59	1.94
D-Phe-D-Phe-Gly	7.31	2.85

bonded phases, because of slower stationary phase mass transfer. The 5-μm ISRP columns can typically achieve 30 000 plates/m, whereas conventional alkyl bonded phases can exhibit twice this amount. The column-to-column reproducibility of the packing is comparable to other silica-bonded phases. When comparing the 15-cm and 25-cm ISRP columns of this study, which were manufactured from different lots of packing, it was found that relative retentions of peptide components varied by an average of 5% between columns, but the slopes of log k *vs.* % acetonitrile for single components were identical between columns.

For the peptide-bonded phases produced by Grushka and co-workers[10–12] and Howard *et al.*[14], chemical stability was a limitation, because of the hydrolysis of the ester linkage connecting the peptides to the support spacers. The peptide-bonded phases produced in this manner were found to display a 50% drop in performance after about two months of use[14]. With the diol-Gly-Phe-Phe-bonded phases, the tripeptide is bound to a glycerylpropyl group by means of a carbonyldiimidazole reaction, producing a carbamate linkage between the peptide and the spacer, which is more stable[24]. A cursory evaluation of the diol-Gly-Phe-Phe-bonded phase stability can be obtained from the 15-cm ISRP column used in this study. After one year of periodic use for *ca.* 350 separations, retention times had decreased by an average of 40%. However, the relative retention between components varied by only 6%, and original retention times could be restored by decreasing the mobile phase strength. In some cases, resolution could not be restored between closely eluted components because of lost efficiency. It should be noted, that all separations were conducted without the use of guard columns. Previous studies have shown that efficiency loss can be prevented by the use of guard columns, even when serum is directly injected[30]. The diol-Gly-Phe-Phe-bonded phase with the carbamate linkage does appear to be more chemically stable than peptide-bonded phases produced with ester linkages, but definitive conclusions in this regard must await further investigation.

CONCLUSION

It was found that the diol-Gly-Phe-Phe silica bonded phase packings provide unique selectivity in the separation of positively charged hydrophobic peptides (<2000 a.m.u.) through multifunctional reversed-phase and cation-exchange partitioning mechanisms. The retention of peptide components can be controlled by alteration in either the mobile phase ionic strength or organic solvent composition. The use of ion-pairing agents, organic amine modifiers, or low pH is unnecessary, because selectivity differences are generated by the peptide-bonded phase itself. The disadvantages of the diol-Gly-Phe-Phe phases, compared to conventional alkyl-bonded phases, are lower efficiency, greater expense, and a lack of established theory for predicting multifunctional retention characteristics. These disadvantages are typical of specialty columns, and customarily, this is the price one pays for achieving a desirable end. In the case of the diol-Gly-Phe-Phe ISRP columns, it may be either the greater selectivity necessary to gain a desired separation between specific analytes with subtle structural differences or the reduction of sample clean-up procedures normally required for matrices containing unwanted proteins. In addition to blood serum or plasma, the latter category also includes plant samples, such as that recently analyzed by Meriluoto and Eriksson[31] with the ISRP separation of peptide toxins from cyanobacterial blooms.

ACKNOWLEDGEMENTS

The authors wish to express their gratitude to F.W. Crow, R. Lehrman, K.D. Evans and R.A. Conradi for providing various peptide samples; and to K.D. Evans for conducting the reversed-phase C_8 separation, illustrated in Fig. 7. Particular thanks are also extended to H. Nakamura of the University of Tokyo for permission to include Table I and Fig. 3.

REFERENCES

1 M.T.W. Hearn, in Cs. Horváth (Editor), *High-Performance Liquid Chromatography: Advances and Perspectives*, Vol. 3, Academic Press, New York, 1983, p. 88.
2 I. Molnár and Cs. Horváth, *J. Chromatogr.*, 142 (1977) 623.
3 M.J. O'Hare and E.C. Nice, *J. Chromatogr.*, 171 (1979) 209.
4 J.L. Meek and Z.L. Rossetti, *J. Chromatogr.*, 211 (1981) 15.
5 M.A. Stadalius, M.A. Quarry and L.R. Snyder, *J. Chromatogr.*, 327 (1985) 93.
6 Cs Horváth, W. Melander and I. Molnár, *J. Chromatogr.*, 125 (1976) 129.
7 R.F. Rekker, *The Hydrophobic Fragmental Constant*, Elsevier, Amsterdam, 1977, p. 31.
8 T.R. Floyd and R.A. Hartwick, in Cs. Horváth (Editor), *High-Performance Liquid Chromatography: Advances and Perspectives*, Vol. 4, Academic Press, New York, 1987.
9 J.B. Crowther and R.A. Hartwick, *Chromatographia*, 16 (1982) 349.
10 E.J. Kikta and E. Grushka, *J. Chromatogr.*, 135 (1977) 367.
11 G.W.-K. Fong and E. Grushka, *J. Chromatogr.*, 142 (1977) 299.
12 G.W.-K. Fong and E. Grushka, *Anal. Chem.*, 50 (1978) 1154.
13 J.A. Corbin, J.E. Rhoad and L.B. Rogers, *Anal. Chem.*, 43 (1971) 327.
14 W.A. Howard, T.B. Hsu, D.A. Nelson and L.B. Rogers, *Anal. Chem.*, 57 (1985) 606.
15 I.H. Hagestam and T.C. Pinkerton, *Anal. Chem.*, 57 (1985) 1757.
16 T.C. Pinkerton, T.D. Miller, S.E. Cook, J.A. Perry, J.D. Rateike, T.J. Szczerba, *Biochromatography*, 1 (1986) 98.
17 T. Nakagawa, A. Shibukawa, N. Shimono, T. Kawashima and H. Tanaka, *J. Chromatogr.*, 420 (1987) 297.
18 S.E. Cook and T.C. Pinkerton, *J. Chromatogr.*, 368 (1986) 233.
19 S.H. Chang, K.M. Gooding and F.E. Regnier, *J. Chromatogr.*, 120 (1976) 321.
20 G. Gubitz, W. Jellenz and W. Sant, *J. Liq. Chromatogr.*, 4 (1981) 701.
21 J. Hermansson, *J. Chromatogr.*, 269 (1983) 71.
22 D.E. Schmit, R.W. Giese, D. Conron, B.L. Karger, *Anal. Chem.*, 52 (1980) 177.
23 K.K. Unger, *Porous Silica* (*Journal of Chromatography Library*, Vol. 16), Elsevier, Amsterdam, 1979, Ch. 6, p. 219.
24 G.S. Bethell, J.S. Ayers, M.T.W. Hearn and W.S. Hancock, *J. Chromatogr.*, 219 (1981) 361.
25 H. Tanaka, M. Koike, T. Nakajima, *Anal. Sci.*, 2 (1986) 385.
26 T.C. Pinkerton and I.H. Hagestam, *U.S. Pat.*, 4 544 485 (1985).
27 R.A. Sams and L.L. Evec, *ISRP Application Note No. 25*, Regis Chemical Company, Morton Grove, IL, August 31, 1987.
28 H. Nakamura, presentation delivered to the 30th Annual Symposium on Liquid Chromatography in Japan, Kyoto, Japan, January 27–28, 1987, Abstracts, p. 63.
29 R.B. Merrifield, L.D. Vizioli and H.G. Boman, *Biochemistry*, 21 (1982) 5020.
30 T.J. Szczerba, *Regis Application Notes No. 9*, Regis Chemical Company, Morton Grove, IL, June 5, 1986.
31 J.A.O. Meriluoto and J.E. Eriksson, *J. Chromatogr.*, 438 (1988) 93.

Journal of Chromatography, 458 (1988) 147–167
Elsevier Science Publishers B.V., Amsterdam — Printed in The Netherlands

CHROMSYMP. 1425

COMPUTER SIMULATION OF HIGH-PERFORMANCE LIQUID CHROMATOGRAPHIC SEPARATIONS OF PEPTIDE AND PROTEIN DIGESTS FOR DEVELOPMENT OF SIZE-EXCLUSION, ION-EXCHANGE AND REVERSED-PHASE CHROMATOGRAPHIC METHODS

ROBERT S. HODGES*, J. M. ROBERT PARKER, COLIN T. MANT and RENU R. SHARMA
Department of Biochemistry and the Medical Research Council of Canada Group in Protein Structure and Function, University of Alberta, Edmonton, Alberta T6G 2H7 (Canada)

SUMMARY

A computer program, called Pro Digest-LC, has been developed which assists scientists in devising methods of size-exclusion, cation-exchange and reversed-phase high-performance liquid chromatography for the analytical separation and purification of biologically active peptides and peptide fragments from enzymatic and chemical digests of proteins. Pro Digest-LC accurately predicts the retention behaviour of peptides of known composition, containing 2–50 amino acid residues, and simulates the elution profiles in all three modes of chromatography. In addition, Pro Digest-LC is a user-friendly program, designed as a teaching aid for both students and researchers in selecting the correct conditions for chromatography, that is, the mode of chromatography, column selection, mobile-phase selection, and has the ability to examine the effects of flow-rate, gradient-rate, and sample size on the separation.

We have designed a set of peptide standards for each mode of chromatography to aid the researcher in eliminating non-specific interactions, to standardize retention behaviour on the user's columns, to monitor column performance and to compare packing materials. In the development of each prediction mode, experimental peak heights, peak widths, and retention times from model synthetic peptide standards were incorporated directly into the program and can be used as default values.

Pro Digest-LC is an interactive program, in that researchers can run peptide standards on their particular columns and enter the peak width at half-height, peak height, retention time and quantity injected to adjust the simulation to their particular column. The simulated experiments eliminate the time-consuming trial-and-error methods used to suitable separation or purification procedures. The researcher would perform the actual experiment only after predicting the optimized conditions, thereby saving valuable sample and research time. The general concepts of the program along with representative separations of protein digests are displayed.

INTRODUCTION

The efficient isolation of peptides has become increasingly important for an ever-widening range of research disciplines in recent years. High-performance liquid

0021-9673/88/$03.50

chromatography (HPLC) has proved very versatile in the separation and purification of peptides from a great variety of sources. Peptide mixtures derived from different sources differ widely in complexity and quantity, and the approach to their separation must be tailored to the separation goals.

Separation of peptides from a chemical and/or proteolytic digest of a protein is a very common requirement. Investigation of the properties of peptides is vital in structure–function relationship studies of proteins, and one approach to locating biologically active regions of proteins is to purify all the fragments from a protein digest for subsequent testing of biological or binding activity. After incorporation of structural probes, during chemical modification studies, identification of the position and percent labelling in the protein is required. By digesting the protein and separating the digest fragments, the location of the labelled peptide and amount of labelling can be determined. Purified native protein fragments can be used to screen native polyclonal or monoclonal antisera for locating immunogenic determinants in proteins. In addition, purified native protein fragments can be used for the preparation of antipeptide antibodies, which can, in turn, be used in structure–function relationship studies, as diagnostics, or in the development of synthetic vaccines for viral and bacterial pathogens.

Advances in biotechnology have provided the ability to prepare proteins for therapeutic purposes. However, during biosynthesis, impurities very close to the desired protein will be present. These impurities can arise from host-cell proteins, expression errors, incomplete post-translational modification, and chemical modification during purification. Separation systems are required to detect small changes in the polypeptide chain, such as deletion or substitution of one amino acid, deletion or addition of carbohydrate, oxidation of a single methionine or cysteine residue, or deamidation at a single site. Thus, peptide mapping, following protein digestion by chemical or proteolytic agents, is one way to verify the structure of a genetically engineered protein.

Peptides obtained from biological tissues are often found in only very small quantities and may require extensive purification. Thus, being able to predict the location of a biologically active peptide from various tissue sources in chromatograms obtained by different modes would be extremely beneficial.

The wide use of automated solid-phase peptide synthesis in recent years has also necessitated efficient isolation of peptides from various impurities. An efficient peptide synthesis should result in only a small number of synthetic impurities. However, these impurities are usually closely related to the peptide of interest (deletion, terminated, or chemically modified peptides), perhaps missing only one amino acid residue, and may be difficult to separate by any single HPLC mode.

Peptides derived from various sources differ widely in size, net charge, and hydrophobicity, and purification of a single peptide from a complex mixture will require an approach different from that necessary for separating all components of a mixture. The former approach may require the application of only a single HPLC mode. In contrast, the latter will require a combination of separation modes (multimode HPLC) for efficient resolution of all desired peptides[1–3]. The three main modes of HPLC used for peptide separations utilize differences in peptide size (size-exclusion HPLC or SEC), net charge (ion-exchange HPLC or IEC), or hydrophobicity (reversed-phase HPLC or RPC). Within these modes, mobile-phase conditions may be

manipulated to maximize the separation potential of a particular HPLC column. Although a desired peptide separation may be obtained by trial and error, this may take many attempts, with subsequent loss of time and final peptide yield. This could be a particular problem where only limited amounts of sample are available.

A computer software program, Pro Digest-LC, has been developed which assists scientists in devising methods for the analytical separation and purification of biologically active peptides and peptide fragments from enzymatic and chemical digests of proteins by SEC, IEC, or RPC. The experiments simulated on the computer eliminate the time-consuming trial-and-error methods involved in obtaining suitable separation or purification methods. In addition, Pro Digest-LC is also a teaching aid for chromatographers, designed to help the student or researcher to select the correct conditions for chromatography, *i.e.*, the mode of chromatography, column and mobile phase, and to allow him the ability to examine the effect of flow-rates, gradient-rates and sample size on the separation.

This paper introduces the user-friendly program, Pro Digest-LC, reviews the concepts which led to its development, and demonstrates many of its simulation capabilities.

EXPERIMENTAL

Materials

HPLC-grade water and acetonitrile were obtained from Fisher Scientific (Fairlawn, NJ, U.S.A.). HPLC-grade trifluoroacetic acid (TFA) was obtained from Pierce (Rockford, IL, U.S.A.).

The peptide standards described were synthesized on a Beckman Model 990 peptide synthesizer (Beckman Instruments, Berkeley, CA, U.S.A.) by means of the general procedure for solid-phase synthesis, described by Parker and Hodges[4].

Two sets of peptide standards were obtained from Synthetic Peptides Incorporated (Department of Biochemistry, University of Alberta, T6G 2H7, Canada). A mixture of four synthetic undecapeptide standards (1–4) was utilized for RPC and IEC. Peptides 1 and 2 were based on the sequence, X^1-X^2-Gly-Leu-Gly-Gly-Ala-Gly-Gly-Leu-Lys, where X^1-X^2 were substituted with G^1-G^2- (peptide 1) or Lys^1-Tyr^2- (peptide 2); peptides 3 and 4 were based on the sequence, X^1-X^2-Ala-Leu-Lys-Ala-Leu-Lys-Gly-Leu-Lys, where X^1-X^2- were substituted with G^1-G^2- (peptide 3) or Lys^1-Tyr^2- (peptide 4). Each peptide contained and N^{α}-acetylated N-terminal and a C-terminal amide. A polymer series of five synthetic peptides was used for SEC. The sequence of the standards was Ac-(Gly-Leu-Gly-Ala-Lys-Gly-Ala-Gly-Val-Gly)$_n$-amide, where n = 1–5.

Apparatus

The HPLC instrument consisted of a Varian (Walnut Creek, CA, U.S.A.) Vista Series 5000 liquid chromatograph coupled to a Hewlett-Packard (Avondale, PA, U.S.A.) HP1040 detection system, HP85B computer, HP9121 disc drive, HP2225A Thinkjet printer and HP7470A plotter. Samples were injected with a 500-μl injection loop (Model 7125, Rheodyne, Cotati, CA, U.S.A.).

Peptide mixtures were separated on four columns: (1) SynChropak GPC60 size-exclusion column (300 × 7.8 mm I.D., 10-μm particle size, 60-Å pore size; Syn-

Chrom, Linden, IN, U.S.A.); (2) SynChropak S300 strong-cation-exchange column (250 × 4.1 mm I.D., 6.5-μm particle size, 300-Å pore size; SynChrom); (3) Aquapore RP-300 C_8 reversed-phase column (220 × 4.6 mm I.D., 7-μm particle size, 300-Å pore size; Brownlee Labs., Santa Clara, CA, U.S.A.); (4) SynChropak RP-P C_{18} reversed-phase column (250 × 4.6 mm I.D.; 6.5-μm particle size, 300-Å pore size; SynChrom).

HPLC-derived data for program development

(1) SEC: mobile phase, 50 m*M* KH_2PO_4 (pH 6.5), containing 0.1 *M* potassium chloride. A mixture of three synthetic peptide polymers (10, 20 and 50 residues) was chromatographed (total sample loads of 2–16 nmol of peptides) in sample volumes of 10, 25, 50, 100 and 200 μl at flow-rates of 0.2, 0.5 and 1.0 ml/min.

(2) IEC: mobile phase, buffer A was 5 m*M* KH_2PO_4 (pH 3.0 or pH 6.5) and buffer B was 5 m*M* KH_2PO_4 (pH 3.0 or pH 6.5), containing 1.0 *M* sodium chloride. The mixture of four synthetic undecapeptide standards (+1 to +4 net charge) was subjected to strong-cation-exchange chromatography (pH 3.0 and pH 6.5) at flow-rates of 0.5, 1.0 and 2.0 ml/min and linear gradient-rates of 5, 10 and 20 m*M* sodium chloride/min. Total sample loads ranged from 2 to 40 nmol of each peptide.

(3) RPC: mobile phase, eluent A was 0.1% aq. TFA and eluent B was 0.05% TFA in acetonitrile (pH 2.0). The mixture of four synthetic undecapeptide standards was subjected to RPC at flow-rates of 0.5, 1.0 and 2.0 ml/min and linear gradient-rates of 0.5, 1.0 and 2.0% acetonitrile/min. Total sample loads ranged from 2 to 40 nmol of each peptide.

Absorbances were measured at 210 nm for SEC, and at 210 and 280 nm (to detect tyrosine absorbance) for IEC and RPC.

Data from these chromatographic experiments were used to derive equations predicting the effects of experimental parameters (sample size, sample volume, flow-rate and gradient-rate) on peptide retention times, peak heights, peak widths and resolution. Simulated elution profiles, generated by the program, are based on the mobile phases used to derive the equations.

Computer hardware requirements

The minimum requirement for operating this program is an IBM-AT or compatible computer with 256K memory, equipped with two floppy disk drives and a monitor with graphics capability. We strongly recommend a math coprocessor (for example, calculations that take approximately 2 min on the IBM-AT can be done in *ca.* 15 s with the math coprocessor).

General features of the program

The most important requirement of any computer program is that it be user-friendly. Each menu is self-explanatory in Pro Digest-LC, providing simple instructions and one-letter keying to access any particular section of the program. An example of the clarity of the Pro Digest-LC presentation is illustrated in Fig. 1. This figure demonstrates the rapid access to a stored protein file, starting from the HPLC Main Menu (section A). Depressing the "Digest" key ("D") selects the Protein Menu (section B). Depressing the "L" key (for loading/viewing/editing a stored protein file) in the Protein Menu brings up the option of scrolling to the desired protein (TnI, in this

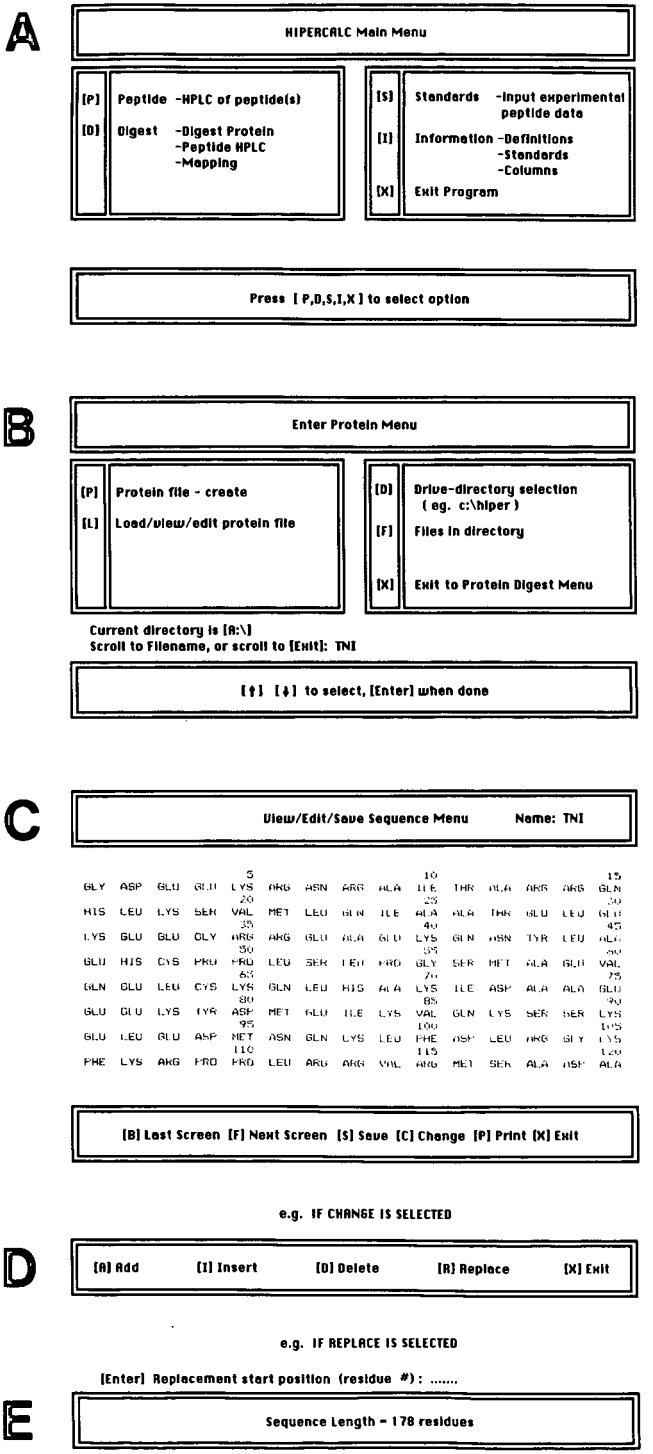

Fig. 1. Examples of the menus of Pro Digest-LC. Panel A shows the main menu of the program. Panel B shows the protein menu, where protein files are created or loaded for subsequent analysis. Panel C shows how protein sequences may be viewed and, if required, modified (panels D and E).

case), followed by pressing "enter". The sequence of the protein now appears on the screen (section C). Various options are now open to the researcher. When viewing the protein sequence, depressing "F" advances the display to the next screen for more of the protein sequence. Depressing "B" returns it to the screen showing the previous part of the protein sequence. The protein sequence can also be printed ("P") on an external printer. If a change in the sequence is required, depressing "C" brings up the options shown in section D. Amino acid residues may be added ("A"), inserted ("I"), deleted ("D"), or replaced ("R"). Depressing any of these keys brings up self-explanatory instructions similar to those shown for replacement of an amino acid residue (section E). It should be noted that during any manipulation of the protein sequence (*e.g.*, sections D and E), the protein sequence is always shown on the computer screen. This enables the operator to verify that the required change has been made. Depressing "X" exits the screen being displayed to the previous options or menu. Once section C has been reached again, the researcher can save ("S") a particular modified protein sequence for future work under a new file name.

From the HIPERCALC Main Menu screen (HIPERCALC stands for high-performance calculations in liquid chromatography), the operator has four options (Fig. 1, section A).

Option 1: Information menu

Pro Digest-LC is a teaching aid for chromatographers, designed to help them to select the correct conditions for chromatography, *i.e.*, the mode of chromatography, column, mobile-phase and to provide them with the ability to examine the effect of flow-rates, gradient-rates and sample size on the elution profile. From the information menu, the operator can select the following sections.

(a) Definitions. This section provides definitions of HPLC parameters used in the program.

(b) Standards information menu. This section describes peptide standards that are available for SEC, IEC and RPC. Once the operator is in the Standards information menu, he has a choice of SEC, IEC, RPC and a list of references. For each method of chromatography, the design features of the standards are described; the reasons for the development of the standards are described, together with examples of separations of the standards by means of various mobile phases, to demonstrate the importance of standards in selecting mobile-phase conditions. In addition, ordering information is provided for the peptide standard kits.

(c) The columns and conditions screen. In this section, the mode of chromatography (SEC, IEC and RPC) or column maintenance and storage conditions can be selected. For each mode of chromatography, reasons are given for using a particular mode for the separation of peptides and for choosing a particular column; the utility of peptide standards for monitoring the resolving power of a column under various mobile-phase conditions and the value of peptide standards in detecting non-specific interactions with column packings are described; and detailed instructions are given for changing the composition of the mobile phase to avoid any non-specific interactions observed, together with examples of appropriate mobile phases, flow-rates and gradient-rates suitable for achieving a desired separation. All relevant references are listed, so that the researcher can quickly access more detailed information, if he desires.

Option 2: Standards data menu

On accessing the Standards data menu, the operator can create a Standards file or load/view/edit Standard data files in the program. The purpose of the Standards data file is to provide the researcher with the option of either using our default file or entering data on standards chromatographed on his columns with his instrumentation. For example, after chromatographing a set of standards on a particular column, the quantity injected, peak heights, peak widths, retention times and other parameters necessary for the program to adjust the predicted elution profiles to the researcher's particular column can be entered.

Option 3: Protein digest menu

Once in the protein digest menu, the operator has the option of entering a protein sequence and performing an enzymatic or chemical digestion of a particular protein sequence (Fig. 1, section B).

(a) Enter protein data

Create protein file: the particular protein sequence can be entered by a one-letter or three-letter code.

Load/view/edit protein file: on selecting this option, the operator can scroll through the list of proteins stored in the program and select the desired protein file. The computer requests the quantity of protein to be digested and applied to the HPLC column. The protein sequence is automatically displayed on the screen, and the sequence can be printed, changed and saved as a new file of required changes. The options of protein sequence manipulation have already been described (Fig. 1, sections C, D and E).

After loading the protein file, the operator exits to the Protein digest menu and selects "Digest" and then cyanogen bromide cleavage or an enzymatic cleavage by trypsin. The computer performs the digestion and then requests in the Protein HPLC column selection menu the mode of chromatography by which the digest is to be separated (SEC, IEC and RPC) and asks whether the peptide mapping option is desired. After the mode of chromatography is selected, the program requests the flow-rate and gradient-rate for RPC and IEC, or the flow-rate and sample volume for SEC. The elution profile is calculated and displayed within 1–15 s, depending on the complexity of the separation. The elution profile is always displayed initially on a time axis to the nearest 10 min after the last peak. After observing the profile, the user has the option of scrolling a cursor backwards or forwards under the peptide peaks to view the sequence, peptide length, and retention time for each peptide (Figs. 5 and 6). He has the option of listing the fragments and their retention times on an external printer (Table I) or of selecting the zoom option. The zoom option allows the researcher to enlarge any particular section of the chromatogram, changing the X-axis (elution time in min) and the Y-axis (milli-absorbance units) to any desired value (Figs. 5 and 6).

If the separation is unsatisfactory, the researcher has the option of trying other conditions to obtain an optimal separation. Once these conditions have been found, the researcher can then perform the actual experiment in the laboratory with great saving in methodology development time.

If the operator selects the peptide mapping option, he has the ability to add the particular digest of the mutant protein to the same digest of the native protein se-

TABLE I

COMPUTER-PREDICTED REVERSED-PHASE RETENTION TIMES OF CYANOGEN BROMIDE CLEAVAGE FRAGMENTS OF RABBIT SKELETAL TNI (SLOW AND FAST)

File: TnI + Slow TnI (mutant).

No.	*Residue*	*Retention time**	*Mutant*	*Fragment*
1	168–173	2.40	No	EGRKKM
2	166–168	2.44	Yes	SGM
3	117–121	6.84	No	SADAM
4	174–178	7.24	No	FESES
5	175–184	9.74	Yes	FDAAKSPTSQ
6	1–21	18.25	No	GDEEKRNRAI...ARRQHLKSVM
7	82–95	19.28	No	EIKVQKSSKELEDM
8	135–167	22.11	No	DLRANLKQVK...RKNIEEKSGM
9	121–133	22.68	Yes	LRALLGSKHKVSM
10	122–134	23.32	No	LKALLGSKHKVCM
11	1–20	24.67	Yes	PEVERKSKITASRKLLKSLM
12	134–165	25.02	Yes	DLRANLKSVK...GDWRKNVEAM
13	58–81	26.44	No	AEVQELCKQL...DAAEEEKYDM
14	96–116	26.85	No	NQKLFDLRGK...KRPPLRRVRM
15	21–120	28.80	Yes	LAKAKECQQE...RRVRVSADAM
16	22–57	31.10	No	LQIAATELEK...CPPLSLPGSM

* The computer simulates reversed-phase elution profiles obtained with a linear aq. TFA to TFA in acetonitrile gradient (1% acetonitrile/min) at a flow-rate of 1 ml/min.

quence. The reversed-phase and ion-exchange mode options can be selected and the elution profile calculated. The peptides found in the mutant that are different from those in the native sequence will be marked on the elution profile (Fig. 6). This can be extremely helpful when one is interested in only identifying the mutant peptides.

If the operator selects the "Compute column selection option" the program separates the digest by RPC and IEC (cation-exchange HPLC at pH 7.0) at the resolution selected by him. The program then indicates for each mode the number of peptides resolved out of the total number of peaks in the elution profile, and if both chromatographic modes are used, the total number of peptides resolved. This option is extremely useful in aiding the researcher in his decision whether multi-modal approaches are necessary for carrying out the separation.

Option 4: Peptide HPLC menu

This section of the program is designed so that the researcher can enter a single or multiple peptide sequences for separation by a particular mode of chromatography.

(a) Enter peptide data

Create peptide or working file: (i) Peptide file. (Enter the particular peptide sequence by a one-letter or three-letter code); (ii) working file. There are two options: one can group already entered peptides into a working file to examine separations of any group of desired peptides, or one can group together more than one working file of peptides. These options provide maximum flexibility to create groups of peptides one wishes to separate.

Load/view/edit file. In this section, one can load/view/edit any particular peptide or group of peptides in a working file. On viewing a particular working file, all the amino acid sequences are displayed on the screen for making sequence changes or printing out the sequences in the file. Peptides can be added to or deleted from the working file. In the peptide file, one can add, insert, delete, or replace any amino acids desired. Of course, after the files or the amino acid sequence of a particular peptide are changed, the information can be saved for future work.

(b) HPLC column and conditions section. In this section, one can select the mode of chromatography by which the particular peptide or group of peptides should be separated (SEC, IEC or RPC). After the mode of chromatography is selected, the flow-rate, gradient-rate, or sample volume desired is entered. As described previously, the elution profiles are calculated and displayed. The peptide sequences and retention times can be listed on an external printer or the zoom option can be used to expand a particular region of the chromatogram.

In a peptide file or a working file, containing a group of peptides, the quantity of the peptide(s) entered can be varied, thus making the program completely versatile.

The program is available from S.P.I. Synthetic Peptides Incorporated (Department of Biochemistry, University of Alberta, Edmonton, Alberta, Canada T6G 2H7).

RESULTS AND DISCUSSION

General concepts

Though RPC is, by far, the most widely-used mode of HPLC for peptide separations, it is unlikely that a single HPLC technique will resolve a very complex peptide mixture. As mentioned previously, it is often easier, even in the case of less complex mixtures, to utilize a combination of two or more HPLC modes, which utilize different selectivities, rather than attempt to optimize a single mode[1–3]. In addition, if only a single peptide or a few peptides in a complex mixture are desired, a particular HPLC mode which, on its own, may not resolve the whole mixture as well as another mode may still be the method of choice for the desired peptide(s)[3].

The standard trial-and-error approach to developing a HPLC purification method is costly in terms of sample loss as well as expenditure of time and effort. Thus, any methodology that can aid the researcher in selecting HPLC mode(s) and chromatographic conditions without using precious sample or requiring an extensive method development time would be advantageous.

For this reason, we have developed a computer simulation program based solely on predicting peptide retention behaviour in SEC, IEC and RPC. In order to predict peptide retention behaviour successfully, any deviations from ideal column behaviour, *i.e.*, non-specific interactions between the sorbent and solute, must be identified and suppressed or eliminated. This can be best accomplished by using peptide standards specifically designed to monitor column performance and non-specific interactions. In addition, the major breakthrough in our ability to predict retention times for peptides of 2–50 residues has resulted from the design and use of a series of synthetic peptide polymers.

Size-exclusion chromatography. Separation of peptides by a mechanism based solely on peptide size (ideal SEC) occurs only when there are no non-specific interac-

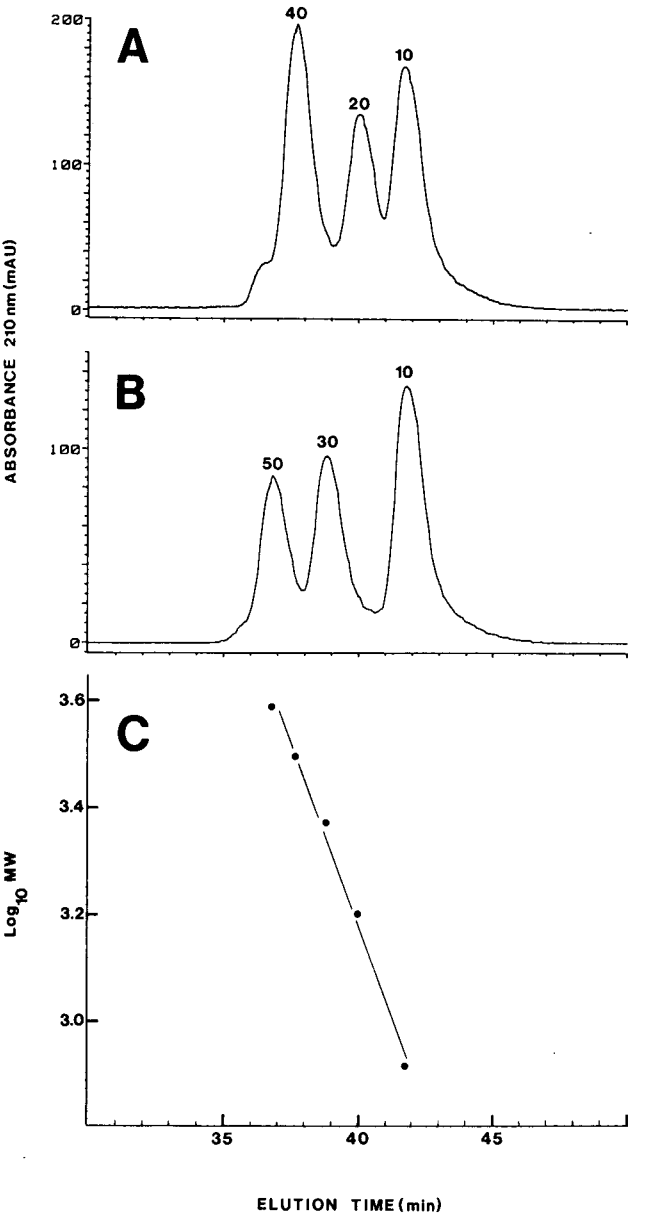

Fig. 2. Ideal SEC of mixtures of synthetic peptide standards. Conditions: column, SynChropak GPC60 (300 × 7.8 mm I.D.); mobile phase, 5 m*M* KH_2PO_4 (pH 7.0), containing 0.15 *M* sodium chloride; flow-rate, 0.2 ml/min; temperature, 26°C. Panel A: mixture of peptides containing 10, 20 and 40 residues. Panel B: mixture of peptides, containing 10, 30 and 50 residues. Panel C: plot of log molecular weight *versus* retention time of the peptide standards. The sequence of the peptide standards is Ac-(G-L-G-A-K-G-A-G-V-G)$_n$-amide, where *n* denotes the number of decapeptide repeating units (n = 1–5).

tions between the solutes and the column matrix. Although SEC columns are designed to minimize non-specific interactions, most modern SEC columns are weakly anionic (negatively charged) and slightly hydrophobic. This results in deviations from ideal size-exclusion behaviour, *i.e.*, non-ideal SEC[5–10]. The volume of solvent required to elute small molecules in ideal SEC is the total permeation volume of the column. This column parameter is a combination of the void volume of the column (elution volume of a totally excluded species) and the pore volume of the size-exclusion matrix. By definition, under ideal size-exclusion conditions, no molecule will be retained beyond the total permeation volume of the column.

A series of synthetic peptide standards (Ac-[G-L-G-A-K-G-A-G-V-G]$_n$-amide, where n = 1–5), designed for monitoring both non-ideal and ideal SEC behaviour, has proved extremely beneficial in enabling rapid development of optimal conditions for SEC of peptides[2,10]. The increasing size of the peptide standards (800–4000 daltons) enables an accurate molecular weight calibration of a column in ideal SEC; the increasingly basic character of the standards (+1 to +5) makes them sensitive to the anionic character of size-exclusion matrices; the increasing hydrophobicity of the polymer series enables a determination of column hydrophobicity.

The chromatographic profiles of mixtures of the size-exclusion standards (10, 20 and 40 residues in Fig. 2a); 10, 30 and 50 residues in Fig. 2b) on a SynChropak GPC60 silica-based size-exclusion column, coupled with the linear character of the $\log_{10}$ molecular weight *versus* peptide retention time plot (Fig. 2c), clearly demonstrates the ability of the polymer series to monitor pure size-exclusion behaviour on SEC columns.

A mixture of the 10-, 20- and 50-residue peptide standards was utilized for the GPC60 column to derive all the parameters required for the computer program. The sensitivity of the standards to any undesirable non-ideal SEC behaviour has already been clearly demonstrated[10]. Aqueous solvents and buffers containing 100–400 m*M* salt are commonly employed as the mobile phase for SEC to eliminate non-specific interactions. The mobile phase which produced the elution profiles shown in Fig. 2, for instance, consisted of 5 m*M* KH_2PO_4 (pH 7.0) containing 150 m*M* sodium chloride (flow-rate = 0.2 ml/min). In fact, efficient separation of peptide mixtures in the absence of salt is the exception rather than the rule[2,10].

Ion-exchange chromatography. The use of peptide standards in monitoring the retention characteristics of ion-exchange columns is twofold: firstly, to confirm that the column can, indeed, retain charged species and determine whether the column can retain peptides with net charges in the 0–1 range; secondly, to assess the effect of pH variations on the resolving capability and load capacity of an ion-exchange column. The latter is particularly important in cation-exchange chromatography, where manipulation of the mobile phase over the acidic to neutral pH range is frequently employed for peptide separations[1–3,11].

Fig. 3a demonstrates the elution profile of the five synthetic peptides described above on a SynChropak S300 strong-cation-exchange column (pH 7.0). The increasingly basic character of the standards makes them sensitive to the anionic character of the cation-exchange column. The standards were subjected to linear gradient elution (buffer A = 5 m*M* KH_2PO_4; buffer B = Buffer A + 1 *M* sodium chloride) at 20 m*M* salt/min and a flow-rate of 1 ml/min, following a 10-min isocratic elution with buffer A. At pH 7.0, peptides 2–5 (+2 to +5 net charge, respectively) were eluted by the salt

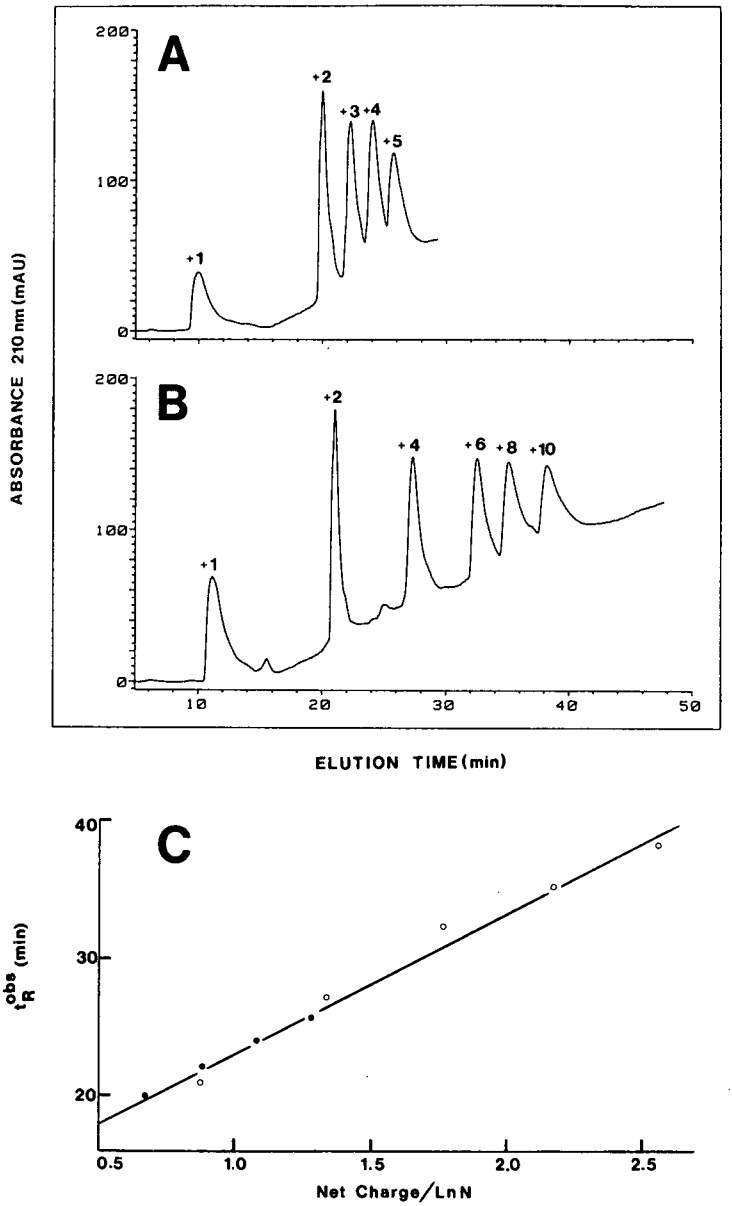

Fig. 3. Strong-cation-exchange chromatography of mixtures of synthetic peptide polymers. Conditions: column, SynChropak S300 (250 × 4.1 mm I.D.); mobile phase, linear AB gradient (20 m*M* salt/min), where buffer A is 5 m*M* KH_2PO_4 (pH 7.0), and buffer B is buffer A plus 1 *M* sodium chloride; flow-rate, 1 ml/min; temperature, 26 °C. Panel A: mixture of five synthetic peptide polymers (+1 to +5 net charge), where the sequence is Ac-(G-L-G-A-K-G-A-G-V-G)$_n$-amide, and *n* denotes the number of decapeptide repeating units (n = 1–5). Panel B: mixture of six synthetic peptide polymers (+1 to +10 net charge), where the sequence is Ac-(G-K-G-L-G)$_n$-amide, and *n* denotes the number of pentapeptide repeating units (n = 1–10). Panel C: plot of observed peptide retention time (t_R^{obs}) *versus* peptide net charge, divided by the log of the number of residues (net charge/ln *N*).

gradient, while peptide 1 (+1 net charge) was eluted during the initial isocratic elution.

An advantage of using IEC for peptides that is not shared by proteins is that, under benign mobile-phase conditions, the overall net charge on a peptide is generally fully expressed[2]. Indeed, Mant and Hodges showed that, under benign conditions [linear potassium chloride gradient (5 m*M*/min) in 5 m*M* KH_2PO_4 buffer], the elution times of several basic peptides (9–21 residues) on the cation-exchange column described above were linear with respect to their charges at pH 3.0 and pH 6.5. Similar observations have been made for a series of acidic peptides (−2 to −5 net charge) chromatographed on a strong-anion-exchange column.

The retention times of the four peptide standards retained by the IEC column (peptides 2–5) were also found to vary linearly with their net charges (+2 to +5, respectively). However, recent observations in this laboratory have suggested that charge density is also a factor affecting the retention behaviour of basic peptides on cation-exchange columns. To investigate this further, another set of peptide polymers was synthesized (Ac-[G-K-G-L-G]$_n$-amide, where n = 1, 2, 4, 6, 8 and 10, *i.e.*, 5–50 residues), with an overall hydrophobicity similar to that of the standards shown in Fig. 3a, but a higher charge density (+2/10 residues, as opposed to +1/10 residues for the initial polymer series). Fig. 3b shows the elution profile of this new polymer series on the S300 column, obtained under the same chromatographic conditions as the elution profile shown in Fig. 3a. Although the elution times of the five peptides retained by the column (+2 to +10 net charge) demonstrate satisfactory linearity with net charge (Fig. 3b) comparison of this elution profile with that in Fig. 3a clearly shows a charge density effect. For instance, the 50-residue peptide (+5 net charge) of the initial polymer series (Fig. 3a) is not retained as long as the 20-residue peptide (+4 net charge) of the new peptide series (Fig. 3b). From Fig. 3c, it can be seen that dividing the net charge of the peptides from the two polymer series by the logarithm of the number of residues they contain (ln N) and plotting this value against the observed retention time (t_R^{obs}) results in a single, straight-line plot, *i.e.*, plotting t_R^{obs} *versus* net charge/ln N instead of simply net charge corrects for charge density and peptide chain length. Additional confirmatory data have been collected to test this relationship more rigorously and will be submitted for publication in the near future.

These results, useful in correlating the overall net charge on a peptide at a given pH with its amino acid composition, have been used in the computer program to predict peptide retention times at pH 7.0 in cation-exchange chromatography.

Reversed-phase chromatography. Though excellent resolution of peptide mixtures may be obtained at both acidic or neutral pH, the majority of researchers have carried out RPC at pH values <3.0, using volatile buffers and linear AB gradients where A = 0.1% aq. TFA and B = 0.1% TFA in acetonitrile[2,3]. Reversed-phase silica-based packings may contain surface silanols which act as weak acids and are ionized above pH 3.5–4.0[9]. These negatively charged silanols may interact with the basic residues of peptides chromatographed on RPC columns and have an adverse effect on resolution, characteristically producing long retention times and peak broadening. Apart from the suppression of silanol ionization, acidic conditions are reasonable, because silica-based columns are more stable at low pH than at pH values close to neutrality.

As well as differing in selectivity, RPC columns may also vary in performance

characteristics due to non-specific interactions. Mant and Hodges[12], using synthetic peptide standards, have demonstrated non-specific interactions even at pH 2.0 with columns from different manufacturers, and have developed procedures to monitor the degree of these interactions at higher pH values.

The ability to separate peptides closely related in hydrophobicity (*e.g.*, differing by only one methyl group) should be a prerequisite of a reversed-phase column[2,3]. A mixture of five synthetic decapeptide RPC standards, S1–S5, has proved extremely useful in monitoring the peptide separation capabilities of reversed-phase columns[13–16]. The hydrophobicity of the standard increases only slightly between S2 and S5, between S2 and S3 there is an increase of two methyl groups, and between S4 and S5 there is an increase of an isopropyl group-enabling very precise determination of the resolving power of a reversed-phase column. Peptide S4 has also been used extensively in this laboratory as an internal peptide standard to correct for column and instrumentation variations in peptide retention time predictions for RPC[17–20].

Several research groups have determined sets of coefficients for predicting peptide retention times in RPC, on the assumption that the chromatographic behaviour of a peptide is mainly or solely dependent on amino acid composition, and this assumption holds well enough for small peptides (up to *ca.* 15 residues)[17,18,21–28]. Retention values have generally been obtained by computer-calculated regression analyses of the retention times of a wide range of peptides of varied composition[21–27]. These methods have not been successful for two reasons: first, the sampling of peptides has not been large enough to ensure a high frequency of occurrence of all amino acid residues; second, if there is a polypeptide-chain-length effect on retention behaviour, this effect would be averaged into values obtained for the retention coefficients, resulting in substantial errors[20,28]. The most precise set of coefficients currently available was reported by Guo *et al.*[17], who measured the contribution of individual amino acid residues to the retention time of a synthetic model peptide at a given chain length. The eight residue octapeptide sequence, Ac-G-X-X-L_3-K_2-amide, was substituted at position X by all 20 naturally occurring amino acids. The predicted retention time (τ) of a peptide in RPC was then equal to the sum of the retention coefficients (ΣR_c) for the amino acid residues in the peptide, plus the time correction (t_s) for the internal peptide standard (S4; see above).

Several researchers have noted that peptides larger than 15–20 residues tended to be eluted more rapidly than predicted from hydrophobic considerations alone[2,20,23–25,28–32]. Fig. 4a demonstrates an exponential relationship between peptide chain length and peptide retention time in RPC of the series of five size-exclusion standards (10–50 residues), described previously (Figs. 2a, b and 3a), on a SynChropak RP-P C_{18} column. The effect on peptide retention of increasing peptide length decreases progressively with each ten-residue addition. The intimate relationship between peptide hydrophobicity and chain length and their combined effect on peptide retention behaviour, already detailed by Mant *et al.*[20], is illustrated in Fig. 4b. Plotting the difference between predicted (τ) and observed (t_R^{obs}) retention time *versus* the product of peptide hydrophobicity (expressed as ΣR_c, the sum of the coefficients of Guo *et al.*[17]) and the logarithm of the number of residues ($\ln N$) results in a straight line plot. This relationship holds for peptides much greater in hydrophobicity than the size-exclusion polymer series, and is consistent for RPC columns of varying dimensions and hydrophobic functionalities (*n*-alkyl chain length) and ligand density[20].

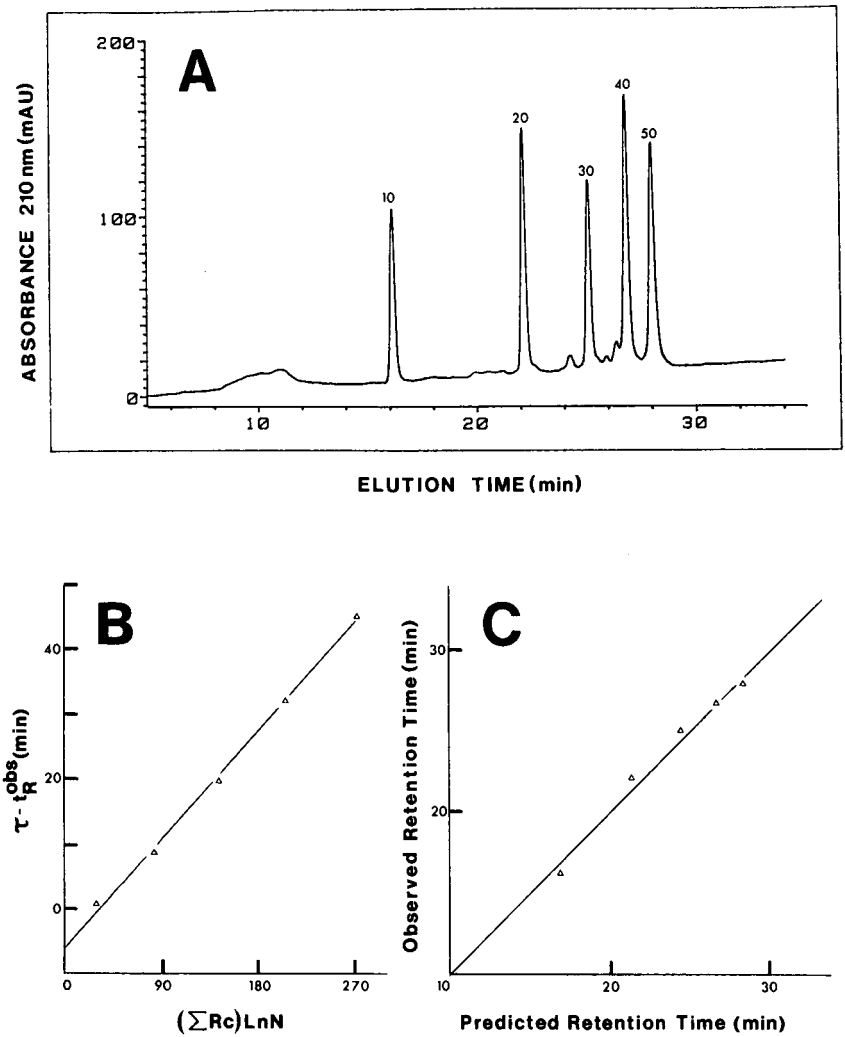

Fig. 4. RPC of a mixture of synthetic peptide polymers. Conditions: column, SynChropak RP-P C_{18} (250 × 4.6 mm I.D.); mobile phase, linear AB gradient (1% B/min), where eluent A is 0.1% aq. TFA and eluent B is 0.1% TFA in acetonitrile; flow-rate, 1 ml/min; temperature, 26°C. Panel A: elution profile of five peptide polymers (10–50 residues). Panel B: plot of predicted minus observed retention time ($\tau - t_R^{obs}$) *versus* the sum of the retention coefficients (ΣR_c) times the log of the number of residues (ln N). Panel C: correlation of predicted and observed retention times of the peptide polymers. The sequence of the peptide polymers is Ac-(G-L-G-A-K-G-A-G-V-G)$_n$-amide, where n denotes the number of decapeptides (n = 1–5).

Using the slope and intercept from such a plot, we can predict the retention behaviour of peptides up to 50 residues in length. Fig. 4c shows the good correlation between predicted and observed retention times of the polymer series, once peptide chain length has been taken into account. This predictive method formed the basis for simulation of reversed-phase peptide elution profiles by the computer program.

Though Figs. 2–4 only show the general concepts used to develop the computer

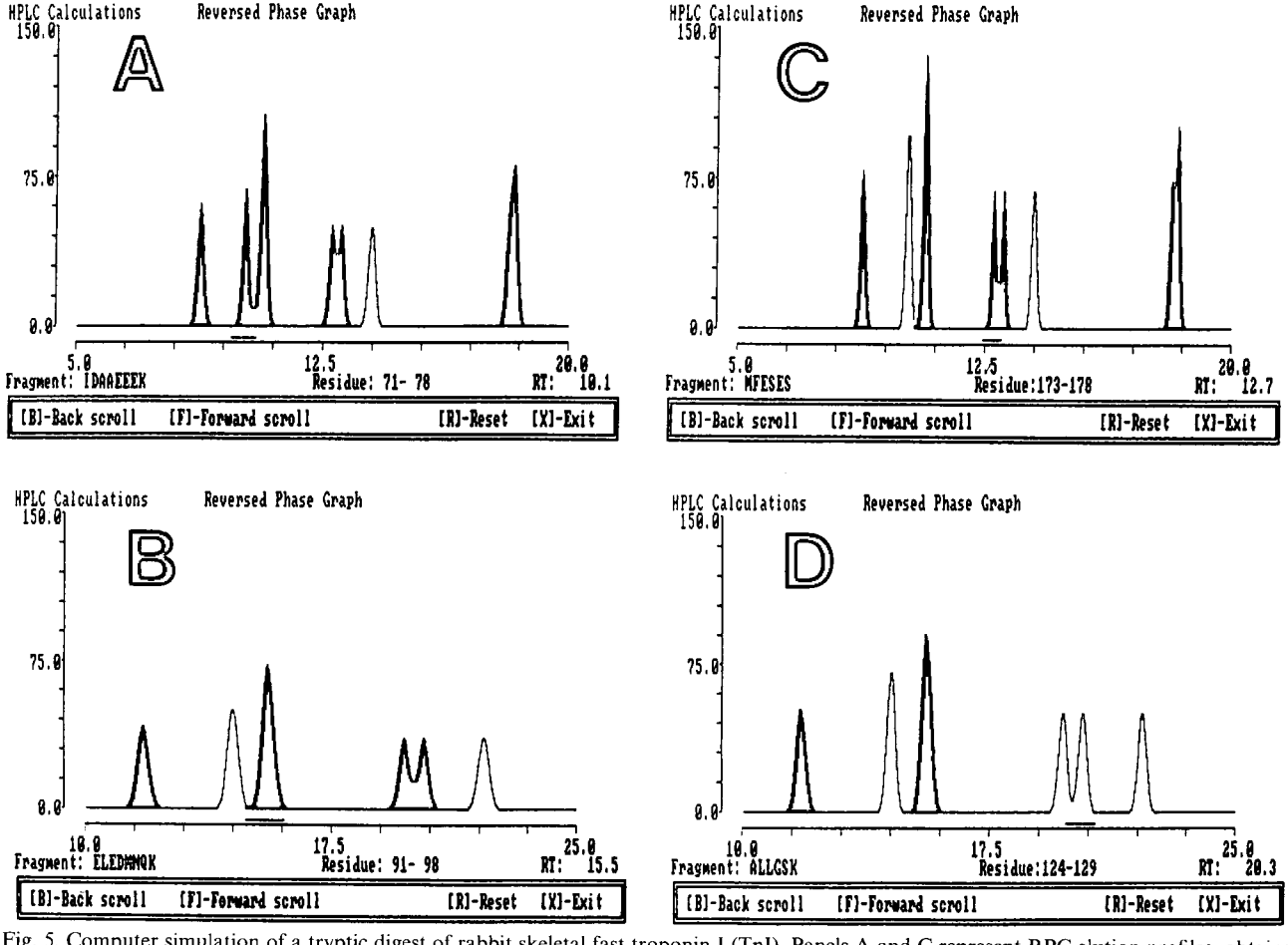

Fig. 5. Computer simulation of a tryptic digest of rabbit skeletal fast troponin I (TnI). Panels A and C represent RPC elution profiles, obtained with a linear AB gradient (1% B/min) at 1 ml/min, where eluent A is 0.1% aq. TFA and eluent B is 0.1% TFA in acetonitrile. Panels B and D represent elution profiles obtained with a linear gradient of 0.5% B/min. Panels A and B represent elution profiles obtained with a peptide standard peak-width ($W_{\frac{1}{2}}$) and peak height parameters of 0.28 min and 87 mAU, respectively. Panels C and D represent elution profiles obtained with standard parameters of 0.20 min ($W_{\frac{1}{2}}$) and 122 mAU (peak height). Specified peptide resolution is 1.0. Shaded peak areas denote unresolved peptides. The zoom option of the program has been selected to show only a section of the protein digest.

program, the success of these approaches to the prediction of peptide retention times has been well documented by our laboratory on the basis of a large number of peptides.

Computer simulation of peptide elution profiles

A demonstration of all the simulation capabilities of the Pro Digest-LC computer program would require considerable space. For the present, we simply wish to demonstrate several of the features of the Pro Digest-LC program in as concise a manner as possible. To this end, we have chosen to illustrate the protein digest and peptide mapping features of the program, coupled with RPC of the peptide fragments. As outlined in the Introduction, efficient separation of protein digests is an important consideration in many research disciplines. In addition, the flexibility and resolving power of RPC makes it the ideal mode of HPLC for demonstrating many of the simulation capabilities of the Pro Digest-LC program.

Tryptic digest of proteins. Prior to running the tryptic digest feature, peak width at half height, $W_{\frac{1}{2}}$, and peak height parameters for a known amount of our peptide standard, S4, were entered into the "Standards" section of the main menu (Fig. 1a), together with the desired resolution (1.0, in this case). The program will then refer to these stored parameters when it simulates the protein digest elution profile.

From the Pro Digest-LC main menu (Fig. 1a), the "Digest" option was chosen to enter the protein menu (Fig. 1b). A stored protein file (rabbit fast skeletal troponin I [TnI]) was loaded (Load/view/edit protein file) at a sample level of 5 nmoles. Troponin I is an inhibitory protein involved in the regulation of muscle contraction. The quantity of protein loaded can, of course, be varied, depending on the researcher's requirements. The tryptic digest option was chosen, followed by a request for a simulated elution profile of the resulting peptide fragments in reversed-phase chromatography. Fig. 5 demonstrates sections of the simulated elution profiles of the tryptic digest of TnI, obtained by RPC.

The profiles shown in Fig. 5a and b represent simulated results for a column (column 1) different from that used in Fig. 5c and d (column 2). For column 1, the $W_{\frac{1}{2}}$ and peak-height parameters entered into the Standards file (Fig. 1a) were 0.28 min and 87 mAU, respectively; in contrast the parameters entered for column 2 were 0.20 min and 122 mAU, respectively. This is not an unusual range of peak width parameters to be investigated, since we have observed the $W_{\frac{1}{2}}$ and peak height of the peptide standard, S4, to change by a factor of 2 between C_8 and C_{18} columns. If one routinely runs peptide standards, one can enter peak width and height information into the program to see how well a particular column would perform a peptide separation.

The entire tryptic digests profiles are not shown in Fig. 5. The zoom option has been selected to narrow the simulated chromatogram down to a small section of the whole peptide elution profile. Fig. 5a and c illustrate the profiles for columns 1 and 2, respectively, which are predicted to be obtained with a 1% acetonitrile/min linear gradient (aq. TFA to TFA in acetonitrile gradient) at a flow-rate of 1 ml/min; Fig. 5b and d illustrate the profiles for a 0.5% acetonitrile/min linear gradient. The separation of the peptides is improved by using a shallower gradient-rate or a column that provides decreased peak widths. This can best be observed by noting the position of the cursor. For column 1, the separation of peptide 71–78 (*i.e.*, residues 71–78) (Fig. 5a) from peptide 91–98 (Fig. 5b) is shown. The position of the cursor is con-

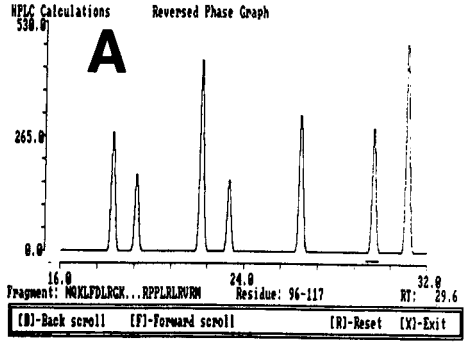
HPLC Calculations
Reversed Phase Graph
530.0
A
265.0
0.0
16.0
24.0
32.0
Fragment: MQKLFDLRGK...RPPLRLRVRM
Residue: 96-117
RT: 29.6
[B]-Back scroll
[F]-Forward scroll
[R]-Reset
[X]-Exit

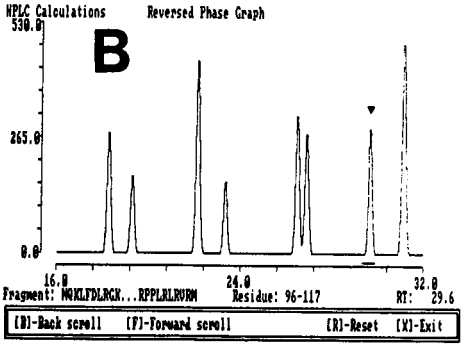
HPLC Calculations
Reversed Phase Graph
530.0
B
265.0
0.0
16.0
24.0
32.0
Fragment: MQKLFDLRGK...RPPLRLRVRM
Residue: 96-117
RT: 29.6
[B]-Back scroll
[F]-Forward scroll
[R]-Reset
[X]-Exit

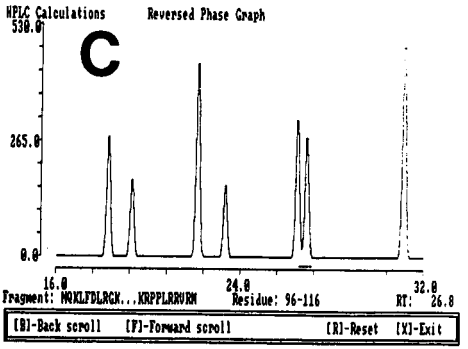
HPLC Calculations
Reversed Phase Graph
530.0
C
265.0
0.0
16.0
24.0
32.0
Fragment: MQKLFDLRGK...KRPPLRRVRM
Residue: 96-116
RT: 26.8
[B]-Back scroll
[F]-Forward scroll
[R]-Reset
[X]-Exit

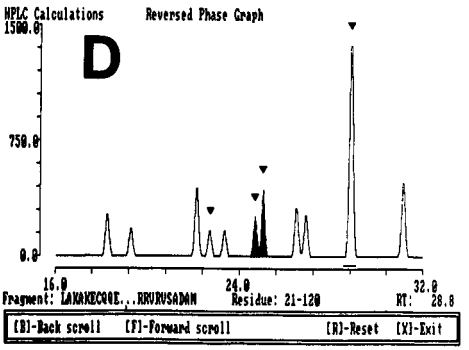
HPLC Calculations
Reversed Phase Graph
1500.0
D
750.0
0.0
16.0
24.0
32.0
Fragment: LAKAKECQQE...RRVRVSADAN
Residue: 21-120
RT: 28.8
[B]-Back scroll
[F]-Forward scroll
[R]-Reset
[X]-Exit

trolled by scrolling it forwards ("F") or backwards ("B"). As the gradient-rate is decreased from 1% acetonitrile/min (Fig. 5a) to 0.5% acetonitrile/min (Fig. 5b), the separation improves. Peaks are shaded to show that peptides are not resolved at a specified resolution (1.0) in the present example. Thus, the peak marked by the cursor in Fig. 5B contains more than one peptide. If the cursor is moved forward, all the peptides under a shaded peak are listed. For column 2, the separation of peptides 173–178 (Fig. 5c) from peptides 124–129 (Fig. 5d) is shown. Peptides 71–78 and 91–98 are already resolved on this column by a linear gradient of 1% acetonitrile/min (Fig. 5c), unlike the chromatogram for column 1 under the same conditions (Fig. 5a). As the gradient-rate is lowered to 0.5% acetonitrile/min (Fig. 5d), the separation of peptides 173–178 and 124–129 is complete (at a specified resolution of 1.0). The unshaded character of the two peptides at the lower gradient-rate shows that no other peptides lie under these peptide peaks. The separation of these two peptides was not obtained on column 1, even at the shallower 0.5% acetonitrile/min gradient-rate (Fig. 5b).

All manner of permutations of sample load, gradient-rate, and flow-rate, coupled with specified standard parameters of $W_{\frac{1}{2}}$, peak height, and desired resolution may be investigated without actually chromatographing a sample.

Peptide mapping. Troponin I (TnI) is a 178-residue protein, involved in the regulation of muscle contraction. This laboratory has identified the region of amino acid residues 105–114 being responsible for the inhibitory activity of TnI[33,34]. Through the use of peptide analogues of the inhibitory region of TnI, Talbot and Hodges[35] have demonstrated that differences in relative inhibitory activity of rabbit skeletal fast and cardiac TnI can be at least partially and perhaps solely explained by a single amino-acid insertion, a leucine residue, between positions 112 and 113 of the skeletal sequence. To investigate this point further, it would be appropriate to engineer, by site-specific mutagenesis, a skeletal protein containing the cardiac leucine insertion. Following site-specific mutagenesis, peptide mapping would be carried out on the engineered protein to verify that the change has indeed been made. It would also be of interest to isolate the inhibitory peptides from the mutant and native protein for biological activity measurements. Thus, being able to predict the retention behaviour of these peptides relative to the other peptides in the digest would be advantageous.

The mutant protein was created by inserting a leucine residue between positions 112 and 113 of the native TnI sequence (Fig. 1C–E) and saving this sequence as TnI-179 (for 179 residues, as opposed to 178 residues in the native sequence). Cyano-

Fig. 6. Computer simulation of peptide mapping. All panels represent simulated RPC elution profiles, obtained with a linear AB gradient (1% B/min) at a flow-rate of 1 ml/min, where eluent A is 0.1% aq. TFA and eluent B is 0.1% in acetonitrile. Panel A: cyanogen bromide digest of a mutant protein, obtained by site-specific mutagenesis of rabbit skeletal fast troponin I (TnI); this mutant protein, the result of a leucine insertion between position 112 and 113 is denoted as TnI-179 in the text. Panel B: overlay of cyanogen bromide digests of a mutant protein (TnI-179) and the native TnI protein; the inverted triangle identifies the mutant peptide fragment. Panel C: cyanogen bromide digest of the native TnI protein. Panel D: overlay of cyanogen bromide digests of protein isoforms (rabbit skeletal fast and slow troponin I); the inverted triangles identify the fragments obtained from the slow troponin I protein. Peptide standard peak width ($W_{\frac{1}{2}}$) and peak height parameters are 0.14 min and 174 mAU, respectively; specified peptide resolution is 1.0. (These are the default values already present in the program.) Shaded areas denote unresolved peptides. The zoom option of the program has been selected to show only sections of the protein digests.

gen bromide cleavage was chosen, followed by a request to simulate the reversed-phase elution profile at a gradient-rate of 1% acetonitrile/min and a flow-rate of 1 ml/min. A section of the simulated profile, following operation of the zoom option, is shown in Fig. 6a. The cursor shown by the bar below the peak at 29.6 min, marks the inhibitory fragment (residues 96–117) of the mutant protein. Rabbit skeletal fast TnI was then loaded (5 nmol), followed by cyanogen bromide cleavage and selection of the RPC option (1% acetonitrile/min and 1 ml/min) (Fig. 6c). The cursor marks the inhibitory fragment (residues 96–116) of the native protein. The differences in the retention times of the native fragment and the mutant fragment (26.8 min and 29.6 min, respectively), clearly show that a change in the native sequence by site-specific mutagenesis can easily be detected. To highlight this, the peptide mapping option, following cyanogen bromide cleavage of the native TnI, was used to produce the simulated chromatogram shown in Fig. 6b. This elution profile is an overlay of the cyanogen bromide cleavage fragments of both proteins (*i.e.* an overlay of Fig. 6a and c). Any mutant fragment not observed in the native sequence is identified by an inverted triangle above the peak (Fig. 6b).

The isolation of protein isoforms is very common, and different isoforms have been shown to have different biological activities. It has been shown, for instance, that rabbit skeletal slow muscle TnI inhibits rabbit skeletal actomyosin ATPase poorly, compared to rabbit skeletal fast muscle TnI[36]. Thus, even though the inhibitory region 105–114 is identical in both proteins[37], the inhibitory activities are different. Since the slow and fast TnI proteins are very homologous, and since they come from the same tissue source (although they occur in different percentages), extensive purification is often necessary if pure proteins are required. However, if it is desired to isolate only biologically active regions, *i.e.*, peptide fragments of the proteins, this extensive purification may not be required. A digestion of a mixture of the two proteins, followed by HPLC, can be quickly simulated by the Pro Digest-LC program. The cyanogen bromide fragments of the two proteins were overlaid, producing the simulated reversed-phase elution profile shown in Fig. 6d. The inverted triangles above the peaks denote peptide fragments of the slow TnI protein. Table I summarizes the information obtained when a listing of the fragments obtained by cyanogen bromide cleavage is requested. The RPC retention times of the fragments are given, as well as the residue numbers and sequences of the peptides. "Yes" in the column marked "Mutant" denotes a mutant fragment (slow TnI fragments, in this example). The two inhibitory peptides (residues 21–120 for slow TnI and residues 96–116 for fast TnI) are readily separated by using the standard conditions of RPC.

CONCLUSIONS

The Pro Digest-LC computer software program assists scientists in devising methodologies for the analytical separation and purification of biologically active peptides and peptide fragments from enzymatic and chemical digests of proteins by size-exclusion, ion-exchange, and reversed-phase HPLC. The program allows changing the sample volume, sample quantity, flow-rates, gradients, and desired resolution. If further optimization is required, optimization programs, such as those described by Dolan and Snyder[38] may be applied following Pro Digest-LC.

Pro Digest-LC is also an interactive program, in that researchers can chroma-

tograph peptide standards on their columns and enter values of retention time, peak width, peak height, and other parameters in the program, in order to adjust the simulation to their particular column. Any deviations from the simulation can provide the researcher with valuable information on the completeness of protein digestion or unique conformations of a particular fragment. Above all, Pro Digest-LC is user friendly and should be very useful to workers involved in peptide and protein research.

ACKNOWLEDGEMENTS

This work was supported by the Medical Council of Canada, S.P.I. Synthetic Peptides Incorporated and by the Alberta Heritage Foundation for Medical Research.

REFERENCES

1 C. T. Mant and R. S. Hodges, *J. Chromatogr.*, 326 (1985) 349.
2 C. T. Mant and R. S. Hodges, in K. Gooding and F. Regnier (Editors), *High-Performance Liquid Chromatography of Biological Macromolecules: Methods and Applications*, Marcel Dekker, in press.
3 C. T. Mant and R. S. Hodges, *J. Liq. Chromatogr.*, in press.
4 J. M. R. Parker and R. S. Hodges, *J. Protein Chem.*, 3 (1985) 465.
5 E. Pfannkoch, K. C. Lu and F. E. Regnier, *J. Chromatogr. Sci.*, 18 (1980) 430.
6 H. Engelhardt and D. Mathes, *Chromatographia*, 14 (1981) 325.
7 H. Engelhardt, G. Ahr and M. T. W. Hearn, *J. Liq. Chromatogr.*, 4 (1981) 1361.
8 W. Kopaciewicz and F. E. Regnier, *Anal. Biochem.*, 126 (1982) 8.
9 F. E. Regnier, *Methods Enzymol.*, 91 (1983) 137.
10 C. T. Mant, J. M. R. Parker and R. S. Hodges, *J. Chromatogr.*, 397 (1987) 99.
11 C. T. Mant and R. S. Hodges, *J. Chromatogr.*, 327 (1985) 147.
12 C. T. Mant and R. S. Hodges, *Chromatographia*, 24 (1987) 805.
13 C. T. Mant and R. S. Hodges, *LC, Liq. Chromatogr. HPLC Mag.*, 4 (1986) 250.
14 C. T. Mant, J. M. R. Parker and R. S. Hodges, *LC · GC*, 5 (1986) 1004.
15 C. T. Mant and R. S. Hodges, *J. Chromatogr.*, 409 (1987) 155.
16 H. Hagestam Freiser and K. M. Gooding, *BioChromatography*, 2 (1987) 186.
17 D. Guo, C. T. Mant, A. K. Taneja, J. M. R. Parker and R. S. Hodges, *J. Chromatogr.*, 359 (1986) 499.
18 D. Guo, C. T. Mant, A. K. Taneja and R. S. Hodges, *J. Chromatogr.*, 359 (1986) 519.
19 D. Guo, C. T. Mant and R. S. Hodges, *J. Chromatogr.*, 386 (1987) 205.
20 C. T. Mant, T. W. L. Burke, J. A. Black and R. S. Hodges, *J. Chromatogr.*, in press.
21 J. L. Meek, *Proc. Natl. Acad. Sci. U.S.A.*, 77 (1980) 1632.
22 J. L. Meek and Z. L. Rossetti, *J. Chromatogr.*, 211 (1981) 15.
23 K. J. Wilson, A. Honegger, R. P. Stötzel and G. J. Hughes, *Biochem. J.*, 199 (1981) 31.
24 S-J. Su, G. Grego, B. Niven and M. T. W. Hearn, *J. Liq. Chromatogr.*, 4 (1981) 1745.
25 T. Sasagawa, T. Okuyama and D. C. Teller, *J. Chromatogr.*, 240 (1982) 329.
26 C. A. Browne, H. P. J. Bennett and S. Solomon, *Anal. Biochem.*, 124 (1982) 201.
27 T. Sasagawa, L. E. Ericsson, D. C. Teller, K. Titani and K. A. Walsh, *J. Chromatogr.*, 307 (1984) 29.
28 C. T. Mant and R. S. Hodges, in M. T. W. Hearn (Editor), *HPLC of Proteins, Peptides and Polynucleotides*, VCH Publishers, in press.
29 M. J. O'Hare and E. C. Nice, *J. Chromatogr.*, 171 (1979) 209.
30 E. C. Nice, M. W. Capp, N. Cooke and M. J. O'Hare, *J. Chromatogr.*, 218 (1981) 569.
31 K. J. Wilson, A. Honegger and G. J. Hughes, *Biochem. J.*, 199 (1981) 43.
32 C. T. Wehr, L. Correia and S. R. Abbott, *J. Chromatogr. Sci.*, 20 (1982) 114.
33 J. A. Talbot and R. S. Hodges, *J. Biol. Chem.*, 254 (1979) 3720.
34 J. A. Talbot and R. S. Hodges, *J. Biol. Chem.*, 256 (1981) 2798.
35 J. A. Talbot and R. S. Hodges, *J. Biol. Chem.*, 256 (1981) 12374.
36 H. Syska, S. V. Perry and I. P. Trayer, *FEBS Lett.*, 40 (1974) 253.
37 J. M. Wilkinson and R. J. A. Grand, *Nature (London)*, 271 (1978) 31.
38 J. W. Dolan and L. R. Snyder, *LC · GC*, 5 (1987) 971.

Journal of Chromatography, 458 (1988) 169–174
Elsevier Science Publishers B.V., Amsterdam — Printed in The Netherlands

CHROMSYMP. 1528

PROTEIN IMMOBILIZATION ON SILICA SUPPORTS

A LIGAND DENSITY STUDY

DANLIN WU
Department of Chemistry, Iowa State University, Ames, IA 50011 (U.S.A.)
and
RODNEY R. WALTERS*
Drug Metabolism Research, The Upjohn Company, Kalamazoo, MI 49001 (U.S.A.)

SUMMARY

The immobilization of proteins on diol-bonded silica matrices containing carboxyl groups (spacer arms) was studied. It was found that the activated ester coupling method worked best with N,N′-dicyclohexylcarbodiimide as the condensing agent in the activation step. During protein coupling, the amount of protein immobilized was highest below pH 6. The optimum pore size of the silica was 300–1000 Å. The spacer arm ligand density was varied over as much as a 100-fold range and the effects on the total activities and specific activities of several proteins were studied. Two proteins exhibited up to two-fold increases in specific activity at low ligand densities. However, the total amounts of activity and protein immobilized decreased at low ligand densities.

INTRODUCTION

Immobilized proteins have found important applications over the past several decades. These applications include biochemical purification by affinity chromatography, biochemical analysis by immunoassay methods, and the use of immobilized enzymes for the catalysis of reactions of industrial interest.

An immobilized protein may have a lower specific activity than the soluble protein. This may be due to multipoint attachment, which causes distortion of the three-dimensional structure of the immobilized protein, or to an immobilized orientation which results in steric hindrance of the binding site[1]. By using a low surface concentration of spacer arms or activated sites for immobilization, multipoint attachment can be minimized and the steric hindrance diminished to some extent, so that the specific activity of the immobilized protein should be increased. This has been observed for several proteins immobilized on hydroxyalkyl methacrylate gels[2], Sepharose CL[3], and aminoethylcellulose[4].

In a previous report[5], silica was silanized to produce diol-bonded silica and further derivatized with diglycolic anhydride to yield a matrix of variable ligand

0021-9673/88/$03.50

density, *i.e.*, variable surface concentration of spacer arms. This has made it possible to investigate the effects of spacer arm concentration on the activity of immobilized proteins over a very broad surface concentration range. In this study, several proteins were immobilized on silica supports of varying spacer arm concentration by first activating the carboxylate spacer arms with a carbodiimide and N-hydroxysuccinimide. The specific activities of these immobilized proteins were studied as a function of spacer arm surface concentration. The influence of the carbodiimide, pore size, and pH on the immobilization yield were also examined. In this paper, the term "ligand density" is defined as the initial surface concentration of the carboxylate spacer arms.

EXPERIMENTAL

Reagents

Eel acetylcholinesterase, soybean trypsin inhibitor, bovine pancreas α-chymotrypsin, bovine pancreas trypsin, *Staphylococcus aureus* protein A, rabbit immunoglobulin G (IgG), goat anti-human serum albumin (anti-HSA, immunoglobulin fraction), bovine pancreas ribonuclease A, porcine pepsin, human serum albumin (HSA), 1-ethyl-3-(3-dimethylaminopropyl)carbodiimide (EDC), acetylcholine iodide, N-succinyl-L-alanyl-L-alanyl-L-prolyl-L-phenylalanine-*p*-nitroanilide, and N-acetyl-L-phenylalanyl-3,5-diiodo-1-tyrosine were from Sigma (St. Louis, MO, U.S.A.). Ninhydrin, 1-cyclohexyl-3-(2-morpholinoethyl)carbodiimide metho-*p*-toluenesulfonate (CMC), dithio bis-2-nitrobenzoic acid, 1,1′-carbonyldiimidazole (CDI), hydrindantin, and 2-methoxyethanol were from Aldrich (Milwaukee, WI, U.S.A.). N,N′-dicyclohexylcarbodiimide (DCC), Triton X-100, and phenol reagent solution were from Fisher (Fair Lawn, NJ, U.S.A.). Nucleosil 1000-5 (1000 Å pore size, 25 m^2/g surface area, 5 μm particle diameter) and 300-5 (300 Å, 100 m^2/g, 5 μm) were obtained from Alltech (Deerfield, IL, U.S.A.). LiChrospher SI-4000 (4000 Å, 10 m^2/g, 10 μm) and SI-1000 (1000 Å, 30 m^2/g, 10 μm) were from Rainin (Woburn, MA, U.S.A.). N-hydroxysuccinimide (NHS) was from Eastman Kodak (Rochester, NY, U.S.A.).

Methods

Carboxylated silica of variable ligand density was prepared and quantitated as described previously[5]. The NHS ester was synthesized according to a published procedure[6] with the following modifications: the silica was suspended in dioxane and degassed by sonication under aspirator vacuum for 10 min prior to reaction, and the NHS ester silica was dried under vacuum at room temperature overnight. The activated silica (0.1 g) was suspended in 2 ml of the coupling buffer (0.1 *M* sodium phosphate of the desired pH) and degassed for 10 min. The protein was added and the suspension shaken in a wrist action shaker. In the pH study, the trypsin (10 mg) and acetylcholinesterase (2 mg) reaction mixtures were shaken at 4°C for one day, trypsin inhibitor (30 mg) at 4°C for 6 h, and anti-HSA (30 mg) at room temperature for 18 h. In the pore size study, the reactions with trypsin inhibitor (30 mg protein, pH 3.0 buffer) and anti-HSA (30 mg, pH 5.0) were shaken at room temperature for 18 h. In the activity study, the α-chymotrypsin (14 mg, pH 4.0, 7 days), pepsin (10 mg, pH 4.0, 7 days), ribonuclease A (20 mg, pH 5.0, 7 days), anti-HSA (30 mg, pH 7.0, 24 h), acetylcholinesterase (10 mg, pH 6.0, 18 h), and trypsin inhibitor (30 mg, pH 3.0, 5 days) were shaken at 4°C, and protein A (20 mg, pH 5.0, 18 h) at room temperature.

In the pore size study, 0.1 g diol-bonded silica was also activated with CDI as described previously[7] and used for the immobilization of anti-HSA at 4°C (30 mg, pH 5.0, 6 days), or oxidized with periodate[8] and used for the immobilization of the anti-HSA at 4°C (30 mg, pH 5.7, 6 days) by the Schiff base method[8,9]. The protein-silica products were washed with 2 *M* sodium chloride, followed by water in the pH and pore size studies, or with 1 *M* sodium chloride in 0.1 *M* sodium phosphate buffer of the appropriate pH in the activity study.

Immobilized glucosamine was quantitated as described previously[5]. Immobilized protein was determined by a modified Lowry protein assay[10] in which all of the reaction times were increased by 50% and the silica was removed by centrifugation prior to absorbance measurement. In both of these assays, blank values were determined using diol-bonded silica.

The activities of immobilized acetylcholinesterase and pepsin were determined by enzyme assay[11,12]. Sodium arsenate was used as the buffer rather than triethanolamine for the assay of α-chymotrypsin[13]. The activities of immobilized trypsin inhibitor, protein A, and anti-HSA were determined from chromatographic breakthrough curve[14] analyses using trypsin, IgG, and HSA, respectively.

RESULTS AND DISCUSSION

Selection of carbodiimide

It was reported in the case of a succinylated agarose matrix that some of the carbodiimide reagents were more effective than others in the formation of NHS esters[15]. Nucleosil 300-5 (carboxyl group content: 310 μmol/g) was similarly examined using the carbodiimides DCC, CMC, and EDC at concentrations of 0.2 *M* and NHS at a concentration of 0.12 *M*. Glucosamine (0.1 *M*) was immobilized at pH 7.4 and assayed by the ferricyanide method[11] as a measure of the effectiveness of each carbodiimide in forming the activated ester. The quantities of glucosamine immobilized with each carbodiimide were: DCC, 124 ± 10 μmol/g; CMC, 61 ± 5 μmol/g; EDC, 54 ± 5 μmol/g. Therefore, DCC was chosen for use in this study. The overall immobilization yield for glucosamine using DCC was 40%.

Comparison of the activated ester method with other immobilization methods

The immobilization of anti-HSA by three different immobilization methods was compared using 4000 Å (LiChrospher) and 300 Å (Nucleosil) pore size silicas. As shown in Table I, the amount of protein immobilized was approximately the same regardless of the coupling method. Since both the CDI and Schiff base methods result in excellent coupling efficiency of immunoglobulins[7–9], it is clear that the N-hydroxysuccinimide method is similar in coupling efficiency. In the case of the carboxylate-silica, it should be noted that high ligand density matrices were used (Table I). These tend to favor high coverage of immobilized protein.

Effect of pore size

The two silicas described above plus silica of 1000 Å pore size (LiChrospher) were used to immobilize trypsin inhibitor and anti-HSA (Table I). The protein content decreased for the largest pore size matrix. However, when corrected for the surface area of the silica (Table I), the amount immobilized per unit of surface area

TABLE I

EFFECT OF PORE SIZE AND COUPLING METHOD ON PROTEIN IMMOBILIZATION

Protein	*Silica*	*Pore size (Å)*	*Carboxyl content* (μmol/g)*	*Protein (mg/g silica)*			*Protein* (mg/m²)*
				NHS	*CDI*	*Schiff base*	
STI	LiChrospher	4000	40	15			1.5
		1000	90	39			1.3
	Nucleosil	300	310	38			0.4
Anti-HSA	LiChrospher	4000	40	30	32		3.0
		1000	90	80			2.7
	Nucleosil	300	310	81	71	66	0.8

* NHS coupling method only.

was actually higher for the larger pore diameter. This is explained by the distribution of pore diameters in each silica[16]. Especially for the 300-Å pore size silica, a fraction of the pores were too small or were blocked by protein molecules, thereby diminishing the available surface area of the matrix. In this case, either the 300-Å or 1000-Å pore size materials were optimal in terms of total protein immobilized.

Effect of pH on the immobilization of proteins

The amount of each protein immobilized was found to increase as the pH of the reaction mixture decreased (Table II). It is well-known that hydrolysis of the ester bond of the activated silica is substantially faster at higher pH so that coupling of proteins should decrease with an increase in pH. On the other hand, higher pH values promote the deprotonation of amino groups of proteins, which would favor the nucleophilic attacking reaction and thus produce a higher coupling yield[15]. The data in Table II indicate that hydrolysis was the more important factor in determining the amount of protein immobilized.

TABLE II

EFFECT OF pH ON THE IMMOBILIZATION OF SEVERAL PROTEINS

Nucleosil 300-5 with a carboxyl content of 310 μmol/g as used.

Protein	*Protein immobilized (mg/g silica)*					
	pH					
	3	*4*	*5*	*6*	*7*	*8*
Trypsin inhibitor	24	–	11	5	4	2
Acetylcholinesterase	32	–	27	–	14	–
Trypsin	9	8	9	8	–	6
Anti-HSA immunoglobulin	90	–	89	–	26	–

Activities of immobilized proteins

Several proteins were immobilized on matrices of spacer arm densities covering a range of up to 100-fold (Table III). At the lowest ligand densities, the average distance between spacer arms was approximately the same as the diameters of the proteins, thus multipoint attachment should have been minimized. Examining first the specific activities of the proteins, it is apparent that the specific activities of several of the proteins (acetylcholinesterase, trypsin inhibitor, protein A, and anti-HSA) were independent of ligand density. However, α-chymotrypsin and pepsin increased in specific activity as the ligand density decreased. A previous fluorescence study of α-chymotrypsin immobilized on Sephadex G-200 has shown that this can be attributed to multiple covalent attachment of the enzyme molecule to the matrix, which disturbs the tertiary structure of the protein[17]. Also, the enzyme molecule may be oriented on the surface in a way that renders it less accessible to the substrate. This may explain the partial loss of enzyme activity even at the lowest ligand density.

TABLE III

SPECIFIC ACTIVITY AND COUPLING YIELD AS A FUNCTION OF LIGAND DENSITY

Protein	*Pore size (Å)*	*Ligand density (μmol/g)*	*Average distance* (Å)*	*Protein coupled (mg/g)*	*Specific activity***
α-Chymotrypsin	1000	3	40	1.5	0.39
		10	19	14.7	0.25
		50	9	31.8	0.19
Pepsin	1000	3	40	0.8	0.59
		10	19	1.5	0.51
		50	9	6.1	0.42
Acetylcholinesterase	300	3	75	1.1	0.97
		50	18	8.7	1.01
		310	7	14.5	1.04
Ribonuclease A	1000	3	40	22.1	–
		20	15	10.2	–
		50	9	0.7	–
Trypsin inhibitor	300	3	75	2.9	0.92
		310	7	38.4	0.92
Protein A	1000	3	40	1.0	3.4
		10	19	3.6	3.5
		50	9	22.1	3.6
Anti-HSA immunoglobulin	300	3	75	13.1	0.044
		50	18	20.8	0.041
		310	7	20.9	0.041

* Average distance between spacer arms based on surface area and ligand density.

** Listed as the ratio of immobilized/native as determined by enzyme assay for the enzymes, or as mg test solute adsorbed/mg immobilized protein as determined by breakthrough curve analysis for the other proteins.

Alternatively, since the carboxylate groups on the silica may not be evenly distributed on the surface, it may be that there is still significant multipoint bonding even at the lowest ligand density.

Although the specific activity increased as much as two-fold at low ligand density, the amount of protein coupled decreased two- to twenty-fold (Table III). Therefore, the total immobilized activity was in all cases lower at low ligand densities. Although the spacer arm density is high enough at the low densities to potentially immobilize a monolayer of protein, hydrolysis of the active ester groups prevents the coupling yield from being high. Therefore, from a practical point of view, it appears that the conventional method of using a high density of activated groups will usually yield a material of the highest total activity. This is usually a more important concern than the specific activity.

REFERENCES

1 R. R. Walters, *Anal. Chem.*, 57 (1985) 1099A.
2 O. Valentova, J. Turkova, R. Lapka, J. Zima and J. Coupek, *Biochim. Biophys. Acta*, 403 (1975) 192.
3 A.-C. Koch-Schmidt and K. Mosbach, *Biochemistry*, 16 (1977) 2101.
4 C. K. Glassmeyer and J. D. Ogle, *Biochemistry*, 10 (1971) 786.
5 M. E. Landgrebe, D. Wu and R. R. Walters, *Anal. Chem.*, 58 (1986) 1607.
6 H. H. Weetall, *Methods Enzymol.*, 44 (1976) 134.
7 S. C. Crowley, K. C. Chan and R. R. Walters, *J. Chromatogr.*, 359 (1986) 359.
8 S. Ohlson, L. Hansson, P.-O. Larsson and K. Mosbach, *FEBS Lett.*, 93 (1978) 5.
9 D. S. Hage, R. R. Walters and H. W. Hethcote, *Anal. Chem.*, 58 (1986) 274.
10 O. H. Lowry, N. J. Rosebrough, A. L. Farr and R. J. Randall, *J. Biol. Chem.*, 193 (1951) 265.
11 G. L. Ellman, K. D. Courtney, V. Andres and R. M. Featherstone, *Biochem. Pharmacol.*, 7 (1961) 88.
12 A. P. Ryle, in H. U. Bergmeyer (Editor), *Methods of Enzymatic Analysis*, Vol. 5, Verlag Chemie, Weinheim, 3rd ed., 1984, p. 223.
13 R. Geiger, in H.U. Bergmeyer (Editor), *Methods of Enzymatic Analysis*, Vol. 5, Verlag Chemie, Weinheim, 3rd ed., 1984, p. 99.
14 U. Lund, *J. Liq. Chromatogr.*, 4 (1981) 1933.
15 P. Cuatrecasas and I. Parikh, *Biochemistry*, 11 (1972) 2291.
16 F. V. Warren, Jr. and B. A. Bidlingmeyer, *Anal. Chem.*, 56 (1984) 950.
17 D. Gabel, I.Z. Steinberg and E. Katchalski, *Biochemistry*, 10 (1971) 4661.

Journal of Chromatography, 458 (1988) 175–183
Elsevier Science Publishers B.V., Amsterdam — Printed in The Netherlands

CHROMSYMP. 1471

Note

Automated high-performance liquid chromatographic method for the determination of iodotyrosines and iodothyronines

P.R. KOOTSTRA*

Experimental Pediatric Endocrinology, Academic Medical Centre (AMC), Meibergdreef 9, 1105 AZ Amsterdam (The Netherlands)

H.H. VAN DEN BROEK, E.A. HOGENDOORN and C.E. GOEWIE

Laboratory of Organic/Analytical Chemistry, National Institute of Public Health and Environmental Protection (RIVM), P.O.Box 1, 3720 BA Bilthoven (The Netherlands)

and

J.J.M. DE VIJLDER

Experimental Pediatric Endocrinology, Academic Medical Centre (AMC), Meibergdreef 9, 1105 AZ Amsterdam (The Netherlands)

Research at the Experimental Pediatric Endocrinological Laboratory involves various aspects of thyroid metabolism. One of the research projects is the study of the iodination of thyroglobulin, catalysed by TPO*. Thyroglobulin is a protein with a molecular weight of 660 000. In a thyroglobulin molecule, there are about 120 tyrosine residues, of which maximally 40 can be iodinated to MIT and DIT[1]. This iodination reaction is catalysed by TPO in the presence of iodide and hydrogen peroxide[2]. In addition to this iodination reaction, TPO catalyses the formation of the thyroid hormone thyroxine from two DIT residues, the so-called coupling reaction. The reactions take place within the thyroglobulin molecule. Thyroxine is released after an enzymatic hydrolysis of the thyroglobulin molecule[3]. MIT, DIT and T4 are not the only reaction products. The formation of other (iodinated) components such as T0, T2, T3 and rT3 is possible. In order to study the kinetics of the different reactions catalysed by TPO, we required a method of analysing the possible reaction products in one chromatographic run. As kinetic studies involve many samples, automation was necessary. Several (HPLC) procedures for the separation of these compounds have been described since 1974[4–8]. These methods were usually developed to assess the purity of pharmaceutical preparations or to study and quantitate thyroid hormones and their metabolites in extracts of biological samples, such as serum and urine. In most instances DIT and T0 are not separated. Most of the quoted procedures involve complicated off-line sample preparation.

We present here a method for the determination of six iodotyrosines and io-

* Abbreviations: Tyr, tyrosine; MIT, 3-monoiodotyrosine; DIT, 3,5-diiodotyrosine; T0, L-thyronine; T0, 3,5-diiodo-L-thyronine; T3, 3,3′,5-triiodo-L-thyronine; rT3, 3,3′,5′-triiodo-L-thyronine; T4, thyroxine; HSA, heptanesulphonic acid; TPO, thyroid peroxidase (E.C. 1.11.1.7).

0021-9673/88/$03.50

dothyronines in reaction mixtures of the model substrate tyrosine and thyroid peroxidase used for kinetic studies, in urine samples from patients and in samples of enzymatically hydrolysed thyroglobulin, isolated from thyroid glands. The method described is a fully automated reversed-phase ion-pairing HPLC procedure and includes sample clean-up and preconcentration on a small C_{18} precolumn.

EXPERIMENTAL

Chemicals

Acetonitrile and methanol were of analytical-reagent grade from J. T. Baker (Deventer, The Netherlands). HPLC-quality water was obtained from doubly distilled water, further purified in a Milli-Q (Millipore, Bedford, MA, U.S.A.) purification system with a Norganic filter. Tyr, MIT, DIT, T3, rT3 and T4 were purchased form Sigma (St. Louis, MO, U.S.A.) and T2 from Serva (Heidelberg, F.R.G.).

Standard solutions of the (iodo)amino acids were prepared in HPLC-quality water with a few drops of concentrated ammonia solution added. Standards were kept in the dark at −20°C.

Buffer solution (Titrisol, pH 4) and orthophosphoric acid (89% pure) were obtained from Merck (Darmstadt, F.R.G.) and HSA disodium salt from Sigma. Pronase P and E were bought from Serva.

Liquid chromatography

The set-up for automated sample clean-up and preconcentration and subsequent LC analysis is shown in Fig. 1. The apparatus consisted of the following components: a Model 9208 HPLC pump, used for loading and flushing the precolumn (Kipp, Delft, The Netherlands); a Perkin-Elmer (Norwalk, CT, U.S.A.) Series 10

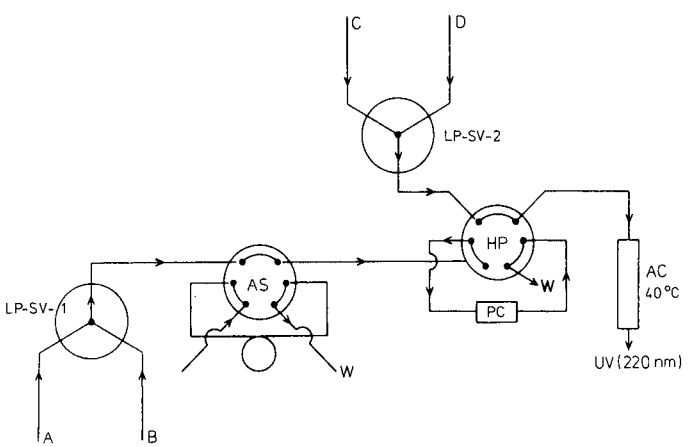

Fig. 1. Schematic representation of the eluent streams used for preconcentration and LC analysis. A = 2.5 m*M* HSA in 0.03 *M* phosphate buffer (pH 2.2); B = 2.5 m*M* HSA in methanol; C = methanol–buffer/HSA (30:70, v/v); D = methanol–acetonitrile–buffer/HSA (34:17:49, v/v/v); LP-SV = low-pressure selector valve; HP = high-pressure six-port switching valve, equipped with a C_{18} precolumn; AS = autosampler high-pressure six-port switching valve, equipped with sample loop; AC = analytical column; W = waste; UV = UV detector.

eluent pump; a Perkin-Elmer LC-235 photodiode array UV–VIS detector; a Gilson ASPI 232-401 autosampler, equipped with four programmable valves, [three Rheodyne 7010 (Cotati, CA, USA) high-pressure injection valves and one Rheodyne 5011 low-pressure solvent selection valve]. A 150-μl sample loop was used for loading the sample on the precolumn; a 15 x 3.2 mm I.D. MPLC New Guard RP-18 precolumn (Brownlee, Santa Clara, CA, U.S.A.) and an analytical (AC) column (150 x 4.6 mm I.D.), laboratory-packed with 5-μm Hypersil ODS (Shandon, Runcorn, U.K.). The column was kept at 40°C in a thermostatted water-bath.

The carrier solvent, A, used for precolumn concentration, was 0.03 *M* sodium phosphate buffer (pH 2.2), containing 2.5m*M* HSA. The clean-up solvent, B, was methanol, containing 2.5 m*M* HSA. The buffer used with the analytical column was a sodium phosphate buffer (pH 2.5) containing 2.5 m*M* HSA; it is referred to as "buffer/HSA" throughout this paper. The following mobile phases were used with the analytical column: eluent C was a mixture of methanol and buffer/HSA (30:70, v/v), containing 0.25% acetone in order to level the absorption of eluent C with solvent D; eluent D was methanol–acetonitrile–buffer/HSA (34:17:49, v/v/v). At the start of the analysis, a sample was injected into the precolumn and flushed with 1 ml of solvent A. After 1 min, the precolumn was switched on-line with the analytical column and desorbed for 6 min with eluent C. Then the eluent for both columns was changed (by switching the valve) to eluent D for 13 min. Twelve minutes after the start of the chromatographic run, the precolumn was switched off-line and cleaned with the clean-up solvent, B, for 3 min, while the analytical run continued. After that, the selector valve 1 was switched back to the initial position, carrier solvent A. On completion of the analytical run (after 18 min), the analytical column was reconditioned for 7 min with 30% of methanol in buffer/HSA (eluent C).

TABLE I

CHARACTERIZATION OF THE UV SPECTRA OF (IODO)TYROSINES AND (IODO)THYRONINES

Compound	*Peak height at selected wavelength**				*Solvent***
	230 nm	*240 nm*	*254 nm*	*280 nm*	
Tyr	0.54	0.03	0.04	0.14	1
MIT	0.36	0.10	0.03	0.11	1
DIT	0.60	0.31	0.06	0.08	1
T0	1.0	0.54	0.13	0.18	1
T2	0.84	0.40	0.14	0.11	2
T3	0.84	0.38	0.12	0.10	2
rT3	0.76	0.46	0.12	0.11	2
T4	0.80	0.43	0.12	0.10	2

* Peak heights are expressed in arbitrary units. Spectra were recorded with a photodiode array detector after injection of 10 μl of a standard solution of 1 mg/ml of each component into a C_{18} column.

** The spectra were measured in (1) methanol–0.05 *M* ammonium acetate buffer (pH 5.0) (30:70; v/v) and (2) methanol–0.05 *M* ammonium acetate buffer (pH 5.0) (60:40, v/v).

RESULTS AND DISCUSSION

Optimization of the analytical LC separation

As the methods described in the literature[4–8] did not meet our requirements, we developed another HPLC procedure, by using a systematic approach, based on the eluent optimization strategy described by Schoenmakers *et al.*[9] and Drouen *et al.*[10]. Because of the chemical nature of the compounds, it can be expected that the pH of the eluent will influence their retention. During optimization, the pH, the composition of the mobile phase and the nature of the stationary phase were chosen as variables. At this stage, we used a photodiode array detector to trace the compounds in the chromatogram. All eight compounds have similar UV spectra, with a pronounced broad band at 200–230 nm and no significant additional absorption maxima. The measured relative absorption values, at selected wavelengths, are given in Table I.

Using a C_{18} column, we found that separation in a single isocratic chromatogram was not possible. There were two groups of peaks present in the chromatogram. The first group, Tyr, MIT, DIT and T0, could be eluted with a low percentage of methanol in the eluent, whereas for the second group, T2, T3, rT3 and T4 a stronger eluent was needed. The peaks of this last group were tailing in all isocratic chromatograms and also with linear gradient elution. We then varied the stationary phase. On a C_8 column the two groups of peaks are positioned closer together, as was expected, but the peak shapes were still not very good. On a C_1 column (Hypersil SAS), the peaks could be separated isocratically, using a mixture of 0.01 *M* ammonium acetate buffer (pH 5.0) and methanol (60:40, v/v). However, owing to bad batch-to-batch reproducibility of the C_1 stationary phase used, this method, unfortunately, had to be rejected. Remarkably, with acetonitrile as modifier, poor peak shapes were observed on all stationary phases tested. Next, ion-pair chromatography was investigated, with HSA as the ion-pair reagent. Because HSA is negatively charged, the compounds must be present as positively charged ions in the solution. This is achieved at low pH. A phosphate buffer of pH 2.5 was used as the aqueous phase and methanol was chosen as modifier. Again, we started with a Hypersil ODS column and again we found two groups of peaks in isocratic runs. However, all eight compounds could be separated in one ion-pair chromatogram with a one step-gradient solvent programme. The retention times were Tyr, 3.08 $\pm$ 0.06; MIT, 5.42 $\pm$ 0.16; DIT, 9.36 $\pm$ 0.008; T0, 9.61 $\pm$ 0.07; T2, 12.02 $\pm$ 0.10; T3, 16.38 $\pm$ 0.13; rT3, 19.70 $\pm$ 0.17; T4, 22.60 $\pm$ 0.21 min (n = 10). We preferred to use stepwise gradient elution over other forms of gradients, as this requires the least costly equipment (one isocratic pump and a low-pressure solvent selector valve) and also because we have the experience, from previous work, that a better reproducibility of eluent conditions is obtained. A one-step gradient from 30 to 60% of methanol in the aqueous buffer mixture, changing after elution of the first group of peaks, gave the required result.

After this result we did not further investigate ion-pair chromatography on other stationary phases, such as C_8, which also is a good candidate, because of the implications that this would have for the precolumn conditions. First, when using a C_8 column, the modifier content necessary for the separation would probably not be higher than 15–20%. This would limit the choice of solvent conditions for the clean-up step within the range 0–15 (20)% of modifier and would thus not be favourable in

the clean-up of actual samples. Second, in order to avoid unnecessary band broadening, retention on the precolumn should not be higher than that on the analytical column. A C_8 precolumn would have a lower volumetric loading capacity than a C_{18} precolumn. The use of a C_8 precolumn would mean a lower clean-up efficiency than is attainable with C_{18} and also a lower concentration factor. Another practical argument in favour of the use of C_{18} material was that we have had good experience with the stability of this type of C_{18} phase in previous ion-pair chromatographic applications and none with C_8 phases.

Optimization of on-line sample preparation

From the descriptions in the literature, it was expected that the real samples would contain a large number of interfering compounds, present in high concentrations. At the Laboratory of Organic/Analytical Chemistry of the RIVM, the experience and equipment for on-line preconcentration and clean-up in HPLC are available. In analogy with our previously published methods for on-line sample preparation[11,12], a precolumn sample pretreatment method was developed. All compounds involved could be sorbed from a buffered aqueous solution on a C_{18} precolumn, equilibrated with 0.03 *M* phosphate buffer (pH 2.2)–2.5 m*M* HSA ("buffer/HSA"). On this column, the first-eluted compound, Tyr, had a retention volume of 2ml, when eluted with this buffer–HSA mixture. We therefore concluded that the boundary condition for sampling without loss of analytes on the precolumn was *ca.* 1 ml of buffer–HSA (a 1-ml margin was arbitrarily adopted). The compounds sorbed could be quantitatively desorbed from the precolumn with 30% methanol in buffer–HSA.

The actual solvent program for clean-up of the samples with the use of a precolumn was derived empirically, within these two boundary solvent conditions. The

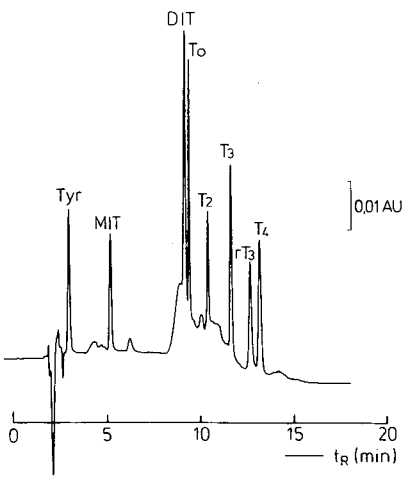

Fig. 2. LC separation of 75 μl of a standard solution containing 1 μg/ml of each of the iodoamino acids in water, carried out by the precolumn switching and ion-pair chromatography procedure described under Experimental. Flow-rate 1 ml/min. Clean-up was accomplished by flushing the loaded precolumn with 1ml of buffer/HSA. Detection, UV at 220 nm, 10 mV, 0.1 a.u.f.s.

result from the experimental optimization was the solvent program we described under Experimental.

With the method described, a test sample of thyroglobulin, enzymatically hydrolysed with pronase P (a protease mixture), was run. The first-eluted analyte, Tyr, could not be seen because of interference from unknown compounds, eluted at t_0. Fortunately, for our study the determination of Tyr is not essential. Further, the chromatogram showed an interfering peak (a compound with the same retention time as T3, but with a different UV spectrum). In order to improve the selectivity of the system towards this peak pair, without having to change the procedure essentially, the use of an iso-eluotropic eluent was indicated, in the step in which T3 is eluted[9,13]. Acetonitrile and THF are the most commonly used alternatives for methanol[9,13,14]. As elution with acetonitrile was found to give poor peak shapes (see above), we only partially replaced methanol with acetonitrile, thus creating a ternary mobile phase, as the second part of the analytical step-gradient procedure. The optimal composition of the ternary eluent was found by trial and error. Satisfactory results were obtained with methanol–acetonitrile–0.05 *M* buffer/HSA (34:17:49, v/v/v). With this eluent the resolution (R_s) between T3 and the unknown peak was 1.1.

The chromatographic behavior and potential interference of other UV-absorbing aromatic amino acids (proline, phenylalanine, histidine and tryptophan) was also investigated. None of them appeared in the chromatogram, because they were not trapped by the precolumn. Standard mixtures of the iodoamino acids can be analysed in a maximum volume of 1000 µl (see above). Samples containing thyroglobulin hydrolysate were in one instance limited to a maximum volume of 100µl, because of a matrix component being eluted close to T3.

A typical chromatogram of a standard mixture is shown in Fig. 2, where the baseline rise indicates the solvent switch from eluent C to D (the step gradient started at $t = 5$ min; the dead volume of the system was 3 ml).

The chromatographic behaviour of the analytes was significantly influenced by the thyroglobulin hydrolysate. Retention values were increased by 0.1 min for MIT, DIT and T0, by 0.5 min for T2, by 1.5 min for T3, by 2 min for rT3 and by 2.5 min for T4 owing to the presence of the matrix. This behaviour was repeatable for Tyr, MIT, DIT and T0, with relative standard deviations of 2–2.5%. The relative standard deviations for the later eluting compounds, T2, T3, rT3 and T4 (peaks 5–8 in Fig. 2), however, are larger (up to 4.25%). Therefore, when analysing samples, measurement of a reference sample (with standards added) after every fifth run, is strongly recommended. No matrix effects were observed in the analysis of tyrosine incubation mixtures.

Quantitative analysis

Plots for 50-µl standard injections of each of the iodoamino acids into the automated clean-up–chromatography system were measured in the ranges 10–180 ng for Tyr, 10–600 ng for DIT and MIT, 5–300 ng for T2 and 10–1000 ng for T3, rT3 and T4 (quantitation of T0 was, unfortunately, not possible owing to the lack of a standard solution of known concentration). Linearity was observed when either peak height or peak area was plotted *vs.* concentration ($R \geqslant 0.98$). The repeatability of the retention values for each compound in the chromatographic precolumn switching–analysis system were determined from ten injections of *ca.* 50 ng of each of the

analytes. The relative standard deviations were less than 1% (0.73–0.93%) for DIT, MIT, T0, T2, T3, rT3 and T4 (see above). The retention times of the two compounds eluted first, Tyr and MIT, showed a much higher variability, 1.95 and 2.95% (R.S.D.), respectively. This can be explained by the susceptibility of the least retained compounds to minor fluctuations in the eluent conditions and the fact that the procedure involves several switches in solvent composition during the precolumn flushing steps.

The sensitivity of the spectrophotometric detection at 220 nm was determined. As little as 10 ng/ml of each of the compounds could be detected in a standard mixture after the injection of 50-μl aliquots.

Calibration graphs for 25–250 ng of each of the analytes in thyroglobulin hydrolysate samples, measured after standard addition, were also linear for all components ($R \geqslant 0.98$) with the exception of Tyr (as mentioned above, Tyr could not be detected at these levels in this matrix, as it is co-eluted with a large amount of a matrix component). The sensitivity of the method for each of the components MIT, DIT, T2, T3, rT3, and T4 in thyroglobulin hydrolysates was 20 ng/ml when 50 μl of sample were injected.

Applications

The method developed was applied to the analysis of dog thyroglobulin, treated with pronase E or with pronases obtained from other manufacturers. A typical chromatogram is shown in Fig. 3. Remarkably, these samples were all much cleaner than was the initial test sample, treated with pronase P. Therefore, the ternary eluent after the gradient step, could be changed back to the binary methanol–buffer/HSA mixture. In the chromatogram shown in Fig. 3, three peaks are present with retention

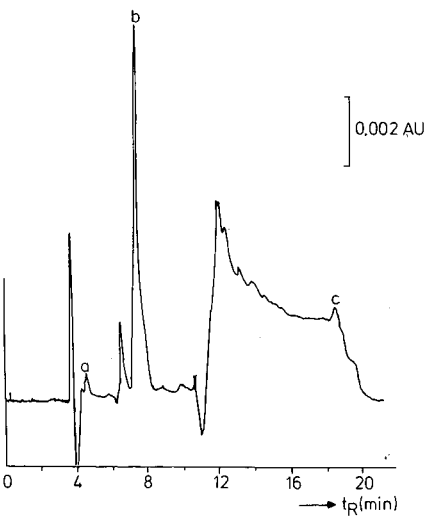

Fig. 3. LC separation of 250 μl of hydrolysed thyroglobulin (50 μg), carried out by the column switching procedure described. Details as under Experimental, except solvent D was replaced by the binary mixture methanol–buffer/HSA (60:40, v/v) and no acetone was added to eluent C. Detection, UV 220 nm, 10 mV, 0.02 a.u.f.s. Flow-rate 1 ml/min. The retention times of peaks a, b and c correspond to those of Tyr, MIT and T4, respectively.

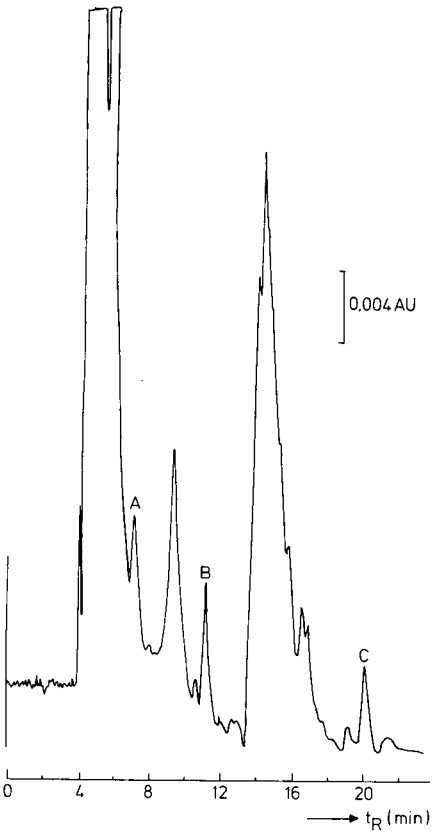

Fig. 4. LC separation of 250 μl of untreated human urine. Conditions as in Fig. 3. UV detector setting: 0.04 a.u.f.s. Flow-rate, 1 ml/min. The retention times of peaks A, B and C are identical with those of MIT, DIT and rT3, respectively.

times identical with those of Tyr, MIT and T4. Experiments are currently being undertaking to confirm the presence of these three compounds.

Another application was the analysis of a urine sample from a patient with a probable de-iodase defect. The chromatogram is shown in Fig. 4. In this chromatogram MIT, DIT and rT3 are probably present.

ACKNOWLEDGEMENTS

This work was supported in part by the Foundation for Medical Research (MEDIGON) subsidized by the Netherlands Organization for Scientific Research (NWO) and the Ludgardine Bouwman Stichting.

REFERENCES

1 K. Kok, *Academic Thesis*, University of Amsterdam, 1987.
2 A. Taurog, M. Dorris and L. Lamas, *Endocrinology*, 94 (1974) 1286.

3 S. H. Wollman, in J. T. Dingle and H. B. Fell (Editors), *Lysosomes in Biology and Pathology*, Vol. 2, Elsevier/North-Holland, Amsterdam, 1969, p. 483.
4 M. R. Hadj-Mohammadi, J. L. Ward and J. G. Dorsey, *J. Liq. Chromatogr.*, 6 (1983) 511.
5 N. M. Alexander and M. Nishimoto, *Clin. Chem.*, 25 (1979) 1757.
6 I. D. Hay, T. M. Annesley, N. S. Jiang and C. A. Gorman, *J. Chromatogr.*, 226 (1981) 383.
7 R. Bianci, N. Molea, F. Cazzuola, L. Fusani, M. Lotti, P. Bertelli, M. Ferdeghini and G. Mariani, *J. Chromatogr.*, 297 (1984) 393.
8 B. R. Hepler, S. G. Weber and W. C. Purdy, *Anal. Chim. Acta*, 138 (1982) 221.
9 P. J. Schoenmakers, A. C. J. H. Drouen, H. A. H. Billiet and L. de Galan, *Chromatographia*, 15 (1982) 680.
10 A. C. J. H. Drouen, H. A. H. Billiet, P. J. Schoenmakers and L. de Galan, *Chromatographia*, 16 (1982) 48.
11 C. E. Goewie and E. A. Hogendoorn, *J. Chromatogr.*, 404 (1987) 352.
12 C. E. Goewie and E. A. Hogendoorn, *J. Chromatogr.*, 410 (1987) 211.
13 L. R. Snyder and J. J. Kirkland, *Introduction to Modern Liquid Chromatography*, Wiley, New York, 1979.
14 P. J. Schoenmakers, *Optimization of Chromatographic Selectivity (Journal of Chromatography Library*, Vol. 35), Elsevier, Amsterdam, 1986.

Journal of Chromatography, 458 (1988) 185–192
Elsevier Science Publishers B.V., Amsterdam — Printed in The Netherlands

CHROMSYMP. 1416

HIGH-PERFORMANCE AFFINITY ISOLATION OF LYMPHOCYTE MEMBRANE RECEPTORS ON BIOTINYLATED ANTIGEN AND AVIDIN-COATED BEADS

T. M. PHILLIPS* and S. C. FRANTZ
Immunochemistry Laboratory, George Washington University Medical Center, Washington, DC 20037 (U.S.A.)
J. V. BABASHAK
Kontes Scientific Glassware, Vineland, NJ (U.S.A.)
and
J. J. CHMIELINSKA
Immunochemistry Laboratory, George Washington University Medical Center, Washington, DC 20037 (U.S.A.)

SUMMARY

Isolation of lymphocyte membrane receptors can be achieved by high-performance liquid chromatography using immobilized streptavidin as the ligand and biotinylated antigen. Activated lymphocytes were allowed to react with biotin-labelled antigen prior to harvesting. The cells were disrupted and their membranes solubilized before passing the suspension through the avidin affinity column. The biotinylated antigen acted as an efficient receptor probe, which helped to maintain the integrity of the receptor during the isolation procedure. The biotin also acted as the substrate that attaches to the immobilized avidin. Recovery of the bound receptor was achieved by dissociation of the receptor from the antigen and recovery of the receptor in the effluent during the elution phase of the separation.

INTRODUCTION

Affinity chromatography, with a variety of different ligands, ranging from immobilized plant lectins[1–3] to receptor substrates[4–6], has been used to isolate cell membrane receptors. In a similar manner, immunoaffinity chromatography, using immobilized antibodies, can also be used to isolate specific receptors[7–9]. The latter technique accomplishes the isolation by means of antibodies directly against the receptor itself, or against the substrate, which is complexed to the receptor. This has led to an interest in using the biotin–avidin system for the isolation of receptors, with biotinylated probes and immobilized avidin as the ligand[10,11].

Streptavidin is a form of avidin, isolated from *Streptomyces avidinii*, which has the ability to bind up to four molecules of biotin[12]. This binding has been shown to be strong enough to withstand the conditions encountered during the elution phase of

0021-9673/88/$03.50

high-performance affinity chromatography (HPAC)[8,13]. We have previously reported the development of an avidin-coated glass bead that can be used to absorb biotinylated antibodies[7,9]. In this paper, we describe the use of immobilized avidin as an affinity ligand for the isolation of membrane receptors that have previously been allowed to bind biotinylated antigen.

EXPERIMENTAL

Materials

Glass beads (1 mm) were obtained from Kontes Scientific Glassware (Vineland, NJ, U.S.A.). Purified streptavidin was purchased as a lyophilized, pure product from Bethesda Research Labs. (Gaithersburg, MD, U.S.A.) and reconstituted in 50 m*M* carbonate buffer (pH 9.0). The biotin derivatives and the laboratory chemicals were obtained from Sigma (St. Louis, MO, U.S.A.). 3-Aminopropyltriethoxysilane and 1,1′-carbonyldiimidazole were obtained from Pierce (Rockford, IL, U.S.A.). All columns and column fittings were purchased from Jones Chromatography (Littleton, CO, U.S.A.).

Derivatization of the glass beads

The glass beads were washed by sedimentation in doubly distilled water, to remove manufacturing impurities from the beads surface, before preparing the beads for silanization and derivatization[14]. Briefly, this was performed by placing 10 g of the washed beads in 50 ml of 1 *M* hydrochloric acid and gently sonicating for 25 min. The beads were then washed by sedimentation in 200-ml portions of 1 *M* hydrochloric acid until the suspension became clear. The beads were removed, air-dried and refluxed for 30 min in 200 ml of 1 *M* nitric acid with constant agitation, then recovered, air-dried and suspended in 50 ml of 10% 3-aminopropyltriethoxysilane dissolved in toluene. This suspension was refluxed for 16 h with constant agitation.

Following silanilization, the beads were washed twice in 200 ml of 95% methanol, then refluxed for 20 min in 95% methanol to remove the excess of silanizing agent. The beads were recovered, washed three times in doubly glass-distilled water and air-dried prior to derivatization of the reactive side-groups.

The reactive carbonyldiimidazole (CDI) side-groups were attached to the bead surface by suspending the beads in 5 ml of dioxane and adding 100 mg of 1,1′-carbonyldiimidazole. The mixture was placed in a 15-ml capped glass tube and incubated for 6 h at room temperature in an overhead mixer. The beads were then recovered and washed thoroughly in dioxane by sedimentation and decantation. The beads were air-dried and used immediately for immobilization of the streptavidin.

Column construction

CDI-derivatized beads (10 g) were suspended in 5 ml of doubly distilled water and 5 ml of 50 m*M* carbonate buffer (pH 9.0) containing 2.5 mg of streptavidin were added. The mixture was placed in a 15-ml capped glass tube and incubated for 18 h at 4°C in an overhead mixer. The beads were then allowed to settle and washed ten times in 0.01 *M* phosphate buffer by sedimentation and decantation. Attachment of the streptavidin to the beads was checked by incubating a 25-μl drop of the bead

suspension, obtained from the last wash, with fluorescein-labelled biotin and examining 100 beads under a fluorescence microscope. Following satisfactory coating of the beads, they were sedimented, recovered, resuspended in 5 ml 0.01 *M* phosphate buffer and slurry-packed into 10 cm × 4.6 mm I.D. high-performance liquid chromatographic (HPLC) columns at 250 p.s.i.

Biotinylation of antigen

The antigen was biotinylated with four different forms of biotin: (a) N-hydroxysuccinimide biotin, (b) long-chain N-hydroxysuccinimide biotin, (c) cleavable iminobiotin and (d) hydrazine biotin. The first three biotinylations were performed in a similar manner by incubating 100 μg of the antigen with 1 mg of the biotin derivative in 1 ml of 0.05 *M* carbonate buffer (pH 9.0). The mixture was placed in a rotating mixer for 2 h at room temperature, and the reaction was stopped by overnight dialysis at 4°C against 0.01 *M* phosphate buffer (pH 7.0).

The hydrazine biotinylation required modification of the carbohydrate portion of the glycoprotein antigen, which was performed by suspending 100 μg of antigen in 1 ml of 0.1 *M* sodium acetate buffer (pH 5.0) and cooling to 4°C. A 1-ml volume of a 10 m*M* solution of cold sodium metaperiodate was added to the antigen before incubation for 20 min at 4°C in the dark. The reaction was stopped by adding 10 ml of 5% ethylene glycol and dialyzing the solution against 0.01 *M* phosphate buffer for 18 h at 4°C, with five changes of the dialysate. The antigen was then removed from the dialysis tubing and placed in a capped glass tube. To this was added 1 ml of phosphate buffer containing 1 mg/ml of sodium cyanoborohydride and 1 ml/ml biotin hydrazine, and the mixture was placed in a rotating mixer for 1 h at room temperature. The reaction was stopped by dialysis against 0.01 *M* phosphate buffer overnight at 4°C.

Isolation of lymphocyte membrane receptors

Prior to disruption and solubilization of their membranes, active lymphocytes were isolated from whole blood by centrifugation at 400 *g* for 15 min in a Ficoll gradient. The lymphocyte band was recovered and the specific receptors were localized by allowing them to interact with the biotinylated antigen for 1 h at 37°C. Following this incubation, the cells were collected, washed twice in 0.01 *M* phosphate buffer (pH 7.0) and pelleted by centrifugation at 600 *g* for 15 min. The pellet, containing 10^8 lymphocytes, was frozen and thawed three times and then sonicated for 2 min at maximum power. The sonicated pellet was resuspended in 2 ml of 0.01 *M* phosphate buffer and the membrane fraction was isolated by centrifugation at 10 000 *g* for 30 min. The membrane-enriched supernatant was mixed with an equal volume of 1% sodium deoxycholate solution and incubated for 30 min at room temperature. Finally, the solubilized membrane sample was centrifuged for 1 h at 10 000 *g* and the supernatant was applied to the avidin columns.

Chromatography

The avidin bead-packed column was installed in a Beckman (Palo Alto, CA, U.S.A.) Model 340 isocratic HPLC system equipped with a Model 112 pump, a Model 160 UV detector (set at 280 nm) and a Shimadzu C-R1B recording peak integrator (Shimadzu Scientific Instruments, Columbia, MD, U.S.A.). The elution profile was automatically controlled by a Model III OPG/S solvent selector/gradient controller

(Autochrom, Milford, MA, U.S.A.). Samples were introduced into the system by injection through an Altex 210 injection port, equipped with a 100-μl sample loop. The column was developed isocratically in 0.01 *M* phosphate buffer, containing 10 m*M* sodium deoxycholate at pH 7.0 for 15 min at a flow-rate of 0.5 ml/min. Throughout the entire run, the column temperature was maintained at 4°C by a glass column jacket attached to a recycling ice-bath.

Following the initial 15-min run, during which the biotinylated antigen–membrane receptor complex was absorbed to the immobilized avidin, an elution recovery phase was started. In all instances except for iminobiotin, a chaotropic ion gradient was developed by adding 0–2.5 *M* sodium thiocyanate to the running buffer over a further 15 min. Recovery of the cleavable iminobiotin complex was achieved using a pH gradient from pH 7.0 to 3.0[15], developed by the addition of 0.5 *M* hydrochloric acid over the same 15-min period.

Recovery of the bound materials was accomplished during the gradient phase, and the upper limits of both gradient types were maintained for a further 5 min before recycling the column by returning it to the initial running conditions. Fractions of the eluted material were collected in 500-μl Beckman microfuge tubes, in a modified ISCO Cygnet fraction collector (ISCO, Lincoln, NB, U.S.A.). The recovered receptors were dialyzed overnight at 4°C against 0.01 *M* phosphate buffer, to which 25 m*M* sodium deoxycholate had been added. The purity of the isolated receptors was checked by polyacrylamide gel electrophoresis[16] and their activity was measured by radiolabelled antigen binding studies[17].

RESULTS

Even coating of the glass beads with the streptavidin was achieved, as demonstrated by microscopic examination of the localization of fluorescein-labelled biotin. The biotin binding capacity of the columns were found to be between 500 and

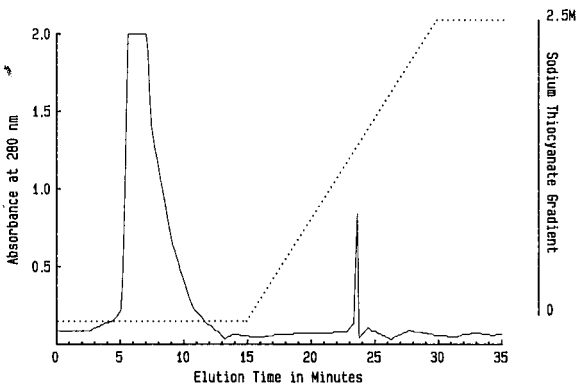

Fig. 1. HPAC isolation of lymphocyte membrane receptors with N-hydroxysuccinimide biotin-labelled antigen as the probe. The chromatogram was produced by passing 100 μl of biotinylated antigen receptor complex through a 10 cm × 4.6 mm I.D. column containing immobilized streptavidin as the ligand. The column was developed in running 0.01 *M* phosphate buffer (pH 7.0) at a flow-rate of 0.5 ml/min. The elution was monitored at 280 nm with the detector set at 0.005 a.u.f.s. The column was maintained at 4°C throughout the experiment. The dotted line indicates the 0–2.5 *M* sodium thiocyanate elution gradient.

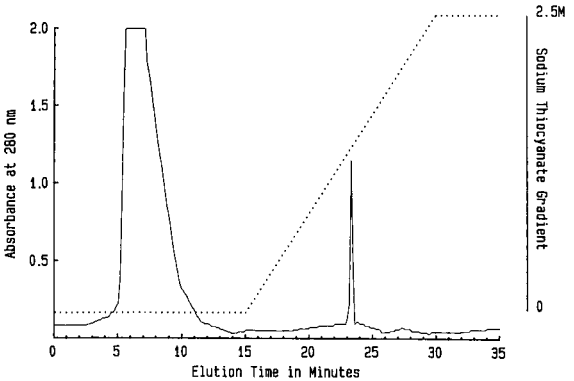

Fig. 2. HPAC isolation of membrane receptors with long-chain biotin-labelled antigen as the probe. Chromatographic conditions as in Fig. 1.

545 μg per column. This coating was stable over ten runs at flow-rates of up to 1.5 ml/min and storage at 4°C for 3 months. However, studies have shown that the CDI-activated beads need to be coated within 48 h of derivatization of the bead surface because the diimidazole side-groups are unstable and the protein binding efficiency will decrease drastically with time.

Affinity isolation of specific receptors, with either the N-hydroxysuccinimide biotin or the hydrazine biotin-labelled antigen, could easily be achieved by using immobilized streptavidin as the ligand. Both biotinylations had the same degree of efficiency and produced similar elution profiles. Fig. 1 shows a typical chromatogram produced by this technique. The primary peak contains the non-reactive membrane components and the sharp, secondary peak contains the isolated receptor eluted from the biotin-labelled antigen. The antigen remains in the column, attached to the immobilized avidin.

Similar results were obtained with long-chain biotin as the antigen label. Fig. 2 shows a typical chromatogram of receptor isolation with this form of biotinylation.

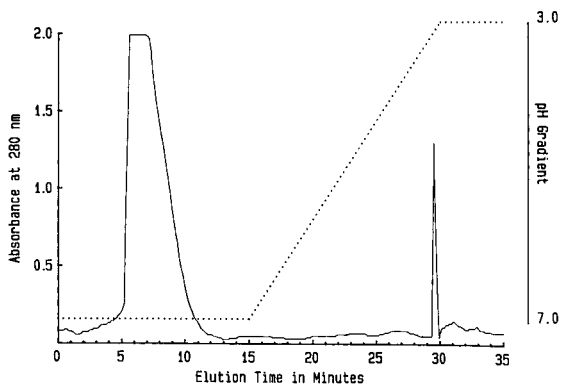

Fig. 3. HPAC isolation of receptors with cleavable iminobiotin as the antigen probe label. Chromatographic conditions as in Fig. 1. The dotted line indicates the pH 7–3 elution gradient.

The secondary peak, which contains the receptor, is slightly larger than that produced by standard N-hydroxysuccinimide or hydrazine biotin labels.

The chromatogram shown in Fig. 3 is representative of the elution profile produced by using cleavable biotin-labelled antigen as the receptor probe. In this chromatogram, the biotinylated antigen receptor complex is eluted from the avidin column by a pH gradient. The second peak, which contains the complexed receptor and antigen, is eluted later in the chromatogram. It was found that further dissociation by chaotropic agents and/or detergents was necessary in order to dissociate the receptor from the antigen probe.

Polyacrylamide gel electrophoresis of the second peak, produced by all of the biotinylated antigen probes, demonstrated the presence of a single protein band, except for the cleavable biotin probe, which also produced a second minor band. This second band was subsequently found to correspond to the biotinylated antigen. All of the major bands were found to consist of 90–92 kDa material by comparison with molecular weight. markers. No comparable bands were found in the first peak of the chromatograms.

Radiolabelled antigen binding studies (Fig. 4) demonstrated differences in the binding efficiency of the different receptor isolates. The receptors isolated by the long-chain biotinylated probe demonstrated the highest degree of antigen binding, which was shown to be approximately 60% of that demonstrated by intact lymphocytes. Receptors isolated by both the standard N-hydroxysuccinimide ester and hydrazine biotin-labelled antigen probes demonstrated comparable binding characteristics. These receptors bound *ca.* 50% of the antigen bound by intact cells. Receptors isolated by cleavable biotin probes appeared to have lost a large amount of their antigen-binding capacity. These receptors demonstrated binding capacities of *ca.* 30% of that shown by intact cells. We postulate that the additional step required to remove the antigen probe from the receptor caused damage to the receptor structure, although we have not been able to prove this.

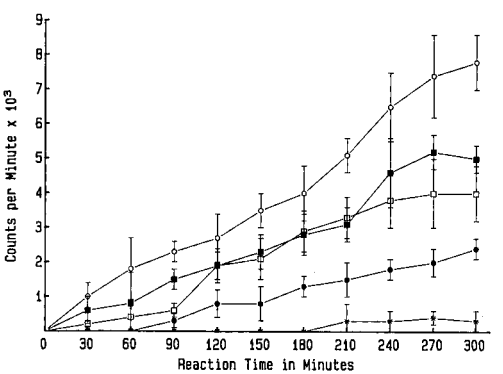

Fig. 4. Comparison of antigen-binding capacities of HPAC-isolated receptors. Points represent the mean of ten experiments ± the standard error of the mean. Receptors isolated by N-hydroxysuccinimide biotin-labelled antigen (□), long-chain biotin-labelled antigen (■) and aminobiotin labelled antigen (●). The binding of the isolated receptors was corrected for the amount of receptor present in each sample and compared a similar number of intact stimulated (○) and normal, unstimulated lymphocytes (★). All cells and receptors were incubated with 50 μg of ^{125}I-labelled antigen.

DISCUSSION

HPAC on avidin-coated glass beads is a rapid technique for isolating membrane receptors that have been complexed with biotinylated antigen. The use of large glass beads (1 mm diameter) was found to have an advantage over smaller packing media, such as controlled-pore glass beads. The larger solid beads were found to help to maintain reasonable flow-rates, reduce column running pressures and provide a large surface area for avidin attachment. However, the advantage of this technique over conventional lectin or biochemical techniques is questionable. In most instances, once the biotin-labelled antigen has attached itself to the biotin receptors on the immobilized avidin, this material is bound so tightly that its removal often damages the avidin coat. This means that the HPAC column is usable only once and must then be discarded. Even when cleavable biotin derivatives are used, the column is reusable, but the isolated membranes are often damaged during the second step, which is required to rid the receptor of the biotinylated probe. The loss of antigen-binding capacity in the receptors isolated with the cleavable biotin-labelled probe was probably caused by a combination of the pH and the chaotropic agent used for elution of the bound antigen. The effects of both of these factors on protein structures and function have been reported previously[18,19]. Steric hindrance also plays a part in the efficiency of biotin binding on the immobilized avidin. In this study, this was seen when long-chain biotinylation was used.

However, the material isolated by all four biotin-labelled probes demonstrated a single band in polyacrylamide gel electrophoresis in the region of 90 kDa, which is comparable to that found by other workers who isolated T cell receptors by other means[20,21].

In conclusion, we believe that the biotin–avidin system is useful for the isolation of membrane receptors, but care must be taken in planning the isolation procedure. The disadvantage of the technique is that, in most instances, the column packing can be used only once and great difficulty is experienced in recycling the packing media. However, the materials isolated by this technique are reasonably pure and in many instances still active. Long-chain biotin derivatives were found to give the most reproducible results and the highest yields of bioactive receptors. Cleavable biotins are not as useful as reported because they require another step for removal of the antigen.

The avidin-coated beads are useful and provide an excellent support for the immobilization of biotinylated ligands or for the isolation of biotin-labelled biological material.

REFERENCES

1 D. Allen, J. Auger and M. J. Crumpton, *Nature New Biol.*, 236 (1972) 23.
2 W. L. Adair and S. Kornfeld, *J. Biol. Chem.*, 249 (1974) 4686.
3 R. Lotan and G. L. Nicolson, *Biochem. Biophys. Res. Commun.*, 559 (1979) 329.
4 R. J. Schneider, A. Kulczycki, S. K. Law and J. P. Atkinson, *Nature (London)*, 290 (1981) 789.
5 G. Ashwell and J. Harford, *Annu. Rev. Biochem.*, 51 (1982) 531.
6 R. M. Graham, H.-J. Hess and C. J. Homcy, *Proc. Natl. Acad. Sci. U.S.A.*, 79 (1982) 2186.
7 T. M. Phillips and S. C. Frantz, *J. Chromatogr.*, 444 (1988) 13.
8 J. V. Babashak and T. M. Phillips, *J. Chromatogr.*, 44 (1988) 21.
9 T. M. Phillips, S. C. Frantz and J. J. Chmielinska, *Biochromatography*, 3 (1988) 149.
10 R. Zeheb, V. Chang and G. A. Orr, *Ann. Biochem.*, 129 (1983) 156.

11 K. Hoffman and F. M. Finn, *Ann. N.Y. Acad. Sci.*, 447 (1985) 359.
12 M. Wilchek and E. A. Bayer, *Immunol. Today*, 5 (1984) 39.
13 T. M. Phillips, *Adv. Chromatogr.*, 29 (1989) in press (Ch. 3).
14 R. R. Walters, in P. D. G. Dean, W. S. Johnson and F. A. Middle (Editors), *Affinity Chromatography*, IRL Press, Washington, DC, 1985, p. 25.
15 G. A. Orr, *J. Biol. Chem.*, 256 (1981) 761.
16 A. Chrambach and D. Rodbard, in B. D. Hames and D. Rickwood (Editors), *Gel Electrophoresis of Proteins: A Practical Approach*, IRL Press, Washington, DC, 1981, p. 93.
17 J. Haberman, C. R. Pickardt and P. C. Scriba, *Acta Endocrinol.*, 2324 (1980) 26.
18 S. Lapanje, *Physicochemical Aspects of Protein Denaturation*, Wiley, New York, 1978, p. 56.
19 Rouslahti, in E. Rouslahti (Editor), *Immunoadsorbents in Protein Purification*, University Park Press, Baltimore, 1976, p. 3.
20 K. Haskins, R. Kubo, J. White, M. Pigeon, J. Kappler and P. Marrack, *J. Exp. Med.*, 157 (1983) 1149.
21 E. Reinherz, S. Meuer, K. Fitzgerald, R. Hussey, J. Hodgdon, O. Acuto and S. Schlossman, *Proc. Natl. Acad. Sci. U.S.A.*, 80 (1983) 4104.

Journal of Chromatography, 458 (1988) 193–205
Elsevier Science Publishers B.V., Amsterdam — Printed in The Netherlands

CHROMSYMP. 1470

EFFECT OF PEPTIDE CHAIN LENGTH ON PEPTIDE RETENTION BEHAVIOUR IN REVERSED-PHASE CHROMATOGRPHY

COLIN T. MANT, T. W. LORNE BURKE, JAMES A. BLACK and ROBERT S. HODGES*
MRC Group in Protein Structure and Function, Department of Biochemistry, University of Alberta, Edmonton, Alberta T6G 2H7 (Canada)

SUMMARY

The use of amino acid retention or hydrophobicity coefficients for the prediction of peptide retention time and/or the elution order on hydrophobic stationary phases is based on the premise that amino acid composition is the major factor affecting peptide retention in reversed-phase chromatography. Although this assumption generally agrees well for small peptides (up to *ca.* 15 residues), the retention times of increasingly larger peptides are less than expected from a simple summation of retention coefficients. In the present study, we report the synthesis of four series of peptide polymers which vary significantly in overall hydrophobicity and polypeptide chain length (5–50 amino acid residues, Ac = acetyl): Ac-(G-L-G-A-K-G-A-G-V-G)$_n$-amide (n = 1–5), Ac-(G-K-G-L-G)$_n$-amide (n = 1, 2, 4, 6, 8, 10), Ac-(L-G-L-K-A)$_n$-amide (n = 1, 2, 4, 6, 8, 10) and Ac-(L-G-L-K-L)$_n$-amide (n = 1, 2, 4). From the retention behaviour of these peptide polymers on C_4, C_8 and C_{18} stationary phases under gradient elution conditions, we have clearly established the effect of polypeptide chain length and hydrophobicity on peptide retention. This, in turn, has enabled us to extend the utility of retention time prediction for peptides containing up to 50 residues by introducing a peptide chain-length correction.

INTRODUCTION

The versatility of reversed-phase chromatography (RPC) is reflected in its successful application to the isolation of peptides from a wide variety of sources. Knowledge of the contribution of individual amino acids to peptide retention behaviour on hydrophobic stationary phases, enabling prediction of elution profiles of peptides of known composition, greatly enhances the value of RPC. A major advantage of peptide retention predictions, for instance, is that the position of a peptide(s) of interest in the elution profile of a peptide mixture is narrowed down to a small section of the chromatogram, saving much time and effort in subsequent purification. In addition, information about the relative order of peptide elution from a complex mixture may be obtained. In conjunction with detection by UV absorbance of aromatic residue-containing peptides, fluorescence detection and/or amino acid-specific colour reactions, the identification of specified peptides in a complex mixture may be greatly simplified.

0021-9673/88/$03.50

A major factor governing the retention behaviour of peptides during RPC is the relative hydrophilic/hydrophobic contribution that the side-chains of individual amino acid residues make to the overall hydrophobicity of the peptide. Indeed, several research groups[1–10] have determined sets of coefficients for predicting peptide retention times during RPC, on the assumption that the chromatographic behaviour of a peptide is mainly or solely dependent on amino acid composition. Although this assumption holds up well enough for small peptides (up to *ca.* 15 residues), it could be expected that amino acid sequence may also have an effect on peptide retention. In fact, deviations from predicted retention times and/or elution order for small peptides are generally explained in terms of sequence-specific conformational differences, leading to preferential interaction sites, or anomalous stationary phase interactions[2,3,11–15]. In addition, a non-polar environment, such as a hydrophobic stationary phase, may induce helical structures in potentially helical molecules[16].

Sequence-dependent effects can be divided into two categories: conformational and nearest-neighbour effects. Nearest-neighbour effects can be defined as a reduction in the contribution that an individual side-chain makes to the overall hydrophobicity of the peptide by the close proximity of neighbouring side-chains in the amino acid sequence. For example, when comparing the peptides Gly-Leu-Gly and Leu-Leu-Leu, is the contribution of each leucine side-chain identical in both peptides, or is the average contribution of each leucine in the latter peptide reduced due to nearest-neighbour effects of adjacent leucines? Our definition of nearest-neighbour effects is that they are amino acid sequence-dependent, but independent of conformation. In other words, to prove the existence of amino acid sequence-dependent nearest-neighbour effects, the lack of any defined peptide conformation on interaction of a peptide with the reversed-phase sorbent must be demonstrated. By comparison, amino acid sequence-dependent conformational effects would be a reduction in the overall hydrophobicity of a peptide as a result of the peptide adopting a unique conformation on interacting with the hydrophobic stationary phase, compared to the hydrophobicity of the peptide if it existed as a random coil, *i.e.*, lacking a unique conformation.

Several researchers have noted that peptides larger than 15–20 residues tended to be eluted more rapidly than predicted from hydrophobic considerations alone[3,4,6,13,16–19]. This non-ideal behaviour is generally assumed to be due to stabilized secondary and tertiary structures in the polypeptide which remove certain amino acid residues from contact with the hydrophobic stationary phase. However, it is also possible that there is a peptide chain length effect on retention behaviour of polypeptides, independent of any conformational considerations. Lau *et al.*[20] reported a linear relationship between $\log_{10}$MW and peptide retention time during RPC for a series of five peptide polymers of 8–36 residues. Mant and Hodges[16] demonstrated a similar exponential relationship for a series of five peptide polymers of 10–50 residues. The effect on peptide retention of increasing peptide length decreased progressively with each ten-residue addition.

To understand peptide retention behaviour during RPC completely, it is not sufficient merely to demonstrate that various factors (nearest-neighbour, conformational, peptide chain length) have an effect on peptide retention; it is also necessary to quantitate the relative contribution each factor makes to retention behaviour. Most reported amino acid retention coefficients derived from observed peptide retention

values during RPC have been obtained by computer-calculated regression analysis of the retention times of a wide range of peptides of varied composition and length[1–7,10]. If nearest-neighbour, conformational and peptide chain length effects were present in individual peptides in these peptide mixtures, the coefficients derived by using this approach would be in error and vary among different research groups, depending on the particular peptides used. In addition, because of the low occurrence of certain amino acid residues in any small group of peptides examined, substantial errors may be created for these residues when computer-calculated regression analysis is used to generate the coefficients. A more precise approach to determining retention coefficients was developed by Guo *et al.*[8], who examined the contribution of individual amino acid residues to peptide retention on reversed-phase columns by measuring their effect on retention of a model synthetic peptide (Ac = acetyl): Ac-Gly-X-X-$(Leu)_3$-$(Lys)_2$-amide, where X was substituted by the 20 amino acids found in proteins. This approach overcame many of the problems associated with computer-calculated regression analysis and eliminated any effect of peptide chain length.

In the present study, we wished to examine the effect of polypeptide chain length on peptide retention times during RPC. We have, therefore, synthesized four series of peptide polymers (5–50 residues) of varying hydrophobicity and subjected them to RPC on C_4, C_8 and C_{18} silica-based columns. From the observed retention times of the polymer sets, we have gained a clearer understanding of the effect of both peptide chain length and overall peptide hydrophobicity on peptide retention behaviour during RPC, enabling the accurate prediction of retention times for peptides up to 50 residues in length.

EXPERIMENTAL

Materials

HPLC-grade water and acetonitrile were obtained from J. T. Baker (Phillipsburg, NJ, U.S.A.). HPLC-grade trifluoroacetic acid (TFA) was obtained from Pierce (Rockford, IL, U.S.A.). A synthetic decapeptide reversed-phase standard, S4, and a mixture of five synthetic size-exclusion standards (10–50 residues) were obtained from Synthetic Peptides Inc. (Department of Biochemistry, University of Alberta, Edmonton, Canada).

Peptide synthesis

The peptide polymers described were synthesized on a peptide synthesizer Model 430A (Applied Biosystems, Foster City, CA, U.S.A.) using the general procedure for solid-phase synthesis described by Parker and Hodges[21] and Hodges *et al.*[22].

Apparatus

The HPLC instrument consisted of a Varian Vista Series 5000 liquid chromatograph (Varian, Walnut Creek, CA, U.S.A.) coupled to an HP 1040A detection system, HP 9000 Series 300 computer, HP 9133 disc drive, HP 2225A Thinkjet printer and HP 7440A plotter (Hewlett-Packard, Avondale, PA, U.S.A.). Samples were injected with a 200-μl injection loop (Model 7125; Rheodyne, Cotati, CA, U.S.A.).

Columns

Peptide mixtures were separated on three columns: (1) SynChropak RP-4 (C_4), 250 mm × 4.1 mm I.D., particle size 6.5 μm, pore size 300 Å, carbon loading *ca.* 7.5% (SynChrom, Linden, IN, U.S.A.); (2) Aquapore RP-300 C_8, 220 mm × 4.6 mm I.D., 7 μm, 300 Å (Brownlee Labs., Santa Clara, CA, U.S.A.); (3) SynChropak RP-P (C_{18}), 250 × 4.6 mm I.D., 6.5 μm, 300 Å, carbon loading *ca.* 10% (SynChrom).

RESULTS AND DISCUSSION

Design of peptide polymers

The effect on peptide retention of increasing peptide length is clearly illustrated in the RPC profile (Fig.1) of a mixture of five synthetic peptide size-exclusion standards[16,23] on a C_{18} column at pH 2.0 [linear AB gradient at 1% B/min and 1 ml/min, where eluent A is 0.1% aq. trifluoroacetic acid (TFA) and eluent B is 0.1% TFA in acetonitrile]. The amino acid sequence of the standards is Ac-(G-L-G-A-K-G-A-G-V-G)$_n$-amide, where n = 1–5, *i.e.*, 10–50 residues in length. As reported previously by Mant and Hodges[16], the effect of increasing peptide length on the retention times of these peptides decreased progressively with each addition of a ten-residue repeating unit.

In order to examine further the effect of peptide chain length, as well as peptide hydrophobicity, on peptide retention behaviour, it was necessary to design series of peptide polymers covering a similar range of chain length, but differing in overall hydrophobicity. The design of these polymers, in turn, required the application of an accurate set of amino acid side-chain hydrophobicity parameters. The model peptide approach of Guo *et al.*[8] would be expected to have produced the most accurate set of retention coefficients currently available. Subsequent application of these coefficients resulted in the design and synthesis of three sets of peptide polymers: (a) Ac(G-K-G-L-G)$_n$-amide, where n = 1, 2, 4, 6, 8, 10 (5–50 residues); (b) Ac-(L-G-L-K-A)$_n$-amide,

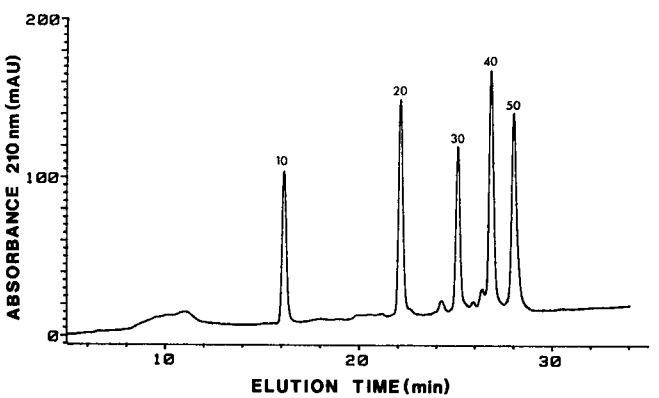

Fig. 1. RPC of a mixture of synthetic peptide polymers. Column: SynChropak RP-P C_{18} (250 mm × 4.6 mm I.D.). Mobile phase: linear AB gradient (1% B/min), where eluent A is 0.1% aq. TFA and eluent B is 0.1% TFA in acetonitrile (pH 2.0); flow-rate, 1 ml/min; 26°C. The numbers labelling the peptide peaks denote 10, 20, 30, 40 and 50 residues, respectively. The sequence of the polymer series is Ac-(G-L-G-A-K-G-A-G-V-G)$_n$-amide, where n = 1–5.

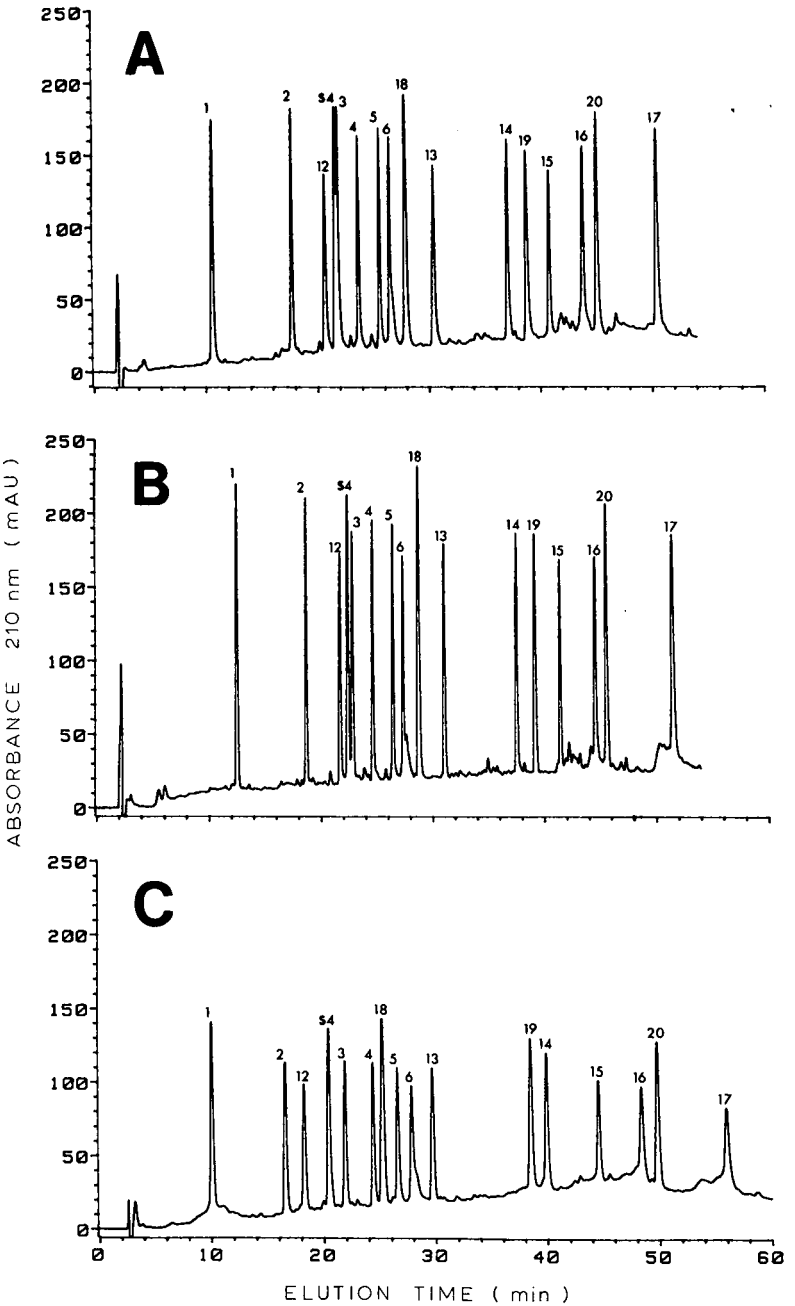

Fig. 2. RPC of a mixture of synthetic peptide polymers. Column: (A) SynChropak RP-4 C_4 (250 mm × 4.1 mm I.D.); (B) Aquapore RP-300 C_8 (220 mm × 4.6 mm I.D.); (C) SynChropak RP-P C_{18} (250 mm × 4.6 mm I.D.). Mobile phase: linear AB gradient (1% B/min), where eluent A is 0.1% aq. TFA and eluent B is 0.1% TFA in acetonitrile (pH 2.0); flow-rate, 1 ml/min; 26°C. Numbers denote peptides listed in Table I.

where $n = 1, 2, 4, 6, 8, 10$ (5–50 residues); (c) Ac-(L-G-L-K-L)$_n$-amide, where $n = 1$–4 (5–20 residues). The retention coefficients reported by Guo *et al.*[8] (obtained with aq. TFA to TFA–acetonitrile gradients, pH 2.0) for Lys, Gly, Ala and Leu were −2.1, −0.2, 2.0 and 8:1 min, respectively, *i.e.*, in order of increasing hydrophobicity, K < G < A ≪ L. Thus, the hydrophobicity of the polymer series increased in the order, Ac-(G-K-G-L-G)$_n$-amide ("G" series) < Ac-(L-G-L-K-A)$_n$-amide ("A" series) < Ac-(L-G-L-K-L)$_n$-amide ("L" series). For the purposes of this study, each peptide is referred to by a number and letter which denote, respectively, the number of residues it contains and to which polymer series it belongs. Thus, 5G refers to the five-residue "G" series peptide, 30A refers to the 30-residue "A" series peptide, etc. The presence of a Leu residue in the five-residue repeating unit in the "G" series ensured that this series was sufficiently hydrophobic to be retained by the reversed-phase columns; the presence of a Lys residue in the five-residue repeating units of the polymer sets ensured that the peptides were soluble in 0.1% aq. TFA (pH 2.0); finally, the replacement of a Leu residue by an Ala residue in the five-residue repeating unit of the "A" series ensured that this polymer set was intermediate in hydrophobicity between the hydrophilic "G" series and the very hydrophobic "L" series.

Effect of polypeptide chain length on peptide retention time

Fig. 2 shows elution profiles of a mixture of the "G", "A" and "L" series of peptide polymers on C_4 (A), C_8 (B) and C_{18} (C) reversed-phase columns. The peptides were chromatographed under conditions identical with those employed by Guo *et al.*[8] to obtain their coefficients (linear AB gradient of 1% B/min at a flow-rate of 1 ml/min, where solvent A is 0.1% aq. TFA and solvent B is 0.1% TFA in acetonitrile). Since the coefficients of Guo *et al.*[8] were obtained on a particular column on a particular high-performance liquid chromatographic (HPLC) instrument, an internal synthetic decapeptide standard, S4, was included in each run as an internal peptide standard to correct for different columns and instrumentation[8,9]. The five size-exclusion standards (plus S4) from Fig. 1 (denoted "X" series for the present study) were also chromatographed on all three columns under the same conditions. Observed retention times for all four peptide polymer series are shown in Table I. The peptide elution profiles are very similar on all three columns. The few selectivity differences that are observed between the three columns are the result of a larger change in retention of the five-residue peptides compared to the longer 10- to 50-residue peptides.

Predicted peptide retention times were determined by use of the rules for prediction of peptide retention times, developed by Guo *et al.*[8]

$$\tau = \Sigma R_c + t_s$$

where the predicted retention time, τ, equals the sum of the retention coefficients, ΣR_c, for the amino acid residues, plus the time correction for the internal peptide standard, t_s. The value t_s is obtained by subtracting the sum of the retention coefficients for the peptide standard S4, ΣR_c^{std}, from the observed retention time of the same peptide, t_R^{std}

$$t_s = t_R^{std} - \Sigma R_c^{std}$$

thus, combining these equations:

$$\tau = \Sigma R_c + t_R^{std} - \Sigma R_c^{std}$$

TABLE I

COMPARISON OF PREDICTED AND OBSERVED RETENTION TIMES*

Peptide number	*Peptide designation***	C_4**			C_8			C_{18}		
		t_R^{obs}	τ_c§	Δt§§	t_R^{obs}	τ_c	Δt	t_R^{obs}	τ_c	Δt
1	5G	10.6	9.4	1.2	12.5	10.3	2.2	10.0	8.4	1.6
2	10G	17.7	14.8	2.9	18.7	15.7	3.0	16.6	13.8	2.8
3	20G	21.8	20.6	1.2	22.8	21.3	1.5	21.9	20.5	1.4
4	30G	23.6	22.4	1.2	24.6	23.0	1.6	24.4	22.9	1.5
5	40G	25.5	23.4	2.1	26.5	24.1	2.4	26.6	24.5	2.1
6	50G	26.4	23.9	2.5	27.4	24.6	2.8	27.8	25.6	2.2
7	10X	17.1	18.2	1.1	17.9	19.1	1.2	16.1	16.9	0.8
8	20X	22.2	23.4	1.2	22.6	24.0	1.4	22.1	23.3	1.2
9	30X	24.6	25.7	1.1	25.0	26.4	1.4	25.1	26.3	1.2
10	40X	25.9	27.0	1.1	26.3	27.8	1.5	26.8	28.4	1.6
11	50X	26.8	27.7	0.9	27.1	28.4	1.3	28.0	29.9	1.9
12	5A	20.6	19.9	0.7	21.7	20.8	0.9	18.3	18.9	0.6
13	10A	30.4	29.1	1.3	31.0	29.8	1.2	29.7	29.2	0.5
14	20A	37.0	37.6	0.6	37.5	38.3	0.8	39.9	39.1	0.8
15	30A	40.8	42.9	2.1	41.4	43.6	2.2	44.6	45.9	1.3
16	40A	43.8	46.0	2.2	44.6	46.7	2.1	48.4	50.7	2.3
17	50A	50.4	47.5	2.9	51.5	48.3	3.2	56.0	54.0	2.0
18	5L	27.9	26.0	1.9	28.7	26.9	1.8	25.2	25.0	0.2
19	10L	38.7	35.7	3.0	39.2	36.4	2.8	38.5	36.1	2.4
20	20L	45.0	47.5	2.5	45.6	48.3	2.7	49.8	49.8	0
Average error				1.7			1.9			1.4

* The observed retention times (min) were obtained under conditions of linear AB gradient elution (1% B/min), where eluent A is 0.1% aq. TFA and eluent B is 0.1% TFA in acetonitrile (pH 2.0); flow-rate, 1 ml/min; 26°C; absorbance at 210 nm.

** Separations were carried out on a SynChropak RP-4 C_4 column (250 mm × 4.1 mm I.D.; particle size 6.5 μm; pore size 300 Å), an Aquapore RP-300 C_8 column (220 mm × 4.6 mm I.D., 7 μm, 300 Å) and a SynChropak RP-P C_{18} column (250 mm × 4.6 mm I.D.; 6.5 μm; 300 Å).

*** G, X, A and L denote the "G" series of peptide polymers [Ac-(G-K-G-L-G)$_n$-amide], the "X" series of polymers [Ac-(G-L-G-A-K-G-A-G-V-G)$_n$-amide], the "A" series of polymers [Ac-(L-G-L-K-A)$_n$-amide] and the "L" series of polymers [Ac-(L-G-L-K-L)$_n$-amide], respectively. 5G refers to the five-residue "G" series peptide; 30A refers to the 30-residue "A" series peptide, etc.

§ τ_c is the predicted retention time of a peptide, taking peptide chain length into account: $\tau_c = \Sigma R_c + t_s + (m\Sigma R_c \ln N + b)$, where ΣR_c is the sum of the retention coefficients of Guo *et al.*[8] for the amino acid residues in a peptide; N is the number of residues in a peptide; t_s is the time correction for the internal peptide standard (S4; see text for details); m and b are the slope and intercept, respectively, obtained from the semilogarithmic plots [$\tau - t_R^{obs}$ *versus* $\Sigma R_c \ln N$ (Fig. 5)] for each column.

§§ Δt is the error, in min, between the predicted (τ_c) and observed (t_R^{obs}) peptide retention times ($\tau_c - t_R^{obs}$).

The approach to determining the t_s value in the present study was a slight modification of that reported in the study by Guo *et al.*[8]. These researchers expressed the predicted peptide retention time τ as

$$\tau = \Sigma R_c + t_s + t_0$$

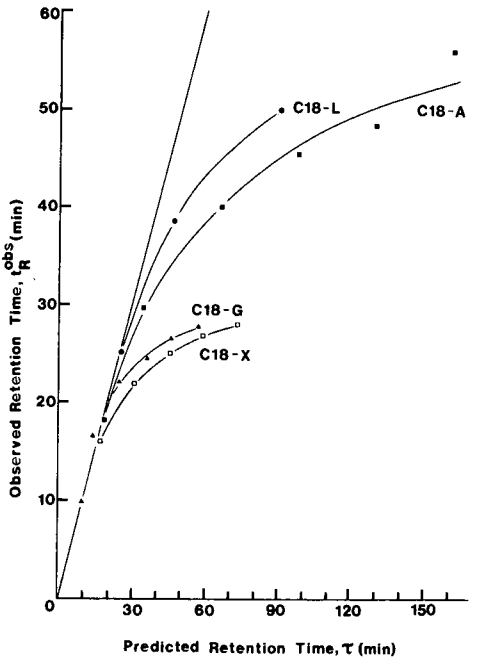

Fig. 3. Deviation of observed from predicted peptide retention times due to polypeptide chain length effect. Column: SynChropak RP-P C_{18} (250 mm × 4.6 mm I.D.). Mobile phase: linear AB gradient (1% B/min), where eluent A is 0.1% aq. TFA and eluent B is 0.1% TFA in acetonitrile (pH 2.0); flow-rate, 1 ml/min; 26°C. Absorbance: 210 nm. C18-X, C18-G, C18-A and C18-L denote results for the "X", "G", "A" and "L" series of peptide polymers, respectively, on the C_{18} column. Sequences of the peptide series are described in the text. The straight line represents a perfect correlation between predicted and observed retention times.

where t_0 was the time correction for unretained compounds only. In the present study, the elution time for unretained compounds was not determined independently, being included instead in the overall time correction, t_s, for the internal peptide standard.

If each addition of a repeating unit in the peptide polymers increased peptide hydrophobicity in a linear manner, then a plot of observed *versus* predicted peptide retention time would also show a linear relationship. Fig. 3 illustrates that this is clearly not the case. The results shown were obtained on the C_{18} column (thus, C18-L denotes "L" series peptide polymers on the C_{18} column, etc.), but are also representative of the C_4 and C_8 columns. Although there is generally a good correlation of observed and predicted retention times for the five-residue peptides (5G, etc.) and also the ten-residue peptides of the least hydrophobic "G" and "X" series (10G, 10X), this correlation falls off rapidly as the peptide chain length increases up to 50 residues. This good correlation for small peptides reflects the work of Guo *et al.*[9], who showed excellent correlation of observed and predicted retention times of 58 peptides of 2–16 residues, 43 of these peptides lying in the 5–12 residue range. It is interesting to note that peptides 10A and 10L, though fairly small, showed significant differences between observed and predicted retention times (5 and 8 min, respectively). These peptides are quite hydrophobic, particularly as compared to peptides 10G and 10X. It should also

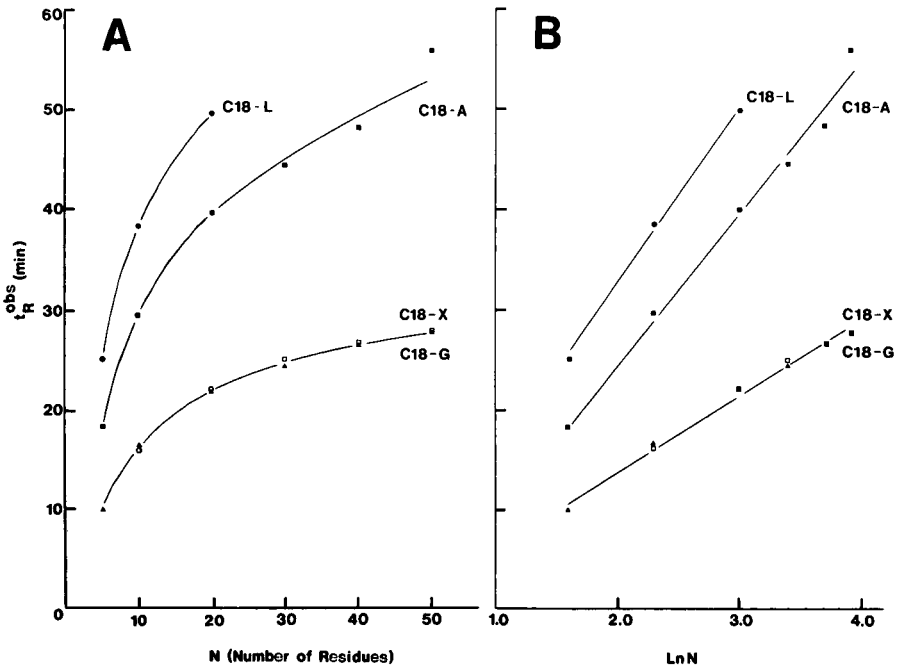

Fig. 4. Effect of polypeptide chain length on observed peptide retention times in RPC. Observed peptide retention time, t_R^{obs}, *versus* N (number of residues) (A) or ln N (B). Conditions as in Fig. 3.

be noted that the greater the hydrophobicity of a peptide at a particular chain length, the greater the deviation of observed from predicted retention time. Tchapla *et al.*[24] reported a similar increasing deviation of expected solute retention time with increasing length of solute molecule during RPC of various homologous series of non-peptide molecules. In addition, the shorter the alkyl ligand of the RPC sorbent (C_6–C_{18}), the earlier the observed deviations. The authors postulated a change in the retention process as the length of the molecules increased. However, in the present study, the deviation from linearity of the predicted *versus* observed peptide retention time plot for the C_{18} (Fig. 3), C_8 and C_4 columns all occurred at the same peptide chain length. This suggests that the above authors' explanation[24] for the retention behavior of non-peptide molecules is probably not applicable to the present study involving RPC of peptide polymers.

The relationship between observed peptide retention time on the C_{18} column and peptide chain length is illustrated in Fig. 4. These results are again representative of all three reversed-phase columns used in this study. Fig. 4A shows the non-linear relationship between observed peptide retention time and the number of residues, N, the peptides contain. Not surprisingly, given the linear relationship between τ and N, the curved profiles resulting from these plots are similar to those illustrated in Fig. 3. The exponential nature of the relationship between peptide retention time and peptide chain length is illustrated in Fig. 4B. Plotting observed peptide retention time *versus* the logarithm of the number of residues (ln N) resulted in straight-line plots with different slopes, depending on the hydrophobicity of a particular peptide polymer

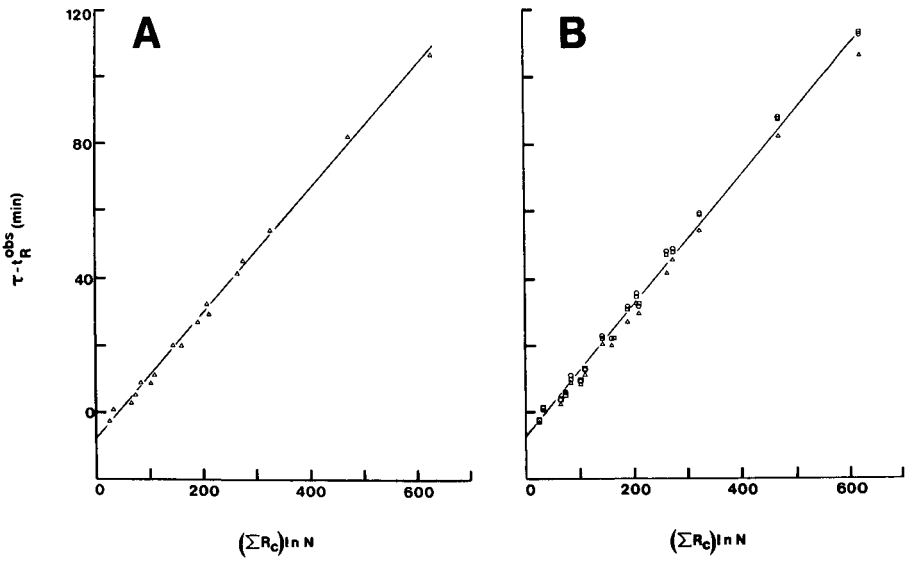

Fig. 5. Correlation of peptide retention time with peptide chain length and hydrophobicity. Predicted minus observed peptide retention time ($\tau - t_R^{obs}$) *versus* $\Sigma R_c \ln N$, where ΣR_c is the sum of the retention coefficients of Guo *et al.*[8] for the amino acid residues in a peptide, and N is the number of residues in a peptide. (A) Results for four series of peptide polymers ("X", "G", "A" and "L" series; see text for details) on a SynChropak RP-P C_{18} column (250 mm × 4.6 mm I.D.). (B) results for four series of peptide polymers on a SynChropak RP-4 C_4 column (250 mm × 4.1 mm I.D.), Aquapore RP-300 C_8 column (220 mm × 4.6 mm I.D.) and SynChropak RP-P C_{18} column (250 mm × 4.6 mm I.D.). The five-residue peptides were not included in the plots. Mobile phase conditions as described in Fig. 3. Absorbance at 210 nm.

series. The "G" and "X" series of polymers are very similar in hydrophobicity, resulting in overlapping profiles in Fig. 4. The slopes of the plots shown in Fig. 4B increased with increasing hydrophobicity of the peptide polymers, *i.e.*, "G" ≈ "X" < "A" < "L" series.

Correlation of peptide retention time with peptide chain length and hydrophobicity

From Fig. 3 it was apparent that a clearer understanding of peptide retention behaviour during RPC required clarification of the effects of both peptide chain length and peptide hydrophobicity on observed retention times. Although the observed peptide retention time data could be linearized with respect to peptide chain length (t_R^{obs} *versus* ln N) (Fig. 4B), the resulting straight-line plots diverged, with the slopes dependent on the hydrophobicity of a particular peptide polymer series.

The intimate relationship between peptide hydrophobicity and chain length and their combined effect on peptide retention behaviour is clearly illustrated in Fig. 5. Plotting predicted (τ) minus observed (t_R^{obs}) peptide retention time *versus* the product of peptide hydrophobicity (expressed as ΣR_c, the sum of the coefficients of Guo *et al.*[8]) and the logarithm of the number of residues (ln N) resulted in a single, straight-line plot. Thus, the discrepancy between predicted and observed peptide retention times is linearly related to $\Sigma R_c \ln N$. Fig. 5A demonstrates the plot for the C_{18} column. All four sets of peptide polymers fall on the line, with an overall correlation of 1.00 (determined

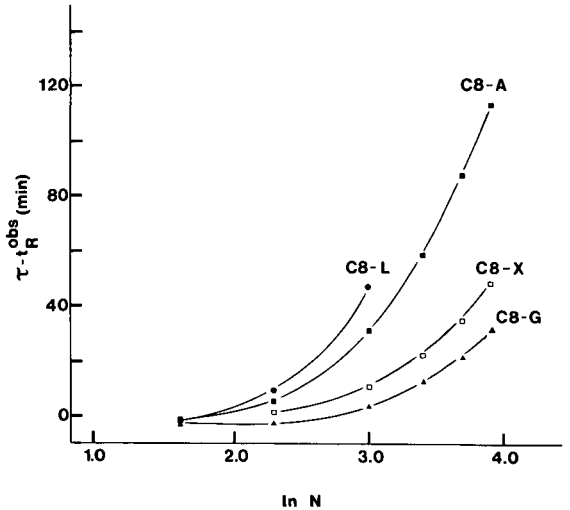

Fig. 6. Plot of predicted minus observed peptide retention time ($\tau - t_R^{obs}$) *versus* the logarithm of the number of residues (ln N). Column: Aquapore RP-300 C_8 (220 mm × 4.6 mm I.D.). Mobile phase conditions as described in Fig. 3; absorbance at 210 nm. C8-X, C8-G, C8-A and C8-L denote "X", "G", "A" and "L" series of peptide polymers, respectively, on the C_8 column. Sequences of the peptide series are described in the text.

by linear least-squares fitting). The profile shown in Fig. 5B was obtained by plotting the data for all three columns. The high correlation (r = 0.99) highlights the consistency of the ($\tau - t_R^{obs}$) *versus* ΣR_c ln N relationship on different reversed-phase columns, varying in dimensions, hydrophobic functionalities (n-alkyl chain length) and ligand density. If ln MW (logarithm of peptide molecular weight) replaces ln N in the above relationship, the correlation of the resulting plot is not as high. The five-residue peptides were not included in these plots, since there was essentially no discrepancy between their observed and predicted retention values (Fig. 3).

When the expression denoting peptide hydrophobicity (ΣR_c) is removed from the relationship producing the straight-line plots demonstrated in Fig. 5, *i.e.*, plotting ($\tau - t_R^{obs}$) *versus* ln N, the profiles for the four peptide series become non-linear and diverge (Fig. 6). Results are shown for the C_8 column only, although, once again, the plots shown are also representative of the C_4 and C_{18} columns. Fig. 6 again stresses the importance of taking the hydrophobicity of a polypeptide into account when attempting to correlate its retention time with the number of residues it contains.

Prediction of polypeptide retention time in RPC

From Fig. 5:

$$\tau - t_R^{obs} \propto \Sigma R_c \ln N$$
$$\tau - t_R^{obs} = m\Sigma R_c \ln N + b$$
$$t_R^{obs} = \tau - (m\Sigma R_c \ln N + b) \quad (1)$$

As described above

$$\tau = \Sigma R_c + t_s \quad (2)$$

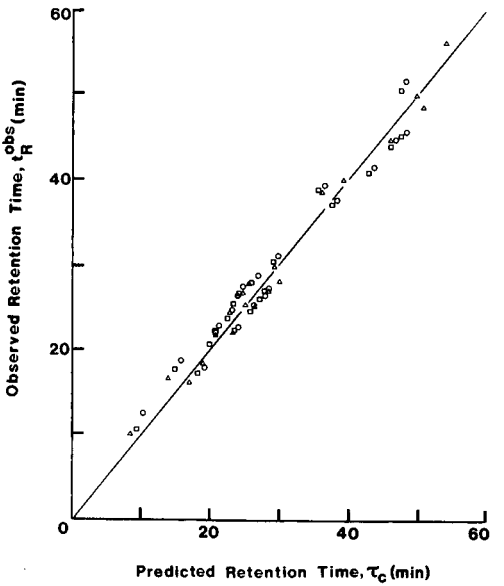

Fig. 7. Correlation of predicted and observed peptide retention times in RPC. Results shown are for four series of peptide polymers ("X", "G", "A" and "L" series; see text for details) on a SynChropak RP-4 C_4 column (250 mm × 4.1 mm I.D.), Aquapore RP-300 C_8 column (220 mm × 4.6 mm I.D.) and SynChropak RP-P C_{18} column (250 mm × 4.6 mm I.D.). The predicted retention times, taking peptide length into account (τ_c), were calculated as described in the text. Mobile phase conditions as described in Fig. 3. Absorbance at 210 nm.

where t_s is the time correction for the peptide standard, S4. Substituting eqn. 2 into eqn. 1 produces the expression:

$$t_R^{obs} = \Sigma R_c + t_s - (m\Sigma R_c \ln N + b) \quad (3)$$

When predicting the retention time of peptides, taking into account peptide chain length, t_R^{obs} in eqn. 3 becomes τ_c (predicted polypeptide retention time)

$$\tau_c = \Sigma R_c + t_s - (m\Sigma R_c \ln N + b) \quad (4)$$

where $(m\Sigma R_c \ln N + b)$ is the correction factor for peptide chain length.

Eqn. 4 was applied to retention time prediction of all four series of peptide polymers on all three reversed-phase columns used in this study, and the results are shown in Table I. The average deviations, Δt, of predicted values, τ_c, from observed peptide retention times, t_R^{obs}, were only 1.7, 1.9 and 1.4 min for the C_4, C_8 and C_{18} columns, respectively. These small deviations are indicative of the high predictive accuracy of this method for peptides up to 50 residues in length. This accuracy is again highlighted by the high correlation ($r = 0.99$) of predicted *versus* observed peptide retention times for the peptide polymers on all three columns (Fig. 7). Comparison of Fig. 7 with Fig. 3 demonstrates the impressive improvement in prediction of

polypeptide retention times when peptide chain length is taken into account. This improvement is especially gratifying, considering the stringent test conditions for this method, covering as it does an extremely wide range of peptide hydrophobicities to values far exceeding those of most peptides encountered.

This study has clearly demonstrated that, if a peptide is not subject to sequence-dependent conformation or nearest-neighbour effects, its reversed-phase chromatographic behaviour can be correlated with its amino acid composition and the number of residues in the polypeptide chain.

ACKNOWLEDGEMENTS

This work was supported by the Medical Research Council of Canada and equipment grants from the Alberta Heritage Foundation for Medical Research.

REFERENCES

1 J. L. Meek, *Proc. Natl. Acad. Sci. U.S.A.*, 77 (1980) 1632.
2 J. L. Meek and Z. L. Rossetti, *J. Chromatogr.*, 211 (1981) 15.
3 S. J. Su, B. Grego, B. Niven and M. T. W. Hearn, *J. Liq. Chromatogr.*, 4 (1981) 1745.
4 K. J. Wilson, A. Honegger, R. P. Stötzel and G. J. Hughes, *Biochem. J.*, 199 (1981) 31.
5 C. A. Browne, H. P. J. Bennett and S. Solomon, *Anal. Biochem.*, 124 (1982) 201.
6 T. Sasagawa, T. Okuyama and D. C. Teller, *J. Chromatogr.*, 240 (1982) 329.
7 T. Sasagawa, L. H. Ericsson, D. C. Teller, K. Titani and K. A. Walsh, *J. Chromatogr.*, 307 (1984) 29.
8 D. Guo, C. T. Mant, A. K. Taneja, J. M. R. Parker and R. S. Hodges, *J. Chromatogr.*, 359 (1986) 499.
9 D. Guo, C. T. Mant, A. K. Taneja and R. S. Hodges, *J. Chromatogr.*, 359 (1986) 519.
10 C. T. Mant and R. S. Hodges, in M. T. W. Hearn (Editor), *HPLC of Proteins, Peptides and Polynucleotides*, VCH, Weinheim, in press.
11 S. Terabe, R. Konaka and K. Inouye, *J. Chromatogr.*, 172 (1979) 163.
12 M. T. W. Hearn and B. Grego, *J. Chromatogr.*, 203 (1981) 349.
13 E. C. Nice, M. W. Capp, N. Cooke and M. J. O'Hare, *J. Chromatogr.*, 218 (1981) 569.
14 M. T. W. Hearn and M. I. Aguilar, *J. Chromatogr.*, 359 (1986) 31.
15 M. T. W. Hearn and M. I. Aguilar, *J. Chromatogr.*, 392 (1987) 33.
16 C. T. Mant and R. S. Hodges, in K. Gooding and F. Regnier (Editors), *High-Performance Liquid Chromatography of Biological Macromolecules: Methods and Applications*, Marcel Dekker, New York, in press.
17 M. J. O'Hare and E. C. Nice, *J. Chromatogr.*, 171 (1979) 209.
18 K. J. Wilson, A. Honegger and G. J. Hughes, *Biochem. J.*, 199 (1981) 43.
19 C. T. Wehr, L. Correia and S. R. Abbott, *J. Chromatogr. Sci.*, 20 (1982) 114.
20 S. Y. M. Lau, A. K. Taneja and R. S. Hodges, *J. Chromatogr.*, 317 (1984) 129.
21 J. M. R. Parker and R. S. Hodges, *J. Protein Chem.*, 3 (1985) 465.
22 R. S. Hodges, R. J. Heaton, J. M. R. Parker, L. Molday and R. S. Molday, *J. Biol. Chem.*, 263 (1988) 11768.
23 C. T. Mant, J. M. R. Parker and R. S. Hodges, *J. Chromatogr.*, 397 (1987) 99.
24 A. Tchapla, H. Colin and G. Guiochon, *Anal. Chem.*, 56 (1984) 621.

Journal of Chromatography, 458 (1988) 207–215
Elsevier Science Publishers B.V., Amsterdam — Printed in The Netherlands

CHROMSYMP. 1506

RAPID HIGH-PERFORMANCE AFFINITY CHROMATOGRAPHY ON MICROPELLICULAR SORBENTS

LÁSZLÓ VÁRADY*, KRISHNA KALGHATGI and CSABA HORVÁTH*
Department of Chemical Engineering, Yale University, P.O. Box 2159, New Haven, CT 06520 (U.S.A.)

SUMMARY

Short columns (30 × 4.6 mm I.D.), packed with 2-μm fluid-impervious silica microspheres with surface-bound Protein A or a lectin were used for fast separation and quantitation of immunoglobulins and glycoproteins by biospecific interaction chromatography. With stepwise elution, the total analysis time including column reequilibration did not exceed 3 min. In the assay of IgG with a stepwise change in pH best results were obtained with citrate buffer, which facilitated not only fast but also very sensitive analysis. The calibration curve was linear in the range 0.5–40 μg of human IgG. By using morpholinoethanesulfonic acid–4-(2-hydroxyethyl)-1-piperazineethanesulfonic acid–acetic acid buffer with a linear decrease in pH from 6.0 to 4.0 and an increase in magnesium chloride concentration to 200 m*M* for elution, the subclasses of human IgG were separated at 40°C above pH 4.0 in 3 min. Micropellicular concanavalin A and wheat germ agglutinin were used for rapid affinity chromatography of horseradish peroxidase and fetuin, respectively. The results suggest that micropellicular affinity sorbents afford fast and sensitive high-performance liquid chromatographic analysis by biospecific interaction chromatography. Although developed primarily for rapid analysis, the micropellicular Protein A exhibited unexpectedly high adsorption capacity (*e.g.*, 4.5 mg human IgG per ml of wet bed volume). This suggests that such columns could be employed in preparative protein chromatography as well.

INTRODUCTION

Reduction of analysis time with concomitant increase in separation efficiency and detection sensitivity has been a major objective in the development of high-performance liquid chromatographic (HPLC) methods. In the 1960s, columns packed with pellicular sorbents and the use of elevated temperature played an important role in reaching this goal first in the chromatography of small molecules[1–3]. Later, the scope of HPLC was extended to biopolymer separations, and more recently, micropellicular sorbents based on fluid-impervious microspheres of 1.5–7 μm in

* Present address: Department of Biochemistry, Purdue University, West Lafayette, IN 47907, U.S.A.

0021-9673/88/$03.50

diameter for reversed-phase[4–6] and ion-exchange [7–9] chromatography were introduced for separation of proteins and for rapid peptide mapping.

Protein A from *Staphylococcus aureus*, which binds specifically at the Fc region of immunoglobulin G (IgG), is widely used for purification and analysis of antibodies by biospecific interaction chromatography[10–12]. Affinity chromatography on immobilized Protein A is also used for separation of human IgG subclasses and monoclonal antibodies from mouse ascites and tissue culture supernatants[13–17]. Lectins, in particular concanavalin A (Con A) are used in affinity chromatography for isolation of carbohydrates or glycoconjugates[18,19]. Recently, Con A and wheat germ agglutinin (WGA), immobilized on a microparticulate macroporous support, were used in biospecific HPLC for the separation of a variety of substances having an appropriate carbohydrate moiety[20–24].

The main goal of our present work was to examine the feasibility of using micropellicular stationary phases for rapid biospecific HPLC with Protein A, Con A or WGA covalently bound to the surface of fluid-impervious 2-μm silica microspheres. Stepwise elution was used to isolate and assay IgG and glycoproteins, and gradient elution was used to resolve subclasses of human IgG.

EXPERIMENTAL

Materials

Horseradish peroxidase, fetuin from fetal calf thymus, purified human IgG, α-methyl-D-glucopyranoside, α-methyl-D-mannopyranoside, N-acetyl-glucosamine, tris(hydroxymethyl)aminomethane (Tris), 2-(N-morpholino)ethanesulfonic acid (MES), and 4-(2-hydroxyethyl)-1-piperazine ethanesulfonic acid (HEPES) were obtained from Sigma (St. Louis, MO, U.S.A.). Protein A, concanavalin A, and wheat germ agglutinin were purchased from Boehringer Mannheim (Indianapolis, IN, U.S.A.). The tissue culture supernatant containing mouse monoclonal antibody was donated by Prof. M. Constantine-Paton, Department of Biology, Yale University. Octyl sodium sulfate was purchased from Eastman Kodak (Rochester, NY, U.S.A.); the silica microspheres from Glycotech (Hamden, CT, U.S.A.); γ-glycidoxypropyl trimethoxy silane from Dow Corning (Midland, MI, U.S.A.); sodium cyanoborohydride and sodium borohydride from Aldrich (Milwaukee, WI, U.S.A.); and HPLC grade acetonitrile, reagent grade phosphoric acid, magnesium chloride, manganese chloride, calcium chloride sodium chloride and hydrochloric acid from Fisher (Pittsburgh, PA, U.S.A.). Mobile phases were prepared with NanoPure (Barnstead, Boston, MA, U.S.A.) deionized water which was filtered through 0.45-μm membranes and deaerated by sparging with helium before use.

The following instruments were used.

(a) A Model HP 1090, Hewlett-Packard (Palo Alto, CA, U.S.A.) liquid chromatograph with diode-array detector and autosampler. The column effluent passed through the heat exchanger in the diode-array detector before entering the flow-cell. The chromatograms were evaluated by a ChemStation and recorded on a ColorPro graphics plotter. No modification of this instrument was necessary.

(b) A Series 400 pump and Model LC-95 spectrophotometric detector, both from Perkin-Elmer (Norwalk, CT, U.S.A.), were assembled with a heat exchanger coil and a Model 7125 injection valve (Rheodyne, Cotati, CA, U.S.A.) with a 20-μl loop

detector, injector, and column were kept in a Model DL-8 constant-temperature bath (Haake Buchler, Saddlebrook, NJ, U.S.A.).

(c) Two Model 2150 pumps and a Model 2152 HPLC controller, (all from LKB Instruments, Gaithersburg, MD, U.S.A.), a Rheodyne Model 7125 injection valve and a Kratos (Ramsey, NJ, U.S.A.) Model SF 770 variable-wavelength detector were assembled. The column, heat exchanger coils, a 10-μl Visco Jet micromixer (Lee Co., Westport, CT, U.S.A.) and the injection valve were thermostatted as described for (b) above.

The flow-cells in detectors for (b) and (c) were pressurized and the chromatograms were processed by a Model C-R3A integrator (Shimadzu, Columbia, MD, U.S.A.). Actual pH gradient profiles were determined with the column in place by measuring the pH of 200-μl effluent fractions.

Methods

A suspension of fluid-impervious silica microspheres (d_p *ca.* 2 μm) in an aqueous solution of γ-glycidoxypropyl trimethoxysilane was acidified and heated at 95°C for 2 h[25]. The diol silica thus obtained was oxidized to aldehyde silica by periodic acid at room temperature for 2 h[26]. The proteins (2 mg of Protein A or 5 mg of lectin per g of silica) were attached to the surface by reductive amination using sodium cyanoborohydride at 4°C[26]. The proteinaceous silica microspheres were packed from a slurry in 0.1 *M* phosphate buffer (pH 7.0) into 30 × 4.6 mm I.D. No. 316 stainless-steel columns at 10 000 p.s.i.

The 25 m*M* MES–HEPES–acetic acid buffer[27] was prepared by mixing equal volumes of 75 m*M* of each MES, HEPES, and acetic acid. It was titrated to the desired pH with 1 *M* sodium hydroxide. Sample injections were made to coincide with the start of the gradient at the column inlet, as established by tracer experiments described earlier[6].

In experiments where a decreasing pH gradient was used, the starting eluent was 25 m*M* MES–HEPES–acetic acid buffer (pH 6.0). The gradient former was the same buffer, containing 200 m*M* magnesium chloride and titrated to pH 4.0. In the case of stepwise elution, the starting buffer was 100 m*M* sodium citrate (pH 7.4) followed by the same buffer titrated to pH 2.2 with 1.0 *M* hydrochloric acid. After each run, the column was regenerated with the starting buffer at a flow-rate of 1 ml/min in 2 min. The time of equilibration can be reduced by using higher flow-rates. The Protein A column showed no changes upon regular use over a period of three months.

The binding capacity of the Protein A column was determined by frontal chromatography with a solution of human IgG (2 mg/ml) in 100 m*M* citrate buffer (pH 7.4) at a flow-rate of 0.15 ml/min and at 25°C. The experiment was repeated three times and in each case the IgG bound to the column was eluted with 100 m*M* citrate buffer (pH 2.2).

The glycoproteins were bound to the Con A stationary phase from 25 m*M* Tris–HCl (pH 7.0), containing 150 m*M* sodium chloride, 1 m*M* manganese chloride, and 1 m*M* calcium chloride. The stepwise elution was carried out with 50 m*M* α-methyl-D-glucopyranoside in the starting buffer. For the WGA column the starting buffer was 25 m*M* Tris–HCl (pH 7.0), containing 0.15 *M* sodium chloride and 100 m*M* N-acetyl-α-D-glucosamine. The column was reequilibrated in 1 min with the binding buffer at a flow-rate of 1 ml/min.

RESULTS AND DISCUSSION

Chromatography on the Protein A column

Purification of IgG on a Protein A column is commonly carried out in two steps: binding under alkaline conditions in the pH range 7.0–9.0, followed by desorption at pH 2.2–3.0 by either stepwise or gradient elution. Whereas stepwise elution is employed for the isolation of IgG in analysis or large scale purification[15–17], gradient elution is mainly used to effect the separation of IgG subclasses[13]. In either case, the enrichment factor of IgG is high, but the acidic eluents used to desorb IgG may cause a loss in immunological activity and reduce the stability of Protein A columns[15–17].

Our goal was to enhance the speed of affinity chromatography of IgG on the Protein A column, to increase the analytical sensitivity, and to elute IgG at a pH as high as possible. According to the literature[13], the subclasses of human IgG are desorbed from Protein A in the pH range 3.0–4.5[13]. For the present work pH 4.0 was selected as the lower pH limit for desorption.

The composition of the buffer system was critical for reaching the goals stated above. The buffer capacities as a function of pH, calculated in terms of β[28] for the MES–HEPES–acetic acid[27] and citrate[13] buffers used in gradient and stepwise elution, are shown in Fig. 1. According to the calculations, the MES–HEPES–acetic acid buffer has a higher and more uniform buffering capacity than citrate in the pH range 4.0–7.0. However, neither buffer in the concentration range 25–50 m*M* was strong enough to elute human or rabbit IgG at pH 4.0 or above.

The interaction between IgG and Protein A is believed to involve all the tyrosine and some of the lysine residues of Protein A and the Fc fragment of IgG[12]. Thus,

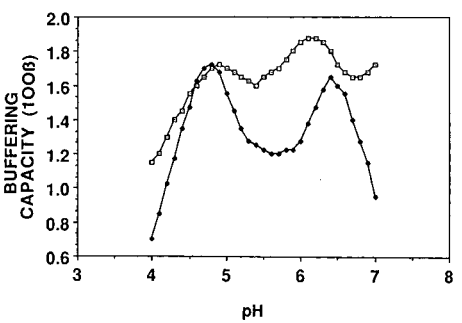

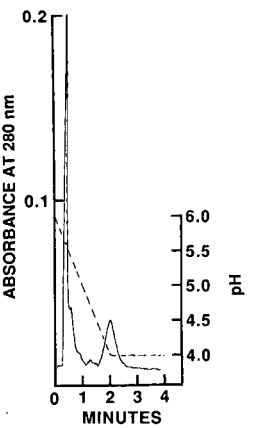

Fig. 1. Calculated buffering capacities as a function of pH: (□) 25 m*M* MES–HEPES–acetic acid and (■) 25 m*M* citrate buffer at 25°C.

Fig. 2. Biospecific interaction chromatography of rabbit IgG on a Protein A column with gradient elution. Column, 30 × 4.6 mm, 2-μm silica based micropellicular Protein A; starting eluent 25 mM MES–HEPES–acetic acid, pH 6.0, gadient former, 25 mM MES–HEPES–acetic acid, 200 mM magnesium chloride (pH 4.0); linear gradient from 0 to 100% B in 2 min; flow-rate, 1 ml/min; temperature, 25°C; sample, 20 μl of serum, diluted 1:40.

besides coulombic interactions, the binding is likely to include hydrophobic interactions as well. For this reason, an increase in buffer concentration and the addition of neutral salts, such as sodium chloride, or ammonium sulfate, to the mobile phase are not expected to facilitate desorption[29]. On the other hand, addition of magnesium chloride to the eluent is expected to reduce electrostatic interactions without promoting hydrophobic interactions between the eluite and the stationary phase. It is believed that magnesium chloride exhibits anomalous behavior and, unlike the other neutral salts, it attenuates hydrophobic interactions between proteins at neutral pH[30,31]. Indeed, a gradient with a magnesium chloride concentration increasing to 200 m*M* and a pH decreasing to 4.0 resulted in the elution of rabbit IgG from Protein A, as shown by the chromatogram in Fig. 2.

In affinity chromatography, extensive band broadening is often attributed to slow kinetics[21,22]. At elevated column temperatures, the kinetics become faster and the efficiency is concomitantly improved[32]. With increasing temperature, the viscosity of the mobile phase decreases, and the faster diffusion rates thus obtained are also expected to improve column performance. The effect of column temperature is illustrated in Fig. 3, which shows chromatograms of rabbit serum at 40 and 60°C. Comparison with the results in Fig. 2 shows that by increasing the temperature to 40°C the IgG peak becomes sharper. At 60°C, another peak appears after that of IgG. It is possible that some IgG undergoes denaturation at this temperature. According to our experiments, a gradient with a pH decreasing from 6.0 to 4.0 and a magnesium chloride concentration increasing from 0 to 200 m*M* at 40°C affords the best results. Under these conditions, the proteins are expected to be more stable than under these commonly used in IgG purification on Protein A. Affinity chromatography of IgG on the micropellicular Protein A column was also carried out with human serum at 40°C according to the same procedure. As seen in Fig. 4, the human IgG subclasses, IgG_1 and IgG_2, were separated in 2 min under the these conditions. As compared with previously published methods[13], our method is not only faster by one order of

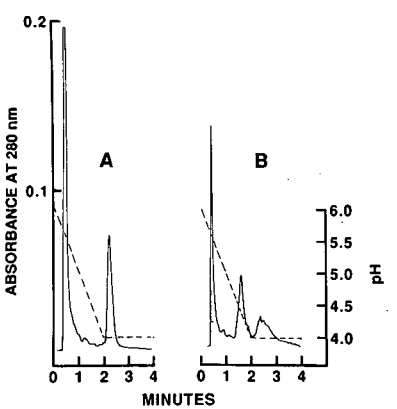

Fig. 3. Biospecific interaction chromatography of rabbit IgG on protein A column with gradient elution at 40°C (A) and 60°C (B). Other conditions as in Fig. 2.

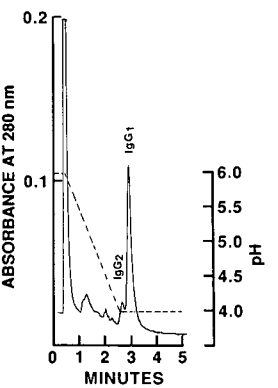

Fig. 4. Biospecific interaction chromatography of human IgG on a Protein A column with gradient elution. Conditions as in Fig. 2, except for 0.5 min isocratic elution, preceding the gradient and at 40°C.

magnitude but also employs milder conditions, *i.e.* a less acidic medium for elution and subsequent recovery of IgG.

Analytical affinity chromatography with stepwise elution is often hampered by extreme changes in refractive index of the mobile phase that occur at the commencement of the desorption step due to the high salt concentration in the debinding buffer. In our case, the baseline drift caused by magnesium chloride interfered with the detection of the IgG peak and greatly reduced the sensitivity of the analysis. This observation prompted us to investigate the requirements of buffer systems of highly sensitive analytical affinity chromatography with stepwise elution.

In stepwise elution, the debinding buffer should have a buffering capacity as high as that of the binding buffer in order to bring about the sudden pH change required to obtain a sharp peak and rapid elution. On the other hand, the binding and debinding buffers should have similar refractive indices to give higher sensitivity of analysis. Buffers such as phosphate–glycine[13], glycine–hydrochloric acid[15], phosphate–acetic acid[16,17], which are frequently employed in affinity chromatography on Protein A columns, fulfil the first requirement but engender excessive changes in refractive index in the desorption step. Therefore, with such buffers large samples size and low detector sensitivity must be used, because the overall sensitivity of the method is quite low. On the other hand, 100 m*M* citrate buffer, which has the buffering capacity of 0.0194 and 0.0186 β at pH 2.2 and 7.4, repectively, is eminently suitable to obtain high analytical sensitivity with stepwise elution of IgG. Furthermore, at low pH, IgG is more stable in citrate[15] than in the other debinding buffers.

The use of citrate buffer in the assay of IgG from human serum and from tissue culture supernatant by high speed affinity chromatography with stepwise elution is illustrated by the chromatograms in Fig. 5. It is seen that IgG appears as a single peak in 2 min after sample introduction. The serum was diluted 40 times and the sample volume was 20 μl in both cases. The response was linear in the range 0.5–40 μg of

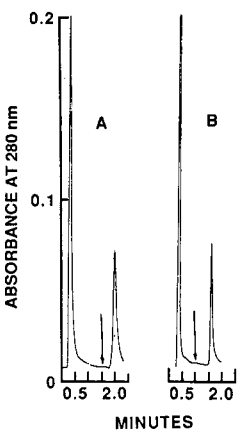

Fig. 5. Biospecific interaction chromatography of human IgG from serum (A) and mouse monoclonal antibody (B) on a Protein A column with stepwise elution. Column, 30 × 4.6 mm I.D., 2-μm silica based micropellicular Protein A; binding buffer 100 m*M* citrate (pH 7.4); debinding buffer, (introduced at the arrow) 100 m*M* citrate (pH 2.2); flow-rate, 1 ml/min; temperature, 25°C, sample 20 μl of tissue culture supernatant or serum, diluted 1:40.

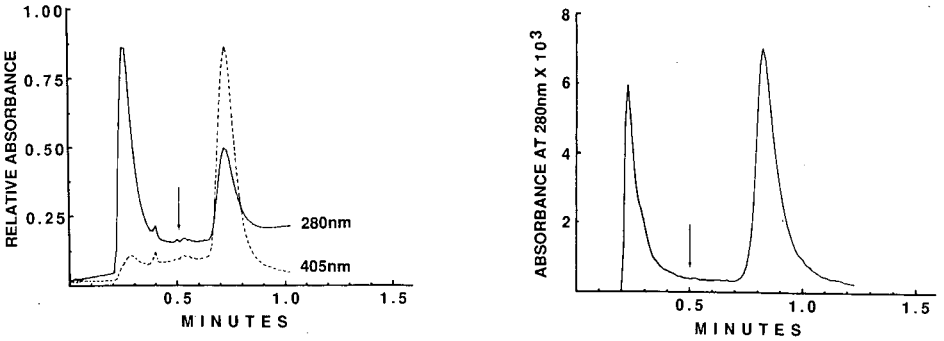

Fig. 6. Biospecific interaction chromatography of horseradish peroxidase on a Con A column by stepwise elution. Column, 30 × 4.6 mm I.D., 2-μm fluid-impervious silica-based micropellicular Con A; binding buffer, 25 m*M* Tris–HCl (pH 7.0)–150 m*M* sodium chloride–1 m*M* manganese chloride–1 m*M* calcium chloride; debinding buffer (introduced at the narrow), 50 m*M* α-methyl-D-glucopyranoside in the binding buffer; flow-rate, 1 ml/min; temperature, 25°C; detector sensitivities, 0.1 and 0.05 a.u.f.s. for 1.0 relative absorbance at 280 and 405 nm, respectively; sample, 20 μg.

Fig. 7. Biospecific interaction chromatography of fetuin from fetal calf serum on WGA column by stepwise elution. Column, 30 × 4.6 mm I.D., 2-μm silica based micropellicular WGA; binding buffer, 25 m*M* Tris–HCl, pH 7.0; debinding buffer (introduced at the arrow), 100 m*M* N-acetyl-α-D-glucosamine in the debinding buffer; flow-rate, 1 ml/min, temperature, 25°C; sample, 20 μg.

human IgG. The correlation coefficient of the calibration curve was 0.995. Therefore, this analytical technique is not only more rapid but also more sensitive than other chromatographic methods[15–17].

The binding capacity of micropellicular sorbents containing Protein A for human IgG was measured by frontal chromatography. It was found that the total human IgG binding capacity of a 30 × 4.6 mm I.D. column was 2.25 ± 0.1 mg, as measured by frontal chromatography at pH 7.4. This represents a capacity of 4.5 mg IgG/ml of bed volume or 3.2 mg IgG/g of dry column packing. The capacity of the column, measured in the presence and absence of 10 mg/ml bovine serum albumin in the IgG solution, was essentially the same, so that non-specific binding did not interfere with the capacity measurement. This IgG binding capacity is about 1/2 or 1/3 of that of commercially available affinity sorbents containing Protein A immobilized on a totally porous silica support[13]. As the binding capacity of the porous and micropellicular sorbents are commensurate for such a large molecule as IgG, the latter type of stationary phase could be useful not only in analytical but also in preparative chromatography.

Chromatography on lectin columns

The potential of silica-supported micropellicular Con A and WGA stationary phases for rapid affinity chromatography was investigated by using commercial horseradish peroxidase and fetuin as sample mixtures, respectively. Since peroxidase contains a protohemin group, which absorbs strongly at 405 nm[8], this protein could be specifically detected at that wavelength. Fig. 6 shows a typical chromatogram of commercial peroxidase on micropellicular Con A silica, while Fig. 7 depicts the chromatogram of fetuin on micropellicular WGA silica. In both cases stepwise elution

was used and the time of the separation was less than 1 min. The total analysis time, including the reequilibration of the column, was about 2 min. Thus, it was much shorter than that reported in literature[20,24]. Moreover, the sensitivity of analysis was also significantly higher.

CONCLUSIONS

The results of this study have demonstrated that micropellicular affinity sorbents are also suitable for rapid biospecific interaction chromatography under appropriate conditions with stepwise elution. IgG could be analyzed with high sensitivity by using a short column, packed with silica supported micropellicular Protein A, within 3 min, including reequilibration time. In a similar fashion, glycoproteins were rapidly analyzed by using micropellicular lectin columns. The binding capacity of a micropellicular Protein A column for IgG was similar to that reported for Protein A, immobilized on totally porous silica. Thus, such columns may be useful, not only for analysis but also for preparative chromatography of proteins and may be expected to facilitate fast separations with high recovery.

ACKNOWLEDGEMENTS

The authors are grateful to Prof. M. Constantine-Paton for the kindly gift of tissue culture supernatant containing monoclonal antibody. This work was supported by Grants Nos. GM 20993 and CA 21948 from the National Institute of Health, US Department of Health and Human Services.

REFERENCES

1 Cs. Horváth, B. A. Preiss and S. R. Lipsky, *Anal. Chem.*, 39 (1967) 1422.
2 Cs. Horváth and S. R. Lipsky, *J. Chromatogr. Sci.*, 7 (1969) 109.
3 Cs. Horváth and S. R. Lipsky, *Anal. Chem.*, 41 (1969) 1227.
4 K. K. Unger, G. Jilge, J. N. Kinkel and M. T. W. Hearn, *J. Chromatogr.*, 359 (1986) 61.
5 K. Kalghatgi and Cs. Horváth, *J. Chromatogr.*, 398 (1987) 335.
6 K. Kalghatgi and Cs. Horváth, *J. Chromatogr.*, 443 (1988) 343.
7 D. J. Burke, J. K. Duncan, L. C. Dunn, L. Cummings, C. J. Siebert and G. S. Ott, *J. Chromatogr.*, 353 (1986) 425.
8 D. J. Burke, J. K. Duncan, C. S. Siebert and G. S. Ott, *J. Chromatogr.*, 359 (1986) 533.
9 I. Mazsaroff, M. A. Rounds and F. E. Regnier, *J. Chromatogr.*, 411 (1987) 452.
10 J. W. Goding, *J. Immunol. Methods*, 20 (1978) 241.
11 R. Lindmark, K. Thoren-Tolling and J. Sjoquist, *J. Immunol. Methods*, 62 (1983) 1.
12 J. Sjoholm, A.-K. Ekenas and J. Sjoquist, *Eur. J. Biochem.*, 29 (1972) 455.
13 S. Ohlson, in I. Chaiken, M. Wilchek and I. Parikh (Editors), *Affinity Chromatography and Biological Recognition*, Academic Press, New York, 1983, p. 255.
14 C. L. Villemez, M. A. Russel and P. L. Carlo, *Mol. Immunol.*, 21 (1984) 993.
15 S. Ohlson and J. Wieslander, *J. Chromatogr.*, 397 (1987) 207.
16 H. Thompson, *Am. Lab.*, 20(5) (1988) 113.
17 R. F. Hammen, D. Pang, K. Remington, H. Thompson, R. C. Judd and J. Szuba, *Biochromatography*, 3 (1988) 54.
18 K. O. Lloyd, in H. Bittiger and H. P. Schnebli (Editors), *Concanavalin A as a Tool*, Wiley, New York, 1976, p. 323.
19 T. Kristiansen, *Methods Enzymol.*, 34 (1974) 331.
20 A. Borchert, P. O. Larsson and K. Mosbach, *J. Chromatogr.*, 244 (1982) 49.

21 A. J. Muller and P. W. Carr, *J. Chromatogr.*, 284 (1984) 33.
22 D. J. Anderson and R. R. Walters, *J. Chromatogr.*, 376 (1986) 69.
23 S. Honda, S. Suzuki, T. Nitta and K. Kakehi, *J. Chromatogr.*, 438 (1988) 73.
24 Z. El Rassi, Y. Truei and Cs. Horváth, *Macromol. Chem., Macromol. Symp.*, 17 (1988) 305.
25 F. E. Regnier and R. Noel, *J. Chromatogr. Sci.*, 14 (1976) 316.
26 P. O. Larsson, M. Glad, L. Hansson, M. D. Hansson, S. Ohlson and K. Mosbach, *Adv. Chromatogr.*, 21 (1982) 41.
27 A. Figueroa, C. Corradini, B. Feibush and B. Karger, *J. Chromatogr.*, 371 (1986) 335.
28 J. N. Butler, *Ionic Equilibrium-A Mathematical Approach*, Addison-Wesley, Reading, MA, 1964, p. 238.
29 W. Melander and Cs. Horváth, *Arch. Biochem. Biophys.*, 183 (1977) 200.
30 T. Arakawa and S. N. Timasheff, *Biochemistry*, 21 (1982) 6545.
31 T. Arakawa and S. N. Timasheff, *Biochemistry*, 23 (1984) 5912.
32 F. D. Antia and Cs. Horváth, *J. Chromatogr.*, 435 (1988) 1.

Journal of Chromatography, 458 (1988) 217–223
Elsevier Science Publishers B.V., Amsterdam — Printed in The Netherlands

CHROMSYMP. 1513

DETERMINATION OF PTERINS IN URINE BY HIGH-PERFORMANCE LIQUID CHROMATOGRAPHY ON C_{18} COLUMNS CONDITIONED WITH CETYLTRIMETHYLAMMONIUM BROMIDE

B. CAÑAS MONTALVO*, C. IMAZ VILLAR, R.C. IZQUIERDO HORNILLOS and L. POLO DIEZ
Facultad de Ciencias Químicas, Departamento de Química Analítica, Universidad Complutense de Madrid, 28040 Madrid (Spain)

SUMMARY

A method is proposed for the determination of pterins in urine without clean-up by reversed-phase high-performance liquid chromatography on a C_{18} column previously conditioned with cetyltrimethylammonium bromide. Other endogenous compounds are retained in the column, preventing interference. Xanthopterin, neopterin, isoxanthopterin, monapterin, biopterin, 6-hydroxymethylpterin, pterin and lumazine can be determined. Retention and separation mechanisms are discussed.

INTRODUCTION

The importance of pterins in tracking diseases that involve changes in the immunological response and neurological diseases is well accepted[1,2]. The technique most often used to determine oxidized pterins in synthetic samples is reversed-phase high-performance liquid chromatography (RP-HPLC) with fluorimetric[3] detection, but there is a lack of selectivity between some pterins on different C_{18} columns and also interference from endogenous compounds in urine samples[4]. In the method described here, interference from other urine components in the determination of several pterins (I–VII) and lumazine (VIII) is minimized, so that clean-up is unnecessary, by conditioning a C_{18} column with cetyltrimethylammonium bromide (CTAB). Moreover, the selectivity of the resolution of some pterin pairs is improved. Other cationic surfactants such as benzetonium chloride gave similar results, but CTAB was chosen because it does not absorb at 235 nm, the wavelength used to measure creatinine, the compound to which measurements on analytes in urine are usually referred. The structures and pK_a values of the compounds studied are summarized in Table I.

EXPERIMENTAL

Materials

Pterins were purchased from Sigma (St. Louis, MO, U.S.A.), except monapterin, which was purchased from Fluka (Buchs, Switzerland), and were of chroma-

0021-9673/88/$03.50

TABLE I

STRUCTURES AND pK_a VALUES[5] OF THE PTERINS AND LUMAZINE

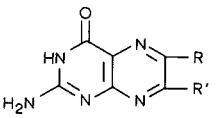

Pterins

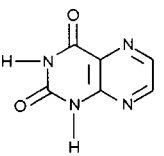

Lumazine

No.	*Compound*	*R'*	*R*	*pK_a*
I	Pterin	H	H	2.20;7.86
II	D-Neopterin	H	$CHOHCHOHCH_2OH$	2.23;7.97
III	L-Monapterin	H	$CHOHCHOHCH_2OH$	2.23;7.97
IV	Biopterin	H	$CHOHCHOHCH_3$	2.25;7.98
V	Xanthopterin	H	OH	1.6;6.3;9.23
VI	6-Hydroxymethylpterin	H	CH_2OH	–
VII	Isoxanthopterin	OH	H	−0.5;7.34;10.06
VIII	Lumazine	–	–	7.95

tographic grade. CTAB was obtained from Serva (Heidelberg, F.R.G.) and monosodium dihydrogenphosphate and disodium hydrogenphosphate from Merck (Darmstadt, F.R.G.). Water was purified with a Milli-Q system (Millipore, Bedford, MA, U.S.A.). Sep-Pak C_{18} cartridges were obtained from Waters Assoc. (Milford, MA, U.S.A.). A Waters liquid chromatograph was used, consisting of the following components: a Model 590 solvent-delivery pump, a Model 420 fluorescence detector, provided with excitation filter at 365 nm and an emission band pass at 420 nm, a Model 481 variable-wavelength detector, set at 235 nm, and a Model 730 data module. A Selecta thermostated bath from Pacisa (Madrid, Spain) was used to control the column temperature in the range 14–25°C. All separations were performed on a Hypersil ODS 100 × 4 mm I.D. column from Technocroma (Barcelona, Spain).

Methods

A 5 m*M* CTAB solution was passed through the column for 16 min at a flow-rate of 1.5 ml/min (the amount of CTAB thus retained in the column was 50 mg), then 200 ml of 1.5 m*M* phosphate buffer (pH 7.2) were passed through the column to equilibrate it and prepare it for use. After 40 urine sample injections, the column was regenerated by the passage of 60 ml of methanol and reconditioning with CTAB.

The urine samples were diluted 10-fold with deionized water and filtered through a 0.45-μm filter; 10 μl of the resulting solutions were injected into the chromatograph. The peak area ratio between the fluorescent emission of pterins and the absorbance of creatinine at 235 nm was determined.

RESULTS AND DISCUSSION

Preliminary experimental work

Preliminary experiments to determine the eight pterins (Table I) in urine samples, based on experimental conditions for C_{18} columns cited in the literature, led to

several conclusions. First, their separation is impossible without a buffered mobile phase, and even then the selectivity depends significantly on the commercial C_{18} column used. Moreover, when separation is achieved and the method is applied to urine samples, interference from other endogenous compounds requires clean-up of samples. Ion-pair chromatography with a mobile phase containing anionic counter ions such as heptanesulphonate makes it necessary to work at pH 2–3 for the best selectivity, but under these conditions a significant decrease in the fluorescence quantum efficiency is observed.

When a C_{18} column was conditioned by passing cationic surfactants, such as CTAB, through it, several important effects were observed. The elution order of pterins and their separation were clearly affected. Endogenous compounds which had previously caused interference were retained on the column. In the following sections, experiments designed to optimize the separation of pterins are presented.

Effect of the amount of CTAB in the column

In order to determine the amount of CTAB retained in the column, the tubing ahead of it was first filled with CTAB solution. After connecting the column, a volume of CTAB solution was passed through it and the eluate was collected to determine its CTAB content by indirect photometry[6]. When the CTAB concentration in this eluate was lower than 0.1 m*M*, it had to be concentrated in a Sep-Pak C_{18} cartridge and eluted with a methanol–1.2 *M* hydrochloric acid (9:1, v/v) solution. The retention mechanism of CTAB must involve not only non-polar interactions, but also exchange between CTAB and silanol groups. When the amount of CTAB retained in the column (Hypersil C_{18}, 5 μm, 100 × 4 mm I.D.) was less than 50 mg, the mobile phase did not elute significant amounts of CTAB (<0.01 m*M*), so it is unnecessary to add CTAB in the mobile phase.

The effect of the amount of CTAB retained in the column on the capacity factors (k') is shown in Fig. 1. Regarding the behaviour of pterins in a conditioned column, three groups may be distinguished. The k' values of xanthopterin (pK_a = 6.3) and isoxanthopterin (pK_a = 7.4) increase with increasing amount of CTAB in the column at pH 6.5. For the non-ionized pterins two different types of behaviour were observed. First, the k' values of the four pterins containing hydroxylated carbon at position 6 (neopterin, monapterin, biopterin and 6-hydroxymethylpterin) decrease as the amount of CTAB in the column increases. This is probably due to progressive masking of free silanol groups. On the other hand, the k' values of pterin and lumazine, which do not contain hydroxylated chains, remain almost constant with variation in the amount of CTAB in the column.

Obviously, the control of CTAB retained in the column offers several practical possibilities for determining these eight compounds, depending on the conditions chosen and on the pterins present in the sample. The control of the other variables, such as pH, phosphate concentration in the mobile phase and temperature of the column, may allow optimization of the separations.

Effect of pH

The influence of pH on the k' values was studied for two different amounts of CTAB retained in the column, as shown in Figs. 2 and 3. The behaviour is similar, although small differences can be observed. The selectivity of some pairs (neopterin–

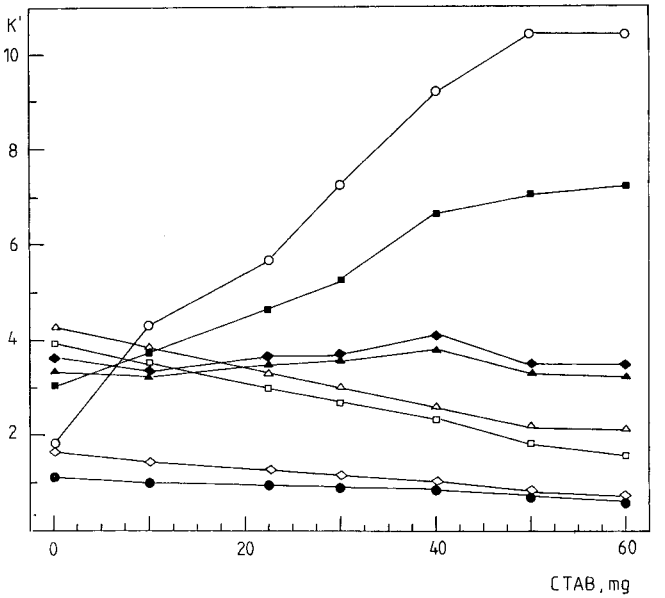

Fig. 1. Effect of the amount of CTAB in the column on the k' values of pterins. Mobile phase, 1.5 mM phosphate (pH 6.5); column, Hypersil ODS, 5 μm (100 × 4 mm I.D.). ○, Xanthopterin; ●, neopterin; ◇, monapterin; □, biopterin; ■, isoxanthopterin; △, lumazine; ◆, pterin; △, 6-hydroxymethylpterin.

monapterin and biopterin–6-hydroxymethylpterin) does not change with pH. To explain the behaviour of pterins at various pH values two main factors have to be taken into account. As the pH increases the ionization increases, causing greater ionic interaction, and hence the k' values increase. Increasing the pH, however, also in-

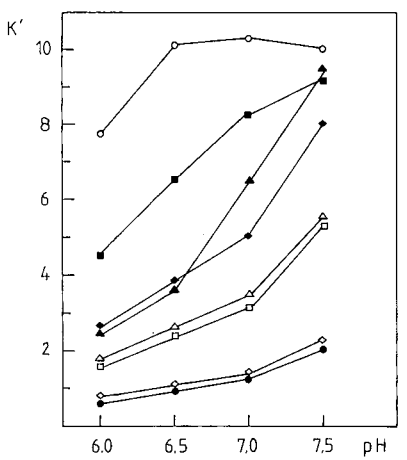

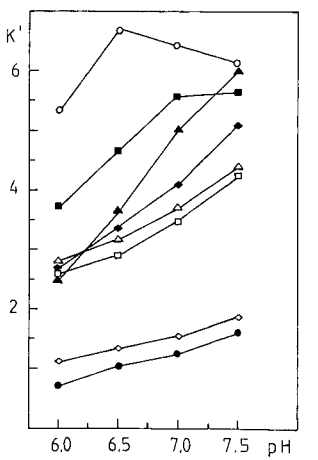

Fig. 2. Effect of pH on k' values. Amount of CTAB in the column, 50 mg; other conditions and compounds as specified in Fig. 1.

Fig. 3. Effect of pH on k' values. Amount of CTAB in the column, 20 mg; other conditions and compounds as specified in Fig. 1, except for the phosphate concentration, which was 0.5 mM.

creases the ionic strength of the mobile phase by changing the hydrogen to dihydrogenphosphate ratio, disturbing the ionic interactions, and this decreases the k' values. The combination of these two opposing effects is apparent in Figs. 2 and 3.

Effect of the phosphate concentration

As ionic interactions are important in retention mechanisms, the ionic strength of the mobile phase must affect separations significantly. As expected, decreasing the buffer concentration increases the k' values and improves the selectivity (Fig. 4). The practical limit of reducing buffer concentration arises from difficulties in adjusting the pH in a reproducible manner. A good compromise is obtained by using a 1.5 m*M* phosphate buffer.

Effect of temperature

The column was placed in a thermostated water-bath and studies were made at different temperatures. The results (Fig. 5) show that the k' values increase slightly with decrease in temperatures, this effect being most important for 6-hydroxymethylpterin and negligible for lumazine. The selectivity of the pair biopterin–6-hydroxymethylpterin, which was difficult to improve by changing other variables, such as pH and phosphate concentration, may be adjusted by controlling the temperature.

Application to pterins in urine

Taking into account the above results, the experimental conditions chosen for the determination of pterins in urine are those specified under *Methods*. The k' values obtained for two columns with different CTAB contents are summarized in Table II. As can be seen, for the column with 50 mg of CTAB, the selectivity is satisfactory except for the neopterin–monapterin pair. In order to separate these two pterins the amount of CTAB must be limited to 20 mg, although the selectivity for separations of

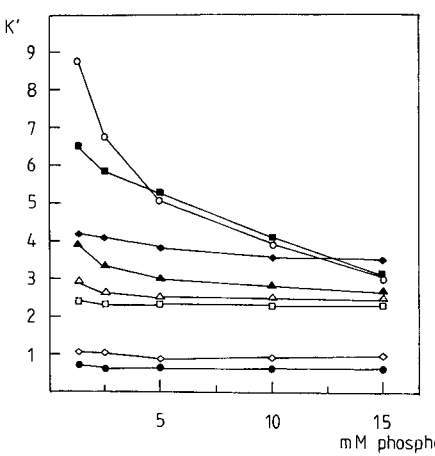

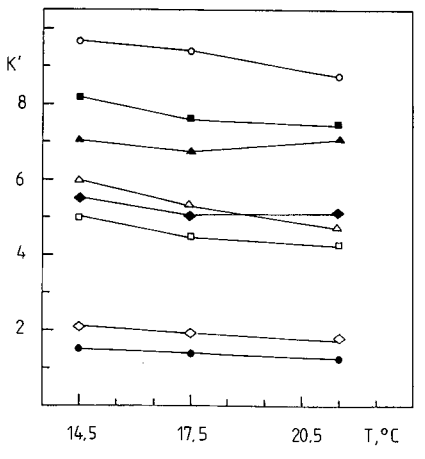

Fig. 4. Effect of phosphate concentration (pH 6.5) on k' values. Conditions and compounds as specified in Fig. 1, with 50 mg of CTAB in the column.

Fig. 5. Effect of temperature on k' values. Conditions: CTAB, 20 mg; mobile phase, 0.5 m*M* phosphate (pH 7). Pterins as in Fig. 1.

TABLE II

k' VALUES OBTAINED FOR PTERINS WITH TWO DIFFERENT AMOUNTS OF CTAB IN THE COLUMN AND TWO DIFFERENT MOBILE PHASE CONDITIONS

Conditions: (A) 22 mg of CTAB (0.5 m*M* phosphate, pH 7); (B) 50 mg of CTAB (1.5 m*M* phosphate, pH 7.2).

Compound	*k' value*	
	A	*B*
Neopterin	1.50	1.12
Monapterin	2.11	1.19
Biopterin	4.98	3.14
6-Hydroxymethylpterin	5.97	3.90
Pterin	5.59	5.70
Lumazine	7.12	6.57
Isoxanthopterin	7.12	7.90
Xanthopterin	9.64	9.90

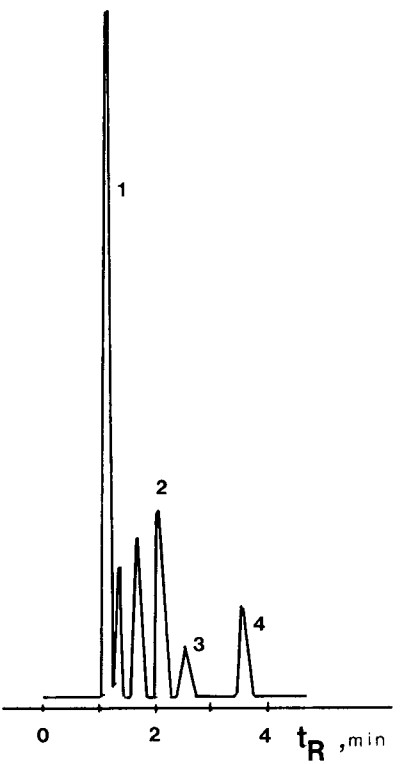

Fig. 6. Separation of some pterins in urine. Peaks: 1 = neopterin; 2 = biopterin; 3 = pterin; 4 = isoxanthopterin. For conditions, see *Methods*.

other pairs may then diminish. Presumably, these problems can be minimized by using a longer column with the same packing.

The calibration graphs were linear in the range 0.1–40 ppm. Depending on the pterin, the correlation between concentration and peak area was 2–8% and the detection limit was 0.01–0.2 ng.

Fig. 6 shows a chromatogram obtained by direct injection of a urine sample, diluted and filtered as indicated under *Methods*.

REFERENCES

1 C. Huber, J. R. Batchelor, D. Fuchs, A. Hausem, A. Lang, D. Niederwieser, G. Ribemegger, P. Swetly, J. Trompair and H. Watcher, *J. Exp. Med.*, 160 (1984) 310.
2 A. Hansen and H. Watcher, *J. Clin. Biochem.*, 20 (1982) 593.
3 B. Andondonskaja-Ranz and H. Zeitler, *Anal. Biochem.*, 133 (1983) 68.
4 T. Fukushima, *Anal. Biochem.*, 102 (1980) 176.
5 W. Pfeleiderer, in S. J. Barkevic and R. L. Blakley (Editors), *Chemistry and Biochemistry of Pterines*, Vol. 2, Wiley, New York, 1985, p. 43.
6 P. Helboe, *J. Chromatogr.*, 261 (1982) 117.

Journal of Chromatography, 458 (1988) 225–240
Elsevier Science Publishers B.V., Amsterdam — Printed in The Netherlands

CHROMSYMP. 1519

STABILIZATION OF REVERSED PHASES FOR LIQUID CHROMATOGRAPHY

APPLICATION OF INFRARED SPECTROSCOPY FOR THE STUDY OF BONDED-PHASE STABILITY

N. SAGLIANO, Jr. and R. A. HARTWICK*
Department of Chemistry, Rutgers University, Busch Campus, Piscataway, NJ 08854 (U.S.A.)
and
R. E. PATTERSON, B. A. WOODS, J. L. BASS and N. T. MILLER
The PQ Corporation, Research and Development Center, Lafayette Hill, PA 19444 (U.S.A.)

SUMMARY

This paper examines the spectroscopic characterization of chromatographic silica gels at three stages: before bonding of an *n*-butyl group to the silica surface, after bonding, and after exposure to hydrolytic conditions expected to lead to some loss of the alkyl groups from the surface. Hydrolysis was achieved by circulating an aqueous acetonitrile solution containing 0.5% (v/v) trifluoroacetic acid at 27°C through a loosely packed bed of the *n*-butyl-bonded silica. This hydrolytic treatment results in a rapid partial loss of bonded phase over about 1 day, followed by a much more gradual loss over the next six days. The extent of hydrolysis depends upon the silica used and the initial degree of coverage of the bonded phase. The results show that a portion of the bonded sites of the bonded phase are hydrolyzed more rapidly under acidic conditions, and that higher initial bonded-phase coverages lead to shielding of the more reactive sites and thus less overall hydrolytic loss. Diffuse-reflectance infrared Fourier transform (DRIFT) spectroscopy was used to study three different silicas before and after hydrolysis of the bonded phase. On one of these silicas, rapid hydrolysis of the *n*-butyl bonded phase was associated with reemergence of isolated silanol groups on the silica surface. On the other two silicas, the same hydrolytic conditions led to much slower loss of coverage, and spectroscopy did not detect a reemergence of lone silanol groups. Although all three unbonded silicas apparently had similar physical and chemical properties, one of them was clearly different from the others in stability of a subsequently attached alkyl phase. This difference could only be detected by bonding, followed by hydrolysis. One possible explanation of these results is that different manufacturing conditions lead to a different distribution of silanol groups on the silica surface, which is not detectable by routine physical and chemical characterization methods, yet nevertheless affects bonded-phase stability.

0021-9673/88/$03.50

INTRODUCTION

Interest in the design, synthesis and use of chemically bonded silica gels in high-performance reversed-phase liquid chromatography remains high. A sizable body of data has been developed on the synthesis of organosilane coatings on the surface of silica gel[1–3]. Recent studies have focused on the role of the silica gel used to prepare the bonded phase as well as the type of organosilane and reaction conditions employed[1,4–7]. A limited number of studies is available on the characterization of hydrolyzed bonded phases[8]. Advances in these areas will lead to better characterized stationary phases with extended lifetime in chromatographic use.

Improved stability of alkyl-bonded silicas in reversed-phase chromatography may be achieved in a variety of ways, including: use of a fully hydroxylated silica[9], use of high-coverage synthetic conditions[6], use of bulky alkylsilanes (*e.g.*, those containing ethyl[10] or isopropyl[7] side groups), multi-reactive silanes (*e.g.*, dichloro- or triethoxysilanes[11]) or siloxane polymer coatings[12,13]. Although all of these approaches can lead to improved stability in individual experiments, they should also be evaluated for their ability to be incorporated into a reproducible manufacturing process.

The silica gel used for bonding plays an important role in the preparation of improved alkyl-bonded phases. Several studies have characterized chromatographic behavior associated with "good" or "bad" silica gel precursors and attempted to relate silica surface chemistry to observations in chromatographic peak shape of basic compounds and column stability[6,14,15].

The early literature[16,17] suggests that differences exist in adsorptive behavior and chemical reactivity of the various silica surface species, including siloxanes ($\equiv$Si–O–Si$\equiv$), isolated or one silanols ($\equiv$SiOH), vicinal silanols (=Si(OH)–O–(OH)Si=) and geminal silanols ($=Si(OH)_2$)[18]. Geminal groups have usually been classified as more like isolated silanols in their IR and chemical behavior[16,19]. "Associated silanols" is a general term for those silanol groups capable of interacting with neighbors through hydrogen bonding[5,6]. The distinction between isolated and associated silanols is one of proximity: neighboring silanols separated by 2.6 to 3.1 Å are close enough to interact, while silanols separated by more than 3.1 Å are isolated on the surface[20]. Spectroscopic methods, such as IR, NMR and fluorescence provide complementary qualitative data on these surface species; identification of specific spectroscopic peaks can be provided by a variety of thermal[20–23], adsorptive[17,24,25], and isotopic exchange[26,27] techniques. Unfortunately, quantitative analysis of surface species is still difficult, although progress has been reported by several groups[28,29].

More recent studies, which often employ spectroscopic techniques, show that a fraction of the total silica surface silanols is more reactive in the typical silanization reaction used for alkyl-bonded phase preparation. Interestingly, published reports disagree on the relative reactivity of isolated, geminal, and vicinal silanols toward a typical monochloro-organosilane [4–6,20,23,27]. Many studies have shown the presence of a more reactive subset of silanols; reports are divided on the identity of this subset. Finally, it must be noted that in these studies silica gels containing variable impurity levels, produced by variable manufacturing processes, were used.

The goal of this research is the generation of a reproducible silica surface chemistry for the preparation of high-coverage, acid-stable alkyl-bonded phases. As a critical use of reversed phases today is in the area of biopolymer separations, which

commonly require the use of acidic conditions, we felt that reversed-phase stability under acid conditions is an appropriate starting point for the general study of stationary phase stability. In particular, we examined the role of the silica gel used in the reaction and the role of initial coverage of the bonded phase on its stability under acidic conditions. We assessed stability directly by measuring the loss of bonded phase upon hydrolysis, using a hydrofluoric acid dissolution/gas chromatography sampling technique. Fourier transform (FT) IR spectroscopy of the unbonded silica and the bonded silica before and after hydrolysis suggests pathways by which the reaction proceeds. Taken together, the results provide greater insight into the variable surface reactivity that underlies stationary-phase instability.

EXPERIMENTAL

Chemicals and materials

n-Butyldimethylchlorosilane was obtained from Petrarch Systems (Bristol, PA, U.S.A.) and was used without further purification. Trifluoroacetic acid (TFA), orthophosphoric acid and acetonitrile were "Baker Analyzed"-reagent grades (J. T. Baker, Phillipsburg, NJ, U.S.A.). HPLC-grade water was prepared in-house. Three experimental silica gel batches were supplied by PQ Corp. (Valley Forge, PA, U.S.A.) and used as received. Their physical and chemical characteristics are listed in Table I.

TABLE I

CHARACTERISTICS OF SILICA GELS STUDIED

	Batch 1	*Batch 2*	*Batch 3*
Date of manufacture	March, 1984	February, 1986	May, 1986
Pore volume (ml/g)*	1.3	1.21	1.39
Surface area (m^2/g)*	261	238	254
Median pore diameter (Å)*	186	197	188
Particle size properties			
Dv, 50 (μm)**	19.2	17.0	16.4
Dv, 50/Dp, 50**	1.09	1.16	1.18
Dv, 10/Dv, 90**	1.55	1.76	1.72
Metals, anions (ppm)***			
Al	45	50	88
Ca	38	7	<25
Fe	53	33	50
Na	10	31	41
SO_4^{2-}	25	<25	31
Cl^-	27	<25	17
pH§	4.0	5.2	4.7
Loss on drying§§	<5	4.2	4.4

* Porisimetry determined by nitrogen sorption (BET method).

** Particle-size analysis by Coulter counter.

*** Cation analysis was by hydrofluoric acid digestion of silica followed by flame atomic absorption spectroscopy for Na and inductively coupled plasma spectroscopy for Al, Ca, Fe and Mg determination. Anion analysis was by ion chromatography of water extracts.

§ pH measured of a 10% slurry of silica in water.

§§ Determined from the weight change of the silica after heating at 105°C for 2 h.

The silica gels were bonded by the procedure of Kinkel and Unger[1]. Before bonding, the silica gel was dried for about 12 h under vacuum at 120°C.

Hydrolysis procedure

In our hydrolysis procedure, which was discussed in a previous paper[10], the bonded phase was exposed to a recirculating hydrolysis solvent, composed of 32% aq. acetonitrile, the aqueous component being 10 m*M* orthophosphoric acid, and, in the final solution, the TFA concentration being 0.5% (v/v). The aqueous component was adjusted to a pH of 1.6, using potassium hydroxide prior to addition of the acetonitrile. The hydrolytic mobile phase was prepared freshly at frequent intervals to prevent any equilibration with the bonded phase during the hydrolysis experiment. Aliquots of the bonded silica gel (*ca.* 500 mg) were sampled at various intervals and washed with 50 ml each of water, methanol and acetone. Bonded-phase coverage was determined by a previously developed HF digestion/gas chromatographic method[30].

DRIFT Studies

Spectra were obtained on a Model 20SXB spectrometer (Nicolet, Madison, WI, U.S.A.) operating at 2 cm^{-1} spectral resolution with full aperture opening. A Happ-Genzel apodization function was used and 100 scans were collected on the typical sample. Approximately 30 mg of the stationary phase was added with minimal packing as a 10% (w/w) mixture in dry potassium chloride to a sample cell, connected to a vacuum pump. Typically, several hours of pumping at room temperature were needed to remove physically adsorbed water to enhance observation of the isolated and vicinal bands. Peak position was assigned by comparison of the characteristic spectra obtained with literature data[31].

RESULTS AND DISCUSSION

The goal of this paper is to relate the spectroscopic properties of silica-based bonded phases to chromatographic stability of the stationary phase. The hydrolysis technique developed previously[10] serves as a testing procedure for the assessment of stability and as a method for preparing various hydrolyzed surfaces. The acid achieves hydrolysis of the bonded ligands in a reasonable time and mimics typical mobile phases used in the reversed-phase HPLC of proteins. Determination of alkyl group coverage is achieved via hydrofluoric acid digestion/headspace gas chromatography[30]. The technique directly measures surface group coverages with the advantage of ligand chain speciation by use of the gas chromatography separation. Thus, a quantitative measure of bonded-phase stability may be generated by appropriate use of the hydrolysis and hydrofluoric acid/gas chromatographic procedures. We next turn to a discussion of the roles of the silica gel precursor used as well as alkyl group coverage level on the stability of the resultant bonded phase.

Effect of base silica gel

Three prototype silicas (batches 1, 2 and 3) were allowed to react with *n*-butyldimethylchlorosilane to the maximum coverage achievable by our procedure, and the bonded phases were subjected to the hydrolysis evaluation described previously. Fig. 1 presents the loss in bonded phase coverage as a function of hydrolysis time.

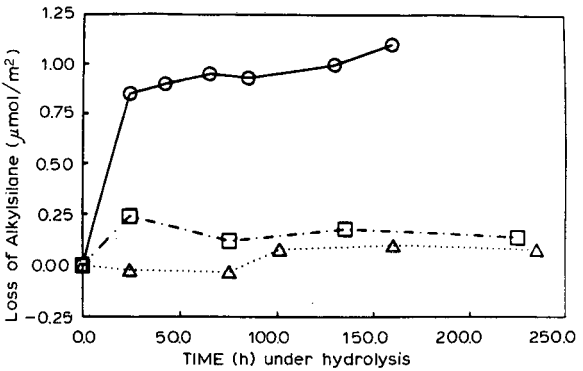

Fig. 1. Hydrolysis response of batch 1, 2 and 3 silicas, bonded with *n*-butyldimethylchlorosilane. Initial coverages are as noted in the figure. ○ = Silica batch 1 (initial concentration, 3.67 μmol/m²); △ = batch 2 (2.83 μmol/m²); □ = batch 3 (4.04 μmol/m²). For conditions, see text.

Note that initial coverage levels varied between silicas, which may reflect type and amount of surface silanols available for reaction. C_4-bonded batch 1 exhibited a rapid loss of coverage from 3.67 to about 2.8 μmol/m² (about 25% over 25 h), followed by a much more gradual loss of coverage. Interestingly, C_4-bonded batches 2 and 3 exhibit losses of only about 0.1 μmol/m² in the course of the experiment. While different manufacturing conditions were used in the production of these silica gels, Table I shows no great differences in the characteristics typically measured on these 200-Å pore diameter, 20-μm particles. Analysis of metals and anions in the gels revealed low levels of these impurities with some variability in the Al, Ca, Fe and Na content. Results obtained by other investigators[6] prompted us to examine silica surface phenomena as a possible source of variability. We next turned to the examination of the influence of coverage levels on the stability of the C_4-bonded batch 1 silica.

Effect of alkyl group surface concentration

The influence of bonded-phase coverage on stability of the material was studied by synthesizing a series of bonded phases on several quantities of batch 1 silica to levels of 1.95, 3.00, 3.17, and 3.67 μmol/m² of *n*-butyldimethylsilyl groups. Fig. 2 presents the loss in bonded-phase coverage of these packings as a function of hydrolysis time. For initial coverages on the same silica of 1.95, 3.00, and 3.17 μmol/m², a similar rapid loss in coverage of ca. 1.6 μmol/m² over 30 h is observed, followed by a much more gradual loss. For the bonded phase initially bonded to highest coverage (3.67 μmol/m²), a rapid loss of coverage of only 0.8 μmol/m² occurs over the same 30 h period, followed again by a much more gradual loss. Fig. 3 provides selected data of Fig. 2 including a plot of initial coverage, the coverage loss at 137 h of hydrolysis, and the remaining surface coverage as a function of initial bonding coverage. First, each of the three partially bonded phases showed about the same 1.6 μmol/m² "average" loss of coverage over the course of the hydrolysis experiment, suggesting the presence of a subset population of more easily hydrolyzed alkylsilylsiloxanes on the surface. Note that the magnitude of this population remains constant, even though the initially bonded coverage increases from 1.95 to 3.17 μmol/m². The residual coverage levels

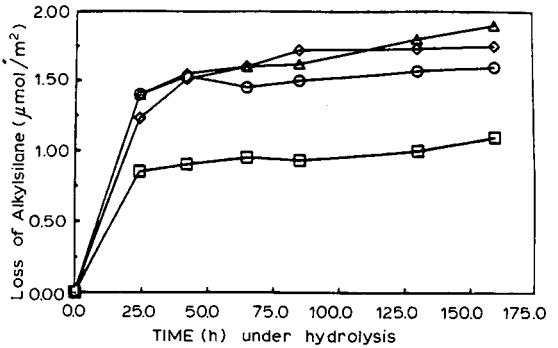

Fig. 2. Hydrolysis response of batch 1 silica, bonded with *n*-butyldimethylchlorosilane to different coverages. Bonded phases of 1.95, 3.00, 3.17 and 3.67 μmol/m^2 initial coverage were evaluated. Initial ligand concentrations: ○ = 1.95 μmol/m^2; △ = 3.00 μmol/m^2; ◇ = 3.17 μmol/m^2; □ = 3.67 μmol/m^2. For conditions, see text.

after hydrolysis of *ca.* 0.35, 1.4 and 1.6 μmol/m^2, corresponding to the partial initial coverages of 1.95, 3.00 and 3.17 μmol/m^2, respectively, represent a less reactive population of sites, which is not hydrolyzed as easily as the first set of sites. The observation that hydrolysis behavior does not proceed more readily after about 30 h suggests that a shielding effect of initially higher but not maximum coverage is not significant. However, evidence of such a shielding effect is noted for the maximum coverage of 3.67 μmol/m^2, where coverage loss has been decreased to about 1 μmol/m^2 over 137 h. For this phase, a relatively greater proportion of the less reactive sites has been bonded so that steric hindrance reduces the easily hydrolyzed population from about 1.6 to about 1 μmol/m^2.

The results indicate that the most densely covered phases will exhibit better stability, but that coverage increases to less than the maximum level will not necessarily result in better stability. Furthermore, even at maximum coverage, some silicas give better stability than others that appear to be similar in typically measured properties. Thus, while improved bonding methods can serve to increase stability[10], it is

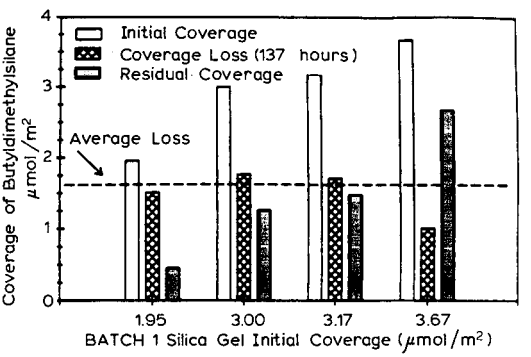

Fig. 3. Comparison of initial coverage level, coverage loss after 137 h of hydrolysis, and residual coverage for batch 1 silicas, bonded with *n*-butyldimethylchlorosilane to variable coverage levels. See text for further discussion.

obviously an advantage to use a silica (*e.g.*, batches 2 or 3) that provides alkylated surfaces of greater stability.

We decided to explore the capability of modern spectroscopic methods for the further identification of differences observed in the stability of bonded phases based on batches 1, 2 and 3. Note that for the remainder of this paper, batches 2 and 3 are grouped as silicas that are "good" or "stable", while batch 1 silica is "bad" or "unstable". The subsequent spectroscopic results therefore use batches 2 and 3 interchangeably as examples of desirable silica gel precursors.

Fourier transform infrared spectroscopic studies

An evaluation of the bare silicas, butyl-bonded phases, and hydrolyzed stationary phases was untertaken by the FT-IR method. Previous literature studies have shown how this method can be used to identify different types of silanol groups on the silica surface. The paper of McDonald[31] provides a useful summary of peak assignments in the IR region. Recent work has shown the value of the FT-IR technique in characterizing the *n*-alkyl-bonded phase, especially as it relates to various pre-treatment procedures of the silica gel precursor[28,32]. FT-IR provides a rapid qualitative analysis of silica surfaces, particularly in the identification of isolated silanol groups compared to other associated or hydrogen-bonded silanol sites. Fig. 4 provides DRIFT spectra of the three unbonded silica surfaces used in this study.

Three bands of interest are evident in each of the three spectra. The sharp band centered at 3735 cm^{-1} is assigned to the isolated silanol sites, while the more diffuse band centered at 3655 cm^{-1} has been tentatively identified as weakly hydrogen-bonded silanols or vicinal silanols[31]. The broad peak at around 3500 cm^{-1} is assigned to physically adsorbed water.

The assigment of IR band intensity to geminal silanols has generated some contradictions in the literature[4,18]. It appears that the predominant view is that the position of the geminal silanol band in the IR is closer to that of the isolated silanol

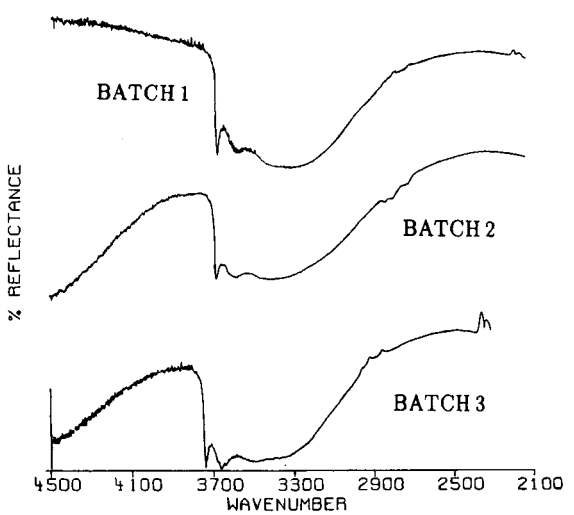

Fig. 4. DRIFT spectra of batch 1, 2 and 3 silicas. See text for discussion.

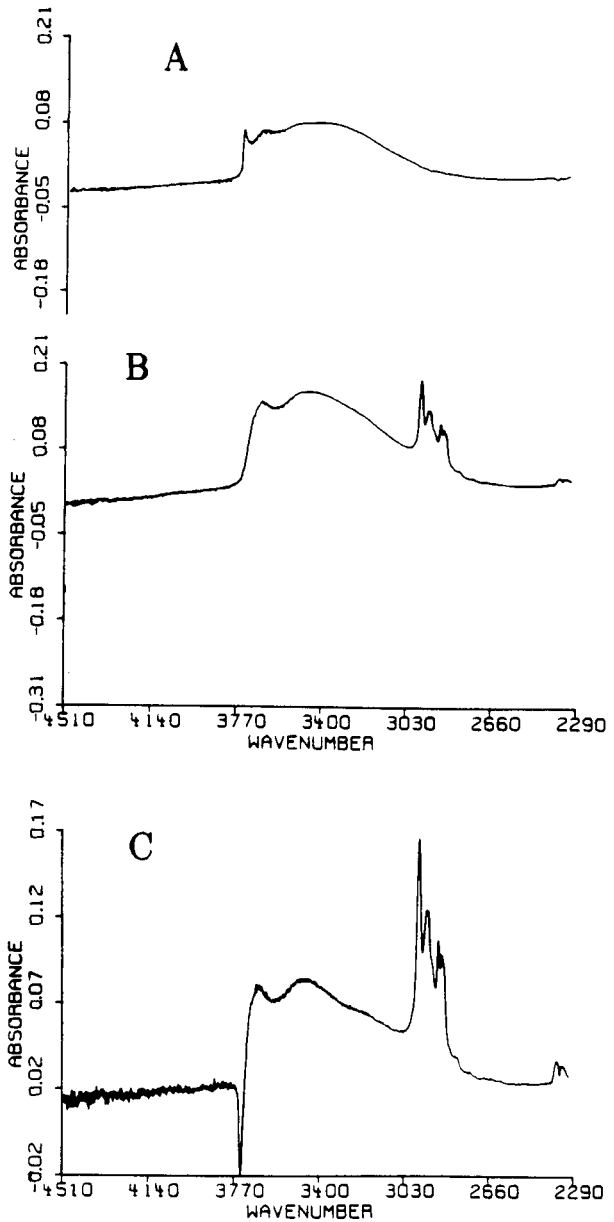

Fig. 5. FT-IR spectra of unbonded and bonded batch 1 silica. (A) Silica batch 1; (B) batch 1 silica, bonded to a coverage of 3.67 μmol/m^2 butyldimethylsilyl groups; (C) difference spectrum, B−A.

rather than the associated silanols[6,16,19]. The IR spectra presented here do not allow any conclusions to be made with respect to the presence of geminal silanols on these silicas.

While we did not attempt to quantitate the observed bands in the IR spectra, a

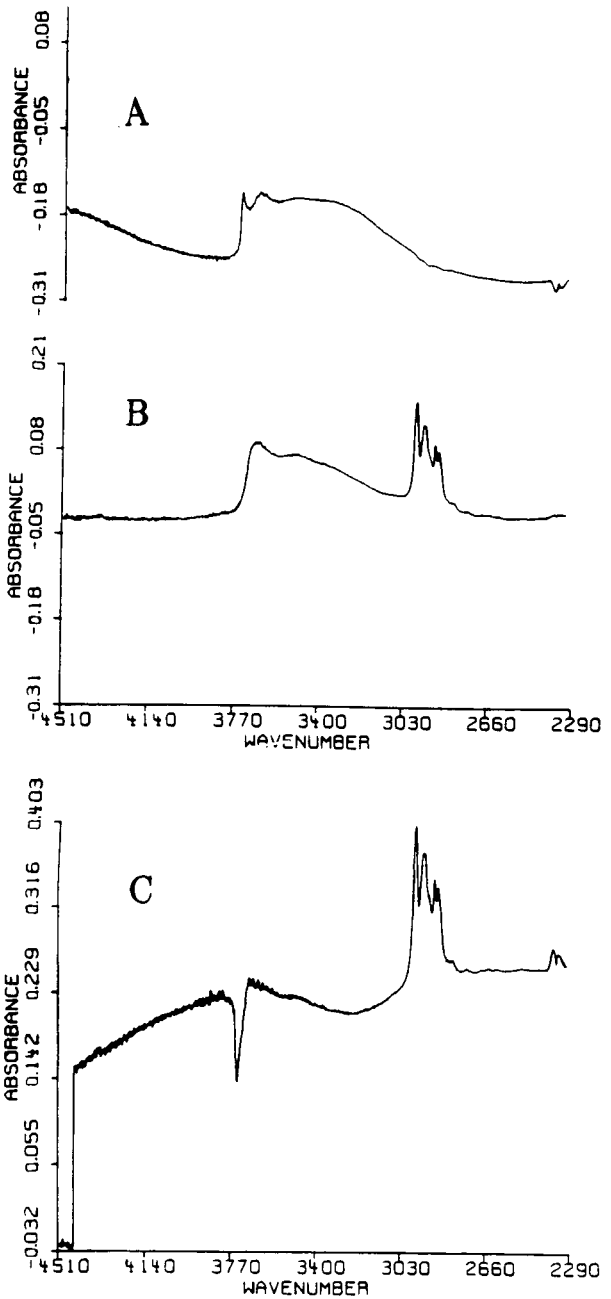

Fig. 6. FT-IR spectra of unbonded and bonded batch 3 silica. (A) Silica batch 3; (B) batch 3 silica, bonded to a coverage of 4.0 μmol/m^2 with butyldimethylsilyl groups; (C) difference spectrum, B – A.

qualitative comparison indicates that there are minimal changes from spectrum to spectrum for these three silicas. Interestingly, silica batches 2 and 3 appear to have a more pronounced band at 3655 cm^{-1} than batch 1. This observation may indicate a greater proportion of vicinal silanols.

Figs. 5 and 6 present IR spectra of unbonded and *n*-butyl-bonded phases, based on batch 1 and batch 3 silicas, respectively. As may be readily observed in both spectra, isolated silanol band intensity is decreased upon bonding the silica with *n*-butyldimethylchlorosilane, with the resultant appearance of CH group stretches at about 2900 cm^{-1}. Interestingly, the associated silanol band intensity does not seem to change significantly. Spectral subtraction of the unbonded silica spectrum from the bonded phase spectrum confirms that the major observable change between the spectra is the loss of isolated silanol intensity and gain in hydrocarbon intensity as indicated by FT-IR. Several other researchers have made this observation in the bonding of monochloroalkylsilanes to silica gel[5,6,20,23].

We next examined the FT-IR of *n*-butyl-bonded phases as a function of hydrolysis time. Figs. 7 and 8 provide spectra of hydrolyzed bonded phases, corresponding to points for batches 1 and 2, respectively, in Fig. 1. Fig. 7 shows that the hydrolysis of *n*-butyl-bonded batch 1 silica leads to a reemergence of isolated silanol intensity at the expense of the hydrocarbon peak area. As short a hydrolysis time as 18 h produces isolated silanols with a corresponding 17% decrease in alkyl group coverage. The isolated silanol peak appears to grow as the hydrolysis of the bonded phase is extended to 137 h.

Interestingly, Fig. 8 shows that a much longer hydrolysis time of 35 days on the *n*-butyl-bonded batch 2 silica for a similar loss of coverage of *ca.* 24% does not lead to a large increase in isolated silanol intensity (although the inflection of the lower spectrum of Fig. 8 suggests that some isolated silanols are present). Figs. 9 and 10 clarify these observations by providing the difference spectrum of the hydrolyzed stationary phases, subtracted from the freshly prepared bonded phase for batches 1 and 2, respectively. After 35 days, batch 2 shows about 37% of the isolated silanol intensity observed for batch 1 after only 137 h (about 6 times less) of hydrolysis. Chromatography of basic amine solutes on both packings indicates that the bonded phase has deteriorated to the extent that broad and tailed peak shapes were observed (data not shown). Thus, while the bonded phases on both batches 1 and 2 have deteriorated, only batch 1 shows a rapid instability associated with the reappearance of isolated silanols. Slow hydrolysis (<6 times longer than for batch 1) of the batch 2 material under the same hydrolytic solution conditions does not lead to a significant reappearance of isolated silanols and suggests that hydrolysis occurs by a different mechanism or occurs on different sites than in batch 1.

One may speculate that the isolated (and/or geminal) silanol population may represent a more reactive set of sites on the surface and are among the first to bond in the typical silanization reaction. This hypothesis is supported by the FT-IR data (Figs. 5 and 6). It is possible that these sites are more reactive even as the bonded siloxane species and so are among the first groups to be hydrolyzed. Hence, isolated and/or geminal silanol intensity reemerges in the IR (Fig. 7) upon hydrolysis of the bonded phase. The lengthy time scale of hydrolysis for bonded phases on batch 2 suggests that a different set of siloxane sites undergoes reaction, and therefore implies the absence of isolated siloxane sites on this silica. Fig. 3 suggests that the population

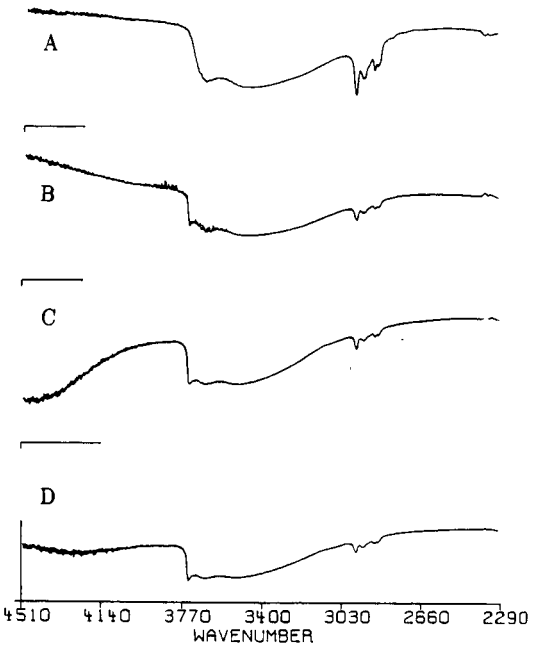

Fig. 7. DRIFT spectra of bonded and hydrolyzed batch 1 stationary phases. (A) *n*-Butyldimethylsilyl-bonded batch 1 silica, 3.67 μmol/m^2; (B) same phase as in A after 18 h of hydrolysis, 3.03 μmol/m^2; (C) same stationary phase as in A after 42 h of hydrolysis, 2.77 μmol/m^2; (D) same stationary phase as in A after 137 h of hydrolysis, 2.64 μmol/m^2. Hydrolysis conditions are described in the Experimental section.

of easily hydrolyzed bonded sites on batch 1 is *ca.* 1.6 μmol/m^2, reflecting a population of *ca.* 1.6 μmol/m^2 of isolated and/or geminal silanols on the surface.

Fig. 11 presents a set of IR spectra, corresponding to a series of *n*-butyl-bonded batch 1 silicas synthesized to coverage levels of 0, 0.83, 2.0 and 3.67 μmol/m^2. The major loss in intensity from spectrum A to spectrum B is at the isolated silanol

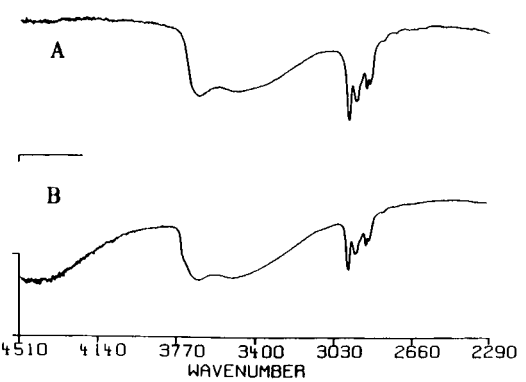

Fig. 8. DRIFT spectra of bonded and hydrolyzed batch 2 stationary phases. (A) *n*-Butyldimethylsilyl-bonded batch 2 silica, 2.83 μmol/m^2; (B) same stationary phase as in A after 35 days of hydrolysis, 2.15 μmol/m^2. Hydrolysis conditions are as described in the Experimental section.

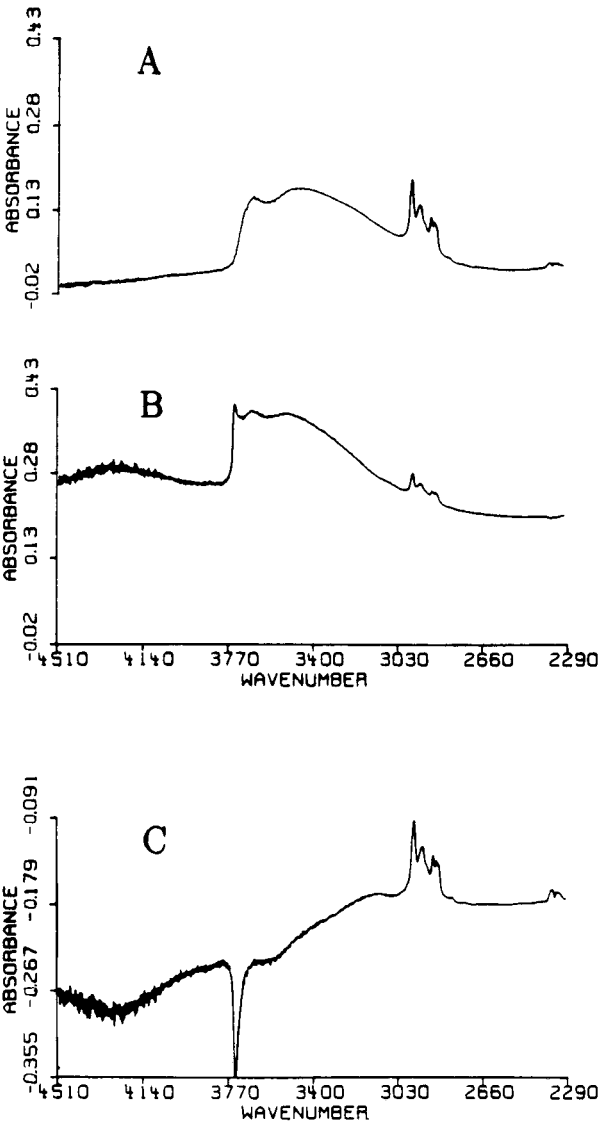

Fig. 9. FT-IR spectra of bonded and hydrolyzed batch 1 stationary phases. (A) *n*-Butyldimethylsilyl-bonded batch 1 silica, 3.67 μmol/m^2; (B) same stationary phase as in A after 137 h of hydrolysis, 2.64 μmol/m^2; (C) difference spectrum, A – B.

position, which reflects the preferential bonding of these silanol sites on the silica surface. It is evident that the lone silanol intensity is lost after silanization of the surface to between 0.83 (spectrum B) and 2.0 (spectrum C) μmol/m^2 coverage, in rough agreement with the 1.6 μmol/m^2 of hydrolyzable sites. These data suggest that the lone or geminal silanol sites react first in bonding and are also hydrolyzed first; consequently, stable stationary phases should contain a minimum of these sites. This

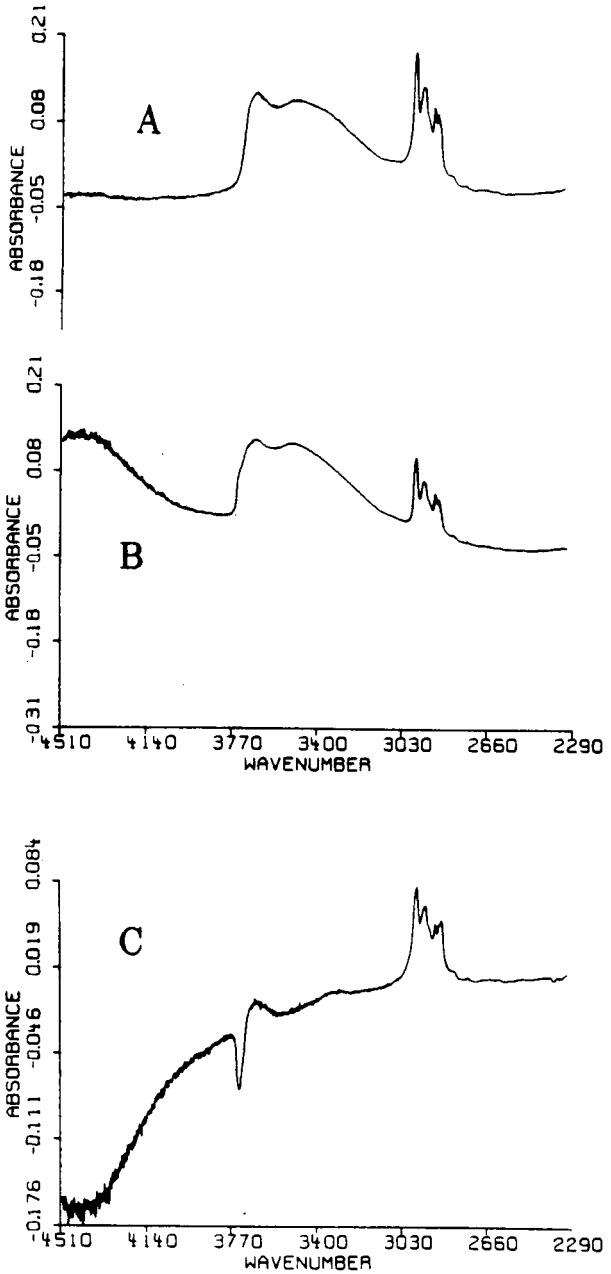

Fig. 10. FT-IR spectra of bonded and hydrolyzed batch 2 stationary phases. (A) *n*-Butyldimethylsilyl-bonded batch 2 silica, 2.83 μmol/m^2; (B) same stationary phase as in A after 35 days of hydrolysis, 2.15 μmol/m^2; (C) difference spectrum, A – B.

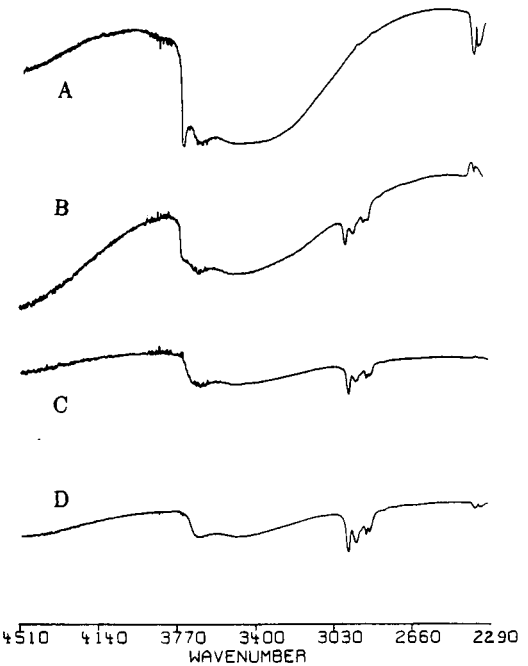

Fig. 11. DRIFT spectra of unbonded and partially *n*-butyldimethylsilyl-bonded batch 1 silicas. (A) Batch 1 silica; (B) C_4-bonded batch 1 silica, 0.83 μmol/m^2; (C) C_4-bonded batch 1 silica, 2.0 μmol/m^2; (D) C_4-bonded batch 1 silica, 3.67 μmol/m^2. See Experimental section for synthesis conditions.

conclusion is in agreement with the literature[6]. Further work to confirm this hypothesis including the use of ^{29}Si NMR spectroscopy is under way in our laboratories.

The main difference between the manufacturing processes used to produce batch 1 silica and batches 2 and 3 silica is in the presence or absence of salts (*e.g.*, sodium sulfate) during drying of the hydrogel. Interestingly, only batch 1 silica possessed about 1000 ppm sodium sulfate as the silica was being dried, and subsequent washing gave the values listed in Table I. One hypothesis now under study in our laboratory is that the presence of salts during drying gives rise to a disadvantageous silanol population on the silica gel surface, perhaps by a "template effect" in which ionic species from the salts that are adsorbed on the silica surface interact with the silanol groups that are forming during the drying process, preventing those silanol groups from interacting with each other. Thus, a higher proportion of isolated groups may form and remain even after the salts are later washed away.

CONCLUSIONS

This paper examined the DRIFT spectroscopic characterization of three batches of *n*-butyl-bonded silica gels before bonding, after bonding, and after hydrolytic removal of the alkyl chains from the surface. Batch 1 silica, when bonded with C_4 chains, yields a characteristic and rapid 25% loss of alkyl groups upon hydrolysis

over a period of *ca.* 25 h, followed by a much more gradual loss. DRIFT results reveal that the rapid hydrolysis of the bonded phase is associated with the reemergence of the isolated silanol groups on the silica gel surface. Initial bonded-phase coverage levels on this silica affect the magnitude of the bonded group loss but not the time scale. A shielding effect is evident at high coverage, which serves to diminish alkyl group loss by hydrolysis. Bonded phases, based on silica batches 2 and 3, manufactured under different conditions, exhibited much slower losses of coverage and did not show reemergence of isolated silanol intensity in spectroscopy. The results indicate that improved coverage serves to decrease coverage losses by hydrolysis and that the silica gel precursor selected has a major role to play in the resultant bonded-phase stability. The data suggest that direct characterization of silica gel products is necessary but not sufficient to quantitate the stability of the bonded phase. Differences in the inherent stability of bonded phases on these two types of silica were only evident after bonding and hydrolysis studies.

ACKNOWLEDGEMENTS

The authors gratefully acknowledge the technical expertise of Margaret M. King in producing some of the FT-IR spectra as well as valuable discussions with Dr. Louis W. Yu. R.A.H. acknowledges the support provided in part by the Center for Advanced Food Technology and the Busch Memorial Fund, both of Rutgers, the State University of New Jersey.

REFERENCES

1 J. N. Kinkel and K. K. Unger, *J. Chromatogr.*, 316 (1984) 193.
2 L. C. Sander and S. A. Wise, *CRC Crit. Rev. Anal. Chem.*, 18 (1987) 299.
3 J. Gobet and E. Kováts, *Adv. Sci. Technol.*, 1 (1984) 77.
4 M. L. Miller, R. W. Linton, G. E. Maciel and B. L. Hawkins, *J. Chromatogr.*, 319 (1985) 9.
5 D. B. Marshall, C. L. Cole and D. E. Connolly, *J. Chromatogr.*, 361 (1986) 71.
6 J. Köhler, D. B. Chase, R. D. Farlee, A. J. Vega and J. J. Kirkland, *J. Chromatogr.*, 352 (1986) 275.
7 J. L. Glajch and J. J. Kirkland, *7th International Symposium on HPLC of Proteins, Peptides and Polynucleotides, Washington, DC, November 2–4, 1987*, paper 129.
8 H. A. Claessens, J. W. de Haan, L. J. M. van de Ven, P. C. de Bruyn and C. A. Cramers, *J. Chromatogr.*, 436 (1988) 345.
9 J. Köhler and J. J. Kirkland, *J. Chromatogr.*, 385 (1987) 125.
10 N. Sagliano, T. R. Floyd, R. A. Hartwick, J. M. DiBussolo and N. T. Miller, *J. Chromatogr.*, 443 (1988) 155.
11 T. G. Waddell, D. E. Leyden and M. T. DeBello, *J. Am. Chem. Soc.*, 103 (1981) 5303.
12 H. Figge, A. Deege, J. Köhler and G. Schomburg, *J. Chromatogr.*, 351 (1986) 393.
13 Y. Ohtsu, H. Fukui, T. Kanda, K. Nakamura, M. Nakano, O. Nakata and Y. Fujiyama, *Chromatographia*, 24 (1987) 380.
14 M. A. Stadalius, J. S. Berut and L. R. Snyder, *LC·GC, Mag. Liq. Gas Chromatogr.*, 6 (1988) 494.
15 J. Nawrocki, *J. Chromatogr.*, 407 (1987) 171.
16 M. L. Hair and W. Hertl, *J. Phys. Chem.*, 73 (1969) 2372.
17 M. L. Hair and W. Hertl, *J. Phys. Chem.*, 73 (1969) 4269.
18 R. K. Iler, *The Chemistry of Silica*, Wiley, New York, 1979, p. 639.
19 J. Sauer and K. P. Schroder, *Z. Phys. Chem. (Leipzig)*, 266 (1985) 379.
20 M. Mauss and H. Engelhardt, *J. Chromatogr.*, 371 (1986) 235.
21 D. W. Sindorf and G. E. Maciel, *J. Am. Chem. Soc.*, 105 (1983) 1487.
22 S. P. Boudreau and W. T. Cooper, personal communication.
23 C. H. Lochmuller and M. T. Kersey, *Langmuir*, 4 (1988) 572.

24 W. Hertl and M. L. Hair, *J. Phys. Chem.*, 72 (1968) 4676.
25 M. L. Hair, in D. E. Leyden (Editor), *Silanes, Surfaces and Interfaces*, Vol. 1, Gordon and Breach, New York, 1986, p. 25.
26 I. Tsuchlya, *J. Phys. Chem.*, 86 (1982) 4107.
27 S. Kondo, H. Yamauchi, Y. Kahiyama and T. Ishikawa, *J. Chem. Soc. Faraday Trans., 1*, 80 (1984) 2033.
28 J. P. Blitz, R. S. S. Murthy and D. E. Leyden, *J. Colloid Interface Sci.*, 121 (1988) 63.
29 D. W. Sindorf and G. E. Maciel, *J. Phys. Chem.*, 86 (1982) 5208.
30 S. D. Fazio, S. A. Tomellini, H. Shih-Hsien, J. B. Crowther, T. V. Raglione, T. R. Floyd and R. A. Hartwick, *Anal. Chem.*, 57 (1985) 1559.
31 R. S. McDonald, *J. Phys. Chem.*, 62 (1958) 1168.
32 J. W. de Haan, H.M. van den Bogaert, J. J. Ponjee and L. J. M. van de Ven, *J. Colloid Interface Sci.*, 110 (1986) 591.

Journal of Chromatography, 458 (1988) 241–253
Elsevier Science Publishers B.V., Amsterdam — Printed in The Netherlands

CHROMSYMP. 1419

ANION-EXCHANGE SELECTIVITY IN LATEX-BASED COLUMNS FOR ION CHROMATOGRAPHY

ROSANNE W. SLINGSBY* and CHRISTOPHER A. POHL
Dionex Corporation, 1228 Titan Way, Sunnyvale, CA 94088-3603 (U.S.A.)

SUMMARY

The anion-exchange columns employed in suppressed ion chromatography contain packings which are agglomerations of anion-exchange latexes and functionalized polymeric substrate. Differences in anion-exchange selectivity studied here are achieved through variations of the properties of the ion-exchange sites and charge density. Column capacity is influenced by the particle sizes of the latexes and substrate. Efficiency is most strongly effected by size of the substrate resin. This paper discusses selectivity variations that are associated with differences in the nature of the quaternary ammonium ion-exchange sites of the latexes and their relationships with various eluents employed in suppressed ion chromatography. Hypotheses are proposed to explain retention behavior of model analyte anions.

INTRODUCTION

Selectivity in a ion-exchange system is often quantified through use of the selectivity coefficient, $K_{A/B}$, as described by a number of authors[1–3]. The selectivity coefficient $K_{A/B}$, is defined as

$$K_{A/B} = \frac{[A]_r[B]_s}{[B]_r[A]_s} \cdot \frac{\gamma_{A,r}\gamma_{B,s}}{\gamma_{B,r}\gamma_{A,s}} \quad (1)$$

where the brackets represent concentration terms for two monovalent ions, A and B, "γ" represents the activity terms for ions A and B, "r" represents the resin phase, and "s" represents the solution phase.

When the selectivity coefficient of eqn. 1 is greater than unity, preference is expressed for ion A over ion B in the resin phase *versus* the solution phase in the concentration range studied. Discussions of parameters that affect the selectivity coefficient deal with the parameters that affect the activity coefficients of the ions in the one phase relative to the other. The selectivity coefficient expresses the net effect of all parameters operating in both phases that are responsible for creating selectivity.

In a chromatographic process, the ionic components of the eluent determine the form of the ion exchanger, *e.g.*, ion B, against which selectivity for the analyte, A, is

0021-9673/88/$03.50

measured. Selectivity between two analyte ions, A and C, is usually expressed as the ratio

$$a = \frac{V_A - V_0}{V_C - V_0} \tag{2}$$

where V_A and V_C are the retention volumes of ions A and C, respectively and V_0 is the void volume. Implicit in this relationship is the affinity of the resin phase for each analyte ion relative to that for the eluent ion.

The capacity factor in chromatography is expressed as k' where

$$k' = \frac{V_A - V_0}{V_0} \tag{3}$$

V_A is the retention volume of the analyte A, and V_0 is the void volume of the column. Capacity factors are used to compare relative selectivities of chromatographic systems for the different analyte ions.

Some authors[2–4] have discussed various models for explaining ion-exchange selectivity in resins. Diamond and Whitney[2] have described selectivity in the ion-exchange process which relies on thermodynamic properties of ions in water as well as properties of water itself. They describe the selectivity order for various anions in terms of the relative basicity of these anions, the degree of hydration of the ions, and the hydration of a trimethylammonium resin. Reichenberg[3] has shown that the elution order of halides and ClO_4^- may be explained in terms of hydration enthalpies. Pearson[5] has discussed his concept of hard and soft acids and bases in several papers. These papers lend considerable insight into the behavior of harder, less polarizable ions such as NO_3^- relative to that of somewhat softer, more polarizable ions, such as ClO_3^-. Walton[4] has assembled a group of papers which deals with the application of ion-exchange selectivity to the chromatographic process.

There is no known literature discussing chromatographic selectivity differences for anions with different quaternary ammonium anion-exchange sites using small, hydrophilic eluent anions. Barron and Fritz[6] have discussed chromatographic selectivity using various quaternary ammonium-functionalized resins relative to eluent ions used in non-suppressed ion chromatography. These eluent anions *e.g.*, benzoate, phthalate and succinate, are larger, in two cases, aromatic, and generally less hydrated than those studied here.

Other authors have discussed the role of matrix effects in selectivity[7], selectivity of resins for organic ions[8], exchange equilibria[9], and schemes for predicting ion-exchange selectivity in resins relative to linear polyelectrolyte analogues[10].

In 1973, Small and Stevens[11] developed and subsequently patented the process for producing ion-exchange materials which, unlike conventional ion-exchange resins, were actually agglomerations of small anion-exchange latexes and larger cation-exchange resin. This type of ion-exchange material is held together by electrostatic forces between the two types of particles. Due to the high charge on both the latexes and resin, this type of packing was found to be very stable. This development produced pellicular anion-exchange packings with higher efficiencies than conventional, micro-

porous, styrene-based anion-exchange resins. The higher efficiencies result from faster kinetics and greater permeability of the pellicular layer.

In this type of packing, the only anion-exchange sites are those in the pellicular layer. Therefore, when substituting in the concentration terms for the resin phase (*e.g.*, $[A_r]$ and $[B_r]$) in eqn. 1, one must use the concentration in the active pellicular layer rather than the bulk composition. This distinction becomes important in calculating distribution ratios in the packing.

In developing useful selectivities for ion chromatography, the main consideration is the selectivity for the chosen eluent ion relative to each analyte ion. Often in designing special-selectivity columns, certain convenient eluents systems, (*e.g.*, OH^-), are essentially pre-determined by cost, availability etc. before the latex-phase is designed. This constraint serves to guide column development. Creating the ion-exchange selectivity required for major applications cannot be separated from the chromatographic need for high efficiency and the practical need for a relatively short analysis time.

The selectivity of a particular packing is the end result of varying several parameters. These include the chemical nature of the monomers in both the substrate resin and the latex, the ratios of the functionalized monomers to crosslinking monomers and the chemical nature of the ion-exchange functionalities.

In this paper, we discuss the effect of varying the quaternary anion-exchange site on a styrene-based polymer latex, keeping the percentage of crosslinking and backbone polymeric structure constant. Our approach is to study the elution behavior of several different types of analytes in four different eluent systems in an attempt to describe the major factors involved in determining anion-exchange selectivity as related to the nature of the anion-exchange site.

EXPERIMENTAL

Apparatus

The 4000i gradient-ion chromatograph (Dionex, Sunnyvale, CA, U.S.A.), equipped with a conductivity detector and a Dionex micromembrane suppressor (AMMS), was used for all work. A Dionex AI400 data system was used for data collection and reduction. A helium headspace was maintained on the eluents by means of a Dionex eluent degas module.

Reagents

The sodium hydroxide (50%) was of analytical grade (J. T. Baker, Phillipsburg, NJ, U.S.A.). The hydrochloric acid and sulfuric acid were of J. T. Baker Instra-analyzed grade.

Substrate resin used in this study was polymerized from styrene and divinylbenzene monomers (Dow Chemical, Midland, MI, U.S.A.) and sulfonated to 5 μequiv./g using sulfuric acid. The latexes were synthesized from divinylbenzene and vinylbenzyl chloride (Dow Chemical). Trimethylamine (TMA), triethylamine (TEA), methyldiethanolamine (MDEA), and dimethylethanolamine (DMEA) were of reagent grade (Aldrich, Milwaukee, WI, U.S.A.).

The column capacity was determined for each packing by use of a breakthrough experiment. After the materials were packed into a polymeric tube, 150 × 4 mm I.D.,

the anion-exchange sites were converted to the OH^- form. Each column was washed with deionized water until the effluent was neutral, and then it was connected to the conductivity detector. A solution of 0.0005 *M* hydrochloric acid was pumped through the columns at 1 ml/min until breakthrough occurred.

RESULTS

The basic structure of the packings under discussion in this paper is that of an anion-exchange latex, agglomerated to cation-exchange-functionalized substrate resin. This type of structure creates an anion-exchange pellicular layer within which the ion-exchange separation takes place and an oppositely charged under-layer which excludes anions through Donnan forces. Table I summarizes the characteristics of the latexes synthesized for this study.

TABLE I

CHARACTERISTICS OF THE LATEXES

Column	*Amine*	*% Cross-linking*	*Size (nm)*		*Column capacity (μequiv./column)*
			Raw	*Functionalized*	
1	MDEA	4	38.0	59.0	24.5*
2	DMEA	4	38.0	64.5	15.1
3	TMA	4	38.0	66.5	16.7
4	TEA	4	38.0	67.7	16.3

* For 5 μm substrate resin.

Fig. 1a, b and c are photographs taken with a scanning electron microscope. Fig. 1a shows unagglomerated 5-μm sulfonated styrene–divinylbenzene substrate resin at 4500 × magnification. In Fig. 1b, substrate agglomerated with 0.2 μm latex is shown at 9000 × magnification. When the magnification is increased to 15 000 ×, a close-up of the anion-exchange latex itself is obtained, as shown in Fig. 1c. The latexes in these photographs are larger than the 60-nm latexes actually used in this study, as the larger latexes produce clearer photographs.

Substrate

The size of the substrate resin was varied in this study, and column capacity and efficiency were evaluated. These data are summarized in Table II. The resin was synthesized with 2% divinylbenzene, a difunctional monomer which provides the crosslinking. The two packings in Table II contain the same latex on different substrates. As can be seen from the efficiency data, the smaller-diameter substrate yields a higher efficiency, assuming that the packing technique used for each material was equally optimized. In general, this latter point is of great importance and considerable skill was required to optimize column packing.

TABLE II

COMPARISON OF COLUMN CAPACITIES AND EFFICIENCIES WITH SUBSTRATE SIZE

Chromatographic conditions: eluent, 5 m*M* sodium carbonate, 1 ml/min; suppression with anion micromembrane suppressor, regenerant 20 m*M* sulfuric acid, 10 ml/min; detection, conductivity; column dimensions, 250 mm × 4 mm I.D.

Substrate size (μm)	*Latex*	*N**	*Column capacity (μequiv./column)*
5	MDEA	8200	24.5
15	MDEA	2290	10.0

* Efficiency was calculated by $N = 5.54\,(t_R/w_{1/2})^2$ where t_R is the retention time for sulfate and $w_{1/2}$ is the width at half height for sulfate.

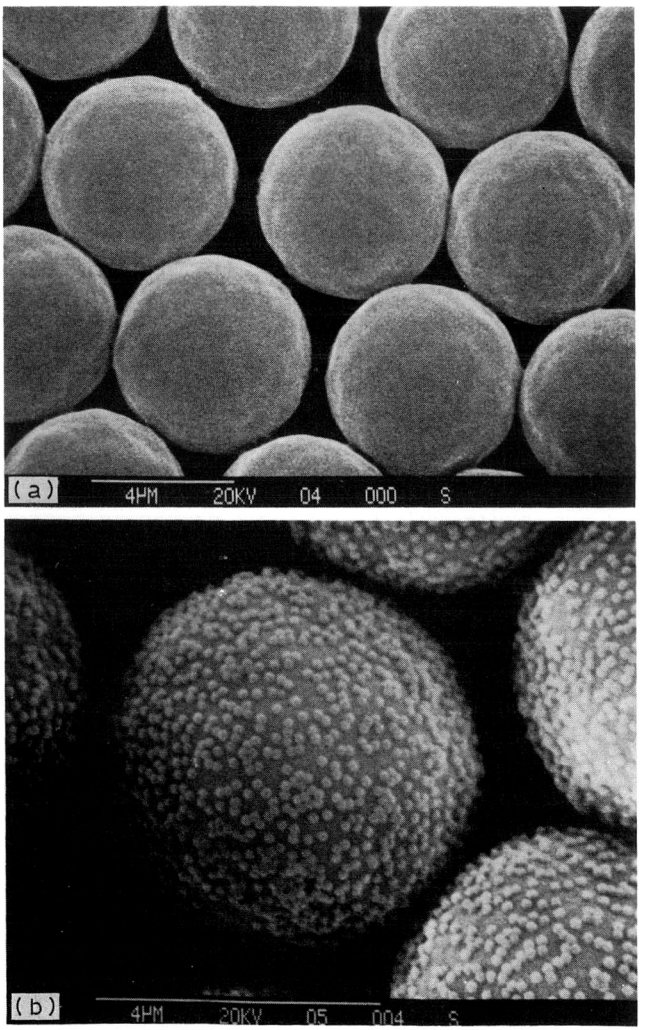

Fig. 1.

(*Continued on p. 246*)

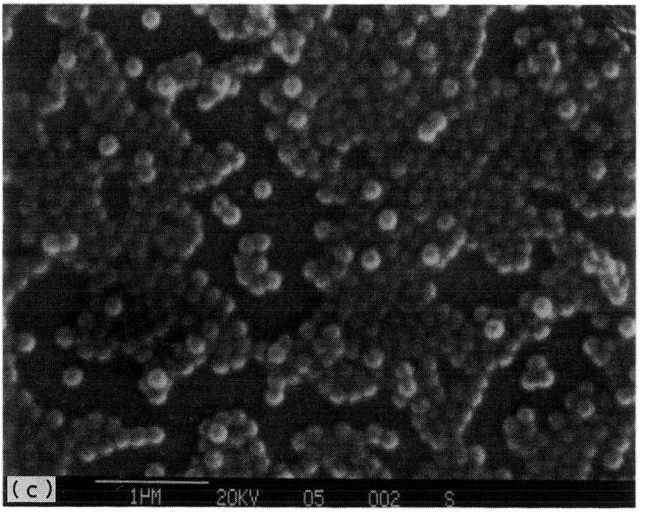

Fig. 1. (a) Scanning electron microscopy (SEM) photograph of 5-μm substrate resin before latex agglomeration; magnification is 4500 ×. (b) SEM photograph of 5-μm substrate resin agglomerated with 0.2 μm anion-exchange latex; magnification is 9000 ×. Note that this material contains larger latex than that under discussion in this paper. (c) SEM photograph of 0.2 μm anion-exchange latex particles; magnification is 15 000 ×.

Latex

The amines used in the quaternization of the latexes and other important characteristics of these latexes are summarized in Table I. The tertiary amines used to quaternize the vinylbenzylchloride-based resin, MDEA, DMEA, TMA and TEA, represent a range of hydrophilicity. Triethylamine is also larger than TMA. This difference provides a variation in charge density.

The percentage of crosslinking and the size before and after functionalization are shown in Table I. As can be seen from these data, functionalization increases the diameter of the 4% crosslinked latexes by about 60%. The volume of a latex in the column, the pellicular layer, in these columns is about 57 μl. This calculation is based on the assumption of hexagonal, closed packing of substrate particles and complete coverage of the 5-μm substrate with 60-nm latex particles. A calculation of about 28 000 latex particles per 5-μm substrate resin particle is obtained. The SEM photographs indicate that coverage of 5-μm substrate by the larger latex used for Fig. 1a–c is not 100% although coverage is reproducible.

Eluents and analytes were selected to give information on the nature of the retention mechanisms operating in the latexes. These topics are discussed in the following sections.

Analyte selection

A standard mixture of analytes was needed which would provide information on basic features of the retention mechanisms. The standard mixture contained F^-, Cl^-, Br^-, NO_3^-, ClO_3^-, PO_4^{3-}, and SO_4^{2-}. Cl^- and SO_4^{2-} were used to evaluate monovalent–divalent selectivity and Br^-–NO_3^-–ClO_3^- were used to study parameters

TABLE III

RETENTION DATA* WITH 5 m*M* SODIUM CARBONATE AS ELUENT

Chromatographic conditions as described in Table II; column designations as in Table I.

Column	*Analyte*						
	F^-	Cl^-	Br^-	NO_3^-	ClO_3^-	SO_4^{2-}	PO_4^{3-}
1	0.09	0.54	2.2	2.6	2.6	5.2	3.3
2	0.18	1.0	3.7	4.4	4.2	5.3	6.4
3	0.16	1.2	4.5	5.4	5.3	3.3	7.6
4	0.13	1.9	9.6	16.8	9.6	3.7	5.6

* k' Corrected for column capacity , normalized to column 2.

that effect monovalent selectivity for analytes with different polarizabilities, degrees of hydration and other features which will be described later. Tables III–VI list k' (normalized for column capacities) for these analytes on each of the packings for various eluent systems.

TABLE IV

RETENTION DATA* WITH 100 m*M* SODIUM HYDROXIDE AS ELUENT

Chromatographic conditions as described in Table II, except for eluent; column designations as in Table I.

Column	*Analyte*						
	F^-	Cl^-	Br^-	NO_3^-	ClO_3^-	SO_4^{2-}	PO_4^{3-}
1	0.06	0.24	0.92	1.1	1.0	0.20	0.31
2	0.14	1.1	4.5	5.0	4.9	3.0	6.7
3	0.30	4.4	19.2	22.5	21.2	51.4	>100
4	0.30	5.8	26.1	55.8	35.7	24.9	>100

* k' Corrected for column capacity, normalized to column 2.

TABLE V

RETENTION DATA* WITH 20 m*M* SODIUM HYDROXIDE–5 m*M* *p*-CYANOPHENOL AS ELUENT

Chromatographic conditions as described in Table II, except for eluent; column designations as in Table I.

Column	*Analyte*						
	F^-	Cl^-	Br^-	NO_3^-	ClO_3^-	SO_4^{2-}	PO_4^{3-}
1	0.13	0.38	0.86	0.74	0.40	1.3	6.5
2	0.30	0.92	2.4	2.1	2.1	6.5	38.2
3	0.34	1.4	3.4	3.3	3.3	15.0	112
4	0.24	0.77	2.4	2.8	2.6	13.8	>150

* k' Corrected for column capacity, normalized to column 2.

TABLE VI

RETENTION DATA* WITH 100 m*M* SODIUM HYDROXIDE–5% METHANOL AS ELUENT

Chromatographic conditions as described in Table II, except for eluent; column designation as in Table I.

Column	*Analyte*						
	F^-	Cl^-	Br^-	NO_3^-	ClO_3^-	SO_4^{2-}	PO_4^{3-}
1	0.06	0.23	0.99	1.1	1.2	0.25	0.86
2	0.14	1.2	4.7	5.3	5.2	3.5	7.6
3	0.34	4.6	19.2	23.6	21.4	58.2	n.d.
4	0.34	5.9	33.9	55.7	54.6	27.1	n.d.

* k' Corrected for column capacity, normalized to column 2.

Eluent compositions

Four eluent compositions were used in the evaluations: 100 m*M* sodium hydroxide, 20 m*M* sodium hydroxide with 5 m*M* *p*-cyanophenol, 100 m*M* sodium hydroxide with 5% methanol, and 5 m*M* sodium carbonate. The k' data from Table IV can be used to show the enhanced OH^- selectivity of the alkanolammonium latexes relative to the alkylammonium latexes. The k' values with 100 m*M* sodium hydroxide as eluent increase in the order of MDEA < DMEA < TMA < TEA, with exceptions, because the alkanolammonium sites are more OH^- selective than the alkylammonium sites. As the fixed sites become more selective for the eluting ion, k' values decrease. This topic is discussed at greater length below.

The *p*-cyanophenate ion is a strong eluting ion. This is evident from the lower k' values for all analytes in Table V relative to Table IV. The *p*-cyanophenate ion also competes effectively with NO_3^- and ClO_3^- for sites in the latexes that have high selectivity for these oxyanions. The k' values for NO_3^- and ClO_3^- are lowered by a greater percentage than those of the other analytes.

The addition of methanol to the 100 m*M* sodium hydroxide eluent was used to study the possible role of a nonaqueous protic solvent in anion-exchange selectivity.

DISCUSSION

When selectivity is viewed in terms of the thermodynamic properties of hydration, comparisons are necessarily made between the resin (fixed site) phase and the eluent (solution) phase. For our purposes here, a highly hydrated ion is viewed as having a large negative free energy of hydration from the gaseous state. Reichenberg noted that the use of free energies versus enthalpies has been a matter of discussion.

The free energy that is driving retention can be viewed as the difference in free energies between the resin phase and the solution phase. Entropy-driven processes often occur in the solution phase; that is, processes associated with a disturbance of the structure of water. An example of an enthalpy-driven process is that of the stabilization of charge through interactions with the resin phase.

A highly hydrated ion will prefer to remain in the aqueous solution phase (low k') where molecules of water of hydration are readily available, if some other interaction with the resin phase which has a larger negative free energy associated with it, is not

available. Discussion of selectivity in view of thermodynamics must be within the context of the relationship between the thermodynamic properties of the various analytes in both phases. Hypotheses for retention behavior are included throughout the following text.

Discussion of these data may be divided into several parts. These include the types of quaternary ammonium sites and their features, the types of analytes and their classification, and types of eluents.

Anion-exchange sites

The anion-exchange functionalities in the four latexes studied are, in the order of decreasing hydrophilicity, MDEA > DMEA > TMA > TEA. With increasing hydroxyl content, the sites become more hydrated as a result of increased hydrogen-bonding. The more hydrated latexes show increased OH^- selectivity in several ways. For example, in Table III the retention of SO_4^{2-} is stronger on MDEA and DMEA than on TMA and TEA. This could be explained by considering that the OH^--selective phases concentrate OH^- from the CO_3^{2-} eluent; monovalent OH^- is a less effective eluent than divalent CO_3^{2-}, especially for divalent analytes. For the OH^--based eluent systems (Table III–VI), the k' data of all analytes are lower on the alkanolammonium latexes than on the alkylammonium latexes.

Another difference between the latexes is that of size. For example, between TMA and TEA functionalities the TEA sites are larger than the TMA sites, assuming the radius values available for the analogous free molecules serve as valid reference. Because the TEA sites are larger than the TMA sites, the charge density of the former latex is lower, thereby reducing the selectivity for multivalent species, such as SO_4^{2-} and PO_4^{3-}. This is evident from the k' data, shown in Table III–VI. The k' values for SO_4^{2-} are lower on TEA than on TMA, except with CO_3^{2-} as eluent. A highly hydrated eluting ion, such as CO_3^{2-} would be expected to be less effective on less hydrated ion exchangers, such as TEA, if other factors, such as OH^- selectivity and charge density do not mask the effect.

Analytes

The multivalent ions, SO_4^{2-} and PO_4^{3-}, most clearly show the effect of OH^- selectivity of the anion-exchange sites. As seen in the k' data (Table III–VI), SO_4^{2-} is eluted much earlier from the alkanolammonium latexes than are the monovalent analytes. The enormity of the selectivity change between the MDEA latex and the other three latexes (Table IV) with OH^- as eluent indicates the value of the MDEA phase for systems with OH^- as eluent.

The pH dependence of the PO_4^{3-} ion is also evident. The PO_4^{3-} ion has its third pK at 12.67 so that at high eluent pH this ion becomes trivalent. The k' values for this trivalent ion are shown only as a > value for the TMA and TEA latexes (Table IV–VI) due to the extremely long retention times. The SO_4^{2-}–PO_4^{3-} elution order for the MDEA latexes with CO_3^{2-} (Table III) as eluent suggests that this latex concentrates OH^- from the eluent resulting in a higher pH in the latex than in the eluent.

The elution order of F^-, Cl^-, Br^-, I^- and ClO_4^- can be explained by differences in enthalpy of hydration from the gaseous state of these ions[3], although most authors make little or no reference to chromatographic eluents. Table VII shows thermodynamic properties for the anions under discussion. It is worthy to note that if

TABLE VII

THERMODYNAMIC PROPERTIES OF SELECTED MONOVALENT ANIONS[2,11,12]

Ion	ΔH^{0}* *(kcal/mole)*	$-\Delta H^{i}$** *(kcal/mole)*	$-\Delta S^{i}$*** *(e.u.)*	$-\Delta G^{i}$§ *(kcal/mole)*
H^+	0	265	–	–
F^-	– 78.7	116	30.7	107
Cl^-	– 40.0	84	17.1	79
Br^-	– 28.9	76	13.42	72
I^-	– 13.4	67	8.05	64
NO_3^-	– 49.4	74	16.9	69
ClO_3^-	– 23.7	69	–	–
ClO_4^-	– 31.4	54	13.4	50
CO_3^{2-}	–161.6	127	65.3	108
OH^-	– 54.9	122	37.6	111

* Heat of formation of the aquo ion[11,15].

** Enthalpy of hydration of the gaseous ion; generally accepted value for H^+ is 260.7, although ref. 12 uses values as shown. Values at infinite dilution and 25°C[12]; values from ref. 14 vary slightly.

*** Entropy of hydration of the gaseous ion at infinite dilution and 25°C[12].

§ Free energy of hydration of the gaseous ion at infinite dilution and 25°C[12].

enthalpies of formation of the aquo ion are compared[11], the elution order cannot be predicted for ClO_4^- although the halide elution order remains the same. This suggests that the crystal lattice energies included in the enthalpies from the gaseous state are very important in the thermodynamics of ion-exchange for ClO_4^-.

In our study, which includes aspects of the chromatographic process, *i.e.* relative selectivity between analyte and eluting ion, the $F^- < Cl^- < Br^-$ elution order is maintained on all four of these latexes for all eluent compositions studied. I^- and ClO_4^- are not included in our data because of their extremely long retention times but they are in fact eluted in that order after Br^- as expected from the hydration enthalpies.

The discussion of the relative retention behaviour of ClO_3^- and NO_3^- deals with attempts to explain variations in relative k' values for the four different latexes. The enthalpies of formation of the aquated ions (Table VII) from the gas state suggest that the order of hydration is $ClO_3^- < NO_3^- \sim Br^-$. Following the hypothesis used for halide elution, these hydration enthalpies would suggest an elution order of $Br^- \approx NO_3^- < ClO_3^-$ with eluent ions that also compete on the basis of hydration enthalpy. (Although we were interested in the relationships between free energies and entropies for these ions, we were unable to find these values from the gaseous state for ClO_3^- in the literature. However, the values for Br^- and NO_3^- are listed in Table VII.) Although it is apparent that the elution order of the halides with CO_3^{2-} and OH^- as eluting ions can be explained by enthalpies of hydration from the gaseous state, it seems that in the case of NO_3^-–ClO_3^- with eluent systems of 5 m*M* sodium carbonate, 100 m*M* sodium hydroxide and 100 m*M* sodium hydroxide containing 5% methanol, this notion fails completely. In addition, when *p*-cyanophenate is added to the eluent (Table V), the elution order is reversed for Br^- and ClO_3^- between the MDEA and TEA latexes; ClO_3^- is affected more than Br^-. The conclusion here is that the retention mechanisms for NO_3^- and ClO_3^- are different from those of the halides. Some insight may be

obtained from examining the geometries of these ions and ion-pairing as a major retention mechanism.

Retention data based on the different eluents used in this study suggest that ClO_3^- and NO_3^- are retained by somewhat different mechanisms. Conventional ion-pair chromatography may give a clue as to these differences. Ion-pair chromatography may be viewed as a dynamic ion-exchange[16] technique which is dependent on the formation of ion-pairs at the low dielectric resin–water interface. This technique then is capable of distinguishing among the retention mechanisms of various ions by identifying those which form more stable ion pairs.

In conventional ion-pair chromatography with quaternary ammonium ion-pairing reagents, ClO_3^- is eluted after NO_3^-. This suggests that ClO_3^- forms more stable ion pairs than NO_3^-. Considering that the stereochemical structure of ClO_3^- is pyramidal[13] while that of NO_3^- is planar and that a less hydrated ion should be able to form an ion pair more efficiently, this ion-pairing hypothesis seems plausible.

Diamond and Whitney[2] have described water-structure-enforced ion pairing, which becomes stronger as ions become larger and less able to become involved in electrostatic, Bjerrum-type ion pairing. According to Diamond and Whitney[2], the less-hydrated ions disturb the normal structure of water more than more-hydrated ions. The associated thermodynamic terms serve to drive these ions to the resin phase where water is less structured. This type of mechanism would be consistent with the retention behavior of ClO_3^- relative to Br^- on our latexes shown in Table III–V. However, the large k' values for NO_3^- require further explanation.

On the latexes used in this study, the k' values for NO_3^- increase dramatically as the quaternary ammonium group becomes more hydrophobic and larger (Table III–V). Selectivity in terms of hydration energies would dictate that ions with the highest hydration energies should prefer to remain in the aqueous external phase or eluent rather than give up part of their water of hydration to enter the dehydrated water-structureless environment of the anion exchanger. Nitrate, therefore, is behaving like a softer, less polarizable, less hydrated ion than any of its thermodynamic properties (Table VII) would suggest.

A hypothesis for the retention of NO_3^- may be made based on molecular geometry. Looking at the planar structure of NO_3^- ion it is evident that three resonance hybrids, viewed in terms of valence bond theory, create an extended π-cloud (with 2 π-electrons) similar to that created in the aromatic ring of the benzyl chloride monomer. Overlap of the π-clouds of NO_3^- with those of the benzyl monomer coincident with close association with the ion-exchange site should cause significant stabilization energies. If this stabilization drives the retention of NO_3^-, then it must have a larger negative free energy associated with it than the energy of hydration, which is fairly large for NO_3^- (Table VII).

The remaining question, that of why retention of NO_3^- is greater on the TEA latex, may perhaps be answered as follows. As there is less water in the vicinity, there is more room for the NO_3^- to maneuver into an overlapping position near enough to the ion-exchange site for ion-exchange, and also to the aromatic π-cloud. It also seems that a more dehydrated environment would help to stabilize the π-overlap. Associated, polarized water serves to delocalize some of the charge throughout the water network. In this scheme, the more hydrophobic the ion-exchange site, *i.e.* TEA > TMA > DMEA > MDEA, the greater the probability that orbital overlap would occur. The

π-overlap concept also explains the especially strong eluting power of the *p*-cyanophenate ion for NO_3^- (Table V). This point is discussed below. This unusual retention mechanism may explain the unusually low overload capacities of NO_3^- relative to other anions on most columns; that is, statistically fewer sites are available which can fulfill both requirements for NO_3^- retention.

Eluents

As Table VII shows, CO_3^{2-} and OH^- are hydrated similarly in the free energy term from the gaseous ion. Both of these ions are more hydrated than the analyte anions. It seems then that the increased retention of anions on increasingly hydrophobic latexes can be explained not only in terms of increased affinity of the ion-exchange sites for less hydrated anions but also in terms of the diminished eluting power of highly hydrated eluent ions. Carbonate remains a very effective eluting ion, because it is divalent, although as the charge density of the latexes increases (*e.g.*, TEA >TMA), the divalent-ion eluting power is somewhat diminished.

Increased selectivity of the alkanolammonium latexes for OH^- may be considered in terms of the extraordinary interaction of OH^- with water. This interaction is evidenced by the high electrical conductivity in water relative to other anions. The powerful elution of anions with OH^- eluents from these latexes is evident when comparing the k' data in Table IIIb for the various latexes. Lower k' values indicate higher selectivity for the eluting ion compared to the analyte ion.

The *p*-cyanophenate ion, with its aromatic structure can interact with the π-orbitals to a greater extent than NO_3^-. The *p*-cyanophenate ion reduces the retention of NO_3^- and ClO_3^- to a much greater extent than that of the other analytes (Table V). The enhanced elution of ClO_3^- may suggest a stereochemical retention mechanism for ClO_3^- similar to but weaker than that for NO_3^-, in addition to ion pairing.

The addition of methanol to the 100 m*M* sodium hydroxide eluent has the effect of increasing the retention of all ions except Cl^- and NO_3^- in this study (Table VI). If we use hydration theories to help provide a model, it seems that the hydration of the latexes is decreasing relative to the eluent phase. This should have a large effect on retention mechanisms based on ion pairing. This also has the effect of making highly hydrated eluting ions, such as OH^-, less effective eluents for reasons already discussed. From these points it seems that the retention of all ions should have been increased. The fact that the retentions of Cl^- and NO_3^- were not increased suggests a retention mechanism not yet identified. This is a subject for further study.

CONCLUSION

Ion-exchange packings can be made by agglomeration of anion-exchange latexes and cation-exchange resin. This paper discusses selectivity that can be varied by changing the quaternary ammonium group on the latex, although other parameters not under discussion here, such as crosslinking, also affect selectivity.

Monovalent anions, as analytes or as eluents, can be categorized on the basis of their thermodynamic properties, their geometries and their abilities to interact with the anion-exchanger phase in specific ways, *i.e.* polarizability, π–π interactions etc. By probing the anion-exchange of various types of analytes on several different quaternary ammonium latexes with different eluent systems for suppressed ion

chromatography, we have attempted to identify selectivity differences among the various types of anion-exchange sites. Of special note is the high selectivity of the alkanolammonium latices for OH^-. There are many areas for continued research, including the role of different types of solvents on ion-exchange and the selection of better probes for the elucidation of retention mechanisms for a wider variety of oxyanions.

ACKNOWLEDGEMENTS

We thank Pam Johnson for the SEM photographs and Steven Papanu for much of the work on synthetic routes to the latexes.

REFERENCES

1 O. Samuelson, *Ion Exchange Separations in Analytical Chemistry*, Wiley, New York, 1963.
2 R. M. Diamond and D. C. Whitney, in J. Marinsky (Editor), *Ion Exchange, A Series of Advances*, Marcel Dekker, New York, NY, 1966, Vol. 1, Ch. 8.
3 D. Reichenberg, in J. Marinsky (Editor), *Ion Exchange, A Series of Advances*, Marcel Dekker, New York, NY, 1966, Vol. 1, Ch. 7.
4 H. F. Walton (Editor), *Benchmark Papers in Analytical Chemistry, Vol. 1, Ion-Exchange Chromatography*, Dowden, Hutchinson & Ross, Stroudsburg, PA, 1976.
5 R. G. Pearson (Editor), *Hard and Soft Acids and Bases*, Dowden, Hutchinson & Ross, Stroudsburg, PA, Wiley, distributor, 1973.
6 R. E. Barron and J. S. Fritz, *J. Chromatogr.*, 284 (1984) 13–25.
7 B. R. Green and R. D. Hancock, *Hydrometallurgy*, 6 (1981) 353–63.
8 M. J. Semmens, *AIChE Symp. Ser.*, 71 (1975) 214–223.
9 A. Delyannis (Editor), *Proc. Int. Symp. Fresh Water Sea, 4th*, 3 (1973) 25–48.
10 R. Yang and J. A. Marinsky, *J. Phys. Chem.*, 83 (1979) 2737.
11 H. Small and T. Stevens, *U.S. Pat.*, 4252644 (1981).
12 D. D. Wagman, W. H. Evans, V. B. Parker, I. Halow, S. M. Bailey and R. H. Schumm, *Selected Values of Chemical Thermodynamic Properties*, National Bureau of Standards, Washington, DC, Circular 500, 1968.
13 V. P. Vasil'ev, E. K. Zolotarev, A. F. Kapustinskii, K. P. Mischenko, E. A. Podgornaya and K. B. Yatsimirskii, *Russ. J. Phys. Chem.*, 34 (1960) 840 (English translation).
14 F. A. Cotton and G. Wilkinson, *Advanced Inorganic Chemistry*, Wiley-Interscience, 3rd ed., 1972.
15 G. Anderegg, in A. E. Martell (Editor), *Coordination Chemistry*, Vol. 1, Van Nostrand Reinhold Co., New York, 1971, p. 464.
16 G. M. Barrow, *Physical Chemistry*, McGraw-Hill, New York, 3rd ed., 1973, p. 783.
17 C. P. Terweij-groen, S. Heemstra and J. C. Kraak, *J. Chromatogr.*, 161 (1978) 69–82.

Journal of Chromatography, 458 (1988) 255–266
Elsevier Science Publishers B.V., Amsterdam — Printed in The Netherlands

CHROMSYMP. 1468

ELECTRON SPIN RESONANCE STUDIES UNDER DYNAMIC MOBILE PHASE CONDITIONS ON CHEMICALLY MODIFIED SILICA

C. MILLER, R. DADOO, R. G. KOOSER* and J. GORSE*
Department of Chemistry, Knox College, Galesburg, IL 61401 (U.S.A.)

SUMMARY

The electron-spin resonance (ESR) techniques of spin labeling and probing are shown to be powerful methods for the study of bonded silicas used in chromatographic separations under dynamic solvent flow conditions. Microscopic information gained from these studies includes solvation composition of the bonded phase at various locales in the bonded phase, configuration of the bonded phase and solvent-flow effects. In the spin-label study, 2-(2,2-dimethyloxazolidine-N-oxy)hexylsilane (DOXYL hexyl siloxane) was used as the label. ESR spectra show changes in the motional freedom of the bonded surface as a function of mobile phase composition and elution time and demonstrate chain stiffening with the introduction of water, as infered by other studies. In the spin-probe work, various nitroxide compounds of the 2,2,6,6-tetramethyl-1-piperidinyloxyl (TEMPO) family were introduced under flow conditions as a 0.1 m*M* solution in various water–methanol mobile phases. C_{18} sample columns were equilibrated with this mixture. Interpretation of the spectra yielded information about the solvated environment on the surface that was sampled by the probes as a function of both the mobile phase and the polarity of the probe.

INTRODUCTION

The development of spectroscopic techniques to study the solid–liquid interface is considered to have a high priority in the understanding of separation mechanisms in bonded phase liquid chromatography[1]. The microscopic views that the application of spectroscopy to bonded phase systems can give will aid the design of more efficient separation techniques.

The most useful stationary phase for liquid chromatography has been the reversed-phase material which is made by bonding long chain hydrocarbons to the porous silica surface by silanization[2]. These stationary phases have been studied extensively by chromatographic means[3,4] and more recently by various spectroscopic methods[5–9]. While providing valuable insights concerning the nature of the bonded silica interface, these techniques often suffer from the need to be performed under

* Present address: Department of Chemistry, Baldwin-Wallace College, Berea, OH 44017, U.S.A.

0021-9673/88/$03.50

conditions that are not representative of those that are useful to chromatographers. As an example, in order to perform most nuclear magnetic resonance (NMR) experiments, the sample must be spinning. This makes it difficult to experiment with solvents flowing through the system. Thus, many of the initial NMR investigations were performed with the bonded phase either dry or in a solvent that wets the hydrophobic modified silica under static (ambient pressure) conditions. Most often these solvents are too "strong", *i.e.*, non-polar, to permit useful separations as chromatographic mobile phases. Mixed solvents that contain 50% or more water are seldom, if ever, useful for these studies[10,11]. It should be mentioned in this connection that Lochmuller *et al.*[12] have been able to construct a fluorescence sample cell that allowed them to maintain sample geometry and also to operate under high pressure and flowing conditions.

Other problems with spectroscopic techniques, as applied to modified silicas, include lack of sensitivity, opacity or light scattering properties of silica and a limited range of probes and labels. Often, the presence of a label, such as a large fluorescent molecule, can significantly alter the nature of the solid–liquid interface that is being characterized. The use of such molecules as probes limits their usefulness in fluorescence studies to mobile phases containing high concentrations of organic modifiers because of quenching at very high stationary phase concentrations when mobile phases with high water content are used[7].

One spectroscopic technique that has only been sparingly applied to chromatographic systems is electron spin resonance (ESR) spectroscopy. The technique has been used to study a wide variety of chemical systems, such as membranes, liquid crystals, polymers, zeolites and biological macromolecules, and has been extensively reviewed[14–16]. The ESR studies of the dynamics, configuration and phase interface properties of systems have been carried out chiefly by two techniques: spin probe and spin label experiments. In the spin-probe experiment, a relatively small paramagnetic molecule, often a nitroxide, is introduced into the system where it is partitioned, adsorbed or intercalated into various regions. The resulting ESR spectrum contains information about the environment(s) of the probe. In a spin-label experiment, a small number of molecules in the system under study have a paramagnetic center chemically bonded to the units. The label density is kept at a very low level to avoid significant perturbation of the system so that the spectroscopic observations on the label reflect the properties of the unlabeled majority of molecules.

Early label experiments were performed on modified silicas with the use of polymers[17–20] and hydrocarbon modifiers under static conditions[21]. These studies demonstrated the existence of two dynamic domains of nitroxide labels: inside bonded clusters and on the perimeter of the cluster, capable of interacting with the unmodified silica surface. Spin probes have been used to investigate unmodified hydrated silicas[22–25] and have demonstrated that the nature of the water on the surface differs greatly from "bulk" water. Ion-exchange resins have also been spin probed[26] and have revealed very anisotropic behavior. Recently, Gilpin *et al.*[27] have sparsely labeled silica surfaces to probe the surface and interface dynamics of normal bonded phases. They found that the nitroxide label strongly interacted with the silanol surface in non-polar solvents, but in polar, hydrogen-bonding solvents the solvent was competitive for the surface sites. Also, Malcom *et al.*[28] reported a true reversed-phase that was sparsely labeled with a nitroxide. They confirmed the two site model and

were able to demonstrate dramatic changes in bonded chain mobility with the introduction of wetting solvents.

In this paper, we show the ESR technique to be very versatile and robust for the investigation of chromatographic systems. We make two important points: first, the technique is very senstive, requiring only minimal disturbance of the system under study by the label or probe and secondly, the technique can be applied under conditions that accurately reflect those in actual chromatographic separations. The requirement that an unpaired electron must be present is satisfied by the use of nitroxide spin-labeled surfaces or nitroxide spin-probes as solutes, dissolved in typical chromatographic mobile phases. The spin-labels are synthesized *in situ* and are present in <0.5 mole percent of the untagged hydrocarbon chains, perturbing the surface very little. The spin-probes exist in a wide range of polarities and sizes, mimicking a wide variety of chromatographic behaviors. We demonstrate that considerable information about the chromatographic surface is available from ESR studies.

The dynamic label/probe studies presented here show various results of interest to chromatographers. Label studies give insight into conditioning effects and well as changes in surface configuration with mobile phase composition. Spin-probe studies give pictures of the microenvironments sampled by chromatographic solutes and offer opportunities to make traditional liquid–solid interface determinations, such as isotherm studies, by spectroscopic means.

EXPERIMENTAL

The ESR spectra were obtained on a Varian V-4500 ESR spectrometer with 100 kHz modulation (Varian Associates, Palo Alto, CA, U.S.A.). The usual precautions were taken to insure that saturation and overmodulation effects were absent.

The dynamic ESR cell inserted into the spectrometer consisted of a 1 mm I.D. quartz tube fitted with a 1/16-in. frit at the outlet end and high pressure plastic tubing and fittings at each end. The column end fittings were made by carefully boring out the plastic coupling fittings (Model P-110; Upchurch Scientific, Oak Harbor, WA, U.S.A.) out to accomodate the frit and the nominal 2 mm O.D. quartz tube in order to provide a seal against the pressures used in the experiments. The quartz tube was filled with spin labeled silica or a typical bonded phase by aspirating the silica into the tube and then conditioning it under higher flow-rates than were actually used for running spectra in order to pack it tightly in the tube. A Beckman 110B Solvent Delivery Module (Beckman Instruments, Altex Div., San Ramon, CA, U.S.A.) was used to pump mobile phase through the column at various flow-rates ranging from 0.1 to 0.6 ml/min.

The labeled, bonded monomeric C_6 silica was synthesized *in situ* by a previously described method[28]. The label was DOXYL hexyl silane[28]. The silica used was Davisil (Aldrich, Milwaukee, WI, U.S.A.) which had a particle size of 36–74 μm, a pore diameter of 150 Å and a pre-derivatization surface area of 300 m^2/g. The % C by weight was determined to be 5.45% which means *ca.* 1.25 bonded chains per 100 $Å^2$ or *ca.* 31% derivatized. This material is surprisingly durable. A batch made 1.5 years ago is still ESR-active. ESR spectra were recorded after equilibrating the column with either 100% methanol or 50% (v/v) aq. methanol at a flow-rate of 0.3 ml/min for 0.5 h. The mobile phases were sparged with helium to remove oxygen. After initial condi-

tioning, the column was left standing overnight, and the ESR spectra were recorded at regular intervals after pumping a mobile phase through the column. In the time-dependence studies, when a steady state had been reached (as seen by the peak heights of the spectra), the pump was shut off and the spectra monitored until the initial time zero state had been reached.

All spin-probe studies were performed in the "isotherm" mode by pumping a degassed solution (see above) of the mobile phase and chosen probe through the dynamic ESR cell. Observations were made when a time-invarient signal was observed. The stationary phase was Bond Elut C_{18} (Analytichem International, Harbor City, CA, U.S.A.), a highly loaded polymerically modified silica marketed for solid-phase extraction. The stationary phase was packed into a 1 mm I.D. ESR quartz column, as described above, and attached to the pump for dynamic probe investigations.

The probes used were TEMPO, 4-hydroxy-TEMPO (TEMPOL) and 4-amino-TEMPO (TEMPAMINE) (Aldrich) and used as received. Solutions in various compositions of methanol and water were made at $< 1 \cdot 10^{-4}$ *M*.

Chromatographic capacity factors, k', were determined for the spin-probes and other solutes on Bond Elut C_{18}. This stationary phase was dry-packed and conditioned with at least 100 column volumes of methanol. The column consisted of a 50 mm × 4.6 mm I.D. guard column. Methanol used in the mobile phase was filtered and water was doubly deionized and filtered. The mobile phase consisted of a 50:50 (v/v) mixture, which was sonicated and allowed to stand overnight. A 1% sodium nitrate solution was used to determine V_0.

RESULTS AND DISCUSSION

Considerable information is available from the ESR spectrum of a free radical. The ESR spectrum of a nitroxide free radical undergoing rapid rotational reorientations ($< 10^{-9}$ s mean rotational correlational time) contains three lines separated by the ^{14}N coupling constant (symbolized by a_N) from the interaction of the unpaired electron with the ^{14}N nucleus in the –NO group (Fig. 1). Readily available information about the microenvironment of the system is as follows.

Solvent polarity

It has been well established that the value of the ^{14}N splitting constant of nitroxides, a_N, is affected by (a) solvent polarity and (b) the extent of hydrogen bonding[29] and that the relationship is linear between the coupling constant and solvent polarity[30]. The more polar the environment of the nitroxide, the greater is the coupling constant; therefore, the coupling constant is a sensitive measure of the character of the solvation in the neighborhood of the nitroxide. Hence, measurements of the changes in the coupling constant provide a means to explore the solvation composition of the bonded phase by various spin-probes and label experiments.

Lineshape anisotropy and rotational correlation times

The three lines of a nitroxide spectrum are of equal integrated intensity, but often of unequal width, hence unequal amplitude. The extent of this spectral anisotropy is related, for a given nitroxide, to the rate of rotational tumbling and to the

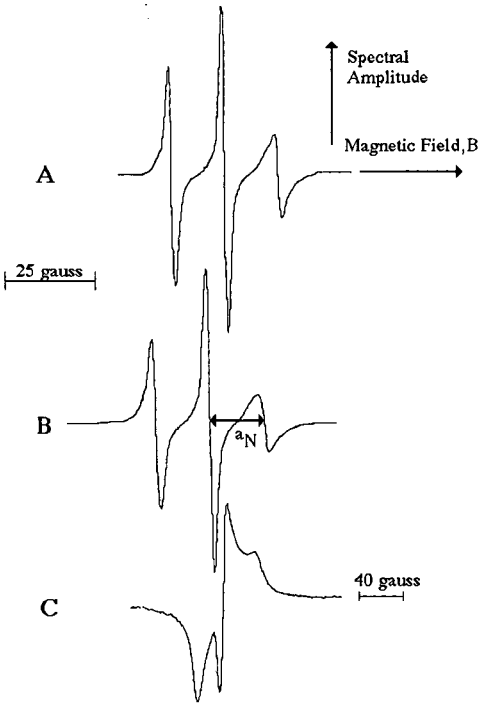

Fig. 1. ESR spectra of the C_6 spin-labeled silica. Magnetic field axis increases to the right, and the three lines arise from the interaction of the electron spin with the three possible N nuclear spin states. The magnitude of the electron nuclear interaction is measured by the hyperfine coupling constant, a_N, and is sensitive to the polarity of the label environment. (A) The bonded silica under flow conditions with pure methanol; (B) the C_6 bonded silica under flow conditions with 50% (v/v) aq. methanol; (C) the C_6 bonded silica in the dry state (note the magnetic field axis scale is different in A and B than in C).

anisotropy of that tumbling about the three mutually perpendicular rotational axes of the molecule. In the case of small, nearly spherical molecules such as TEMPO, rotating rapidly (rates in the range of 10^9–10^{11} s^{-1}) in isotropic media, the three lines are of nearly equal amplitude, reflecting a rotation that is the same about the three molecular axis directions. In the case of more rapid rotation about one axis, the character of the spectrum is determined by the relationship between the rotation axis system of the molecule and the magnetic axes, fixed on the nitroxide group (Fig. 2). Rapid rotation about either the magnetic y or z axis is distinguishable from rotation about the magnetic x axis, parallel to the NO bond[31–33].

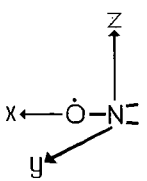

Fig. 2. Nitroxide fragment, showing the magnetic axes associated with the nitroxide group. The molecular (rotation) axes may or may not coincide with the magnetic axes on the NO group.

In the case of dilute solutions, the variation of the widths of the three spectral lines in the nitroxide radical undergoing rapid rotational motion can be used to determine the exact rotational anisotropy as well as a rotational correlation time. Such a correlation time gives information about the effective microviscosity of the environment about the radical. When the radical exhibits slower tumbling (less than 10^9 s^{-1}), similar information is available but must be extracted by spectral simulation, based on the theory of Freed and co-workers[33]. In both cases, changes in rotational anisotropy can be correlated to changes in the configuration of the bonded surface.

Multiple radical sites

If there is more than one environment accessible to the radical and if the rate of exchange among the sites is not rapid, then the ESR signal consists of a superposition of signals from the different sites. Such information provides a picture of the heterogeneity of the surface, as well as information about the relative fraction in each site[31].

Exchange rates

In the case of multiple sites in equilibrium with each other, the rate of jumping among the sites can be gotten from the widths of the spectral lines. If the radical concentration is high enough, radical–radical encounters become frequent enough that spin exchange begins to appear as an equal broadening of all three lines. The rate of exchange is related to, among other things, the rate of diffusion of the radicals together, *i.e.*, translational mobility.

Label studies

Label studies on C_6 and C_{11} DOXYL-labeled silica have been reported recently by us[28]. These studies were performed statically, *i.e.*, run either on dry silica or silica wetted with a solvent. This system is typical of most previous spectroscopic studies on modified silica in that the sample is neither under pressure nor influenced by the motion of a flowing mobile phase. The results of these studies confirmed the two-site models proposed by Gilpin and co-workers[6,34] and the effect of the solvent on reducing the rigid nature of the bonded phase. However, our labeled silicas were the first true reversed-phase silicas reported which are ESR active and have a spacer chain of five or more methylene groups. Gilpin *et al.*[27] have also reported a static ESR study on silica, but this involved the use of TEMPOL which was modified through a reaction with the hydroxy group to form a silane with essentially no hydrocarbon spacer.

Typical spectra of the labeled C_6 silica are shown in Fig. 1 after conditioning with 100% methanol and 50% (v/v) aq. methanol as mobile phases. The first thing to note is that there is not a large difference in these spectra indicating that the labels are in relatively the same solvated environment. There is a small but measurable change in spectral anisotropy with the introduction of water indicating an increase in the rigidity of the system as expected[9]. Further studies are being conducted with various labeled phases, variable coverage and differing chain lengths in order to investigate bonded phase dynamics as a function of mobile-phase composition.

After initial conditioning and relaxation to a non-flow condition, upon sudden application of solvent flow and examination of the amplitude of the central line of the nitroxide label as a function of time shows that the amplitude of the center peak increases in time until a plateau is reached in about 30 min (Fig. 3). A calculation of

the area under the spectral peak shows no change with time so that the increase in amplitude is not from an increase in the number of radicals but rather must come from a narrowing of the central line. This indicates that the labeled environment is undergoing a reorientation that is somehow dependent upon pumping methanol through the system. If the pump is then shut off and the system is continually monitored as a function of time, the peak amplitude will then slowly decay over a period of several hours until the initial "relaxed" state is achieved. We have found this effect to be very reproducible in different columns. The same experiment with 50% methanol shows a similar, but greatly diminished, effect that is barely measurable in our system. The coupling constants for these series of spectra remain the same throughout the experiment indicating no significant change in the solvation of the environment of the label due to pumping the methanol through the silica.

One possible cause of the line narrowing effect with solvent flow is that the pores of the silica might not be filled at ambient pressure. This type of effect is seen in mercury porosiometry. With poorly wetting solvents, such as pure or nearly pure water, this effect has manifested itself as an increase in void volume with increasing head pressure on a column and increasing retention volume for solutes in mobile phases with high water content. (This is the opposite of what one would expect in a typical reversed-phase system[35,36].) One flaw in the pore filling argument is that methanol is a very effective wetting solvent, and normally no pressure is required to wet reversed-phase silica with methanol. Pressure is another possible cause. To find out whether pressure had an effect, the column was capped off at the outlet, and the inlet was connected to a reservoir containing methanol. The reservoir was, in turn, pressurized with compressed gas up to 700 p.s.i. No change in the ESR line amplitude

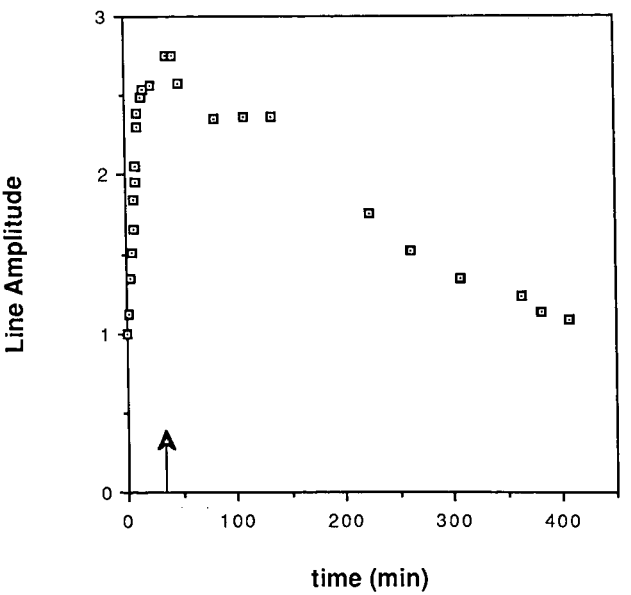

Fig. 3. Amplitude of the center line of the C_6 label as a function of time, beginning from a no-flow state and going to a flow-rate of 0.6 ml/min of methanol. After the maximum was reached, the pump was turned off (shown by the arrow), and the figure shows the decay of the amplitude to the original no-flow state.

was seen after 4 h under pressure. Since the maximum head pressure in the column was estimated to be about 200 p.s.i. under flow conditions, the restructuring of the bonded silica surface is not a pressure effect.

It is possible that the flowing methanol is causing a buildup of charge on the surface which, in turn, causes a reorientation of the hydrocarbon chains, similar to the effects of a charge on liquid crystals. Since our system is in a plastic and glass column with plastic inlets and outlets, the dissipation of this charge would be slow. Streaming potential is the term applied to the potential caused by a flowing stream of liquid and charge buildup has been a problem with non-aqueous solvents in contact with non-metallic surfaces[37]. Discharges caused by the high-speed fueling of jet aircraft is one example of the effects of streaming potential. These effects have been noted in the packing of reversed-phase columns (*cf.*, ref. 2, p. 214). This effect is reduced when aqueous solvents are used and/or when ions are present in the solvent. This is consistent with the fact that the ESR line amplitude increase with the flow-rate is greater in the 100% methanol than with 50% aq. methanol as the mobile phase. In previous studies, Gilpin and Squires[38] found that changes in bonded chain orientation can have chromatographic significance. At present, we are exploring the retention and band broadening effects of the orientational changes which we observe in the ESR spectra. The outcome of this study may add to our understanding of the need to "equilibrate" a column by passing several column volumes of mobile phase through before injecting samples in order to achieve reproducibility. An interesting possibility might be the eventual ability to control column selectivity characteristics through the use of an applied electric or magnetic field to orient the bonded moieties.

Probe studies

This work was performed by dissolving a small amount of a nitroxide compound, such as TEMPO, TEMPAMINE or TEMPOL in a typical chromatographic stationary phase and eluting this mixture through a test column until the ESR signal reached a maximum. It should be mentioned that at the concentrations used (*ca.* 10^{-4} *M*) no ESR signal could be seen from the nitroxide alone in solution. Therefore the spectra are assumed to be representative of the nitroxide sorbed on the solvated bonded silica surface only. Examples of the spectra in 50% aq. (v/v) methanol are seen in Fig. 4. Close examination of the spectrum of TEMPAMINE indicates that it is due to the superposition of two signals from different environments. TEMPO shows no effects from a second site and, in the 50:50 solvent, TEMPOL shows a barely visible hint of a second site. In the case of TEMPAMINE, the two sites differ markedly in the rotational mobility of the probe, as seen by the differences in lineshapes. The second probe site that appears with the introduction of water is very immobile (see the "wings" in Fig. 4). These immobile probes are sorbed at sites in which they are held more energetically. Fig. 5 shows the probes in a pure water solvent. An increase in the number of probes in the more energetic environment is noted. For instance, TEMPOL now shows an appreciable immobile component, although the separation of the wings is not as great as in the case of TEMPAMINE, indicating great rotational mobility for TEMPOL[39]. Hence, we note that the rotational mobility of the immobile site is in order of increasing rotational rate: TEMPAMINE < TEMPOL < TEMPO. This leads to an assignment of this second site to an environment where hydrogen bonding can occur. Most likely it is a region near the

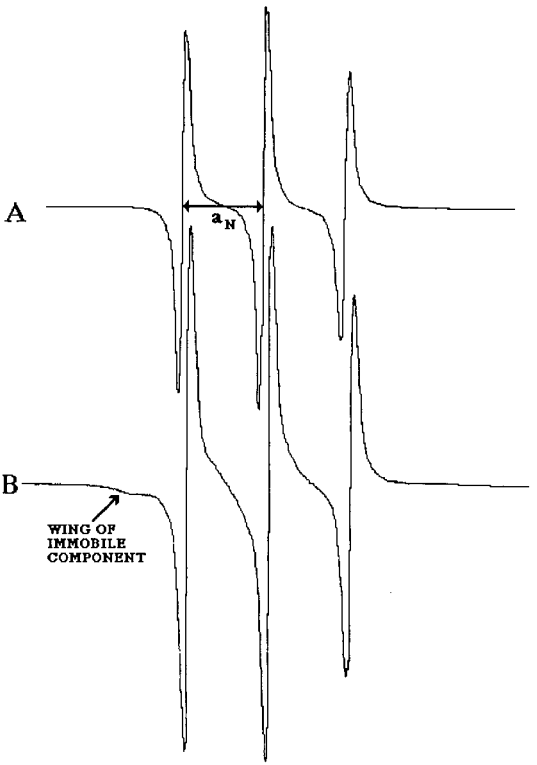

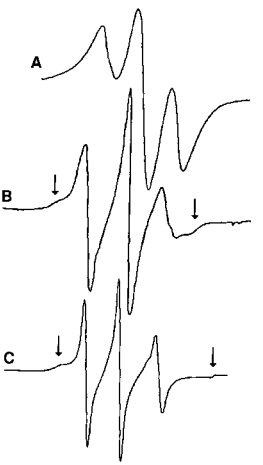

Fig. 4. ESR spectra of the TEMPO (A) and TEMPAMINE (B) spin probes, sorbed on the C_{18} bonded phase from 50% (v/v) aq. methanol mobile phase, flowing through the ESR sample-cell column. Magnetic field increases to the right. B shows a bump on the low-field side of the low-field sharp line from the second immobile site. The spectrum of TEMPOL probe is not shown, but differed little from TEMPO.

Fig. 5. ESR spectra of the TEMPO (A), TEMPOL (B) and TEMPAMINE (C) spin probes, sorbed on the C_{18} bonded phase from 100% water as the mobile phase, flowing through the ESR sample-cell column. The magnetic field increases to the right. The arrows indicate the locations of the low- and high-field extremes from probes in a second immobile site. The TEMPO spectrum is spin-exchange broadened because of the large increase in the sorption equilibrium of TEMPO in pure water as the solvent.

surface that is richer in water or a water-rich solvated region of the stationary phase, probably very near the mobile–stationary phase interface. The immobility of the two probes with polar tails probably reflects hydrogen bonding with surface silanols or imbibed mobile phase. The greater rigidity of TEMPAMINE could be due to actual proton transfer from the acidic silanol hydrogens to the amine group. We note that in bonded-phase liquid chromatography, amines will often "tail", due to interactions with the underivatized silanols. These results directly confirm that interaction.

In Fig. 6 the nitroxide coupling constant, a_N, of the free probe, TEMPO, as a function of solvent composition is plotted for the methanol–water system. Windle's[29] value for water is included in the figure to establish the extreme for highly polar solvents. To establish what the coupling constant would be in a pure hydrocarbon environment, we measured TEMPO $a_N = 15.3 \pm 0.2$ G in octane at room temperature. For the free probe in solution, Fig. 6 shows, as expected[29,30], that the coupling

constant increases monotonically with the water content. Using these results, we can then use the measured a_N value of the sorbed probe to determine the nature of the stationary phase solvation, *i.e.*, % methanol. Examination of the TEMPO probe behavior in the C_{18} bonded phase shows that the coupling constant is not a function of the water content of the mobile phase and that it is, within experimental error, the same as the coupling constant in pure methanol —well above the measured value in pure hydrocarbon environment of 15.3 G. We conclude that the C_{18} phase becomes well solvated with methanol above 25% methanol and that the water content of the polymeric stationary phase in which TEMPO is sorbed does not change significantly. This is consistent with the results of others, who have determined the extent of solvation of the stationary phase in reversed-phase systems[35,36,40,41]. It should be noted that the probe method is a vastly easier method of establishing stationary phase composition. It is interesting to note that the solvated environment for the probe is pure methanol, unmodified by the hydrocarbon bonded phase. This suggests that a relatively non-polar solute like TEMPO appears to dissolve in "pools" of organic solvent embedded in the non-polar stationary phase.

Beyond the consideration of the preferential sorption of the organic component of the mobile phase in the hydrocarbon environment, attention must be given to the nature of the solute. Table I shows a list of the capacity factors for a number of typical test solutes and the probes used in this study. It is seen that k' decreases for

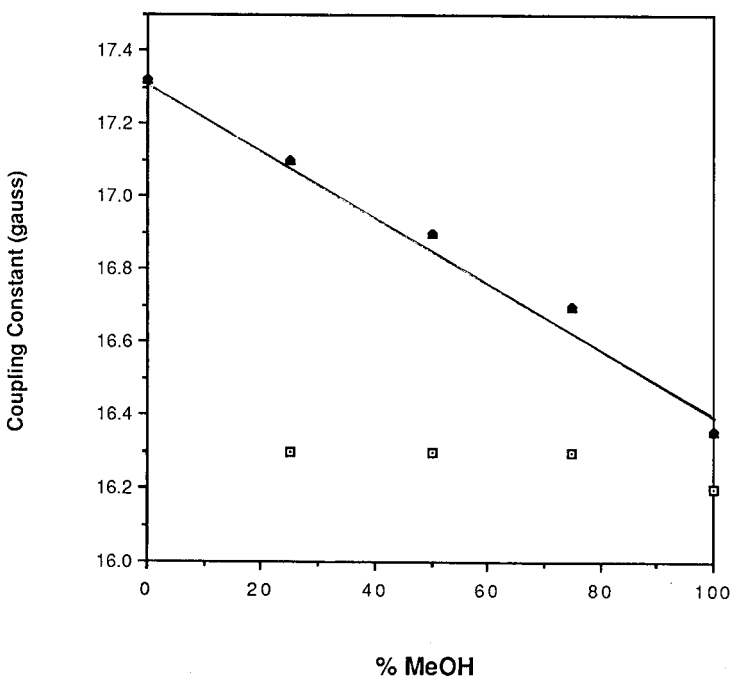

Fig. 6. Coupling constants, in gauss, for the sorbed TEMPO spin probe as a function of mobile phase composition for the methanol (MeOH)–water system in C_{18} bonded phase (squares) under flow conditions. Also shown are the values for free TEMPO, dissolved in the mixed solvent (triangles). Coupling constant for the free probe in pure water is from ref. 29.

TABLE I

CAPACITY FACTORS FOR TYPICAL SOLUTES AND ESR PROBES ON BOND ELUT C_{18} WITH 50% (v/v) AQ. METHANOL

Solute	*Capacity factor (k')*
Aniline	2.61
Acetophone	5.20
Nitrobenzene	7.13
Benzene	11.1
Toluene	25.2
TEMPOL	1.83
TEMPAMINE	2.16
TEMPO	19.9

TEMPO > TEMPOL > TEMPAMINE in the order given. It should be noted that TEMPO is quite hydrophobic, since it has a k' value of 19.9 that is comparable to toluene at 25.2 and greater than benzene at 11.1 (all determined on a C_{18} Bond Elut phase). Previous studies have indicated that different solutes appear to contact different zones on the solvated stationary phase[13,41]. Using the linear correlation between a_N and % methanol (see Fig. 6) and interpolating the a_N *vs.* % methanol found individually for TEMPO, TEMPAMINE and TEMPOL, a value for the effective concentration of methanol in the zone where the probe is sorbed can be determined. The most non-polar probe, TEMPO, is sorbed in a surface region where the environment is *ca.* 90% methanol, even though the mobile phase contained only 50% methanol in this case. The polar probes TEMPOL and TEMPAMINE, on the other hand, are sorbed into a region that contains *ca.* 60% methanol. This type of behavior has been observed before by Schunk[41], who noted significant differences in the retention of various solute probes as a function of temperature. He suggested that solute probes that penetrated the solvated surface more deeply would respond to temperature-induced phase changes at a higher temperature and *vice versa*. Our method can give similar information and we believe that we can eventually probe the surface in depth as well as determine the "topography" of the surface.

CONCLUSIONS

ESR label studies have shown the existence of flow-induced structuring of the stationary phase. These studies also show a change in the configuration of the stationary phase upon the introduction of water into the mobile phase, demonstrating spectroscopically the chain-stiffening infered from other techniques. The ESR probe studies have allowed us to develop a convenient polarity scale for the solute environment, based on coupling constants. This polarity scale can be used along with a variety of nitroxide probes to study the solvation of any permeable material that can be packed into a small tube. This work demonstrates the utility of the spin-label/probe technique to characterize surfaces of interest to chromatography.

ACKNOWLEDGEMENTS

The authors acknowledge the support of Knox College, E. I. du Pont de Nemours and NIH AREA grant No. GM37479-01 for this work.

REFERENCES

1 *Separation & Purification Critical Needs and Opportunities,* National Academy Press, Washington, DC, 1987.
2 L. R. Snyder and J. J. Kirkland, *Introduction to Modern Liquid Chromatography,* Wiley, New York, 2nd ed., 1979.
3 H. Colin and G. Guiochon, *J. Chromatogr.,* 141 (1977) 289.
4 W. R. Melander and Cs. Horváth, in Cs. Horváth (Editor), *High Performance Liquid Chromatography —Advances and Perspectives,* Vol. 2, Academic Press, New York, 1980, p. 113.
5 R. K. Gilpin, *J. Chromatogr. Sci.,* 22 (1984) 371.
6 R. K. Gilpin, *Anal. Chem.,* 57 (1985) 1465A.
7 J. W. Carr and J. M. Harris, *Anal. Chem.,* 58 (1986) 626.
8 J. W. Carr and J. M. Harris, *Anal. Chem.,* 59 (1987) 2546.
9 R. K. Gilpin and M. E. Gangoda, *J. Chromatogr. Sci.,* 22 (1983) 352.
10 R. K. Gilpin and M. E. Gangoda, *J. Magn. Reson.,* 64 (1985) 408.
11 L. C. Sander, J. B. Callis and L. R. Field, *Anal. Chem.,* 55 (1983) 1068.
12 C. H. Lochmuller, A. S. Colburn, M. L. Hunnicutt and J. M. Harris, *Anal. Chem.,* 55 (1983) 1344.
13 T. C. Schunk, *Ph.D. Dissertation,* University of Arizona, Tucson, AZ, 1985.
14 L. J. Berliner (Editor), *Spin Labeling: Theory and Applications,* Academic Press, New York, 1976.
15 L. J. Berliner (Editor), *Spin Labeling II,* Academic Press, New York, 1979.
16 R. F. Boyer and S. E. Keinath (Editors), *Molecular Motion in Polymers by ESR (MMI Press Symposium Series,* Vol. I), Harwood Academic Press, New York, 1980.
17 H. Hommel, A. P. Legrand, H. Balard and E. P. Papirer, *Polymer,* 25 (1984) 1297.
18 H. Hommel, A. P. Legrand, P. Tougne, H. Balard and E. P. Papirer, *Macromolecules,* 17 (1984) 1578.
19 H. Hommel, A. P. Legrand, H. Balard and E. P. Papirer, *Polymer,* 24 (1983) 959.
20 H. Hommel, L. Facchini, A. P. Legrand and J. Lecourtier, *Eur. Polym. J.,* 4 (1978) 803.
21 N. Sistovaros, W. O. Riede and H. Sillescu, *Ber. Bunsenges. Phys. Chem.,* 79 (1975) 882.
22 G. Martini, M. F. Ottaviani and M. Romanelli, *J. Colloid Interface Sci.,* 94 (1983) 105.
23 M. Romanelli, M. F. Ottaviani and G. Martini, *J. Colloid Interface Sci.,* 96 (1983) 373.
24 G. Martini and M. Bindi, *J. Colloid Interface Sci.,* 108 (1985) 133.
25 G. Martini, M. Bindi, M. Francesca and M. Romanelli, *J. Colloid Interface Sci.,* 108 (1985) 140.
26 J. S. Hwang, W. A. Al-Rashid and M. M. Saleem, *J. Phys. Chem.,* 92 (1988) 3630.
27 R. K. Gilpin, A. Kasturi and E. Gelerinter, *Anal. Chem.,* 59 (1987) 1177.
28 T. Malcom, J. Gorse and R. G. Kooser, *J. High Resolut. Chromatogr. Chromatogr. Commun.,* 11 (1988) 416.
29 J. Windle, *J. Magn. Reson.,* 4 (1981) 432.
30 S. A. Zager and J. H. Freed, *J. Phys. Chem.,* 77 (1982) 3344.
31 O. H. Griffith and P. C. Jost, in L. J. Berliner (Editor), *Spin Labeling: Theory and Applications,* Academic Press, New York, 1976, pp. 453–523.
32 S. A. Goldman, G. V. Bruno and J. H. Freed, *J. Chem. Phys.,* 56 (1972) 716.
33 J. S. Hwang, R. P. Mason, L. P. Hwang and J. H. Freed, *J. Phys. Chem.,* 79 (1975) 489.
34 B. R. Suffolk and R. K. Gilpin, *J. Chromatogr. Sci.,* 24 (1986) 423.
35 R. M. McCormick and B. L. Karger, *Anal. Chem.,* 52 (1980) 2249.
36 R. P. W. Scott and C. F. Simpson, *J. Chromatogr.,* 197 (1980) 11.
37 A. W. Adamson, *A Textbook of Physical Chemistry,* Academic Press, New York, 2nd ed., 1979, p. 919.
38 R. K. Gilpin and J. A. Squires, *J. Chromatogr. Sci.,* 19 (1981) 195.
39 J. H. Freed, in L. J. Berliner (Editor), *Spin Labeling: Theory and Applications,* Academic Press, New York, 1976, pp. 53–132.
40 C. R. Yonker, T. A. Zwier and M. F. Burke, *J. Chromatogr.,* 241 (1982) 257.
41 J. Gorse and M. F. Burke, *J. Liq. Chromatogr.,* 10 (1987) 1049.

Journal of Chromatography, 458 (1989) 267–279
Elsevier Science Publishers B.V., Amsterdam — Printed in The Netherlands

CHROMSMP. 1449

INSIGHTS INTO THE SLURRY PACKING AND BED STRUCTURE OF CAPILLARY LIQUID CHROMATOGRAPHIC COLUMNS

DENNIS C. SHELLY*, V. L. ANTONUCCI, T. J. EDKINS and T. J. DALTON
Department of Chemistry and Chemical Engineering, Stevens Institute of Technology, Hoboken, NJ 07030 (U.S.A.)

SUMMARY

New techniques have been developed for studying filtration phenomena and packing structure in slurry-packed fused-silica microcolumns. Filtration was studied by direct measurement of packing pressure, flow-rate, bed height and time using a computer-interfaced packing apparatus. Optical microscopy methods and image analysis techniques were used to study packing structure. These results plus chromatographic figures of merit were combined in order to learn more about the packing process and its relationship to chromatographic performance.

INTRODUCTION

Fused-silica microcolumns have recently been used to study the slurry-packing technique. Shelly and Edkins[1] have identified some of the unique features of these columns which influence the way in which they are packed and a novel method by which the packing process can be studied. The reproducible preparation of stable, efficient fused-silica microcolumns packed with 5-μm reversed-phase material[2] and various polar bonded phases[3] has been reported. In the papers cited, details of the slurry and pump solvent choices, nature of the pressure–time profile and post-packing conditioning schemes were given. Verzele *et al.*[4] examined some new aspects of slurry packing, such as particle shape and size effects. A comprehensive review of microcolumn technology was presented by Novotny[5]. The packing of several types of "microscale" columns was described by Ishii *et al.*[6].

Despite these advances, the reproducible preparation of efficient and stable microcolumns containing 3-μm and smaller particles remains elusive. We have attempted to develop an improved understanding of slurry packing, especially the packing of 3-μm octadecylsilane (ODS)-bonded particles, using an array of techniques and concepts from several technologies. Slurry packing can be viewed as a complex process involving three distinct phenomena: (a) colloid chemistry, (b) slurry rheology and (c) particle filtration[1]. When slurries have a low solids content, rheological effects tend to be minimal. However, colloid chemistry (interfacial tension and electrostatics) and particle filtration are critically important to the preparation of good chromatographic beds (filter cakes)[1]. A tetrahydrofuran–methanol slurry–packing solvent combination, followed by water conditioning, yields very stable fused-silica micro-

0021-9673/88/$03.50

columns with a performance reproducibility of 1.33% (relative standard deviation on the minimum reduced plate height, h_{min}, where $h_{min} = 4.8$)[1]. In an effort to obtain more efficient columns, we have focused on particle filtration and the resulting bed structure associated with our approach to slurry packing. Recently, Hoffman and Blomberg[7] suggested that filtration, influenced by slurry density, is particularly important in the packing of 3-μm particles.

This paper deals explicitly with our efforts to understand particle filtration and structural effects of the fused-silica microcolumn chromatographic beds. Our first objective was to develop a fully instrumented packing apparatus with which we could control and measure pressure, flow-rate, bed-height and time during packing. The development of novel bed visualization techniques was our second objective. Our third objective was to identify those unique material properties which are fundamentally important to the packing process. These studies are a logical extension of our previous attempts[1] to develop an improved understanding of the packing of 3-μm particles in fused-silica microcolumns.

EXPERIMENTAL

Computer-controlled pump

An ISCO (Lincoln, NE, U.S.A.) μLC-500 syringe pump was interfaced to a Leading Edge (Canton, MA, U.S.A.) Model D computer using a Model INST 54 analog-to-digital interface (Cyber Research, New Haven, CT, U.S.A.). The computer was equipped with version 3.10 of MS-DOS and version 3.11 of BASIC. A Model DT707 screw terminal panel (Data Translation, Marlboro, MA, U.S.A.) was used to connect the interface to the pump via a 3-m long shielded cable.

A BASIC program (*ca.* 950 lines) was written for pump control and monitoring. The pump was operated in the controlled-pressure mode in which the pressure–time relationship was defined by any of three options: linear, logarithmic or a logarithmically-modified linear. Pressure, flow-rate and time were stored to disk during a pressurization cycle. All packing experiments began at atmospheric pressure and proceeded to a defined pressure. For the linear profile, the slope of the curve, in p.s.i./s, was selected in addition to the final pressure. For the logarithmic profile, the pressure (P)–time (t) relationship was defined by $P = a(t^{3/2} - t^{6/5})$, where $1.0 < a < 1.15$ and a was user-selectable. This function and the values of a were chosen from extensive modeling of a desired logarithmic pressure *vs.* time profile that would allow a maximum pressure to be achieved in about 15 min. The logarithmically modified linear profile was implemented by beginning with a linear profile (with a selectable slope) and converting to a logarithmic profile (using the relationship described above) at the desired switch-over pressure. Thus, three variables were selected for this option: slope, a and switch pressure. Three consecutive analog-to-digital conversions were averaged for each stored pressure and flow-rate data point. After pressurization, a monitoring period of varibable duration could be implemented. All stored data could be restored and displayed in tabular form or as pressure *vs.* time and flow-rate *vs.* time plots. Other features included pump stop and start, automatic shutdown at over-pressure (9500 p.s.i.) and pressure transducer compensation control.

Bed visualization measurements

A photographic enlarger–mask combination was developed to visualize sections of packed fused-silica microcolumns. The mask was fabricated by means of photographic techniques and standard laboratory hardware. Fig. 1 shows a line drawing of the mask design. The mask image was defined from a 1.4 mm wide line, photographically reproduced on to Kodalith negative film (Eastman Kodak, Rochester, NY, U.S.A.), resulting in an average line width of 0.2 mm. Four strips of paper tape were positioned as shown in order to form a channel in which the fused-silica microcolumn would be reproducibly positioned in the mask opening. The mask was attached to a frame-type film holder, supplied with the enlarger.

A Model 67C enlarger (Charles Beseler, Florham Park, NJ, U.S.A.) was controlled by a Model 300 darkroom timer (DIMCO*Gray, Dayton, OH, U.S.A.). A mask was used to isolate light from a 0.2 mm wide, 35 mm long portion of the column. Each segment was enlarged to 0.9 mm wide and 225 mm long. Black-and-white photographic paper (Eastman Kodak) and a No. 2 contrast enhancement filter (Ilford, Cheshire, U.K.) were used to produce the prints. A 12 ± 0.5 s exposure time (aperture = $f/8$) was used for each segment. Translation from one column segment to the next was accomplished by partially releasing tension in the mask–frame sandwich and pulling the column through in 35 ± 3 mm portions. Prior to visualization, each column was flushed with acetonitrile followed by carbon tetrachloride, the latter being used as a refractive index matching liquid.

Material properties studies

A series of experiments that compared material properties of two commercial packings were designed. Two commonly used spherical 3-μm ODS packings were chosen: Spherisorb ODS-2 (Lot 26/79) and Hypersil (Lots 1743 and 11 1383). Both were obtained from Keystone Scientific (State College, PA, U.S.A.).

Specific gravity measurements. Moore/van Slyke specific gravity bottles (National Glass and Plastic, Camden, NJ, U.S.A.) were used for both solvents and slurries. After the specific gravity of solvent alone (tetrahydrofuran, THF) and of the solvent + particles had been determined, the specific gravity of the particles was calculated by difference. THF was chosen because the particles approximate defloculated behavior when suspended in this solvent, thus minimizing errors caused by air entrapment or non-uniform wetting during agglomeration.

Sediment quotient study. A sediment quotient study[1] was performed in order to obtain the settling tendencies of the materials. The solids content was 120 mg/ml, representing the actural slurry concentration used when packing a fused-silica microcolumn.

Interfacial tension measurements. The technique described by Absolom and Barford[8] was used, except that the 1-propanol–water mixtures spanned the surface tension range 25–31 mJ/m^2. For each of the packing materials, 160 mg were suspended in 400 μl of solvent (400 mg/ml). All slurries were degassed, sonicated and then transferred to settling tubes. Surface tension measurements of the solvent were performed with a Kruss (Hamburg, F.R.G.) Interfacial-Tensiometer K8. Final sediment quotient measurements were obtained after a 24–48-h settling time.

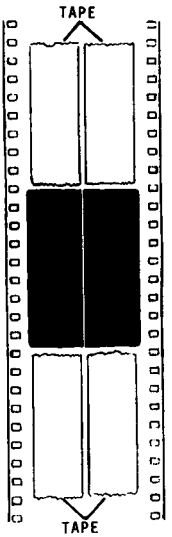

Fig. 1. Mask design.

On-column injector

A new on-column injector was fabricated which permitted convenient, dispersion-free sample injections. A modified stopped-flow technique[9,10] was used in which the top 2–3 mm of the column contained the sample, introduced using a micro-plunger. The details of this device will be given in a separate publication.

Chemicals and reagents

High-performance liquid chromatography-grade solvents (Burdick & Jackson, Muskegon, MI, U.S.A.) were used for all packing, slurry and elution solvents. All photographic chemicals (Eastman Kodak) were prepared and used according to manufacturer's directions. The column test mixture has been described previously[1]. Details of the column fabrication, including the fused-silica capillaries (Polymicro Technology, Phoenix, AZ, U.S.A.) and epoxy (Epoxy Technology, Billerica, MA, U.S.A.) that were used, has been described[1,11].

RESULTS AND DISCUSSION

Computer-controlled packing

Linear packing profile. The computer-controlled pump was used to pack fused-silica microcolumns, simultaneously storing pressure, flow-rate and time data for subsequent analysis.

Column 1 was packed using a linear pressurization profile with a slope of 19 p.s.i./s. Fig. 2A shows the pressure *vs.* time plot and Fig. 2B shows the flow-rate *vs.* time plot for the preparation of column 1. As pressure was the control parameter, we would expect the profile in Fig. 2A. The profile in Fig. 2B is also expected in that there is initially a high flow-rate, corresponding to slurry flowing to meet the frit, followed by a dramatic decrease in flow-rate as the bed begins to form. A steadily decreasing

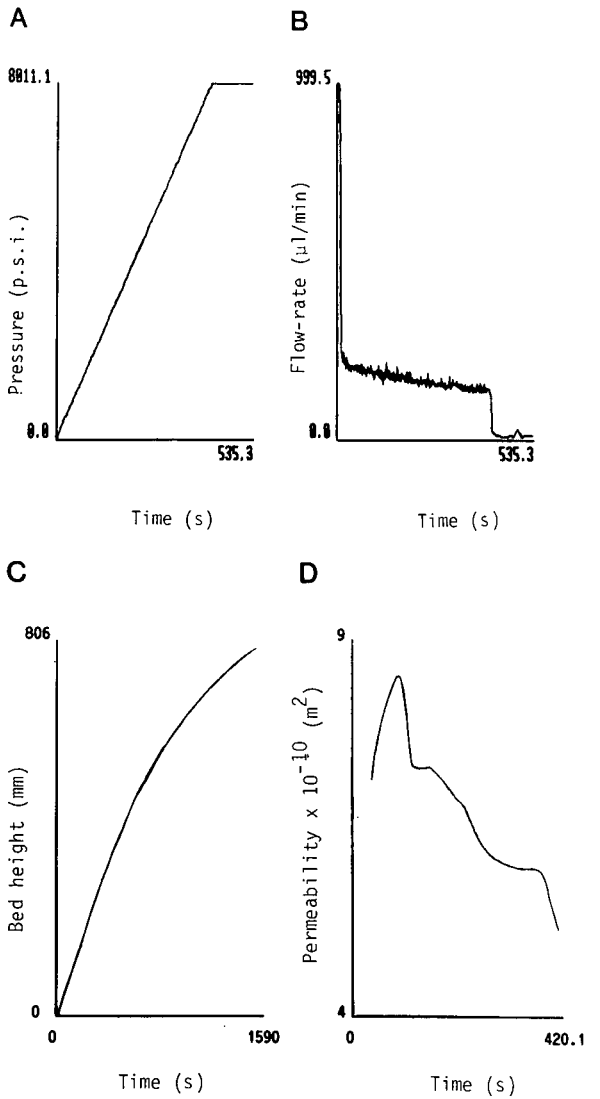

Fig. 2. Linear profile packing data. A, Pressure *versus* time plot; B, flow-rate *versus* time plot; C, bed-height *versus* time plot; D, permeability *versus* time plot.

flow-rate is seen, which indicates increasing resistance from a continuously increasing bed length. At 8000 p.s.i., the pressure remained constant, which explains the plateau in Fig. 2A and the drop in flow-rate in Fig. 2B. The bed height was recorded (manually) every 30 s by marking a length of tape, attached along the edge of a meter stick, which was placed next to the column. Fig. 2C shows a plot of bed height or length *vs.* time for the entire length of the column. The column required 1590 s to pack, hence approximately one third of the column was packed during the period indicated in Fig. 2A and B. Note that the bed height profile is not linear, especially over the last 300 mm.

It is reasonable to expect that the packing density in that region would be different from that in the rest of the column.

Integration of all the data can yield useful information concerning the permeability of the column. Bristow and Knox[12] gave two equations, which have a common variable, t_0. Eqn. 1 defines the total porosity, ε_T:

$$\varepsilon_T = \frac{4 f_v t_0}{\pi d_c^2 L} \tag{1}$$

where f_v is the volumetric flow-rate, t_0 is the void time, d_c is the column diameter and L is the column length. Eqn. 2 relates the specific column permeability, K^0, in terms of measurable parameters:

$$K^0 = \frac{\eta L^2}{\Delta p\, t_0} \tag{2}$$

where η is the mobile phase viscosity and Δp is the pressure differential. Solving both equations for t_0, setting them equal to each other and rearranging gives

$$\varepsilon_T K^0 = \frac{4 \eta f_v L}{\pi d_c^2 \Delta p} \tag{3}$$

According to Cramers *et al.*[13], K^0 is equal to $K/(\varepsilon_u + \varepsilon_i)$, where K is the bed permeability and ε_u and ε_i are the inter- and intra-particle porosities, respectively. Considering that $\varepsilon_T = \varepsilon_u + \varepsilon_i$, the left-hand side of eqn. 3 is simply K, the bed permeability. Using this information, we calculated permeability at several intervals, up to 8000 p.s.i., from the data shown in Fig. 2A, B and C. These results are shown in Fig. 2D. A predictable trend towards lower permeability with increasing time is shown in this plot. As yet, we have no adequate explanation for the steep rise in permeability in the first 100 s of the plot. Fluctuations in the flow-rate measurements could have caused some of the features of the plot. Two assumptions must hold for our approach to be valid, *i.e.*, that the measured system pressures and system flow-rates are solely attributable to the chromatographic bed. Any other contributions, such as clogging of the slurry reservoir or column, would introduce significant errors.

Logarithmic packing profile. By means of the computer-interfaced pump, another column was packed, using a logarithmic profile. Column 2 was packed using the logarithmic pressure–time profile with $a = 1.15$ and a final pressure of 8000 p.s.i. Fig. 3A, B, C and D show the same type of data, corresponding to column 1 and Fig. 2. The differences in Figs. 2 and 3 are remarkable. Fig. 3B shows an increasing flow-rate after the initial surge, attributable to the increasingly more rapid rate of pressurization as the pressure approaches 8000 p.s.i. However, there is a distinct flattening of the flow-rate curve as the pressure approaches the maximum. In Fig. 3C, there is greater linearity in the bed height–time profile than in Fig. 2C. Nonetheless, 2388 s were required to pack column 2. The differences indicated in Fig. 3B and C, compared with the same data in Fig. 2, could imply that the longitudinal uniformity of the packing density of the two columns would be very different. As in Fig. 2D, we calculated the

permeability at several intervals, using the data from Fig. 3A, B and C. Fig. 3D shows a shape that is very different from that in Fig. 2D. There is relatively constant permeability in the logarithmically packed column. This may suggest that the formation of the first few centimeters of the column dramatically affects the formation kinetics of the remainder of the bed. The filtration rate for the first 5 cm of column 2 was nearly half that for column 1. Hence the slope of the pressure–time profile influences the packing kinetics of the bed.

Column evaluation. The chromatographic performance of the two columns was evaluated as in a previous study[1]. Fig. 4 shows Van Deemter and Knox plots for both

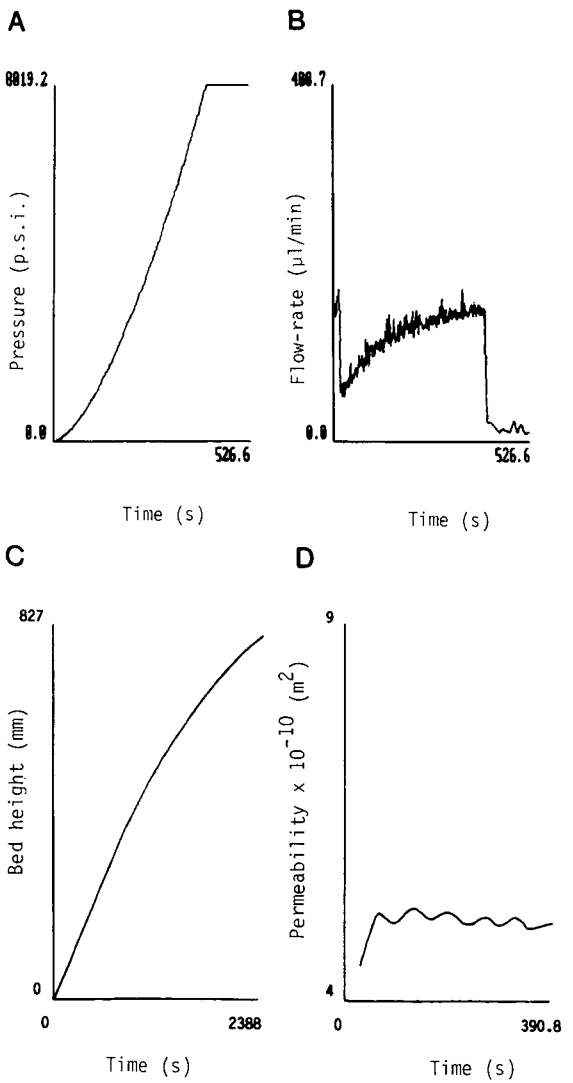

Fig. 3. Logarithmic profile packing data. A, Pressure *versus* time plot; B, flow-rate *versus* time plot; C, bed-height *versus* time plot; D, permeability *versus* time plot.

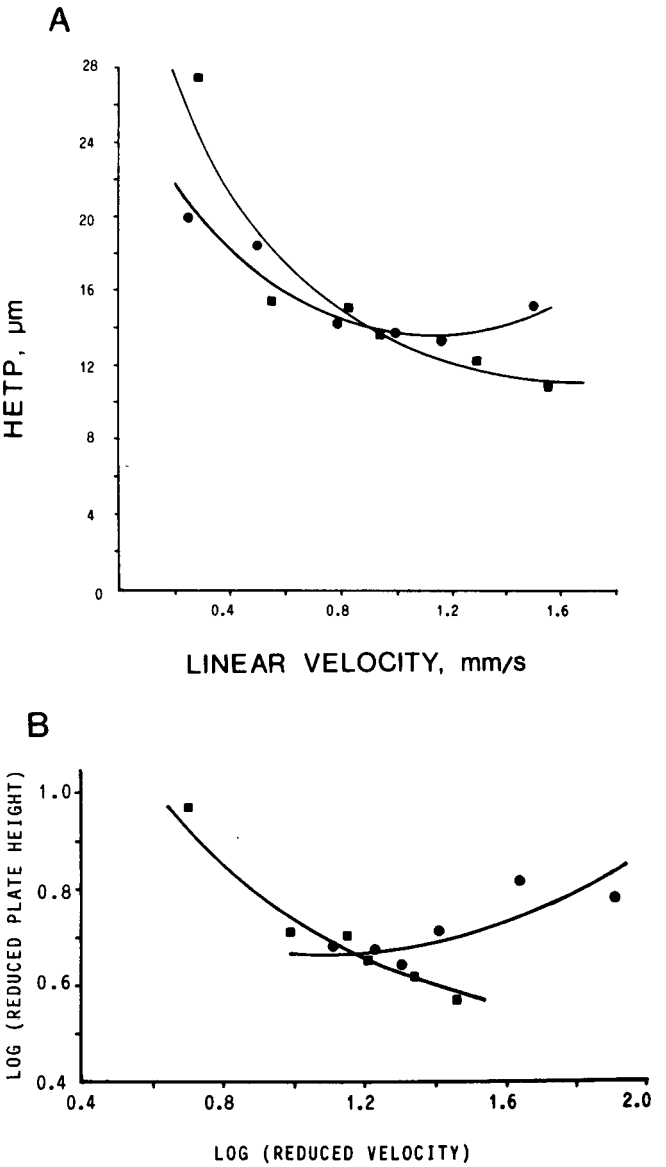

Fig. 4. Column performance analysis. ● = column 1, linear packing profile; ■ = column 2, logarithmic packing profile. A, Van Deemter plot; B, Knox plot.

columns. The linear column seems to display a fairly typical kinetic performance. However, the logarithic column shows significant longitudinal dispersion contributions and no distinct minima in either plot. Other pertinent performance data are listed in Table I. It can be seen from these data that the two columns are roughly equivalent, except for their optimal efficiencies. These results are the best we have obtained for 3-μm materials, but it is possible that Spherisorb material (this study) produces slightly

TABLE I

COLUMN PERFORMANCE DATA

Column	h_{min}	$K^0 \cdot 10^{-10}$ (cm^2)	ε_T	φ	E
1	4.45	1.49	0.94	602	11954
2	3.67	1.54	0.98	584	7886

more efficient columns than Hypersil material (see ref. 1). We suspect that our void volume marker is partly retained, hence the ε_T values are unusually high. However, lower t_0 values would also decrease the flow resistance factor, φ, and the separation impedance, E, and increase K^0. We observed no changes in bed height during column evaluation with the new on-column injector design. However, during repeated injections at 1000 p.s.i. some movement of the bed (in both columns) was noted.

Bed visualization measurements

The packing or bed structure of a chromatographic column has rarely been studied in a direct fashion. However, fluidized beds have been studied photographically with respect to mass transport[14] and phase structure[15]. Electron microscopy has been employed to illustrate the differences in packing columns with flocculated and deflocculated slurries[1]. Although this technique affords excellent resolution, the destructive nature of the sampling cannot be avoided. We have been pursuing the development of non-destructive techniques for viewing the particle packing structure of packed columns. Fused-silica microcolumns are an ideal test structure because of optical transparency, mechanical stability and ease of manipulation and handling. It is well known that the optical density of a packed bed changes, depending on the difference in refractive index of the mobile phase relative to that of the packing material. Hence it should be possible to observe directly differences in packing density by properly matching refractive indices and measuring a refractive-index-specific parameter, such as optical density.

Preliminary results from several experiments are presented here. Fig. 5 shows the projections of four segments from column 1. Keeping in mind that the segment from 70 to 105 mm was packed in the linear (constant filtration rate) portion of Fig. 2C and the segment extending from 735 to 770 mm was packed in a region of decreasing filtration rate, it is apparent that the optical differences in segments A and D are due to differences in filtration rate. As the mask–projection apparatus functions like a negative, the darker the image, the lighter is the exposure. Hence, more light propagates through the column in segment A than in segment D, primarily owing to a greater packing density in segment D than in segment A. Segment B shows the presence of bubbles, which completely disrupted the bed. This occurred although both ends were completely sealed with epoxy resin and despite the fact that this segment is approximately in the middle of the column. The mere presence of a bubble, under these conditions, may be indicative of mechanical stresses on the bed in this region of the column. Little direct evidence of the mechanical stability of packed fused-silica microcolumns is available from the literature. Segment C is darker than segment D, implying that a gradation of optical density and packing density occurs, roughly

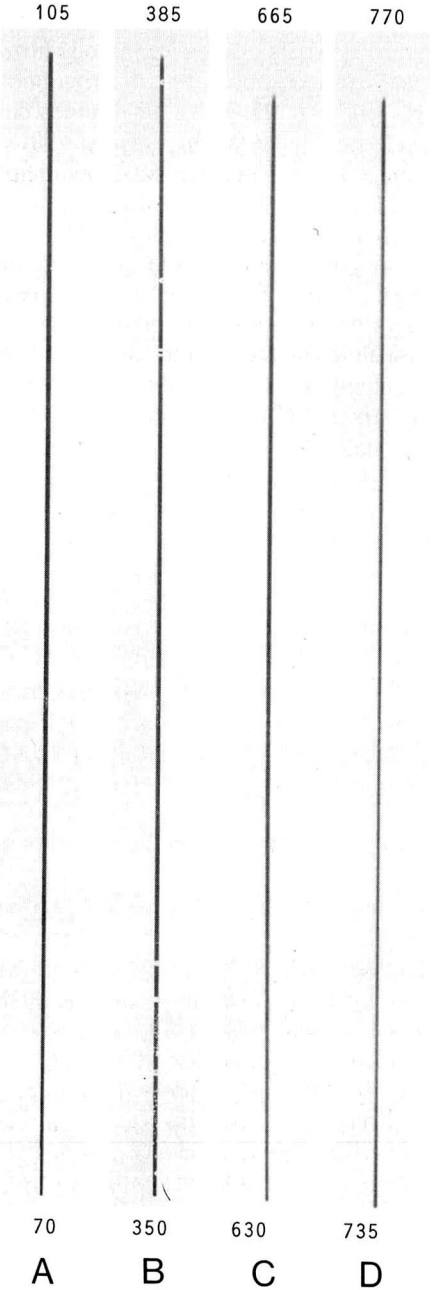

Fig. 5. Column projections for column 1, linear packing profile. A, 70–105 mm segment; B, 350–385 mm segment; C, 630–665 mm segment; D, 735–770 mm segment.

corresponding to the profile in Fig. 2A. The exposure-to-exposure reproducibility of the technique was very good. The positioning reproducibility of the technique was not as good, primarily owing to the inability to position the column accurately, because the column was not marked in any way along its length. However, the positioning accuracy within the mask was fairly good, as evidenced by the fact that segments A and B are similarly dark, yet separated by more than 200 mm. Bed structure, as evidenced by particle density, relates to porosity of the bed in a fairly straightforward manner. However, particle density relates to bed permeability in a more complex fashion. The data in Fig. 5 should be interpreted in this context. Unfortunately, column 2 could not be examined using this technique because its bed structure was accidently disrupted after the column evaluation studies.

Material property studies

Specific gravity measurements. Moore/van Slyke bottles were used to measure the specific gravity (ρ) of the solvent (THF), yielding excellent agreement with literature values ($\rho_{lit.} = 0.889$, $\rho_{expt.} = 0.883$ at 20°C)[16]. Although these bottles are routinely used for liquids, we also obtained reliable results for slurries. A value of 1.63 g/ml was measured for the Hypersil material compared with a value of 1.69 g/ml for the 3-μm Spherisorb. Based on a duplicate of Spherisorb, the precision was estimated to be better than 0.5%, indicating that there is a significant difference in their specific gravities. These results are in agreement with a previous report[7] in which a balanced-density technique was employed to pack 3-μm particles.

Sediment quotient study. Fig. 6A is a bar graph of sediment quotients (SQ) for two lots of Hypersil and one lot of Spherisorb. For both materials, methanol gave a higher SQ than THF. This is to be expected because methanol slurries exhibit flocculated properties and THF slurries show nearly deflocculated behavior[1]. It is important to note that the THF–Spherisorb slurry (bar C) gave a lower SQ than THF–Hypersil (bars A and B), because columns packed with Spherisorb have given better efficiencies than Hypersil-packed columns[17], indicating that there may be a relationship between extent of deflocculation and ultimate chromatographic efficiency.

Interfacial tension measurements. As indicated in Fig. 6B, both particle types gave identical interfacial tension (γ) results ($\gamma = 27.5$ mJ/m^2) although, as noted in the sediment quotient study, the absolute SQ values were different. A local maximum is reached at 27.5 mJ/m^2 and the curves steeply approach an SQ of 1000 as the interfacial tension extends beyond 28.25 mJ/m^2. This sharp increase is due to the vanishing wettability of the particles, which results in air and solvent bubbles becoming trapped in the particle aggregates. These data (Fig. 6B) also reflect the decreasing wettability of the reversed-phase packing by an increasingly aqueous medium. There may also be surface area and shape dependences on the measured interfacial tension, as our data for 3-μm spherical particles are much lower than for 5-μm irregular materials[8,18]. Our data suggest that the different sediment quotient values would appear to be related to differences in particle density rather than interfacial tension. Studies are in progress to confirm this relationship.

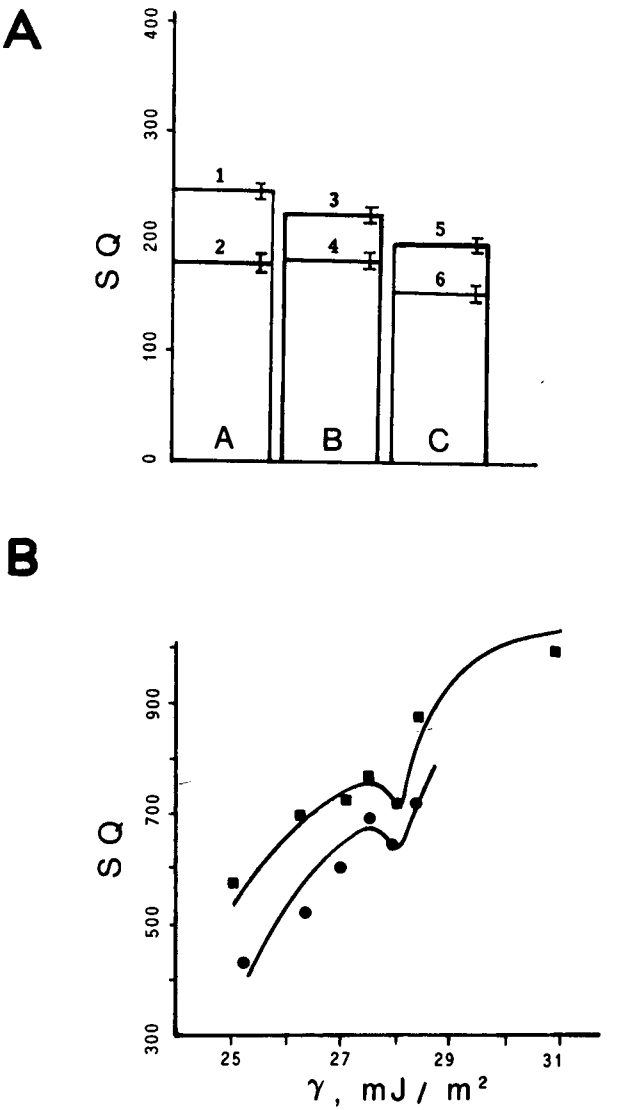

Fig. 6. Data on materials properties for 3-μm packings. A, Sediment quotient study. Section A, Shandon Hypersil ODS, Lot 1743; 1, methanol slurry; 2, tetrahydrofuran slurry. Section B: Shandon Hypersil ODS, Lot 11 1383: 3, methanol slurry; 4, tetrahydrofuran slurry. Section C: Spherisorb ODS2, Lot 26/79: 5, methanol slurry; 6, tetrahydrofuran slurry. B, Interfacial tension measurements ■ = Shandon Hypersil ODS, Lot 11 1383; ● = Spherisorb ODS 2, Lot 26/79.

CONCLUSIONS

Several important conclusions can be formulated from our work. First, more details of particle filtration, as a component of slurry packing, have been revealed. Constant-rate filtration appears to be very important, mainly to the extent of assuring

longitudinal uniformity of the packing density. The rate of filtration is also important, as evidenced by slightly lower reduced plate heights for the logarithmic profile packed column, which packed more slowly than the linear profile column. A lower slurry density should accomplish the same objective in a shorter time. Second, we have obtained direct evidence of a relationship between particle filtration rate and packing density. It appears that the faster the bed forms, the looser is the packing structure. To confirm this, we should have packed columns under the same kinetic constaints, *i.e.*, allowing the pressure to reach 8000 p.s.i. after 15 min for both the linear and logarithmic profiles. Third, a more complete description of slurry packing is emerging, a picture which contains three major components: colloid chemistry, slurry rheology and particle filtration. A unifying element in this description is basic materials properties, which can be used to explain why the particles behave as they do under various conditions. As we learn more about the materials aspects of chromatographic particles, we shall be better prepared to design and implement new column structures.

ACKNOWLEDGEMENTS

We express appreciation to Richard Henry of Keystone Scientific for many consultations and suggestions regarding the materials studies. We are also grateful to Richard A. Hartwick (Rutgers University) and Peter Carr (University of Minnesota) for their many helpful suggestions. We appreciate financial support, provided by the National Institutes of Health and the Governor's Commission on Science and Technology of New Jersey–Innovative Partnership Program.

REFERENCES

1 D. C. Shelly and T. J. Edkins, *J. Chromatogr.*, 411 (1987) 185.
2 C. Borra, S. M. Han and M. Novotny, *J. Chromatogr.*, 385 (1987) 75.
3 F. Andreolini, C. Borra and M. Novotny, *Anal. Chem.*, 59 (1987) 2428.
4 M. Verzele, C. Dewaele and D. Duquet, *J. Chromatogr.*, 391 (1987) 111.
5 M. Novotny, *Anal. Chem.*, 60 (1988) 500A.
6 D. Ishii, T. Takeuchi and A. Wada, in D. Ishii (Editor), *Introduction to Microscale High-Performance Liquid Chromatography*, VCH, New York, NY, 1988, Ch. 3, pp. 33–67.
7 S. Hoffmann and L. Blomberg, *Chromatographia*, 24 (1987) 417.
8 D. R. Absolom and R. A. Barford, *Anal. Chem.*, 60 (1988) 210.
9 Y. Hirata and M. Novotný, *J. Chromatogr.*, 186 (1979) 521.
10 Y. Hirata and K. Jinno, *J. High Resolut. Chromatogr. Chromatogr. Commun.*, 6 (1983) 196.
11 D. C. Shelly, J. C. Gluckman and M. V. Novotny, *Anal. Chem.*, 56 (1984) 2990.
12 P. A. Bristow and J. H. Knox, *Chromatographia*, 10 (1977) 279.
13 C. A. Cramers, J. A. Rijks and C. P. M. Schutjes, *Chromatographia*, 14 (1981) 439.
14 L. Massimilla and J. W. Westwater, *AIChE J.*, 6 (1960) 134.
15 P. L. Yue, L. Rizzuti and V. Augugliaro, *Chem. Eng. Sci.*, 41 (1986) 171.
16 R. C. Weast (Editor), *CRC Handbook of Chemistry and Physics*, CRC Press, Cleveland, OH, 54th ed., 1973, p. C306.
17 T. J. Edkins and D. C. Shelly, unpublished results, 1988.
18 R. A. Barford, personal communication, 1988.

Journal of Chromatography, 458 (1988) 281–286
Elsevier Science Publishers B.V., Amsterdam — Printed in The Netherlands

CHROMSYMP. 1440

NEW PACKING AND COLUMN FOR FAST PROTEIN HIGH-PERFORMANCE LIQUID CHROMATOGRAPHY

TED J. SZCZERBA*, DAVID N. BAEHR, LOUIS J. GLUNZ and JOHN A. PERRY
Regis Chemical Company, 8210 Austin Avenue, Morton Grove, IL 60053 (U.S.A.)
and
MICHAEL J. HOLDOWAY
Exmere Ltd., Hawarden, Clwyd (U.K.)

SUMMARY

Macromolecules can be quickly and effectively separated using packings with very small (either non-porous or wide-pore) particles in short columns. However, exploitation of this capability has until now been hampered by a lack of commercial availability. The first commercially available 3-μm, 300 Å, bonded-phase, spherical silicas and the capabilities of a 1-cm column (5-cm columns are also commercially available) packed with these silicas at pressures used in high-performance liquid chromatography are described. The particle pore size and size distribution of the silicas are highly reproducible; the resulting bonded-phase silicas are efficient and yield high protein recoveries. The 1-cm column, which can handle normal sample loads (we used up to 50 μl), can be used for either extremely rapid or slower, more discriminating separations. With a fast gradient, a baseline separation of a standard protein mixture is achievable in less than 90 s with only standard commercial instrumentation. The slow-gradient separations produced by the 1-cm column are virtually indistinguishable from those of a similarly packed 5-cm column.

INTRODUCTION

In an introduction to a study involving applications of 2-μm, 200-Å silica, Danielson and Kirkland[1] reviewed the concepts[2] and practices associated with the use of such small particles (diameter < 5 μm) for the separation of macromolecules. Because of improved mass transfer, such small particles should be able to separate macromolecules very quickly when packed into short columns[2]. Toward this end, Unger *et al.*[3] developed non-porous 1-μm silica microspheres and concluded that with them protein separations could indeed be fast and effective. However, the low load capacity of such non-porous particles limits their applicability, even aside from requirements for adequate peak retention and resolution[1]. Column length is another salient variable; Pearson[4] concluded that a column less than 1 cm long can provide not only increased recovery of but also sufficient resolution for molecules that are sufficiently different from each other. Stevens *et al.*[5] emphasized the importance of fast

0021-9673/88/$03.50

separations of proteins, peptides and other natural macromolecules in, for instance, certain clinical analyses.

Although small, wide-pore particles and short columns have great potential for the fast separation of macromolecules, their use has hitherto been severely hampered by a lack of commercial availability[1]. As a result of this study, a range of bonded phases, based on 3-μm, 300-Å silica, have become available and are marketed as Rexchrom (Regis, Morton Grove, IL, U.S.A.). We report here an evaluation of this first commercially available 3-μm, 300-Å bonded-phase, spherical silica, and the performance of a high-performance liquid chromatographic (HPLC) 1-cm column packed with this material (both 1- and 5-cm columns are commercially available).

EXPERIMENTAL AND RESULTS

Materials

Mobile phases were prepared with HPLC-grade water, acetonitrile, methanol (EM Science, Cherry Hill, NJ, U.S.A.) and trifluoroacetic acid (TFA) (Pierce, Rockford, IL, U.S.A.). Proteins (ribonuclease, insulin, lysozyme, myoglobin and ovalbumin) and dibutyl phthalate were purchased from Sigma (St. Louis, MO, U.S.A.).

Chromatographic experiments were carried out with standard commercial equipment. The Kratos (Ramsey, NJ, U.S.A.) gradient system used consisted of a Model 783G detector (flow-cell, 12 μl internal volume) that controls two Kratos Spectroflow 400 gradient pumps, and a dynamic high-pressure gradient mixer that combines the flow from the pumps. The internal diameter of the capillary tubing throughout the system was 0.01 in. Samples of 10 and 50 μl were injected with a Model 7010 injection valve (Rheodyne, Calabasas, CA, U.S.A.).

The 3-μm, 300-Å, wide-pore silica (Exsil A300) was specially manufactured and supplied by Exmere (Hawarden, Clwyd, U.K.). The particle-size distribution of this batch (1 kg) was determined by microscopy, and the mean diameter was found to be 3.2 μm, mode 3.1 μm, median 3.2 μm, with a standard deviation of 0.653 μm.

Size-exclusion chromatography (SEC) (Fig. 1) was carried out with polystyrene standards (Polymer Laboratories, Shropshire, U.K.) and tetrahydrofuran as mobile phase. The SEC data were transformed by the method developed by Jerebek[6] and showed a very narrow pore-size distribution with a mean pore diameter of 300 Å. Mercury porosimetry (Fig. 2) confirmed the extremely narrow pore-size distribution and indicated a mean pore diameter of 310 Å and a surface area of 97 m^2/g.

The pore volume, determined by titration with methanol by the method of Motlau[7], was 0.777 ml, compared with a differential volume of 0.79 ml found between 10 and 200 nm by mercury porosimetry.

Methods

By proprietary means to ensure a high protein recovery and a truly monomeric coating, an octadecyl stationary phase was bonded to the Exsil A300 silica to produce Rexchrom S3-300-ODS packing (Regis). Columns of 5 cm × 4.6 mm I.D. and 1 cm × 3.0 mm I.D. were packed with this material by proprietary means to achieve a high column efficiency with good peak symmetry. The efficiency of the columns was determined by the half-height method. With dibutyl phthalate (0.85 mg/ml) as the test

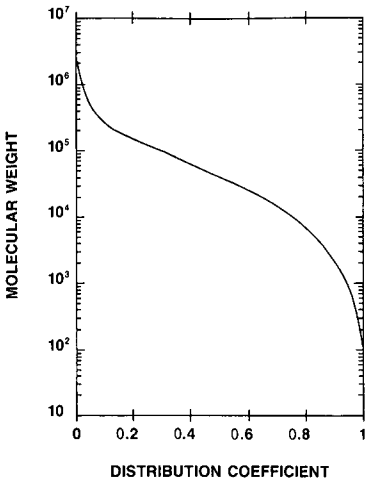

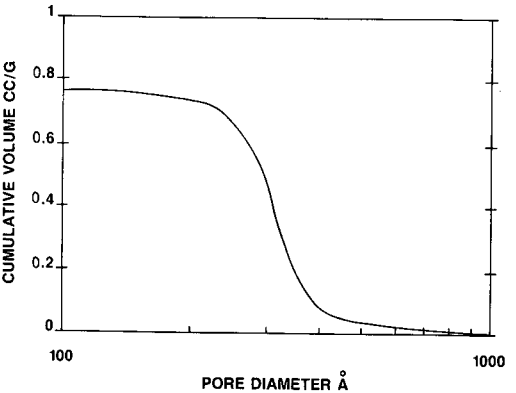

Fig. 1. Size-exclusion calibration graph for 3-μm, 300-Å silica (Exsil A300/3), obtained by using polystyrene standards in THF.

Fig. 2. Pore-size distribution of 3-μm, 300-Å silica (Exsil A300/3) obtained by mercury porosimetry.

substance, the column efficiency was measured with 70% methanol at a flow-rate of 0.5 ml/min with detection at 254 nm.

The protein test mixture was prepared by dissolving 15 mg of ribonuclease, 5 mg of insulin, 5 mg of lysozyme, 10 mg of myoglobin and 25 mg ovalbumin in 50 ml 0.1% TFA.

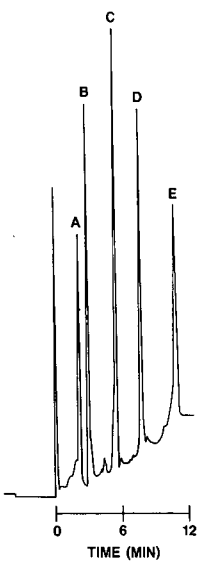

Fig. 3. Chromatogram of a five-component protein mixture: A = ribonuclease; B = insulin; C = lysozyme; D = myoglobin; E = ovalbumin. Column, 1 cm × 3.0 mm I.D. S3-300-ODS; gradient, from A–B (25:75) to 100% B in 25 min (A = 0.1% TFA, B = 0.1% TFA in 95% aq. acetonitrile; flow-rate, 1.0 ml/min; sample, 10 μl containing 12 μg of protein; pressure, 500 p.s.i.

For the chromatogram shown in Fig. 3, 10 μl of the test solution containing 12 μg of proteins were injected into a 1 cm × 3.0 mm I.D. column. For the chromatograms shown in Figs. 4 (1-cm column) and 5 (5-cm column), 50 μl of test solution containing 60 μg of proteins were injected. For the separation shown in Fig. 4, the sample was eluted with a combination of two linear gradients; this took only 2.25 min. Eluent A was 0.1% TFA and eluent B was 0.1% TFA in acetonitrile. The first gradient went from A–B (75:25) to A–B (25:75) in 1.00 min; the second proceeded to 100% in the next 1.25 min.

For Figs. 3 and 5, one 25-min linear gradient was used, from A–B (25:75) to 100% B, where eluent A was 0.1% TFA and eluent B was 0.1% TFA in 95% acetonitrile.

DISCUSSION

Silica

The previously outlined advantages that accrue from the development of

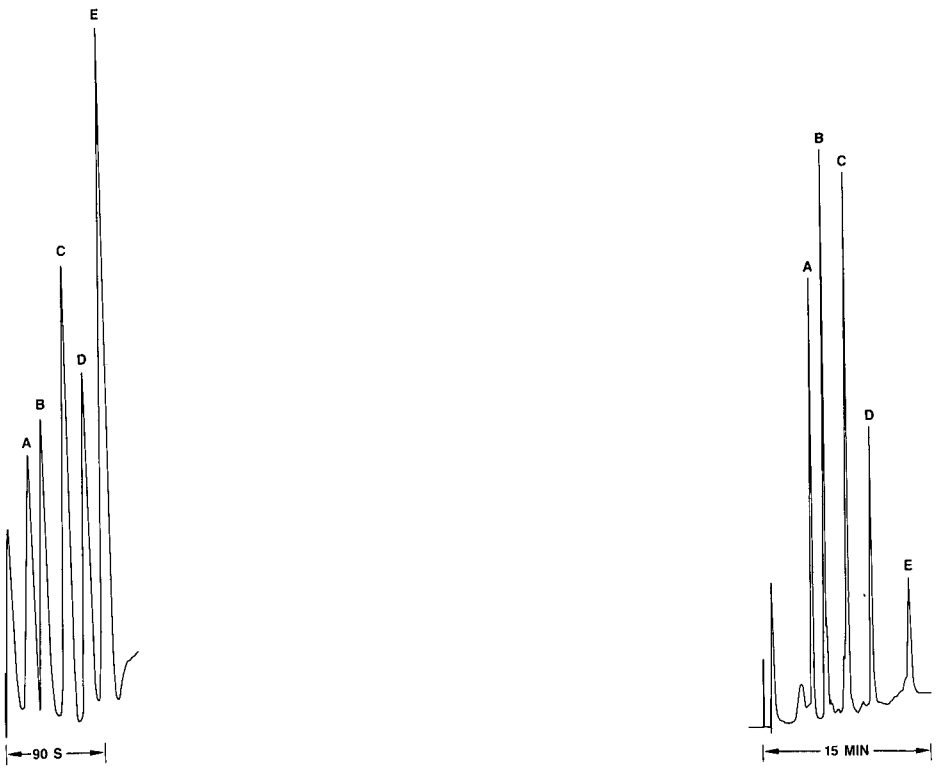

Fig. 4. Chromatogram of the same five-component protein mixture as in Fig. 3 with the same column but with a gradient from A–B (75:25) to A–B (25:75) in 1.00 min, then to 100% B in the next 1.25 min (A and B as in Fig. 3). Flow-rate, 3.5 ml/min; sample, 50 μl containing 60 μg of protein; pressure, 1900 p.s.i.

Fig. 5. Chromatogram of the same five-component protein mixture as in Fig. 3 with a 5 cm × 4.6 mm I.D. S3-300-ODS column and the same gradient as in Fig. 3. Flow-rate, 1.0 ml/min; sample, 50 μl containing 60 μg of protein; pressure, 1400 p.s.i.

a wide-pore silica based on 3-μm particles prompted Exmere to carry out a feasibility study on its manufacture as part of a joint study between Exmere and Regis. The proprietary processes developed by Exmere for the manufacture of 5- and 10-μm wide-pore silicas (Exsil A300) were extended to the preparation of 3-μm, 300-Å silica. The resulting silica was used in the work reported here.

The intrinsic properties of this new 3-μm silica were found to be identical with those of the larger diameter products. The extremely narrow pore-size distribution established for the Exsil A300 5-μm product (which compared favorably in this regard with competitive 5-μm, 300-Å silicas) was found to be maintained in the new 3-μm silica.

Bonding. Having found that the bonding procedures that heretofore had led to satisfactorily high chromatographic efficiency did not yield satisfactory protein recovery, we re-examined and recast the bonding methods in every detail. The new methods finally adopted, including end-capping, yield a strictly monomeric stationary phase, with a carbon load of 5.75% for ODS. Perhaps because each part of this strictly monomeric coating participates with equal effect in chromatography, proteins are retained more strongly by this packing than they are by comparable products. We found that the reproducibility of each stage of the bonding process could not be taken for granted but had to be, and was, separately established.

The 80 000 plates/m chromatographic efficiency of the new 3-μm, 300-Å ODS packing is much higher than that of other commercially available products. Nevertheless, it is much lower than the comparably tested, *ca.* 125 000 plates/m efficiency of the 3-μm, 100 Å ODS packing that we have bonded in exactly the same way. We cannot at present explain the discrepancy.

Performance of the 1-cm column

Fig. 4 illustrates both the rapid resolving ability of the 1-cm column and its high capacity. A baseline separation of the protein test mixture was achieved in less than 90 s with a sample load of 50 μl, containing 60 μg of protein.

Fig. 3 shows the relatively high resolution achievable with the 1-cm column when a slower gradient is employed. Indeed, it is not easy to distinguish between the chromatogram in Fig. 3, obtained with the 1-cm column, and that in Fig. 5, obtained with the 5-cm column. These results support Pearson's[4] conclusion that very short columns can provide sufficient resolution for pairs of molecules that show adequate differences in retention indices.

Shorter columns have another significant advantage over longer columns, *viz.* the back-pressure was 500 p.s.i. for the 1-cm column (Fig. 3) but 1400 p.s.i. for the 5-cm column (Fig. 5). Because these columns can easily withstand imposed pressures of 5000 p.s.i., flow-rates much higher than the 0.5 ml/min actually used could be tolerated. Under constant use and testing for 4 days, the columns performed consistently. No increase in back-pressure or loss of resolution was observed.

ACKNOWLEDGEMENTS

Thanks are due to G. O. Tame and E. M. Holdoway (both of Exmere) for much of the preparation and characterization of the silica support.

REFERENCES

1 N. D. Danielson and J. J. Kirkland, *Anal. Chem.*, 59 (1987) 2501–2506.
2 L. R. Snyder and J. J. Kirkland, *Introduction to Modern Liquid Chromatography*, Wiley, New York, 1979, Ch. 5.
3 K. K. Unger, G. Jilge, J. N. Kinkel and M. T. W. Hearn, *J. Chromatogr.*, 359 (1986) 61.
4 J. D. Pearson, *Anal. Biochem.*, 152 (1986) 189.
5 A. Stevens, T. Morrill and S. Parlante, *Biochromatography*, 1 (1986) 50.
6 K. Jerebek, *Anal. Chem.*, 57 (1985) 1595.
7 A. Y. Motlau, *Anal. Chem.*, 34 (1962) 714.

Journal of Chromatography, 458 (1989) 287–293
Elsevier Science Publishers B.V., Amsterdam — Printed in The Netherlands

CHROMSYMP. 1495

Note

Liquid chromatographic determination of low-molecular-weight amides in pharmaceutical matrices

S. V. SNOREK, B. A. OLSEN and D. A. PIERSON
Eli Lilly and Company, Tippecanoe Laboratories, P. O. Box 685, Lafayette, IN 47902 (U.S.A.)

Low-molecular-weight amides, such as N,N-dimethylformamide (DMF) and N,N-dimethylacetamide (DMAC), are common solvents in the chemical, agricultural, and pharmaceutical industries. Because of the potentially toxic properties of amides it is necessary to control their concentrations at very low levels in isolated products[1]. This requires a sensitive, accurate, and reproducible analytical method for the separation and quantitation of these analytes in organic matrices.

Gas chromatography (GC) has commonly been used for the separation and quantitation of low-molecular-weight amides in air or aqueous matrices[2,3]. GC methods for more complex matrices suffer from low sensitivity and interferences from the matrix. High-performance liquid chromatography (HPLC) was investigated as an alternative to GC for the determination of amides in several pharmaceutical compounds. In this note, we report methods for the separation and quantitation of acetamide, DMF and DMAC in complex matrices by HPLC. As examples, we present three applications of the method which have been studied in detail, including comparisons of HPLC and GC methods.

EXPERIMENTAL

Materials

Acetonitrile (HPLC grade) was purchased from Burdick & Jackson Labs. (Muskegon, MI, U.S.A.). All other chemicals employed were of reagent grade and were used without further purification. The water used was deionized and passed through a Millipore (Bedford, MA, U.S.A.) Milli-Q water purification system. All samples were powders of the bulk material obtained from Eli Lilly (Lafayette, IN, U.S.A.).

Chromatographic systems

HPLC experiments were conducted using a Spectra-Physics 8700 solvent-delivery system (San Jose, CA, U.S.A.) with a Micromeritics 728 autosampler (Norcross, GA, U.S.A.), a Valco fixed-loop injection valve (Houston, TX, U.S.A.) and a Kratos 757 variable-wavelength UV detector (Ramsey, NJ, U.S.A.). The chromatographic conditions were as follows: column, 250 mm × 4.6 mm I.D. Zorbax C_8 (DuPont, Wilmington, DE, U.S.A.) or Alltech C_{18} (Deerfield, IL, U.S.A.); mobile phase, 3–5% acetonitrile in 0.1 *M* phosphate buffer; flow-rate, 1–1.5 ml/min; temperature, ambi-

0021-9673/88/$03.50

ent; injection volume, 10–50 μl. All samples and standards were dissolved in 0.1 *M* phosphate buffer.

GC experiments were conducted using a Hewlett-Packard 5880 gas chromatograph with a flame ionization detector (Palo Alto, CA, U.S.A.) or a Tracor 570 gas chromatograph equipped with a nitrogen–phosphorus detector (Austin, TX, U.S.A.). The data were collected and processed with a Hewlett-Packard 1000 computer and analytical software developed in-house. The GC columns were obtained from the following sources: DB columns, J&W Scientific (Folsom, CA, U.S.A.); Porapak, Chromosorb, and OV-101 columns, Supelco (Bellefonte, PA, U.S.A.); Tenax, Scientific Products (McGaw Park, IL, U.S.A.).

RESULTS AND DISCUSSION

Determination of amides by HPLC

In the analysis of pharmaceutical samples for low-molecular-weight amides, separation of the analyte from the sample matrix is an important factor in obtaining adequate sensitivity. In this study, a reversed-phase HPLC system was developed which strongly retained the sample matrix while allowing the analyte to be eluted and detected. The baseline remained stable and free from interferences from the sample matrix for *ca.* ten injections before matrix components began to be eluted from the column. When these interferences were observed, the sample matrix was removed from the column by increasing the strength of the mobile phase. Although more time-consuming, the method could be automated by utilizing gradient elution after each injection as described in the section on the determination of DMAC. A wavelength of 210 nm was necessary for the detection of amides. As shown in Fig. 1, seven different amides were resolved under the conditions given. When this method was applied to different products, only slight modifications were necessary. The strength of the mobile phase, pH and flow-rate were adjusted to resolve the peak from the

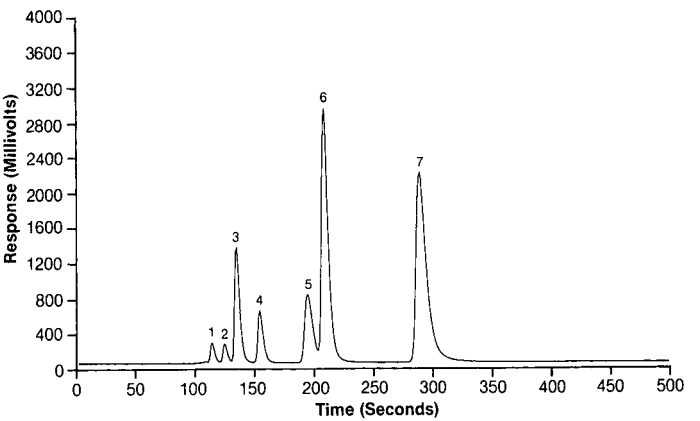

Fig. 1. HPLC chromatogram of low-molecular-weight amides. Column, Zorbax C_8 (5 μm, 250 mm × 4.6 mm I.D.); eluent, acetonitrile–0.1 *M* phosphate buffer, pH 2.5 (5:95); flow-rate, 1.5 ml/min; detection, 210 nm; temperature, ambient; injection volume, 10 μl. Peaks: 1 = formamide; 2 = acetamide; 3 = N-methylformamide; 4 = N-methylacetamide; 5 = N-ethylformamide; 6 = N,N-dimethylformamide; 7 = N,N-dimethylacetamide; all at a concentration of 0.1 mg/ml.

sample matrix, impurities, and baseline disturbances at the void volume. When increased sensitivity was required, the injection volume was increased.

Determination of acetamide

Previous methods for the determination of acetamide by GC utilized Tenax or a porous polymer, such as Poropak or Chromosorb, as the column packing material[4]. However, it was noted that with porous polymer packings quantitation of polar compounds, such as acetamide, was difficult. Below 100 μg/g, non-linear behavior and adsorption of the compounds by the column packing material were observed[5].

A Tenax column was evaluated for the GC determination of acetamide in a pharmaceutical product. The peak shape was acceptable but acetamide gave a low response in the flame ionization detector. A linearity and matrix study was performed by preparing a set of standards and spiked samples, covering a range from 10 to 200% of the target level in the sample. For example, if the maximum target level for the amide was 100 μg/g, standards and spiked samples were prepared covering a range of 10 to 200 μg/g of amide in the sample. Log–log slopes and coefficients of determination (r^2) were calculated from the least-squares line of the response–concentration plot for both standards and spiked samples. A linear response was indicated when the log–log slope of the least-squares line did not differ significantly from 1.0 and the coefficient of determination approached 1.0. To determine whether there was a matrix effect, the least-squares slope of the spiked samples was compared to that of the standards. Slope ratios differing significantly from 1.0 indicate the presence of a matrix effect[6,7]. The linearity and matrix validation are summarized in Table I. In this example, the slope ratio of 0.94 corresponded to a 6% error in the determination of the concentration over the concentration range tested. The negative intercept and the depressed log–log slope observed could be indicative of adsorption at low levels. Based on the sample concentration of 100 mg/ml, the detection limit was 50 μg/g for the GC–flame ionization detection of acetamide. In an effort to improve the sensitivity and eliminate the matrix effects, a nitrogen–phosphorus detector was evaluated. No improvement in sensitivity was observed. For this application, a detection limit of 10 μg/g or less, based on the sample weight was required.

Attempts to increase the sensitivity by increasing the sample concentration were not successful. At sample concentrations greater than 100 mg/ml, interferences from

TABLE I

SUMMARY OF VALIDATION STATISTICS

Analyte	*Method*	*Concentration range (μg/g)*	*Sample set*	*Slope*	*y intercept*	r^2	*log–log slope*	*Slope ratio*
Acetamide	GC	100–2000	Standards	$5.3 \cdot 10^4$	$-6.8 \cdot 10^2$	0.9964	0.84	
			Spikes	$5.0 \cdot 10^4$	$-7.6 \cdot 10^2$	0.9857	0.81	0.94
Acetamide	HPLC	10–200	Standards	9.1	$-2.4 \cdot 10^1$	0.9998	1.00	
			Spikes	8.2	$-1.5 \cdot 10^1$	0.9986	1.11	0.90
DMAC	HPLC	60–1300	Standards	$2.3 \cdot 10^6$	$-9.7 \cdot 10^1$	0.9993	1.01	
			Spikes	$2.3 \cdot 10^6$	$5.0 \cdot 10^4$	0.9985	1.05	1.01
DMF	HPLC	1–55	Standards	$8.1 \cdot 10^2$	$1.4 \cdot 10^2$	1.0000	1.00	
			Spikes	$8.0 \cdot 10^2$	$1.5 \cdot 10^2$	1.0000	1.02	0.98

TABLE II

GC CONDITIONS EVALUATED FOR THE DETERMINATION OF ACETAMIDE IN A PHARMACEUTICAL MATRIX

Solvent	*Column*	*Temperature (°C)*	*Comments*
Water	30 m × 0.32 mm I.D., 0.25-μm film DB-1	100	Detection limit 100 μg/g
Water	60 m × 0.32 mm I.D., 1-μm film DB-1	40–200	Detection limit 250 μg/g
Water	30 m × 0.53 mm I.D., 1.5-μm film DB-1	100	Irreproducible peaks
Methanol	30 m × 0.53 mm I.D., 1.5-μm film DB-1	40–250	Poor peak shape
Water	30 m × 0.53 mm I.D., 5-μm film DB-1	40–100	Poor peak shape
Water	15 m × 0.53 mm I.D., 1-μm film DB-17	40	Poor peak shape
Water	15 m × 0.53 mm I.D., 1-μm film DB-Wax	40	Poor peak shape
Methanol	15 m × 0.53 mm I.D., 1.5-μm film DB-1	40–80	Poor peak shape
Water	15 m × 0.53 mm I.D., 1.5-μm film DB-1	40–80	Irreproducible peaks
DMF	15 m × 0.53 mm I.D., 1.5-μm film DB-1	40–80	Coelutes with solvent
Water	6 ft. × 2 mm I.D., Porapak Q	100–250	Not eluted
Water	6 ft. × 2 mm I.D., Chromosorb 104	200–240	Sample builds up on column
Methanol	6 ft. × 2 mm I.D., 3% OV-101	40–200	Coelutes with solvent
DMF	6 ft. × 2 mm I.D., 3% OV-101	40–200	Coelutes with solvent
Water	6 ft. × 2 mm I.D., 3% OV-101	40–200	Irreproducible peaks

the sample matrix were severe. This was mainly due to the buildup of non-volatilized sample on the column and decomposition of the sample in the injector. As shown in Table II, other attempts to increase the sensitivity included: alternate column packings, narrow- and wide-bore capillary columns, and different sample solvents.

The HPLC method was explored as an alternative to GC. Conditions were developed for the determination of acetamide, and a linearity and matrix study was conducted covering the range from 10 μg/g to 200 μg/g, based on the sample concentration of 100 mg/ml. An example of the resulting HPLC elution profile is shown in

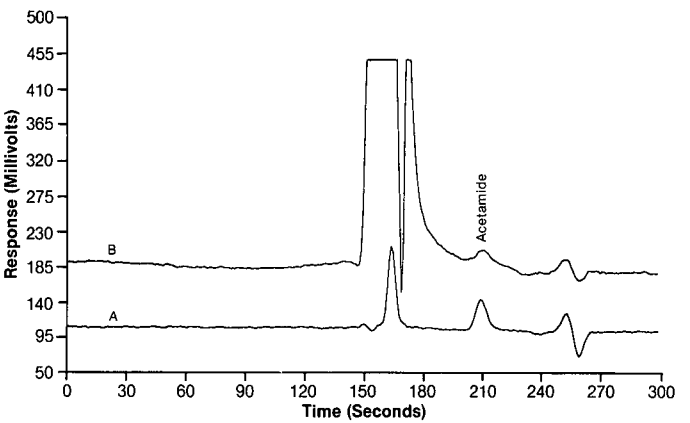

Fig. 2. HPLC chromatograms of acetamide in a pharmaceutical product. Column, Alltech C_{18} (10 μm, 250 mm × 4.6 mm I.D.); eluent, acetonitrile–0.1 *M* phosphate buffer, pH 4.4 (3:97); flow-rate, 1.0 ml/min; detection, 210 nm; temperature, ambient; injection volume, 10 μl. Samples: (A) standard acetamide solution (1 μg/ml); (B) sample (100 mg/ml) in phosphate buffer. Peak corresponds to a spike of 10 μg/g acetamide.

Fig. 2. The validation summary given in Table I indicates a matrix effect by HPLC, comparable to that observed by GC. However, a significant improvement in the detection limit by HPLC was observed. The detection limit by HPLC for acetamide in the pharmaceutical product was statistically determined to be 10 $\mu g/g$[8].

Determination of DMAC

Another application of the HPLC method for amides was the determination of DMAC in an antibiotic pharmaceutical product. GC has been the traditional method of choice for determining DMAC[9]. GC determinations were attempted with both packed columns containing Chromosorb 102 and DB-1 wide-bore capillary columns. Good resolution was obtained on both types of column. Unfortunately, the non-volatile product matrix built up at the front of the column and led to gradually increasing baselines and analyte carryover from one injection to the next. DMAC was observed in solvent blanks injected after sample injections. Fig. 3 is an illustration of the effect of sample injection on the baseline response and analyte carryover. Scan B shows a positive response for a sample which, because of the synthesis used, contained no DMAC. Scan C shows a spiked sample, which indicated a recovery of 140%. On a new DB-1 column, a detection limit of 0.2 mg/g was obtained. However, the sensitivity gradually decreased as samples were injected into the column. A level of detection of *ca.* 0.1 mg/g DMAC in the sample matrix was required.

The HPLC assay was developed and tested for linearity and matrix effects. Validation covered a concentration range of 0.06 to 1.3 mg/g, based on a sample concentration of 10 mg/ml. As shown in Table I, both spiked and unspiked calibration curves were linear with adequate coefficients of determination. A matrix effect was not observed in this application. The reproducibility of the method was estimated from results for control samples generated over a 6-month period. The assay was performed on ten separate days by two different analysts. The same instrument and column were used in each case. The resulting mean was 0.46 mg/g with a standard

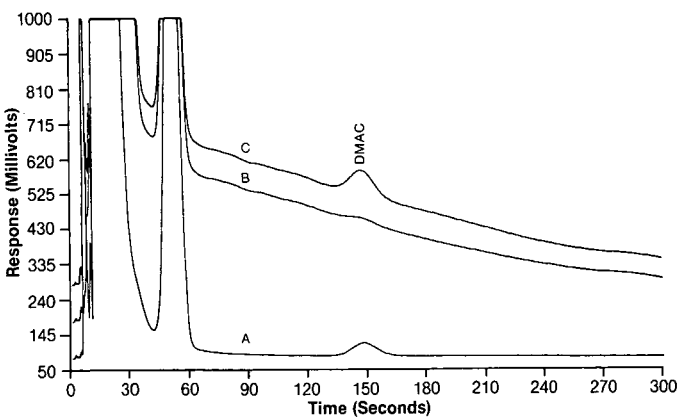

Fig. 3. GC chromatograms of DMAC in an antibiotic matrix. Column, Chromosorb 102 (3 ft. × 2 mm I.D., 80–100 mesh); carrier gas, helium; flow-rate, 25 ml/min; flame ionization detection; temperature, 200°C; injection volume, 12 μl. Samples: (A) standard DMAC solution (10 $\mu g/ml$); (B) sample (10 mg/ml) in dichloromethane; (C) sample spiked with the 10 $\mu g/ml$ DMAC standard.

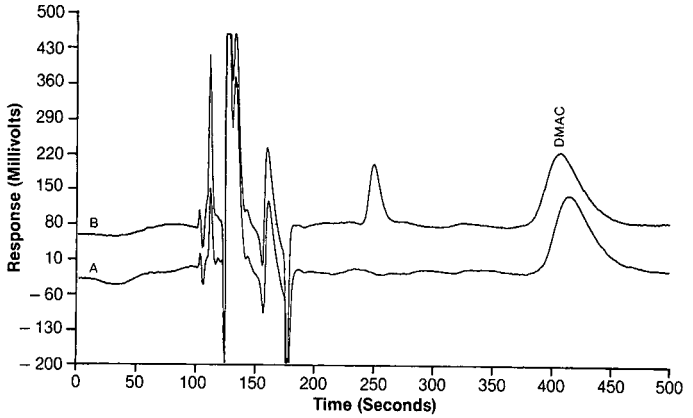

Fig. 4. HPLC chromatograms of DMAC in an antibiotic product. Column, Zorbax C_8 (5 μm, 250 mm × 4.6 mm I.D.); eluent, acetonitrile–0.1 *M* phosphate buffer, pH 2.5 (5:95); flow-rate, 1.5 ml/min; detection, 210 nm; temperature, ambient; injection volume, 10 μl. Samples: (A) standard DMAC solution (3 μg/ml); (B) sample (10 mg/ml) in methanol. Peak corresponds to a level of *ca.* 0.3 mg/g DMAC.

deviation of 0.05 mg/g. Chromatograms of standard and sample solutions are shown in Fig. 4. After *ca.* ten sample injections, gradient elution was used to remove matrix components. Acetonitrile in the mobile phase was increased from 5% to 50% over 5 min. After holding at 50% for 5 min, the acetonitrile was reduced to 5% over 5 min. The system was allowed to reequilibrate for 5 min prior to the next injection. The detection limit for DMAC in the product was *ca.* 0.05 mg/g in the HPLC method.

Determination of DMF

Residual DMF has also been determined in bulk pharmaceuticals by GC[9,10]. Following the successful use of HPLC in the previous two applications, the method was also evaluated for the determination of DMF in an agricultural product. There

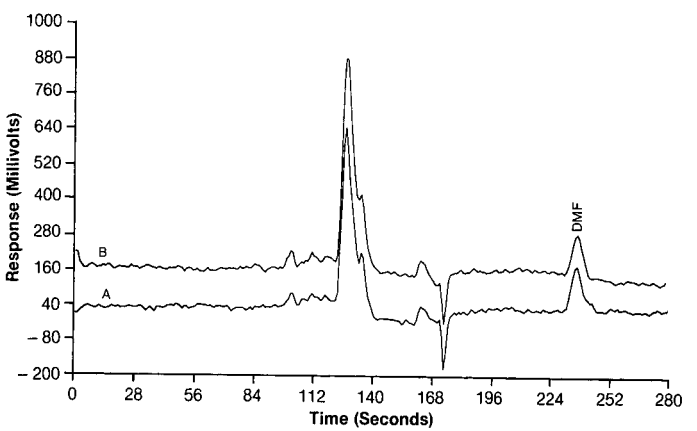

Fig. 5. HPLC chromatograms of DMF in an agricultural product. Column, Zorbax C_8 (5 μm, 250 mm × 4.6 mm I.D.); eluent, acetonitrile–0.1 *M* phosphate buffer, pH 2.5 (5:95); flow-rate, 1.5 ml/min; detection, 210 nm; temperature, ambient; injection volume, 50 μl. Samples: (A) standard DMF solution (0.05 μg/ml); (B) sample (50 mg/ml) in methanol. Peak corresponds to a spike of 1 μg/g DMF.

were no attempts to develop a GC method. The HPLC method was evaluated in terms of linearity, matrix effects, and sensitivity. The detection limit for the assay was *ca.* 0.2 μg/g DMF in the sample matrix, which relates to a total of 0.5 ng of DMF on the column. This increased sensitivity was achieved by injecting 50 μl of the sample solution as opposed to 10-μl injections in the previous two applications. In addition, a larger relative response was observed for DMF as compared to the other amides tested (Fig. 1). Assay validation results are given in Table I. Chromatograms of standard and spiked sample solutions are shown in Fig. 5.

CONCLUSION

The use of HPLC with UV detection has been described as an effective method for the determination of low-molecular-weight amides in organic matrices, such as pharmaceutical and agricultural products. By strongly retaining the sample matrix and allowing the amide analyte to elute, the method can be generally applied to many types of organic matrix. This method was found to exhibit greater sensitivity and freedom from matrix interferences than GC in the examples described.

REFERENCES

1 F. A. Patty (Editor), *Industrial Hygiene and Toxicology, Vol. II, Toxicology*, Interscience, New York, 1963, 2nd ed., Ch. XL.
2 J. F. O'Donnel and C. K. Mann, *Anal. Chem.*, 36 (1964) 2097.
3 D. G. Taylor, R. E. Kupel and J. M. Bryant, *Documentation of the NIOSH Validation Tests* (Stanford Research Institute, Menlo Park), National Institute for Occupational Safety and Health, Cincinnati, 1977.
4 M. L. Knuth and M. D. Hoglund, *J. Chromatogr.*, 285 (1984) 153.
5 W. R. Supina, *The Packed Column in Gas Chromatography*, Supelco, Inc., 1974, pp. 45–52.
6 M. H. Cardone, *J. Assoc. Off. Anal. Chem.*, 66 (1983) 1283.
7 R. W. Souter, *J. Chromatogr.*, 193 (1980) 207.
8 E. L. Inman and E. C. Rickard, *J. Chromatogr.*, 447 (1988) 1.
9 F. Butcher, *Perkin-Elmer Anal. News*, 11 (1977) 9.
10 J. E. Haky and T. M. Stickney, *J. Chromatogr.*, 321 (1985) 137.

Journal of Chromatography, 458 (1988) 295–301
Elsevier Science Publishers B.V., Amsterdam — Printed in The Netherlands

CHROMSYMP. 1431

HIGH-PERFORMANCE LIQUID CHROMATOGRAPHY OF THE ANTITUMOUR AGENT TRIETHYLENETHIOPHOSPHORAMIDE AND ITS METABOLITE TRIETHYLENEPHOSPHORAMIDE WITH SODIUM SULPHIDE, TAURINE AND *o*-PHTHALALDEHYDE AS PRE-COLUMN FLUORESCENT DERIVATIZATION REAGENTS

AKIRA SANO*, SATOSHI MATSUTANI and SHOJI TAKITANI
Faculty of Pharmaceutical Sciences, Science University of Tokyo, 12, Ichigaya-funagawara-machi, Shinjuku-ku, Tokyo 162 (Japan)

SUMMARY

The method described is based on the reaction of triethylenethiophosphoramide (ThioTEPA) and triethylenephosphoramide (TEPA), through their ethyleneimine groups, with sodium sulphide, taurine and *o*-phthalaldehyde to give fluorescent products, and separation of the derivatives by reversed-phase high-performance liquid chromatography. The method was successfully applied to the determination of ThioTEPA and TEPA in rabbit plasma samples after clean-up with an Extrelut 3 column. The recoveries of ThioTEPA and TEPA from plasma were 66.1–80.3% and the limits of determination in plasma were *ca.* 10 and 20 ng/ml, respectively.

INTRODUCTION

The alkylating antitumour agent triethylenethiophosphoramide (ThioTEPA) (Fig. 1) has been used in cancer treatment. ThioTEPA is metabolized to triethylenephosphoramide (TEPA) (Fig. 1), which is also an alkylating agent. Because of their high cytotoxicity, the simultaneous determination of these two compounds is desirable for pharmacokinetic studies[1]. Previously reported methods, such as spectrophotometric[2] and fluorimetric[3] methods, did not distinguish between the parent drug and its metabolite unless a cumbersome procedure[3] was used. An assay method based on the use of radiolabelled drugs[4] is not easy to perform. Recently, gas

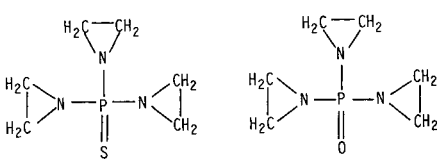

Fig. 1. Structures of ThioTEPA and TEPA.

0021-9673/88/$03.50

chromatography (GC) with nitrogen–phosphorus detection[5,6] was reported. The method is very sensitive and permits the determination of both ThioTEPA and TEPA. The GC method, however, requires a high operating temperature and accordingly it may cause undesirable problems in biological analysis because of the thermal instability of ThioTEPA and TEPA and many endogenous substances which can inactivate the column packings.

Despite the utility of high-performance liquid chromatography (HPLC) for determining thermally unstable compounds, no application of HPLC for ThioTEPA and TEPA has been reported so far, perhaps because they have no specific ultraviolet-active or fluorescent functional groups in their molecule. Recently, a fluorigenic reaction of ThioTEPA, based on the S-alkylation reaction of its ethyleneimine group with sodium sulphide and subsequent condensation with *o*-phthalaldehyde (OPA) and taurine was reported[7]. This reaction seemed promising as a method for the pre-column derivatization of ThioTEPA and TEPA for HPLC. This work was aimed at devising an HPLC method for the simultaneous determination of ThioTEPA and TEPA by using the fluorigenic reaction described above. An application to rabbit plasma was also examined.

EXPERIMENTAL

Chemicals and materials

All chemicals were of analytical-reagent grade, unless stated otherwise. Water was purified on a Milli RO-Milli Q system (Millipore, Bedford, MA, U.S.A.). ThioTEPA was kindly supplied by Simitomo Pharmaceuticals (Osaka, Japan). TEPA was synthesized according to the published method[8] with a slight modification: the crude product obtained was purified on a LiChroprep RP-18 (40–63 μm) column 310 mm × 25 mm I.D. (Merck, Darmstad, F.R.G.) with 30% aqueous methanol as the eluent (flow-rate, 1.0 ml/min). Mass spectra of TEPA gave a molecular weight of 173 (M^+) (calculated for $C_6H_{12}N_3PO$, 173.0717; found, 173.0719). Standard solutions of ThioTEPA and TEPA were prepared in 1-propanol. An Extrelut 3 column was obtained from Merck. The solutions used for the fluorescent derivatization reaction were prepared as follows.

Sodium sulphide (40 mM)–ethylenediaminetetraacetic acid, tetrasodium salt (Na_4EDTA) (50 mM) solution. Equal volumes of aqueous 80 m*M* sodium sulphide nonahydrate and aqueous 100 m*M* Na_4EDTA were mixed (prepared daily).

Taurine solution (0.2 mM). Taurine was dissolved to give a 0.2 m*M* solution in 0.1 *M* phosphate buffer (pH 8.0).

OPA solution (0.3 mM). OPA was dissolved to give a 0.3 m*M* solution in 0.1 *M* phosphate buffer (pH 8.0).

Fluorescent derivatization

To 100 μl of sample solution in a 1.5-ml glass-stoppered test-tube were added 10 μl of sodium sulphide–EDTA solution. The tube was heated in a water bath at 80°C for 30 min and then cooled in an ice–water bath. To the mixture, 400 μl each of taurine and OPA solutions were added about 10 min before injection of the sample (20 μl) into the HPLC system.

HPLC apparatus and conditions

The HPLC system consisted of a Shimadzu LC-6A pump (Shimadzu, Kyoto, Japan), a Rheodyne Model 7125 injector with a 20-μl sample loop (Rheodyne, Cotati, CA, U.S.A.) and a 5-μm Hibar LiChrosorb RP-18 (250 mm × 4 mm I.D.) (Merck) with a guard column (LiChroCART RP-18) (Merck). The mobile phase was 0.1 *M* phosphate buffer (pH 5.7)–acetonitrile (72:28). The column temperature was ambient and the flow-rate was 1.0 ml/min. Detection was carried out with a Hitachi F-1000 fluorescence spectrophotometer equipped with a flow cell (12 μl) and a xenon lamp (Hitachi, Tokyo, Japan), operated at 440 nm emission and 340 nm excitation.

Extraction of ThioTEPA and TEPA from plasma samples

A plasma sample (1 ml) was diluted with water (2.2 ml) and 3 ml of the solution were applied to the Extrelut 3 column. After 15 min, chloroform was passed through the column. The first 8 ml of effluent were collected and dried under nitrogen at *ca.* 20°C. The residue obtained was dissolved in 500 μl of 1-propanol. A 100-μl aliquot of the solution was then examined by the above methods.

RESULTS AND DISCUSSION

Derivatization

The method used in this study was essentially the same as that described in a previous paper dealing with a manual procedure for the determination of ThioTEPA[7]. TEPA was also derivatized by this method, although its fluorescence intensity was *ca.* 45% of the value for ThioTEPA. The OPA reaction for the products resulting from ThioTEPA and TEPA with sodium sulphide was carried out in the presence of taurine at basic pH. In the manual procedure, borate–phosphate buffer (pH 8.0) was used for the preparation of the OPA and taurine reagents. However, in this study, 0.1 *M* phosphate buffer (pH 8.0) was used instead of borate–phosphate buffer, because phosphate buffer was used as a component of the eluent for HPLC. The fluorophores obtained by the proposed method are assumed to be isoindole derivatives, which are known to be very unstable[9,10]. The final fluorescence obtained for ThioTEPA and TEPA was stable for 20 min at room temperature. On the other hand, alkylated products of ThioTEPA and TEPA with sodium sulphide were stable for at least 8 h in an ice–water bath. Therefore, after the alkylation reaction, the reaction mixture was stored in an ice–water bath without addition of taurine and OPA reagents. Both of the reagents were added about 10 min prior to injection of the sample into the HPLC system, because a reaction time of 10 min at room temperature was required to give the maximum fluorescence intensity.

Separation

The simultaneous separation of the fluorescent derivatives was studied to revesred-phase HPLC, because the derivatization reaction was carried out in aqueous solution. Also, isoindole fluorophores are known to separate efficiently on reversed-phase columns with a mobile phase consisting of aqueous methanol[11] or acetonitrile[12] containing phosphate or acetate buffers. Therefore, phosphate buffer solutions (0.02–0.2 *M*, pH 5.7–8.0) mixed with acetonitrile (25–30%, v/v) or methanol (50–60%, v/v) were tested as eluents. Although the derivatives of ThioTEPA and TEPA were

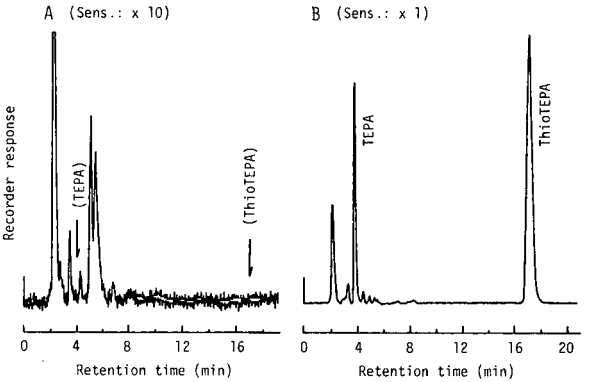

Fig. 2. HPLC traces of (A) reagent blank and (B) derivatives resulting from a standard solution containing ThioTEPA (189 ng) and TEPA (173 ng) in 100 μl of 1-propanol.

easily separated in both instances, significant problems were encountered with the interference of a few minor peaks originating from the reagents. The retention times of the derivatives and reagent blank decreased with either increasing concentrations of organic solvents and pH or decreasing phosphate concentration in the mobile phase. It was found that acetonitrile–0.1 *M* phosphate buffer (pH 5.7) (28:72) permitted the satisfactory resolution of peaks for TEPA and the reagent blank (Fig. 2). The retention times of ThioTEPA and TEPA were 17.0 and 4.0 min, respectively. Other ionic media, such as borate, acetate and citrate buffers, were examined, but no improved separation from the interfering peaks was obtained.

Calibration graphs for standard solutions

Linear calibration graphs were obtained for ThioTEPA and TEPA over the concentration ranges 1.5–378 ng (8–2000 pmol) and 3.5–346 ng (200–2000 pmol), respectively, in 100 μl of 1-propanol, with a relative standard deviation of *ca.* 5%. When the calibration graphs were analysed by least-squares linear regression, the equations of the lines were $y = 2.84x + 0.39$ ($r = 0.9993$) for ThioTEPA and $y = 2.47x - 0.83$ ($r = 0.9998$) for TEPA. The detection limits were 1.5 and 3.5 ng of ThioTEPA and TEPA, respectively, in 100 μl of 1-propanol at a signal-to-noise ratio of 2.

Clean-up of ThioTEPA and TEPA in plasma samples

In previous work[7] the utility of an Extrelut 3 column for the clean-up of plasma ThioTEPA was demonstrated. It was more effective and easier to use than other methods, such as chloroform extraction[6] and the use of Sep-Pak C_{18} cartridges[5]. The column was therefore examined for the simultaneous extraction of ThioTEPA and TEPA from plasma samples. When rabbit plasma (1 ml) to which 945 ng of ThioTEPA and 865 ng of TEPA had been added was diluted with water (2.2 ml) and then applied to the column, maximum recoveries (*ca.* 70–80%) were obtained by elution with 7 ml of chloroform. Dichloromethane and ethyl acetate gave low recoveries, especially for TEPA (below 50%), and therefore chloroform (8 ml) was used. The use of a stream of nitrogen is recommended instead of a rotary evaporator for evaporating the eluent.

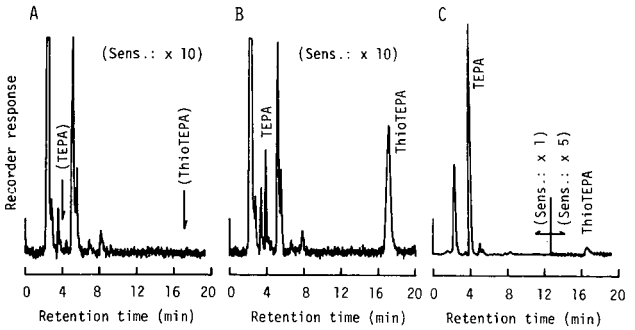

Fig. 3. HPLC traces of extracts of rabbit plasma: (A) control plasma; (B) control plasma with ThioTEPA (94.5 ng) and TEPA (86.5 ng) added; (C) plasma sample obtained 1 h after intravenous injection of 1 mg/kg of ThioTEPA, containing 8 ng/ml of ThioTEPA and 1250 ng/ml of TEPA.

The latter gave poor reproducibility of the recovery of TEPA, probably because of the greater volatility of TEPA. As shown in Fig. 3, this clean-up procedure was effective for the removal of endogenous substances, which could interfere with the derivatization reaction and the chromatographic separation. For example, the HPLC trace resulting from blank plasma (Fig. 3A) was essentially the same as that of the reagent blank itself (Fig. 2A). ThioTEPA and TEPA were detected successfully without interferences (Fig. 3B and C). From the chromatogram of plasma to which were added ThioTEPA (94.5 ng) and TEPA (86.5 ng), the limits of determination were estimated to be *ca.* 10 and 20 ng/ml for ThioTEPA and TEPA, respectively, in plasma (Fig. 3B). Although significant losses of ThioTEPA and TEPA occurred during the evaporation stage, owing to their volatility, about 66–80% recoveries were obtained for ThioTEPA and TEPA added to plasma at concentrations of 86.5–945 ng/ml (Table I). The standard deviations were also satisfactory. By employing a clean-up procedure similar to that in the present method, we previously obtained a linear calibration graph for plasma ThioTEPA[7]. Therefore, this method presumably permits the determination of ThioTEPA and TEPA at concentrations up to *ca.* 2500 ng/ml in plasma with a mean recovery of *ca.* 70% (corresponding to 330 ng per 100 μl in the final solution after dissolving the dried residue in 500 μl of 1-propanol).

TABLE I

RECOVERIES OF ThioTEPA AND TEPA FROM RABBIT PLASMA

Experiment No.	*ThioTEPA or TEPA added [nmol/ml (ng/ml)]*	*Recovery (%)**
1	ThioTEPA 0.5 (94.5)	66.1 ± 8.2
	TEPA 0.5 (86.5)	72.3 ± 4.6
2	ThioTEPA 5 (945)	80.3 ± 9.8
	TEPA 5 (865)	72.1 ± 8.4

* Mean ± standard deviation (n = 4).

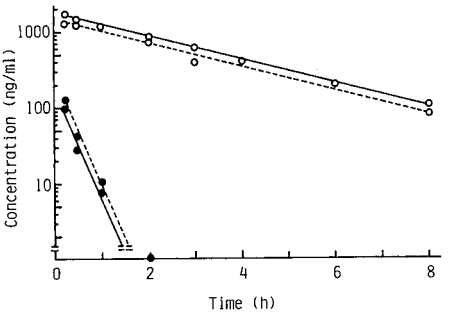

Fig. 4. Plasma concentrations of (●) ThioTEPA and (○) TEPA in two rabbits (solid line, 3.7 kg; broken line, 3.8 kg) following a single intravenous injection of 1 mg/kg of ThioTEPA.

Determination of ThioTEPA and TEPA in rabbit plasma

In order to test the applicability of the proposed method to plasma samples, it was used to analyse plasma from two male rabbits (3.7 and 3.8 kg) that had been given an intravenous injection of a ThioTEPA preparation (1 mg/kg). Venous blood specimens were collected in heparinized tubes just before and up to 8 h after the drug administration. A typical chromatogram and time courses of plasma levels of the drug and its metabolite are shown in Figs. 3C and 4, respectively. It should be noted that the concentrations of ThioTEPA and TEPA indicated in Figs. 3C and 4 were not corrected for recovery. Plasma concentrations of ThioTEPA and TEPA declined exponentially. By 2 h after injection, there was little ThioTEPA in the plasma, but *ca.* 100 ng/ml of TEPA was detected, even 8 h after injection. These results are similar to those reported for mice[5]. In previous work, 200–400 ng/ml of ThioTEPA were detected, even 5 h after intravenous administration of ThioTEPA to three female rabbits (5 mg/kg). However, as suggested in that paper[7], it seems that the values determined as ThioTEPA must include considerable amounts of TEPA, because it is also eluted from the Extrelut column under the conditions used in the study.

Chromatographic procedures are considered to be the most suitable for the simultaneous determination of ThioTEPA and TEPA in biological fluids. A few methods based on GC with nitrogen–phosphorus detection have been reported[5,6], but apparently no application of HPLC methods has been described. This study provides the first HPLC method for determining ThioTEPA and TEPA. The proposed method permits the determination of 10 and 20 ng/ml of ThioTEPA and TEPA, respectively, in rabbit plasma. This sensitivity is greater than that of the method based on capillary GC with nitrogen–phosphorus detection and temperature-programmed elution (the detection limits were 1–5 ng/ml in human plasma for both compounds)[5], but it is comparable to that obtained by conventional and isothermal GC with nitrogen–phosphorus detection (the detection limits were 10 and 100 ng/ml of ThioTEPA and TEPA, respectively, in human plasma)[6]. Probably there is not a marked difference between the recoveries obtained by our method and by the GC method[5,6], except for ThioTEPA treated by the method of McDermott *et al.*[5] (in which more than 90% recoveries were reported), because in both the GC method and our method the evaporation of the extracts from plasma is necessary in order to improve the sensitivity, and this step causes significant losses of the analytes.

Pharmacokinetic studies of ThioTEPA and TEPA were recently performed with such GC procedures. Probably the HPLC method described here is also capable of determining ThioTEPA and TEPA in plasma samples from patients following a therapeutic dose of ThioTEPA. The method should be useful for clinical studies.

REFERENCES

1 S. Eksborg and H. Ehrsson, *J. Chromatogr.*, 340 (1985) 31.
2 Y. L. Tan and D. R. Cole, *Clin. Chem.*, 11 (1965) 58.
3 L. B. Mellett and L. A. Woods, *Cancer Res.*, 20 (1960) 524.
4 I. U. Boone, B. S. Rogers and D. L. Williams, *Toxicol. Appl. Pharmacol.*, 4 (1962) 344.
5 B. J. McDermott, J. A. Double, M. C. Bibby, D. E. V. Wilman, P. M. Loadman and R. L. Turner, *J. Chromatogr.*, 338 (1985) 335.
6 M. J. Egorin, B. E. Cohen, E. A. Kohlhepp and P. L. Gutierrez, *J. Chromatogr.*, 343 (1985) 196.
7 A. Sano and S. Takitani, *Anal. Chim. Acta*, 201 (1987) 77.
8 A. W. Craig and H. Jackson, *Br. J. Pharmacol.*, 10 (1955) 321.
9 S. S. Simons, Jr. and D. F. Johnson, *Anal. Biochem.*, 90 (1978) 705.
10 J. F. Stobaugh, A. J. Repta, L. A. Sternson and K. W. Garren, *Anal. Biochem.*, 135 (1983) 495.
11 P. Lindroth and K. Mopper, *Anal. Chem.*, 51 (1979) 1667.
12 K. Mopper and D. Delmas, *Anal. Chem.*, 56 (1984) 2557.

Journal of Chromatography, 458 (1988) 303–312
Elsevier Science Publishers B.V., Amsterdam — Printed in The Netherlands

CHROMSYMP. 1454

SEPARATION AND DETECTION OF DNA BY CAPILLARY ELECTROPHORESIS

THOMAS J. KASPER*, MARA MELERA, PHILIPPE GOZEL and ROBERT G. BROWNLEE
Microphoretic Systems, Inc., 750 North Pastoria Avenue, Sunnyvale, CA 94086 (U.S.A.)

SUMMARY

The use of capillary electrophoresis for the separation and detection of nucleic acids has been investigated. Lab-model instruments have been built, using commercially available UV absorbance and fluorescence detectors which were modified for use with 50–100 μm I.D. fused-silica capillary tubing. The sensitivity of these instruments (signal-to-noise ratio = 3) was measured as 15 μg/ml for fluorescence detection of ethidium bromide-stained herring-sperm DNA and 3 μg/ml for UV absorbance detection. With the former instruments a variety of strategies has been used to attain rapid separations of bases, oligonucleotides, restriction fragments and whole phage, viral and plasmid DNAs.

INTRODUCTION

Since 1981 there has been a great increase in interest in electrophoresis in fused-silica capillaries of small inner diameter[1–4]. Capillaries of 50–100 μm I.D. have several beneficial properties, among which are rapid dissipation of Joule heat, elimination of thermal and gravitational convection, and a flat electro-endosmotic flow profile. These properties make fused-silica capillaries an ideal medium for electrophoresis in free solution[2,5]. Separations have been demonstrated for proteins, peptides, amino acids, oligonucleotides, nucleosides and several other small organic molecules[2,3,6,7]. These separations have utilized high voltages (up to 30 kV) in order to achieve rapid separation at extremely high resolution. The theoretical limit of the efficiency of capillary electrophoresis (CE) has been estimated to be over two million theoretical plates, and separations have been reported with efficiencies of nearly one million plates[8,9]. Another feature of CE is the great variety of separation strategies that may be used, including zone electrophoresis[2,9], isotachophoresis[10,11], isoelectric focusing[11,12] and micellar electrokinetic capillary chromatography (MECC)[6,7,13]. More recent work has demonstrated the feasibility of gel electrophoresis of proteins in capillaries[14].

We are interested in the separation and detection of nucleic acids by CE. Earlier work has shown that oligonucleotides and nucleic acid constituents (bases, nucleosides and nucleotides) can be efficiently separated in zone or micellar systems[6,13,15].

0021-9673/88/$03.50

However, these systems have thus far failed to separate large DNA molecules. This may be attributed primarily to the fact that nucleic acids over twenty bases in length have essentially the same charge-to-mass ratio. In this paper, we describe separations which we have achieved for nucleic acids and their constituents, ranging from nucleosides to large restriction fragments (up to 23 kb). Also detailed are the techniques we have used for the detection of nucleic acids and the properties of these various optical techniques.

EXPERIMENTAL

Materials

Nucleic acid bases and Hoechst 33258 were purchased from Sigma (St. Louis, MO, U.S.A.). Herring sperm DNA and ethidium bromide were obtained from Serva (Westbury, NY, U.S.A.). All other nucleic acids were supplied by Bethesda Research Labs (Gaithersburg, MD, U.S.A.). Acrylamide and bis-acrylamide were purchased from Bio-Rad (Richmond, CA, U.S.A.). Ammonium persulfate and N,N,N′,N′-tetramethylethylenediamine (TEMED) were supplied by International Biotechnologies (New Haven, CT, U.S.A.). All other reagents were obtained either from Fisher (Pittsburgh, PA, U.S.A.), Sigma, or Serva. Fused-silica capillary tubing was purchased from Polymicro Technologies (Phoenix, AZ, U.S.A.).

For detection either a modified Kratos Spectroflow 757 UV absorbance detector (Applied Biosystems, Foster City, CA, U.S.A.) or a modified HP1046A fluorescence detector (Hewlett-Packard, Palo Alto, CA, U.S.A.) was used. Modification of the detectors involved replacement of the flow cells with capillary holders, which immobilized the capillary in the light beams. For simplicity, these capillary holders were of similar geometry to the original flow cells. The UV detector capillary holder had a 0.50 mm × 0.15 mm slit placed adjacent to the capillary, between it and the photodiode. In the fluorescence detector, the lenses from the original flow cell were placed in the capillary holder, in order to focus the excitation and emission beams. A fused-silica capillary bridged the gap from the high-voltage electrolyte at the injection end to the ground electrolyte at the detector end. At the point where the capillary passed through the detector beam, a small segment of the polyimide coating was burned off and the capillary was cleaned with methanol, which allowed detection directly through the capillary tube. The ground electrolyte reservoir was sealed and connected to a vacuum pump (Model N79MVI, KNF Neuberger, Princeton, NJ, U.S.A.), which was used to purge, fill, and inject the capillaries, except in the polyacrylamide gel experiments, where injection was accomplished by electrophoresis. Power supplies (±30 kV) were obtained from either Hipotronics (Brewster, NY, U.S.A.) or Gamma High-Voltage Research (Mt. Vernon, NY, U.S.A.).

Methods

New capillaries were cleaned by sequentially rinsing for 5–10 min, first with water, then with 0.1 *M* sodium hydroxide, again with water, and finally with the buffer to be used for the subsequent separation. This procedure was also used to recondition capillaries after every 2–4 runs. For gel electrophoresis, tubes were treated with 0.4% (v/v) 3-methacryloxypropyltrimethoxysilane in water, adjusted to pH 3.5 with acetic acid[16].

Polyacrylamide gels were prepared by a standard method[17]. Monomer mix was degassed under vacuum in an ultrasonic bath. Gel mixture was drawn into the capillary under vacuum immediately after the addition of TEMED and ammonium persulfate.

For cetyltrimethylammonium bromide (CTAB)-MECC and gel electrophoresis applications the high voltage (injection end of capillary) was at a negative potential. All other applications utilised high voltage at positive potentials.

Commonly used buffers were TPE (80 m*M* Tris-phosphate, 2 m*M* EDTA, pH 8.0), and a 1:10 dilution of TBE (9 m*M* Tris, 9 m*M* boric acid, 0.2 m*M* EDTA, pH 8.0). All solutions were made from water which had been highly purified by ultrafiltration (Barnstead NANOpure II System, Sybron Corp., Newton, MA, U.S.A.).

UV absorbance detection was carried out at 260 nm. Fluorescence detection was performed at excitation and emission wavelengths of 250 nm and 585 nm, respectively, except as noted.

RESULTS AND DISCUSSION

In general, CE separations have been characterized by high speed and high resolution. Another potential benefit of CE is the ability to obtain real-time quantitative analysis. In order to test this ability for nucleic acid analyses, calibration curves were plotted for the absorbance and fluorescence detectors. Serial dilutions of herring-sperm DNA in TPE were drawn by vacuum through capillaries inserted into the detectors. The absorbance detector displays a linear response over three orders of magnitude, up to 2.0 mg DNA/ml (data not shown). Its sensitivity limit is 3 μg/ml (measured at 3:1 signal-to-noise ratio in a 50-μm I.D. capillary). Since the detection volume of this detector is around 1 nl (based on 0.5 mm slit length and 50 μm I.D.), this limit would correspond to detection of peaks containing as little as 3 pg of DNA. However, since this measurement was made in a static system, it must be considered the idealized limit for this detector. During actual separations, higher noise levels were observed, and this resulted in a somewhat higher detection limit, which was dependent on the particular buffer system being used. This additional noise may be due to electrical impulses transmitted to the detector when the high voltage is applied, or to effects of the buffers. It should be noted also that some buffers may attenuate the response, in particular those buffers which contain additives that significantly alter the refractive index of the aqueous solution or chaotropic agents which affect the structure of nucleic acid, such as urea.

Fig. 1 shows the response of the fluorescence detector to DNA in varying concentrations of ethidium bromide (EB) and also in 20 μg/ml Hoechst 33258 (H33258). The latter is a nuclear stain which is seldom used in electrophoresis, since its emission is at a wavelength which is not as easily seen by the naked eye as that of EB. For EB staining, the greatest sensitivity is obtained at low concentrations of the dye. However, with increasing concentrations of DNA, the dye solution becomes saturated with DNA, and linearity is lost. Thus, for higher DNA concentrations, higher concentrations of EB are required in order to obtain a linear response. This is contrary to the results for gel staining in which a linear response is suggested for low EB concentration over a wide range of DNA concentrations[18]. This may be attributed to the large volume excess of EB solution used in these procedures. In contrast to

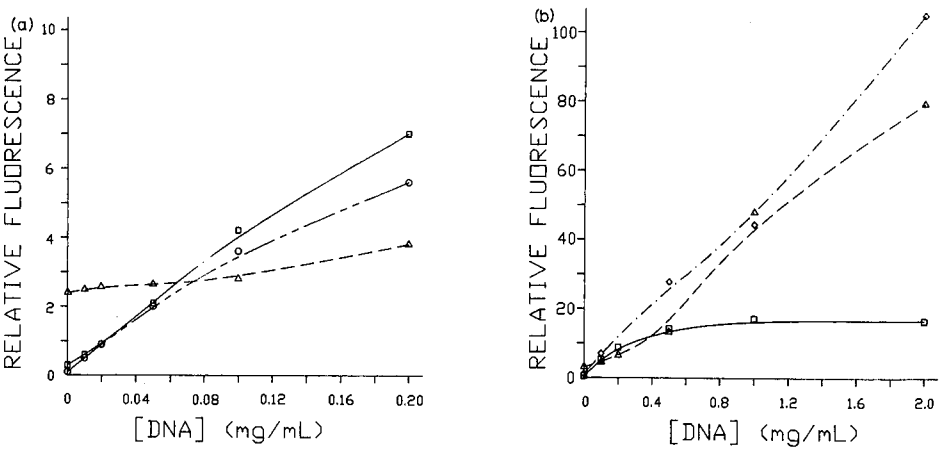

Fig. 1. Response of modified HP1046A fluorescence detector to DNA for various dye concentrations. Serial dilutions of herring-sperm DNA in TPE, with dye, were drawn through the detector under vacuum in a 75-μm-I.D. capillary. (a) Low concentration range. (b) High concentration range. Fluorescence measurements for H33258 stained samples at excitation and emission wavelengths of 232 and 458, respectively. (○) EB 10 μg/ml; (□) EB 20 μg/ml; (△) EB 200 μg/ml; (◇) H33258 20 μg/ml.

EB, staining with H33258 apparently shows a wide linear range, and thus merits further investigation. Sensitivity levels for fluorescence were measured as 15 μg/ml DNA for 10 μg/ml EB or 30 μg/ml DNA in 20 μg/ml H33258. For comparison, sensitivity was also measured for fluorescein as $7 \cdot 10^{-7}$ *M* (260 ng/ml), using broad-band UV excitation and monitoring emission at 515 nm.

These results, in combination with other data we have obtained, suggest that greater sensitivity and linearity of response is obtained by using absorbance detection, whereas fluorescence detection of stained DNA has the benefits of reduced background noise and elimination of certain artifacts (such as peaks caused by protein contaminants). The lower sensitivity of absorbance detection is surprising, considering that fluorescence detection of EB-stained gels is the most popular detection method for DNA gel electrophoresis. However, the popularity of this technique is principally due to its simplicity compared to densitometric analysis. Furthermore, the high absorptivity of nucleic acid polymers is well documented, and is the basis for the most common technique for accurate quantification of dilute DNA samples of manageable volume[18]. On the other hand, the high sensitivity limit obtained for EB staining may be caused by inadequacies in the optics of this design. Future detectors should include tighter focusing of the excitation beam into the detection volumes as well as elimination of scattered light which may contribute to background. It will be interesting to see if this sensitivity level will be significantly improved in upgraded detectors.

A variety of methods has been utilised for the separation of nucleic acids and their constituents, the strategy used being primarily dependent upon the size range being analysed. Fig. 2 shows a MECC separation of nucleic acid bases in a sodium dodecyl sulphate (SDS)-containing buffer. The mechanism of this separation method is well understood, and has been documented elsewhere[6,19,20]. Briefly, the separation

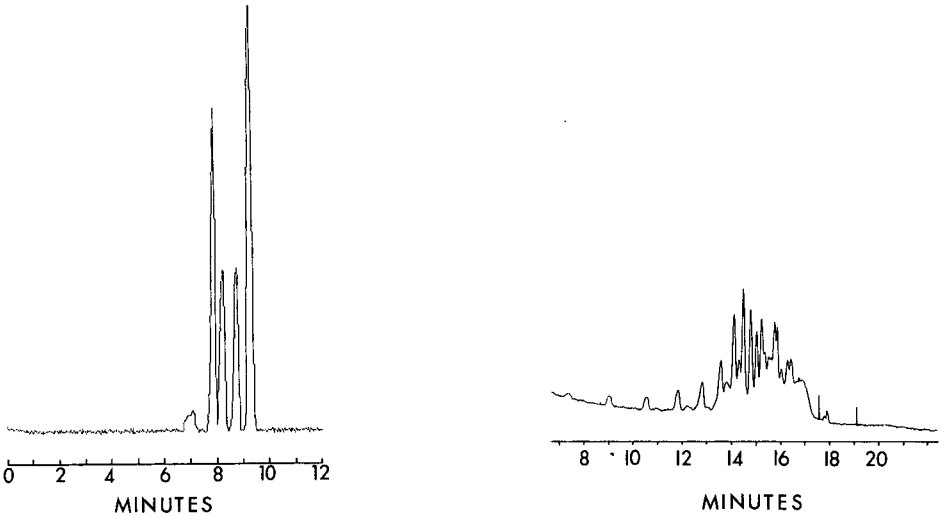

Fig. 2. MECC of nucleic acid bases. Peaks are from left to right: uracil, cytosine, thymine and adenine. Approximately 5 ng each was injected in 5 nl. Electrophoresis at 24 kV, 57 μA, in 25 m*M* $Na_2B_4O_7$–50 m*M* NaH_2PO_4–0.1 *M* SDS (pH 7.0), in a 50 cm × 50 μm I.D. capillary. Detection by UV absorbance.

Fig. 3. Zone electrophoresis of BRL oligo dT ladder. Approximately 12 ng was injected in 50 nl. Electrophoresis at 16 kV, 36 μA, in 50 m*M* phosphate buffer, in a 50 cm × 50 μm I.D. capillary. Detection by UV absorbance.

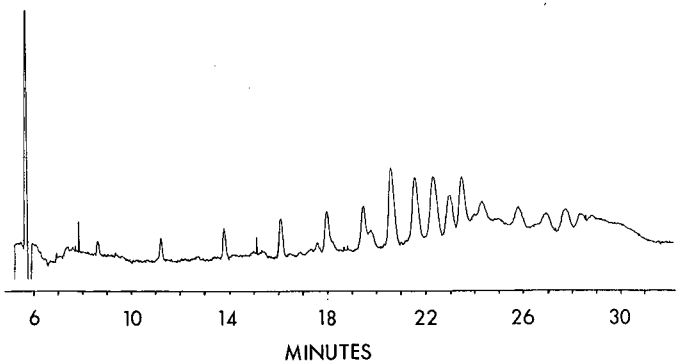

Fig. 4. Same as Fig. 3, except that buffer included 5% ethylene glycol, and electrophoresis conditions were 17 kV and 50 μA.

is based on the ability of the bases to partition into a SDS micelle. Since bases are uncharged at neutral pH, and SDS micelles are negatively charged, bases which partition more efficiently into the micelles (*e.g.*, purines) will be retarded, due to the electrophoretic motion of the micelles against the electroosmotic flow. In addition to bases, MECC has been shown to efficiently separate nucleosides and nucleotide phosphates[6,13], and oligonucleotides[6], as well as basic, acidic and (net) uncharged peptides[21].

Separation of large DNAs (*i.e.*, plasmids, restriction fragments and larger molecules) in capillaries has proven to be a formidable problem. Early conjecture was

that separations of nucleic acids over eight bases long would not be possible without the "sieving effect of a high density gel"[15]. (Unlike size-exclusion chromatography, gel electrophoresis apparently utilizes a sieving mechanism, whereby smaller polymers move more quickly and larger ones are more highly retained.) However, the separation of oligonucleotides by CE with continuous, non-partitioning buffers, as well as more complex systems, has been successfully accomplished. Fig. 3 shows a separation of oligodeoxythymidines ranging in size from 4 to 22 bases. In Fig. 4, the same electropherogram is shown with the addition of 5% ethylene glycol, which increases the viscosity and thus reduces the electroosmotic flow. It can be seen that, while the total elution time is increased, the later-eluted peaks are significantly better resolved. The mechanism of these separations is not yet fully understood, but is likely to involve a combination of mobility and viscous drag. Nevertheless, separations of larger DNAs have been difficult and elusive.

Early attempts in this laboratory have involved the use of simple buffers, such as 10 m*M* Tris-borate. It was felt that the differences in viscous drag could cause sufficient variations in migration velocities of fragments of differing sizes. Fig. 5 shows a separation of SV40 DNA in a 1:10 dilution of TBE. In this figure, two major peaks can clearly be distinguished, as well as a smaller, early-eluted peak and a range of peaks of intermediate migration rate. Although these fractions have not yet been isolated and analysed, it may be conjectured that the three principal peaks correspond to linear, open-circular, and supercoiled forms. It is well known that the tertiary structure of these different forms of DNA causes large differences in the Stokes radius of these molecules, and this results in increasing viscous drag as follows:

$$\text{linear} \geqslant \text{open-circular} > \text{supercoiled}.$$

Since all of these DNAs have the same mass and essentially the same charge, it seems likely that the resultant differences in frictional forces are the cause of the observed separation. (These tertiary structure differences are known to affect migration rates

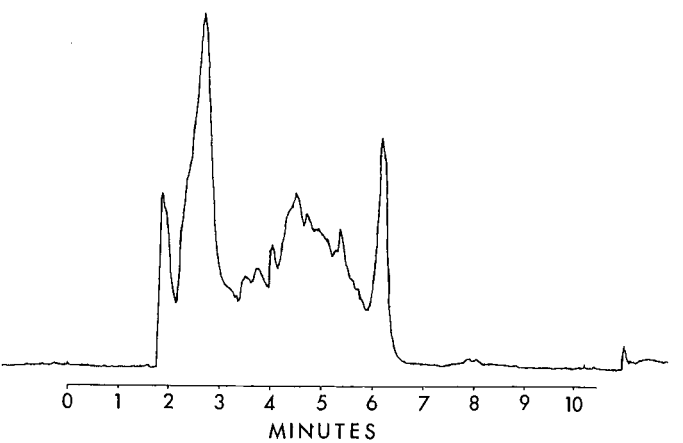

Fig. 5. SV40 RF DNA electrophoresed in a 50 cm × 75 μm I.D. capillary, containing a 1:10 dilution of TBE and 100 μg/ml EB. Electrophoresis at 30 kV and 10 μA. Sample, *ca.* 40 ng of DNA. Detection by fluorescence.

for agarose gel electrophoresis, as well as sedimentation coefficients for ultracentrifugation[22].) The source of the range of intermediate peaks is not known. Attempts at performing the same separation with viscous buffers, such as 5% ethylene glycol or 5% glycerol, or buffers containing high-molecular-weight reagents, such as Ficoll or polyvinylpyrrolidone, have resulted in reduced resolution, and also, in certain instances, the appearance of artifacts, or precipitation, leading to loss of current.

Attempts to separate large linear DNAs by this mechanism have thus far failed, presumably due to the direct proportionality between charge, drag, and mass. In one series of experiments, in a capillary treated with 3-methacryloxypropyltrimethoxysilane, Hind III fragments of λ-DNA were electrophoresed for varying amounts of time, ranging from 1 to 40 min. In this tube, the electroosmotic flow was only slightly greater than the electrophoretic velocity of the DNA, and this resulted in an extremely slow net migration of the sample. After electrophoresis, the sample was drawn past the detector under vacuum. Even after 40 min of electrophoresis, only a single peak was observed (data not shown).

Since these mechanisms had failed to resolve linear DNAs, it was our opinion that the remaining options for these separations were either gel electrophoresis or chromatography based on specific complexation. Presently, gel electrophoresis is the method of choice for separating linear DNAs. Furthermore, gel electrophoresis in capillaries has been demonstrated to be an effective way of obtaining rapid size separations of proteins[14] and oligonucleotides[23]. Fig. 6 shows a separation of the Hae III restriction fragments of φ-X DNA in a polyacrylamide gel. In this electrophe-

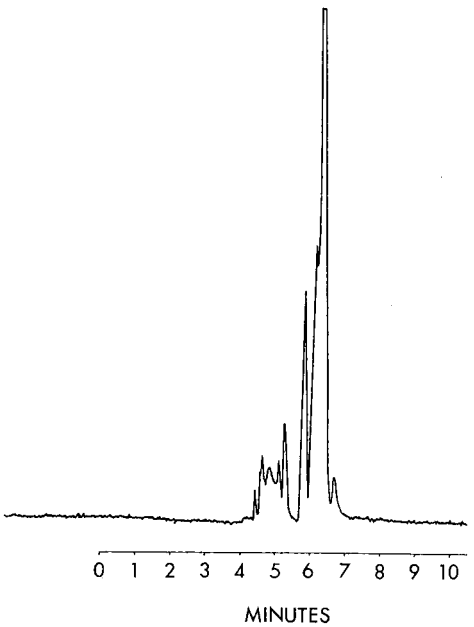

Fig. 6. Hae III fragments of φ-X DNA, electrophoresed in a 3%T, 5%C polyacrylamide gel-filled 20 cm × 100 μm I.D. capillary. Electrophoresis at 10 kV and 10 μA in 0.1 X TBE, containing 10 μg/ml EB. Detection by fluorescence.

rogram, nine different fractions can clearly be distinguished. Elution time is quite rapid as compared to conventional polyacrylamide gel electrophoresis. However, compared to the latter technique, a significant compression of DNA bands is observed. This is probably due to the high voltage applied, and may be a phenomenon similar to the compression of high-molecular-weight DNAs in agarose gels. A possible solution of this problem, which has not yet been investigated, is the use of pulsed field inversion.

Additional problems have also been encountered in these experiments. First, the effective separation range of polyacrylamide gels is around 2000 base pairs, whereas larger molecules require a larger pore matrix, such as agarose, for efficient separation. However, agarose gels have proven to be a poor medium for CE, since they are relatively unstable at high temperature and field strength. Thus, separations in agarose gels have been extremely difficult to reproduce. Additionally, the investigation of separations in acrylamide gels has been hindered by the difficulty of preparing gels of adequate quality, and associated problems with reproducibility from gel to gel. Further experiments in this direction will most likely focus on alternative gel matrices as media for capillary gel electrophoresis.

The final apparent candidate for the separation of linear DNAs is specific complexation. Many cations, including magnesium and tetra-alkylammonium ions have displayed strong interactions with DNA and nucleic acid constituents. Most intriguing has been the success of reversed-phase ion-pair high-performance liquid chromatography (HPLC) in the separation of DNA restriction fragments[24]. In light of the analogies between MECC and reversed-phase (RP)-HPLC, it seems likely that a mechanism similar to ion-pairing chromatography may be utilised to enable the separation of DNA restriction fragments in micellar buffer systems. There are two prime choices for such buffer systems: either a SDS-micelle buffer, containing tetraalkylammonium ions, or a CTAB-micelle buffer, in which CTAB would serve both as micelle and as ion-pairing reagent. Previous work has demonstrated that CTAB at concentrations above $3.5 \cdot 10^{-4}$ *M* effectively reverses the electroosmotic flow[25]. Thus, using a negative potential at the injection end of the capillary, a CTAB-micelle system will behave like a SDS system. We have chosen the CTAB system because of its inherent simplicity compared to a multi-component system. Fig. 7 shows a separation of φ-X DNA Hae III fragments in a phosphate–borate buffer containing 20 m*M* CTAB and 4 *M* urea. Our experience has shown that inclusion of urea enhances the resolution of this separation. This was an expected result, since partial unzipping of the DNA helix will allow hydrophobic interaction between the interior of the micelles and the bases as well as ion pairing between the surface of the micelles and the phosphate backbone.

Several features of the electropherogram in Fig. 7 are notable. First, the separation is very rapid, and is completed in less than 8 min. Second, it is extremely efficient. The number of theoretical plates for this separation was estimated as 1 000 000 plates, on the basis of the formula

$$N = 5.54\,(t/w)^2$$

where t is the elution time and w is the full peak-width measured at half-maximum[1]. Finally, it should be noted that all fractions are eluted in a total elapsed time of less than 1 min. This is a reflection of the minuteness of the differences which are the basis

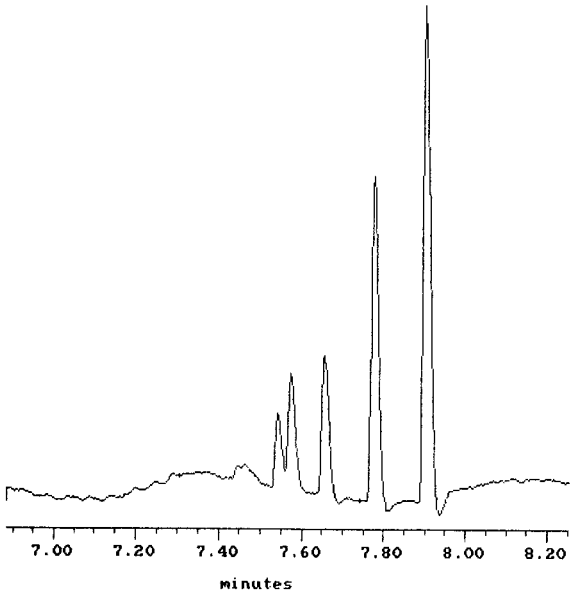

Fig. 7. Hae III fragments of φ-X DNA, electrophoresed in 20 m*M* CTAB–10 m*M* NaH_2PO_4–6 m*M* $Na_2B_4O_7$–4 *M* urea (pH 7.0). Previous to injection, DNA was heated to 95°C for 2 min. Electrophoresis at 15 kV and 12 μA in a 40 cm × 50 μm I.D. capillary. Sample, *ca.* 20 ng in 25 nl. Detection by UV absorbance.

for this separation. Similarly, in ion-pair RP-HPLC of restriction fragments, all fractions are generally eluted within a tight range of acetonitrile percentage[24]. It is interesting to note that in recent experiments, Cohen and Karger have obtained similar high-efficiency separations of Hind III fragments of λ-DNA in a SDS–urea system containing Tris–borate[26]. These separations are especially intriguing and are currently under intensive investigation.

CONCLUSIONS

CE can potentially be used to separate nucleic acids, ranging from small oligonucleotides to linear and circular DNAs of greater than 2000 base pair length. Separations have been demonstrated for these molecules, although in most cases the separation mechanisms are thus far poorly understood. A better understanding of these mechanisms will come with continued investigation in this and other labs. Linearity of absorption and fluorescence detection has been demonstrated for static systems. However, this capability has yet to be shown to yield quantitative results under actual operating conditions. This topic is currently under investigation. Although no work has been done on separations of RNAs in this lab, due to the difficulties involved with the handling of RNA samples, it is assumed that the same techniques should also result in successful separations of oligoribonucleotides and RNA molecules.

REFERENCES

1 J. W. Jorgenson and K. D. Lukacs, *Anal. Chem.*, 53 (1981) 1298.
2 J. W. Jorgenson and K. D. Lukacs, *Science (Washington, D.C.)*, 222 (1983) 266.
3 H. H. Lauer and D. McManigill, *Trends Anal. Chem.*, 5 (1986) 11.
4 S. W. Compton and R. G. Brownlee, *BioTechniques*, 6 (1988) 432.
5 Y. Walbroehl, *Ph.D. Dissertation*, University of North Carolina, Chapel Hill, NC, 1986.
6 A. S. Cohen, S. Terabe, J. A. Smith and B. L. Karger, *Anal. Chem.*, 59 (1987) 1021.
7 K. Otsuka, S. Terabe and T. Ando, *J. Chromatogr.*, 348 (1985) 39.
8 A. S. Cohen, A. Paulus and B. L. Karger, *Chromatographia*, 24 (1987) 15.
9 H. H. Lauer and D. McManigill, *Anal. Chem.*, 58 (1986) 166.
10 F. M. Everaerts and Th. P. E. M. Verheggen, in J. W. Jorgenson and M. Phillips (Editors), *New Directions in Electrophoretic Methods*, American Chemical Society, Washington, D.C., 1987, p. 199.
11 S. Hjertén, K. Elenbring, F. Kilár and J.-L. Liao, *J. Chromatogr.*, 403 (1987) 47.
12 S. Hjertén and M.-D. Zhu, *J. Chromatogr.*, 346 (1985) 265.
13 K. H. Row, W. H. Griest and M. P. Maskarinec, *J. Chromatogr.*, 409 (1987) 193.
14 A. S. Cohen and B. L. Karger, *J. Chromatogr.*, 397 (1987) 409.
15 K. D. Lukacs, *Ph.D. Dissertation*, University of North Carolina, Chapel Hill, NC, 1983.
16 S. Hjertén, *J. Chromatogr.*, 347 (1985) 191.
17 T. Maniatis, E. F. Fritsch and J. Sambrook, *Molecular Cloning, A Laboratory Manual*, Cold Spring Harbor Laboratory, Cold Spring Harbor, NY, 1982, p. 174.
18 T. Maniatis, E. F. Fritsch and J. Sambrook, *Molecular Cloning, A Laboratory Manual*, Cold Spring Harbor Laboratory, Cold Spring Harbor, NY, 1982, p. 468.
19 S. Terabe, K. Otsuka, I. Ichikawa, A. Tsuchiya and T. Ando, *Anal. Chem.*, 56 (1984) 111.
20 S. Terabe, K. Otsuka and T. Ando, *Anal. Chem.*, 57 (1985) 834.
21 T. J. Kasper and M. Melera, unpublished results.
22 C. R. Cantor and P. R. Schimmel, *Biophysical Chemistry, Part 3: The Behavior of Biological Macromolecules*, W. H. Freeman and Co., San Francisco, CA, 1980, p. 1278.
23 A. S. Cohen and B. L. Karger, submitted for publication.
24 S. Eriksson, G. Glad, P.-A. Pernemalm and E. Westman, *J. Chromatogr.*, 359 (1986) 265.
25 T. Tsuda, *J. High Resol. Chromatogr. Chromatogr. Commun.*, 10 (1987) 622.
26 B. L. Karger and A. S. Cohen, results presented at *The 2nd Annual Seminar on Analytical Biotechnology, Baltimore, MD, 1988.*

Journal of Chromatography, 458 (1988) 313–321
Elsevier Science Publishers B.V., Amsterdam — Printed in The Netherlands

CHROM. 1446

ON-LINE CAPILLARY ZONE ELECTROPHORESIS–ION SPRAY TANDEM MASS SPECTROMETRY FOR THE DETERMINATION OF DYNORPHINS

EDGAR D. LEE, WOLFGANG MÜCK* and JACK D. HÉNION*
Equine Drug Testing and Toxicology Program, New York State College of Veterinary Medicine, Cornell University, 925 Warren Drive, Ithaca, NY 14850 (U.S.A.)
and
THOMAS R. COVEY
Sciex, 55 Glencameron Road, Thornhill, Ontario L3T 1P2 (Canada)

SUMMARY

Capillary zone electrophoresis–mass spectrometry and capillary zone electrophoresis–tandem mass spectrometry with ionization at atmospheric pressure are demonstrated as being feasible for the separation and determination of small peptides such as dynorphins (1–6, 1–7, 1–8, 1–9) and leucine enkephalin at low picomole levels by full-scan mass spectrometry and tandem mass spectrometry and at the low femtomole range under selected ion monitoring conditions. Ion evaporation resulting from the ion spray liquid chromatography–mass spectrometry interface exhibits primarily molecular weight information as singly and multiply charged ions and is shown to be a sensitive and mild ionization method for peptides. The full-scan daughter ion mass spectrum of leucine enkephalin is shown to contain fragment ions consistent with the sequence of the peptide. Parent ion scanning in the tandem mass spectrometry mode is a promising technique for the screening of related peptides.

INTRODUCTION

About 10 years ago, one of the classical papers introducing high-performance electrophoresis as the electrophoretic counterpart of high-performance liquid chromatography (HPLC)[1] confronted its readers with the following statement: "Many of the problems in the development of electrophoresis can be reduced to convection and detection". The concept of high-performance capillary electrophoresis[2], for which the most commonly known mode of operation is capillary zone electrophoresis (CZE)[3], includes the alleviation of the convection problem by using narrow-bore open tubes as the separation chamber, thereby allowing rapid dissipation of the joule heat generated by the applied electric field. This approach guarantees stable electrophoresis performance owing to the "anti-convective wall-effect"[1], in contrast to the more

* On leave from the Department of Pharmacy and Food Chemistry, Würzburg University, 8700 Würzburg, F.R.G.

0021-9673/88/$03.50

common solution of using such anti-convective stabilizers as paper, cellulose acetate and gels to suppress convective zone broadening in electrophoresis techniques. This approach also brought about the realization of a powerful instrumental version of electrophoresis[4], analogous to modern column chromatography, with its appreciated high standard of automation. Recently published studies focusing on different aspects of CZE instrumentation still emphasize this key concern for present and future developments[5–8].

With regard to the above-mentioned detection problem, the principle of on-column detection feasibility in CZE again opened new possibilities for analyte characterization. The readily installed optical detectors based on UV absorption and fluorescence emission[9,10] were soon followed by other techniques promising to fulfil the requirements of universal detection on the one hand and high sensitivity on the other. This capability is especially challenging owing to detection volumes in the low nanoliter to picoliter range[11,12].

Smith and co-workers[13,14] were the first to report the successful interfacing of CZE with mass spectrometry (CZE–MS). Their interface was based on the electrospray ionization liquid interface for mass spectrometry developed by Whitehouse *et al.*[15]. There should be little need here to review the merits of mass spectrometric detection with regard to universality, high sensitivity and outstanding selectivity. The success of gas chromatography–mass spectrometry (GC–MS) and high-performance liquid chromatography–mass spectrometry (HPLC–MS) easily attests to the importance of the mass spectrometer as the preferred detector for modern on-line separation techniques.

Although HPLC, another powerful separation technique, has become more widely used in the biochemical field in the last decade owing to advances in instrumentation and automation, there is no doubt that electrophoresis in its various forms is still the premier method for the separation and analysis of peptides, proteins and polynucleotides. The impact of mass spectrometry on the analytical demands in the life sciences has become increasingly important[16–19]. Research in the area of endogenous peptides, for example, has frequently profited from progress in mass spectrometry[20] since the successful identification of enkephalins in brain tissues by Hughes *et al.*[21]. An excellent overview of state-of-the-art mass spectrometric determination of peptides and proteins was recently published by Biemann and Martin[22].

The potential of CZE to separate peptides, proteins and polynucleotides has already been demonstrated[3,23,24]. The new technique of CZE–MS, which combines the separation efficiency of electrophoresis for charged species with the well known capability of mass spectrometry for structure elucidation, should be well suited for the analysis of complex mixtures of charged biochemical compounds.

Here we describe in brief the instrumental and experimental aspects of our approach to on-line CZE–MS coupling, which will be presented in more detail elsewhere[25]. We also present results demonstrating the feasibility of this technique for the determination of small peptides.

EXPERIMENTAL

Electrophoresis

The capillary electrophoresis system consisted of a 0–60 kV voltage regulated

power supply (Spellman, Model RHR60P30/EI, Plainview, NY, U.S.A.). The high-voltage lead was connected directly to a 2-ml carbon vessel which served a dual purpose as buffer reservoir and electrode. The separation column, a 100 cm × 100 μm I.D. length of uncoated fused-silica capillary (Polymicro Technologies, Phoenix, AZ, U.S.A.), was suction-filled with buffer and the anode end of the column was suspended in the carbon vessel containing the buffer medium. The cathode end of the column was connected to the ion spray LC–MS interface[26] via a liquid junction coupling described in more detail elsewhere[25]. The buffer used was acetonitrile–30 m*M* acetate buffer (pH 4.8) (1:1). Sample volumes of 2 to 30 nl were introduced into the column at the anode end by hydrostatic injection (siphoning)[27]. The injection volume was determined by injecting a narrow band of a dark dye and measuring the time required for it to pass through a given length of the column while in the inject mode. A potential of 30 kV was applied to the anode end of the separation column through the carbon buffer reservoir and 3 kV was applied to the cathode end through the ion spray interface, which produced a net CZE voltage of 27 kV. A CZE voltage of 27 kV was used for all separations reported and the current (20–40 μA) passing through the CZE column was measured with an in-line analog ammeter (Model 260; Simpson, Chicago, IL, U.S.A.).

Mass spectrometry

A SCIEX TAGA 6000E triple quadrupole mass spectrometer (Thornhill, Ontario, Canada) equipped with an atmospheric pressure ionization (API) source was used to sample ions produced from the ion spray LC–MS interface. In this system ions in the gas phase are drawn into the vacuum of the mass spectrometer through a 100 μm I.D. orifice. The atmospheric side of the orifice is bathed with a curtain of high-purity, dry nitrogen gas. The nitrogen curtain acts as a barrier that restricts contaminants and solvent vapor from entering the mass spectrometer vacuum. High vacuum in the analyzer region of the mass spectrometer is achieved by cryogenically cooled surfaces, maintained at 19–20 K, surrounding the quadrupoles. During routine operation the indicated vacuum was $7 \cdot 10^{-6}$ Torr and during collision-induced dissociation (CID) the vacuum was $1.5 \cdot 10^{-5}$ Torr with a target gas thickness of $230 \cdot 10^{12}$ atoms/cm^2 of argon in the collision cell. A collision energy of 50 V was used for all CID experiments.

Chemicals

The peptides dynorphin 1–6, 1–7, 1–8 and 1–9 and leucine enkephalin (dynorphin 1–5) were obtained from Sigma (St. Louis, MO, U.S.A.) and used without further purification. HPLC-grade ammonium acetate, glacial acetic acid, water and acetonitrile were obtained from Fisher (Rochester, NY, U.S.A.).

RESULTS AND DISCUSSION

The injection reproducibility for the system described above was determined by triplicate 10-s hydrostatic injections at a height of 5 cm for three different concentrations of leucine enkephalin (Fig. 1). As the flow of the CZE system can be stopped during operation by simply turning off the high voltage, serial injections can be made at close intervals. Amounts of 24, 120 and 600 fmole of leucine enkephalin were

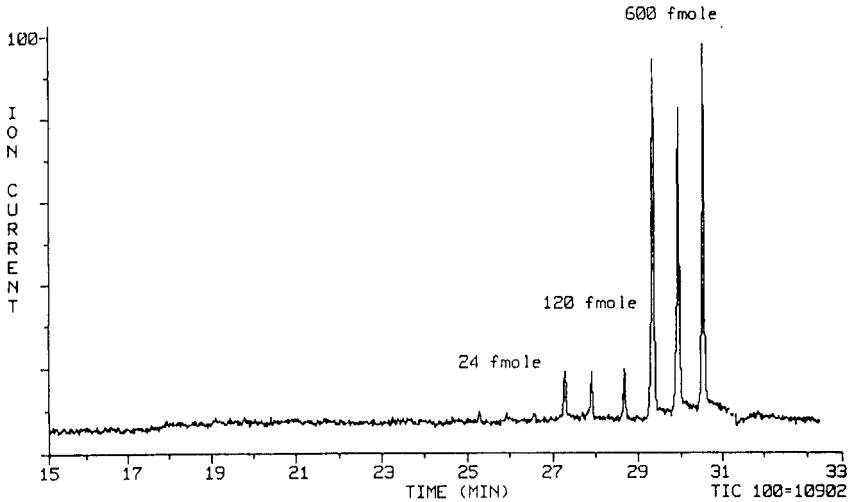

Fig. 1. SIM CZE–MS electropherogram for repetitive triplicate injections of 24, 120 and 600 fmole levels of leucine enkephalin. The $(M+H)^+$ ion at *m/z* 556 was monitored.

injected with mass spectral acquisition of its protonated molecular ion at *m/z* 556. The peak widths at half-height for all peaks in the serial injection electropherogram (Fig. 1) were measured and found to be the same (1.2 mm). This demonstrates that band broadening from each injection was not observed. The peak heights and areas

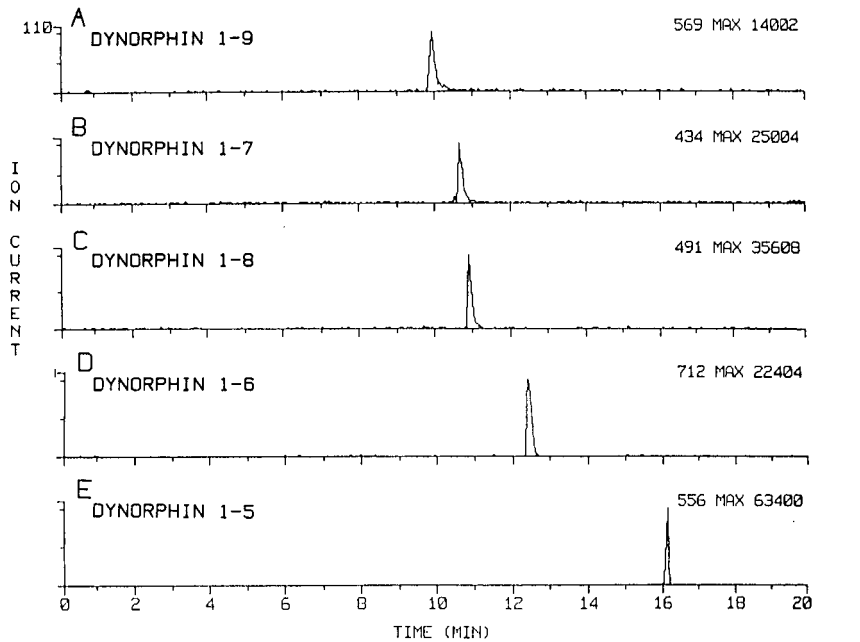

Fig. 2. Full-scan CZE–MS extracted ion electropherograms for 5 pmole per component of (A) dynorphin 1–9, (B) dynorphin 1–7, (C) dynorphin 1–8 (D) dynorphin 1–6 and (E) leucine enkephalin (dynorphin 1–5).

within each triplicate (Fig. 1) are within 10% of the other two peaks, demonstrating satisfactory reproducibility from the system. All injections were made by manual operation. If this system were automated it should follow that reproducibility would be within 1–2%.

A CZE separation was obtained for 5 pmole each of dynorphin 1–9, 1–7, 1–8 and 1–6 and leucine enkephalin under full-scan CZE-MS conditions (Fig. 2). The mass spectrometer was scanned from m/z 300 to 750 at a rate of 2 s per scan. The

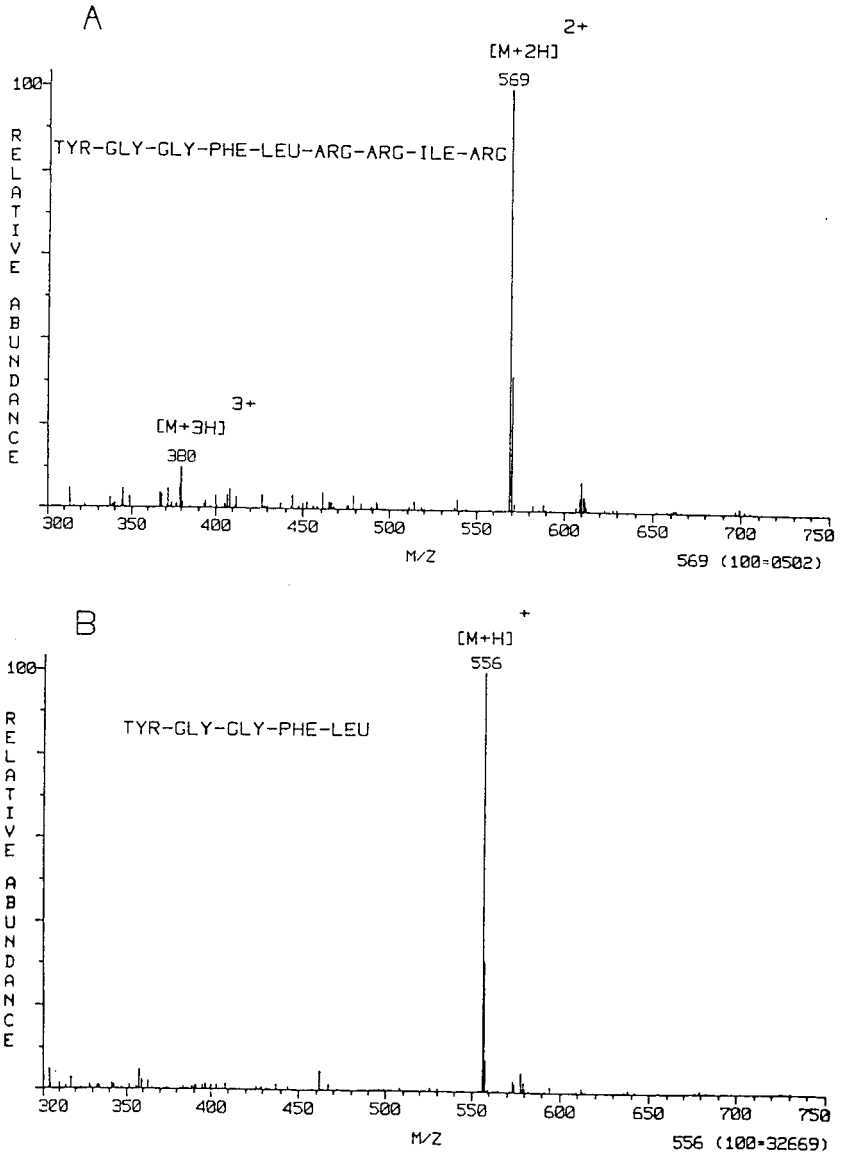

Fig. 3. CZE–MS mass spectra for (A) dynorphin 1–9 and (B) leucine enkephalin from Fig. 2. Ions are formed by ion evaporation at atmospheric pressure via the ion spray LC–MS interface.

individual extracted ion current electropherograms from this CZE–MS experiment show good separation for all five components. Because the capillary electrophoresis separation was developed with the anode end at high positive voltage (30 kV) and the cathode at low voltage (3 kV), the net electroosmotic flow of the system was from the anode to the cathode and species with more positive electrophoretic mobilities were eluted first. Electrophoretic mobility is a function of charge and size, and the more positively charged species should be eluted first[3]. As shown in the corresponding CZE–MS mass spectra (Fig. 3), obtained from the electropherogram shown in Fig. 2, the mass spectrum of the first-eluted peak, dynorphin 1–9 (Fig. 3A), contains both triply protonated, triply charged (*m/z* 380) and doubly protonated, doubly charged (*m/z* 569) molecular ions and the last-eluted peak, leucine enkephalin (Fig. 3B) contains only the singly charged, protonated molecular ion (*m/z* 556). Under the acidic CZE conditions used the charge on each peptide in solution is a function of the number of terminal amino functionalities. This is evidenced by the fact that dynorphin 1–7 (Fig. 2B) is eluted before dynorphin 1–8 (Fig. 2C). Both dynorphin 1–7 and dynorphin 1–8 contain three terminal amino groups; however, the mass of dynorphin 1–8 is greater. Therefore, dynorphin 1–8 has a lower mobility than dynorphin 1–7, so it is eluted later. As can be seen, the elution order is a function of the charge and size of the species with the most positively charged and small size species being eluted first.

The ion spray LC–MS interface utilizes a form of electrospray ionization where gaseous ions are produced by the mechanism of ion evaporation[28]. This is a mild form of ionization where predominantly singly protonated, singly charged and/or multiply protonated, multiply charged molecular ions are formed. This provides an opportunity for operating the mass spectrometer in the selected ion monitoring (SIM) mode with high sensitivity, as the ion current is concentrated into only a few species which are characteristic of the analyte. By operating in the SIM mode lower CZE–MS detection limits can be achieved with higher separation efficiencies. This is evidenced in the SIM electropherogram (Fig. 4) for 2 pmole per component of the mixture

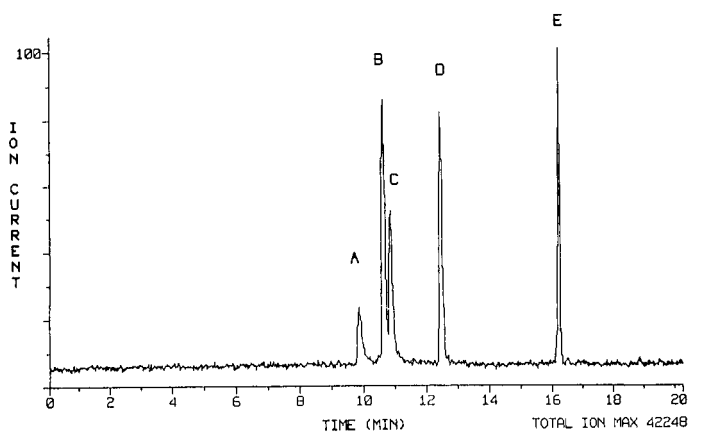

Fig. 4. Total SIM CZE–MS ion electropherogram for 2 pmole per component of (A) dynorphin 1–9 (*m/z* 380 and 569), (B) dynorphin 1–7 (*m/z* 434), (C) dynorphin 1–8 (*m/z* 491), (D) dynorphin 1–6, (*m/z* 356 and 712) and (E) leucine enkephalin (*m/z* 556).

described in Fig. 2, where the last-eluted peak (E) exhibits efficiencies in excess of 250 000 theoretical plates.

Another advantage of having the molecular ion carry most of the ion current is that sensitivity is increased for tandem mass spectrometry (MS–MS) experiments. By monitoring the protonated molecular ion of leucine enkephalin at *m/z* 556 with the first quadrupole, performing collision-induced dissociation (CID) in the second qua-

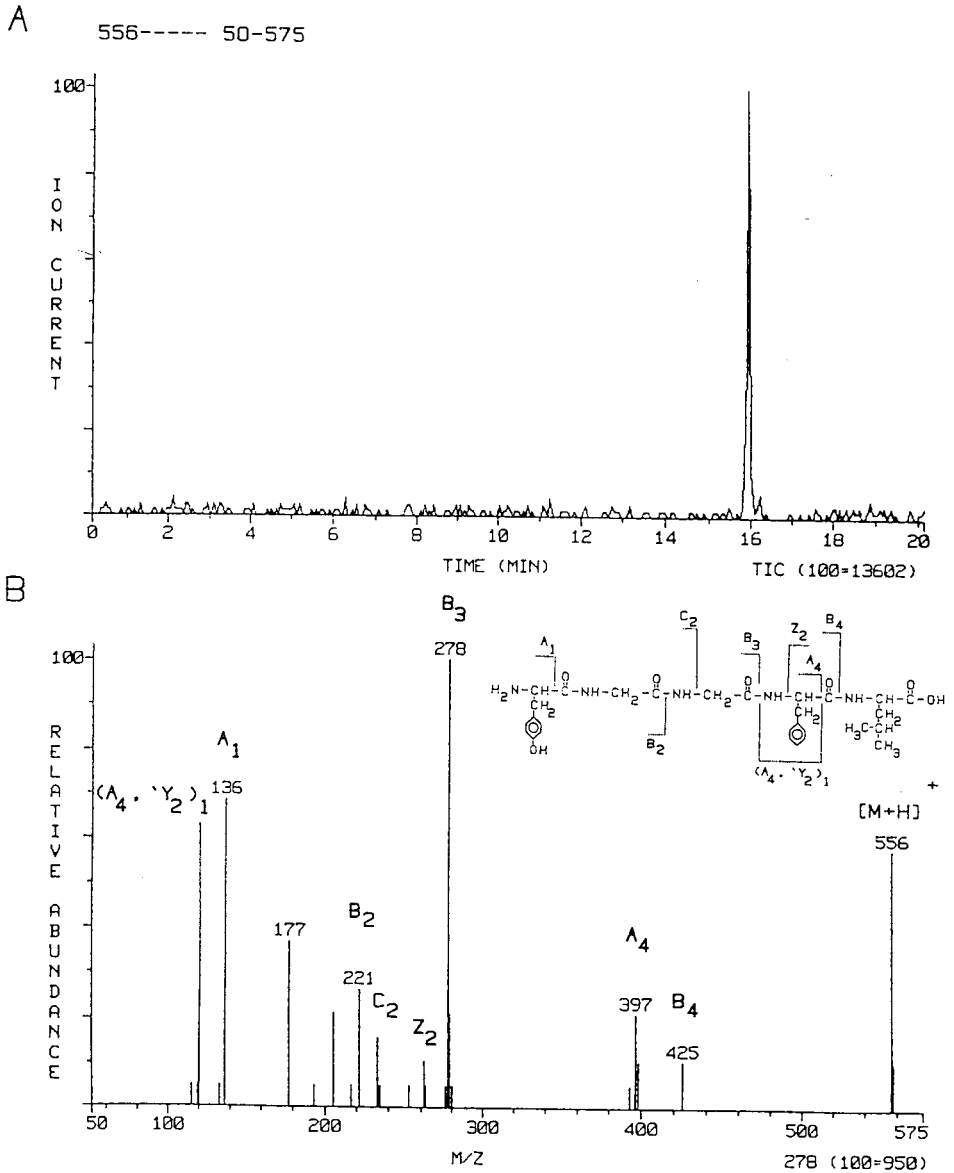

Fig. 5. (A) Full-scan CZE–MS–MS (from *m/z* 50 to 556) total daughter ion current electropherogram and (B) collision-induced-dissociation mass spectrum for 5 pmole of leucine enkephalin. The parent ion for CID was $(M+H)^+$ ion at *m/z* 556.

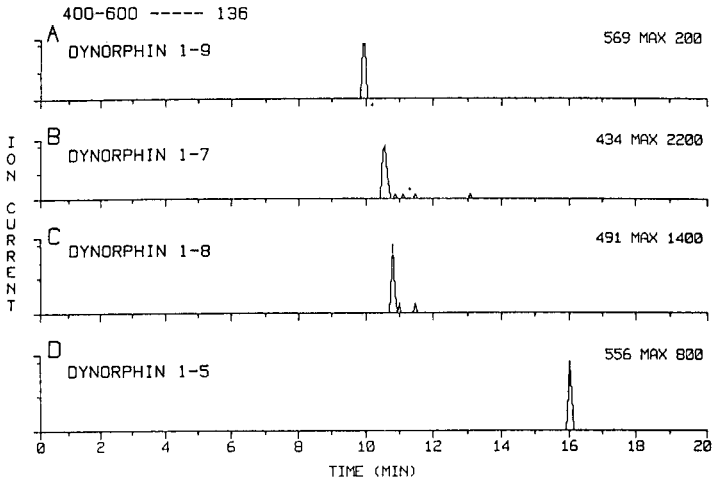

Fig. 6. CZE–MS–MS extracted parent ion electropherograms for the common daughter ion at *m/z* 136 for (A) dynorphin 1–9, (B) dynorphin 1–7, (C) dynorphin 1–8 and (D) leucine enkephalin. Quadrupole 1 was scanned from *m/z* 400 to 600 and Quadrupole 3 monitored *m/z* 136.

drupole, and scanning the third quadrupole from *m/z* 50 to 556 the total ion electropherogram (Fig. 5A) and the daughter ion mass spectrum (Fig. 5B) for 5 pmole of leucine enkephalin were acquired[29]. The daughter ion mass spectrum (Fig. 5B) is consistent with the sequence of the pentapeptide, leucine enkephalin, and provides the necessary information required to identify its structure. The nomenclature scheme proposed by Roepstorff and Fohlman[30] was used to label the sequence ions of the CID daughter ion mass spectrum of leucine enkephalin (Fig. 5B). The daughter ions B_2, Z_2, B_3, A_4 and B_4 are consistent with fragment ions from fast atom bombardment linked-field scanning of leucine enkephalin reported in the literature[31].

Because $(A_4, {}^{\prime}Y_2)_1$ at *m/z* 120 and A_1 at *m/z* 136 are common CID daughter ions of all dynorphins, parent ion scans can be performed as a screen for possible components in a mixture[29]. The parent ion experiment (Fig. 6) for 5 pmole per component of dynorphin 1–9, 1–7 and 1–8 and leucine enkephalin was performed by scanning the first quadrupole from *m/z* 400 to 600 and monitoring *m/z* 136 in the third quadrupole. Dynorphin 1–9, 1–7 and 1–8 were identified by their doubly protonated, doubly charged molecular ions at *m/z* 569, 434 and 491, respectively, and leucine enkephalin was identified by its singly protonated, singly charged molecular ion at *m/z* 556.

CONCLUSIONS

These results demonstrate the feasibility of using CZE–MS and CZE–MS–MS with an atmospheric pressure ionization (API) triple quadrupole mass spectrometer for the determination of small peptides. CZE is capable of separating small peptides with high efficiencies, from 50 000 to 250 000 theorectical plates, relatively rapidly. The ion spray LC–MS interface is well suited for CZE and API mass spectrometry owing to its high sensitivity for species which exist charged in solution. Quantitation

with this system should be possible owing to the satisfactory reproducibility of injection. CZE–MS–MS complements CZE–MS by producing additional structural and sequence information. At present, concentrations of the analytes of interest in the sample solution are still in the high parts per billion to low parts per million range. Improved sensitivity of the mass spectrometer and higher sample capacity of the CZE column would improve the utility of the combined CZE–MS system. Future efforts should be directed towards these goals.

ACKNOWLEDGEMENTS

We thank Waters Chromatography Division for providing a modified Model 440 detector cell for on-line UV detection. W. M. thanks the Deutsche Forschungsgemeinschaft for providing a post-doctoral scholarship.

REFERENCES

1 F. E. P. Mikkers, F. M. Everaerts and Th. P. E. M. Verheggen, *J. Chromatogr.*, 169 (1979) 11–20.
2 S. Hjérten, *J. Chromatogr.*, 270 (1983) 1–6.
3 J. W. Jorgenson and K. D. Lukacs, *Science*, 222 (1983) 266–272.
4 J. W. Jorgenson and K. D. Lukacs, *Anal. Chem.*, 53 (1981) 1298–1302.
5 R. A. Wallingford and A. G. Ewing, *Anal. Chem.*, 59 (1987) 678–681.
6 T. Tsuda, T. Mizuno and J. Akijama, *Anal. Chem.*, 59 (1987) 799–800.
7 D. J. Rose and J. W. Jorgenson, *Anal. Chem.*, 60 (1988) 642–648.
8 D. J. Rose and J. W. Jorgenson, *J. Chromatogr.*, 438 (1988) 23–24.
9 Y. Walbroehl and J. W. Jorgenson, *J. Chromatogr.*, 315 (1984) 135–143.
10 J. S. Green and J. W. Jorgenson, *J. Chromatogr.*, 352 (1986) 337–343.
11 R. A. Wallingford and A. G. Ewing, *Anal. Chem.*, 59 (1987) 1762–1766.
12 X. Huang, T.-K. J. Pang, M. J. Gordon and R. N. Zare, *Anal. Chem.*, 59 (1987) 2747–2749.
13 J. A. Olivares, N. T. Nguyen, C. R. Yonker and R. D. Smith, *Anal. Chem.*, 60 (1987) 1230–1232.
14 R. D. Smith, J. A. Olivares, N. T. Nguyen and H. R. Udseth, *Anal. Chem.*, 60 (1988) 436–441.
15 C. M. Whitehouse, R. N. Dreyer, M. Yamashita and J. B. Fenn, *Anal. Chem.*, 57 (1985) 675–679.
16 H. R. Schulten, *Int. J. Mass Spectrom. Ion Phys.*, 32 (1979) 97–283.
17 C. Fenselau, *Anal. Chem.*, 54 (1982) 105A–116A.
18 M. Barber, R. S. Bordoll, G. J. Elliot, R. D. Sedgwick and A. N. Tyler, *Anal. Chem.*, 54 (1982) 645A–657A.
19 P. Roepstorff, *Eur. Spectrosc. News*, 73 (1987) 18–23.
20 D. M. Desiderio and G. H. Fridland, in S. J. Gaskell (Editor), *Mass Spectrometry in Biomedical Research*, Wiley, New York, 1986, pp. 443–458.
21 J. Hughes, T. W. Smith, H. W. Kosterlitz, L. A. Fothergill, B. A. Morgan and H. R. Morris, *Nature (London)*, 258 (1975) 577–579.
22 K. Biemann and S. A. Martin, *Mass Spectrom. Rev.*, 6 (1987) 1–76.
23 H. H. Lauer and D. McManigill, *Anal. Chem.*, 58 (1986) 166–170.
24 A. S. Cohen, S. Terabe, J. A. Smith and B. L. Karger, *Anal. Chem.*, 59 (1987) 1021–1027.
25 E. D. Lee, W. Mück, T. R. Covey and J. D. Henion, *Anal. Chem.*, submitted for publication.
26 A. P. Bruins, T. R. Covey and J. D. Henion, *Anal. Chem.*, 59 (1987) 2642–1646.
27 X. Huang, M. J. Gordon and R. N. Zare, *Anal. Chem.*, 60 (1988) 375–377.
28 B. A. Thomson and J. V. Iribarne, *J. Chem. Phys.*, 71 (1979) 4451–4463.
29 R. A. Yost and C. G. Enke, *Anal. Chem.*, 51 (1979) 1251A–1264A.
30 R. Roepstorff and J. Fohlman, *J. Biomed. Mass Spectrom.*, 11 (1984) 601.
31 D. M. Desiderio and I. Katakuse, *Mass Spectrom.*, 33 (1985) 351–369.

Journal of Chromatography, 458 (1988) 323–333
Elsevier Science Publishers B.V., Amsterdam — Printed in The Netherlands

CHROMSYMP. 1530

RAPID SEPARATION OF DNA RESTRICTION FRAGMENTS USING CAPILLARY ELECTROPHORESIS

A. S. COHEN
Barnett Institute, Northeastern University, Boston, MA 02115 (U.S.A.)
D. NAJARIAN
Department of Molecular Biology, Massachusetts General Hospital, and Department of Genetics, Harvard Medical School, Boston, MA 02114 (U.S.A.)
JOHN A. SMITH
Department of Molecular Biology and Pathology, Massachusetts General Hospital, and Department of Pathology, Harvard Medical School, Boston, MA 02114 (U.S.A.)
and
B. L. KARGER*
Barnett Institute, Northeastern University, Boston, MA 02115 (U.S.A.)

SUMMARY

Open-tube capillary electrophoresis has been applied to the separation of restriction fragments of DNA with a Tris–borate buffer containing 7 *M* urea and 0.1% sodium dodecyl sulfate. The importance of sample pretreatment and of the injection of heated samples has been demonstrated. In one separation, a DNA restriction fragment mixture from 72 to 23 130 base pairs (DRIgest™ III) (molecular weight range from $4.6 \cdot 10^4$ to $1.5 \cdot 10^7$) has been electrophoresed in 10 min on a column of 15 cm effective length. Over 600 000 plates have been obtained for individual peaks. Several of the peaks have been identified, by spiking slab gel electrophoretically purified components. Other examples of restriction fragment separations are illustrated in this paper. The results of this study when further validated with full characterization of individual species, open up the possibility of rapid restriction enzyme mapping.

INTRODUCTION

The ability to analyze and manipulate DNA conveniently and rapidly is the cornerstone of the recent revolution in the biological sciences. With the discovery of restriction endonucleases, the molecular scissors of biology[1,2], a route was opened for characterization and use of fragments of large DNA molecules. Since individual restriction enzymes cleave at specific DNA base sequences, separation and analysis of individual fragments provides important information on the structure of DNA. Interestingly, the characterization of DNA is not only of importance in molecular biology but has also recently been promoted as a tool in forensic science for human identification[3].

0021-9673/88/$03.50

Restriction mapping, a method of separation and analysis of DNA fragments, is currently a major application of slab gel electrophoresis[4]. The basis of separation is believed to be size related since the charge density of large individual fragments is similar, except for conformational changes[5]. While successful, the slab gel method can be characterized as long and tedious, prone to error (particularly in not detecting all fragments), non-quantitative and cumbersome to use for isolation of individual fragments.

Capillary electrophoresis has recently emerged as an instrumental approach to electrophoresis (*e.g.*, refs. 6–13). Both open-tube and gel-filled capillaries can be used for separation. Remarkably high-performance separations are possible due to the high applied electric fields and operation in a manner that axial diffusion is the main cause of band broadening[14]. The method can be automated and used both for analysis and isolation of purified fragments.

This laboratory has previously separated small oligonucleotides by open-tube capillary electrophoresis using a metal–sodium dodecyl sulfate (SDS) micelle system[15]. In addition, we have used polyacrylamide gel-filled columns for separation of oligonucleotides differing by single bases and have isolated purified fractions[16]. The time required for isolation was greatly reduced over conventional methods for slab gel electrophoresis, elution and desalting. Others have separated small oligonucleotides[17] and eluted λ DNA [48 kilobase (kb) pairs][18] in open-tube electrophoresis. Since samples of restriction fragments will normally consist of polynucleotides with a wide molecular weight range, we decided to examine the possibility of DNA restriction fragment separations with open-tube capillaries. This approach should in principle permit the migration of all molecular weight species. In this paper we report initial studies on the rapid separation of restriction fragments using open-tube capillary electrophoresis. These promising results offer the potential of a new approach to restriction mapping. Relative to slab gel electrophoresis the possibility exists of higher speed of separation, higher resolution, greater ease of isolation of individual fragments and a greatly increased dynamic molecular weight range for separation.

EXPERIMENTAL

Apparatus

Capillary gel electrophoresis was performed in fused-silica tubing (Scientific Glass Engineering, Austin, TX, U.S.A.), 75 μm I.D. with column lengths of 300–650 mm, depending on the experiment. The polyimide coating was carefully burned off at approximately the midpoint of the capillary for on-column detection. A 30-kV high-voltage d.c. power supply (Model LG-30R-5, Glassman, Whitehouse Station, NJ, U.S.A.) was used to produce the potential across the capillary. A plexiglass lock system with cut-off the circuit when opened was placed on the high-voltage side for safety. A UV detector (Soma S-3702, IR & D, Kingston, MA, U.S.A.), modified as previously described[15], was employed at a wavelength of 260 nm. The tubing and the detector were cooled using a thermostated air bath. The power supply outlets were connected to platinum electrodes, immersed in buffer reservoirs (for analytical runs) or in a microfuge vial (for collection). An analog–digital interface (Nelson Analytical, Cupertino, CA, U.S.A.) attached to a recorder and IBM PC/XT computer system were used to record the results and process the data.

Materials

DRIgest™ III (λ DNA-Hind III/ΦX174 DNA-Hae III), DRIgest™ II (λ DNA-Hind III/ΦX174 DNA-Hinc II) and ΦX174 DNA-Hinc II digest were purchased from Pharmacia, (Piscataway, NJ, U.S.A.) and used as received. All other reagents were of protein-research grade (Schwartz/Mann Biolab, Cambridge, MA, U.S.A.). All buffer solutions were filtered through a Nylon GC filter unit of 0.2 μm pore size (Schleicher and Schuell, Keene, NH, U.S.A.). Samples were kept frozen at -20°C and sample solutions were stored at 4°C before use. Samples were heated at 60–65°C for 20 min prior to injection and were injected hot. Buffer solutions were carefully vacuum degassed.

Procedure

The fused-silica capillary tubing was filled with the desired buffer (0.1 *M* Tris–borate pH 8.1, 2.5 m*M* EDTA, 7 *M* urea and 0.1% SDS = buffer A). Both ends of the tube were then dipped into separate 5-ml reservoirs filled with buffer. The end in which the sample was introduced was connected with a platinum electrode to the positive high voltage side of the power supply. The reservoir at the detector end was connected with a platinum electrode to ground. Hot samples at a concentration of 0.25 mg/ml were introduced by siphoning with an estimated injection volume of 3–4 nl.

Before each run, the capillary was purged with 100 μl of 0.1 *M* sodium hydroxide solution followed by 250 μl of triply distilled water. Care was taken to equilibrate the capillary with buffer prior to operation. The reproducibility of retention was better than $\pm$ 3% relative standard deviation from run to run. It has been found that reproducibility is sensitive to temperature control.

RESULTS AND DISCUSSION

We selected for study a standard digest —DRIgest III, which consists of a combination of the restriction enzyme, Hind III, digest of λ DNA (48 kb) and the enzyme Hae III digest of ΦX174 DNA (5 kb). This mixture, based on the known sequences of the DNAs, is expected to yield 19 fragments from 72 to 23 130 base pairs; however, the molecular weight difference of several pairs is not great (and generally not resolved) and several only appear faintly on gels upon staining[19]. It is to be noted that the molecular weight range of this sample is very wide ($4.6 \cdot 10^4$ to $1.5 \cdot 10^7$), necessitating different polyacrylamide or agarose gel compositions to encompass the whole mixture[20].

It is known that a sample of DNA fragments must first be carefully treated in order to break aggregated base-pair species. Moreover, DNA can break into smaller fragments as a result of shear forces, the lability being a function of the size of the DNA. Care must therefore be exercised in sample handling. In addition, samples were always freshly used and stored at -20°C.

Direct injection of an untreated sample of the DRIgest III mixture resulted in poor separation, with very broad bands under a variety of buffer and column temperature conditions. This is possibly due to the sticky ends of λDNA aggregating together[19]. We then turned to the standard pretreatment procedure for dissociating aggregates, namely heating the sample at 60°C for 15–20 min. This approach most likely does not break base-paired fragments, since 7 *M* urea is not present[21].

Fig. 1 shows an electropherogram after cooling the heat treated sample to 25°C and then injecting into a column at room temperature containing buffer A. Improved separation resulted over an untreated sample; however, a broad early eluting band was observed. This band was suspected to be aggregated fragments of deoxyoligonucleotides, perhaps arising from reaggregation of the small fragments upon cooling.

Successful separation required injection of the hot sample solution on the column and rapid application of the electric field. In this work, 3–4 nl of the heat-treated sample was siphoned into the column, and an electric field of 500 V/cm was immediately applied. In this manner high-performance separations were achieved, as shown in Fig. 2A. Evidently, the applied electric field is able to act as a counterbalancing force to aggregation by providing rapid separation of individual fragments. Not only were the sample pretreatment and injection steps important, but the composition of the buffer was also significant. For example, removing 7 *M* urea from buffer A caused formation of a broad band as in Fig. 1. Similarly, 0.1% SDS was found to be a necessary ingredient for achieving successful separation. Finally, substitution of Tris–phosphate for Tris–borate at pH 8 caused a significant loss in

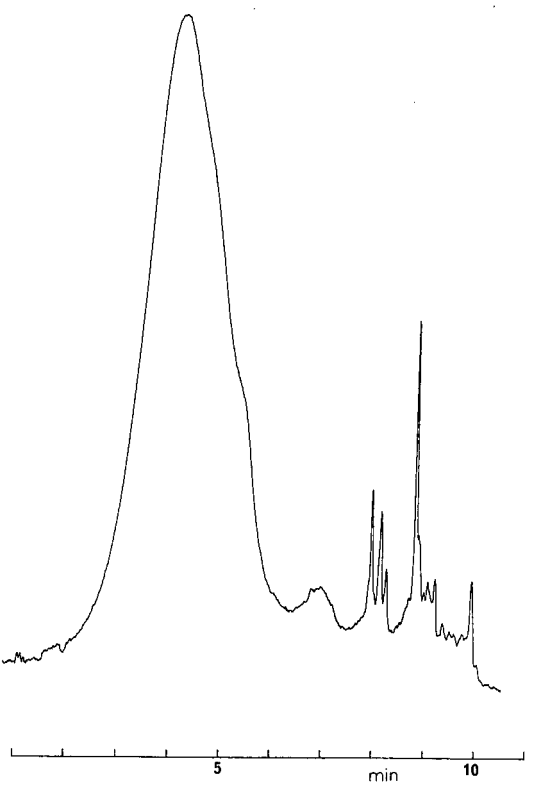

Fig. 1. Influence of sample pretreatment on electropherogram of DRIgest III. Sample heated for 20 min at 60°C, cooled to room temperature, and injected by siphoning. Conditions: Buffer: 0.1 *M* Tris–borate, pH 8.1, 2.5 m*M* EDTA, 0.1% SDS, 7 *M* urea; column 300 × 0.075 mm I.D., effective length 150 mm; applied voltage, 15 kV, 30 μA; detection, UV, 260 nm; temperature, 27 ± 0.5°C.

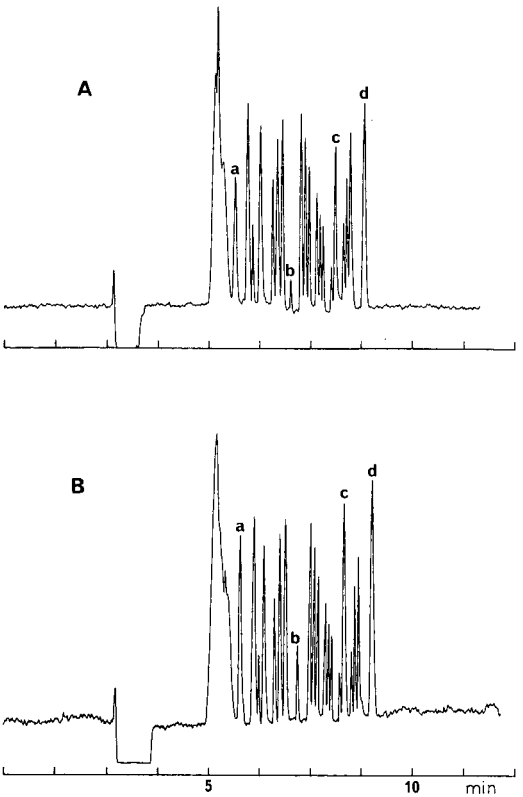

Fig. 2. (A) Separation of DRIgest (λ DNA-Hind III/ΦX174 DNA-Hae III). Sample heated for 20 min at 60°C, injected hot by siphoning (3–4 nl). All other conditions in Fig. 1. (B) Separation of DRIgest III sample spiked with 4 slab gel electrophoretically purified fragments: 72 (a), 564 (b), 4362 (c) and 23 130 (d) base pairs. Note the increased peak areas for the spiked peaks relative to those (A). All conditions identical to (A).

resolution. Other systems, perhaps involving complexation[15], may also prove useful for resolution purposes.

Returning to Fig. 2A, high-performance separation is observed, with the appearance of 20 peaks, after a small initial broad band. Electroosmotic flow occurs towards the negatively charged electrode (cathode), due to the negative zeta potential on the walls. Since the restriction fragments are also negatively charged, elution order is in increasing electrophoretic mobility towards the positive electrode. In order to demonstrate that restriction fragments are indeed being separated we next examined the elution order of several purified fragments.

Using standard Hind III digest conditions of λ DNA, we separated individual fragments in a conventional manner on a slab gel consisting of 0.8% agarose. Several bands were observed upon staining with ethidium bromide and each band was electroeluted into a dialysis bag. The DNA was recovered by precipitation with ethanol to yield purified fragments.

Two fragments were isolated in sufficient quantity for examination: 564 and

23 130 base pairs. On the agarose gel, these fractions appeared pure on the basis of ethidium bromide staining. Fig. 3B and D show the elution of these two substances from the capillary electrophoresis column, using identical conditions as in Fig. 2A. The electropherograms appear fairly pure in both cases.

Fig. 3A shows the electropherogram of a purified 72-base pair fragment obtained from the plasmid M13 mp18. The fragment was purified by slab gel electrophoresis using 2% agarose. After excision and electroelution into a dialysis bag, the fragment was recovered and further purified by ion exchange. Finally, Fig. 3C shows the electropherogram of a 4362-base pairs fragment obtained from the plasmid pBr 322 which was again digested with Eco RI. Note that for 72 and 4362 base pairs, the base pair number agrees with a fragment of DRIgest III, but the sequence is not the same.

We next added a small amount of each purified fragment to a DRIgest III sample, and the electropherogram of this sample is shown in Fig. 2B. A rudimentary comparison of peaks a–d in Fig. 2A and B reveals that increases in peak height occur for all four bands. This result strongly suggests that elution is in order of increasing molecular weight, *i.e.* the highest molecular weight has the largest electrophoretic mobility. These promising results require further validation, both by examining a larger number of purified fractions and also by collecting fractions from the capillary[16] followed by slab gel electroporesis. Nevertheless, restriction fragment separations have been achieved. Let us next examine several aspects of the separation.

It is generally believed that electrophoretic mobility differences in free solution are independent of the moleclar weight of the restriction fragment.[4] The fact that separation is observed in an open capillary format as in Fig. 2 may in part be related to the high resolving power of the capillary electrophoretic approach. While plate number (N) varies from peak to peak, an average value would appear to be 600 000 plates. With such large plate numbers rapidly generated, the power of the high-performance capillary electrophoresis approach can be understood in the following way.

The resolution (R_s) of two adjacent peaks can be written as

$$R_s = \left(\frac{N^{1/2}}{2}\right)\left(\frac{\Delta\mu}{\bar{\mu}}\right) \tag{1}$$

where $\Delta\mu$ is the difference in electrophoretic mobilities of adjacent pairs and $\bar{\mu}$ is the average mobility for the set of fragments. If $R_s = 1$ is assumed to be minimal resolution, then for $N = 6 \cdot 10^5$, $\Delta\mu/\bar{\mu} = 5.3 \cdot 10^{-3}$. In other words, an electrophoretic mobility difference of 0.5% will lead to baseline resolution. Thus the high plate count permits subtle differences in mobility to be observed.

Based on retention time and a hold-up time (t_0) of 2.8 min, it is possible to calculate the apparent mobility μ_{app} and the true electrophoretic mobility μ_e

$$\mu_{app} = \mu_e + \mu_0^* \tag{2}$$

where μ_0^* is the effective mobility of the electroosmotic flow. For the 72-base pairs fragment $\mu_{app} = 9 \cdot 10^{-5}$ cm^2/V s and for the 23 130-base pairs fragment $\mu_{app} = 5.4 \cdot 10^{-5}$ cm^2/V s. The electrophoretic mobilities μ_e are then $0.9 \cdot 10^{-4}$cm^2/V s and

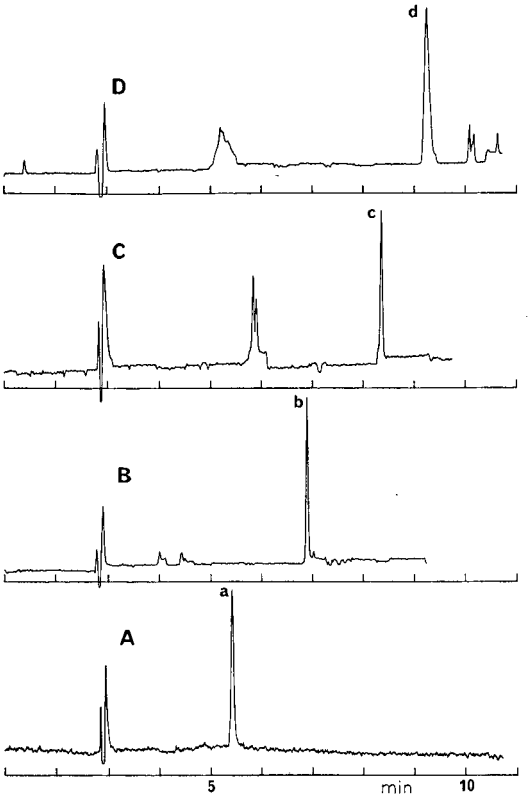

Fig. 3. Electropherograms of individual restriction fragments used in the spiked sample of Fig. 2B. Conditions as in Fig. 2A. (A) 72-base pairs gel-purified fragment from plasmid M13 mp18 DNA. After electroelution the fragment was further purified using an ion-exchange column. (B) 564-base pairs fraction purified from a λ DNA-Hind III digest using slab gel electrophoresis, 0.8% agarose. Gel slice of this fraction (stained with ethidium bromide) was electroeluted into a dialysis bag. The fraction was recovered by precipitation with ethanol. The precipitate was then washed with 80% aq. ethanol, suspended in deionized water and lyophilized. (C) 4362-base pairs fraction from plasmid DNA pBr 322 was linearized by Eco RI digestion. (D) 23 130-base pairs fraction purified from a λ DNA-Hind III using a slab gel electrophoresis.

$1.3 \cdot 10^{-4}$cm^2/V s for the smaller and larger fragments, respectively. These values are in the proper order of magnitude for base pair restriction fragments in solution[22]. The mobility change is seen to be small given a molecular weight variation of 300-fold. In terms of electrophoretic mobility, the column is thus able to achieve baseline resolution of differences of *ca.* $5 \cdot 10^{-7}$cm^2/V s. Clearly, column efficiency is very important in restriction fragment separations. Further improvement in resolution and column performance may be anticipated.

A second factor in the high resolution of the restriction fragments is the buffer selected. As already noted, Tris–phosphate did not yield the resolving power of Tris–borate. Undoubtedly, borate complexation with the sugar moieties affects mobility (charge and conformation) in a manner to alter electrophoretic mobility differences[23]. Secondly, SDS and urea were both found to be important in yielding

sharp bands. This may be related to the disaggregating effect of these species[24]. In addition, it is possible that SDS hydrophobically binds to oligonucleotides resulting in mobility changes. Further studies are underway to understand in more depth the retention and separation mechanism, as well as to examine other possible chemistries for selectivity.

Returning to Fig. 2B, four peaks have been identified by spiking of a DRIgest III sample. Interestingly, there are three peaks observed between 4362 and 23 130 base pairs. Theoretically, two peaks are expected (6557 and 9416 base pairs). The extra peak could arise from an impurity in the sample; however, collection and identification would be necessary to clarify this point.

That extra peaks can occur after slab gel purification can be seen in Fig. 3. The electropherogram for the 23 130-base pairs fraction reveals several peaks eluting later than the major peak, and these peaks presumably represent higher-molecular-weight polynucleotides. These could arise from incomplete cleavage (*e.g.*, a 2000-base pairs fragment is adjacent to the 23 130-base pairs fragment) as well as association of the sticky ends of λ DNA after fragmentation. It is interesting to note that only a single stained band of the 23 130-base pairs fragment was observed on agarose and this was excised from the gel; however, extra peaks are observed in capillary electrophoresis.

We also note two extra bands of presumably lower-molecular-weight fragments with the 4362-base pairs peak (Fig. 3C). These species arise either from further fragmentation upon sample handling or the possibility of entrapment of small fragments in the duplex helical structure.

Finally, in Fig. 2 the broad peak eluting early in the electropherogram of DRIgest III was investigated. The peak was collected in water (2 μl) and then analyzed by polyacrylamide slab gel electrophoresis. The peak was assumed to consist of small oligonucleotide fragments (less than 72 base pairs) based on ethidium bromide staining. Thus, the band may be broad as a result of incomplete resolution of small fragments.

Having examined DRIgest III, we next turned to several other restriction fragments to assess separation. Fig. 4 shows the separation under identical mobile phase conditions of Fig. 2 of DRIgest II which is a combination of λ DNA-Hind III and ΦX174 DNA-Hinc II. A total of 21 peaks are expected, again with a few components either difficult to resolve or detect. A total of 21 peaks are observed with high resolution in a narrow time window. It is to be noted that for this example (as well as for Fig. 5), a longer column was employed and a slightly lower field (300 *vs.* 500 V/cm). Hence, elution required a longer time than in Fig. 2. Finally, Fig. 5 shows a corresponding separation of ΦX174-Hinc II. Here, a maximum total of 13 peaks are expected (though several are quite difficult to observe by slab gel electrophoresis). A separation with 12–13 peaks is found in this figure. As with DRIgest III, it was necessary to inject hot into the column samples in both Figs. 4 and 5.

CONCLUSIONS

This paper has presented initial results on the open-tube capillary separation of restriction fragments. An open tube has been selected in order to encompass the wide molecular weight range in one run. Successful operaton required careful attention to

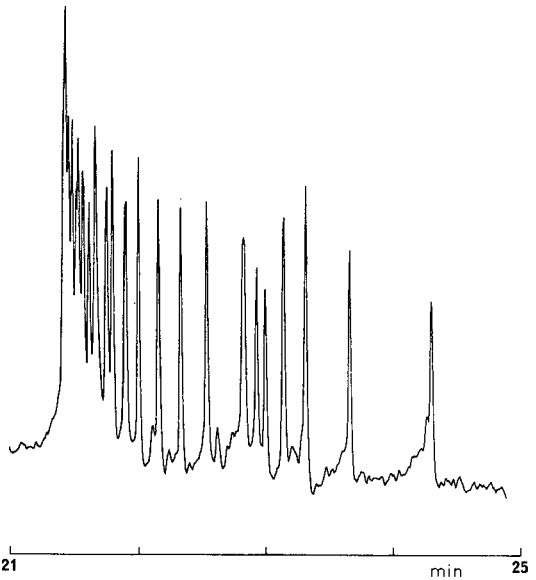

Fig. 4. Separation of DRIgest II (λ DNA-Hind III/ΦX174 DNA-Hinc II). Conditions as in Fig. 2A except column: 500 × 0.075 mm I.D., effective length 250 mm; applied voltage 15 kV, 18 μA.

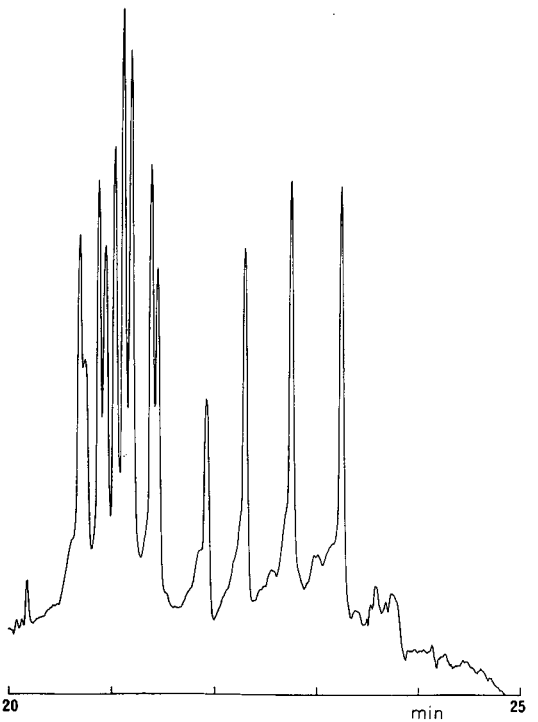

Fig. 5. Separation of ΦX174 DNA-Hinc II. Conditions as in Fig. 4.

sample handling and pretreatment. Hot sample injection produced the best results.

Given the similarity of mobilities of the restriction fragments, even with a molecular weight difference of 300-fold, high efficiency was found to be essential for success. With columns of 600 000 plates, mobilities differing by 0.5% or less should be resolvable. This translates to $5 \cdot 10^{-7}$ cm^2/V s difference with a restriction fragment mobility of $1 \cdot 10^{-4}$ cm^2/V s.

We have been able to identify several peaks in the electropherogram of DRIgest III by spiking the sample with purified fragments. More work is necessary in identifying a number of other fragments. The strategy to be taken will be to use other purified fragments, as well as a collection of electropherogram peaks (or peak clusters) and identification by agarose or polyacrylamide slab gel electrophoresis.

Ultimately, capillary electrophoresis should be useful in restriction mapping as well as optimization of digestion conditions for DNA. In addition, with appropriate resolution, it should be possible to isolate individual fragments[16] for further study (*e.g.* sequencing) as well as for subcloning. Work is continuing in our laboratory in this area.

ACKNOWLEDGEMENTS

B.L.K. gratefully acknowledges support by Beckman Instruments, Inc. and the James L. Waters Chair in Analytical Chemistry. J.A.S. gratefully acknowledges support by Hoechst AG (F.R.G.). Contribution No. 359 from the Barnett Institute.

REFERENCES

1 D. Nathans, *Science (Washington, D.C.)*, 206 (1979) 903.
2 H. Smith, *Science (Washington, D.C.)*, 205 (1979) 455.
3 B. Merz, *J. Am. Med. Assoc.*, 259 (1980) 2193.
4 N. C. Stellwagen, in A. Chrambach, M. J. Dunn and B. J. Radola (Editors), *Advances in Electrophoresis*, Vol. I, VCH, New York, 1987, p. 177.
5 P. Serwer and J. L. Allen, *Biochemistry*, 23 (1984) 922.
6 F. E. P. Mikkers, F. M. Everaerts and Th. P. E. M. Verheggen, *J. Chromatogr.*, 169 (1979) 11.
7 J. W. Jorgenson and K. D. Lucas, *Science (Washington, D.C.)*, 222 (1985) 266.
8 S. Tanaka, K. Otsuka and T. Ands, *Anal. Chem.*, 57 (1985) 834.
9 A. S. Cohen, A. Paulus and B. L. Karger, *Chromatographia*, 24 (1987) 15.
10 S. Hjertén, K. Ellring, F. Kilár, J. L. Liao, A. J. C. Chen, C. J. Siebert and M.-D. Zhu, *J. Chromatogr.*, 403 (1987) 47.
11 J. A. Olivares, N. T. Nguyen, C. R. Yonker and R. D. Smith, *Anal. Chem.*, 59(1987) 1232.
12 R. A. Wallingford and A. G. Ewing, *Anal. Chem.*, 59 (1987) 1767.
13 X. H. Huang, T. K. J. Pang, M. J. Gordon and R. N. Zare, *Anal. Chem.*, 59 (1987) 2747.
14 H. H. Lauer and D. McManigill, *Anal. Chem.*, 58 (1986) 166.
15 A. S. Cohen, S. Terabe, J. A. Smith and B. L. Karger, *Anal. Chem.*, 59 (1987) 1021.
16 A. S. Cohen, D. R. Najarian, A. Paulus, A. Guttman, J. A. Smith and B. L. Karger, *Proc. Natl. Acad. Sci. U.S.A.*, in press.
17 K. H. Row, W. H. Griest and M. P. Maskarinic, *J. Chromatogr.*, 409 (1987) 193.
18 S. Compton and R. Brownlee, *Biotechniques*, 6 (1988) 5.
19 *Certificate of Analysis, DRIgest™ III*, Pharmacia, Molecular Biology Division, Piscataway, NJ, 1988.
20 T. Maniatis, E. E. Fritsch and J. Sambrook, *Molecular Cloning: A Laboratory Manual*, Cold Spring Harbor Laboratory, New York, 1982.
21 D. Rickwood and B. D. James (Editors), *Gel Electrophoresis of Nucleic Acids: A Practical Approach*, IRL Press, Washington, DC, 1983.

22 S. P. Edmondson and D. M. Gray, *Biopolymers*, 23 (1984) 2725.
23 J. Zernik and A. Lichter, *BioTechnique*, 5 (1987) 411.
24 F. Sanger, A. R. Couson, T. Friedman, G. M. Air, B. G. Barell, N. L. Brown, J. C. Fiddes, C. A. Hutchinson, P. M. Slocombe and M. Smith, *J. Mol. Biol.*, 125 (1978) 225.

Journal of Chromatography, 458 (1988) 335–353
Elsevier Science Publishers B.V., Amsterdam — Printed in The Netherlands

CHROMSYMP. 1531

STRATEGIES FOR AUTOMATED OPTIMISATION OF HIGH-PERFORMANCE LIQUID CHROMATOGRAPHIC SEPARATIONS INCORPORATING DIODE-ARRAY DETECTION

A. G. WRIGHT and A. F. FELL*
Department of Pharmaceutical Chemistry, University of Bradford, Bradford BD7 1DP (U.K.)
and
J. C. BERRIDGE
Pfizer Central Research, Sandwich, Kent CT13 9NJ (U.K.)

SUMMARY

An optimisation strategy based on the simplex lattice mixture design is automated by the development of a peak recognition algorithm which utilises multiwavelength detection data. The peak tracking routines are shown to deal with multiple peak overlap and extensive peak cross-over. The utility of these techniques is demonstrated for a model system of seven components. The efficiency of optimisation and quality of separation are compared, for the same test mixture, with an existing automated optimisation strategy, namely the sequential simplex procedure incorporating multichannel detection.

INTRODUCTION

High-performance liquid chromatography (HPLC) is well established as a powerful analytical tool for the separation and quantitation of mixtures. To obtain an adequate separation of all components of interest in an acceptable analysis time it is frequently necessary to adjust or optimise operating conditions. Mobile phase composition in particular is most frequently varied. For situations where a number of variables needs to be optimised simultaneously, there are formal strategies which may prove useful[1,2].

These formal optimisation strategies fall into two main categories: sequential experimental techniques and simultaneous experimental techniques. At least one strategy, however, has been developed[3] which combines both approaches.

Sequential procedures rely on search algorithms to traverse the specified response surface and locate a point of optimum or maximum response. The search is directed by the quality of preceding separations. The principal sequential method applied to HPLC separations is sequential simplex[4] or modified simplex[5]. This method has been widely used for the optimisation of factors such as: proportions of organic modifiers, flow-rate and temperature[6–9]. Sequential simplex has been successfully automated[6] and shown to be suitable for dealing with unknown samples[10].

Simultaneous experimental procedures collect data over the factor space

0021-9673/88/$03.50

according to a pre-defined scheme. These data are then used to fit an appropriate mathematical model. The use of such models allows chromatographic behaviour to be interpolated between the experimental points and optimum separation conditions to be predicted. A number of simultaneous procedures have been developed for use in HPLC and these include factorial design[11] and procedures based on simplex lattice mixture design[12–16]. In all these techniques the retention behaviour of individual solutes is modelled to enable a chromatogram to be predicted for any point on the response surface.

The hybrid technique developed by Schoenmakers *et al.*[13] is an iterative mixture design. A simple model is fitted to individual solute retention data collected from a simultaneous experimental scheme. The model is refined in a sequential, iterative process until a separation of pre-defined quality is located or the model can no longer be improved.

All three categories of optimisation strategy have both advantages and disadvantages. Table I describes some of the strengths and weaknesses for each approach, with reference to a particular technique. Of the three procedures only the sequential simplex procedure has been able so far to deal with unknown samples in a fully automated way[6,10]. Unfortunately, the existence of "local" optima may mean that an acceptable separation is not located. The two other procedures would address this problem but have not been automated for poorly characterised samples (*i.e.* where no reference standards are available) due to the need for solute recognition.

Peak recognition is a major problem which remains to be overcome. The failure of simultaneous and hybrid optimisation strategies to deal with unknown samples stems from the lack of peak recognition tools. This limitation has been widely appreciated by workers in the field of optimisation and a number of attempts have been made to overcome this difficulty. Drouen *et al.*[17] have attempted to utilise the

TABLE I

ADVANTAGES AND DISADVANTAGES OF THE MAJOR OPTIMIZATION APPROACHES

Each type is exemplified by a particular procedure.

Approach	*Advantages*	*Disadvantages*
Sequential (simplex)	No assumptions about retention behaviour	Requires many experiments (20–30)
	Can deal with unknown samples	May locate "local" optima
	Conceptually simple	Automation often limited to mixtures of two modifiers due to hardware
	Can be automated	
Simultaneous (simplex lattice mixture design)	Models whole response surface	Requires solute recognition
	Locates global and local optima	Accuracy dependent on model relationship selected
	Few experiments required (7–10)	Limited as to modifier
Hybrid (iterative regression analysis)	Models whole response surface	Requires solute recognition
	Locates global and local optima	Complex programming required when more than one variable considered
	Few experiments required	
	Models are accurate	

absorbance ratio method[18] for solute recognition. The ratio of absorbance at two detection wavelengths for a pure peak is both constant and characteristic. Drouen *et al.* have employed these ratios for peak recognition. Later work by these workers[19] utilised multichannel diode-array detectors to collect UV spectra for the components. Comparison of spectra allows peak recognition. Unfortunately, the spectral similarity between many components limits the utility of these approaches.

Closely overlapping components present extreme difficulties when it is necessary to obtain pure spectra for peak recognition. Recently powerful deconvolution techniques have been developed which can extract individual peak profiles and the component spectra from a multiple component absorbance–time–wavelength data matrix. Strasters *et al.*[20] have evaluated four of these chemometric approaches as a means of peak recognition. It was concluded that even these techniques have limitations: in most cases spectral differences and a degree of resolution are required if spectra are to be extracted. Once spectra are available recognition of solutes still suffers the problems of spectral similarity.

Other recognition techniques have also been employed: these mostly rely on peak area. Earlier work with the sequential simplex procedure[10] has shown that diode-array detection[21] offers significant potential for simple peak recognition strategies based on comparison of peak integrals determined at different detection wavelengths. Thus it was proposed to develop this strategy in order to automate an optimisation strategy based on the simplex lattice mixture design. This procedure was selected in preference to iterative mixture design as the computer programming required is less complex.

In the present studies an automated peak recognition and data handling program is developed for the optimisation of HPLC separations, on the basis of minimum selectivity, using data collected in a simplex lattice mixture design[16].

THEORY

Peak recognition has previously been attempted, in conjunction with a simplex lattice design optimisation strategy, by Issaq and McNitt[22]. They developed a computer program able to track solutes on the basis of percentage area for peaks at a single detection wavelength. The chromatographic separation that revealed the most peaks was used as a reference and all the peaks in other chromatograms were correlated to these data. Two-component overlap was dealt with by adding two reference components together and assessing the degree of fit with the chromatographic peak. Applicability of the routines was demonstrated by a hypothetical example.

Two questions remain to be answered as a result of this work: (a) how to deal with two or more components of very similar area and (b) how to deal with the case where only partial resolution of peaks is observed in the reference chromatogram itself. The peak recognition algorithm developed by Wright *et al.*[10] aimed to address the peak similarity problem by using multiwavelength detection. The problem of overlap in the reference chromatogram did not arise in this earlier work as only well resolved chromatograms were studied.

Clearly the need for well separated peaks in the reference chromatogram imposes

an impossible constraint on the simplex lattice based optimisation procedures. In order to track peaks using the existing algorithm, every peak in each chromatogram has to be well resolved. If this is the case then optimisation may be unnecessary. Thus, it was proposed to extend the existing procedure to cover both complete and partial peak overlap.

Both procedures described[10,22] require the reference data to be extracted from one of the separations, a major limitation. However, the basic assumption of any area-based recognition approach is that area (or integral) does not change significantly with mobile phase composition. If this fundamental assumption holds then the reference data for a particular solute can, in principle, be taken from any of the chromatograms where the solute is fully resolved from neighbouring peaks. In the proposed procedure complete resolution of all components is not required in a single chromatogram; it is simply necessary that complete resolution of each solute from its neighbours occurs in at least one of the seven chromatograms resulting from the mixture design.

Algorithms for automated optimisation

The programs needed for automated simplex lattice mixture design optimisation can be summarised in six steps: (i) integration of all peaks in each chromatogram at each detection wavelength; (ii) extraction of all apparently resolved peaks; (iii) reduction of resolved peak array to remove any duplicates and any composite peaks, to arrive at a representative set of reference data; (iv) correlation of chromatographic peaks in each separation with the reference data; (v) fitting of the mathematical model to retention data; (vi) calculation of optimum separation conditions.

Routines for steps v and vi are straightforward and will not be discussed further.

Integration of all chromatograms involves the simultaneous handling of several data sets, one for each detection wavelength selected. Absorbance data are encoded as data strings and stored on magnetic disk. Also included in the coded data are peak event markers which signify start of peak, apex, valley, and end of peak, indicating the appropriate points where integration is started and finished. The integration routine employs Simpson's rule for the determination of area under a chromatographic peak.

The peak event codes also offer a convenient way of selecting pure (or apparently pure) peaks for the initial reference array. If a chromatographic peak is recognised by a start code, and the end code occurs without an intervening valley code then the peak is assumed to be pure. If a valley code is observed but the height above baseline corresponds to less than 5 mAU then the peak is also regarded as pure.

Routines for reduction of the array of "pure" peaks to a representative set of reference data form the core of an automated procedure. The principles are best described schematically (Fig. 1). It is necessary to remove any multiple occurrences of the same component so that each solute is represented only once in the reference array. A complication is the presence of composite peaks in the array (Fig. 2). Extra peaks occur which cannot be deleted by comparison with the other solutes present. Combinations of the other peaks (two together, or three together etc.) have then to be compared. These comparisons between peaks require a function which can assess similarity to allow objective decisions as to whether or not a peak should be included in the reference array.

The peak recognition algorithm developed previously[10] provides an assessment

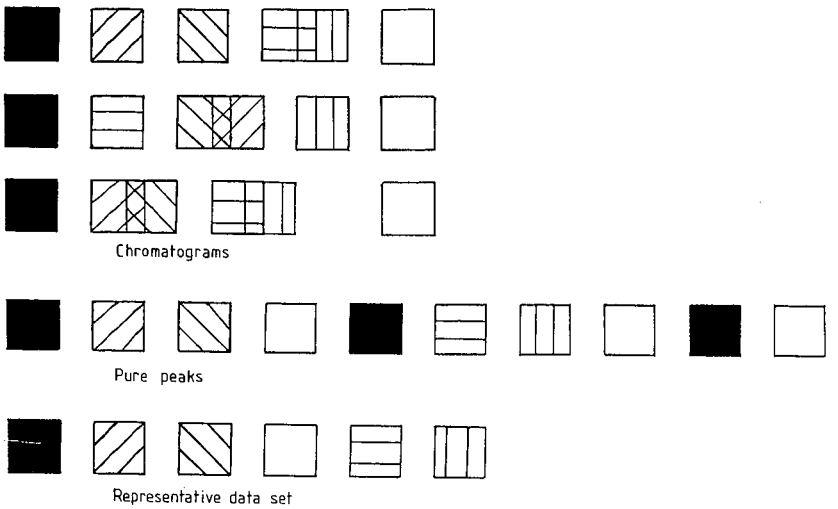

Fig. 1. Schematic diagram representing the basic principle behind the proposed program for extracting reference data from the simplex lattice design. Chromatographic peaks are represented by the squares. Any square exhibiting only one pattern is assumed to be pure. Removal of any pattern occurring more than once leads to a representative data set — a reference archive.

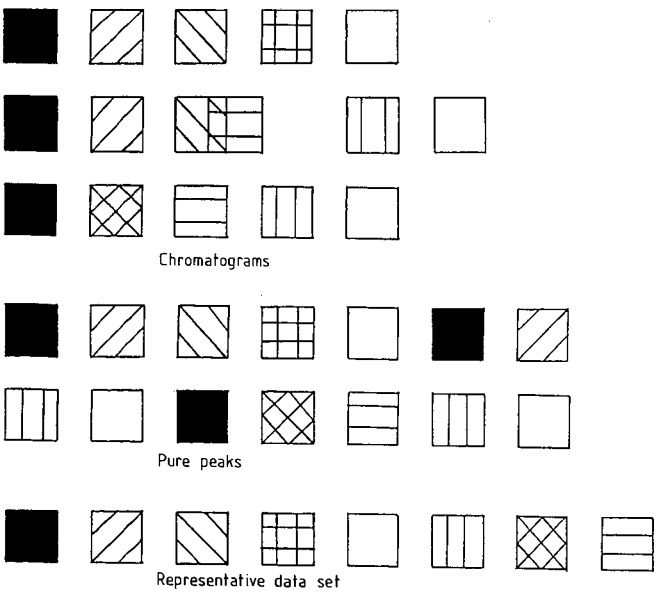

Fig. 2. Similar data showing the problem associated with complete overlap. Completely fused peaks appear to be pure but cannot be removed from the array of pure peaks. In this instance the representative data set consists of eight peaks instead of six.

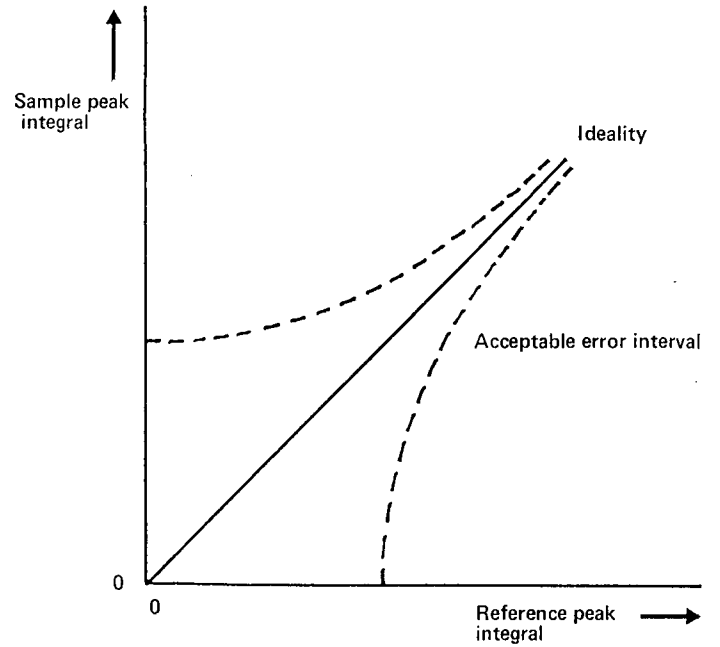

Fig. 3. Sample peak integral as a function of reference peak integral to illustrate the increase in acceptable error which should be included, as reference and sample peak integrals decrease.

of similarity between two peaks but has a major limitation, in that no provision is made for the larger degree of error associated with small relative to larger peaks (Fig. 3). The significance of the degree of difference between two chromatographic integrals is dependent upon the size of the integrals. A 30% difference when each of the integrals is less than 2% of the total chromatographic integral, is clearly less significant than a 30% difference when the integrals are greater than 10% of the total integral. The original algorithm[10] made no allowance for this and so a new algorithm was developed.

The peak percentage areas for a selected reference peak are summated over all the detection wavelengths used:

$$I_R^{tot} = \sum_{i=1}^{n} I_R^{\lambda_i} \tag{1}$$

where I_R^{tot} is total percentage area summated over all wavelengths, $I_R^{\lambda_i}$ is percentage area at wavelength λ_i, and n is the number of wavelengths used. The total percentage area over all detection wavelengths indicates the contribution the reference peak makes to the total chromatographic integral over the same detection channels. The size of this contribution should dictate the degree of difference which can be tolerated between the sample and reference peaks before it must be concluded that they arise from different solutes. The value of I_R^{tot} dictates the value of this maximum acceptable difference

TABLE II

MAXIMUM DIFFERENCES BETWEEN SAMPLE AND REFERENCE PEAK INTEGRALS WHICH MAY BE TOLERATED BEFORE THE PEAKS ARE REGARDED AS DIFFERENT

n is the number of detection wavelengths used.

Range for I_R^{tot}	*Maximum value of D as the fraction of* I_R^{tot}
$< 1.67\ n$	0.475
1.67–2.50 n	0.450
2.50–3.33 n	0.400
3.33–4.00 n	0.325
4.00–4.67 n	0.225
$> 4.67\ n$	0.100

(Table II). The actual difference at each wavelength is determined by the absolute difference in peak area for reference peak and sample peak:

$$D^{\lambda_i} = |I_R^{\lambda_i} - I_2^{\lambda_i}| \tag{2}$$

where: $I_2^{\lambda_i}$ is percentage area for a sample peak at wavelength λ_i. The total difference (D) is defined as:

$$D = \sum_{i=1}^{n} D^{\lambda_i} \tag{3}$$

For the reduction of the reference array it is not necessary to calculate a numerical value for an assessment of similarity. It is sufficient to compare D with the maximum value allowed (Table II). If D exceeds the acceptable maximum then the solutes are regarded as different.

The computer program proposed in this work deals firstly with the reference array of pure (or apparently pure) peaks. The first peak is taken as a reference and values for D are determined with every other peak in the array. Where the difference does not exceed the maximum value allowed (Table II) the subsequent peak is deleted from the array as being a duplicate of the reference peak. Where the value of D exceeds the maximum allowable level the peak is assumed to be due to another component. Repeating the routine for the second and subsequent peaks in the reference array deletes any further duplicate peaks.

Once duplicate peaks have been removed, any extra sets of data, over and above the representative set, are assumed to be attributable to composite peaks. A similar approach to the one above is used to delete these additional data. The percentage areas of two or more of the remaining peaks can be added together and used as a reference for comparison with the other peaks.

The peaks of the reference array are sorted into ascending order on the basis of percentage area for the first detection wavelength selected. It is then assumed that a composite peak will be larger than any of the individual peaks overlapped to produce it. Therefore, if two peaks in the ordered reference array are combined together (*i.e.* 1 and 2), it follows that only larger peaks (*i.e.* 3 onwards) need be considered as

potential composite peaks. Calculation of the maximum allowable differences and assessment of similarity follows the same approach as before, except that the percentage areas for the combined peaks are used as reference data. The current software can consider two and three component overlap. Any peak which may be concluded to arise from a two or three peak combination is deleted from the reference array. After completion of this second process only one set of data should be retained for each solute (a representative set of reference data *i.e.* peak integrals at each detection wavelength).

The availability of a complete and unique set of reference data means that peak recognition in the other chromatograms is possible. The current recognition algorithm does not determine a numerical value, it simply allows a decision as to the inclusion or exclusion of a peak in the reference array. For recognition of peaks in chromatograms it is necessary to calculate a numerical assessment of similarity between reference and chromatographic peaks. To achieve this the recognition algorithm was amended.

To calculate a specific similarity assessment value it is still necessary to determine both I_R^{tot} for the reference peak, and D between the reference and chromatographic peaks. As discussed above the error associated with small percentage areas is less significant than that for larger percentage areas. Thus, I_R^{tot} is used to select a weighting factor to determine how much of the absolute difference should be regarded as significant (Table III).

The numerical value for measuring the similarity is calculated by taking the ratio of significant difference to I_R^{tot}. A value close to zero indicates a good fit. These calculations are not limited to single reference peaks and may be applied to comparisons of two and three reference peak combinations with chromatographic peaks.

Peak recognition in chromatograms may be achieved on the basis of these similarity values. Peak similarity is calculated for each individual reference peak with every chromatographic peak in the seven chromatograms. The three best fitting reference peaks are stored in descending order of fit. Similarity values are calculated between chromatographic peaks and combinations both of two reference peaks, and of three reference peaks. The three best fitting two-peak combinations and the two best fitting three-peak combinations are recorded.

The program for identifying the peaks in the chromatograms contains three sets of routines. Which set is used depends on the number of peaks detected. Where all

TABLE III

DETERMINATION OF THE FINITE DIFFERENCE BETWEEN THE REFERENCE AND SAMPLE INTEGRALS WHICH MAY BE REGARDED AS SIGNIFICANT

Range for I_R^{tot}	*Weighting factor*	*Significant absolute difference (D)*
$< n$	0.2	0.2
1–2 n	0.3	0.3
2–3 n	0.4	0.4
3–4 n	0.5	0.5
4–5 n	0.6	0.6
5–6 n	0.8	0.8
$>6 n$	1.0	1.0

expected peaks are detected in a given chromatogram, only similarity values with single reference peaks need be considered. When one less peak occurs in the chromatogram, this means that two-peak overlap must be considered. The absence of two or more peaks leads to both two and three peak overlap being examined.

The first case is where all peaks are detected. The best similarity value for each chromatographic peak (with single reference peaks) is studied. A value of 0.05 or below is assumed to correspond to a correctly assigned peak. All peaks in the chromatogram are considered in this way and as many peak identities as possible are assigned. Any remaining non-assigned peaks are then studied. The best fitting reference peak is provisionally assigned in each case. The chromatogram is then examined to check that each reference peak has only been assigned once. If this is the case then elution order has been assigned and the process can be halted for this chromatogram. If peaks are assigned more than once then any provisionally identified peak takes its second best identity and the checking procedure is repeated. A third best identity is available if necessary. Eventually an elution order can be assigned even for chromatograms where there is partial overlap of several components. A fit value of less than 0.05 should be very specific for one component. Two solutes would have to have almost identical absorptivity–concentration combinations at the detection wavelengths for both to be fitted by one reference peak.

The second case to be considered is that for one peak less than expected in the sample chromatogram. Single reference peaks are assigned to as many peaks as possible in the same way as before. The two routines diverge at this point. The chromatographic peak with the worst single peak fit is located and two-peak combination data are studied. If the similarity for the best fitting two-peak combination is less than 0.15 then the two peaks are provisionally assigned. A check is made to ensure that these peaks have not already been positively assigned to "single" components. Where these peaks are unused the identity is then positively assigned. If either or both peaks have been used then the next best fitting pair of peaks is considered. The process is repeated provided that the similarity value is less than 0.20. When a two-peak combination cannot be assigned the second worst fitted peak from the single reference peak data is located and these routines repeated. A check that all reference peaks are assigned only once is carried out. A process analogous to the one used with single reference peaks is applied to arrive at the correct elution order.

The third case is for two fewer peaks than expected. As for the previous case, single reference peak fits are used to assign identity to as many peaks as possible. Once this has been done, the worst single peak fit is located and the three-peak combination data examined. The process is analogous to that for two-peak combinations. However, only one peak in the chromatogram is considered and the second to worst fitted peak is not evaluated. If a three-peak combination does not satisfactorily describe the worst fitted peak then it is assumed that the discrepancy is due to two instances of two-peak overlap. Thus, the two worst fitted peaks are studied to see which two combinations fit best. The process is identical with that used for the first part of the routine for fitting two overlapped peaks as described above. Elution order is established by ensuring that each peak is used only once.

These proposed algorithms should enable: peak recognition; the determination of elution orders; and the assignation of the correct retention time to each solute from every chromatogram. When these data are supplied to a routine for fitting to the

special cubic equation[12–14], retention time can be predicted at any point on the response surface for any of the solutes provided that the model employed is adequate[23]. These retention models allow optimisation of the separation.

In the present work a model system exhibiting peak overlap and multiple peak cross-over is used to exemplify the new procedure. Such a sample also provides a very severe test of the sequential simplex procedure since multiple elution orders mean there are many local maxima.

EXPERIMENTAL

Apparatus and materials

Two systems were used for this work. Automated simplex lattice mixture design employed a Hewlett-Packard (Wokingham, U.K.) 1040A diode-array detector, an HP85B computer controller, an LDC (Stone, U.K.) Constametric 3000 pump and a Rheodyne (Alltech, Carnforth, U.K.) 7010 injection valve fitted with a 20-μl loop. Separations were performed at room temperature (*ca.* 21°C) on a 125 × 4.6 mm I.D. Partisphere C_{18} 5-μm column (Whatman). The flow-rate used 1.25 ml/min.

Automated sequential simplex procedures employed a Hewlett-Packard 1090A liquid chromatograph comprised of an HP 1040A diode-array detector, a DR5 ternary pumping system and a 100-position autosampler. The system was controlled by an HP85B computer. Separations were performed at controlled temperature (*ca.* 27°C) also using a Partisphere column. The flow-rate used was 1.25 ml/min.

Mobile phases consisted of different mixtures of methanol, acetonitrile, tetrahydrofuran (THF) (Rathburn Chemicals, Peebles, U.K.) and distilled water. A seven component model system consisting of benzyl alcohol (BA), *p*-cresol (PC), propyl *p*-hydroxybenzoate (PHB), butyl *p*-hydroxybenzoate (BHB), diethyl phthalate (DP), toluene (TOL) and benzophenone (BP) was used throughout.

Software

Programs for the sequential simplex optimisation procedure were written in BASIC as a series of "hook" programs on the HP85B. The quality of separation was assessed using a chromatographic response function (CRF)[10]. The maximum number of injections was limited to 25.

Programs for the simplex lattice mixture design were written in BASIC on the HP85B as separate programs called from a short linking program.

RESULTS AND DISCUSSION

In this study the aim was to demonstrate the applicability and feasibility of an automated simplex lattice mixture design based on simple peak recognition procedures. The model system was selected to provide an exacting test of the proposed procedure.

Techniques based on the simplex lattice mixture design in HPLC require appropriate isoeluotropic eluents of water with each of the following: methanol, acetonitrile and THF. In this instance methanol–water (60:40, v/v) producing an analysis time of *ca.* 8 min was selected by an iterative procedure. A single gradient scan would also allow the appropriate composition to be predicted[24,25], although it does

suffer some limitations. The methanol–water composition found was used to predict the acetonitrile–water and THF–water eluents of the same solvent strength using the rules developed by Schoenmakers *et al.*[19]. These compositions were predicted to be 46:54 (v/v) and 40:60 (v/v), respectively. A "fine tuning" adjustment of composition to obtain three nominally isoeluotropic eluents was required, resulting in the following being selected: methanol–water (60:40, v/v), acetonitrile–water (47:53, v/v), and THF–water (42.5:57.5, v/v). Recently Haddad and Sekulic[26] have published an iterative procedure for the fine tuning of eluent composition which may be more efficient than the process used here.

Chromatograms were run for the seven mobile phases required by the simplex lattice mixture design[12–14]. Data were acquired simultaneously at 240, 260 and 280 nm. Each set of chromatographic data was stored on magnetic disk for subsequent integration and processing.

The number of peaks detected in the chromatograms ranged from five to seven. In no chromatogram were all peaks completely resolved (Fig. 4) and so the sample was a good candidate for optimisation. Applying the suite of programs described above allowed retention data to be determined for each solute from every one of the seven chromatograms. These data enabled a special cubic function[12–14] to be fitted. This function describes retention behaviour for every point on the response surface. Glajch *et al.*[27] found that the most accurate models were those where the logarithm of capacity factor was modelled. Therefore, the special cubic function fitted to these data was:

$$\ln k' = a_1x_1 + a_2x_2 + a_3x_3 + a_{12}x_1x_2 + a_{13}x_1x_3 + a_{23}x_2x_3 + a_{123}x_1x_2x_3 \quad (4)$$

where x_1, x_2 and x_3 are proportions of isoeluotropic eluents 1, 2 and 3 respectively, a_1–a_{123} are coefficients calculated from the seven experimental points of the simplex lattice design.

The optimisation criterion selected for use with this automated procedure was selectivity (α) for the least well separated pair of adjacent peaks (*i.e.* the minimum α). Laub and Purnell[28] first used selectivity as an optimisation criterion, but it was Weyland *et al.*[16] who applied it to a simplex lattice design based procedure to generate minimum alpha plots. The selectivity between the least well separated pair of adjacent peaks was plotted against mobile phase composition. The highest point on the minimum alpha plot (MAP) corresponded to the best separation for the worst separated pair of peaks. All other peaks were better separated.

The use of minimum α as an optimisation criterion has been criticised since the separation of other peaks may suffer by concentrating on just the worst pair. However, in this work an adequate separation of all peaks was the only consideration. Thus, if the worst peak pair could be separated it follows that all other peaks should also be resolved. With this criterion, the only parameter which had to be measured or predicted was the column dead or void time, t_0. Knox[29] proposed a simple relationship which allowed t_0 to be estimated from the column dimensions:

$$t_0 = \frac{\pi d_c^2}{4} \varepsilon_0 \cdot L \cdot \frac{1}{F} \quad (5)$$

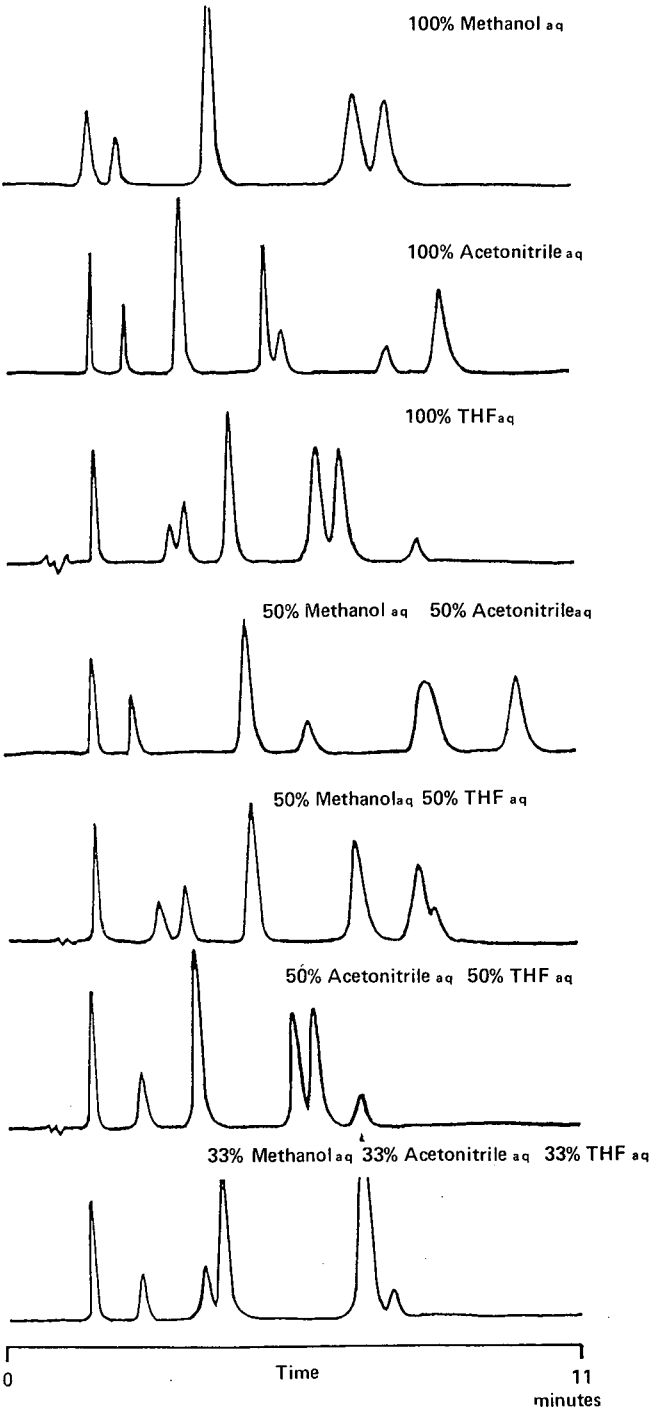

Fig. 4. Seven chromatograms collected according to the simplex lattice mixture design described (aq means aqueous).

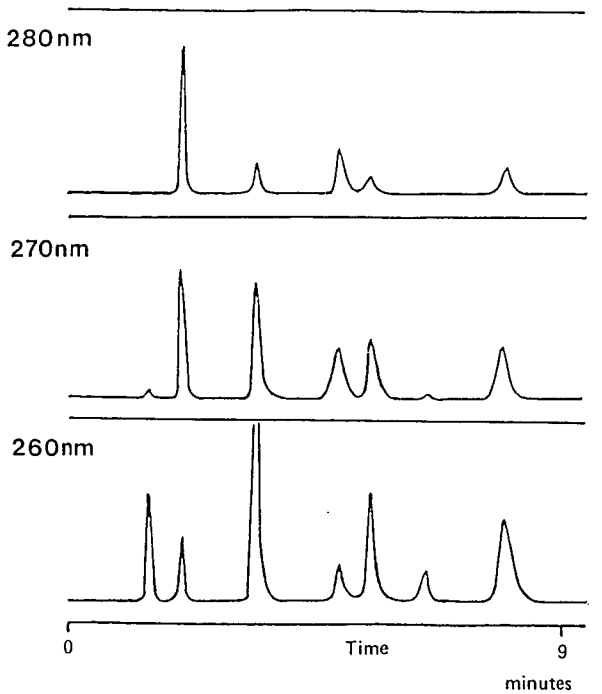

Fig. 5. The predicted optimum separation at different detection wavelengths. Mobile phase: 60% (v/v) aqueous methanol–47% (v/v) aqueous acetonitrile (25:75, v/v). Minimum α: 1.15.

where d_c is the column diameter, ε_0 is total porosity (taken as 0.75 for silica based packings), L is column length, and F is the flow-rate. These variables were known therefore allowing an estimate of t_0 (*ca.* 1.25 min for this column and these conditions).

The recognition algorithm would also allow many different criteria to be used, including those where specific peaks are of particular interest. Weighting factors may be applied to the resolution or separation of these components and a recognition procedure would enable this without the injection of standards.

The final optimisation program in the suite predicts an optimum by grid search of the predicted response surface. The grid uses 5% steps in eluent composition and involves more than 200 points. Optimum separation conditions of 47% (v/v) aq. acetonitrile–60% (v/v) aq. methanol (75:25, v/v) were predicted. The minimum selectivity expected for this point was 1.20. A chromatogram run with these separation conditions produced baseline resolution of all components and a minimum selectivity of 1.15 (Fig. 5). The error in selectivity is due to the lack of fit of the special cubic function and possible errors in the estimated value of t_0.

Absolute identity of the component peaks in each chromatogram was established by examination of the elution orders assigned and injection of individual reference standards for two sets of separation conditions (the methanol–water binary eluent and the optimum separation conditions) (Table IV). The complexity of retention behaviour was immediately apparent.

The programs developed were shown to deal with situations where two-

TABLE IV

ELUTION ORDER ENCOUNTERED FOR THE SEVEN EXPERIMENTS OF THE SIMPLEX LATTICE MIXTURE DESIGN AND THE OPTIMUM, TOGETHER WITH THE THREE CHROMATOGRAMS DESCRIBED BY SNEE TO ASSESS THE DEGREE OF FIT OF THE SPECIAL CUBIC MODEL

Two-letter codes together signify total overlap.

Mobile phase composition			*Peak*						
Methanol (%)	*Acetonitrile (%)*	*THF (%)*	*1*	*2*	*3*	*4*	*5*	*6*	*7*
100	0	0	BA	PC	PHB/DP	BHB/TOL	BP	–	–
0	100	0	BA	PC	PHB	BHB	DP	TOL	BP
0	0	100	BA	PC	DP	PHB	BP	BHB	TOL
50	50	0	BA	PC	PHB	DP	BHB/TOL	BP	–
50	0	50	BA	PC	DP	PHB	BP	BHB	TOL
0	50	50	BA	PC	PHB/DP	BHB	BP	TOL	–
33	33	33	BA	PC	PHB	DP	BHB/BP	TOL	–
25	75	0*	BA	PC	PHB	DP	BHB	TOL	BP
67	16	16	BA	PC	DP	PHB	BHB/TOL/BP	–	–
16	67	16	BA	PC	PHB	DP	BHB	TOL	BP
16	16	67	BA	PC	DP	PHB	BP	BHB	TOL

* Optimum separation conditions with aqueous isoeluotropic organic phases (see text).

component overlap occurs, and where two-component overlap occurs twice in the same chromatogram. Three further chromatograms were run (eluent compositions in Table IV) as potential checks of degree of fit for the special cubic model as outlined by Snee[14]. While these data were not considered in this study they were included for future extensions of the method. Elution orders were correctly assigned for these chromatograms and an instance of three-component overlap was satisfactorily identified. The limited computer memory available on the instrument used for these studies means that more complicated overlap situations cannot be dealt with.

The elution orders encountered over the response surface were plotted (Fig. 6). In all, seven different elution orders were predicted and each had a corresponding local maximum. A contour MAP (Fig. 7) was generated to establish which elution order or orders were capable of yielding an adequate separation. From this plot it was concluded that two of the local maxima would yield adequate separations although the optimisation program had in fact correctly identified the global optimum.

This seven-component test mixture was also optimised using the automated sequential procedure[10]. The use of a ternary solvent delivery system meant that methanol, acetonitrile, THF and water could not all be included in the same procedure unless isoeluotropic binary eluents were used. The isoeluotropic compositions employed were those from the simplex lattice design although column temperature was more than 5°C higher than with the simplex lattice procedure. As a result analysis time was reduced from 8 to 5 min. Thus, minimum α values for separations resulting from the two procedures were taken as the criterion for comparison as a 5°C increase in temperature was not expected to significantly alter selectivity. Comparisons of

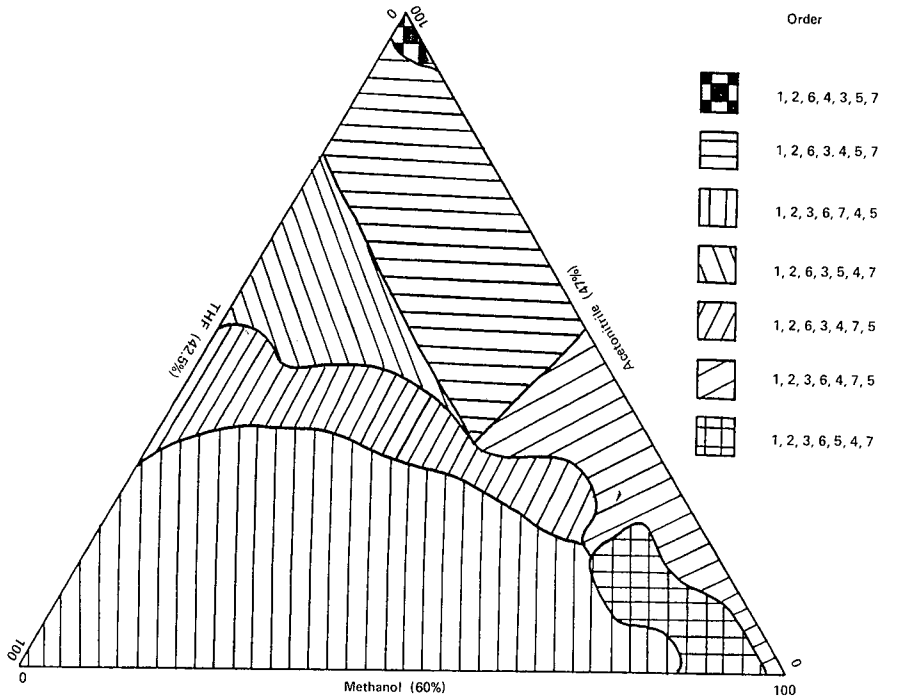

Fig. 6. Plot of elution orders encountered over the entire response surface. Peaks: 1 = benzyl alcohol, 2 = *p*-cresol, 3 = diethyl phthalate, 4 = butyl *p*-hydroxybenzoate, 5 = toluene, 6 = propyl *p*-hydroxybenzoate, 7 = benzophenone.

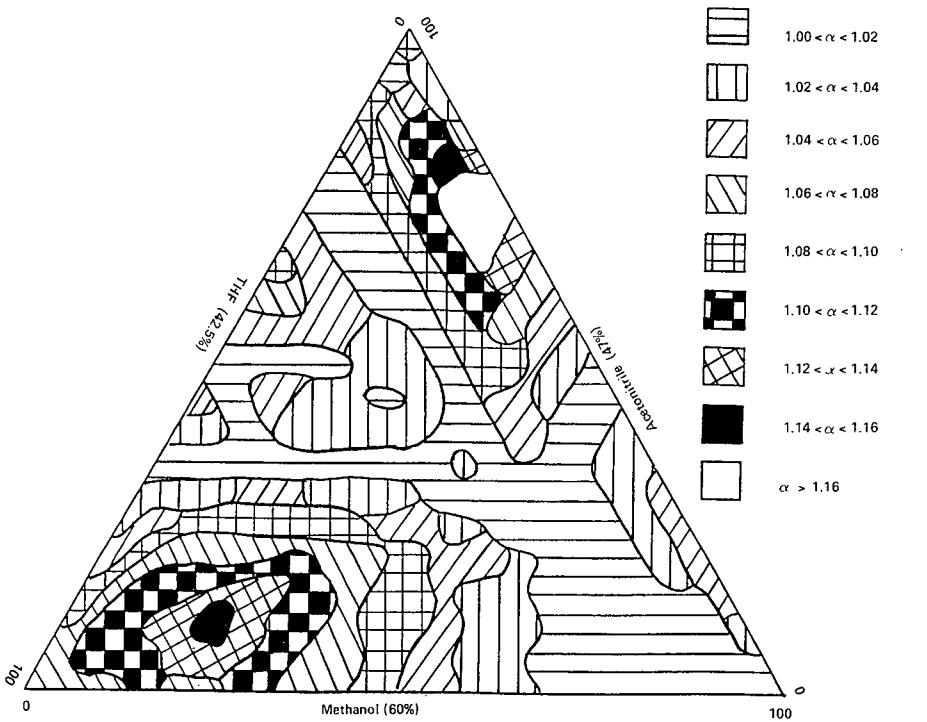

Fig. 7. Contour plot of minimum α values over the response surface.

resolution were not suitable criteria as decreasing the average capacity factor for two peaks leads to a decrease in their separation[2].

The CRF used for the sequential simplex optimisation study was:

$$\mathrm{CRF} = \sum_{i=1}^{n-1} R_s + n - |t_A - t_L| \tag{6}$$

where R_s is the resolution between adjacent peaks (limited to a maximum value of 1), n is the number of peaks detected, t_A is the required retention time for the last peak, and t_L is the actual retention time for the last peak. The final term was only included if it exceeded 1 min. The time term was of little importance to the CRF as the use of iso-eluotropic eluents was designed to constrain analysis time.

On carrying out the sequential simplex optimisation procedure for the separation, the stop criterion[10] halted the search after 20 injections as the CRF had attained values within 5% of the maximum CRF on three occasions. The best separation encountered was selected for comparison with the simplex lattice mixture design optimum. Baseline resolution of all components was not achieved and the minimum α value was 1.10. The eluent composition producing this separation was: 60% methanol–47% (v/v) aq. acetonitrile–42.5 (v/v) aq. THF (7.0:61.1:31.9, v/v/v) (Fig. 8).

The complexity of retention behaviour for this test mixture meant that the sequential simplex procedure was unable to fully optimise the separation. A number of pairs of peaks in the sample proved difficult to resolve. As the separation of one pair of peaks was improved the separation of another pair deteriorated.

Since both simultaneous and sequential experimental optimisation strategies were applied to the same test sample, it was possible to compare them. In this case multiple peak cross-over meant that the simultaneous procedure, capable of modelling the entire response surface, located a better separation than the sequential procedure, which relied on a search algorithm. The problems associated with local optima and the sequential simplex procedure were highlighted by the complex nature of the response surface.

The simplex lattice mixture design requires the selection of appropriate isoeluotropic binary eluents of water with methanol, acetonitrile, and THF. In these studies an iterative procedure was employed, necessitating two chromatograms for each of the three eluents. These six chromatograms required about 2 h to complete. Once isoeluotropic eluents were located seven mixed eluents were prepared and the chromatograms run, taking about 3 h. Programs for predicting optimum separation conditions required about 80 min, while to run the final chromatogram required 30 min. Thus, an adequate separation for this mixture was located within a working day (*ca.* 7 h).

The sequential simplex procedure required 20 injections taking a total time of around 6.5 h. Additionally, the selection of the isoeluotropic binary eluents still has to be considered. As the chromatograph had only three solvent reservoirs, it was necessary to employ isoeluotropic binary eluents if the full range of selectivities (*i.e.* due to methanol, acetonitrile, and THF) were to be exploited. Therefore, the selection of isoeluotropic eluents, as in the earlier procedure, required about 2 h. Thus, the sequential simplex procedure required 9 h for operation (although it was highly automated), but could achieve an adequate separation of the test sample (Fig. 8), even

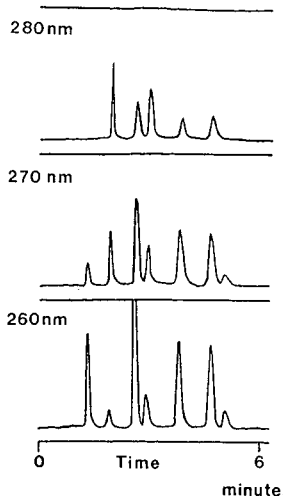

Fig. 8. Best separation located by the sequential simplex optimisation procedure. Mobile phase: 60% (v/v) aqueous methanol–47% (v/v) aqueous acetonitrile–42.5% (v/v) aqueous THF (7.0:61.1:31.9, v/v/v). Minimum α: 1.10.

though this was not the global optimum revealed by the contour plot (Fig. 7).

The sequential simplex procedure did have a major advantage, in that its operation was fully automated once the isoeluotropic eluents were prepared. Simplex lattice mixture design data had to be collected in an interactive process, although with suitable chromatographic hardware its automation would be straightforward. As with sequential simplex the only information required at the outset of optimisation were the column parameters (diameter, length etc.).

CONCLUSIONS

A peak recognition algorithm based on percentage area at a number of detection wavelengths has been developed. This algorithm enabled the simplex lattice mixture design to be automated for a test mixture where individual standards were not available. Separation optimisation was achieved by combining the simplex lattice design with a minimum alpha (selectivity) criterion. Baseline resolution of a seven component test mixture was achieved despite there being seven different elution orders across the response surface.

Automated sequential simplex optimisation was applied to the same sample and was found to be unable to locate the global optimum. A comparison of the two procedures revealed that not only was simplex lattice mixture design able to obtain an adequate separation but it did so in substantially fewer chromatograms and took 20% less time than sequential simplex. With an automated instrument the time reduction could conceivably be greater. Thus, automated simultaneous optimisation procedures incorporating peak recognition algorithms now provide a reasonable alternative to the sequential simplex procedure for unknown samples. Samples producing complex response surfaces can be optimised by the simplex lattice design, more efficiently and more reliably than by the sequential simplex procedure. Simultaneous procedures are

more generally applicable than sequential procedures, provided that appropriate mathematical models can be fitted to the chromatographic data.

The suite of programs currently used was written primarily to demonstrate the feasibility of this approach. A number of problems are associated with the routines: (i) programs take a significant time to run on the HP 85B; (ii) each peak must be detected in at least one of the chromatograms; (iii) the minimum number of peaks which can be dealt with is only two less than the maximum.

These difficulties may all be addressed. A chromatograph with a multiple solvent delivery system would increase the rate of data acquisition, while more efficient programming and a faster computer/program language would speed up data handling. The detection of all peaks in one chromatogram may not be necessary if solvochromic effects are insignificant. Cases of multiple peak overlap may be dealt with if more computer memory were available.

These algorithms described have been successfully applied to the test mixture without any knowledge of the number of components or their UV spectra. However, the optimisation routine is dependent upon the accuracy of the model and if retention behaviour can not be accurately described by the special cubic function adopted, then errors will result. The possibility of using a procedure such as the iterative mixture design[3] remains to be assessed. The basic suite of programs may be elaborated and extended to form a useful and generally applicable automated optimisation procedure. This will form the basis of further work.

ACKNOWLEDGEMENT

A.G.W. is grateful to Pfizer Central Research, U.K. for providing the studentship for this work.

REFERENCES

1 J. C. Berridge, *Techniques for the automated optimisation of HPLC Separations*, Wiley-Interscience, New York, 1985.
2 P. J. Schoenmakers, *Optimization of Chromatographic Selectivity*, Elsevier, Amsterdam, 1986.
3 P. J. Schoenmakers, A. C. J. H. Drouen, H. A. H. Billiet and L. de Galan, *Chromatographia*, 15 (1982) 688.
4 W. Spendley, G. R. Hext and F. R. Himsworth, *Technometrics*, 4 (1962) 441.
5 J. A. Nelder and R. Mead, *Comput. J.*, 7 (1965) 308.
6 J. C. Berridge, *J. Chromatogr.*, 244 (1982) 1.
7 J. C. Berridge and E. G. Morrissey, *J. Chromatogr.*, 316 (1984) 69.
8 J. C. Berridge, *Analyst*, 109 (1984) 291.
9 A. S. Kester and R. E. Thompson, *J. Chromatogr.*, 310 (1984) 372.
10 A. G. Wright, A. F. Fell and J. C. Berridge, *Chromatographia*, 24 (1987) 533.
11 M. Otto and W. Wegscheider, *J. Chromatogr.*, 258 (1983) 11.
12 H. Scheffe, *J. Royal Stat. Soc. B*, 20 (1958) 344.
13 J. W. Gorman and J. E. Hinman, *Technometrics*, 4 (1962) 463.
14 R. D. Snee, *Chemtech*, 9 (1979) 702.
15 J. L. Glajch, J. J. Kirkland, K. M. Squire and J. M. Minor, *J. Chromatogr.*, 199 (1980) 57.
16 J. W. Weyland, C. H. P. Bruins and D. A. Doornbos, *J. Chromatogr. Sci.*, 22 (1984) 31.
17 A. C. J. H. Drouen, H. A. H. Billiet and L. de Galan, *Anal. Chem.*, 56 (1984) 971.
18 R. Yost, J. Stoveken and W. MacLean, *J. Chromatogr.*, 134 (1977) 73.
19 A. C. J. H. Drouen, H. A. H. Billiet and L. de Galan, *Anal. Chem.*, 57 (1985) 962.

20 J. K. Strasters, H. A. H. Billiet, L. de Galan, B. G. M. Vandeginste and G. Kateman, *J. Chromatogr.*, 385 (1987) 181.
21 A. F. Fell, B. J. Clark and H. P. Scott, *J. Chromatogr.*, 316 (1984) 423.
22 H. J. Issaq and K. L. McNitt, *J. Liq. Chromatogr.*, 5 (1982) 1771.
23 P. J. Schoenmakers and T. Blaffert, *J. Chromatogr.*, 384 (1987) 117.
24 L. R. Snyder, J. W. Dolan and J. R. Gant, *J. Chromatogr.*, 165 (1979) 3.
25 P. J. Schoenmakers, H. A. H. Billiet and L. de Galan, *J. Chromatogr.*, 205 (1981) 13.
26 P. R. Haddad and S. Sekulic, *J. Chromatogr.*, 392 (1987) 65.
27 J. L. Glajch, J. J. Kirkland and L. R. Snyder, *J. Chromatogr.*, 238 (1982) 269.
28 R. J. Laub and J. H. Purnell, *J. Chromatogr.*, 161 (1978) 49.
29 J. H. Knox, *J. Chromatogr. Sci.*, 15 (1977) 352.

Journal of Chromatography, 458 (1988) 355–370
Elsevier Science Publishers B.V., Amsterdam — Printed in The Netherlands

CHROMSYMP. 1434

CORRECTION OF THE RESOLUTION FUNCTION FOR NON-IDEAL PEAKS

PETER J. SCHOENMAKERS*
Philips Research Laboratories, P.O. Box 80 000, 5600 JA Eindhoven (The Netherlands)
and
JOOST K. STRASTERS and ÁKOS BARTHA
Delft University of Technology, De Vries van Heystplantsoen 2, 2628 RZ Delft (The Netherlands)

SUMMARY

The resolution function is commonly used to describe the extent of separation between successive peaks in a chromatogram. However, the resolution is usually defined in such a way that it is applicable only to symmetrical (Gaussian) peaks. Moreover, the resolution does not provide a realistic estimate of the extent of separation between two peaks with greatly different areas. Nevertheless, the main advantage of the resolution is that its value can be predicted from retention and efficiency data for the individual peaks. Simple methods are described to correct the resolution function for (i) large variations in peak areas and (ii) peak asymmetry. The corrections are derived as modifications of the resolution equation. An important consequence of these modifications is that the resolution for a pair of peaks has two different values, one for each peak. The new resolution equations were evaluated using computer-generated (exponentially modified Gaussian) peak profiles. The effects of varying degrees of peak asymmetry and varying peak-area ratios were studied.

INTRODUCTION

The most common way to describe the extent of separation between two successive peaks, i and j, in a chromatogram is by the resolution (R_s), which is defined as

$$R_s = \frac{t_j - t_i}{{}^1/_2(w_i + w_j)} \tag{1}$$

where t is the retention time and w is the peak width. For Gaussian peaks the width is usually assumed to equal four times the standard deviation, σ, corresponding to the width of the peak at 13.5% (e^{-2}) of its height. This results in

$$R_s = \frac{t_j - t_i}{2(\sigma_i + \sigma_j)} \tag{2}$$

0021-9673/88/$03.50

When eqn. 2 can be used to describe the extent of separation, the resolution can be predicted if the retention times and the standard deviations are known. For Gaussian peaks, the plate count, which is defined by

$$N_i = \left(\frac{t_i}{\sigma_i}\right)^2 \tag{3}$$

can be substituted for σ, yielding

$$R_s = \frac{t_j - t_i}{2t_i/\sqrt{N_i} + 2t_j/\sqrt{N_j}} \tag{4}$$

If, moreover, the plate count is the same for the two peaks ($N_i = N_j = N$), then

$$R_s = \frac{t_j - t_i}{t_i + t_j} \cdot \frac{\sqrt{N}}{2} \tag{5}$$

or, in terms of the capacity factor, k,

$$R_s = \frac{k_j - k_i}{2 + k_i + k_j} \cdot \frac{\sqrt{N}}{2} \tag{6}$$

Eqns. 5 and 6 are very important for chromatography. Under the assumption of equal N values, they allow the resolution to be calculated if the retention data (in terms of t or k) are known. This is especially important in two areas:

(*i*) *Column optimization.* Chromatographic theory allows the effects of operating parameters (*e.g.*, flow-rate) and column characteristics (column length and diameter, particle size) to be predicted accurately. This allows the optimization of the column and operating parameters in order to obtain sufficient resolution in the shortest possible time, with the highest possible (detection) sensitivity, etc. (see, *e.g.*, ref. 1, Chapter 7). Computer simulation[2] may be used to optimize the conditions. However, in order to optimize the resolution, it must be possible to calculate its value under varying conditions in practical (non-symmetrical peaks of different height) rather than theoretical (Gaussian peaks of equal height) situations.

(*ii*) *Selectivity optimization.* A number of methods have been developed especially for the optimization of chromatographic selectivity[1]. These interpretive methods rely on the observation that the retention of individual solutes can be predicted from a few experimental data. The quality of the separation in the entire chromatogram is a much more complicated function, which can be calculated from the retention data of the individual solutes if a sensible value for the resolution can be calculated from the retention data.

Alternative measures for the extent of separation between successive peaks have been suggested (see ref. 1, section 4.2). In particular, resolution criteria may be defined on the basis of peak-to-valley or valley-to-peak ratios. The main advantage of these empirical functions (abbreviated to P values) is that they are more generally valid for

chromatographic peaks of any shape or size, as long as the required characteristics (valley and peak heights) can be obtained from the chromatogram. A first major disadvantage is that there will be a threshold range in which peaks overlap severely, but not completely. In this range the resolution may differ significantly from zero, but no valley can be observed so that all P values equal zero. Secondly, for non-Gaussian peaks P values cannot be predicted on the basis of retention times and column efficiencies (plate counts), so that they cannot be used in the two important areas outlined above.

In this paper we shall try to define simple equations for calculating the resolution (R_s) in practical situations. In addition to retention and efficiency data, some information will necessarily be required on the size (for peak-height correction) or the asymmetry of the actual peaks, but one of the aims of this work was to keep the corrections as simple as possible and the number of additional parameters to a minimum.

THEORY

Large variations in peak areas

One factor that appears to affect the resolution between two successive peaks in a chromatogram, but which is not taken into account in any of the equations given in the Introduction, is the (relative) height or area of the two peaks (see, *e.g.*, ref. 3, Section 2.5). When two successive peaks have different heights (or areas), the relative overlap is larger for the smaller peak. The relative overlap can be found from the part of the peak area where the two solutes are eluted together (A_{ij}) and the total area of the peak. For example, for the first peak (i) in Fig. 1,

$$RO_i = \frac{A_{ij}}{A_i} \tag{7}$$

The second peak in Fig. 1 overlaps with both the first and third peaks, so that

$$^{i}RO_j = \frac{A_{ij}}{A_j} \tag{8}$$

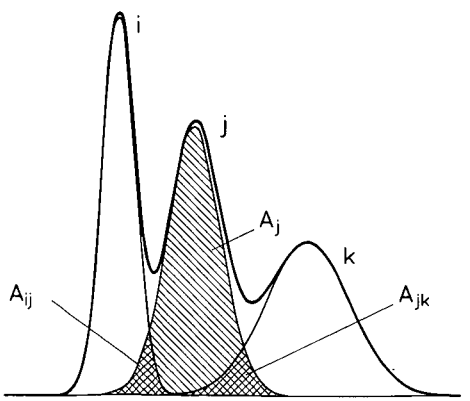

Fig. 1. Illustration of the relative peak overlap (RO).

and

$$^{k}RO_j = \frac{A_{jk}}{A_j} \tag{8a}$$

If the detection sensitivity is similar for the different peaks, then the relative overlap is a good indication of the extent to which solutes are separated. *RO* is not a practical resolution criterion, because it is very difficult to calculate its value from a chromatogram.

It is clear from eqns. 7 and 8 that *RO* will be different for peaks *i* and *j* if the areas A_i and A_j are different. This is different from the resolution, R_s, in the situation of eqns. 5 and 6. Both equations yield a single (absolute) value for each pair of peaks (*i.e.*, $R_{s,ji} = -R_{s,ij}$). If we are to correct the resolution for the difference in height between successive peaks, then this symmetry will no longer be found. Instead, there will be two different resolution values describing the separation between two successive peaks: one describing the extent to which the first peak is separated ($R_{s,i}$) and one to characterize the separation of the second peak ($R_{s,j}$).

A Gaussian peak is described by

$$f_i(t) = h_i \exp -\frac{1}{2}\left(\frac{t - t_i}{\sigma_i}\right)^2 \tag{9}$$

where h_i is the height of the peak, t_i the retention time at the peak maximum and σ_i the standard deviation. The width of the peak is $4\sigma_i$ (*i.e.*, $t - t_i = 2\sigma_i$) when $f_i(t)$ equals $h_i e^{-2} = 0.135h_i$. For a second peak (*j*) we find for the peak width at this height

$$h_i \exp(-2) = h_j \exp -\frac{1}{2}\left(\frac{t - t_j}{\sigma_j}\right)^2 \tag{10}$$

from which we find

$$\left(\frac{t - t_j}{\sigma_j}\right)^2 = 4 + 2\ln(h_j/h_i) \tag{11}$$

or

$$t = t_j \pm \sigma_j\sqrt{4 + 2\ln(h_j/h_i)} \tag{12}$$

so that the width of the second peak at 13.5% of the height of the first peak (indicated by the prefix *i*) is

$$^{i}w_j = 2\sigma_j\sqrt{4 + 2\ln(h_j/h_i)} \tag{13}$$

We may now obtain the resolution of the first peak by applying eqn. 1 at $h = 0.135h_i$:

$$^{i}R_{s,ji} = \frac{t_j - t_i}{2\sigma_i + \sigma_j\sqrt{4 + 2\ln(h_j/h_i)}} \tag{14}$$

If $h_i = h_j$, eqn. 14 reduces to eqn. 2. If we introduce the plate count (eqn. 3) into eqn. 14, we find

$$ {}^{i}R_{s,ji} = \frac{(t_j - t_i)\sqrt{N_i N_j}}{2t_i\sqrt{N_j} + t_j\sqrt{N_i}\sqrt{4 + 2\ln(h_j/h_i)}} \tag{15} $$

and if $N_i = N_j = N$, then

$$ {}^{i}R_{s,ji} = \frac{(t_j - t_i)\sqrt{N}}{2t_i + t_j\sqrt{4 + 2\ln(h_j/h_i)}} \tag{16} $$

An analogous argument for the second peak at $h = 0.135h_i$ leads to

$$ {}^{j}R_{s,ji} = \frac{(t_j - t_i)\sqrt{N}}{t_i\sqrt{4 + 2\ln(h_i/h_j)} + 2t_j} \tag{16a} $$

According to eqns. 16 and 16a, the largest resolution value is obtained for the largest of the two peaks (${}^{i}R_{s,ji} \geqslant {}^{j}R_{s,ji}$ if $h_i \geqslant h_j$ and *vice versa*). Eqn. 16 may be used in interpretive optimization procedures, where the retention surfaces are modelled as a function of the parameters to be optimized. For Gaussian functions there is no need to model the peak heights, as h will vary according to

$$ h_i = \frac{h_i^0}{t_i} = \frac{h_i^0}{1 + k_i} \tag{17} $$

where h_i^0 is the height peak i would have if it were to be eluted at $t_i = t_0$ ($k_i = 0$). Only one experimental chromatogram is necessary to calculate h^0 values for all the peaks and eqn. 16 may be rewritten as

$$ \begin{aligned} {}^{i}R_{s,ji} &= \frac{(t_j - t_i)\sqrt{N}}{2t_i + t_j\sqrt{4 + 2\ln(h_j^0/h_i^0) + 2\ln(t_i/t_j)}} \\ &= \frac{(k_j - k_i)\sqrt{N}}{2 + 2k_i + (1 + k_j)\sqrt{4 + 2\ln(h_j^0/h_i^0) + 2\ln\{(1 + k_i)/(1 + k_j)\}}} \end{aligned} \tag{18} $$

The two separate criteria describing the resolution between two peaks may be used in different situations. If both i and j are relevant peaks in the chromatogram, then the lower value appears to be the more relevant. This implies that only the resolution for the smaller of two peaks should be considered. If, however, the analytical problem is to quantify the amount of solute corresponding to the larger peak and the small peak is a contaminant, the concentration of which is not relevant, then the resolution for the large peak is the relevant number.

Careful considerations are required for using corrected resolution values in criteria describing the quality of separation for complete chromatograms rather than for pairs of successive peaks (see ref. 1, p. 140).

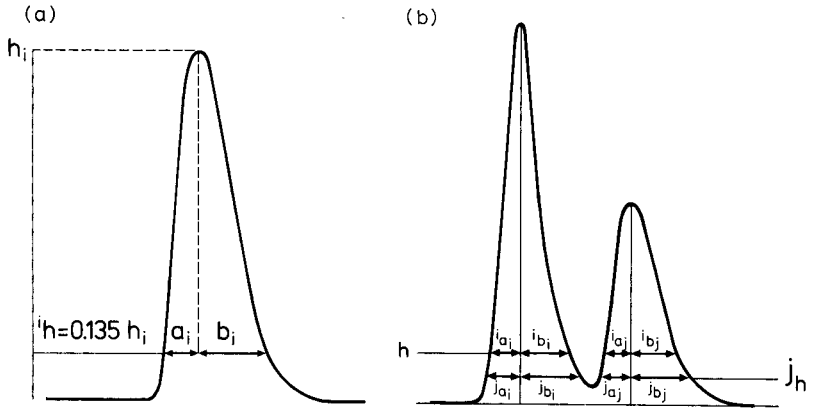

Fig. 2. (a) Illustration of the definition of the peak-width parameters a and b on the ascending and descending slope of a peak, respectively, at a certain fraction of the peak height (here 13.5%). (b) Illustration of the relevant parameters determining the resolution between two asymmetric peaks. ^ia_i, ^ib_i, ^ia_j and ^ib_j are measured at the reference height for peak i, *i.e.*, $^ih = 0.135h_i$ and ^ja_i, ^jb_i, ^ja_j and ^jb_j are measured at the reference height for peak j, *i.e.*, $^jh = 0.135h_j$.

Non-symmetrical peaks

For non-Gaussian peaks eqn. 2 is strictly invalid, but eqn. 1 may be used as long as the peaks are symmetrical. For non-symmetrical peaks $^1/_2w$ is not a good indication of the relevant peak width. Therefore, eqn. 1 may not be used. Instead[4], the relevant widths are those of the descending (end) slope of peak i (b_i) and the ascending (beginning) slope of peak j (a_j). This is illustrated in Fig. 2a, where it can be seen that a and b are defined on one slope of the peak, relative to the peak top. Parameters similar to a and b have been used to correct resolution values for the occurence of large, non-symmetrical peaks in a chromatogram[4]. For Gaussian peaks $a = b = {}^1/_2w$. In the general situation, in which the peaks are not Gaussians, we find

$$R_s = \frac{t_j - t_i}{b_i + a_j} \tag{19}$$

The parameter commonly used to characterize the degree of asymmetry of chromatographic peaks is the asymmetry factor, A_s, which is defined at a certain fraction, x, of the peak height as

$$A_s^x = \frac{b}{a} \tag{20}$$

At different values of x, not only will a and b be different, but their ratio may also change. Often, x is arbitrarily chosen to be 0.1, but $x = 0.135$ appears to be more logical (see above). However, when we define A_s at a certain fraction of the peak height, then the absolute height at which a and b are measured in the chromatogram will generally be different for each peak in the chromatogram. This is illustrated in Fig. 2b. At any given height in the chromatogram we can, in principle, measure a and b values.

If we take peak i as our reference peak (as indicated by the prefix before the symbols), then the obvious "observation height" is $0.135h_i$. At this height A_s can be calculated from eqn. 20 and the plate count from

$$^{i}N_i = 16\left(\frac{t_i}{^{i}a_i + {}^{i}b_i}\right)^2. \tag{21}$$

which for peak i itself is the conventional definition of N, but for all other peaks yields different values:

$$^{i}N_j = 16\left(\frac{t_j}{^{i}a_j + {}^{i}b_j}\right)^2 \tag{21a}$$

Eqn. 21a yields smaller N values ($^{i}N_j < {}^{j}N_j$) if peak j is larger than peak i and larger values ($^{i}N_j > {}^{j}N_j$) if peak j is smaller. Substitution of eqns. 20 and 21 in eqn. 19 yields

$$^{i}R_{s,ji} = \frac{(t_j - t_i)(1 + {}^{i}A_{s,i})(1 + {}^{i}A_{s,j})\sqrt{{}^{i}N_i{}^{i}N_j}}{4{}^{i}A_{s,i}t_i(1 + {}^{i}A_{s,j})\sqrt{{}^{i}N_j} + 4t_j(1 + {}^{i}A_{s,i})\sqrt{{}^{i}N_i}} \tag{22}$$

If the peaks are symmetrical ($A_s = 1$), eqn. 22 reduces to eqn. 4.

Eqn. 22 is fairly complex and it requires four parameters to obtain it from the chromatogram at the reference height (*e.g.*, $^{i}a_i$, $^{i}b_i$, $^{i}a_j$ and $^{i}b_j$). This is not very attractive and it may be difficult if the peaks are poorly resolved. Nevertheless, it has been demonstrated that relative peak widths (similar to a and b values) can be monitored during selectivity optimization procedures, yielding a separate surface next to the retention surfaces[4]. In the most dramatic situations, in which very large solvent or matrix peaks are present in the chromatogram, such a procedure should be followed. However, in situations in which the peaks are asymmetric and in which successive peaks differ significantly (*e.g.*, by more than a factor of two) but not dramatically (*e.g.*, by not more than a factor of ten) in height we should be looking for simplifications.

In practical situations we find it acceptable to require measurements of the width and the asymmetry of each individual peak, if these factors are to be taken into account. Hence, $^{i}N_i$, $^{i}A_{s,i}$, $^{j}N_j$ and $^{j}A_{s,j}$ will usually be determined. However, the width and asymmetry of a peak at a reference height, determined by another peak (*e.g.*, $^{i}N_j$ and $^{i}A_{s,j}$), will not usually be available. From this limited information the most sensible approximation is to assume the asymmetry factors to be independent of the height, *i.e.*, in eqn. 20 A_s^x is assumed to be independent of x, but to correct for differences in the heights between successive peaks. In terms of eqn. 19 this leads to

$$^{i}R_s = \frac{t_j - t_i}{^{i}b_i + {}^{i}a_j} = \frac{t_j - t_i}{^{i}b_i + {}^{j}a_j\sqrt{1 + {}^{1}/_{2}\ln(h_j/h_i)}} \tag{23}$$

With eqns. 20 and 21 we now find for the first peak

$$ {}^{i}R_{s,ji} = \frac{(t_j - t_i)(1 + {}^{i}A_{s,i})(1 + {}^{j}A_{s,j})\sqrt{{}^{i}N_i^{j}N_j}}{4{}^{i}A_{s,i}t_i(1 + {}^{j}A_{s,j})\sqrt{{}^{j}N_j} + 4t_j(1 + {}^{i}A_{s,i})\sqrt{{}^{i}N_i}\sqrt{1 + {}^{1}/_{2}\ln(h_j/h_i)}} \quad (24) $$

The analogous equation for the second peak is

$$ {}^{j}R_{s,ji} = \frac{(t_j - t_i)(1 + {}^{i}A_{s,i})(1 + {}^{j}A_{s,j})\sqrt{{}^{i}N_i^{j}N_j}}{4{}^{i}A_{s,i}t_i(1 + {}^{j}A_{s,j})\sqrt{{}^{j}N_j}\sqrt{1 + {}^{1}/_{2}\ln(h_j/h_i)} + 4t_j(1 + {}^{i}A_{s,i})\sqrt{{}^{i}N_i}} \quad (24a) $$

If, moreover, we assume that ${}^{i}N_i = {}^{j}N_j = N$ and that ${}^{i}A_{s,i} = {}^{j}A_{s,j} = A_s$, then we find a simple expression for a corrected resolution function for peak i:

$$ {}^{i}R_{s,ji} = \frac{(t_j - t_i)(1 + A_s)\sqrt{N}}{4A_s t_i + 4t_j\sqrt{1 + {}^{1}/_{2}\ln(h_j/h_i)}} \quad (25a) $$

For the second peak (j) the corresponding equation is

$$ {}^{j}R_{s,ji} = \frac{(t_j - t_i)(1 + A_s)\sqrt{N}}{4A_s t_i\sqrt{1 + {}^{1}/_{2}\ln(h_i/h_j)} + 4t_j} \quad (25b) $$

Eqns. 25a and b present a simple means of correcting for both the asymmetry of peaks and for variations in peak height. However, unlike eqns. 16 and 18, Eqn. 25a is not exact. If the two peaks considered show vastly different peak widths or asymmetry factors then, strictly, eqn. 22 should be applied.

For optimization purposes, eqns. 25a and b again represent two criteria for the separation between a pair of successive peaks, *i.e.*, one for each peak. Either or both of these may be used for optimization purposes in three different manners:

(1) correcting for differences in peak heights; this can be done if the concentrations in the sample are constant (*e.g.*, in quality control situations);

(2) assuming that $h_i = h_j$ if the concentrations are not constant;

(3) correcting for the largest possible difference in heights between peaks i and j, based on an expected range of possible solute concentrations. In this latter instance one should be aware of the increasingly approximate character of eqns. 25a and b with increasing peak-height ratios.

In the following evaluation the usefulness of the rigorous eqn. 22 and the simplified eqns. 24 and 25a and b will be examined.

EVALUATION PROCEDURE

In order to evaluate the applicability of the equations derived in this paper for characterizing the resolution in non-ideal situations, we used a series of computer-generated peak profiles. Exponentially modified Gaussian (EMG) functions provide a very accurate description of the true peak shape in analytical (reversed-phase) liquid

chromatography (LC). In other forms of chromatography the peak shapes may be different. For example, this will be the case in preparative LC. We have tested the present equations for EMG peaks, because of our intention to apply them for the purpose of optimizating analytical separations. This does not imply that use of the equations should be limited to EMG peaks. For other asymmetric peaks they will almost certainly yield more useful values than the conventional definition for R_s.

A series of EMG peaks were generated, with varying values for the time constant (τ) of the exponential decay[8]. The parameters of the Gaussian function were $t_{max} = 15$ min and $\sigma_t = 0.474$ min (corresponding to 1000 theoretical plates for $\tau = 0$) for the first peak. The values for τ were 0 (Gaussian peak), 1, 2, 3, 4 and 5 min. The t_{max} value of the second peak was increased from 15.8 to 19.0 min, while maintaining a plate count of 1000 for the Gaussian peak ($\sigma_t = t_{max}/\sqrt{1000}$). Different values for τ result in different values for the peak asymmetry, as is illustrated in Fig. 3. The asymmetry factor in this picture was obtained from the simulated peak profiles at a fraction of 13.5% of the peak height. It is seen that the present range of variation for τ corresponds to a range $1 \leqslant A_s < 3.23$. In practical chromatograms all peaks may have similar asymmetry factors, but large variations in A_s between successive peaks in a single chromatogram are also possible. For example, this is often the case in ion-pair chromatography with differently charged solutes. The situations examined in this paper were thought to provide the most severe tests for the proposed equations.

At the heart of the present evaluation method is a comparison between the values obtained from the modified resolution equations (eqns. 22, 24 and 25) and the relative overlap (eqns. 7 and 8), The relative overlap is thought to be the natural measure of chromatographic resolution. It is directly related to the extent to which a peak area can be used correctly for quantitative analysis, or the purity which can be obtained in a preparative separation. However, *RO* can only be determined if the individual peak profiles are known. In the present simulation study, the individual peak profiles are known so that a comparison can be made between the modified resolution functions and the relative overlap criterion. Ideally, a given value of *RO* should correspond to a unique value of the resolution, independent of the peak shape (asymmetry) and the peak-height ratio. If the calculated resolution value is plotted against *RO*, this ideal situation would lead to a single, monotonic line (*i.e.*, no minima or maxima) for all different conditions.

Further details of the evaluation procedure have been described elsewhere[9].

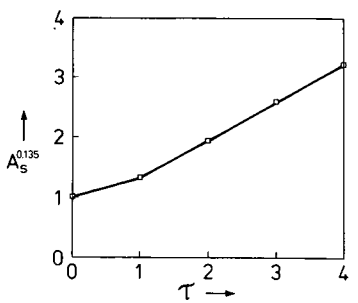

τ min	A_s
0.0	1.000
1.0	1.321
2.0	1.944
3.0	2.591
4.0	3.226

Fig. 3. Relationship between the exponential decay factor τ and the observed asymmetry factor at 13.5% of the peak height. Parameters for the Gaussian peak were $t_{max} = 15$ min and $\sigma_t = 0.474$ min (corresponding to $N = 1000$).

RESULTS

Fig. 4a shows the correlation between the resolution, calculated from eqn. 22, and the relative overlap for the first peak (RO_i) for situations in which the asymmetry of the first peak is varied. In this situation, the two peaks are of equal area. When the asymmetry of the first peak increases, its height decreases and therefore the ratio of peak heights also varies.

Along the horizontal axis, the difference in retention time between the peaks decreases from left to right, causing an increase in the relative overlap and a decrease in the calculated resolution. It is seen that there is little divergence between the different curves, so that the ideal situation of a single, monotonic relationship is approached. Only in the range where strong overlap occurs (*i.e.*, where the relative overlap becomes high and the resolution low) are different values for the resolution obtained for the peaks of different asymmetry with the same *RO* value. In this range a lower value for the resolution is obtained when the first peak becomes less asymmetrical.

Fig. 4b represents the same peak pairs as Fig. 4a, but both the resolution (eqn. 22) and the relative overlap are now calculated for the second peak. Because the tail of the first peak stretches far into (or even beyond) the second peak, the resolution of the latter is usually more difficult to determine, However, the different curves, corresponding to different asymmetry factors for the first peak, are still fairly close together.

In Fig. 5 the same peak pairs are characterized as in Fig. 4b, but the resolution is now calculated for the second peak with the approximated eqn. 24a. The results are seen to be virtually identical with those in Fig. 4b, and hence eqns. 24 and 24a are a good approximation of eqn. 22. This is of great practical value, because eqns. 24 and 24a only require the retention times, plate counts and asymmetry factors for each individual peak. The plate count may be obtained from the peak width at any given fraction of the peak height (in this case N has been obtained from eqn. 21, using the a and b values measured at 13.5% of the peak height). The asymmetry factors should

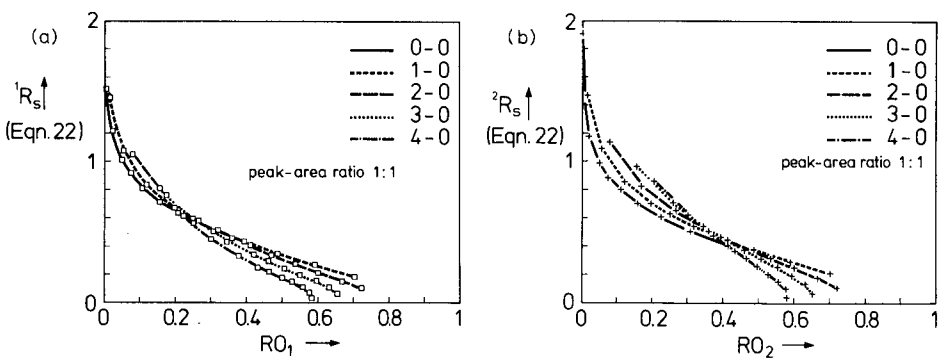

Fig. 4. Relationship between the relative peak overlap and the modified resolution calculated from eqn. 22 for two peaks of equal area. (a) Results for the first peak. (b) Results for the second peak. The exponential decay of the first peak was varied from $\tau = 0$ (———), $\tau = 1$ (·····), $\tau = 2$ (– – –), and $\tau = 3$ (· · · · · ·) to $\tau = 4$ min (— · — · —). The second peak was symmetrical ($\tau = 0$). The retention time of the first peak was 15 min, that of the second peak was varied from 15.8 to 19 min. For both peaks the efficiency for the Gaussian function was taken to correspond to $N = 1000$.

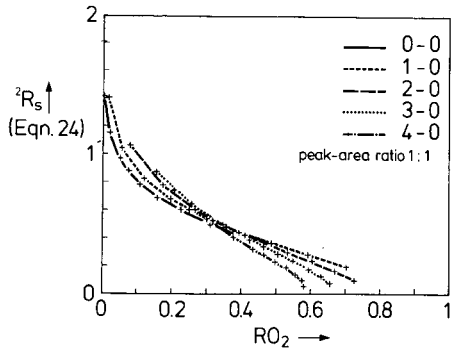

Fig. 5. As Fig. 4b, except that the modified resolution was calculated from eqn. 24a.

be obtained at 13.5% of the peak height. Eqn. 22 is much less attractive in practice, because it also requires the measurement of the peak width and asymmetry at the same fractions of the height of the preceding peak (and at the same fractions of the height of the following peak).

Fig. 6a shows that eqn. 25a is still a useful approximation in this instance. However, eqn. 25b (Fig. 6b) yields resolution values that are poorly correlated with *RO*. This is understandable, because eqn. 25b is based on the peak width and asymmetry of the second peak, which was taken to be symmetrical, while the asymmetry of the first peak increased. Naturally, poor results are obtained if a (strongly) asymmetric peak is assumed to be symmetrical. Nevertheless, this is exactly what is done when the conventional resolution equation is applied in this situation. Conventionally, both peaks are assumed to be symmetrical and the plate count of a symmetrical peak (*e.g.*, the second peak in the present peak pair) is used to calculate a value for *N*. Thus, a comparison of Figs. 4b, 5 and 6a with Fig. 6b serves to illustrate how much better it is to use the (approximated) modified resolution functions than it is to use the conventional resolution (eqn. 2).

It is important to realize that Fig. 4a and b show the resolution values each for one of the two peaks. Both the relative overlap and the modified resolution equations are based on the understanding that the true extent of separation in non-ideal

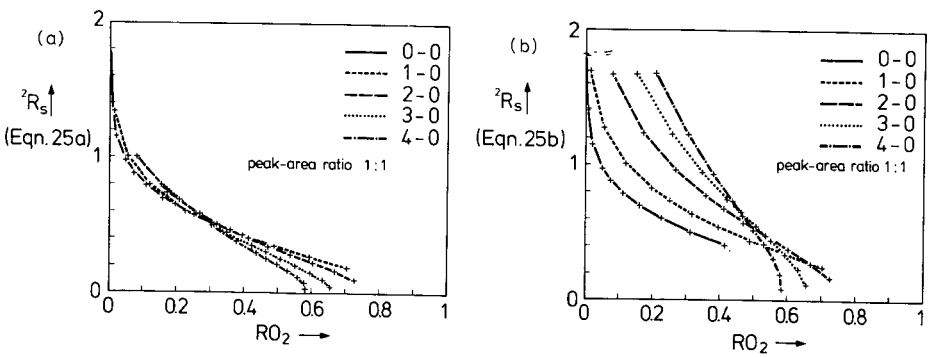

Fig. 6. As Fig. 4b, except that the modified resolution was calculated from (a) eqn. 25a and (b) eqn. 25b.

situations is different for the two peaks constituting a pair. However, because the areas of the two peaks are the same for the peak pairs used to make Fig. 4, the relative overlap is by definition the same for both peaks. Ideally, therefore, the curves in Fig. 4a and b should be identical, which is exactly true for the situation in which both peaks are Gaussian (solid lines). The extent of the deviation of the other curves from this line is a measure of the performance of eqn. 22.

In Fig. 7 we show two sets of curves for a situation which is similar to that in Fig. 4, except for the peak-area ratio. The area of the first peak is now four times larger than that of the second peak. As a result, the relative overlap is now much smaller for the first peak than it is for the second peak. This is seen in Fig. 7a. The highest possible *RO* for the first peak is 0.25. Increasing the asymmetry of the first peak is seen to have only a small effect on the relationship between the resolution calculated from eqn. 22 and *RO*. In Fig. 7b, which represents the data for the second peak, a different set of curves is observed, but again they are found close together, approaching the ideal situation.

Fig. 8 illustrates that eqn. 24a is still a reasonable approximation of eqn. 22 for the second (more difficult) peak in the situation of a 4:1 peak-area ratio. However, a larger variation is found between the different lines in Fig. 8 than in Fig. 7b. If the peak-area ratio becomes 8:1 (not shown), the difference between eqns. 22 and 24 becomes larger. For large peak-area ratios the former, less practical equation does need to be used. Eqn. 22 is essentially identical with the approach previously suggested for dealing with very large solvent or matrix peaks in a chromatogram[4].

Fig. 9 illustrates the effect of varying peak-area ratios. In Fig. 9a the modified resolution is calculated from eqn. 24a for the second in a pair of symmetrical peaks. In this situation the asymmetry factors are equal to 1 and eqn. 24a reduces to eqn. 16a. It can be seen from Fig. 9a that eqns. 16 and 16a perform very well in situations in which two Gaussian peaks of different areas occur.

When the asymmetry of the peaks increases, a less ideal picture of the calculated resolution *vs.* the relative overlap is obtained if eqn. 24 is used. For example, in Fig. 9b results are shown for a situation in which the first peak is asymmetrical ($\tau = 2$ min, *i.e.*, $A_s^{0.125} \approx 2$) and the second peak is symmetrical ($\tau = 0$). Whereas the different curves tend to converge at the high-resolution end (*i.e.*, at resolution values of 1 and higher, different resolution values may be calculated if the relative overlap (*RO*) of the

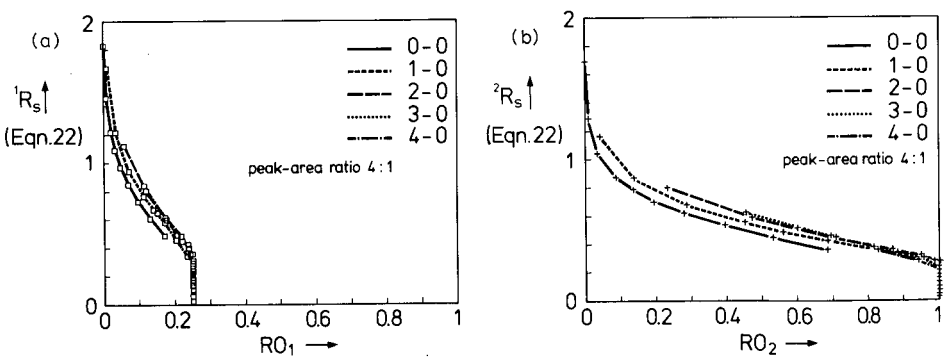

Fig. 7. As Fig. 4, except that the area of the first peak was four times larger than that of the second peak.

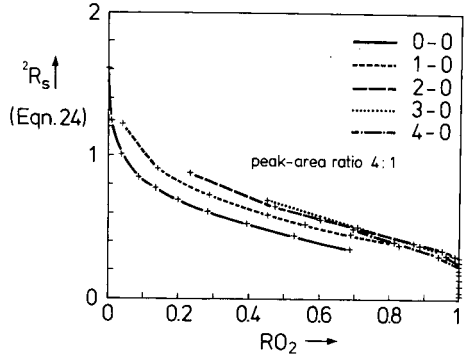

Fig. 8. As Fig. 7b, except that the modified resolution was calculated from eqn. 24a.

second peak is at a constant, high value. If $\tau = 1$ min, the results are in between those in Fig. 9a and b, whereas they become slightly worse is τ is increased further to 4 min (results not shown).

Fig. 9b is an indication of the limitations of eqns. 24 and 24a. If the peak-area ratio starts to differ significantly from 1, the peaks are strongly asymmetric and the resolution is small, than eqn. 24 becomes too much of an approximation and only eqn. 22 will yield good results.

DISCUSSION

We consider the performance of the modified resolution function as defined by eqn. 22, and closely approximated by eqns. 24 and 24a, to be highly satisfactory. Not only do the results compare very favourably with those that would be obtained with the conventional resolution function (compare, *e.g.*, Figs. 5 and 6b), the results

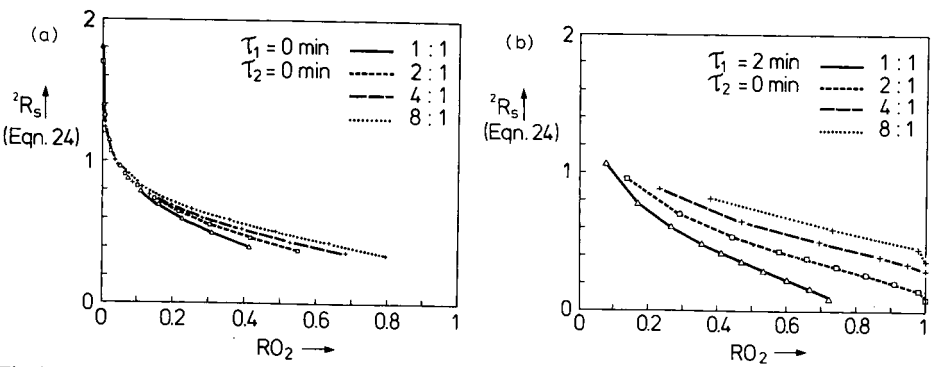

Fig. 9. Relationship between the relative peak overlap and the modified resolution calculated from eqn. 24a for the second of two peaks with different areas. (a) Both peaks symmetrical. (b) First peak asymmetric ($\tau = 2$ min, *i.e.*, $A_s^{0.135} \approx 2$). Peak-area ratios: 1:1 (———), 2:1 (- - - -), 4:1 (— — — —), 8:1 (.....). The second peak was symmetrical ($\tau = 0$). The retention time of the first peak was 15 min, that of the second peak was varied from 15.8 to 19 min. For both peaks the efficiency for the Gaussian function was taken to correspond to $N = 1000$.

obtained with the present modified resolution function also compare favourably with other possible methods of characterizing the resolution[9]. Eqns. 24 and 24a can be used as a more practical alternative to eqn. 22 except in situations in which the peaks are asymmetric or of greatly different areas and the relative overlap is high (Fig. 9b). Eqn. 25 can be used if the plate counts and asymmetry factors are approximately constant throughout the chromatogram. Eqn. 16 can be used for Gaussian peaks of greatly different areas.

Another important consideration is that resolution values can be calculated from eqn. 24 if (i) the retention time (or capacity factor), (ii) the peak width at half-height (plate count) and (iii) the asymmetry factor at 13.5% of the peak height are known. It appears to be feasible to keep track of these three parameters for each individual peak during interpretive optimization procedures[1], so that the present approach can be used for this purpose. Empirical resolution functions, such as the ratio between the (average) peak height and the depth of the valley between peaks (peak-valley ratios) may be used to characterize the extent of separation, but cannot be used in interpretive optimization procedures.

A second advantage of the present resolution functions in the context of optimization procedures is that a value can be calculated, even for very strongly overlapping peaks. The relative overlap will yield a value of $RO = 1$ for the small peak, even if the degree of separation is small. The modified resolution for the small peak will still be different from zero, so that small improvements in separation may be exploited during optimization. However, this will require that the individual peak profiles be known, either from individual injections of each sample component or from the deconvolution of multi-channel data.

Whereas eqn. 24 was found to be an accurate approximation of eqn. 22, eqn. 25 cannot always be used. Eqn. 25 can be used if the plate heights and asymmetries of all peaks are (approximately) the same. However, if the asymmetry varies as dramatically as in Fig. 5, eqn. 25b, in which the smaller of the two asymmetry factors is used, yields very poor results (Fig. 5b). This problem will be even greater if the area of the first peak becomes larger than that of the second (not shown). In this situation the asymmetry factor of the least symmetrical peak may be used (see Fig. 5a), but we prefer to use the more complex eqn. 24 because (i) it is easier not to have to decide which of the two asymmetry factors (and plate counts) should be used and (ii) in order to make such a decision, the values for both peaks would usually need to be calculated anyway, so that there is no practical objection to using eqn. 24.

The present approach has a limitation in the calculation of the peak-height correction for the larger peak in a separation concerning peaks of different height. If a peak is more than e^2 (7.4) times larger than an adjacent peak, the square root in eqn. 24 becomes undefined. This is not a major problem, because it concerns the resolution for the large peak only. A reasonable value can be obtained by defining $\sqrt{1 + {}^1/_2 \ln(h_j/h_i)}$ to be equal to zero if $h_j/h_i \leqslant e^{-2}$.

Chromatograms

In our opinion, we have provided a thorough, objective evaluation of the modified resolution functions in the systematic study described above. Fig. 10 is intended to allow the reader to form a subjective opinion from a visual inspection of a number of peak pairs, with a varying degree of asymmetry of the first peak (τ

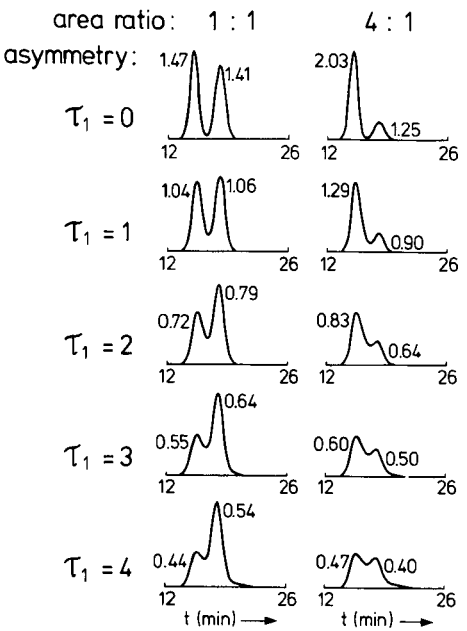

Fig. 10. Calculated resolution values (eqns. 24 and 24a) for each peak in ten different peak pairs. t_1 = 15 min, t_2 = 18 min. N = 1000 (for Gaussian peak). Exponential decay factors (τ) and peak-area ratios vary, as indicated. The conventional resolution value is 1.44 for all peak pairs.

increases from top to bottom) and for two different values of the peak-area ratio (1:1 in the first column, 4:1 in the second). For the Gaussian part of the first peak in each pair the retention time was 15 min and for the second 18 min. All peaks were calculated with a plate count of 1000 for the Gaussian peak. This implies that if the resolution is determined in the conventional way (eqn. 5), using the plate count as measured either from the second peak or from a standard injected separately, the first pair of peaks in Fig. 10 would have a resolution of 1.44. This value will decrease only slightly for asymmetric peaks owing to a marginal increase in the retention time of the peak maximum with increasing peak asymmetry (τ). For all peak pairs the conventional resolution function yields values close to 1.4.

In Fig. 10 the resolution values calculated from eqns. 24 and 24a are indicated for each peak. In the first pair (top left) both peaks are Gaussian. Because of the slightly different peak heights (equal area), the resolution is slightly higher than the conventional value for the first (larger) peak (1.47 instead of 1.44) and slightly lower for the second peak (1.41). However, in this situation there is very little difference between the conventional and modified resolution values.

If the peak-area ratio increases to 4:1 (top right), the modified resolution value increases to 2.03 for the first peak but decreases to 1.25 for the second, indicating that the separation of this pair is better for the first peak than it is for the second. To quantify small peaks next to large ones, a higher resolution is required than in the opposite situation.

When the asymmetry of the first peak increases for two peaks of equal area (top to bottom in the left column), the modified resolution starts to decrease and actually

becomes lower for the first peak than for the second. For a peak-area ratio of 4:1 (top to bottom in the left column) the loss in resolution is also larger for the first (asymmetric) peak.

The reader is invited to make a subjective judgement of the modified resolution values shown for each peak in Fig. 10, bearing in mind that the conventional resolution function yields a value of 1.4 for each of the peak pairs in this figure.

CONCLUSIONS

(1) The modified resolution functions presented in this paper can be used to characterize the resolution in non-ideal situations.

(2) The modified resolution function yields two values for the resolution of a pair of peaks, one for each peak. The largest value (best separation) will be obtained for the largest peak.

(3) A good correlation is obtained between the modified resolution and the relative peak overlap. Variations in the peak asymmetry and the relative peak area are shown to have a minor effect on this relationship. In this respect, the modified resolution behaves better than alternative peak-separation characteristics.

(4) The modified resolution function (eqn. 22) can be adequately approximated by a simpler equation (eqn. 24), which requires only the retention time, peak width and asymmetry factor of each individual peak.

(5) Because of the previous conclusion, the modified resolution function can be used in combination with interpretive optimization procedures.

(6) If the efficiency and the peak asymmetry are (roughly) constant for all peaks in the chromatogram, eqns. 25 and 25b may be used as a further approximation of eqn. 22. If this condition is not met, we recommend the use of eqns. 24 and 24a.

(7) For Gaussian peaks with different areas eqns. 16 and 16a provide a very simple and effective correction for the resolution

(8) If the peaks are strongly asymmetric the peak-area ratio is high and the resolution is low, the more complex eqn. 22 should be used, which requires monitoring of the peak width and asymmetry of each peak at a given fraction of its own height, in addition to that of its neighbours.

REFERENCES

1 P. J. Schoenmakers, *Optimization of Chromatographic Selectivity, A Guide to Method Development*, Elsevier, Amsterdam, 1986.
2 L. R. Snyder, J. W. Dolan and M. A. Quarry, *Trends Anal. Chem.*, 6 (1987) 106.
3 L. R. Snyder and J. J. Kirkland, *Introduction to Modern Liquid Chromatography*, Wiley, New York, 2nd ed., 1979.
4 P. J. Schoenmakers, P. J. Naish and R. J. Hunt, *Chromatographia*, 24 (1987) 579.
5 P. J. Schoenmakers, *J. Liq. Chromatogr.*, 10 (1987) 1865.
6 J. C. Berridge, *Techniques for the Automated Optimization of HPLC Separations*, Wiley, Chichester, 1985.
7 P. J. Naish and S. Hartwell, *Chromatographia*, submitted for publication (presented at the *17th Symposium on Chromatography, Vienna, 25–30 September, 1988).*
8 J. P. Foley and J. G. Dorsey, *Anal. Chem.*, 55 (1983) 730.
9 J. K. Strasters, A. Bartha, H. A. H. Billiet and L. de Galan, *J. Liq. Chromatogr.*, in press.

Journal of Chromatography, 458 (1988) 371–384
Elsevier Science Publishers B.V., Amsterdam — Printed in The Netherlands

CHROMSYMP. 1504

PRACTICAL OPTIMIZATION OF THE SEPARATION OF A LIMITED SUBSET OF COMPONENTS BY USING ISOELUOTROPIC TERNARY ELUENT MIXTURES IN REVERSED-PHASE HIGH-PERFORMANCE LIQUID CHROMATOGRAPHY

AKOS BARTHA*, HUGO A. H. BILLIET* and LEO DE GALAN
Department of Analytical Chemistry, Delft University of Technology, De Vries van Heystplantsoen 2, 2628 RZ Delft (The Netherlands)

SUMMARY

A fully integrated procedure is presented for the separation optimization of all or a limited subset of components by means of isoeluotropic ternary solvent mixtures along with the iterative regression method in reversed-phase high-performance liquid chromatography. The optimization search area is defined for both full and limited optimization by utilizing a statistical approach in combination with an extended gradient isocratic scanning procedure. Starting eluent compositions are selected with respect to the complexity of the sample mixture, and the merits of the procedure are evaluated by performing the full and limited (3-out-of-9) optimization of a nine-component aromatic solute mixture. Three resolution-based optimization criteria are used and selected sequentially to achieve satisfactory resolution for the peaks of interest in the shortest possible analysis time. In order to guide the analyst through the selection of the criteria and to assist in the evaluation of the optimum found, an "expert" algorithm has been integrated in the optimization program. The use of the algorithm in the optimization of the analysis time is also demonstrated (while resolution is maintained at the required level) by applying a suitable criterion and allowing column length variation.

INTRODUCTION

The development and application of computerized optimization procedures in high-performance liquid chromatography (HPLC) is a steadily growing area of research. Most of the currently proposed selectivity optimization schemes revolve around the separation of all components in the sample mixtures with some minimum resolution. However, the analyst is not always interested in the quantification of all the components, but rather in a limited subset of key components. The merits of performing such a "limited" optimization, rather than the separation of all solutes in a complex mixture ("full" optimization), have been evaluated by Herman *et al.*[1] using

* On leave from the University of Chemical Engineering, Veszprem, Hungary.

0021-9673/88/$03.50

computer-simulated examples. It has been shown that the peak capacity (and therefore the analysis time) required to separate a solute mixture at a given probability level can be substantially reduced for moderately complex mixtures when the number of solutes of interest is less than half of the total number of solutes. Generally, the eluent optimization of limited sample subsets will (i) save analysis time (the peak capacity requirement for a successful separation is lower) or (ii) allow mixtures containing a larger number of components to be analyzed. In the same paper, a procedure was formulated for selecting appropriate starting eluent compositions for solvent optimization in reversed-phase (RP) HPLC on a statistical basis[1]. The approach allows also the analyst to define starting conditions for the optimization of a limited subset of key components (NI) in a sample containing more solutes ($M \geqslant NI$).

The application of predictive optimization procedures such as the iterative regression method[2] to limited optimization procedures requires (besides the recognition of the solutes in the successive chromatograms) optimization criteria which reflect only the separation of the peaks of interest. In a recent paper[3], different resolution-based optimization criteria were adapted for limited optimization. To avoid the ambiguity of multi-purpose criteria, a sequential approach was formulated for three resolution-based criteria. As a primary goal, we aim to find satisfactory resolution for the peaks of interest. The secondary goal can be to achieve the shortest possible analysis time, while resolution is maintained at the required level.

In this paper the utilization of the rational selection of the starting eluent compositions on a statistical basis and the sequential use of optimization criteria are evaluated, respectively, by performing both the full and limited optimization of the same sample by using ternary solvent mixtures in RP-HPLC. Another possible approach is the use of the Multi-Criteria Decision Making (MCDM) procedure suggested by Smilde *et al.*[4] which also can perform resolution and time optimization simultaneously. We favour the sequential approach for several reasons. The MCDM plots do not provide information on the ruggedness of the resolution optimum. Also the sequential approach lends itself more readily to automation than the MCDM procedure because it shows directly how the chromatography can be adapted to gain analysis time. To guide the chromatographer through the selection of criteria and to help in the evaluation of the optimum found, an "expert" algorithm has been developed and integrated into the binary and ternary eluent optimization programs. The application of this integrated procedure in the optimization of the (satisfactory) resolution of the sample components and the minimum analysis time, by allowing column length variation, is also demonstrated.

EXPERIMENTAL

HPLC-grade organic solvents were obtained from Rathburn (Walkerburn, U.K.). Distilled, deionized water was prepared by means of a Milli-Q water purification system (Millipore, Molsheim, France). Solutes for the sample mixtures were from Fluka (Buchs, Switzerland) and E. Merck (Darmstadt, F.R.G.).

The stationary phase was 5-μm ODS-Hypersil (Shandon Southern Products, U.K.) slurry-packed into 4.6 mm I.D. HPLC columns of length 7.5, 12.5 or 20 cm. The chromatographic system consisted of a Model 1090 chromatograph, equipped with an auto-injector and a Model 1040A linear photodiode-array UV–VIS spectrometer (Hewlett-Packard, Waldbronn, F.R.G.). All measurements were made at 25°C.

The optimization programs for limited optimization were developed in PRO/BASIC on a Waters 840 Data Management System, equipped with 512K memory, dual diskette drive (2 × 400K), integral 10M Winchester disk drive, extended bit map graphics with colour monitor and a Letterprinter LA-100 (all from Digital Equipment Corporation, Maynard, MA, U.S.A.).

RESULTS AND DISCUSSION

Determination of the optimization search area

Recently, an efficient procedure has been described by Herman *et al.*[5] for predicting solute retention in the three common binary solvent mixtures used for ternary eluent optimization in RP-HPLC. The method combines the results from a single water-to-methanol gradient scan and one or two additional isocratic measurements. The statistical approach[1] and the above procedure have been integrated into a common procedure, which allows selection of the most suitable eluent compositions on a statistical basis for either full or limited optimization at constant or variable eluotropic strength. The operation of this integrated method for the experimental selection of the initial eluent compositions for a full optimization example has been discussed by De Galan *et al.*[6] in detail. Here, the application of this start-up procedure will be demonstrated for both full and limited optimization of ternary eluent mixtures of "fixed"eluotropic strength (isoeluotropic) for the separation of a sample containing nine aromatic solutes.

First, a water-to-methanol gradient scan is carried out in 15 min (Fig. 1). The first solute peak is eluted at 1.21 min, the last one at 13.96 min (see Fig. 1 for other experimental details). The polarity range of this sample (defined according to ref. 1) is found to be 5 from the gradient experiment. Once the polarity range and the number of the solutes are known (the latter can also be estimated as described in ref. 6), the peak capacity needed to solve the separation problem at a preselected probability level can be determined from the probability curves described in ref. 1.

We target the separation of (i) all nine components and (ii) three solutes out of nine at the probability level 0.75. In ref. 1 an empirical relationship was derived to relate a NI-out-of-M limited optimization problem to the equivalent m'-out-of-m' full

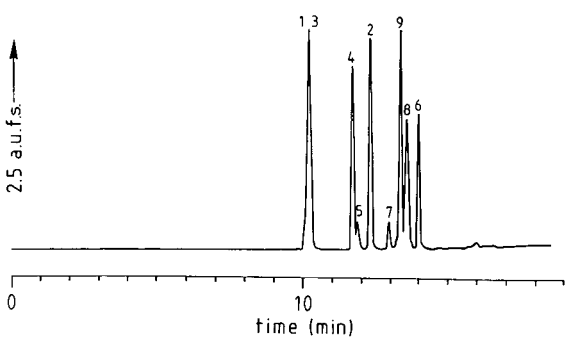

Fig. 1. Gradient elution chromatogram of an aromatic solute mixture. For solutes see Table III. Linear gradient from water to methanol in 15 min; void time, 1.41 min; flow-rate, 1 ml/min; column, 20 cm × 4.6 mm I.D. packed with 5-μm ODS-Hypersil; detection, 210 nm.

TABLE I

DETERMINATION OF THE INITIAL ISOCRATIC BINARY ELUENT COMPOSITIONS FOR THE FULL OPTIMIZATION OF A NINE-COMPONENT SAMPLE MIXTURE

The polarity range of the sample is 5, the preselected level of probability of separation success is 0.75 and the necessary peak capacity is 26.

Organic solvent		*Predicted retention**		*Measured retention**		*Probability*
Type	*Concentration*					
Methanol	57.1	1.71	10.16	1.66	6.00	0.341
	48.5	2.81	11.50	2.40	14.26	0.797
	49.9	2.26	12.39	2.08	11.2	0.738
Acetonitrile	40	2	11	1.41	6.53	0.552
	35.6	1.72	10.20	1.90	13.9	0.858
	37.5	1.67	9.99	1.67	10.03	0.754
THF	33.4	2	11	2.15	9.65	0.623
	30.8	2.46	13.26	2.47	13.9	0.775

* Capacity factors of first and last peaks.

optimization problem, in terms of the total number of components. The 3-out-of-9 separation for ternary optimization was calculated to be equivalent to a full optimization of seven components.

Next, the corresponding plots of probability *vs.* peak capacity (*cf.*, Fig. 2 in ref. 1) are selected according to the polarity range index and the (equivalent) number of the components. The required peak capacities for 0.75 probability are found to be 26 (nine components) and 18 (seven components), respectively. According to the above approach, in order to maintain the same probability of separation success with ternary solvent mixtures, the initial binary eluents should have the same (predetermined) peak capacities. Once the probability level (peak capacity of the chromatogram) is closely identical in each of the three binary mixtures *and* the solute retention is within acceptable limits, the ternary eluent optimization procedure can be initiated.

The results on the determination of the starting eluent compositions are summarized in Tables I and II. In the first line of Table I (9-out-of-9 separation) the

TABLE II

DETERMINATION OF THE INITIAL ISOCRATIC BINARY ELUENT COMPOSITIONS FOR THE LIMITED OPTIMIZATION OF THREE SOLUTES OF INTEREST FROM A NINE-COMPONENT SAMPLE MIXTURE

The polarity range of the sample is 5, the preselected level of probability of separation success is 0.75 and the necessary peak capacity is 18.

Organic solvent		*Predicted retention**		*Measured retention**		*Probability*
Type	*Concentration*					
Methanol	69.1	0.85	3.76	1.14	2.57	0.101
	55.8	2.16	7.12	1.64	6.32	0.797
Acetonitrile	46.1	1.6	6.3	1.37	5.92	0.825
THF	38.2	1.6	6.3	1.85	7.44	0.832

* Capacity factors for first and last peaks.

gradient experiment predicts that the required peak capacity of 26 can be reached with an isocratic binary mobile phase containing 57.1% methanol, where the capacity factors of the first and the last peaks eluted are predicted to be 1.71 and 10.16, respectively. A column plate count of 8000 and a required resolution of 1.25 were used in these calculations. However, the measured data ($k'_{first} = 1.66, k'_{last} = 6.0$) deviate from the predicted, resulting in a much lower peak capacity and, hence, in a probability of successful separation of only 0.34 rather than the 0.75 originally required. Using the results of this isocratic and the gradient experiment, a new prediction is made at 48.5% methanol–water (for the details of this gradient isocratic procedure see ref. 5). This composition results in a high probability of 0.797, but much longer analysis time. It should be pointed out that the higher the probabilities required are (as a result of larger peak capacities), the longer the analysis time will become. Therefore, a compromise must be found between the probability of the separation success and a sensible length of the chromatographic analysis. It is not advisable to ask for a probability of >0.9 (for a maximum success) for any separation, since it can result in very long analysis times.

As a compromise between the probability of separation success and the time needed to record the chromatogram, a final prediction is made, based on both isocratically determined points, again for the probability of 0.75. Now, the result seems quite acceptable [$k'_{last} = 11.2$ (k' = capacity factor) and probability of 0.738] in the 49.9% methanol–water eluent.

The equivalent compositions of acetonitrile–water and tetrahydrofuran (THF)–water binaries (which are expected to elute the sample mixture within the same retention limits, *i.e.*, peak capacities, at $k'_{first} = 2$, $k'_{last} = 11$) are calculated from the empirical transfer rule equations, as described in ref. 5. Again, the original predictions for these binary eluent compositions are refined until the probabilities and the analysis time become acceptable. The results summarized in Table II for the 3-out-of-9 limited optimization problem were obtained in a similar manner, using the same gradient data as a starting point. Since the starting conditions for the isoeluotropic ternary eluent optimization offer reasonably high probabilities (see Tables I and II) of the separation success, no other more complex (*e.g.*, quaternary or variable-eluotropic-strength ternary) optimization parameter space is considered. Therefore, isoeluotropic ternary-eluent optimization is favoured for this sample, and this selection is highly justified by the optimization results discussed below.

Development of an "expert" algorithm

After defining the vector space of the optimization parameters, suitable optimization criteria must be selected which clearly reflect the goal of the analyst. In ref. 3 we suggested a sequential approach to the selection and use of the different optimization criteria, for both full and limited optimization. The goal of the optimization in this scheme is to find satisfactory resolution for the peaks of interest in a minimum analysis time.

First, the optimum resolution, $R_{s_{min}}$, must be found with confidence for the peaks of interest. Weighting factors with a value of 1 (important) or 0 (unimportant) are assigned to each component of the sample, and the resolution between two neighbouring peaks is taken as relevant when (w_i OR w_{i+1}) = 1. The analyst can also specify what resolution is required, $R_{s_{req}}$. When satisfactory minimum resolution is

found with confidence, *i.e.*, $R_{s_{min}} \geqslant R_{s_{req}}$, the optimization can be continued to find the minimum analysis time, using secondary criteria. These criteria can be adapted to the goals and (chromatographic hardware) abilities of the analyst to realize the shortest possible analysis time on the same column as that used for optimization or on another column of different length (preferably leaving the flow-rate and particle diameter unaltered). The threshold separation criterion, S_k, and the required analysis time criterion, $1/T_{nefd}$, suggested by Schoenmakers[7] can be used to optimize for these two goals in limited optimization as well[3].

However, for a given chromatographic system, the resolution at optimum conditions can still be lower than the required value. Most optimization procedures abandon the analyst in such a case without giving him any help on how to improve the current separation. Therefore, it seemed to be valuable to include a special algorithm in the solvent optimization program to combine two goals: (i) to guide the user through the selection of criteria and to help in the evaluation of the optimum found, (ii) to provide options and advice when the required resolution could not be reached in the actual chromatographic system. This "expert" algorithm is not a simple "on-line help" function, since it also reports the status of the optimization process and provides advice on how to continue the optimization procedure.

A simplified flow diagram of some major decision branches of the routine is shown in Fig. 2. The algorithm was integrated into the binary and ternary optimization procedures described elsewhere[3] for both full and limited optimization. When the maximum value of $R_{s_{min}}$ remains below the required level, $R_{s_{req}}$, the (righthand side of the) scheme is designed to accommodate a number of "backtracking" possibilities of revising (incorrect) decisions, made earlier during the optimization procedure. Meaningful suggestions are given in Fig. 2. Overall, a stopping point is provided, where the analyst may have to make even more trenchant decisions, *e.g.*, to change the phase system. Consulting (or interfacing the program) at this point with real expert systems may be a possibility for the future. However, the more elaborate evaluation of all the options and advice that can be given is outside the scope of this paper.

In the following discussion, the use of secondary criteria (left hand side of the scheme) will be evaluated in detail, with respect to the decisions based on the scheme in Fig. 2. All three criteria are calculated over the whole eluent composition range from the beginning of the optimization procedure. The "expert" algorithm keeps track of

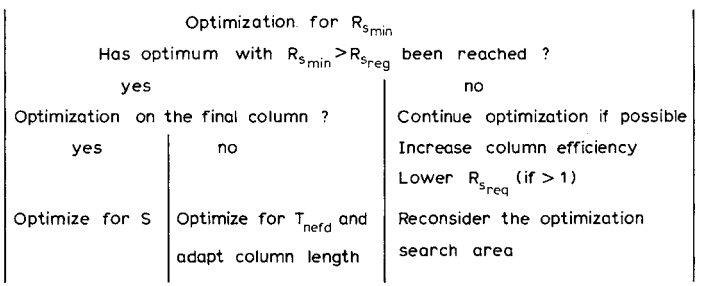

Fig. 2. Major decision branches used by the "expert" algorithm, guiding the analyst through the sequential use of the resolution-based optimization criteria.

the status of each criterion, and once the optimum is found, not only for the $R_{s_{min}}$ but also for (any of) the other two criteria, the option to realize any of these optima can become available without further experiments. This situation can occur when the predicted optimum composition for the analysis time criterion is within the confidence interval of a criterion determined earlier during the search. When a (satisfactory) optimum is found for both the minimum resolution, $R_{s_{min}}$, and the required analysis time criterion, $1/T_{nefd}$, the length of the column (or the flow-rate) may also be adapted in order to reduce the analysis time. The use of these options will be demonstrated on real experimental examples.

Comparison of the full and limited optimization

The last chromatograms determined in the start-up procedure provide the binary limits for the ternary eluent optimization procedure by means of the iterative regression method[2]. It is assumed that in the course of the optimization solute peaks are recognized in sequential chromatograms either on the basis of their UV spectra or by injecting known standards.

The nine-component aromatic solute mixture represents a typical example for ternary-eluent optimization. In each of the three binaries, different solute pairs are unresolved, while (small) variations of the solvent strength in the determination of the initial binaries did not reveal changes in selectivity. Larger variations of the solvent strength, *e.g.*, binary-eluent optimization may result in different band spacing; however, it would cause large changes in the analysis time as well.

Full optimization. The starting binary-eluent chromatograms of the nine-component aromatic mixture are shown in Fig. 3. All solutes are assigned to be of interest ($w_i = 1, i = 1 \ldots 9$) and to be separated from each other and the (imaginary) solvent peak at t_0 with a required resolution of $R_{s_{req}} = 1.25$. The logarithm of solute capacity factors is assumed to be a linear function of the ternary eluent composition (Fig. 4a). These plots are used for calculation of the minimum resolution criterion, $R_{s_{min}}$, in Fig. 4b. Clearly, separation selectivity is strongly influenced by the ternary-eluent composition (the elution order of the components varies) and a maximum value of $R_{s_{min}} = 1.64$ is predicted for a ternary mobile phase containing 24.4% methanol and 19.2% acetonitrile ($X = 1.51$); X is a parameter indicating binary and ternary compositions along the composition axis in the phase selection diagram[2]. After measuring two other chromatograms at "shifted" compositions[2] (see eluent compositions and retention data in Table III), a final optimum is predicted at $X = 1.70$ with a $R_{s_{min}} = 1.60$ (see phase-selection diagram in Fig. 5). The chromatogram verifying this optimum with an analysis time of 18.5 min is shown in Fig. 6a. If this analysis time is acceptable, the procedure stops at this point. However, according to the optimization scheme in Fig. 2, when $R_{s_{min}} \geqslant R_{s_{req}}$ at the optimum conditions, the analysis time can be minimized by using secondary criteria.

The response surfaces of the three criteria (relative plots) are shown in Fig. 5b. We point out that the optimization process can take different directions (eluent compositions), depending on the choice of the secondary (analysis time) criterion. The maximum of the threshold separation criterion, S_k, is in another (the acetonitrile–THF–water) ternary "window" at $X = 2.21$. However, before we continue the optimization, it is worthwhile to examine the possible gain in analysis time (on the given column) at this composition. From the retention plots, we estimate that the

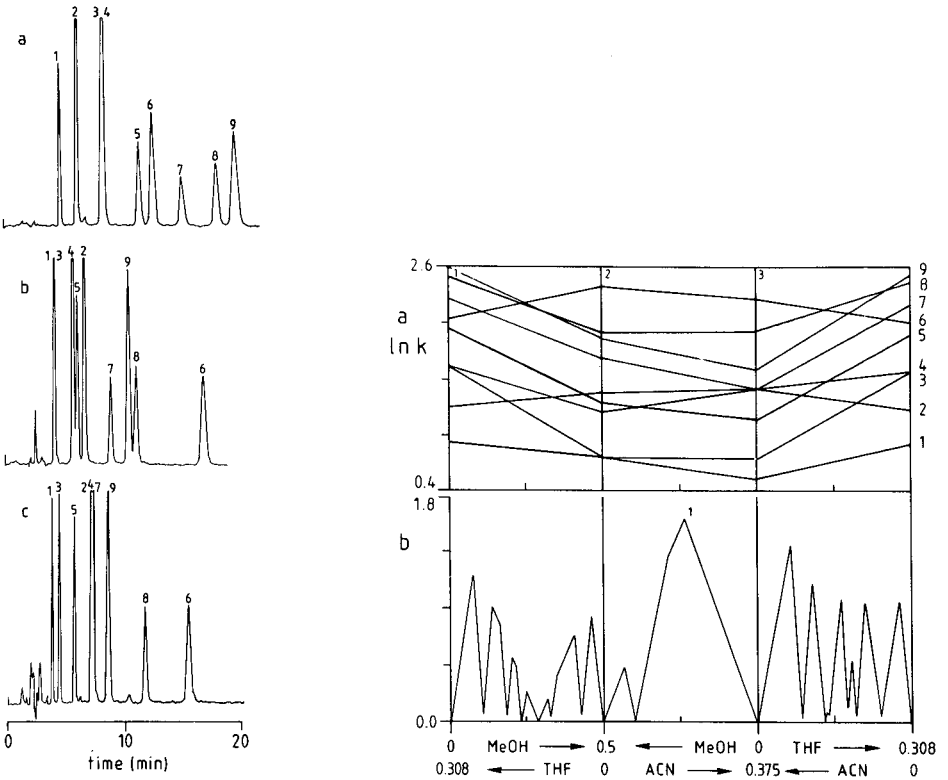

Fig. 3. Isocratic chromatograms of the nine-component mixture of aromatic solutes with the initial binary eluents for full optimization. Eluents: (a) 30.8%; (b) 49.9% methanol; (c) 37.5% acetonitrile. Detection: 260 nm. For other conditions see Fig. 1.

Fig. 4. Phase-selection diagram, constructed from the chromatograms shown in Fig. 3, for the full optimization. (a) Plots of ln k'; (b) response surface for the minimum resolution, $R_{s_{min}}$, criterion. MeOH = Methanol; ACN = acetonitrile; THF = tetrahydrofuran.

predicted optimum composition offers only minor reduction (less than 10%) of the analysis time compared to that already found for the $R_{s_{min}}$ criterion with confidence, since the retention of the last-eluted peak(s) is closely constant in the three isoeluotropic ternary eluent systems. Therefore the optimization is not continued in this direction. On the other hand, the optimum found for the required analysis time criterion, $1/T_{nefd}$, is identical with that for the $R_{s_{min}}$. Since $R_{s_{min}} = 1.6$ is obtained with 6000 plates (in the given ternary system) on a 20-cm column, a value of $R_{s_{req}} = 1.25$ can be realized with 3660 plates on a 12-cm column. The chromatogram obtained with a 12.5-cm column with the same flow-rate and particle diameter is shown in Fig. 6b. The observed $R_{s_{min}} = 1.3$ and analysis time of 12.2 min are in good agreement with the predictions.

When the analysis is to be performed on a routine basis, the saving in time and eluent consumption can be significant, and it pays to adapt the column length. However, if the analysis is to be performed only a few times and/or no shorter column

TABLE III

SOLUTE RETENTION DATA FROM SEQUENTIALLY MEASURED CHROMATOGRAMS, DURING THE FULL OPTIMIZATION PROCEDURE, USING TERNARY SOLVENT MIXTURES IN RP-HPLC

The value of w_i is 1 for the peaks of interest and 0 for the unimportant peaks.

Solute	w_i	*Retention times (min)*					
		*1**	*2*	*3*	*4*	*5*	*6*
1 Benzyl alcohol	1	4.77	4.33	3.77	4.17	3.95	4.02
2 Dimethyl phthalate	1	6.24	6.95	7.23	7.75	7.53	7.81
3 Phenol	1	8.53	4.33	4.35	4.49	4.30	4.49
4 Benzonitrile	1	8.53	5.95	7.23	6.63	6.85	7.04
5 *p*-Cresol	1	11.65	6.33	5.70	6.35	6.00	6.25
6 Diethyl pthalate	1	12.78	17.15	15.55	18.92	17.51	18.48
7 3,4-Dimethylphenol	1	15.30	9.23	7.23	8.87	8.11	8.54
8 Benzene	1	18.25	11.43	11.80	11.42	11.52	11.91
9 2,4-Dimethylphenol	1	19.83	10.80	8.58	10.41	9.50	10.07
Parameter X		0	1	2	1.51	1.736	1.70
Percentage of methanol		0	49.9	0	24.4	13.2	15
Percentage of acetonitrile		0	0	37.5	19.2	27.6	26.3
Percentage of THF		30.8	0	0	0	0	0
Percentage of water		69.2	50.1	62.5	56.4	59.2	58.7

* Number of chromatogram as indicated in Fig. 5.

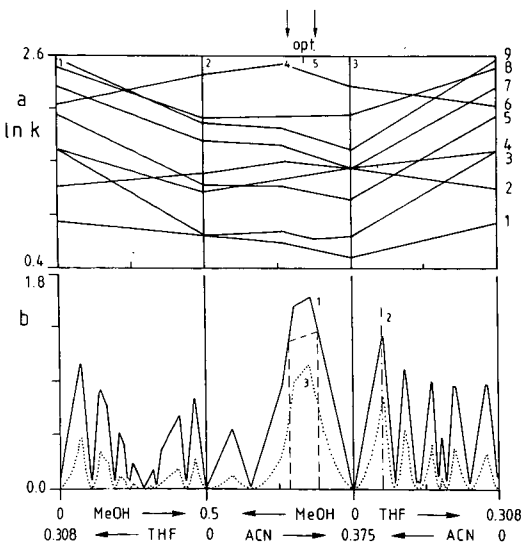

Fig. 5. Phase-selection diagram, showing the final result of the full optimization example. (a) Plots of ln k'; (b) optimization criteria $R_{s_{min}}$ (1), S_k (2) and T_{nefd} (3), normalized to give maximum values between 0.75 and 1.25.

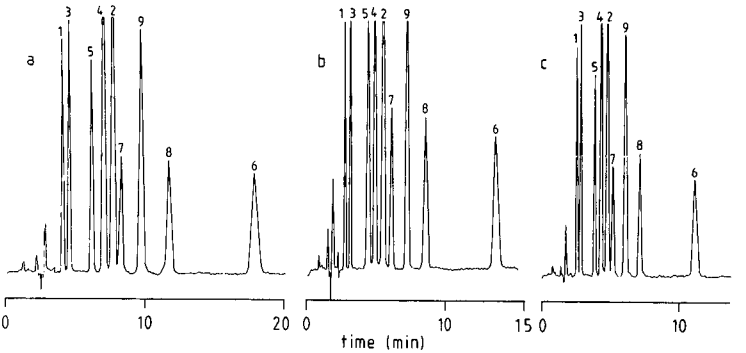

Fig. 6. Separation of all nine aromatic solutes at optimum conditions (15% methanol, 26.3% acetonitrile and 58.7% water) on (a) 20-cm column, flow-rate 1.0 ml/min, (B) a 12.5-cm column, flow-rate 1.0 ml/min and (c) a 20-cm column, flow-rate 1.66 ml/min; column pressure, 200 bar.

is at hand, as an alternative the flow-rate can be increased in order to shorten the analysis time at the expense of higher column pressure and eluent consumption. The limit of flow-rate increase is determined by the decrease in column efficiency (in our case it should not drop below 3660) and/or the increase in the column pressure drop. We decided to allow a pressure of 200 bar as the practical upper limit; the flow could be increased to 1.66 ml/min on the 20-cm column. As a result, the overall analysis time needed for the complete separation of our nine-component sample mixture decreased to 10.8 min (Fig. 6c).

Limited optimization. Three phenolic compounds, phenol (3), 3,4-dimethylphenol (7) and 2,4-dimethylphenol (9), were designated as being of interest for limited optimization of the same nine-component sample mixture. The three initial chromatograms with the starting binary eluents are shown in Fig. 7. In these chromatograms the position of the important solutes is indicated by the symbol (*). Note the much

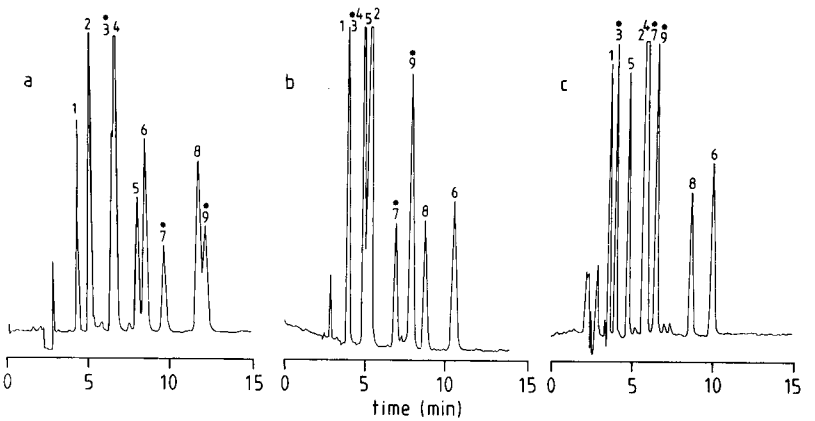

Fig. 7. Isocratic chromatograms of the nine-component mixture of aromatic solutes in the initial binary eluents for limited optimization. The three phenols of interest are marked with an asterisk. Eluents: (a) 38.2% THF; (b) 55.8% methanol; (c) 46.1% acetonitrile. Detection: 260 nm. For other conditions see Fig. 1.

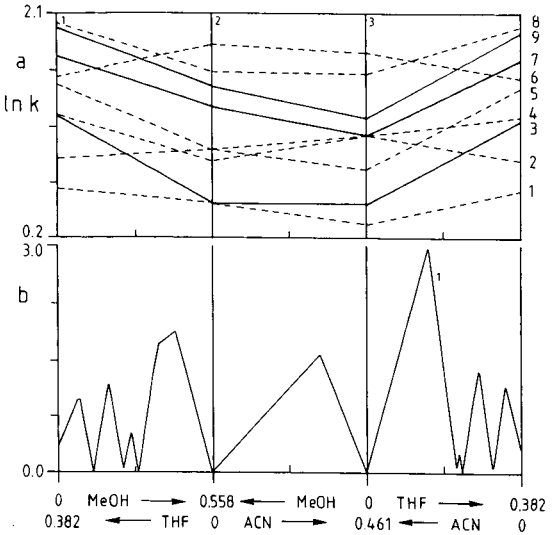

Fig. 8. Phase-selection diagram, constructed from the chromatograms shown in Fig. 7, for the limited optimization. (a) Plots of ln k'; (b) response surface for the minimum resolution, $R_{s_{min}}$, criterion.

smaller separation space,, set by the statistical approach compared to the full optimization problem (*cf.*, Fig. 3).

The phase-selection diagram at the beginning of the optimization is shown in Fig. 8. The response surface of the minimum resolution criterion is also different from that of the full optimization and exhibits a maximum of 2.4 in another ternary system (acetonitrile–THF–water) at $X = 2.39$. In fact, after two additional measurements in this ternary system, the maximum value of $R_{s_{min}}$ for the three peaks of interest (3.0) is located at $X = 2.30$ (11.5% THF and 32.3% acetonitrile), as shown by the final phase-selection diagram in Fig. 9. The chromatogram (No. 6) verifying this optimum is shown in Fig. 10a, with an analysis time of 8.7 min. All retention data are given in Table IV. Comparison of the results of the full and limited optimizations on the same (20-cm) analytical column (see Figs. 6a and 10a, respectively) reveals that the separation of only three components out of nine can be accomplished in about half the analysis time, even before special time optimization or column length variation are invoked. This is achieved simply by (i) defining realistic starting conditions for the less complex (limited) optimization problem, and (ii) allowing other components, which are of no interest, *e.g.*, dimethyl phthalate, benzonitrile and *p*-cresol to remain unresolved.

Optima for the other two criteria have also been found (Fig. 9). Now the optimum composition ($X = 2.24$) predicted for the threshold separation criterion, S_k, is also within the confidence range of points measured earlier. In a way similar to the full optimization, the optimum for S_k offers only a minor decrease in the analysis time, since the overall solute retention is closely constant in this ternary system as well. However, this does not mean that the use of S_k is completely irrelevant in ternary-eluent optimization. When the eluents are less "isoeluotropic", the use of the S_k criterion can lead to significant savings in analysis time on the given column[3]. For instance, when similar peak capacities (probabilities) are set in the initial binary eluents

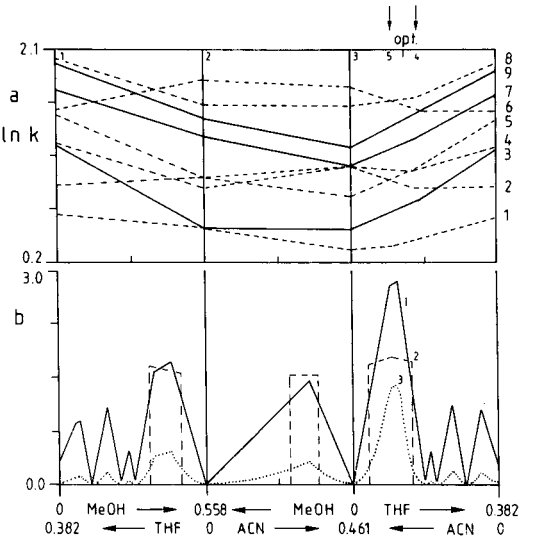

Fig. 9. Phase-selection diagram, showing the final result of the limited optimization example. (a) Plots of ln k'; (b) optimization criteria, $R_{s_{min}}$ (1), S_k (2) and T_{nefd} (3), normalized to give maximum values between 0.75 and 1.25.

or when the eluotropic strength is varied intentionally, different first and last peak retentions may result. On the other hand, the optimum found for the required analysis time criterion, $1/T_{nefd}$, is identical with that of the $R_{s_{min}}$ and allows a dramatic decrease

TABLE IV

SOLUTE RETENTION DATA FROM SEQUENTIAL CHROMATOGRAMS, IN THE LIMITED OPTIMIZATION PROCEDURE, WITH TERNARY SOLVENT MIXTURES IN RP-HPLC

The value of w_i is 1 for the peaks of interest and 0 for the unimportant peaks.

Solute	w_i	*Retention times (min)*					
		*1**	*2*	*3*	*4*	*5*	*6*
1 Benzyl alcohol	0	4.02	3.72	3.34	3.51	3.40	3.45
2 Dimethyl phthalate	0	4.79	5.09	5.49	4.75	5.03	4.94
3 Phenol	1	6.20	3.72	3.72	4.39	4.05	4.18
4 Benzonitrile	0	6.29	4.71	5.49	5.33	5.36	5.33
5 *p*-Cresol	0	7.71	5.05	4.51	5.40	5.00	5.33
6 Diethyl phthalate	0	8.19	10.32	9.76	8.16	8.87	8.73
7 3,4-Dimethylphenol	1	9.37	6.63	5.49	6.67	6.13	6.33
8 Benzene	0	11.91	8.45	8.42	9.07	8.80	8.73
9 2,4-Dimethylphenol	1	11.48	7.59	6.21	7.87	7.09	7.39
Parameter X		0	1	2	2.43	2.22	2.30
Percentage of methanol		0	55.8	0	0	0	0
Percentage of acetonitrile		0	0	46.1	26.1	35.7	32.3
Percentage of THF		38.2	0	0	16.6	8.6	11.5
Percentage of water		61.8	44.2	53.9	57.3	55.7	56.2

* Numberof chromatogram as indicated in Fig. 9.

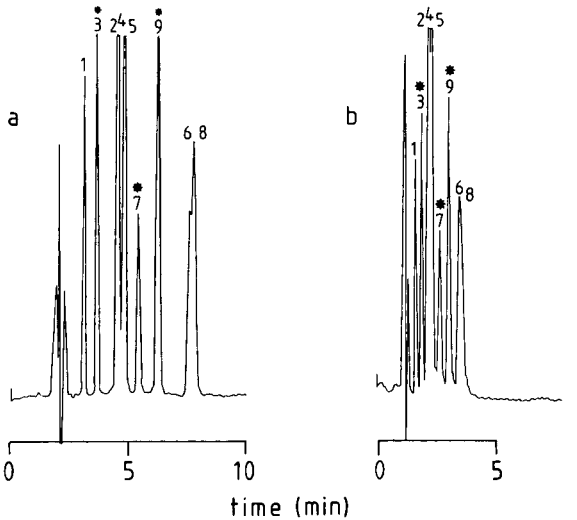

Fig. 10. Separation of the three phenolic compounds of interest (*) in the nine-component sample mixture at optimum conditions (11.5% THF, 32.3% acetonitrile and 56.2% water) on (a) a 20-cm column, flow-rate 1.0 ml/min, (b) a 7.5-cm column, flow-rate 1.0 ml/min.

in column length (plate count is 6500 in this ternary system). In principle, only 1105 theoretical plates (a 4-cm instead of 20-cm column) are needed to maintain a ($R_{s_{req}} = 1.25$) satisfactory resolution of the three peaks of interest within 2 min! Again, one must consider (i) the need for a shorter analysis time and (ii) the necessity of purchasing or packing a shorter column. Obviously, the reduction in column length should be considered carefully, since it is always better to "overscore" by using a column with a practical length than to use a very short (< 5-cm) column. In this study, this optimum was realized with a 7.5-cm (65% shorter) column; the chromatogram is shown in Fig. 10b. The analysis time was 4.0 min, and the three peaks of interest were baseline-separated. The results demonstrate the dramatic gain in analysis time between full and limited optimizations when the number of components of interest is much lower than the number of all solutes.

CONCLUSIONS

The combination of the statistical approach and the extended gradient isocratic scouting procedure results in rapid selection of realistic starting eluent conditions prior to systematic eluent optimization. The main advantage of the statistical approach is best demonstrated by comparing the starting conditions for the full and limited optimization of the same sample mixture. For limited optimization, the chromatograms with the starting binaries are proportionally shorter (in our case by *ca.* 50%) when assigning more realistic starting conditions and allowing a gain in analysis time due to the less complex (3-out-of-9) optimization problem.

The sequential selection and use of resolution-based criteria, which were adapted for limited optimization by assigning weighting factors to each solute in the sample

mixture, allows the efficient optimization of the separation of the peaks of interest when the iterative regression method is applied. In order to help the analyst to achieve the goal of satisfactory/required resolution in the shortest possible analysis time, an ("expert") algorithm has been developed and integrated into the eluent optimization program. The use of this algorithm is demonstrated in the optimization of the analysis time (while resolution is maintained at the required level) by applying suitable criteria and allowing column length variation. By comparing the full and limited optimization of the sample mixture, we have demonstrated that the degree of separation space required to resolve a limited subset of components (and hence the analysis time as well) can be reduced when unimportant solutes are allowed to remain unresolved and the number of the components of interest is much lower than that of all components of the sample.

REFERENCES

1 D. P. Herman, H. A. H. Billiet and L. de Galan, *Anal. Chem.*, 58 (1986) 2999.
2 A. C. J. H. Drouen, H. A. H. Billiet, P. J. Schoenmakers and L. de Galan, *Chromatographia.*, 16 (1982) 48.
3 A. Bartha, H. A. H. Billiet and L. de Galan, *J. Liq. Chromatogr.*, in press.
4 A. K. Smilde, A. Knevelman and P. M. J. Coenegracht, *J. Chromatogr.*, 369 (1986) 1.
5 D. P. Herman, H. A. H. Billiet and L. de Galan, *J. Chromatogr.*, 463 (1989) 1.
6 L. de Galan, D. P. Herman and H. A. H. Billiet, *Chromatographia.*, 24 (1987) 108.
7 P. J. Schoenmakers, *The Optimization of Chromatographic Selectivity*, Elsevier, Amsterdam, 1986.

Journal of Chromatography, 458 (1988) 385–394
Elsevier Science Publishers B.V., Amsterdam — Printed in The Netherlands

CHROMSYMP. 1483

COMPUTER-ASSISTED RETENTION PREDICTION SYSTEM FOR OLIGONUCLEOTIDES IN GRADIENT ANION-EXCHANGE CHROMATOGRAPHY

YOSHINOBU BABA* and MIYUKI FUKUDA
Department of Chemistry, Faculty of Education, Oita University, Dannoharu 700, Oita 870-11 (Japan)
and
NORIMASA YOZA
Department of Chemistry, Faculty of Science, Kyushu University, Hakozaki, Higashiku, Fukuoka 812 (Japan)

SUMMARY

A technique is presented for the retention prediction of single-stranded homo-oligonucleotides under gradient elution conditions in anion-exchange chromatography. The prediction system is based on the theory proposed by Jandera and Churaček. In the present system, the theory was modified by the extrapolation method, utilizing the linear relationship between the log of the capacity factor and the number of nucleotides. The modified theory allowed the prediction of retention times for high-molecular-weight oligonucleotides, which could not be calculated from the original theory. Oligoadenylate was used as a standard oligonucleotide to demonstrate the accuracy of the prediction system. By use of this system, the retention times of oligoadenylates up to 25–35 bases in chain length were predicted within 8% errors under both binary-linear and binary-convex gradient shapes.

INTRODUCTION

In the different steps of cloning and sequencing of nucleic acids, high-performance liquid chromatography (HPLC) is particularly useful for the separation of fragments of DNA and RNA[1–18]. To find suitable separation conditions of these fragments by trial-and-error experiments is a time-consuming and troublesome task. Although computer-assisted retention prediction has been recognized as a powerful tool for optimizing elution conditions[19–31] in isocratic and gradient HPLC, no successful attempts have been reported on a prediction system for fragments of DNA and RNA.

We have developed a computer-assisted retention prediction system for inorganic polyphosphates in isocratic[30] and gradient[29,31] anion-exchange chromatography. The prediction system for inorganic polyphosphates has been successfully applied to the optimization of isocratic[27] and gradient[28] elution conditions and has provided a substantial saving in the time required for optimization over the conventional (trial-and-error) method.

0021-9673/88/$03.50

Oligonucleotides as well as inorganic polyphosphates are anionic species, containing negatively charged phosphate groups. In anion-exchange chromatography, the behaviour of oligonucleotides is expected to be similar to that of inorganic polyphosphates, because the separation is primarily based on the ionic interactions of positively charged groups on the anion exchanger and negatively charged phosphate groups on the solutes.

In the present paper, the theory and procedure of computer-assisted retention prediction under gradient elution conditions are described for the oligomeric series of oligonucleotides, the simplest fragments of DNA or RNA. Oligoadenylate, A_n, in which n is the number of nucleotides, was chosen as a standard oligonucleotide. Fundamental chromatographic parameters necessary for the prediction system were obtained by isocratic elution chromatography. The capacity factor, k', of individual oligoadenylates containing less than eight nucleotides were measured under various isocratic elution conditions: eluent concentrations, C, and column temperature. The log k' values of oligoadenylates were found to be linearly related to the number of nucleotides, n. The k' values for oligoadenylates with n values > 7, which are difficult to obtain, were estimated by extrapolation of the linear relationship between log k' and n. The constants a and b were calculated from the relationship between k' and C. The retention times under gradient elution conditions were predicted by means of the present system, in which fundamental parameters were stored. The predicted retention times in gradient anion-exchange chromatography were compared with the observed ones with binary-linear and binary-convex gradient shapes.

EXPERIMENTAL

Chemicals

Unless otherwise stated, guaranteed reagents from Wako (Osaka, Japan) were used without further purification. Polyadenylate, sodium salt [poly(A)] was obtained from Yamasa Shoyu (Chiba, Japan). Oligoadenylate fragments from poly(A) were prepared by alkaline hydrolysis of poly(A) according to the literature[5]. Poly(A), digested in alkaline solution, gave a series of oligoadenylates, A_n, with varying chain lengths. Each A_n contains 2′- and 3′-terminal phosphates.

HPLC equipment

A TRI-ROTAR II HPLC system (Jasco, Tokyo, Japan) was used. The separations were performed on a commercially available column[10] (Shim-pack WAX-1, a weakly basic anion exchanger, 50 mm × 4 mm I.D.; Shimadzu, Kyoto, Japan). The Shim-pack WAX-1 is packed with a spherical silica support, having a particle diameter of 3 μm and a pore size of 100 Å and tertiary amino groups chemically bonded to the silica support. The column dead-time, t_0, was measured by injecting water and found to be 0.55 min. The separation column was surrounded by a jacket containing circulating water at constant temperature within ± 0.1°C. The sample solution (100 μl) was injected into a separation column and chromatographed at a flow-rate of 1.0 ml/min. Oligoadenylate fragments, eluted from the column, were monitored at 260 nm by means of an UVIDEC-100 spectrophotometric detector (Jasco).

Eluent

Fundamental chromatographic parameters were measured in isocratic elution with phosphate buffer solutions (pH 6.8), containing appropriate concentrations of phosphate and 20% acetonitrile.

The binary gradient elution technique was used for oligoadenylate separations. Buffer A was 0.01 *M* phosphate buffer (pH 6.8) containing 20% acetonitrile and buffer B was 0.3 *M* phosphate buffer (pH 6.8) containing 20% acetonitrile.

Calculation

Retention times and band widths were calculated with a personal computer PC-9801 (NEC, Tokyo, Japan). The program was written in BASIC. The full listings are available on request from the authors.

RESULTS AND DISCUSSION

Procedure for prediction of retention times and band widths

The first step in the procedure for prediction of retention times of oligonucleotides under gradient elution conditions is to determine constants a and b characteristic of each solute. These constants are calculated from the relatonship between the eluent concentratons, C, and the capacity factors, k', measured under isocratic elution conditions[20,27]:

$$k' = aC^{-b} \tag{1}$$

In gradient ion-exchange chromatography, the solute retenton times, t_R (min), for oligonucleotides were calculated from eqn. 2 by means of constants a and b[20–22,29,31].

$$t_R = (1/u)\{(1/B')[(xb + 1)B'\, at_0u + C_i^{(xb + 1)/x}]^{1/(xb + 1)} - C_i^{1/x}/B'\} + t_0 \tag{2}$$

where u is the flow-rate (ml/min) and t_0 is the column dead-time (min); C_i, B' and x are adjustable parameters for the gradient profile.

The following form of the gradient-profile function was chosen so as to be applicable to a great variety of gradient shapes

$$C = (C_i^{1/x} + Bt)^x$$
$$B = (C_f^{1/x} - C_i^{1/x})/t_f \tag{3}$$

where C is the eluent concentration (M) at time t (min), C_i is the initial eluent concentration (M) at the beginning of the gradient elution ($t = 0$ min) and C_f is the final one at the end of gradient elution ($t = t_f$); $B' = B/u$. The parameter x characterizes the shape of the gradient profile: at $x = 1$, the change in eluent concentration is linear, while the concentration gradient is convex for $x < 1$ and concave for $x > 1$. Gradient profiles with the parameters $x = 0.58$ and $x = 1$ were used in the present study, as shown in Fig. 1.

Band widths of oligonucleotides should be estimated to calculate chromato-

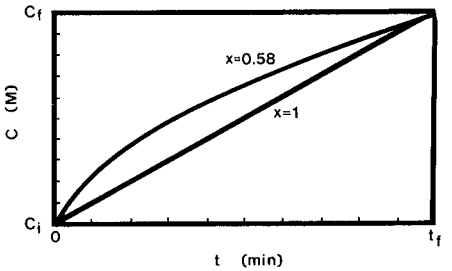

Fig. 1. Gradient profiles used in the present study. For details see text.

graphic resoluton in addition to solute retention time. Band widths, w ($=4\sigma$ in time units) are calculated as follows

$$w = 4t_R/N_g^{1/2} \tag{4}$$

where N_g is the plate number in gradient elution chromatography.

Fig. 2 illustrates the plots of observed band widths against observed retention times in gradient anion-exchange chromatography of oligoadenylates at column temperatures of 40 (Fig. 5), 50 an 60°C. It was surprising that the column temperature did not contribute to a decrease in band widths, as shown in Fig. 2.

The calculated band widths (solid line in Fig. 2) were in good agreement with the observed ones, when N_g was 5000. As a result, in the present system, band widths at all column temperatures were calculated from eqn. 4, using this value of N_g.

The simple expression (eqn. 4) is a first approximation for the estimation of band widths in gradient elution chromatography. Other N_g values should be chosen for the estimation of band widths in other chromatographic systems, because the value of 5000 would be applicable for a specific chromatographic system.

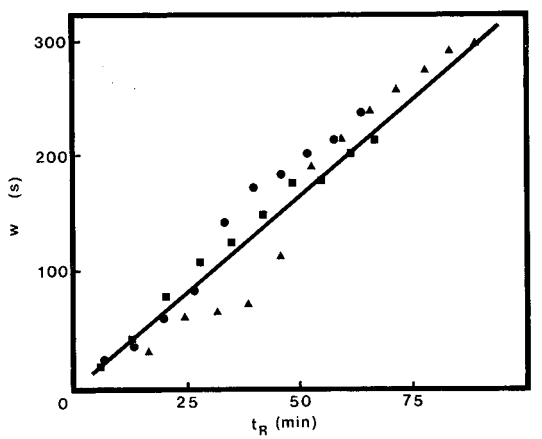

Fig. 2. Relationship between the band width, w, and retention time, t_R, at various temperatures: ● = 40 (Fig. 5); ▲ = 50; ■ = 60°C in gradient elution chromatography. The solid line represents the band width calculated from eqn. 4 using an N_g value of 5000.

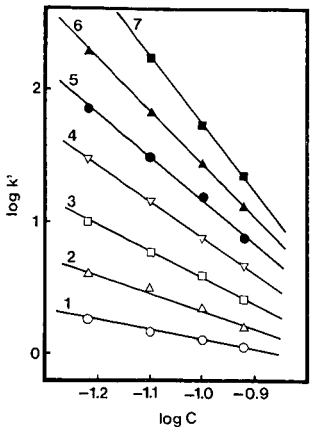

Fig. 3. Plots of log k' *vs.* log C at pH 6.8 and a column temperature of 40°C. Eluent: phosphate buffer solution (pH 6.8) containing 20% acetonitrile. Numbers indicate the number of nucleotides in the oligoadenylates.

Determination of constants a and b in isocratic elution

As described in the above section, constants a and b must be determined prior to the prediction of retention times. As shown in Fig. 3, the plot of log k' *vs.* log C gave straight lines with correlation coefficients between 0.985 and 0.999 at a column temperature of 40°C. Constants a and b for individual solutes of purified low-molecular-weight nucleotides (from A_1 to A_7) were determined from the slope and intercept of the straight line in Fig. 3 and are compiled in Table I.

In previous papers, we demonstrated that the column temperature was an indispensable factor in improving the chromatographic resolution of inorganic polyphosphates in both isocratic[27] and gradient[28] anion-exchange chromatography. However, it scarcely affected the chromatographic behaviour of oligonucleotides. Consequently, constants a and b in Table I were used for the prediction of retention times at all column temperatures.

Isocratic elution experiments to determine k' values were performed for individual oligonucleotides up to seven bases in chain length, as shown in Fig. 3. When individual nucleotides were difficult to obtain, such as the purified higher oligo-

TABLE I

VALUES OF CONSTANTS a AND b IN EQN. 1 AT A COLUMN TEMPERATURE OF 40°C

Solute	*b*	*a*
A_1	0.737	$2.32 \cdot 10^{-1}$
A_2	1.37	$8.95 \cdot 10^{-2}$
A_3	1.92	$4.50 \cdot 10^{-2}$
A_4	2.71	$1.44 \cdot 10^{-2}$
A_5	3.25	$8.09 \cdot 10^{-3}$
A_6	3.90	$3.41 \cdot 10^{-3}$
A_7	5.01	$5.38 \cdot 10^{-4}$

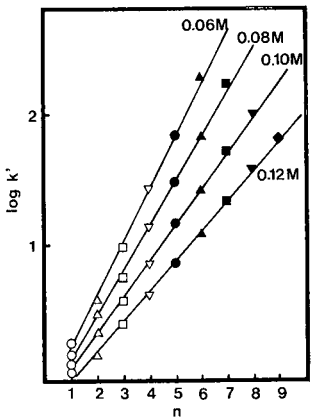

Fig. 4. Plots of log k' *vs.* the number of nucleotides of oligonucleotides, n, at various eluent concentrations (molar concentrations of phosphate buffer, pH 6.8). Column temperature: 40°C. ○ = Mono-; △ = di-; □ = tri-; ▽ = tetra-; ● = penta-; ▲ = hexa-; ■ = hepta-; ▼ = octa-; ◆ = nonaadenylate.

nucleotides or polynucleotides, an extrapolation method was employed to estimate k' values.

In isocratic elution reversed-phase chromatography, the log of the capacity factor for the members of an oligomeric series was related linearly to the polymerization number of the series for various organic compounds[32–37]. The relationship can be written as

$$\log k' = cn + d \tag{5}$$

where c and d are constant and n is the polymerization number. We found a similar relatonship in isocratic anion-exchange chromatography for oligomeric series of inorganic polyphosphates[29] and applied the extrapolation of the relationship to the retention prediction of higher polyphosphates.

The log k' values for the oligomeric series of oligoadenylates were found to increase linearly with increasing number of nucleotides, n, in isocratic anion-exchange chromatography (correlation coefficient = 0.999) at each eluent concentration (Fig. 4). Constants c and d of eqn. 5 were determined by linear regression analysis and are listed in Table II.

TABLE II
VALUES OF c AND d IN EQN. 5 FOR VARIOUS PHOSPHATE BUFFER CONCENTRATIONS

Buffer concentration (M)	c	d
0.06	0.409	−0.189
0.08	0.343	−0.209
0.10	0.278	−0.212
0.12	0.229	−0.252

TABLE III
ESTIMATED LOG *a* AND *b* VALUES AT A COLUMN TEMPERATURE OF 40°C

Solute	*b*	*log a*	*Solute*	*b*	*log a*
A_8	5.10	−3.00	A_{22}	13.4	−7.35
A_9	5.61	−3.33	A_{23}	14.0	−7.86
A_{10}	6.21	−3.65	A_{24}	14.6	−8.18
A_{11}	6.81	−3.97	A_{25}	15.2	−8.51
A_{12}	7.41	−4.30	A_{26}	15.8	−8.83
A_{13}	8.02	−4.62	A_{27}	16.5	−9.15
A_{14}	8.62	−4.94	A_{28}	17.1	−9.48
A_{15}	9.22	−5.27	A_{29}	17.7	−9.80
A_{16}	9.82	−5.59	A_{30}	18.3	−10.12
A_{17}	10.4	−5.92	A_{31}	19.0	−10.96
A_{18}	11.0	−6.24	A_{32}	19.6	−11.30
A_{19}	11.6	−6.56	A_{33}	20.2	−11.65
A_{20}	12.2	−6.89	A_{34}	20.8	−11.99
A_{21}	12.8	−7.21	A_{35}	21.4	−12.33

The capacity factors of oligoadenylates containing more than seven nucleotides at various eluent concentrations were estimated by the extrapolation of the relationships. As a result, constants *a* and *b* for higher oligonucleotides were calculated from eqn. 1 and compiled in Tabe III.

Constants *a* and *b* listed in Tables I and III were stored in the program, which is described in a previous paper[31]. After the constants for solutes are obtained and stored in a computer system, the prediction of the retention time for each solute in gradient anion-exchange chromatography becomes possible.

TABLE IV
OBSERVED (Obs.) AND CALCULATED (Calc.) RETENTION TIMES (min) UNDER GRADIENT ELUTION CONDITIONS

$x = 1$; $C_i = 0.01\ M$; $C_f = 0.3\ M$; $t_f = 128$ min; $T = 40$°C.

Solute	*Obs.*	*Calc.*	*Error(%)*	*Solute*	*Obs.*	*Calc.*	*Error(%)*
A_1	4.72	4.05	−14	A_{14}	76.3	79.9	4.7
A_2	11.6	11.6	0	A_{15}	79.4	82.3	3.7
A_3	19.8	20.3	2.5	A_{16}	82.2	84.4	2.7
A_4	28.2	30.9	9.6	A_{17}	84.9	86.4	1.8
A_5	35.5	40.2	13	A_{18}	87.5	88.1	0.69
A_6	42.1	45.9	9.0	A_{19}	89.8	89.7	−0.11
A_7	47.9	52.3	9.2	A_{20}	92.0	91.2	−0.87
A_8	53.3	57.9	8.6	A_{21}	94.1	92.6	−1.6
A_9	57.2	62.8	9.8	A_{22}	96.1	93.8	−2.3
A_{10}	61.7	67.1	8.8	A_{23}	97.4	94.9	−2.6
A_{11}	65.8	70.9	7.8	A_{24}	99.2	96.0	−3.2
A_{12}	69.5	74.3	6.9	A_{25}	101	97.0	−4.0
A_{13}	73.0	77.2	5.8				

TABLE V
OBSERVED (Obs.) AND CALCULATED (Calc.) RETENTION TIMES (min)
$x=0.58$; $C_i=0.01$ M; $C_f=0.3$ M; $t_f=240$ min; $T=40°C$.

Solute	*Obs.*	*Calc.*	*Error(%)*	*Solute*	*Obs.*	*Calc.*	*Error(%)*
A_1	5.04	3.74	−26	A_{19}	122	116	−4.9
A_2	11.7	8.70	−26	A_{20}	127	120	−5.5
A_3	17.8	14.8	−17	A_{21}	132	123	−6.8
A_4	23.7	23.7	0	A_{22}	136	126	−7.4
A_5	30.7	33.3	8.5	A_{23}	140	130	−7.1
A_6	38.0	39.8	4.7	A_{24}	145	132	−9.0
A_7	45.0	48.1	6.9	A_{25}	149	135	−9.4
A_8	52.0	56.0	7.7	A_{26}	153	137	−10
A_9	58.8	63.8	8.0	A_{27}	158	140	−11
A_{10}	65.1	70.6	8.4	A_{28}	162	142	−12
A_{11}	72.0	77.2	7.2	A_{29}	165	144	−13
A_{12}	78.9	83.4	5.7	A_{30}	169	146	−14
A_{13}	86.0	89.2	3.7	A_{31}	172	147	−15
A_{14}	92.9	94.6	1.8	A_{32}	175	149	−15
A_{15}	99.6	99.6	0	A_{33}	179	151	−16
A_{16}	106	104	−1.9	A_{34}	182	152	−16
A_{17}	112	109	−2.7	A_{35}	185	154	−17
A_{18}	117	113	−3.4				

Prediction of retention times for oligonucleotides

To predict retention times, the following parameters are input into the prediction system: column dead-time (min); flow-rate (ml/min); N_g value; adjustable parameters for the gradient profile (x, C_i, C_f and t_f).

The retention times for oligoadenylates were predicted and compared with the observed t_R values to test the performance of the present system under gradient elution conditions. Tables IV and V list the results with binary-linear ($x=1$) and binary-convex ($x=0.58$) gradient shapes (Fig. 1), respectively. The 60 observed t_R values were predicted with an average error of 7.7%.

To discuss the accuracy of the prediction in more detail, the errors of prediction and the range of n values are 6.4% ($n<25$) and 13.9% ($n\geq 25$). Predictions reported in gradient reversed-phase chromatography[21,25,26,38,39] were achieved in the range of errors from 3 to 8%. In comparison with the reported errors, our result for lower oligoadenylates was satisfactory but that for higher oligoadenylates was slightly poor. The reason is that the constants a and b used in the predictions were extrapolated from the data for the first seven oligoadenylates, while the t_R values reported in reversed-phase chromatography were predicted without extrapolation methods. As a result, we conclude that the extrapolation of the relationship between log k' and n is successful in the estimation of capacity factors for higher oligoadenylates under gradient elution conditions.

As an example, the predicted chromatogram displayed on the monitor screen was compared with a chromatogram observed under the gradient elution conditions in Table V, as shown in Fig. 5. In the predicted chromatogram, the peaks were given gaussian profiles by use of the predicted retention times (Table V) and band widths

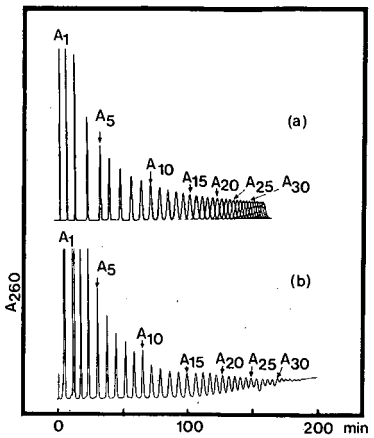

Fig. 5. Predicted (a) and observed (b) chromatograms for a polyadenylate partial hydrolyzate. (a) Gradient elution conditions as in Table V. (b) Column: Shim-pack WAX-1 (weak anion exchanger, 50 mm × 4 mm I.D.). Flow-rate: 1.0 ml/min. Buffer: A, 0.01 *M* phosphate (pH 6.8) containing 20% acetonitrile; B, 0.3 *M* phosphate (pH 6.8) containing 20% acetonitrile. Gradient elution conditions as in Table V. Column temperature: 40°C.

calculated by eqn. 4. The area of each peak was assumed to be the same. The characteristics of each chromatogram are similar with respect to the retention times, band widths and resolution.

When the present prediction system is applied to the other separation variables including stationary phases, mobile phases and equipment, constants *a* and *b* in eqn. 1 will be obtained with a minimum number of experiments (at least three sets of experiments under isocratic elution conditions).

ACKNOWLEDGEMENT

The authors wish to express their thanks to Professor Takami Awa of Beppu University and Professor Teruko Abe of Oita University for their cooperation in assembling the TRI-ROTAR II HPLC system.

REFERENCES

1 J. B. Crowther and R. A. Hartwick, in P. R. Brown (Editor), *HPLC in Nucleic Acid Research*, Marcel Dekker, New York, 1984, Ch. 11, pp. 195–213.
2 L. W. McLaughlin and R. Bischoff, *J. Chromatogr.*, 418 (1987) 51.
3 R. Hecker and D. Riesner, *J. Chromatogr.*, 418 (1987) 97.
4 R. D. Wells, S. C. Hardies, G. T. Horn, B. Klein, J. E. Larson, S. K. Neuendorf, N. Panayotatos, R. K. Patient and E. Selsing, *Methods Enzymol.*, 65 (1980) 327.
5 J. D. Pearson and F. E. Regnier, *J. Chromatogr.*, 255 (1983) 137.
6 M. Colpan, D. Riesner, *J. Chromatogr.*, 296 (1984) 339.
7 R. R. Drager and F. E. Regnier, *Anal. Biochem.*, 145 (1985) 47.
8 R. R. Drager and F. E. Regnier, *J. Chromatogr.*, 359 (1986) 147.
9 P. A. D. Edwardson, C. R. Lowe and T. Atkinson, *J. Chromatogr.*, 368 (1986) 363.
10 T. Ueda and Y. Ishida, *J. Chromatogr.*, 386 (1987) 273.
11 J. B. Crowther, S. D. Fazio and R. A. Hartwick, *J. Chromatogr.*, 282 (1983) 619.

12 R. Bischoff and L. W. McLaughlin, *J. Chromatogr.*, 296 (1984) 329.
13 R. Bischoff and L. W. McLaughlin, *Anal. Biochem.*, 151 (1985) 526.
14 E. Selsing, J. E. Larson and R. D. Wells, *Anal. Biochem.*, 99 (1979) 213.
15 R. Lohrmann and L. E. Orgel, *J. Mol. Biol.*, 142 (1980) 555.
16 H. Sawai, *Nucleic Acids Res. Symp. Ser.*, No. 15 (1984) 105.
17 G. D. McFarland and P. N. Borer, *Nucleic Acids Res.*, 7 (1979) 1067.
18 H.-J. Fritz, R. Belagaje, E. L. Brown, R. H. Fritz, R. A. Jones, R. G. Lees and H. G. Khorana, *Biochemistry*, 17 (1978) 1259.
19 G. D'Agostino, L. Castagnetta, F. Mitchell and M. J. O'Hare, *J. Chromatogr.*, 338 (1985) 1.
20 P. Jandera and J. Churáček, *J. Chromatogr.*, 91 (1974) 223.
21 P. Jandera and J. Churáček, *Adv. Chromatogr. (N.Y.)*, 19 (1981) 125.
22 P. Jandera and J. Churáček, *Gradient Elution in Column Liquid Chromatography*, Elsevier, Amsterdam, 1985.
23 L. R. Snyder, J. W. Dolan and J. R. Gant, *J. Chromatogr.*, 165 (1979) 3.
24 K. Jinno and K. Kawasaki, *J. Chromatogr.*, 316 (1984) 1.
25 S. A. Tomellini, R. A. Hartwick and H. B. Woodruff, *Anal. Chem.*, 57 (1985) 811.
26 K. Jinno and M. Kuwajima, *Chromatograhia*, 21 (1986) 541.
27 Y. Baba, N. Yoza and S. Ohashi, *J. Chromatogr.*, 348 (1985) 27.
28 Y. Baba, N. Yoza and S. Ohashi, *J. Chromatogr.*, 350 (1985) 119.
29 Y. Baba, N. Yoza and S. Ohashi, *J. Chromatogr.*, 350 (1985) 461.
30 Y. Baba, *J. Assoc. Pers. Comput. Chem.*, 7, No. 1 (1985) 119.
31 Y. Baba, *J. Assoc. Pers. Comput. Chem.*, 7, No. 3 (1985) 41.
32 H. Colin and G. Guiochon, *J. Chromatogr. Sci.*, 18 (1980) 54.
33 P. Dufek and E. Smolková, *J. Chromatogr.*, 257 (1983) 247.
34 P. Dufek, *J. Chromatogr.*, 281 (1983) 49.
35 A. Tchapla, H. Colin and G. Guiochon, *Anal. Chem.*, 56 (1984) 621.
36 P. Jandera, *J. Chromatogr.*, 314 (1984) 13.
37 P. Jandera, *Chromatographia*, 19 (1984) 101.
38 P. Jandera, J. Churáček and L. Svoboda, *J. Chromatogr.*, 174 (1979) 35.
39 S. A. Tomellini, S.-H. Hsu and R. A. Hartwick, *Anal Chem.*, 58 (1986) 904.

Journal of Chromatography, 458 (1988) 395–404
Elsevier Science Publishers B.V., Amsterdam — Printed in The Netherlands

CHROMSYMP. 1516

DETERMINATION OF HYDROPHOBICITY PARAMETERS ON POLYBUTADIENE-COATED ALUMINA AND THEIR APPLICATION IN QUANTITATIVE STRUCTURE–ACTIVITY RELATIONSHIPS ANALYSIS

ROMAN KALISZAN * and JACEK PETRUSEWICZ
Medical Academy, K. Marksa 107, 80-416 Gdansk (Poland)
and
ROGER W. BLAIN and RICHARD A. HARTWICK
Department of Chemistry, Rutgers University, Piscataway, NJ 08854 (U.S.A.)

SUMMARY

The reversed-phase high-performance liquid chromatographic (HPLC) method of hydrophobicity evaluation based on polybutadiene-coated alumina columns was applied in quantitative structure–activity relationship (QSAR) studies of a group of pharmacologically active azole derivatives. The solutes (weak organic bases) were chromatographed at pH 7.30 and 11.5. The HPLC data obtained under alkaline conditions correlated well with hydrophobicity parameter calculated for non-ionized forms of the compounds. The same chromatographic data were demonstrated to provide the most significant information on the biological activity of the compounds under study. The polymer-coated alumina stationary phases developed by Schomburg and co-workers, which can be used over a wide range of eluent pH values and which show no tendency to undergo the specific interactions with solutes typical of silica-based materials, offer unique advantages from the point of view of QSAR applications.

INTRODUCTION

Hydrophobicity (lipophilicity) is a structural feature of compounds that has important effects on biological activity. Determination of the hydrophobicity of the compounds considered is often required in order to rationalize the mechanism of pharmacological action at the molecular level, to predict the activity of drug candidates or other xenobiotics, to evaluate the hazards of environmental pollution, etc.

A single, continuous scale for measurement of hydrophobicity (log P) is provided by the n-octanol–water partition system. Numerous limitations of the "shake-flask" method for the determination of log P justified efforts to develop more convenient and reliable chromatographic methods of hydrophobicity characterization[1]. High-performance liquid chromatography (HPLC) is the preferred approach for the determination of lipophilicity, having the following advantages: it is fast and suitable for substances containing impurities, for mixtures and for volatile compounds; it

0021-9673/88/$03.50

requires no quantitative determination; it is highly reproducible and can be applied over a wide hydrophobicity range; and it provides precise control of pH and ionic strength during the separation process.

The reversed-phase HPLC systems most often used for hydrophobicity characterization employ alkyl ligands chemically bonded to the silica support surface[1–4]. There are two main disadvantages of the hydrocarbonaceous silica stationary phases: the possibility of interaction of some solutes with the free silanol sites on the silica support surface and the chemical instability of alkyl-bonded silicas at pH above *ca.* 8 (ref. 5).

In a search for a stationary phase allowing hydrophobicity comparisons of undissociated organic bases, we considered the new generation of polymer-coated reversed-phase stationary phases introduced by Schomburg and co-workers[6,7]. Using such a stationary phase, we proposed[5] an HPLC method for the determination of the hydrophobicity of diverse basic, neutral and acidic solutes of different chemical classes. The capacity factors (log k') determined for a set of 22 test solutes were linearly correlated with the *n*-octanol–water partition coefficients (log P).

In this paper we report the results of studies on the application of the previously proposed method of hydrophobicity evaluation to the determination of quantitative structure–activity relationships (QSAR). The compounds of interest are newly synthesized azole-type organic bases possessing varying circulatory activity[8]. The biological activity data, pIC_{30}, determined independently[9,10], are the negative logarithms of the molar concentrations of the compounds giving 30% inhibition of the human blood platelet aggregation caused by 10^{-5} M adrenaline.

The lipophilicity of the compounds in a non-ionized form, which is assumed to interact with biological receptors, is of interest for QSAR studies. On the other hand, the overall lipophilicity of the non-ionized and ionized species at physiological pH may also be important, as it may be related to the penetration of drug in living systems, and thus to its availability to specific receptors located in various body compartments. With this in mind, we planned our HPLC determinations at pH 7.30 and 11.5. For the sake of comparison the hydrophobicity, Σf, of the agents studied was calculated on the basis of the so-called fragment method of Hansch and Leo[11]. The HPLC data were related to the hydrophobicity data derived from the structural formulae of the agents studied and also to their biological activity data.

EXPERIMENTAL

Chromatography

The chromatographic system (Altex Scientific, Berkeley, CA, U.S.A.) consisted of a single-piston reciprocating pump and a Model 157 UV detector operating at 254 nm. A Rheodyne (Cotati, CA, U.S.A.) Model 7410 injection valve fitted with a 10-μl sample loop was used. A 150 × 4.6 mm I.D. stainless-steel column was slurry-packed using 2-propanol as the slurry solvent and methanol as the packing solvent. Polybutadiene-coated Spherisorb A5Y stationary phase was prepared according to the procedure of Schomburg and co-workers[6,7]. The polybutadiene was immobilized on the alumina support surface with the help of cross-linking reactions involving radical formation.

As a compromise between reasonable retention times for the most strongly

retained solutes and a reliable pH for the control of ionization, a methanol–buffer (1:1, v/v) eluent was used. Two buffers were applied: for pH 7.30 the buffer was 0.1 *M* potassium dihydrogenphosphate–0.1 *M* sodium hydroxide and for pH 11.5 the buffer was 0.05 *M* disodium hydrogenphosphate–0.1 *M* sodium hydroxide.

The structures of the solutes under study are given in Table I; a general procedure for their preparation is described elsewhere[8].

To calculate the capacity factors, k', the solvent disturbance peak was used as a reference. Reproducible data for the solvent disturbance peak were obtained when trace amounts of methanol were injected into the column. The logarithms of the capacity factors, log k', given in Table I are the means of three determinations.

Structural analysis

The method of calculation of the hydrophobicity parameter, Σf, according to Hansch and Leo[11] is illustrated in Fig. 1. The superscript φ denotes substitution in aromatic systems; fragments fused in an aromatic ring are underlined; subscript b is a geometric factor proportional to the length minus 1 of a chain (no superscript) or a ring (superscript ring); the subscript (=) represents unsaturation; F_{HBN} is a correction

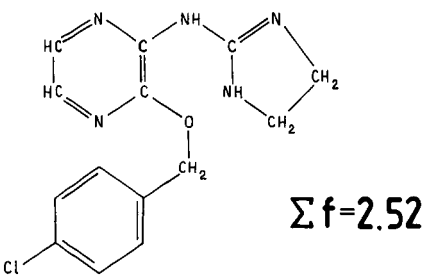

$\Sigma f = 2.52$

f_{Cl}^{φ}	= 0.94
$f_{C_6H_4}$	= 1.67
f_{CH_2}	= 0.66
f_{O}^{φ}	= 0.61
$F_b \times (3-1)$	= −0.24
$f_N \times 2$	= −2.24
$f_{\underline{CH}} \times 2$	= 0.70
$f_{\underline{C}} \times 2$	= 0.26
f_{NH}^{φ}	= −1.03
f_C	= 0.20
f_{NH}	= −2.15
f_N	= −2.38
$f_{CH_2} \times 2$	= 1.32
$F_b \times (2-1)$	= −0.12
$F_b^{ring} \times (5-1)$	= −0.36

$F_{(=)}$	= −0.55
F_{HBN}	= 0.60
F_{p2}^{φ}	= −0.08(−1.12 − 1.12) = 0.18
F_{p2}^{φ}	= −0.08(−1.12 − 0.61) = 0.14
F_{p1}^{φ}	= −0.16(−1.12 − 0.61) = 0.28
F_{p2}^{φ}	= −0.08(−1.03 − 0.61) = 0.13
F_{p2}^{φ}	= −0.08(−1.12 − 1.03) = 0.17
F_{p1}^{φ}	= −0.16(−1.12 − 1.03) = 0.34
F_{p2}^{φ}	= −0.08(−1.12 − 0.61) = 0.14
F_{p1}^{ring}	= −0.32(−2.38 − 1.03) = 1.09
F_{p1}^{ring}	= −0.32(−2.15 − 1.03) = 1.02
F_{p1}^{ring}	= −0.32(−2.38 − 2.15) = 1.45
F_{p2}^{ring}	= −0.20(−2.38 − 2.15) = 0.91

Fig. 1. Sample calculations of the hydrophobicity parameter, Σf, by the fragment method of Hansch and Leo[11]. For details, see text.

TABLE I

STRUCTURES, CAPACITY FACTORS, HYDROPHOBICITY PARAMETERS AND ANTI-AGGREGATORY ACTIVITIES OF PYRAZINYLDIAZACYCLOALKANES

No.	*Structure*	*Log k'*		*Σf*	*pIC_{30}*
		pH 11.5	*pH 7.30*		
1′	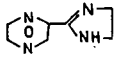	−0.353	−0.125	−1.41	9.68*
2′	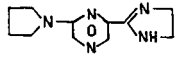	0.160	−0.085	0.49	10.72
3′	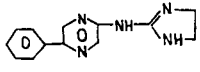	0.708	0.434	0.71	10.22
4′	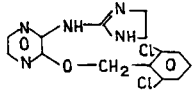	1.163	0.836	3.23	8.80
5′	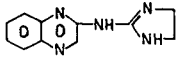	0.054	0.091	0.61	8.13**
6′	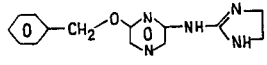	0.582	0.398	0.70	10.20
7′	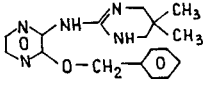	1.050	0.776	2.55	9.96

8′	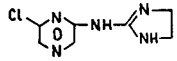	−0.109	−0.262	−0.25	9.68*
9′	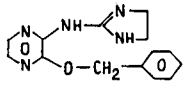	0.755	0.410	1.81	9.33
10′	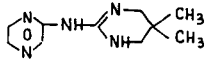	0.301	0.015	0.11	10.22
11′	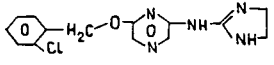	0.831	0.702	1.41	9.12
12′	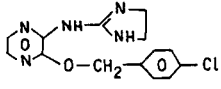	1.270	0.760	2.52	8.11
13′	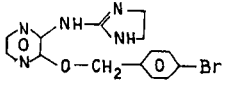	1.402	0.879	2.67	−***
14′	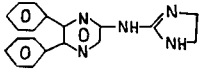	1.145	0.905	2,14	8.66
15′	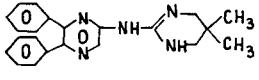	1.913	1.279	3.45	−***

* Partial agonist.
** Full agonist.
*** No 30% antagonist effect attained.

for intramolecular hydrogen bonding; and F_P factors account for the H-polar proximity effects when two H-polar fragments are separated by one (subscript 1) or two (subscript 2) carbon atoms. The sum of individual fragments and correction factors yields the total hydrophobicity, Σf (Table I).

Pharmacological data

Anti-aggregatory activity of the compounds studied was determined independently[9,10] by the turbidimetric method of Born[12]. Of the fifteen compounds studied (Table I), compound 5′ showed significant aggregatory activity. The anti-aggregatory effects of compounds 13′ and 15′ were less than 30% at the highest concentrations obtained. The anti-aggregatory activity data, pIC_{30}, are given in Table I.

RESULTS AND DISCUSSION

The correlation between capacity factors determined at pH 7.30 and 11.5 is shown in Fig. 2. Deviation of the data points from a straight line results from differences in the degree of ionization of the solutes at the two pH values studied. The compounds studied are weak bases, but at pH 7.30 at least some of them are still partially ionized. As pointed out by the referee, the log k' values decreased for compounds 1′ and 5′ when measured at higher pH values. This is opposite to the expected behaviour and may indicate interaction between the solute and the alumina backbone.

Figs. 3 and 4 shows relationships between Σf and log k', as determined at pH 7.30 and 11.5, respectively. Evidently, the correlation between Σf and log k' determined at pH 11.5 is better. For the total number of solutes (n = 15) the correlation coefficient, r, is 0.944, the standard deviation from regression, s, is 0.223 and the

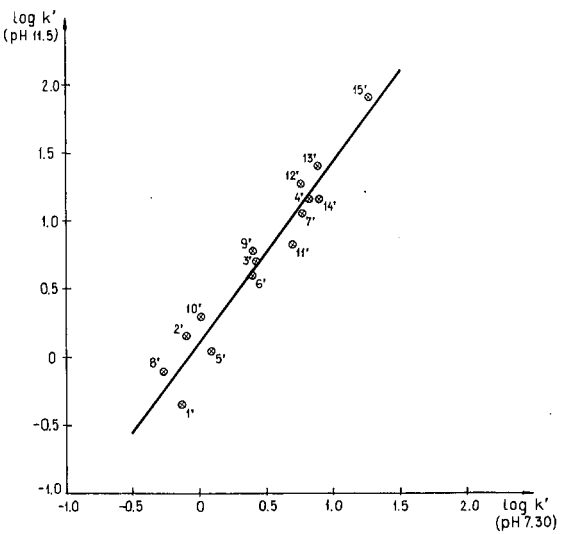

Fig. 2. Correlation between the HPLC capacity factors determined at different pH values for the solutes listed in Table I. log k' (pH 11.5) = 1.323 log k' (pH 7.30) + 0.106 (n = 15, r = 0.969, s = 0.168, p = 5.4 · 10^{-8}).

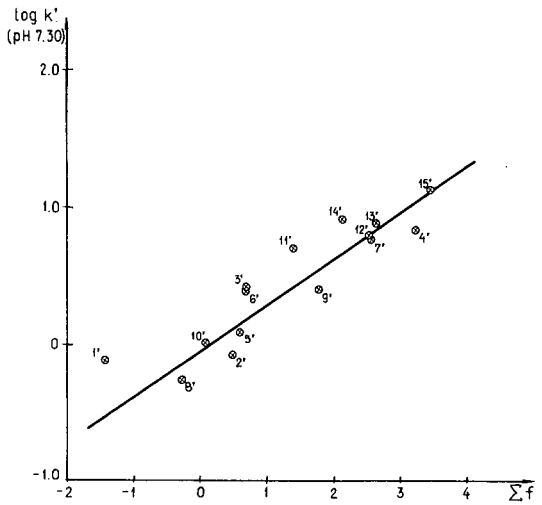

Fig. 3. Relationship between the theoretically calculated hydrophobicity parameter, Σf, and the capacity factor, log k', determined at pH 7.30. Compounds are numbered as in Table I. log k' (pH 7.30) = 0.301 Σf + 0.052 (n = 15, r = 0.915, s = 0.199, $p = 1.8 \cdot 10^{-5}$).

significance level, p, is $1.7 \cdot 102^{-6}$. The respective data for the relationship Σf *vs.* log k' (pH 7.30) are r = 0.915, s = 0.199 and $p = 1.8 \cdot 10^{-5}$. As the Σf values represent hydrophobicities of non-ionized forms of the compounds, the log k' data for bases determined at higher pH shoud correlate better with Σf, as occurs here.

Fig. 5 shows the relationship between Σf and bioactivity data, pIC_{30}. Although the scattering of the data is obvious, some regularities are apparent. Keeping in mind

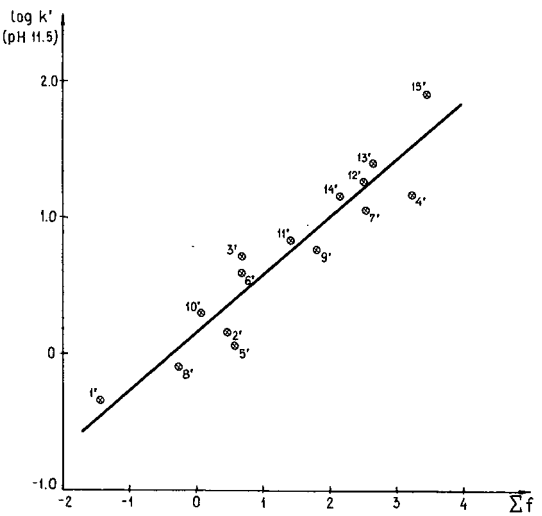

Fig. 4. Relationship between the theoretically calculated hydrophobicity parameter, Σf, and the capacity factor, log k', determined at pH 11.5. Compounds are numbered as in Table I. Log k' (pH 11.5) = 0.424 Σf + 0.139 (n = 15, r = 0.944, s = 0.223, $p = 1.7 \cdot 10^{-6}$).

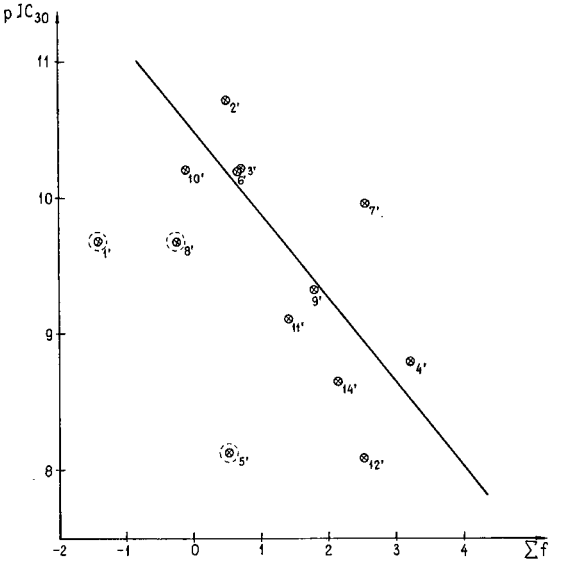

Fig. 5. Anti-aggregatory activity, pIC_{30}, as a function of the theoretically calculated hydrophobicity parameter, Σf. Compounds are numbered as in Table I. Compounds 1′, 5′ and 8′ were excluded from the regression analysis. $pIC_{30} = -0.62\ \Sigma f + 10.50$ ($n = 10$, $s = 0.63$, $r = 0.761$, $p = 4.8 \cdot 10^{-2}$).

the generally limited precision of the determination of hydrophobicity by means of the hydrophobicity parameter, Σf, one may conclude that the anti-aggregatory activity of the compounds studied decreases with increasing hydrophobicity.

A similar trend is observed in Fig. 6, where the same biological activity data are

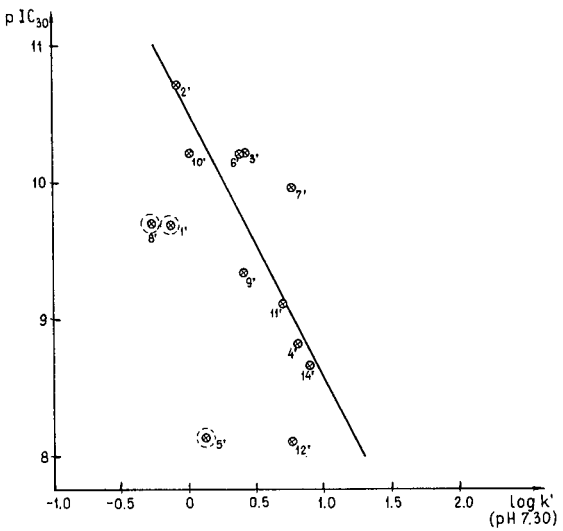

Fig. 6. Anti-aggregatory activity, pIC_{30}, as a function of the HPLC capacity factors determined at pH 7.30. Compounds are numbered as in Table I. Compounds 1′, 5′ and 8′ were excluded from the regression analysis, $pIC_{30} = -1.94 \log k'$ (pH 7.30) + 10.53 ($n = 10$, $s = 0.60$, $r = 0.784$, $p = 3.5 \cdot 10^{-2}$).

plotted against log k' values determined at pH 7.30. The scattering of the data points in Fig. 6 is less than that in Fig. 5, but the predictive value of the pIC_{30} *vs.* log k' (pH 7.30) relationship is not better than the pIC_{30} *vs.* Σf relationship.

The correlation between pIC_{30} and log k' (pH 11.5) is shown in Fig. 7. The observed relationship is satisfactory from the point of view of biological QSAR, especially if one realizes that hydrophobicity is an important but by no means exclusive structural factor affecting biological activity. The obvious outlier is compound 5', which was proved to be an agonist. Compounds 1' and 8' are also outliers. The possible explanation for this is that these compounds possess mixed aggregatory and anti-aggregatory properties. Such a phenomenon was observed independently in pharmacological studies of a group of structurally related imidazoline drugs[13].

Compounds 13' and 15' require separate discussion. For these highly hydrophobic solutes no 30% inhibition of the adrenaline-induced aggregation was obtained at concentrations of up to 10^{-8} *M*. However, if one extrapolates the plot of percentage inhibition against the concentration of the compound to 30% inhibition of aggregation, then the extrapolated biological activity values, pIC_{30} (extrapolated), fit the relationship shown in Fig. 7.

In QSAR studies, the physical interpretation of the relationships is important. The results obtained here clearly indicate that the more hydrophobic the compound, the lower is its ability to produce 30% inhibition of the adrenaline-induced aggregation. Such an observation could appear surprising, as the reverse dependence of biological activity on hydrophobicity is more commonly reported. However, a similar hydrophobicity–biological activity dependence was found by Hansch and Steward[14] as early as 1964. They linked the concentration of penicillin derivatives needed to cure mice of a bacterial infection to the hydrophobicity of the substituents. In subsequent

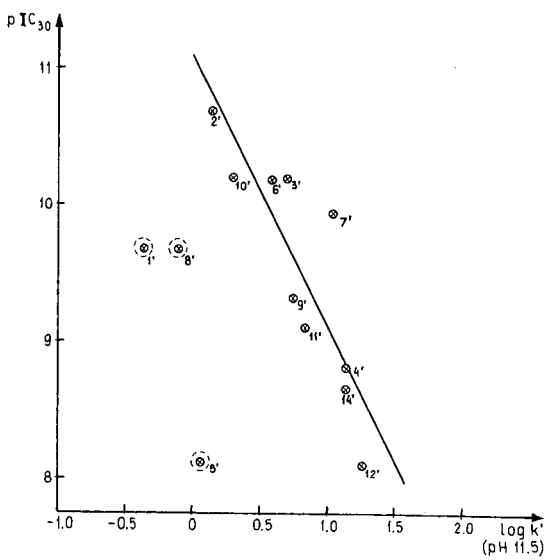

Fig. 7. Anti-aggregatory activity, pIC_{30}, as a function of the HPLC capacity factors determined at pH 11.5. Compounds are numbered as in Table I. Compounds 1', 5' and 8' were excluded from the regression analysis. pIC_{30} = −1.95 log k' (pH 11.5) + 11.09 (n = 10, s = 0.50, r = 0.856, p = 1.0 · 10^{-3}).

studies it was demonstrated that the observed hydrophobicity–biological activity relationship for penicillins resulted from the fact that hydrophobicity promoted binding to a different than the pharmacological receptor site of loss to a greater extent than it promoted antibacterial activity[15]. Similarly, the binding to human serum albumin can also reduce the effective concentration of the compounds studied here, reaching the target, *i.e.*, blood platelet adrenoceptor.

From the chromatographic point of view the most important conclusion is that the HPLC method for the evaluation of hydrophobicity employing polybutadiene-coated alumina columns readily provides structural information directly applicable to QSAR studies. The chemical stability of the new polymer-coated reversed-phase materials over a wide range of eluent pH values, including alkaline environments, is especially valuable. In effect, the hydrophobicity of non-ionized forms of solutes, including organic bases, can be directly quantified by HPLC.

Leaving aside the question of what the hydrophobicity really is, we realize that individual hydrophobicity parameters depend on the method of determination. Also, the semi-empirical fragmental methods for the evaluation of hydrophobicity do not yield absolute quantities because of some ambiguities in fragment and/or correction factor definition and identification. Hence the method of choice should be one that produces the best QSAR. In this work, the HPLC method for the determination of the hydrophobicity of basic solutes at pH 11.5, employing polybutadiene-coated alumina columns, yielded better QSAR than the theoretically calculated hydrophobicity parameter or HPLC data obtained at the pH at which ordinary reversed-phase hydrocarbonaceous silica columns can be operated.

REFERENCES

1 R. Kaliszan, *Quantitative Structure–Chromatographic Retention Relationships*, Wiley, New York, 1987, p. 232.
2 J. J. Sabatka, D. K. Minick, T. J. Shumaker, G. L. Hodgson, Jr. and D. A. Brent, *J. Chromatogr.*, 384 (1987) 349.
3 C. V. Eadsforth, *Pestic. Sci.*, 17 (1986) 311.
4 K. Valkó, *J. Liq. Chromatogr.*, 10 (1987) 1663.
5 R. Kaliszan, R. W. Blain and R. A. Hartwick, *Chromatographia*, 25 (1988) 5.
6 U. Bien-Vogelsang, A. Deege, H. Figge, J. Kohler and G. Schomburg, *Chromatographia*, 19 (1984) 170.
7 G. Heinemann, J. Kohler and G. Schomburg, *Chromatographia*, 23 (1987) 435.
8 R. Kaliszan, H. Foks, B. Damasiewicz, A. Nasal, A. Radwanska, W. Kuzmierkiewicz, D. Pancechowska-Ksepko, W. Rudnicka and K. Wisterowicz, *Pol. J. Pharmacol. Pharm.*, 37 (1985) 79.
9 J. Petrusewicz and R. Kaliszan, *Agents Actions*, 23 (1988) 1.
10 J. Putrusewicz and R. Kaliszan, unpublished data.
11 C. Hansch and A. Leo, *Substituent Constants for Correlation Analysis in Chemistry and Biology*, Wiley, New York, 1979, p. 18.
12 G. V. R. Born, *Nature (London)*, 194 (1962) 927.
13 J. Petrusewicz and R. Kaliszan, *Pharmacology*, 33 (1986) 249.
14 C. Hansch and A. Steward, *J. Med. Chem.*, 7 (1964) 691.
15 A. Leo, *Environ. Health Perspect.*, 61 (1985) 275.

Author Index

PUBLICATION SCHEDULE FOR 1988

Journal of Chromatography and Journal of Chromatography, Biomedical Applications

MONTH	J	F	M	A	M	J	J	A	S	O	N	D
Journal of Chromatography	435/1 435/2 435/3 436/1	436/2 436/3	437/1 437/2	438/1 438/2	439/1 439/2 440 441/1	441/2 442 443	444 445/1 445/2 446	447/1 447/2 448/1	448/2 448/3 449/1	449/2 450/1 450/2 450/3 452	453 454 455	456/1 456/2 457 458 459
Bibliography Section		460/1		460/2		460/3		460/4		460/5		460/6
Cumulative Indexes, Vols. 401–450												451
Biomedical Applications	424/1	424/2	425/1 425/2	426/1 426/2	427/1	427/2 428/1	428/2 429	430/1	430/2 431/1	431/2	432	433 434/1 434/2

INFORMATION FOR AUTHORS

(Detailed *Instructions to Authors* were published in Vol. 445, pp. 453–456. A free reprint can be obtained by application to the publisher, Elsevier Science Publishers B.V., P.O. Box 330, 1000 AH Amsterdam, The Netherlands.)

Types of Contributions. The following types of papers are published in the *Journal of Chromatography* and the section on *Biomedical Applications:* Regular research papers (Full-length papers), Notes, Review articles and Letters to the Editor. Notes are usually descriptions of short investigations and reflect the same quality of research as Full-length papers, but should preferably not exceed six printed pages. Letters to the Editor can comment on (parts of) previously published articles, or they can report minor technical improvements of previously published procedures; they should preferably not exceed two printed pages. For review articles, see inside front cover under Submission of Papers.

Submission. Every paper must be accompanied by a letter from the senior author, stating that he is submitting the paper for publication in the *Journal of Chromatography*. Please do not send a letter signed by the director of the institute or the professor unless he is one of the authors.

Manuscripts. Manuscripts should be typed in double spacing on consecutively numbered pages of uniform size. The manuscript should be preceded by a sheet of manuscript paper carrying the title of the paper and the name and full postal address of the person to whom the proofs are to be sent. Authors of papers in French or German are requested to supply an English translation of the title of the paper. As a rule, papers should be divided into sections, headed by a caption (*e.g.*, Summary, Introduction, Experimental, Results, Discussion, etc.). All illustrations, photographs, tables, etc., should be on separate sheets.

Introduction. Every paper must have a concise introduction mentioning what has been done before on the topic described, and stating clearly what is new in the paper now submitted.

Summary. Full-length papers and Review articles should have a summary of 50–100 words which clearly and briefly indicates what is new, different and significant. In the case of French or German articles an additional summary in English, headed by an English translation of the title, should also be provided. (Notes and Letters to the Editor are published without a summary.)

Illustrations. The figures should be submitted in a form suitable for reproduction, drawn in Indian ink on drawing or tracing paper. Each illustration should have a legend, all the *legends* being typed (with double spacing) together on a *separate sheet*. If structures are given in the text, the original drawings should be supplied. Coloured illustrations are reproduced at the author's expense, the cost being determined by the number of pages and by the number of colours needed. The written permission of the author and publisher must be obtained for the use of any figure already published. Its source must be indicated in the legend.

References. References should be numbered in the order in which they are cited in the text, and listed in numerical sequence on a separate sheet at the end of the article. Please check a recent issue for the layout of the reference list. Abbreviations for the titles of journals should follow the system used by *Chemical Abstracts*. Articles not yet published should be given as "in press" (journal should be specified), "submitted for publication" (journal should be specified), "in preparation" or "personal communication".

Dispatch. Before sending the manuscript to the Editor please check that the envelope contains three copies of the paper complete with references, legends and figures. One of the sets of figures must be the originals suitable for direct reproduction. Please also ensure that permission to publish has been obtained from your institute.

Proofs. One set of proofs will be sent to the author to be carefully checked for printer's errors. Corrections must be restricted to instances in which the proof is at variance with the manuscript. "Extra corrections" will be inserted at the author's expense.

Reprints. Fifty reprints of Full-length papers, Notes and Letters to the Editor will be supplied free of charge. Additional reprints can be ordered by the authors. An order form containing price quotations will be sent to the authors together with the proofs of their article.

Advertisements. Advertisement rates are available from the publisher on request. The Editors of the journal accept no responsibility for the contents of the advertisements.

Analytical Artifacts

GC, MS, HPLC, TLC and PC

by **B.S. MIDDLEDITCH**, *Dept. of Biochemical and Biophysical Sciences, University of Houston, Houston, TX, USA*

(Journal of Chromatography Library, 44)

This encyclopaedic catalogue of the pitfalls and problems that all analysts encounter in their work is destined to spend more time on the analyst's workbench than on a library shelf. The author has dedicated the book to "the innumerable scientists who made mistakes, used impure chemicals and solvents, suffered the consequences of unanticipated side-reactions, and were otherwise exposed to mayhem yet were too embarrassed to publish their findings".

Traditionally, the mass spectroscopist or gas chromatographer learnt his trade by participating in a 4-6 year apprenticeship as graduate student and post-doctoral researcher. Generally, no formal training was provided on the things that go wrong, but this information was accumulated by sharing in the experiences of colleagues. Nowadays, many novice scientists simply purchase a computerized instrument, plug it in, and use it. Much time can be wasted in studying and resolving problems due to artifacts and there is also a strong possibility that artifacts will not be recognized as such. For example, most analysts realize that they should use glass rather than plastic containers; but few of them would anticipate the possibility of plasticizer residues on glassware washed using detergent from a plastic bottle.

This book is an easy-to-use compendium of problems encountered when using various commonly used analytical techniques. Emphasis is on impurities, by-products, contaminants and other artifacts. A separate entry is provided for each artifact. For specific chemicals, this entry provides the common name, mass spectrum, gas chromatographic data, CAS name and registry number, synonyms and a narrative discussion. More than 1100 entries are included. Mass spectral data are indexed in a 6-peak index (molecular ion, base peak, second peak, third peak) and there are also formula, author and subject indexes. An extensive bibliography contains complete literature citations.

The book is designed to be *used*. It will not only allow experienced analysts to profit from the mistakes of others, but it will also be invaluable to other scientists who use analytical instruments in their work.

1989 xxiv + 1028 pages
US$ 241.50 / Dfl. 495.00
ISBN 0-444-87158-6

ELSEVIER SCIENCE PUBLISHERS

P.O. Box 211, 1000 AE Amsterdam, The Netherlands
P.O. Box 882, Madison Square Station, New York, NY 10159, USA